



Luminescent hybrid materials for LED lighting

Qiqiao Lin

► To cite this version:

Qiqiao Lin. Luminescent hybrid materials for LED lighting. Organic chemistry. Université Paris Saclay (COmUE), 2019. English. NNT : 2019SACLX036 . tel-03334741

HAL Id: tel-03334741

<https://theses.hal.science/tel-03334741>

Submitted on 5 Sep 2021

HAL is a multi-disciplinary open access archive for the deposit and dissemination of scientific research documents, whether they are published or not. The documents may come from teaching and research institutions in France or abroad, or from public or private research centers.

L'archive ouverte pluridisciplinaire **HAL**, est destinée au dépôt et à la diffusion de documents scientifiques de niveau recherche, publiés ou non, émanant des établissements d'enseignement et de recherche français ou étrangers, des laboratoires publics ou privés.

Luminescent hybrid materials for LED lighting

Thèse de doctorat de l'Université Paris-Saclay
préparée à l'**École Polytechnique**

École doctorale n°571 Sciences chimiques :
molécules, matériaux, instrumentation et biosystèmes (2MIB)
Spécialité de doctorat: **Chimie**

Thèse présentée et soutenue à Palaiseau, le 04/09/2019, par

M. Qiqiao Lin

Composition du Jury :

Mme. Isabelle Ieray

Directrice de Recherche, CNRS, ENS-Cachan (UMR 8531)

Présidente

Mme. Françoise Le Guen

Professeur, CNRS, Université Rennes 1 (UMR 6226)

Rapporteuse

M. Olivier Maury

Directeur de Recherche, CNRS, ENS de Lyon (UMR 5182)

Rapporteur

M. Alain Ibanez

Directeur de Recherche, CNRS, Institut Néel (UPR 2940)

Examineur

M. Gaël Zucchi

Chargé de recherche, CNRS, École Polytechnique (UMR 7647)

Directeur de thèse

Acknowledgements

For the past years I have enjoyed a lot the research that I was doing and have a good experience working here. My deepest gratitude is to my supervisor Dr. Gaël ZUCCHI, who gave me the precious opportunity to study here, and he helped me a lot to learn the project little by little with patience and good consideration. He gave me a lot of good advices that make me develop the project much more smoothly. Whenever I had questions and problems, he was always there and provided sufficient and effective assistance to me. Thanks very much to him for giving me a so interesting project that opened a new wonderful science-world to me. His intelligence and rich knowledge always inspired me and encouraged me. His great sense of humor made the daily life here much more fascinating.

Especially thanks also to Dr. Xinyang Wang who introduced me to the place. Also much thanks to Dr. Abderrahim Yassar, Dr. Ramachandran Sasikumar, Dr. Guang Hu, Melissa Richard, Shiwei Ren and Choi Jonghyun for sharing much time together in the ChimOrga lab and we always did good to keep everything organized and becoming better in the lab. Thanks for Dr. Bérengère Lebental and Dr. Laurence Bodelot who always kindly provided me suggestions for how to better present my work to people and for their questions and suggestions about my work. Thanks for Dr. Boris Gusarov for helping me with the AFM measurements and training me how to properly work in the Platine lab. And thanks to all OLAE members and Platine members, e.g. Prof. Yvan Bonnassieux, Robert Benda, Cho Gookbin, Massonnet Nicolas, Arruabarrena Patxi, Arikudil Mathew Vivin Varghese, Tanguy Levent, Chloé Dindault, Shirinskaya Anna, Dmitri Daineka, Maëlle Buisson, Sort montenegro Annaël, Nicolas Daveau, Minjin Kim, Nahdi Hindia. We had a lot of fruitful discussions in our group meetings and some of us have shared much wonderful afterwork “drinking” time and concert and movie time. Our good collaboration and much care and assistance to each other made our research day full of warm, humor and sweet. I am also much grateful to all PICM members with who I have shared plenty of works and time and brought a lot of fun to our life, especially the director, Prof. Pere Roca i Cabarrocas, for his good management of the lab with intelligence.

I would also like to thank Prof. Geneviève Chadeyron and her group, especially Rachod Boonsin, Yasmine Khendriche, and Jean-Philippe Roblin for measurements on phosphors at the Clermont Ferrand Institute of Chemistry (ICCF). Much thanks for Prof. Geneviève Chadeyron

who kindly accepted to be my “membre du comité de suivi de thèse”, and thanks for her encouraging positive comments. Also, thanks to Dr. Laurent Bouteiller for a facilitated access to the GPC equipment and to Gaëlle Pembouong for the measurements.

I am also grateful to all the other members in the lab for helping me on the technical or administrative level. Thanks Alain Louis Joseph for NMR training and Cindy Kaimakian in the Centre de travaux expérimentaux de chimie for opening the labs of photoluminescence and NMR promptly each time when I need. Thanks to Jérôme Charliac and Cyril Jadaud for helping me to print posters many times. Thanks to Laurence Gérot, Gabriella Medina and Fabienne Pandolf who work silently behind the scene but importantly to keep everything moving well.

Great thanks also to all members of my jury committee for making the time to read, assess and judge my thesis. All your suggestions are making this work better and much more valuable.

Also I would like to thank many other Chinese friends here that I haven't mentioned above, e.g. Letian Dai, Junkang Wang, Qi Huang (LOS), Bo Liu (LPP), Heng Li (PMC), Wanghua Chen, Hongye Yuan (PMC), Lan Zou (LIPM & UOT), Hongliu Li, Prof. Zhanbing He, Prof. Hong Liu, Jian Tang, Zhaoguo Xue, Yongpeng Liu, Hengyang Xiang, etc. Thanks for their assistance when I needed and many of us have shared a lot of joyful life experiences.

Thanks to the Ecole Polytechnique for providing us a rich research environment and a comfortable living environment here. Thanks to the China Scholarship Council (CSC) for offering me a fellowship to study in France, and the CNRS and the Ecole polytechnique for their financial support.

Of course, my infinite thanks to my family and friends. Thanks for their support and encouragements that made me possible to comfortably focus on my study here. Zhiqian Zhang and Yuxiang Yang are specially thanked for they readily to be guarantors of my abroad study. Particularly thanks also to my beloved fiancée Baochun Wu, a sunny angel in my life.

Thanks to all

Merci à tous

谢谢大家

Qiqiao

Abstract

Conjugated polymers have attracted a great attention for their remarkable optical and semi-conducting properties. They can be highly soluble, thus enabling a facile fabrication of devices from solution processing techniques such as spin-coating and ink-jet printing methods; they usually form films of high quality; they particularly show interesting absorption and emission properties from the near-UV to the near IR ranges. Their electronic properties have made them widely investigated as active materials in electronic devices in the last three decades. Such polymers comprising a regular alternance of donor and acceptor units within their backbone, labelled (D-A)_n copolymers, show a reduced bandgap due to their in-chain donor-acceptor interactions. In consequence, their emission is shifted to the red and can be tuned depending on the relative strength of the donor and acceptor units. 2,2'-bipyrimidine (**BPM**) has been reported in our group as an interesting multifunctional molecule, such as a ligand for designing molecular complexes as well as coordination polymeric lanthanide materials. However, to the best of our knowledge, there was no previous report introducing BPM as an acceptor unit to design conjugated (D-A)_n polymers. In this work, we have thus designed, synthesized and characterized a series of new (D-A)_n conjugated polymers based on BPM as an acceptor unit and various donor units.

The work aimed at designing and synthesizing organic-inorganic hybrid materials with controlled luminescence and at investigating them as phosphors for LED lighting. The final goal was to obtain a white source of light. Indeed, commercial white LEDs are made up of a blue emitting device covered with a yellow phosphor. Combining these two colors yields white light. However, this light is not of good quality as it lacks some red component. This results in a bad rendering of the colors of objects illuminated by these sources of light. In our work, conjugated polymers with different emission colors in the visible such as blue (**PF**, **P11**, **P12**) and green (**P1**, **P8**, **P9**, **P10**) were successfully obtained by the Suzuki coupling reaction. We have also successfully obtained several interesting white emitting materials from different components. Two of the white emitting materials were made with two types of luminescent molecules (**P1** and an **Eu-complex**, or **P10** and **P26**, both contained two emitters only), which avoided the use of polyfluorene, a compound sensitive to light, easy photo-degraded and oxidized, as a blue emitting component. Another three materials were even more interesting and special. They emit

white light, which is relatively rare. Indeed, white emission from a single pure organic polymer has scarcely been reported to date. (**P13**, **P14**, **P15**). They represent a potential interesting alternative to lanthanide-free phosphors. We have investigated the influence of the polymer backbone composition, side chain structure, linearity and different matrices such as PMMA and polystyrene, on their photostability, solubility and photoluminescence (PL) properties. It was concluded that the carbazole unit possesses a better photostability over fluorene or other heterofluorene derivatives thanks to the nitrogen atom that provides a lone electron pair that gives a fully aromatic structure. The solubility and so the processability of the polymers clearly depend on the nature and length of the side chains. Long and bulky side chains can obviously increase their solubility. Concerning the study of the influence of the linearity on the polymer emission properties, we have compared 2,7-carbazole and 3,6-carbazole derivatives as donor groups. It shows that increasing the linearity of the polymer chains is also favorable to decrease their energy bandgaps.

In this thesis, not only the synthetic procedures and chemical characterizations are presented in detail, but also the studies of the photophysical properties of the polymers, either in solution or in the solid state. Solid state studies were performed on the bulk polymers and on the polymers dispersed into a polymeric matrix. These studies will lead to identify the limiting factors that could hamper the use of the materials, and solutions have been proposed to improve the materials performance. And more importantly, this work enhanced the diversity of the conjugated polymers, and represents a new substrate type in palladium catalyzed Suzuki coupling reactions that **BPM** represents.

Keywords: Conjugated polymer, 2,2'-bipyrimidine, Luminescence, Synthesis, Hybrid materials

Résumé

Les polymères conjugués ont suscité un grand intérêt pour leurs remarquables propriétés optiques et semi-conductrices. Ils peuvent être très solubles, permettant l'élaboration aisée de dispositifs électroniques avec des techniques de dépôt comme l'enduction centrifuge ou l'impression jet d'encre. Ils forment des films de très bonne qualité et ils montrent des propriétés d'absorption et d'émission très intéressantes du proche UV jusqu'au proche IR. Grâce à leurs propriétés électroniques, ils ont été très étudiés comme matériaux actifs de dispositifs électroniques ces trente dernières années. De tels polymères comportant une alternance régulière de groupements donneurs et accepteurs d'électrons dans leur chaîne principale, notés (D-A)_n, ont un gap énergétique réduit dû à des interactions donneur-accepteur au sein de la chaîne. De ce fait, l'émission est déplacée vers le rouge et l'importance du déplacement est contrôlée par la capacité du donneur et de l'accepteur à respectivement donner facilement et accepter facilement des électrons.

La 2,2'-bipyrimidine (**BPM**) a été reportée comme étant une molécule multifonctionnelle très intéressante dans notre équipe, elle s'est notamment avérée être un ligand permettant le design de complexes moléculaires et de polymères de coordination des lanthanides fortement luminescents. Cependant, cette unité n'a jamais été utilisée comme entité déficitaire en électrons pour concevoir des polymères conjugués alternés de type (D-A)_n. Dans ce travail, nous avons donc entrepris le design, la synthèse et la caractérisation d'une série de polymères conjugués (D-A)_n comportant la BPM comme unité acceptrice.

Le travail présenté avait pour but d'élaborer des matériaux hybrides organiques-inorganiques dont la luminescence pouvait être contrôlée et d'étudier leur potentialité comme phosphores pour l'éclairage à LED. L'objectif final était d'obtenir une source de lumière blanche. Les LED blanches commercialisées actuellement comportent un dispositif émettant de la lumière bleue sur lequel est déposé un phosphore émettant du jaune. La combinaison de ces deux couleurs fournit un blanc qui est souvent de qualité médiocre par l'absence de composante rouge. Ceci résulte en un indice de rendu des couleurs insuffisant et une couleur faussée des objets éclairés par ces sources lumineuses. Dans ce travail, des polymères conjugués présentant des émissions différentes dans le visible, comme le bleu (**PF**, **P11**, **P12**) ou le vert (**P1**, **P8**, **P9**, **P10**) ont été obtenus par couplage de Suzuki. Nous avons aussi obtenu plusieurs matériaux émettant

de la lumière blanche. Deux d'entre eux comprennent une combinaison de deux émetteurs (**P1** et un complexe d'euporium et **P10** avec **P26**), évitant l'utilisation de polyfluorène, un composé certes, fort émetteur dans le bleu, mais trop instable sous lumière UV. Des matériaux encore plus intéressants ont aussi été obtenus, puisque des polymères (**P13**, **P14**, **P15**) émettant du blanc ont pu être isolés. L'émission blanche d'une unique molécule est généralement très difficile à obtenir et très peu sont reportées dans la littérature. Elles sont potentiellement très intéressantes dans le but d'obtenir des phosphores ne contenant d'ions lanthanides. Nous avons étudié l'influence de paramètres comme la composition de la chaîne conjuguée, de sa structure géométrique et des groupements latéraux sur l'émission des polymères purs en solution et à l'état solide et dispersés dans différentes matrices organiques comme le poly(méthacrylate de méthyle) (PMMA) et le polystyrène sur la photostabilité, la solubilité et les propriétés photophysiques. Nous en avons déduit que l'unité carbazole conférait au polymère une meilleure photostabilité que le fluorène et ses dérivés grâce à la présence du doublet de l'atome d'azote qui permet une structure aromatique.

Dans cette thèse, non seulement toutes les procédures de synthèse et les caractérisations chimiques ont été détaillées, mais également les résultats des mesures d'absorption et de photoluminescence des polymères, en solution ou dopés dans une matrice, puis déposés en film mince sur un substrat de verre. Des solutions ont été proposées pour améliorer les performances des matériaux. Plus important encore, grâce à l'introduction de la **BPM**, ces travaux ont permis de développer une nouvelle famille de polymères conjugués.

Mots-clés: Polymère conjugué, 2,2'-bipyrimidine, Luminescence, Synthèse, Matériaux hybrides

Contents

Acknowledgements.....	I
Abstract.....	III
Résumé.....	V
Contents.....	VII
List of Acronyms and Symbols.....	X
Chapter I Introduction.....	- 1 -
1.1 Luminescent materials: different types of materials for different applications.....	- 2 -
1.1.1 Lighting systems.....	- 2 -
1.1.2 Photocatalysis.....	- 5 -
1.1.3 Sensors.....	- 10 -
1.1.4 Others.....	- 15 -
1.2 Luminescent materials as luminophors.....	- 16 -
1.2.1 Fluorescent lamps.....	- 17 -
1.2.2 Light-emitting diodes (LEDs).....	- 18 -
1.3 Different ways for making white light emitting materials.....	- 19 -
1.4 Polymer matrices.....	- 28 -
1.5 CIE coordinate diagram.....	- 30 -
1.6 Thesis structure.....	- 31 -
Chapter II Experimental part.....	- 33 -
2.0 General information.....	- 34 -
2.1 Synthesis and chemical characterization of the monomers.....	- 37 -
2.2 Synthesis and chemical characterization of the polymers.....	- 48 -
2.2.1 P1 and P2	- 48 -
2.2.2 P3 , P4 , P5 and P6	- 49 -
2.2.3 P7 and P8	- 53 -
2.2.4 P9	- 54 -
2.2.5 P10	- 54 -
2.2.6 P11 and P12	- 55 -
2.2.7 P13 and P14	- 56 -
2.2.8 P15	- 57 -
2.2.9 P16 , P17 and P18	- 58 -
2.3 Synthesis and chemical characterization of metal complexes.....	- 60 -
2.4 Preparation of the liquid materials.....	- 64 -

2.5 Preparation of thin films.....	- 66 -
2.6 Summary and Perspectives.....	- 68 -
Chapter III Photophysical properties of pure polymers.....	- 70 -
3.1 Polymers in Solution.....	- 71 -
3.1.1 Absorption and PL spectra of PF	- 71 -
3.1.2 Absorption and PL spectra of P1	- 74 -
3.1.3 Absorption and PL spectra of P2	- 78 -
3.1.4 Absorption and PL spectra of P5	- 81 -
3.1.5 Absorption and PL spectra of P6	- 85 -
3.1.6 Absorption and PL spectra of P8	- 87 -
3.1.7 Absorption and PL spectra of P9	- 91 -
3.1.8 Absorption and PL spectra of P10	- 95 -
3.1.9 Absorption and PL spectra of P11	- 98 -
3.1.10 Absorption and PL spectra of P12	- 102 -
3.1.11 Absorption and PL spectra of P13	- 106 -
3.1.12 Absorption and PL spectra of P14	- 110 -
3.1.13 Absorption and PL spectra of P15	- 113 -
3.1.14 Absorption and PL spectra of P18	- 116 -
3.1.15 Comparison of absorption and PL spectra of PF and P1	- 119 -
3.1.16 Comparison of absorption and PL spectra of P1 and P2	- 120 -
3.1.17 Comparison of absorption and PL spectra of P1 , P5 , P6 and P8	- 121 -
3.1.18 Comparison of absorption and PL spectra of P8 and P9	- 123 -
3.1.19 Comparison of absorption and PL spectra of P9 and P10	- 124 -
3.1.20 Comparison of absorption and PL spectra of PF , P11 and P12	- 125 -
3.1.21 Comparison of absorption and PL spectra of P6 , P13 and P14	- 126 -
3.1.22 Comparison of absorption and PL spectra of P13 in different solvents.....	- 127 -
3.1.23 Comparison of absorption and emission spectra of P10 , P13 and P15	- 137 -
3.2 Polymers as pure thin films.....	- 138 -
3.2.1 Absorption.....	- 139 -
3.2.2 Excitation and emission of polymers as thin films.....	- 141 -
3.3 Summary.....	- 155 -
Chapter IV Investigations as luminophors.....	- 158 -
4.1 Polymers in different matrices.....	- 159 -
4.1.1 P1 in different matrices.....	- 159 -
4.1.2 P10 in different matrices.....	- 163 -
4.1.3 P13 in different matrices.....	- 169 -

4.1.4 P14 in different matrices.....	- 182 -
4.1.5 P15 in different matrices.....	- 188 -
4.1.6 Summary of the influence of the matrix on the photophysical properties.....	- 195 -
4.2 Investigations on the possibility of Aggregation Induced Emission.....	- 195 -
4.2.1 Introduction.....	- 195 -
4.2.2 Preparation of the samples.....	- 196 -
4.2.3 Absorption and PL results.....	- 197 -
4.2.4 Conclusions.....	- 199 -
4.3 Blends with different emitters for white light emission.....	- 199 -
4.3.1 Blends for white light in solution.....	- 200 -
4.3.2 Blending the emitters in thin films.....	- 205 -
4.4 Quantum yields determination.....	- 206 -
4.4.1 Quantum yields measured in DCM.....	- 207 -
4.4.2 Quantum yields measured in thin film.....	- 208 -
4.5 Photostability studies.....	- 208 -
4.5.1 PF	- 209 -
4.5.2 P1	- 210 -
4.5.3 P8	- 211 -
4.5.4 Influence of the liquid matrix.....	- 213 -
4.5.5 [Eu(tta)₃(L)]	- 214 -
4.6 Thermostability studies.....	- 214 -
4.7 Summary.....	- 216 -
Chapter V Conclusion and perspectives.....	- 217 -
5.1 Conclusion.....	- 218 -
5.2 Perspectives.....	- 219 -
5.2.1 Further improvement of the photostability through chemical design.....	- 219 -
5.2.2 Design and synthesis of new BPM-based metal complexes.....	- 219 -
5.2.3 Design and synthesis of new conjugated polymers with red emission.....	- 221 -
5.2.4 Others.....	- 222 -
Appendix I Polymers discussed in the thesis.....	- 223 -
Appendix II NMR spectra of selected new compounds.....	- 227 -
Appendix III List of publications and conferences.....	- 243 -

List of Acronyms and Symbols

No.	Acronyms/Symbols	Definition
1	ABS	Absorption
2	AcOH	Acetic acid
3	ACQ	Aggregation-caused quenching
4	AFM	Atomic Force Microscopy
5	AIE	Aggregation induced emission
6	Ar	Argon
7	BPM	Bipyrimidine
8	BTB	Benzo-thiadiazole
9	CCT	Calculate color temperature
10	CIE	Commission Internationale de l'Eclairage / International Commission on Illumination
11	C-Si	Carbazole-Silica
12	DCM/CH ₂ Cl ₂	Dichloromethane
13	DIPEA	N,N-Diisopropylethylamine
14	DMF	N,N-Dimethylformamide
15	DMSO	Dimethyl sulfoxide
16	EA	Ethyl acetate
17	EL	Electroluminescence
18	EM	Emission
19	eq	Equivalent weight
20	EtOH	Ethyl alcohol
21	Eu	Europium
22	EX	Excitation
23	FWHM	Full width at half maximum
24	GPC	Gel permeation chromatograph
25	HOMO	Highest occupied molecular orbital
26	IR	Infrared Radiation
27	KOAc	Potassium Acetate

28	LED	Light-emitting diode
29	LUMO	Lowest unoccupied molecular orbital
30	MeOH	Methanol
31	NBS	N-Bromosuccinimide
32	NEt ₃	Triethylamine
33	NMR	Nuclear Magnetic Resonance
34	<i>o</i> -DCB	1,2-Dichlorobenzene
35	OLED	Organic Light Emitting Diode
36	PE	Petroleum ether
37	PEA	Poly(Ethylene-co-vinyl acetate)
38	PeLED	Perovskite Light Emitting Diode
39	PF	Polyfluorene
40	PL	Photoluminescence
41	PLED	Polymer Light Emitting Diode
42	PMMA	Poly(methyl methacrylate)
43	QDs	Quantum dots
44	QY	Quantum yield
45	RT	Room temperature
46	SEC	Size exclusion chromatography
47	TADF	Thermal active delay fluorescent
48	TGA	Thermal Gravity Analysis
49	TsCl	4-Toluenesulfonyl chloride
50	THF	Tetrahydrofuran
51	TLC	Thin-Layer Chromatography
52	TMSCl	Chlorotrimethylsilane
53	tta	4,4,4-trifluoro-1-(thiophen-2-yl)butane-1,3-dione
54	UV	Ultraviolet
55	UV-Vis	Ultraviolet visible spectroscopy
56	WLED	White Light Emitting Diode
57	wt %	Mass fraction of a mixture
58	XRD	X-Ray Diffraction

59	λ	Wavelength
60	$v:v$	The ratio in volume
61	Lu/W	Lumens/watt

Chapter I Introduction

Contents

1.1 Luminescent materials: different types of materials for different applications.....	- 2 -
1.1.1 Lighting systems.....	- 2 -
1.1.2 Photocatalysis.....	- 5 -
1.1.3 Sensors.....	- 10 -
1.1.4 Others.....	- 15 -
1.2 Luminescent materials as luminophors.....	- 16 -
1.2.1 Fluorescent lamps.....	- 17 -
1.2.2 Light-emitting diodes (LEDs).....	- 18 -
1.3 Different ways for making white light emitting materials.....	- 19 -
1.4 Polymer matrices.....	- 28 -
1.5 CIE coordinate diagram.....	- 30 -
1.6 Thesis structure.....	- 31 -

In this first chapter, we will briefly describe the different types of luminescent materials that are used for different applications, especially in lighting, photocatalytic and sensing systems. Then typical lighting systems using phosphors including fluorescent tubes, compact fluorescent lights (CFLs), light emitting diodes (LEDs) will be introduced, followed by a brief summary of different ways to obtain white light and polymeric matrices that are used to protect the organic luminophors from UV degradation. All of these are of significant importance to illustrate the entire work we have done for the project.

1.1 Luminescent materials: different types of materials for different applications

Luminescent materials are widely applied in different areas. A brief introduction of the application of different types of luminescent materials in the three most common used domains, that are lighting systems, photocatalysis and sensors, is presented below.

1.1.1 Lighting systems

Light, as a green and neat energy, is an excellent source for various applications, including product manufacturing and inspection, information communication, medical treatment and analysis, etc.¹ As known to all, light can not only be emitted from the sun but also from the bodies of living organisms (such as fireflies and bioluminescent jellyfish) and various other lighting devices. Luminescent materials possess the characteristic of emitting light when excited by cathode rays, UV radiation, visible light or other stimulus, such as temperature increase, mechanical pressure of friction², or application of an electrical current.³ To date, they have been well studied and vast applications have been revealed. When the luminescent material is irradiated with a suitable stimulus, the activators or sensitizers absorb the energy, reaching an electronic excited state and thus creating an exciton. Afterwards, the exciton goes back to the ground state by releasing the energy in the form of radiative emission (fluorescence) or non-radiative relaxation (kinetic), as an electronic excited state is unstable.⁴ Phosphorescence also occurs via an intersystem crossing of exciton from a singlet excited state into a triplet state, which then relaxes slowly to the ground state, emitting photons in the process. This process is much slower than fluorescence because it involves two states of distinct multiplicity. A diagram

¹ W. Wang, J. Lin, C. Cai, S. Lin. *Eur. Polym. J.*, **2015**, 65, 112–131.

² C. Moretti, X. Tao, L. Koehl, V. Koncar. *Book chapter, Smart Textiles and Their Applications*. Elsevier, **2016**, 539-568.

³ S. Rossi, A. Quaranta, L. Tavella, F. Deflorian, A. M. Compagnoni. *Book chapter, Intelligent Coatings for Corrosion Control*. Elsevier. **2015**. 251-282.

⁴ Y. H.; Z. Y.; L. Y.; W. J.; L. X.; S. J.; Z. B.; F. Y., *CHINESE J ORG CHEM.*, **2017**, 37, 1991-2001.

to illustrate the mechanism of fluorescence and phosphorescence is shown in **Figure 1-1**.⁵

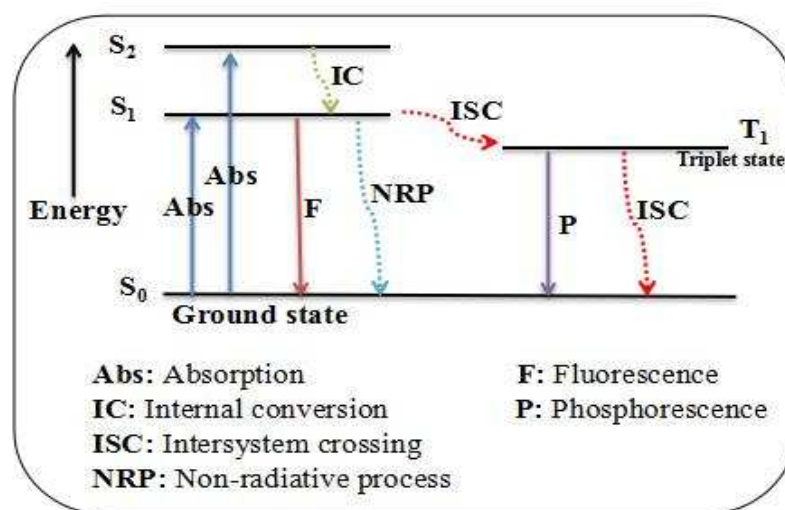


Figure 1-1 A diagram illustrating the mechanism of fluorescence and phosphorescence

Various luminescent materials have been investigated and used in lighting systems to date, as it is one of the main domains of their application, including lanthanide-doped nanoparticles⁶, transition-metal ion doped host matrix⁷, organic or polymeric molecules⁸, quantum dots (size 1-10 nm)⁹ and so forth. Major applications of luminescent materials in lighting systems are in emissive displays, fluorescent lamps and LEDs.¹⁰ They have found a number of applications in smartphones, television and computer screens, oscilloscopes and radar screens, indicating lamps, electron microscope screens, automotive lamps, and decorative lamps and LEDs for general lighting and specific applications, etc.¹¹ Some representative applications of luminescent materials in common lighting systems are shown in **Figure 1-2**. Some specific applications of light from luminescent materials including 1) the use of near-infrared lights in devices in daily life, such as remote controllers for household appliances (air conditioner, light, television, satellite receiver, etc.) and communications between portable terminals (mobile phone network, etc.)¹², 2) the applications of polarized light for metrology in microelectronics and for sensing, measurement and biomedical diagnostics¹³, 3) the use of UV light as a means for purifying or disinfecting the air, water and surfaces by killing or inactivating the pathogenic microorganisms

⁵ S. Parola, B. Julián-López, L. D. Carlos, and C. Sanchez. *Adv. Funct. Mater.*, **2016**, 26, 6506–6544.

⁶ H. Wen and F. Wang, *Book chapter, Nanocrystalline Materials*. Elsevier. **2014**. 121-160.

⁷ A. Rahman. *Module in Materials Science and Materials Engineering*, Elsevier. **2016**. 1-13.

⁸ C. Ronda and A. Srivastava. *The Electrochem. Soc. Interface*. **2006**, 15 (1), 55-57.

⁹ C. R. Ronda, *Book chapter, Luminescence: From Theory to Applications*. WILEY-VCH. **2007**, 35-59.

¹⁰ C. Ronda, *Module in Materials Science and Materials Engineering*, Elsevier. **2017**, 1-9.

¹¹ K. J. D. MacKenzie. *Handbook of Alkali-activated Cements, Mortars and Concretes*. **2015**. 777-805.

¹² M. M. Josephine, *Technol. Eng. Syst. J.*, **2017**, 2 (4), 154-164.

¹³ a. J. S. Baba. The use of polarized light for biomedical applications. *PhD thesis*, **2003**, Texas A&M University.

b. S. Alalia and A. Vitkin. *J BIOMED OPT*, **2015**, 20 (6), 061104.

contained, instead of hazardous chemicals that are harmful to the environment¹⁴. Special UV lamps are also used as insect traps in industries and food-service, as well as in agriculture and other outdoor settings.¹⁵

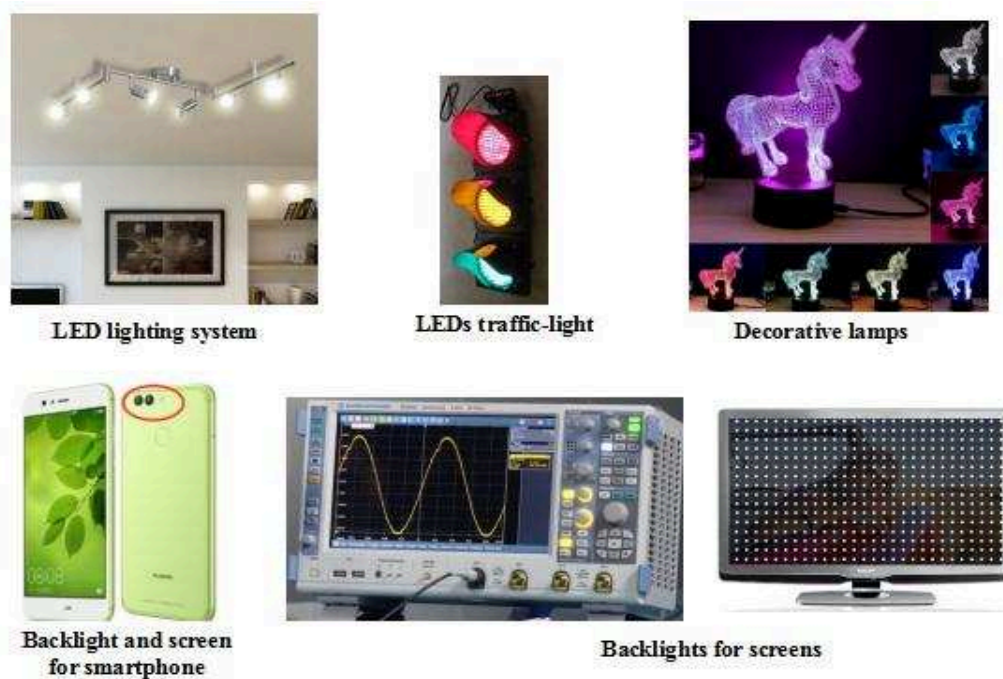


Figure 1-2 Representatives of applications of common lighting systems

Besides, lighting systems are broadly investigated and used to facilitate the growth of plants, especially LEDs (**Figure 1-3**), due to their advantages such as higher efficiency, longer life-time, easy luminescence tuning, less heat and they are environment friendly.¹⁶ Different colors and intensities of light may have different effect on the plants. Generally, as reported, red light is conducive to plant carbohydrate synthesis and can improve the biomass, increase the leaf length and increase the chlorophyll content, thus accelerating the plant growth and development.¹⁷ Far-red light can control the whole process of plant, from germination to vegetative growth and to flowering.¹⁸ Blue light can increase the leaves area and the pigment content of photosynthesis, which has been reported to affect the photomorphogenesis, chlorophyll synthesis, stomatal

¹⁴ a. Guimera D, Trzil J, Joyner J, Hysmith ND. *Am J Infect Control.*, **2018**, 46(2), 223-225.

b. Nicholas G. Reed, *Public Health Rep.*, **2010**, 125 (1), 15–27.

c. Brickner PW, Vincent RL, First M, Nardell E, Murray M, Kaufman W. *Public Health Rep.*, **2003**, 118 (2), 99-114.

d. Miller SL, Linnes J, Luongo J. *Photochem Photobiol.*, **2013**, 89 (4), 777-781.

e. Vilhunen, S., Sarkka, H., Sillanpaa, M., *ENVIRON SCI POLLUT R.Int.*, **2009**, 16 (4), 439-442.

f. N. Areid, A. Peltola, I. Kangasniemi, A. Ballo, T. O. Närhi. *Clin Exp Dent Res.*, **2018**, 4 (3), 78–85.

¹⁵ a. A. Barghini PhD and B. Augusto Souza de Medeiros. UV Radiation as an Attractor for Insects. *LEUKOS*, **2012**, 9 (1), 47-56.

b. David H. Sliney, David W. Gilbert II & Terry Lyon. *J OCCUP ENVIRON HYG*, **2016**, 13 (6), 413-424.

¹⁶ a. L. Sun, B. Devakumar, J. Liang, S. Wang, Q. Sun, and X. Huang. *J. Alloys Compd.*, **2019**, 785, 312-319.

b. Q. Sun, S. Wang, B. Devakumar, L. Sun, J. Liang, X. Huang, Y. Wu. *J. Alloys Compd.*, **2019**, 785, 1198-1205.

¹⁷ L. Shi, Y. Han, H. Wang, D. Shi, X. Geng, Z. Zhang. *J. Lumin.*, **2019**, 208, 307–312.

¹⁸ L. Shi, J. Li, Y. Han, W. Li, Z. Zhang. *J. Lumin.*, **2019**, 208, 201–207.

opening, and secondary metabolism of plants¹⁹, while yellow light can stimulate the synthesis of disaccharides. Green light can enhance plant growth but the absorption of green light is lower compared to others. It was also reported that the adoption of cold LEDs would help plant growth more than warm LEDs.²⁰ On the other hand, it was observed that the increase of the light intensity will improve the biomass of plants in most cases.²¹ Certainly, a proper combination of blue, yellow and red light will be most beneficial to the increase of plant productivity and its fruit quality.²²



Figure 1-3 Applications of LEDs to facilitate the growth of plants

Moreover, when introducing luminescent material into cells, tissues, and living organisms, people can get useful information on what is happening in the biological samples as they can be readily visualized with a luminescence microscope.²³ More interestingly, using new techniques, a mixture of rationally designed nanoparticles can be introduced into living plants to make them as self-powered light sources.²⁴ Also, luminescent materials are very useful and have a variety of potential applications in biochemical and medical science research.²⁵

1.1.2 Photocatalysis

¹⁹ T. Ouzounis, B. Razi Parjikolaei, X. Fretté, E. Rosenqvist and C.-O. Ottosen. *FRONT PLANT SCI*, **2015**, 6, 1-14.

²⁰ C. Burattini, B. Mattoni and F. Bisegna. *Energies*, **2017**, 10, 1383

²¹ S. Muneer, E. J. Kim, J. S. Park and J. H. Lee. *Int. J. Mol. Sci.*, **2014**, 15, 4657-4670.

²² a. M. F. Riadi, R. R. Esyanti and A. Faizal. *MATTER: Int. J. Sci. Technol.* **2015**, 13-23. ISSN 2454-5880.

b. M. Olle, A. Viršile. *Agricultural and Food Science*, **2013**, 22, 223-234.

²³ H. Wen and F. Wang. *Book chapter, Nanocrystalline Materials*. Elsevier. **2014**. 121-160.

²⁴ S.Y. Kwak, J. P. Giraldo, M. H. Wong, V. B. Koman, T. T. S. Lew, J. Ell, M. C. Weidman, R. M. Sinclair, M. P. Landry, W. A. Tisdale, and M. S. Strano. *Nano Lett.*, **2017**, 17, 7951–7961.

²⁵ T. Novikova. *Beilstein J. Nanotechnol.*, **2017**, 8, 1844–1862.

Besides the broad range of applications of luminescent materials in lighting systems, they have found widespread utility in the area of organic synthetic chemistry as an efficient and indispensable photocatalyst for selective small-molecule activation and chemical-bond formation over the past decade.²⁶ This tool enhances photon capture and allows photosensitizers to convert visible light into chemical energy that prompts the generation of reactive radical intermediates which avoids the use of traditionally employed toxic and hazardous chemical reagents.²⁷ Meanwhile, compared to classic chemical approaches, photocatalysis methods are done under much more mild conditions. Normally, they are performed at room temperature in air. Modern advances in visible-light photocatalysis have led to the wide use of selected low-cost high-energy LEDs with specific wavelengths and intensities that best fit to the reactions, which greatly improves the reactions efficiency and rate, holding significant promise for enabling the continued discovery of valuable organic conversions.²⁸ Some representative examples are shown in **Figure 1-4**. Liu *et al*, reported a highly efficient and selective visible-light (3 W blue LEDs ($\lambda = 450$ nm)) irradiated aerobic oxidation of 1,4-dihydropyrimidines and phenolic imines in the presence of TBA-eosinY and a base for the synthesis of 2-substituted pyrimidines.²⁹ In the work of Xia *et al*, a visible-light-induced (blue LED light ($\lambda = 455$ nm)) photochemical cyclization was applied in the establishment of the all-carbon quaternary stereocenter with high efficiency and excellent yield.³⁰ Recently, a conjugated polymer, CPTF, was shown as a good photosensitizer for the oxidation of aromatic aldehyde to aromatic acid with great photostability, excellent recyclability, high O₂ generation efficiency and enables solvent-free reactions in high yields both under direct sunlight and simulated AM 1.5G irradiation.³¹

²⁶ a. F. Chen, H. Huang, L. Guo, Y. Zhang, and T. Ma. *Angew. Chem. Int. Ed.*, **2019**, 10.1002/anie.201901361.

b. C. Shu, A. Noble, and Varinder K. *Angew. Chem.*, **2019**, 131, 3910–3914.

c. J. Luo and J. Zhang. *ACS Catal.*, **2016**, 6 (2), 873–877.

d. X. Wu, Y. Li, G. Zhang, H. Chen, J. Li, K. Wang, Y. Pan, Y. Zhao, Y. Sun, and Y. Xie. *J. Am. Chem. Soc.*, **2019**, 141 (13), 5267–5274.

e. H. Rao, L. C. Schmidt, J. Bonin & M. Robert. *Nature*, **2017**, 548, 74–77.

²⁷ a. C. Le, M. K. Wismer, Z. Shi, R. Zhang, D. V. Conway, G. Li, P. Vachal, I. W. Davies, and D. W. C. MacMillan. *ACS Cent. Sci.*, **2017**, 3, 647–653.

b. R. Hommelsheim, Y. Guo, Z. Yang, C. Empel, and R. M. Koenigs. *Angew. Chem. Int. Ed.*, **2019**, 58, 1203–1207.

c. D. Ravelli, D. Dondi, M. Fagnoni and A. Albini. *Chem. Soc. Rev.*, **2009**, 38, 1999–2011.

d. J. M. R. Narayanam and C. R. J. Stephenson. *Chem. Soc. Rev.*, **2011**, 40, 102–113.

e. X. Lang, X. Chen and J. Zhao. *Chem. Soc. Rev.*, **2014**, 43, 473–486.

f. N. Corrigan, S. Shanmugam, J. Xu and C. Boyer. *Chem. Soc. Rev.*, **2016**, 45, 6165–6212.

²⁸ R. C. McAtee, E. J. McClain, and C. R. J. Stephenson. *Trends in Chemistry*, **2019**, 1(1), 111–125.

²⁹ L. Wang, Z. Ma, X. Wei, Q. Meng, D. Yang, S. Du, Z. Chen, L. Wu and Q. Liu. *Green Chem.*, **2014**, 16, 3752–3757.

³⁰ X. Tong, B. Shi, K. Liang, Q. Liu, and C. Xia. *Angew. Chem. Int. Ed.*, **2019**, 58, 1–5.

³¹ W. Wu, S. Xu, G. Qi, H. Zhu, F. Hu, Z. Liu, D. Zhang, and B. Liu. *Angew. Chem. Int. Ed.*, **2019**, 58, 1–6.

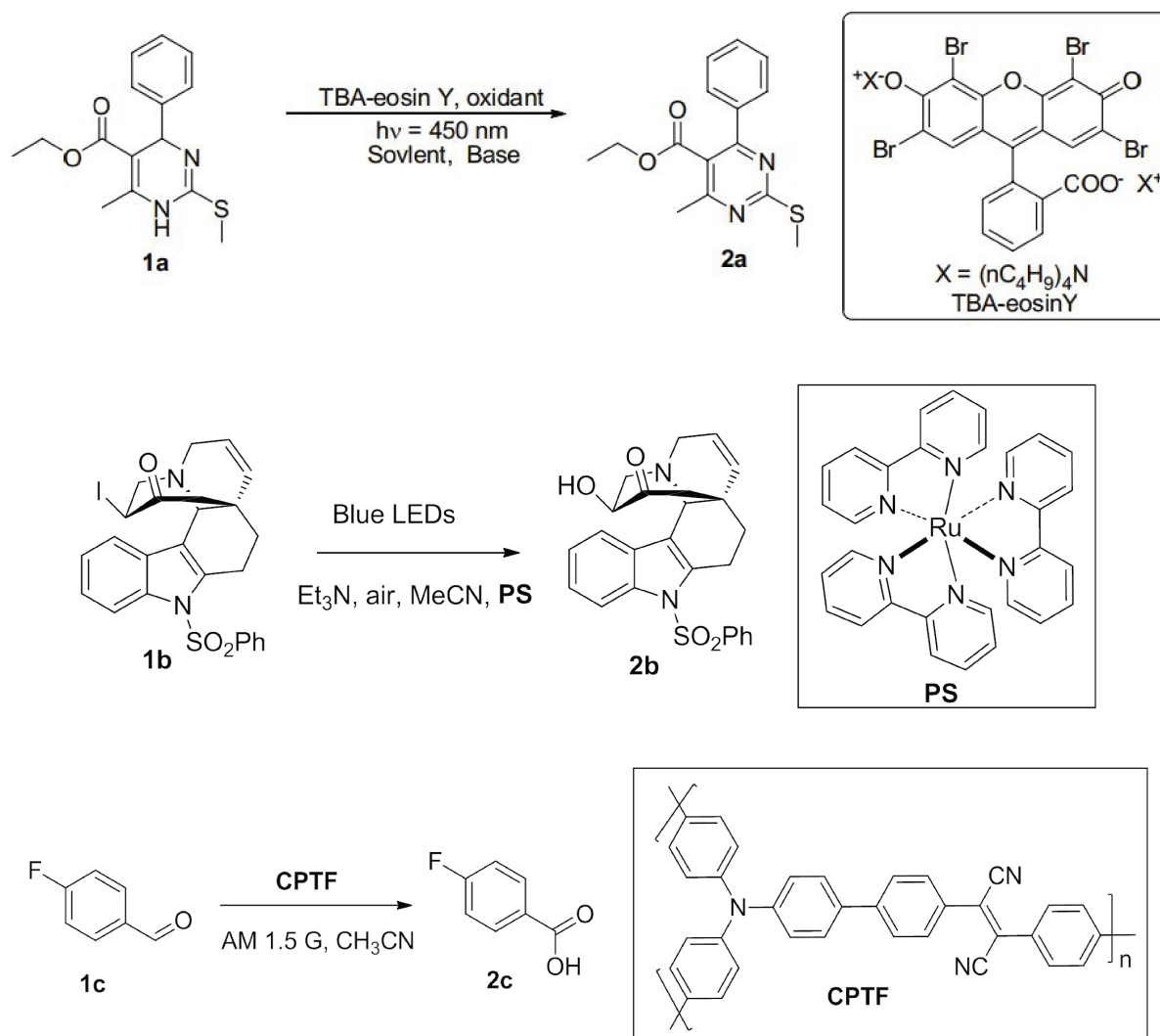


Figure 1-4 Representatives of reported photocatalytic reactions

Moreover, the simultaneous use of photocatalysis in combination with other catalytic methods, e.g., electrocatalysis, transition metal catalysis, Lewis and Brønsted acids, organocatalysis, enzymatic catalysis³², can lead to more reaction breakthroughs.³³ Researchers have developed various methods for making valuable compounds by using a combination of catalysts.³⁴ Some

³² E. Churakova, M. Kluge, R. Ullrich, I. Arends, M. Hofrichter, and F. Hollmann. *Angew. Chem. Int. Ed.*, **2011**, 50, 10716 – 10719.

³³ K. L. Skubi, T. R. Blum, and T. P. Yoon. *Chem. Rev.*, **2016**, 116, 10035-10074.

³⁴ a. I. WILLNER, Z. GOREN, D. MANDLER, R. MAIDAN and Y. DEGANI. *Journal of Photochemistry*, **1985**, 28, 215 - 228.

b. D. Mandler and I. Willner. *J. Am. Chem. Soc.*, **1984**, 106, 5353-5355.

c. D. Mandler and I. Willner. *J. Chem. Soc., Chem. Commun.*, **1986**, 0, 851-853.

d. D. Mandler and I. Willner. *J. Chem. Soc., Perkin Trans. II*, **1986**, 0, 805-811.

e. R. Maidan and I. Willner. *J. Am. Chem. Soc.*, **1986**, 108, 1080-1082.

f. R. Ruppert and E. Steckhan. *J. Chem. Soc., Perkin Trans. II*, **1989**, 0, 811-814.

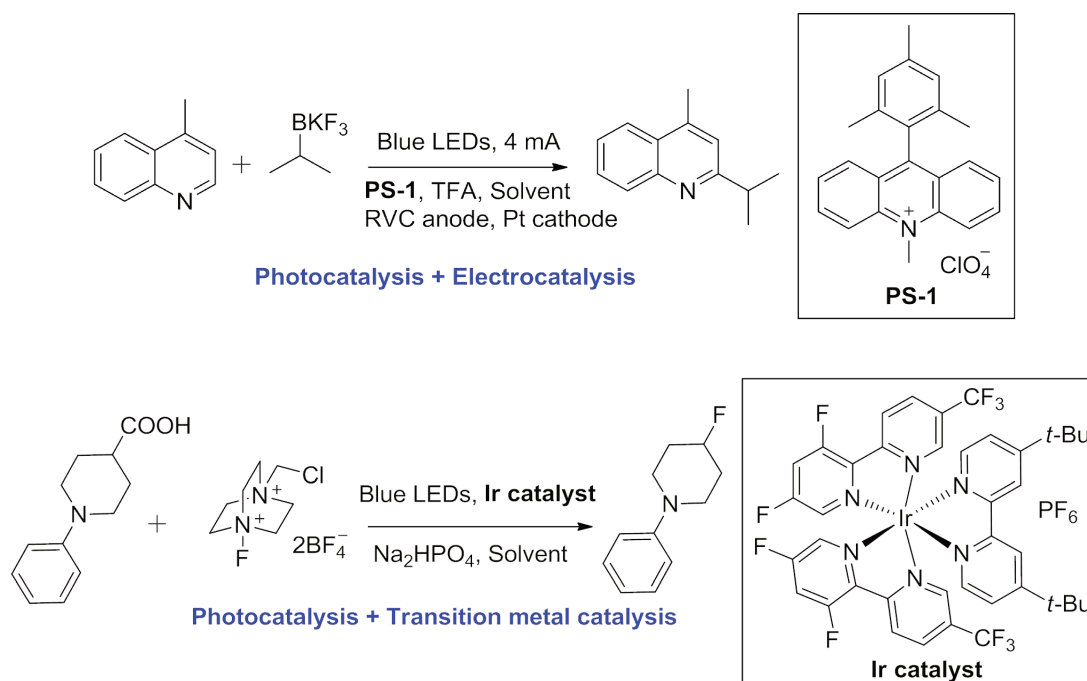
g. A. Taglieber, F. Schulz, F. Hollmann, M. Rusek, and M. T. Reetz. *ChemBioChem.*, **2008**, 9, 565 – 572.

h. J. H. Kim, S. H. Lee, J. S. Lee, M. Lee and C. B. Park. *Chem. Commun.*, **2011**, 47, 10227–10229.

i. R. K. Yadav, J. O. Baeg, G. H. Oh, N. J. Park, K. Kong, J. Kim, D. W. Hwang, and S. K. Biswas. *J. Am. Chem. Soc.*, **2012**, 134, 11455-11461.

j. J. Ryu, D. H. Nam, S. H. Lee, and C. B. Park. *Chem. Eur. J.*, **2014**, 20, 12020 – 12025.

representatives are shown in **Figure 1-5**. Xu *et al* have developed a chemical oxidant-free C-H alkylation reaction of heteroarenes with organotrifluoroborates by merging photoredox catalysis and electrocatalysis, in which a 20 W blue LED was employed as the light source and a constant current of 4 mA in an undivided cell equipped with a reticulated vitreous carbon (RVC) anode and platinum plate cathode was conducted for the electrolysis.³⁵ The direct conversion of secondary carboxylic acids to the corresponding fluorides has been achieved in MacMillan lab via dual catalysis strategy of visible light-promoted photoredox catalysis (with two 34 W blue LEDs) and Ir complex, with excellent yield.³⁶ A visible-light-mediated, organic photocatalytic cascade cyclization of polyenes was realized in the work of Yang *et al.*, in which the addition of Lewis acid LiBr helped to favor the enol tautomer, allowing facile cyclization.³⁷ Rovis demonstrated that asymmetric α -acylation of tertiary amines with aldehydes can be realized by dual catalysis mode with the use of chiral *N*-heterocyclic carbene (NHC) organocatalysis and photoredox catalysis (with a 32 W blue LED lamp ($\lambda = 450$ nm)).³⁸ Zhao and Hartwig *et al.* reported cooperative asymmetric reactions of alkenes in high yield with excellent enantioselectivity, combining photocatalysis (with a 34 W blue LED lamp ($\lambda = 465$ nm)) and enzymatic catalysis that united the advantages of the reactivity of chemical catalysts with the selectivity of enzymes.³⁹



k. M. Aresta, A. Dibenedetto, T. Baran, A. Angelini, P. Labuz and W. Macyk. *Beilstein J. Org. Chem.*, **2014**, *10*, 2556–2565.

³⁵ H. Yan, Z. Hou and H. Xu. *Angew. Chem. Int. Ed.*, **2019**, DOI: 10.1002/anie.201814488.

³⁶ S. Ventre, F. R. Petronijevic, and D. W. C. MacMillan. *J. Am. Chem. Soc.*, **2015**, *137* (17), 5654–5657.

³⁷ Z. Yang, H. Li, L. Zhang, M. Zhang, J. Cheng, S. Luo. *Chem. - Eur. J.*, **2015**, *21* (42), 14723–14727.

³⁸ D. A. DiRocco and T. Rovis. *J. Am. Chem. Soc.*, **2012**, *134* (19), 8094–8097.

³⁹ Z. C. Litman, Y. Wang, H. Zhao & J. F. Hartwig. *Nature*, **2018**, *560*, 355–359.

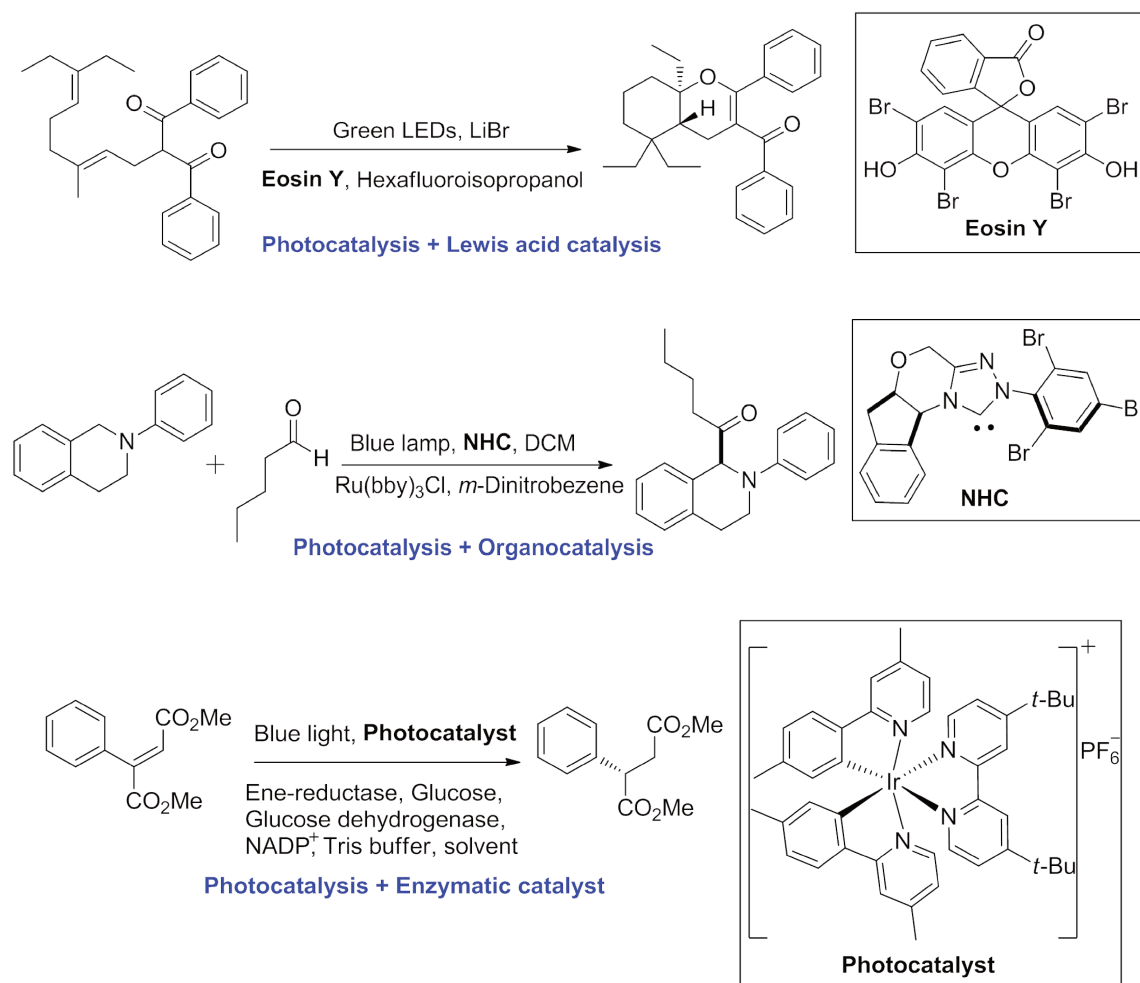


Figure 1-5 Representative of reported photocatalysis combined with other catalytic methods

As shown above, photocatalysis is still a field of high interest and is of great promise in the application for solar fuel production or pollutant degradation.⁴⁰ Continued advancements in excavation of new reaction types is keep extending the application of photocatalyst. Recent advance in photocatalytic decarboxylative alkylation reactions can avoid the use of common photoredox catalysts, such as precious metal complexes and synthetically elaborate organic dyes that are costly, instead, a combination of triphenylphosphine and sodium iodide under 456 nm irradiation by blue LEDs was applied and revealed to function quite well with excellent results (**Figure 1-6**).⁴¹ On the other hand, the development of photocatalytic reaction will help to reduce the waste streams, and decrease the reaction times, ultimately leading chemical synthesis to a more sustainable approach.

⁴⁰ J. A. Macia-Agullo, A. Corma, and H. Garcia. *Chem. Eur. J.*, **2015**, 21, 10940 – 10959.

⁴¹ M. Fu, R. Shang, B. Zhao, B. Wang, Y. Fu. *Science*, **2019**, 363, 1429–1434.

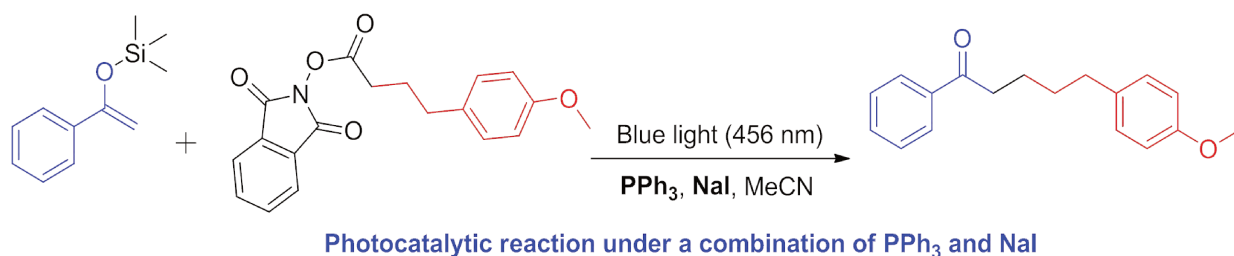


Figure 1-6 Representative of reported photocatalysis with novel type of catalysts

1.1.3 Sensors

Luminescent materials can also be used as sensors. Highly sensitive and selective molecular sensory materials have received considerable attention since the nineties.⁴² Among various detection approaches, the fluorescence technique has received considerable attention due to its prominent advantages, such as high sensitivity and selectivity, low-cost, signal simplification, realtime detection and their operation simplicity and high detection limit.⁴³ In comparison, other methods such as chromatographic and spectroscopic techniques that are, in general, very complex, time-consuming, more expensive⁴⁴ and some of them suffer from non-portability or need post-mortem and destruction of tissues or cells⁴⁵ and require specialized technicians.⁴⁶ There are numerous reports concerning the design and construction of chemosensors using fluorescence and optical changes as output signals. Following are some typical examples. Two terpyridine-containing siloles (**1-C1** and **1-C2** in **Figure 1-7**) have been reported as fluorescent chemosensors with high selectivity and sensitivity for Zn²⁺ in comparison with alkali and alkaline earth metal ions and other transition metal ions. As being chemosensor, **1-C1** with two terpyridine groups at both ends shows better Zn²⁺ sensing properties than **1-C2** that containing only one terpyridine group at the end due to the formation of a metalorganic coordination oligomer or polymer.⁴⁷ 2-((9H-fluoren-2-ylidene) methyl)phenol (**1-C3**, **Figure 1-7**) was reported as a fluorescent chemosensor with high selectivity for detection of Cr³⁺ and Al³⁺ ions.

⁴² a. M. Kimura, T. Horai, K. Hanabusa, and H. Shirai. *Adv. Mater.*, **1998**, *10*, 6.

b. Richard A. Bissell, A. Prasanna de Silva, H. Q. Nimal Gunaratne, P. L. Mark Lynch, Glenn E. M. Maguire, and K. R. A. S. Sandanayake, *Chem. Soc. Rev.*, **1992**, *21*, 187-195.

c. R. Jia, W. Tian, H. Bai, J. Zhang, S. Wang & J. Zhang. *Nature Communications* volume, **2019**, *10*, 795.

⁴³ a. P. F. Li, Y. Y. Liu, W. J. Zhang, and N. Zhao. *ChemistrySelect*, **2017**, *2*, 3788-3793.

b. G. K. Walkup and B. Imperiali. *J. Am. Chem. Soc.*, **1997**, *119*, 3443-3450.

c. X. Sun, Y. Wang and Y. Lei. *Chem. Soc. Rev.*, **2015**, *44*, 8019-8061.

d. H. Nie, Y. Zhao, M. Zhang, Y. Ma, M. Baumgarten and K. Mullen. *Chem. Commun.*, **2011**, *47*, 1234-1236.

e. H. Nie, G. Sun, M. Zhang, M. Baumgarten and K. Mullen. *J. Mater. Chem.*, **2012**, *22*, 2129-2132.

⁴⁴ F. R. Simões, L. H. C. Mattoso, and C. M. P. Vaz. *Sensor Lett.*, **2006**, *4*, 3.

⁴⁵ B. Gua, L. Huang, Z. Xu, Z. Tan, M. Hu, Z. Yang, Y. Chen, C. Peng, W. Xiao, D. Yu, H. Li. *Sensors & Actuators: B. Chemical*, **2018**, *273*, 118-125.

⁴⁶ Y. Luo, C. Li, W. Zhu, X. Zheng, Y. Huang, and Z. Lu. *Angew. Chem. Int. Ed.*, **2019**, *58*, 1 – 6.

⁴⁷ S. Yin, J. Zhang, H. Feng, Z. Zhao, L. Xu, H. Qiu, B. Tang. *Dyes and Pigments*, **2012**, *95*, 174-179.

The addition of Cr^{3+} and Al^{3+} can make a significant increase in the fluorescent intensity while other metal ions have almost no influence on the fluorescence.⁴⁸ A pyrene compound (**1-C4**, **Figure 1-7**) containing piperazine was reported as ratiometric fluorescent chemosensor to recognize Cr^{3+} . The result shows that the fluorescence changes of the chemosensor are remarkably specific for Cr^{3+} in the presence of other metal ions, which meet the selective requirements for practical application. Meanwhile, the response of this chemosensor toward Cr^{3+} is fast (response time less than 2 min).⁴⁹ Recently a new kind of molecule with unique aggregation-induced emission (AIE) feature has emerged as a promising class of fluorescent probe for metal ions, anions, biomolecules, gases and so on. Unlike conventional fluorogens that always suffer from aggregation-caused quenching (ACQ) effect since the strong π - π stacking interaction in the aggregated state, AIE fluorogens show non- or very weak emission in molecularly diluted state, but turn into strong fluorescence when the molecular aggregates are formed, which was mainly attributed to the restriction of intramolecular rotation (RIR).^{43,50} For example, a fluorescent probe based on tetraphenylethylene derivative (**1-C5**, **Figure 1-7**) with AIE characteristics for detection of pyrophosphate with high selectivity and sensitivity. When the fluorescent probe was quenched by the addition of Cu^{2+} , the fluorescence can be selectively recovered upon addition of pyrophosphate.⁴³ A highly selective and sensitive cationic AIE sensor (**1-C6**, **Figure 1-7**) for the detection of I^- and Hg^{2+} ions in aqueous solution was also reported, based on a tetraphenylethylene-functionalized quinolinium salt with hexafluorophosphate (PF_6^-) as the counterion. In the presence of I^- , the emission of **1-C6** is quenched due to the strong electrostatic interaction between **1-C6** and I^- . By the introduction of Hg^{2+} into the system, the fluorescence can be significantly recovered owing to the remove of I^- through formation of HgI_2 . Therefore, the turn-off and turn-on assay for the detection of I^- and Hg^{2+} , respectively, can be established.⁵¹

⁴⁸ M. Tajbakhsh, G. B. Chalmardi, A. Bekhradnia, R. Hosseinzadeh, N. Hasani, *Spectrochimica Acta Part A: Molecular and Biomolecular Spectroscopy*, **2018**, 189:22-31.

⁴⁹ Y. Wu, C. Li, Y. Li, J. Tang, D. Liu, *Sensors and Actuators B*, **2014**, 203, 712–718.

⁵⁰ Y. Hong, S. Chen, C. W. T. Leung, J. W. Y. Lam, J. Liu, N. Tseng, R. T. K. Kwok, Y. Yu, Z. Wang, and B. *ACS Appl. Mater. Interfaces*, **2011**, 3, 3411–3418.

⁵¹ R. Zhang, P. Li, W. Zhang, N. Li, and N. Zhao, *J. Mater. Chem. C*, **2016**, 4, 10479-10485.

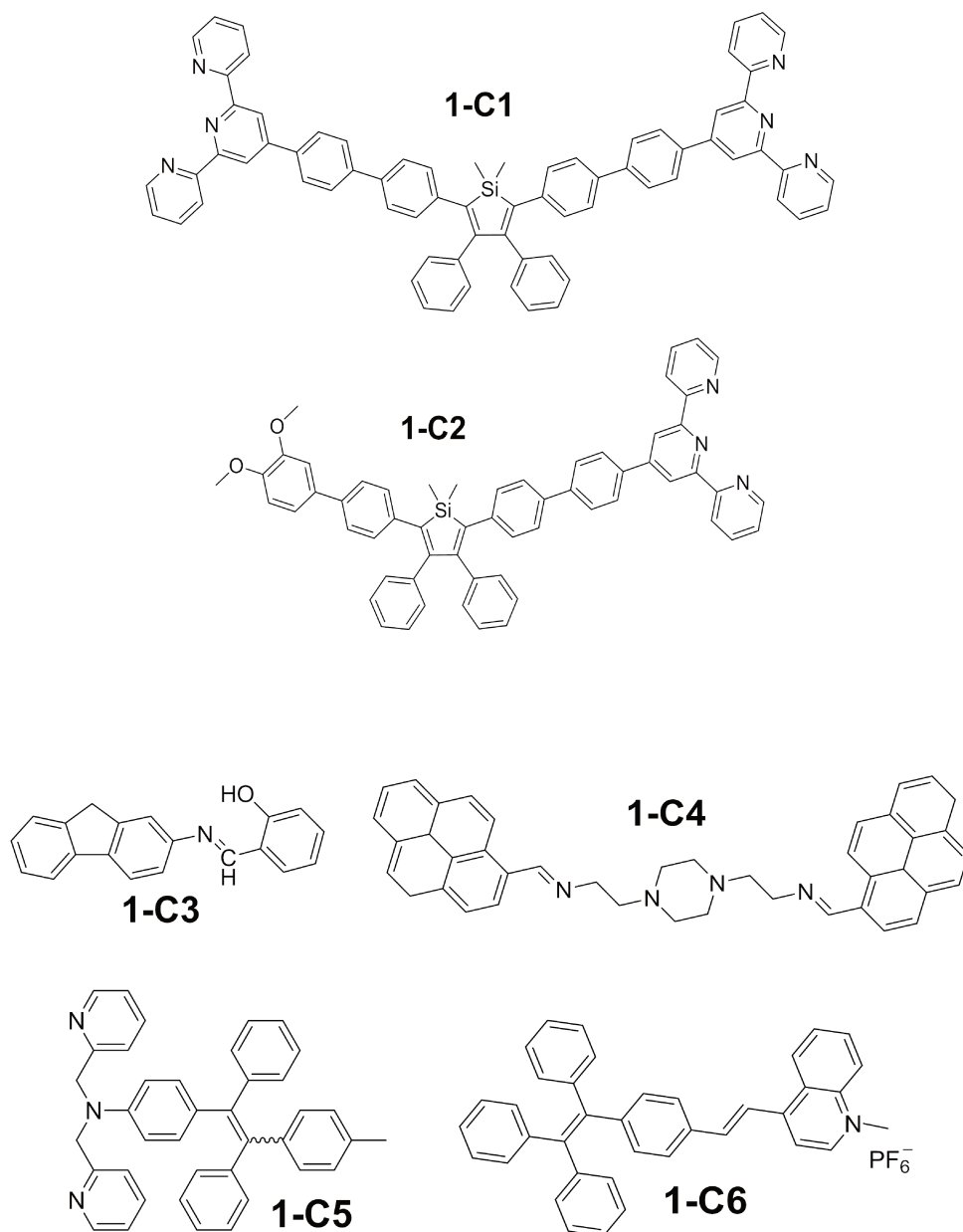


Figure 1-7 Representative small molecules reported as chemosensors

In recent years, polymer-based sensors have attracted much attention because polymers have more advantages than small molecules for sensing applications, such as signal amplification when it comes to use emission properties, and a solubility that is easier adjustable in water or organic solvents.^{52,53} As a consequence, polymers are also deposited from solution deposition techniques more easily and forms films of better quality. Furthermore, polymer-based sensors possess high selectivity and binding efficiency as the polymer chain can incorporate multiple recognition elements for analytes. Some typical examples are shown in **Figure 1-8**. A

⁵² J. Ge, Z. Liu, Q. Cao, Y. Chen, and J. Zhu. *Chem. Asian J.*, **2016**, *11*, 687-690.

⁵³ a. S. Wang, K. Gu, Z. Guo, C. Yan, T. Yang, Z. Chen, H. Tian, and W. Zhu. *Adv. Mater.*, **2018**, 1805735.

b. X. Liu, Y. Xu, and D. Jiang. *J. Am. Chem. Soc.*, **2012**, *134* (21), 8738-8741.

poly(phenyleneethynylene) (**1-P1** in **Figure 1-8**) material and a cyclophane-containing polymer (**1-P2** in **Figure 1-8**) has been shown to display a chemoresistive response with paraquat derivatives.⁵⁴ A pyrene-functionalized polynorbornene (**1-P3** in **Figure 1-8**) bearing sulfonamide NH and triazolium donors has been reported for ratiometric fluorescence recognition and sensing of pyrophosphate anion in aqueous solution.⁵² A monochromophore based ratiometric probe, which consists of a hydrophilic backbone poly(N-vinylpyrrolidone) (PVP) and single chromophore of platinum(II) tetraphenylporphyrin (Pt-TPP) (**1-P4** in **Figure 1-8**) is reported for ratiometric sensing of hypoxia levels.⁵³ A new conjugated polymer-based fluorescent chemosensor incorporating propane-1,3-dione and 2,5-diethynylbenzene moieties (**1-P5** in **Figure 1-8**) was developed for detection of Cu^{2+} and Fe^{3+} over other metal ions with high sensitivity and selectivity. The UV-Vis absorption and PL spectra of **1-P5** could be gradually changed with the increasing concentration of Cu^{2+} and Fe^{3+} .⁵⁵

Noteworthy, conjugated polymers containing terpyridyl segments as molecular recognition sites have also been studied as highly sensitive chemosensors for metal ion sensing. It is well known that low-molecular-weight terpyridyl ligands can easily afford bistridentate-type octahedral bis(terpyridyl)metal complexes with metal ions.^{47,50,56} The remarkably high binding affinity of terpyridines toward most transition metal ions by $d\pi\text{-}\pi\pi^*$ bonding, together with their chelation properties, make terpyridines attractive in metal ions detection.⁵⁶ The conjugated polymer **1-P6** in **Figure 1-8** is reported to be a good sensor for Zn^{2+} ions which can brought about a red shift of the emission peak due to the coordination of Zn^{2+} to terpyridyl ligands in **1-P6** that changed the electron density of the polymer backbone.⁴² An alternating conjugated polymer (**1-P7** in **Figure 1-8**) was reported by our lab recently to have a good sensitivity towards metal ions as it can detect Ni^{2+} and Zn^{2+} down to 2 ppb and 4 ppb, respectively.⁵⁷

Besides, many polymer/metal ion complexes as novel chemosensors have been designed to probe amino acids and their derivatives. For instance, Cu^{2+} and Ni^{2+} metal complex of polymer with 2-(pyridin-2-yl)-1H-benzo[d]imidazole unit (**1-P8**, **Figure 1-8**) was reported as a selectivity-tunable chemosensor for amino acids with high selectivity. The amino acid competes with the transition metal ion present in the complex of the conjugate polymer during the

⁵⁴ Q. Zhou and T. M. Swager. *J. Am. Chem. Soc.*, **1995**, *117*, 12593-12602.

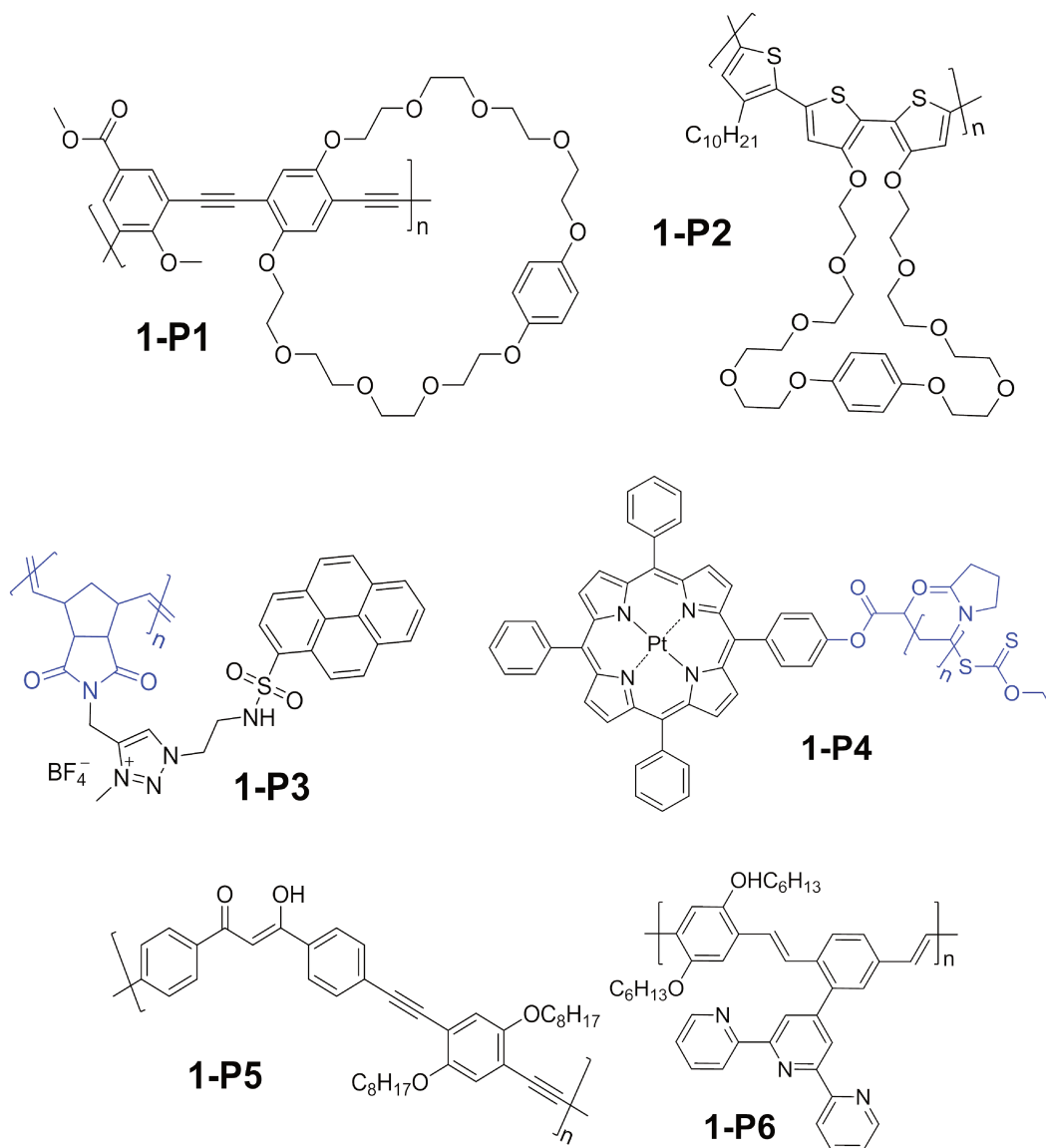
⁵⁵ D. Yang, C. Dai, Y. Hu, S. Liu, L. Weng, Z. Luo, Y. Cheng, and L. Wang. *Polymers*, **2017**, *9*, 267.

⁵⁶ a. P. D. VELLIS, J. A. MIKROYANNIDIS, C.-N. LO, C.-S. HSU. *Journal of Polymer Science: Part A: Polymer Chemistry*, **2008**, *46*, 7702-7712.

b. R. Dobrawa, M. Lysetska, P. Ballester, M. Grune, and F. Wurthner. *Macromolecules*, **2005**, *38*, 1315-1325.

⁵⁷ X. Wang, Q. Lin, S. Ramachandran, G. Pembouong, R. B. Pansu, I. Leray, B. Lebental, G. Zucchi. *Sensors & Actuators: B. Chemical*, **2019**, *286*, 521-532.

recognition process, thereby triggering a change in the optical properties.⁵⁸ Such a phenomenon can be applied to detect more amino acids selectively. To be noted, the *N*-heterocyclic aromatic compounds, such as benzimidazole and its derivatives are the key components of the chemosensors. These compounds are also strongly coordinating ligands that are able to form stable complexes with various metals.^{58,59}



⁵⁸ G. Xiang, S. Lin, W. Cui, L. Wang, L. Zhou, L. Li, De. Cao. *Sensors and Actuators B*, **2013**, 188, 540–547.

⁵⁹ a. S. Liu, J. Zuo, Y. Wang, Y. Li, X. You. *Journal of Physics and Chemistry of Solids*, **2005**, 66, 735–740.

b. S. Liu, J. Zuo, Y. Li, X. You. *Journal of Molecular Structure*, **2004**, 705, 153–157.

c. S. Liu, R. Pan, G. Li, W. Su, and C. Ni. *Journal of Chemistry*, **2017**, ID 8647419, 1–7, <https://doi.org/10.1155/2017/8647419>.

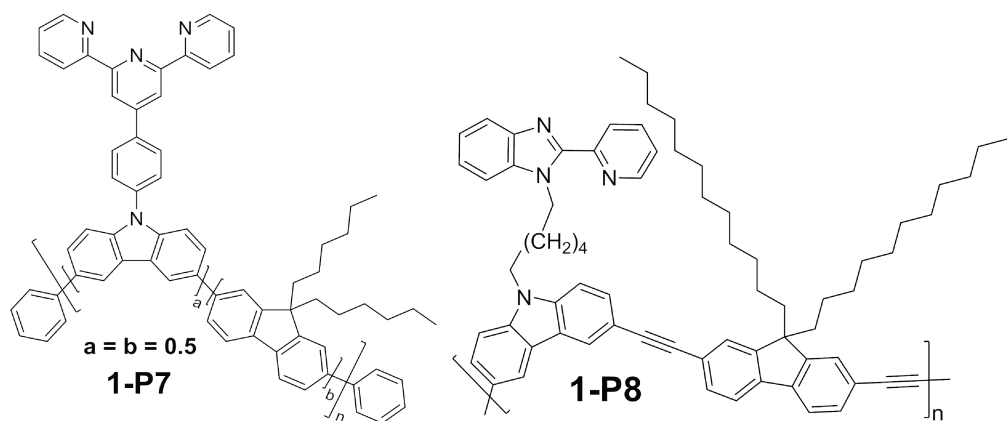


Figure 1-8 Representative polymers reported as chemosensors

1.1.4 Others

There are more applications of the luminescent materials. For examples, recently LED materials of ocular injectable photoreceptor-binding upconversion nanoparticles (pbUCNPs) which were anchored on retinal photoreceptors as miniature naturally invisible near-infrared (NIR) light transducers to create NIR light image vision are reported for the detection of NIR light and that extend the mammalian visual spectrum to the NIR range (**Figure 1-9**).⁶⁰ The mammalian invisible NIR light was transformed in vivo into a short wavelength visible emissions by this way. It was demonstrated that mice with these nanoantennae can not only perceive the NIR light, but also differentiate sophisticated NIR shape patterns. This study in NIR light image detection not only broaden the application of these nanoparticles and provided the potential for human body to extend the visual spectrum, but also open a new wide field for the design and application of LED materials.

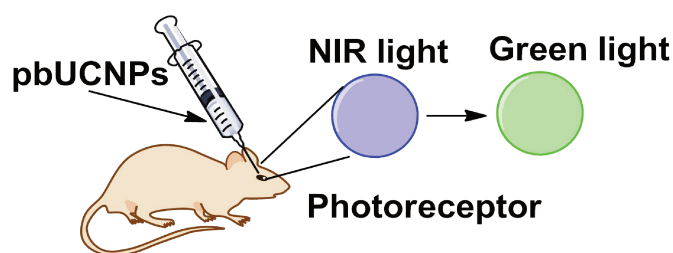


Figure 1-9 Illustration of injection of pbUCNPs in a mouse and the generation of green light upon NIR light illumination of the outer segments of photoreceptors that contains pbUCNPs

When luminescent materials with photochromism, photo-crosslinking or photodegradation

⁶⁰ Y. Ma, J. Bao, Y. Zhang, Z. Li, X. Zhou, C. Wan, L. Huang, Y. Zhao, G. Han, T. Xue. *Cell*, **2019**, 177, 1–13.

properties are incorporated into polymers, self-assemblies also can be changed under light irradiation, which resulted in the transformation of either their shapes or inner structures. This light triggered property is suitable in the application for controllable release of loaded species from assemblies, such as controlled drug delivery and release.¹ In some cases, the self-assemblies can undergo dissociation upon irradiation at lights of some specific wavelength. Following (**Figure 1-10**) is a typical photochromic polymer that can be disrupted upon UV irradiation.¹

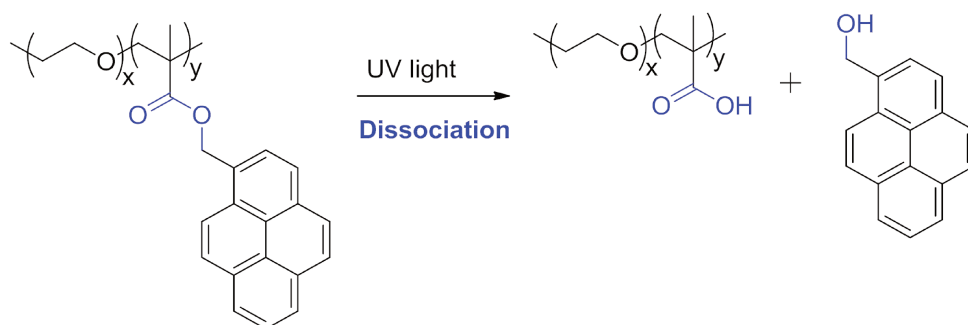


Figure 1-10 Chemical structure of a photochromic polymer and its dissociation under UV light irradiation

As shown, there are a great variety of luminescent materials that are applied for various applications, either in our daily life or in scientific fields. Nevertheless, considering the changing demands of human being, more novel materials and properties are still to be found, and more applications are to be developed, with a very promising prospect not only from a scientific point of view, but also for future lighting strategies.

1.2 Luminescent materials as luminophors

Nowadays, we have the choice between three types of light bulbs (**Figure 1-11**), namely incandescent lamps, fluorescent lamps and LED lamps. Luminescent materials have been widely used as phosphors in electronics and optoelectronics.⁶¹ Phosphors are materials that are able to absorb higher energy (shorter wavelength) emitted by the source of light and down-convert it into lower energy (longer wavelength).⁶² Usually, phosphors accept the energy of ultraviolet photons and emit visible photons. Hereafter, we introduced about several typical examples of light tools that are using luminescent materials as phosphors, including fluorescent lamps and light-emitting diodes (LEDs).

⁶¹ P.P.Zak, V.A.Lapina, T.A.Pavich, A.V.Trofimov, N.N.Trofimova, Yu.B.Tsaplev Russ. Chem. Rev., **2017**, 86 (9) 831 – 844.

⁶² G. Balachandran. *Treatise on Process Metallurgy*, **2014**, 3, 1291-1340.



Figure 1-11 Different types of light bulbs

1.2.1 Fluorescent lamps

Fluorescent tubes and compact fluorescent lights (CFLs) are two types of fluorescent lamps that are most frequently seen. A fluorescent tube is usually a long, straight glass tube that produces white light. It is commonly used in offices, class rooms, libraries, stores and some home fixtures at present. CFLs, are fluorescent tubes bended into various shapes, commonly seen as little curvy twisted bulbs, and were firstly created in 1976 due to the energy shortage caused by the oil crisis. They are more costly than incandescent bulbs, but they possess higher energy efficiency (50-90 lm/W for fluorescent lamps and 12-24 lm/W for incandescent bulbs). Because they create light by exciting gases rather than heating up a wire, they are less easy to break out and they have a nine-year life span, better than incandescent bulbs.

Inside a fluorescent tube or a CFL is low pressure mercury vapor. When ionized by an electric current in the gas, mercury vapor emits the ultraviolet light which is absorbed by phosphors coated on the inside and that further emits visible photons (**Figure 1-12**). The efficiency of a fluorescent lamp to convert electrical energy into useful light is much higher than incandescent lamps but it is more costly.

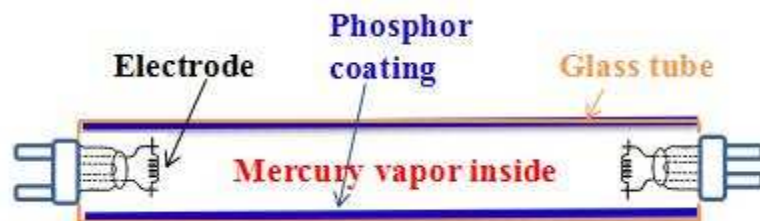


Figure 1-12 Illustration of basic construction of fluorescent tubes

1.2.2 Light-emitting diodes (LEDs)

Light-emitting diodes (LEDs) are made of a semiconductor material that emit light when current flow through it. It is a p-n junction diode that emits light when activated. When electrons in the semiconductor recombine with holes, energy will be released in the form of photons, which is called electroluminescence. The color of the light is determined by the energy band gap of the semiconductor. A typical LED construction is shown in **Figure 1-13**. LEDs are very small in size and usually consume very little power. They possess many advantages over fluorescent and incandescent bulbs, including lower energy consumption (90-100 lm/W for LEDs), improved physical robustness, smaller size, longer lifetime, lower turn-on voltage (normally 1-5 V for LEDs, while normally 220 V or higher for fluorescent and incandescent lamps) and faster switching (they respond rather instantaneously and there is no warm up or cool down period). LEDs are widely used in the society. For example, they are applied in home lighting system, traffic lighting system, backlights for screens, flat-panel displays, medical devices and many other situations. Generally, the efficiency of LEDs is limited by nonradiative recombination, whereby charge carriers recombine without releasing photons, and light trapping.⁶³

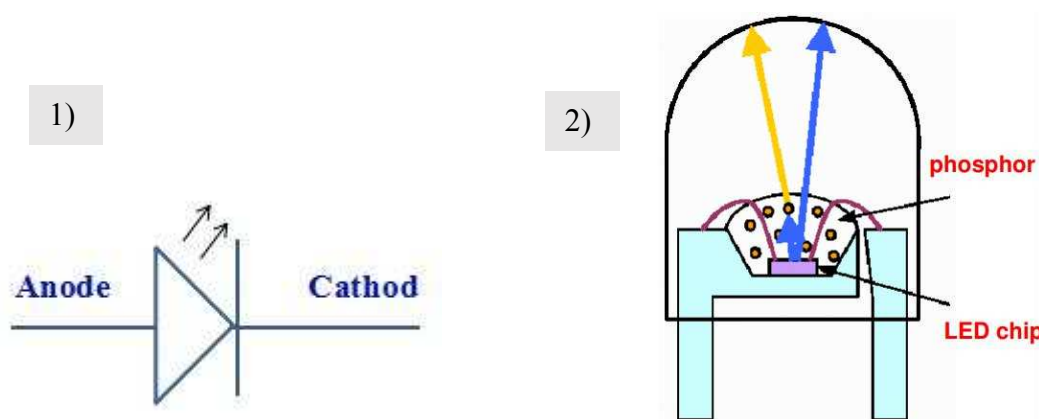


Figure 1-13 1) Diagram of common LED structure; 2) Phosphor position in a white LED⁶¹

Since nearly 25% of the global electricity has been utilized for lightings, causing 1.9 GT of CO₂ emissions,⁶⁴ LEDs with higher efficiency and flexibility are in highly demand. Although history of LEDs goes back more than a century, with the first observation in 1907, by H. J. Round, of the electroluminescence in a silicon carbide junction diode, the first practical visible LEDs appeared in 1962 and was developed by Nick Holonyak. Red, green, and yellow LEDs have

⁶³ Y. Cao, N. Wang, H. tian, J. Guo, Y. Wei, H. Chen, Y. Miao, W. Zou, K. Pan, Y. He, H. Cao, Y. Ke, M. Xu, Y. Wang, M. Yang, K. Du, Z. Fu, D. Kong, D. Dai, Y. Jin, G. Li, H. Li, Q. Peng, J. Wang & W. Huang. *Nature*, **2018**, 562:249-253.

⁶⁴ B. Liu, L. Wang, H. Tao, M. Xu, J. Zou, H. Ning, J. Peng, Y. Cao. *Science Bulletin*, **2017**, 62: 1193-1200.

been available since the 1970s and were used extensively in numerical displays and signaling applications. Then the blue LEDs were developed in 1990s. In 1993, a fundamental step was made by Shuji Nakamura at Nichia who developed the first high-brightness blue LED with p-doping of GaN. This makes it possible for their use in general lighting. In particular, the availability of high-brightness blue sources has made high-efficiency white lighting sources possible. In 1996, Nichia further produced a phosphor-converted white light-emitting diode (pc-WLED) by using a blue InGaN LED chip coated with yttrium aluminium garnet yellow phosphor ($\text{Y}_3\text{Al}_5\text{O}_{12}:\text{Ce}$, YAG:Ce).⁶⁵ The 2014 Nobel Prize in Physics was awarded to the three creators (I. Akasaki, H. Amano and S. Nakamura) of blue LEDs.⁶⁶

LEDs have some advantages over fluorescent lamps, such as lifetimes ten times higher, operating voltages of a few volts, they are mercury-free, no flickering, they do not emit strong UV radiations, and they are almost fully recyclable and are much more safe. In addition, they are shock resistant. LED light bulbs are extremely cost-effective, eco-friendly and have various designs to suit the home atmosphere. It represents a green alternative to other lighting systems used nowadays, especially as they do not use mercury. LED lighting is viewed as the next generation of lighting⁶⁷. Some devices are already on the market. But new materials with good performance that can lead to more decrease of the manufacturing cost are still in high demand. Especially, white-emitting LED materials have received a broad attention for their enormous promising applications in the field of flat-panel displays and solid-state lightings.⁶⁸

1.3 Different ways for making white light emitting materials

To date, white light emitting diodes (WLEDs) have received a broad attention⁶⁹ and are under intensive research for their wide panel of applications (such as flat-panel displays, solid-state lightings, etc.)⁷⁰ and many unique advantages (such as fast response time, wide operation temperature, environment friendliness, wide range of colour temperature, long lifetime, small size and high efficiency, etc.)⁷¹. After decades of the development in lighting systems, currently

⁶⁵ G. C. Righini, U. Caldiño, C. Falcony, M. Ferrari, and S. Pelli. **2014**, *16th International Conference on Transparent Optical Networks (ICTON)*, 1-4.

⁶⁶ E. Gibney. *Nature*, **2014**, *514*, 152–153.

⁶⁷ M. GiShina, K. Thangarajua, S. Kim, J. Park, Y. Kim, S. Kwon. *Organic Electronics*, **2011**, *12*, 785-793.

⁶⁸ a. T. Zhang, S. He, D. Wang, N. Jiang & Z. Lu. *Sci. Rep.*, **2016**, *6*, 20517.

b. S. Reineke, F. Lindner, G. Schwartz, N. Seidler, K. Walzer, B. Lüssem & K. Leo. *Nature*, **2009**, *459*, 234–238.

c. M. Segal, M. Singh, K. Rivoire, S. Difley, T. Van Voorhis & M. A. Baldo. *Nature Materials*, **2007**, *6*, 374-378.

⁶⁹ J. Tydlitát, S. Achelle, J. Rodriguez-Lopez, O. Pytela, T. Mikysek, N. Cabon, F. Robin-le Guen, D. Miklik, Z. Ruzickova, F. Bures. *Dyes and Pigments*, **2017**, *146*, 467-478.

⁷⁰ T. Zhang, S. He, D. Wang, N. Jiang & Z. Lu. *Scientific Reports*, **2016**, *6*, 20517.

⁷¹ P. T. Tin, N. H. K. Nhan, T. H. Q. Minh, T. N. Nguyen, M. Voznak and T. T. Trang. *Proceedings of the Estonian Academy of Sciences*, **2018**, *67*, 4, 337–341.

there are various ways to create white light from LEDs, each has specific advantages. Among them, two primary ways can be concluded. One is to blend the individual LEDs that emit three primary colors to form white light, named as multi-colored white LEDs (sometimes referred to as RGB LEDs). Another is to use phosphor materials to convert the light from a blue or an UV LED to white light similar with fluorescent light bulb, the resultant LEDs are named as phosphor-based white LEDs. The second method is most widely used due to its low cost and simple technology of production and use.⁷²

Following **Figure 1-14** shows the illustration of common strategies for white light⁷³ and basic principle of color mixtures.

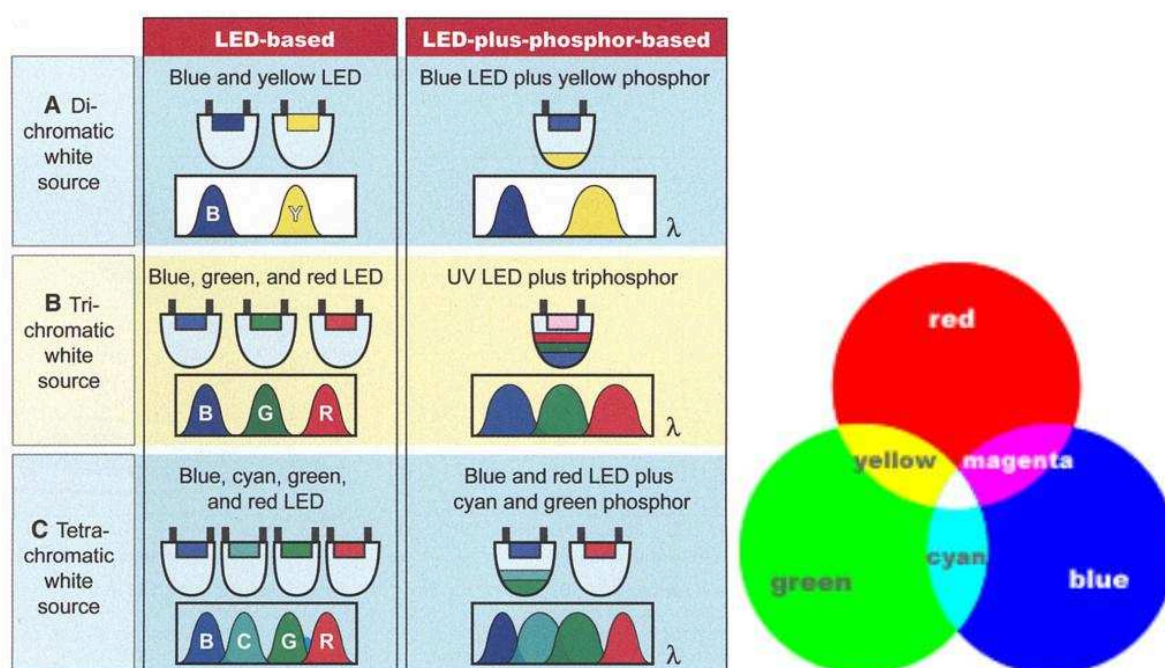


Figure 1-14 Diagram of different strategies for white light (left) and color mixtures (right)⁷³

In summary, common strategies for obtaining white light are

- 1) a near-UV LED with blue and yellow phosphors (or red, green, and blue phosphors);
- 2) a blue LED combined with a yellow phosphor;
- 3) a near-UV LED with white phosphors (polymers, or blends of polymer with metal complexes);

⁷² a. G. Chen, L. Yao, H. Zhong, S. Cui. *Journal of Luminescence*, **2016**, 178, 6–12.

b. S. Singh. **2009**, Chapter In book: Handbook of Light Emitting and Schottky Diode Research, Edition: 1st, Publisher: Nova Scientific Publisher, Editors: N.P. Chen.

⁷³ E. Fred Schubert and J. K. Kim. *Science*, **2005**, 308, 1274-1278.

- 4) a combination of blue and yellow LEDs;
- 5) a combination of red, green, and blue LEDs or more (cyan for example);
- 6) color-tunable luminescent supramolecular hydrogel with white-light emission.⁷⁴

Among them, near-UV LED with di-colour, tri-colour or tetra-colour materials (namely, multi-phase phosphors) often require complex production processes that lead to high costs, have phase separation problem and their white-emitting light changes with input power.⁷⁵ Thus, the development of single white emitter or single phosphor material with several different luminescent molecules, such as different emitting rare earth ions or the combination of different organic luminescent materials, is more desirable and preferable⁷⁶.

Up to now, inorganic luminescent materials contains rare earth elements have been widely reported as luminophors leading to white light.⁷⁷ For example, $(\text{Ce}_{0.2}\text{Gd}_{0.6}\text{Tb}_{0.2})(\text{Mg}_{0.9}\text{Mn}_{0.1})\text{B}_5\text{O}_{10}$ was reported as a single white emitter which was a combination of blue (from Ce ion), green (from Tb ion) and red (from Mn ion) from different rare earth ions. Besides, a blend of $\text{Sr}_4\text{Al}_{14}\text{O}_{25}:\text{Eu}^{2+}$ (Blue, 490nm, 90%)/ $\text{GdMgB}_5\text{O}_{10}:\text{Ce}^{3+}, \text{Mn}^{2+}$ (Red, 633 nm)/ $\text{GdMgB}_5\text{O}_{10}:\text{Tb}^{3+}$ (green) was reported as white light as well, which was a combination of three primary colors from different component.⁷⁸ $(\text{Y,Gd})_3(\text{Al,Ga})_5\text{O}_{12}:\text{Ce}^{3+}$ / $(\text{Ba,Sr,Ca})\text{Si}_2\text{O}_4:\text{Eu}^{2+}$ was also reported as white emitting material.⁷⁹ A phosphor-converted white light-emitting diode (pc-WLED) by using a blue InGaN LED chip coated with yttrium aluminium garnet yellow phosphor ($\text{Y}_3\text{Al}_5\text{O}_{12}:\text{Ce}$, YAG:Ce) was produced by Nichia in 1996⁶⁵ and he won the Nobel Prize in Physics in 2014, shared with two other creators of blue LEDs.⁶⁶ Following **Table 1-1** is a summary of commonly used inorganic luminophors with different emissions which can be commercially used for the constructions of white light systems.⁸⁰

Table 1-1 Summary of commonly used inorganic luminophors

⁷⁴ Zhang Y., Chen Y., Li J., Liang L., Liu Y., *Acta Chim. Sinica.*, **2018**, 76: 622-626.

⁷⁵ S. Achelle, J. Rodriguez-Lopez, C. Katan and F. Robin-le Guen. *J. Phys. Chem. C*, **2016**, 120 (47), 26986–26995.

⁷⁶ S. Fan, C. Yu, D. He, X. Wang, and L. Hu. *Optical Materials Express*, **2012**, 2 (6), 765-770.

⁷⁷ C.R. Ronda, T. Justel, H. Nikol. *J. Alloys Compd.*, **1998**, 669–676.

⁷⁸ <http://ocw.nctu.edu.tw/course/ch-inorganic-phosphors/2010chap6-1applicationI.pdf>, **2019**.

⁷⁹ T. Chen. *Materials Chemistry of Inorganic Phosphors*. <http://ocw.nctu.edu.tw/course/ch-inorganic-phosphors/2010chap1-introduction.pdf>, **2019**.

⁸⁰ a. *Phosphor Materials and Their Applications in Lighting and Displays*, **2019**, http://ocw.nctu.edu.tw/course/ipchemistry/ipchemistry_lecturenotes/ipch-7-1.pdf.

b. W. M. Yen and M. J. Weber. *Inorganic phosphors : compositions, preparation, and optical properties*. **2004**, CRC Press LLC. ISBN 0-8493-1949-8.

c. W. M. Yen, S. Shionoya, H. Yamamoto. *Phosphor handbook*. **2006**, CRC Press. ISBN 0-8493-3564-7.

Color	Blue	Green	Red
Chemical formula (Quantum efficiency)	BaMgAl ₁₀ O ₁₇ :Eu ²⁺ (90%)	(Ce _{0.67} Tb _{0.33})MgAl ₁₁ O ₁₉ (85%)	Y ₂ O ₃ :Eu ³⁺ (100%)
	Sr ₃ (PO ₄) ₅ Cl:Eu ²⁺ (90%)	(Ce _{0.45} La _{0.40} Tb _{0.15})(PO ₄) (86%)	Y ₂ O ₂ S:Eu ³⁺
	Sr ₂ Al ₆ O ₁₁ :Eu ²⁺ (90%)	(Ce _{0.3} Gd _{0.5} Tb _{0.2})MgB ₅ O ₁₀ (88%)	CaSiO ₃ :Pb:Mn (85%)
	Sr ₂ P ₂ O ₇ :Eu ²⁺ (90%)	Zn ₂ SiO ₄ :Mn (70%)	Y ₂ O ₃ :Eu ³⁺ (92%)
	Sr ₂ P ₂ O ₇ :Sn (86%)	(Ce, Tb)MgAl ₁₁ O ₁₉	Cs(BO ₂) ₂ :Mn (78%)
	Ca ₅ F(PO ₄) ₃ :Sb (71%)	(La, Ce)PO ₄ :Tb ³⁺	YVO ₄ :Eu ³⁺ (89%)
	MgWO ₄ :W (83%)	(La, Ce)(P, Si)O ₄ :Tb ³⁺	Y ₂ O ₃ :Eu ³⁺
	CaWO ₄ :W (75%)	ZnS:Cu, Al	Mg ₄ O _{5.5} GeF:Mn ⁴⁺
	(Sr, Ca, Ba) ₁₀ (PO ₄) ₆ Cl ₂ :Eu ²⁺	SrGa ₂ S ₄ :Eu	SrY ₂ S ₄ :Eu ³⁺
	(Ba,Sr,Ca) ₂ MgAl ₁₆ O ₂₇ :Eu ²⁺	Sr ₄ Al ₁₄ O ₂₅ :Eu ²⁺	YVO ₄ :Eu ³⁺ ,Bi
	(Sr,Ca,Ba) (Al,Ga) ₂ S ₄ :Eu ²⁺	Ba ₂ Al ₁₀ O ₇ :Eu ²⁺ ,Mn ²⁺	(Ca,Sr)S:Eu ³⁺
	BaMg ₂ Al ₁₆ O ₂₇ :Eu ²⁺	Ca ₈ Mg(SiO ₄) ₄ Cl ₂ :Eu,Mn	SrS:Eu ³⁺

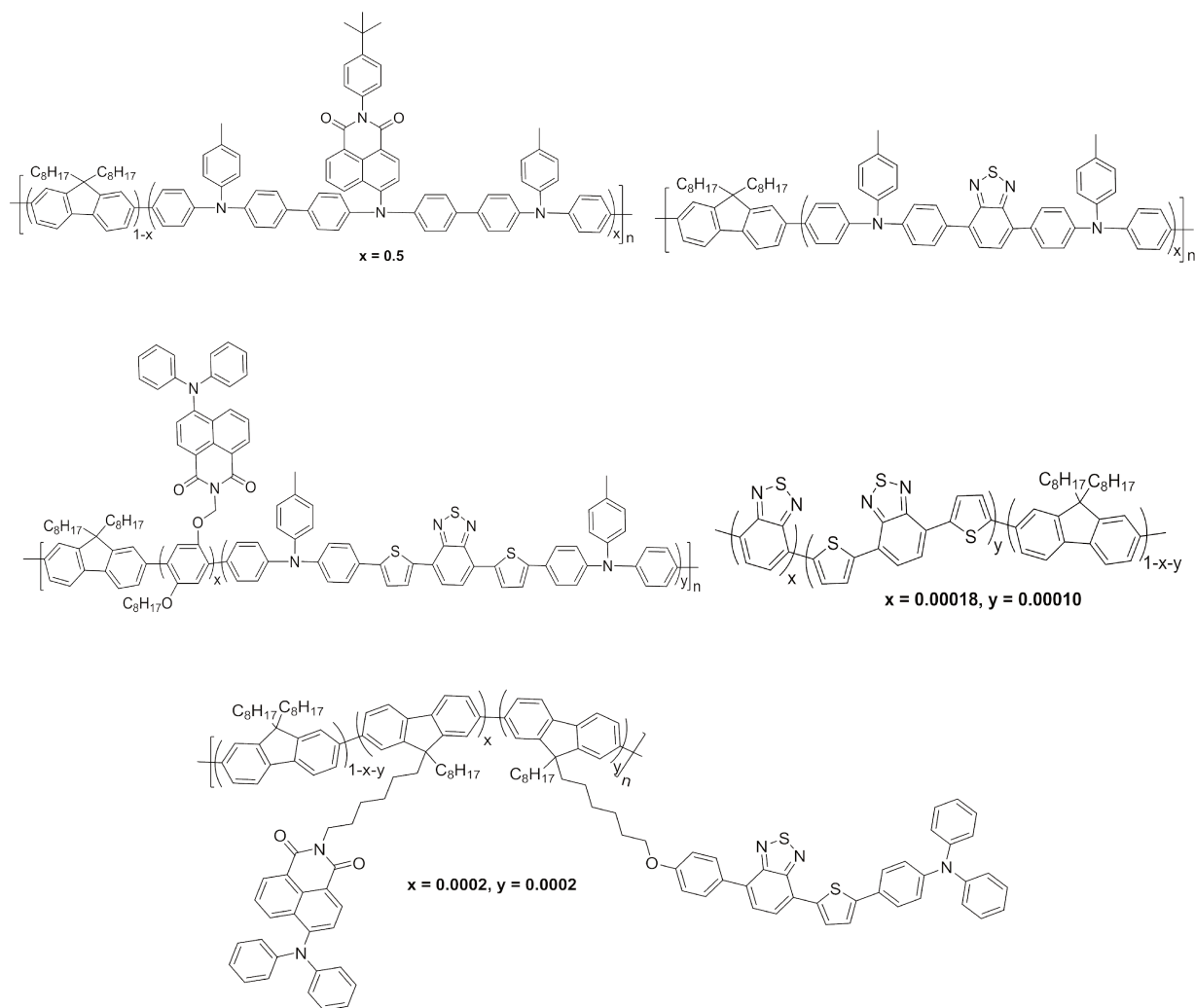
White LEDs actually commercialized combine the blue emission of a LED with the yellow emission of a luminescent material coated on it. The universal phosphor is Y₃Al₅O₁₂:Ce³⁺, which is purely inorganic. These systems suffer from a low color rendering index because of the lack of a red component and some of them have raised a sanitary issue, as too much blue light is emitted. This can potentially creates damages to the eye. Also, the color cannot be tightly tuned and it is not possible to improve the quality of the light emitted by adjusting the composition of these inorganic materials. In the long view, the application of rare earth elements for white light sources is also restricted due to the limited availability of resources of these elements. Besides, the pollution of the costly rare-earth containing materials is a notorious intractable and inextricable problem.^{81,82} Hybrid or organic emissive materials are anticipated to be an interesting alternative to inorganic materials. They are obtained from syntheses that do not demand temperatures as high as those needed for inorganic materials (hundreds of degrees), which lowers their cost. Their color of emission can be easily tuned thanks to an appropriate molecular engineering. The application of hybrid or organic luminophores instead of inorganic materials thus aroused great interest of scientists. Schlotter et al., who used luminescent dyes, and Heeger and co-workers, who employed a polymeric luminescent material as the converter, have demonstrated the applicability of organic luminophores for blue light converters.⁶¹

⁸¹ a. B.C. McLellana, G.D. Corder, A. Golev, S.H. Ali. *Procedia Environmental Sciences*, **2014**, 20, 280 – 287.

b. T. Ault, S. Krahn and A. Croff. *Energies*, **2015**, 8, 2066-2081.

⁸² N. J. Findlay , J. Bruckbauer , A. R. Inigo , B. Breig , S. Arumugam , D. J. Wallis , R. W. Martin , and P. J. Skabara. *Adv. Mater.* **2014**, 26, 7290–7294.

So far, many organic molecules, especially polymers, have been reported as single emitters for white light in electroluminescent devices, such as OLEDs (representatives are shown in **Figure 1-15**)⁸³. But to the best of our knowledge, there have been no reports on white-light photoluminescence from a single polymer. Much attention continues to be paid to the development of white light-emitting diodes (WLEDs) owing to the expectation of replacing the conventional lighting based on fluorescent and incandescent bulbs which show a low electro-optic conversion efficiency.⁸⁴



⁸³ a. G. Tu, C. Mei, Q. Zhou, Y. Cheng, Y. Geng, L. Wang, D. Ma, X. Jing, and F. Wang. *Adv. Funct. Mater.*, **2006**, 16, 101–106.

b. J. Liu, Q. Zhou, Y. Cheng, Y. Geng, L. Wang, D. Ma, X. Jing, and F. Wang. *Adv. Funct. Mater.*, **2006**, 16, 957–965.

c. J. Liu, Q. Zhou, Y. Cheng, Y. Geng, L. Wang, D. Ma, X. Jing, and F. Wang. *Adv. Mater.*, **2005**, 17, 2974–2978.

d. J. Luo, X. Li, Q. Hou, J. Peng, W. Yang, and Y. Cao. *Adv. Mater.*, **2007**, 19, 1113–1117.

e. J. Liu, Z. Xie, Y. Cheng, Y. Geng, L. Wang, X. Jing, and F. Wang. *Adv. Mater.*, **2007**, 19, 531–535.

f. H. Wu, L. Ying, W. Yang and Y. Cao. *Chem. Soc. Rev.*, **2009**, 38, 3391–3400.

⁸⁴ a. S. Jhulki, S. Seth, S. Rafiq, A. Ghosh, T. J. Chow, and J. N. Moorthy. *ACS Omega*, **2018**, 3: 1416–1424.

b. P. Waltereit, O. Brandt, A. Trampert, H. T. Grahn, J. Menniger, M. Ramsteiner, M. Reiche & K. H. Ploog. *Nature*, **2000**, 406, 865–868.

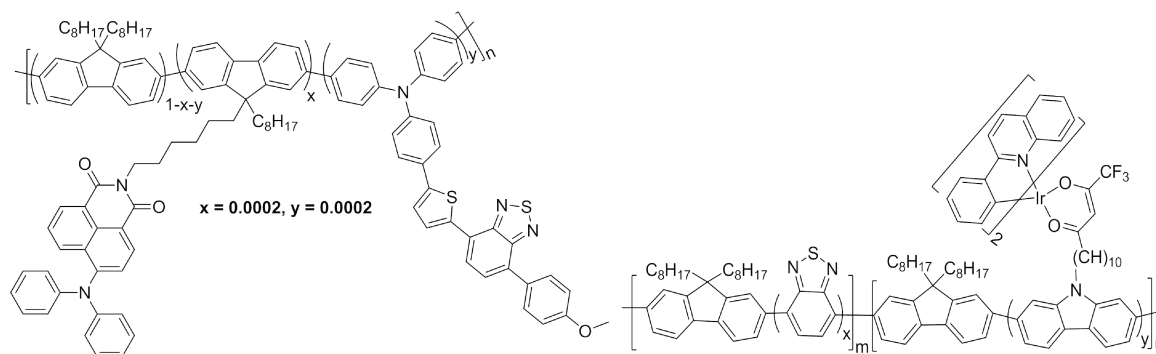


Figure 1-15 Representatives of reported single molecules for WLED

Polymers usually have higher glass transition temperatures. It is also easier to design polymers that emit different colors, which permits the creation of full color displays. Besides, polymers can be easily spin-coated or casted as they possess better solubility. This indicates that polymers have potentially a lower cost to process and are easier to coat on large surfaces for large display applications. Especially, conjugated polymers are very important photoactive materials because they possess a highly delocalized π -electron system and efficiently transport charges.⁸⁵ Hence much attention have drawn on conjugated polymeric materials.⁸³ It is also the main focus of this thesis.

The performance of optoelectronic devices based on donor-acceptor (D-A) conjugated materials has remarkably improved in past years and they represent promising candidates for the elaboration of flexible large-area and low-cost optoelectronic devices, due to their outstanding solution processability, film forming abilities and excellent mechanical properties.⁸⁶ Tremendous efforts have been devoted to develop materials with lower band-gap based on the concept of the (D-A)_n approach⁸⁷. These materials with the combination of donor (D) and acceptor (A) moieties exhibit a narrow optical band-gap with intramolecular charge transfer (ICT) characteristic from the donor to the acceptor⁸⁸ that leads to unique properties, as illustrated in **Figure 1-16**.⁸⁹ The highest occupied molecular orbital (HOMO) of the donor unit interacts with the HOMO of the acceptor unit giving two new HOMOs for the (D-A)_n system. In a similar way, the lowest

⁸⁵ M. Leclerc, A. Lorette (CA); J.-F. Morin, S. Foy (CA); I. Levesque, Q. City (CA); M. D'Iorio, Gloucester (CA); C. Py, Ottawa (CA). **2003**, US 2003/0008172 A1.

⁸⁶ G. L. Schulz, X. Chen, and S. Holdcroft. *American Institute of Physics*, **2009**, 94, 023302.

⁸⁷ X. Long, C. Dou, J. Liu, and L. Wang. *Macromolecules*, **2017**, 50 (21), 8521–8528.

⁸⁸ E. Zhou, K. Hashimoto, K. Tajima. *Polymer*, **2013**, 54, 6501–6509.

⁸⁹ a. J. Dhar, N. Venkatramaiah, A. A. and S. Patil. *J. Mater. Chem. C*, **2014**, 2, 3457–3466.

b. J. Mei, Y. Diau, A. L. Appleton, L. Fang, and Z. Bao. *J. Am. Chem. Soc.*, **2013**, 135, 6724–6746.

c. A. W. Hains, Z. Q. Liang, M. A. Woodhouse and B. A. Gregg. *Chem. Rev.*, **2010**, 110, 6689–6735.

d. E. E. Havinga, W. Tenhoeve and H. Wynberg. *Polym. Bull.*, **1992**, 29, 119–126.

e. E. E. Havinga, W. Tenhoeve and H. Wynberg. *Synth. Met.*, **1993**, 55, 299–306.

f. C. Kitamura, S. Tanaka and Y. Yamashita. *Chem. Mater.*, **1996**, 8, 570–578

unoccupied molecular orbital (LUMO) of the donor unit interacts with the LUMO of the acceptor unit leading to two new LUMOs for the (D-A)_n system. As a consequence, after the electrons redistributed to these new hybridized orbitals, a higher lying HOMO and a lower lying LUMO was formed and resulted in a smaller bandgap.⁹⁰

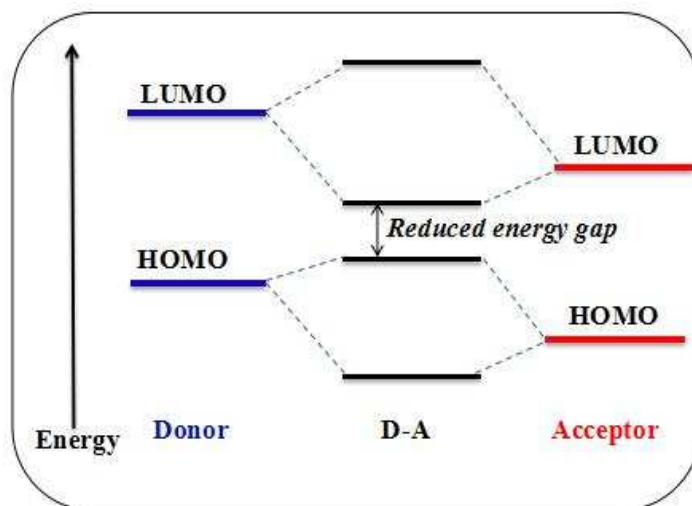


Figure 1-16 Illustration of reduced energy gap of polymer by (D-A)_n conjugation

In (D-A)_n conjugated polymer systems, the HOMO and the LUMO are mainly located at the donor unit and acceptor unit, respectively. Higher energy level of HOMO of the donor and lower energy level of LUMO of the acceptor will lead to a lower band gap of (D-A)_n system due to an intra-chain charge transfer from the donor to acceptor.⁹¹ Therefore, the bandgaps of (D-A)_n copolymers can be easily tuned and developing new acceptor and donor units as building blocks with suitable energy levels becomes crucial for developing high performance copolymers.⁹² Although (D-A)_n copolymers based on electron-deficient blocks such as thienothiophene, benzothiadiazole,⁹³ thienopyrazine, diketopyrrolopyrrole,⁹⁴ naphthalene diimide,⁹⁵ isoindigo⁹⁶,

⁹⁰ Benjamin James Hale, *PhD thesis*, **2015**, Iowa State University.

⁹¹ E. Bundgaard, F. C. Krebs. *Solar Energy Materials & Solar Cells*, **2007**, *91*, 954–985.

⁹² W. Zhang, Y. Sun, C. Wei, Z. Lin, H. Li, N. Zheng, F. Li, G. Yu. *Dyes and Pigments*, **2017**, *144*, 1–8.

⁹³ a. S. Wang, M. Kappl, I. Liebewirth, M. Müller, K. Kirchhoff, W. Pisula, K. Müllen. *Adv. Mater.*, **2012**, *24*, 417.

b. H. N. Tsao, D. M. Cho, I. Park, M. R. Hansen, A. Mavrinskiy, D. Y. Yoon, R. Graf, W. Pisula, H. W. Spiess, K. Müllen. *J. Am. Chem. Soc.*, **2011**, *133*, 2605.

c. H.-R. Tseng, L. Ying, B. B. Y. Hsu, L. A. Perez, C. J. Takacs, G. C. Bazan, A. J. Heeger. *Nano. Lett.*, **2012**, *12*, 6353–6357.

⁹⁴ a. P. Sonar, S. P. Singh, Y. Li, M. S. Soh, and A. Dodabalapur. *Adv. Mater.*, **2010**, *22*, 5409–5413.

b. T. L. Nelson, T. M. Young, J. Liu, S. P. Mishra, J. A. Belot, C. L. Balliet, A. E. Javier, T. Kowalewski, and R. D. McCullough. *Adv. Mater.*, **2010**, *22*, 4617–4621.

c. H. Chen, Y. Guo, G. Yu, Y. Zhao, J. Zhang, D. Gao, H. Liu, and Y. Liu. *Adv. Mater.*, **2012**, *24*, 4618–4622.

⁹⁵ a. H. Huang, Z. Chen, R. P. Ortiz, C. Newman, H. Usta, S. Lou, J. Youn, Y.-Y. Noh, K.-J. Baeg, L. X. Chen, A. Facchetti, T. Marks. *J. Am. Chem. Soc.*, **2012**, *134*, 10966 ;

b. K.-J. Baeg, D. Khim, S.-W. Jung, M. Kang, I.-K. You, D.-Y. Kim, A. Facchetti, Y.-Y. Noh. *Adv. Mater.*, **2012**, *24*, 5433–5439.

⁹⁶ a. T. Lei, J.-H. Dou, Z.-J. Ma, C.-J. Liu, J.-Y. Wang, J. Pei. *Chem. Sci.*, **2013**, *4*, 2447 ;

b. R. Stalder, J. Mei, K. R. Graham, L. A. Estrada, and J. R. R. Isoindigo, *Chem. Mater.*, **2014**, *26* (1), 664–678.

c. T. Lei, J.-H. Dou, Z.-J. Ma, C.-H. Yao, C.-J. Liu, J.-Y. Wang, J. Pei. *J. Am. Chem. Soc.*, **2012**, *134*, 20025 ;

benzobisthiadiazole⁹⁷, corannulene derivatives⁹⁸ and so forth,⁹⁹ (Chemical structures of representatives are shown in **Figure 1-17**) have led to excellent performance in optoelectronic devices, such as improved emission efficiency, tunable emission, high charge-carrier mobilities in smaller bandgap and leading to the red-shift of the emission bands, the types of acceptor units are still limited. Since the development of distinct structures are the basis of new improvements of the conjugated polymers, it is important to develop different new acceptor structures.¹⁰⁰

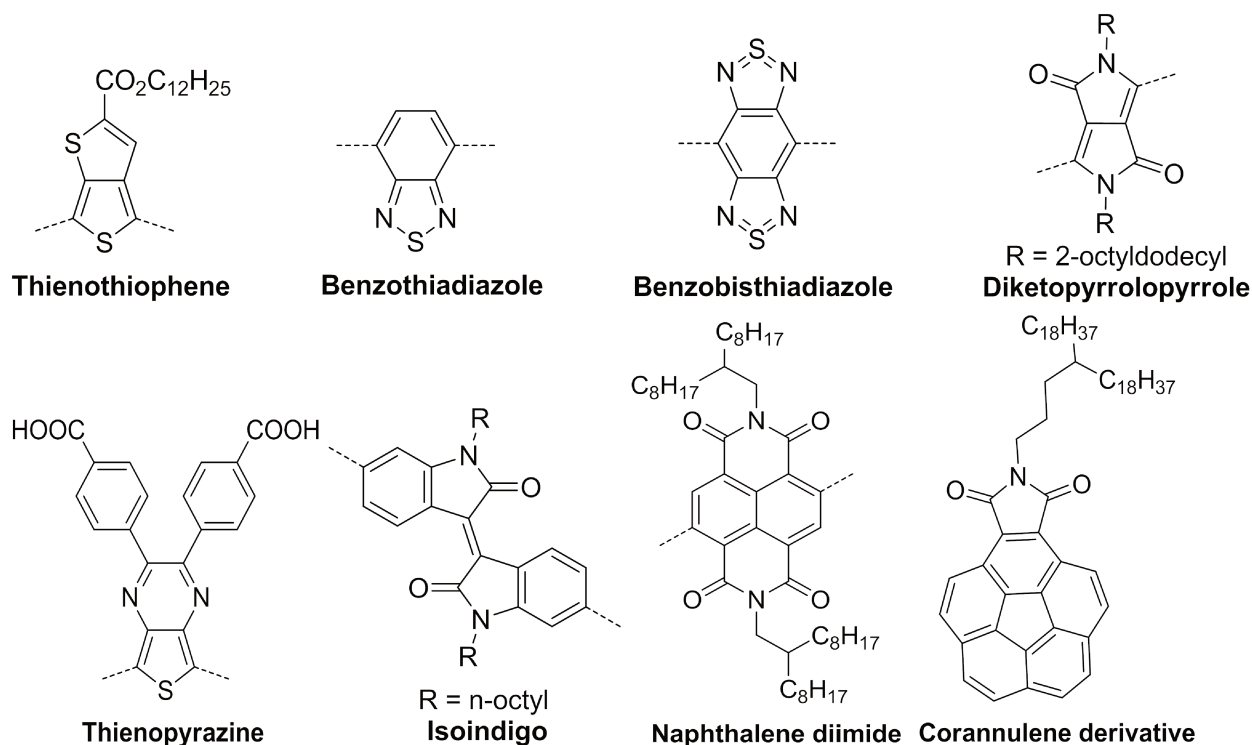


Figure 1-17 Representatives of reported acceptor group

Among others, *N*-based π -deficient heterocycles such as pyridine, pyrimidine, quinazoline, pyrazine, and benzimidazole have been explored as good electron-withdrawing units.^{69,101} In

d. Y. Ren, A. K. Hailey, A. M. Hiszpanski, and Y.-L. Loo. *Chem. Mater.*, **2014**, 26, 6570–6577.

e. J. Mei, D. H. Kim, A. L. Ayzner, M. F. Toney, Z. Bao. *J. Am. Chem. Soc.*, **2011**, 133, 20130 ;

f. T. Lei, Y. Cao, Y. Fan, C. Liu, S. Yuan, and J. Pei. *J. Am. Chem. Soc.*, **2011**, 133, 6099–6101.

⁹⁷ J. Fan, J. D. Yuen, W. Cui, J. Seifter, A. R. Mohebbi, M. Wang, H. Zhou, A. Heeger, and F. Wudl. *Adv. Mater.*, **2012**, 24, 6164–6168.

⁹⁸ a. R. Lu, W. Xuan, Y. Zheng, Y. Zhou, X. Yan, J. Dou, R. Chen, J. Pei, W. Weng and X. Cao, *RSC Adv.*, **2014**, 4, 56749–56755.

b. R. Lu, Y. Zheng, Y. Zhou, X. Yan, T. Lei, K. Shi, Y. Zhou, J. Pei, L. Zoppi, K. K. Baldrige, J. S. Siegel, and X. Cao. *J. Mater. Chem. A*, **2014**, 2, 20515–20519.

c. I. V. Kuvychko, C. Dubceac, S. H. M. Deng, X.-B. Wang, A. A. Granovsky, A. A. Popov, M. A. Petrukhina, S. H. Strauss and O. V. Boltalina, *Angew. Chem. Int. Ed.*, **2013**, 52, 7505–7508.

⁹⁹ a. M. Manceau, E. Bundgaard, F. C. Krebs et al. *J. Mater. Chem.*, **2011**, 21, 4132.

b. T. Lei, J. Dou, X. Cao, J. Wang, and J. Pei. *Adv. Mater.*, **2013**, 25, 6589–6593.

¹⁰⁰ R. Lu, W. Xuan, Y. Zheng, Y. Zhou, X. Yan, J. Dou, R. Chen, J. Pei, W. Weng and X. Cao, *RSC Adv.*, **2014**, 4, 56749–56755.

¹⁰¹ S. Achelle, J.-P. Malval, S. Aloïse, A. Barsella, A. Spangenberg, L. Mager, H. Akdas-Kilig, J.-L. Fillaut, B. Caro, F. Robin-Le Guen. *ChemPhysChem*, **2013**, 14 (12), 2725–36.

particular, pyrimidine derivatives are found with some extra super properties, such as high emission efficiency, and some pyrimidine push-pull derivatives were described as polarity sensors due to their strong emission solvatochromism and *pH* sensors due to the basic character of the nitrogen atoms of the heterocycles.^{75,102} Bipyrimidine derivatives have drawn much attention and have been exploited for the design and synthesis of bipyrimidine-containing conjugated systems (examples are shown in **Figure 1-18**)^{103,104,105} with interesting luminescent properties: (i) the electron affinity of the pyrimidine ring is much higher than that of the pyridine ring due to its higher electron deficient property; (ii) they can be applied as versatile bis-chelating ligands towards metal ions and important building components for the establishment of supramolecular assemblies, as the *N*-heterocyclic aromatic compounds are strongly coordinating ligands that are able to form stable complexes with various metals;^{57,59,106} (iii) the high photostability and thermostability of pyrimidine ring also make it more attractive.¹⁰⁷ But to the best of our knowledge, the BPM molecule has never been used as an electron-deficient unit in conjugated polymers, probably because of their synthetic difficulties and their poor solubility.¹⁰⁸

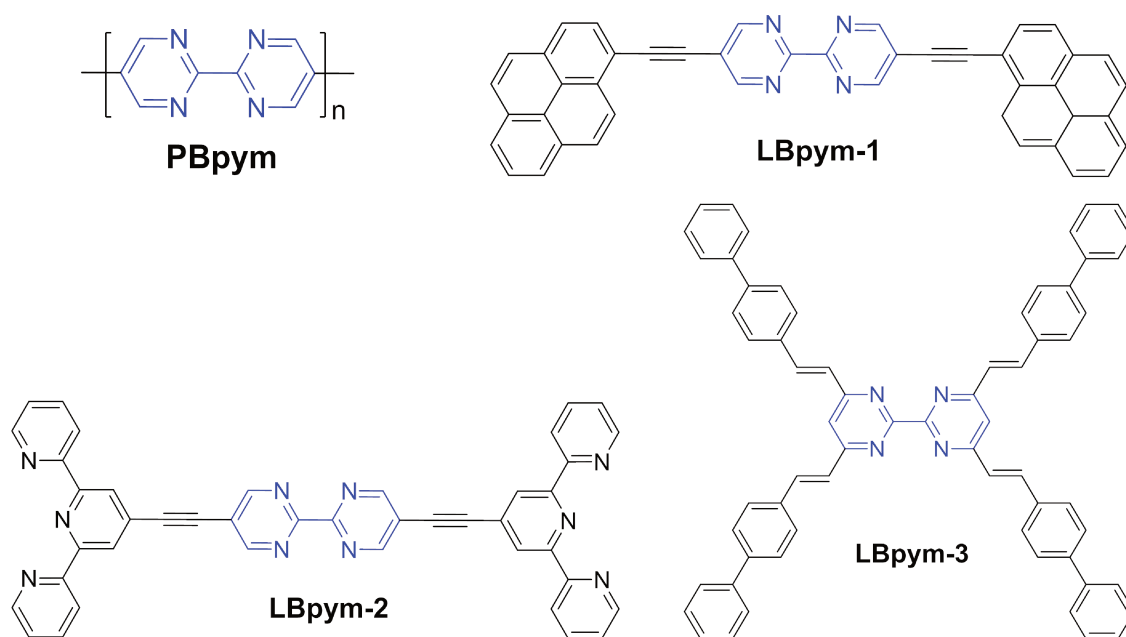


Figure 1-18 Representatives of reported bipyrimidine-containing conjugated systems

In fact only one report of bipyrimidine-based conjugated polymer was found, as shown in **Figure**

¹⁰² S. Achelle, L. Bodiou, J. Charrier, F. Robin-le Guen. *C. R. Chimie*, **2016**, 19, 279-285.

¹⁰³ R. Ziessel and C. Stroh. *Tetrahedron Letters*, **2004**, 45, 4051-4055.

¹⁰⁴ T. Yamamoto, N. Hayashida, T. Maruyama and K. Kubota. *Chemistry Letters*, **1998**, 1125-1126.

¹⁰⁵ T. Yamamoto, T. Koizumi. *Polymer*, **2007**, 48, 5449-5472.

¹⁰⁶ H. Akdas-Kilig T. Roisnel, I. Ledoux and H. L. Bozec. *New J. Chem.*, **2009**, 33, 1470-1473.

¹⁰⁷ R. Gompper, S. Brandl, H. J. Mair. Use of conjugated compounds containing pyrimidine groups as electroluminescence materials. *United States Patent*, **1999**, US5948551A.

¹⁰⁸ M. J. Crosley, S. Gorjian, S. Sternhell and K. M. Tansey. *Aust. J. Chem.*, **1994**, 47, 723-738.

1-18 (PBpym), and it demonstrated poor solubility that only partially soluble in acids.¹⁰³ In this thesis, we have particularly focused on the exploration and development of the use of bipyrimidine derivatives into conjugated polymers as a novel acceptor due to its electron deficient property with improved solubility and processibility, as well as bipyrimidine-based metal complexes.

It is noteworthy that increasing interest has been paid to hybrid materials for their remarkable unique advantages, such as easiness of processing, ultrapure light emission and fine-tuning of their emission color, compared to others, particularly inorganic materials.¹⁰⁹ It has been reported as a feasible avenue to overcome shortages of each material through a hybrid inorganic/organic LED architecture, where a blue emissive inorganic LED is coated with an organic material that has an absorbance band aligned with the emission wavelength of the inorganic structure. The organic material acts as an energy down-converter for the inorganic LED, which converts a part of the blue luminescence emitted by the inorganic LED to lower energy light such as yellow and red, which in combination delivers a high quality output of white light. Through this way, not only the advantages of both materials are combined, for example, the excellent stability and electronic properties of inorganic substrates and the tunable emission and easy fabrication of organic semiconductors, but also new potential properties can be expected.⁸² Based on the above knowledge, we expected that our newly developed polymer-based luminescent materials coated on inorganic LEDs would bring a superior combination of outstanding characteristics and performance to them, and thus leading to some new potential applications.

1.4 Polymer matrices

As we known, a high stability of luminescent materials in optoelectronic devices is of great importance.⁹⁰ The stability of LED lighting materials concerning the severe environment, such as thermal treatment, humidity and UV light exposure, appears to be a bottleneck that impedes their further commercialization. One of the most challenging issue in LED lighting materials is the long-term photostability, which must be cleared up before putting it into practical applications. Various strategies to reduce the UV-induced instability of the devices have been reported, such as composition engineering (synthesizing emitters such as polymers with higher photostability units)¹¹⁰ and device encapsulation (using UV-absorbing molecules to protect the emitters).^{61,111}

¹⁰⁹ a. W. Deng, H. Fang, X. Jin, X. Zhang, X. Zhang and J. Jie. *J. Mater. Chem. C*, **2018**, 6, 4831-4841.

b. M.-S. Wang and G.-C. Guo. *Chem. Commun.*, **2016**, 52, 13194-13204.

¹¹⁰ S.-H. T.-Cruz, A. Hagfeldt, M. Saliba. *Science*, **2018**, 362, 449.

¹¹¹ a. R. Wang, M. Mujahid, Y. Duan, Z.-K. Wang, J. Xue, and Y. Yang. *Adv. Funct. Mater.*, **2019**, 1808843.

Particularly, it has been shown that, through encapsulation, the stability of organic electronic devices, such as perovskite solar cells and OLEDs, can be highly enhanced.^{111c,112} Devices without encapsulation commonly exhibited severe degradation under continuous UV irradiation after several hours, while encapsulated devices exhibited longer lifetimes. Encapsulation strategy plays a vital role in improving the stability of organic electronic devices that will help to accelerate the technology to the goal of commercialization. At present, the encapsulation method of the commercial products such as OLED displays, lighting product, and most of displays is achieved by glass and metal lid. However, this results in a rigid device and hampers the development of applications such as flexible devices.⁶⁰

Recently, much progress has been made in improving organic luminophor interfaces through polymer matrix encapsulation method from UV degradation.¹⁰⁹ A variety of polymer matrix materials have been investigated as device encapsulants, including Polymethyl Methacrylate (PMMA), Polyvinyl butyral (PVB), poly(ethylene naphthalate) (PEN) and polycarbonate (PC) and so on.^{110,111} Structures of investigated polymer matrix materials are shown in **Figure 1-19**. They serve as a solid “solvent” to disperse the luminophors as well as molecule encapsulants to protect them from UV degradation by the absorption and the conversion of part of the UV radiation into harmless heat, and the screen of harmful radiations.¹¹³ Sol-gel polymer matrix material is among the most widely used encapsulating materials available, it offers resistance and reliability under long periods of exposure to different elements, such as heat, wet and UV-light. Also, as they can well combine an inorganic silica network with the organic groups that are easily modifiable, sol-gel materials are very attractive.¹¹⁴

Sol-gel materials that present a liquid character are expected to have a lot of advantages over their common solid counterparts, such as easy-processing, self-healing properties, excellent homogeneity due to the dispersion of the precursors in solution, mild reaction conditions, high transmission and no need of solvent. In this work, we not only have tried to improve the photostability of the materials by composition engineering, but also have studied different polymer matrices containing PMMA, Polystyrene, Poly(Ethylene-co-vinyl acetate) and

b. D. Yu, Y. Yang, Z. Chen, Y. Tao, Y. Liu. *Optics Communications*, **2016**, 362, 43–49.

c. P. E. Burrows, V. Bulovic, S. R. Forrest, L. S. Sapochak, D. M. McCarty, and M. E. Thompson. *Appl. Phys. Lett.*, **1994**, 65 (23), 2922-2924.

¹¹² X. Zhao, A. J. D. Ng, R. H. Friend, and Z. K. Tan. *ACS Photonics*, **2018**, 5 (10), 3866–3875.

¹¹³ a. C. Queant, P. Blanchet, V. Landry and D. Schorr. *Coatings*, **2018**, 8, 265.

b. C. Queant, P. Blanchet, V. Landry and D. Schorr. *J Polym Eng*, **2019**; 39 (1): 94–103.

¹¹⁴ a. X. Huang, G. Zucchi, J. Tran, R. B. Pansu, A. Brosseau, B. Geffroy and F. Nief. *New J. Chem.*, **2014**, 38, 5793-5800.

b. X. Huang, Luminescent Lanthanide Hybrid Sol-gel Materials with Potential Applications in Electronic Devices. *PhD thesis*, Ecole polytechnique, **2015**.

especially the liquid Carbazole-Silica matrix (C-Si matrix) as encapsulating materials in the goal of protecting our lumonophors from UV degradation. An illustration of the formation of the C-Si matrix is shown in **Figure 1-20**. It mainly contains two chemical steps, that are, hydrolysis of the alkoxy silane ($-\text{Si}(\text{OEt})_3$) and poly-condensation. The general procedure for the synthesis of such materials can be found in Xiaoguang Huang's PhD thesis.¹¹⁴

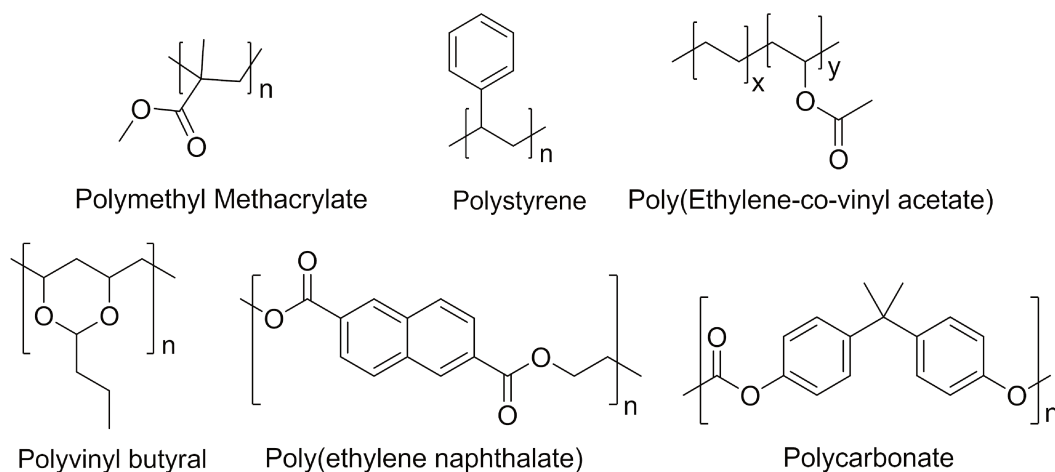


Figure 1-19 Representative reported polymer matrix materials

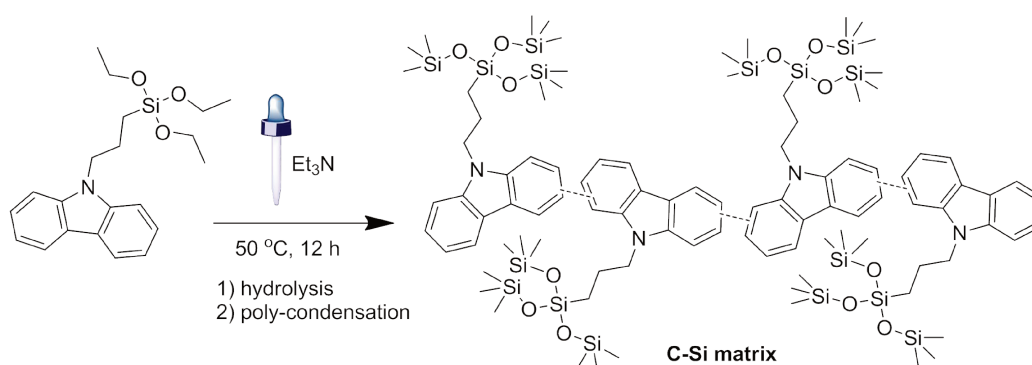


Figure 1-20 Illustration of the preparation of a C-Si matrix

1.5 CIE coordinate diagram

CIE, abbreviated from Commission Internationale de l'Eclairage, was created by the International Commission on Illumination (CIE) in 1931. Nowadays the CIE coordinate diagram is widely applied as a system for the specification of color stimuli. The chromaticity is specified by the two derived parameters as (x, y) . It was resulted from a series of experiments done in the late 1920s by William David Wright using ten observers and John Guild using seven observers. Revisions were made in 1960 and 1976, but the 1931 version remains the most widely used

version.¹¹⁵

Approximate colors can be assigned to areas on the following CIE Chromaticity Diagram.

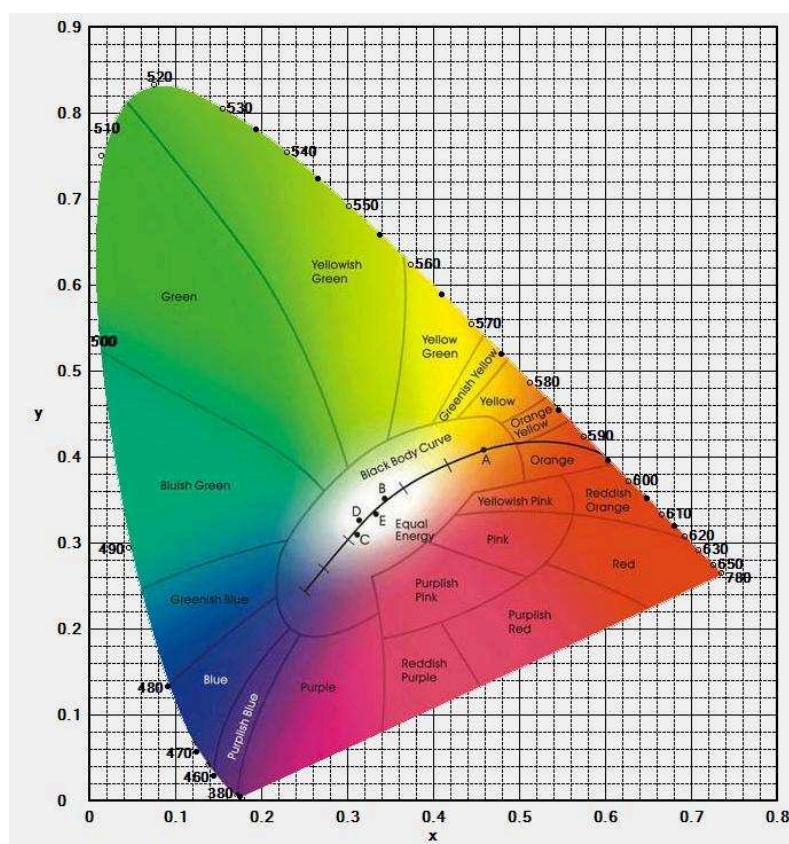


Figure 1-21 Approximate color regions on CIE diagram

In the presented work, the CIE coordinate diagram was applied to define the specific colors, especially the three types of white light, including cool white, neutral white and warm white, according to calculated color temperature (CCT) from CIE data. The CCT is the temperature of the Planckian radiator whose perceived color most closely resembles that of a given stimulus at the same brightness and under specified viewing conditions. It is measured in degrees of Kelvin (K) on a scale from 1,000 to 10,000.

1.6 Thesis structure

The presented work aims at elaborating novel soft and highly luminescent silica-based hybrid materials that could be used as potential phosphors for LED lighting. Soft materials have many advantages, as they are synthesized from neat reactions, they are easily-processed with various

¹¹⁵ a. <http://hyperphysics.phy-astr.gsu.edu/hbase/vision/cie.html>
b. https://en.wikipedia.org/wiki/CIE_1931_color_space

shapes without the use of any solvent, and they are self-healing. The emitters we are investigating are either metal complexes or conjugated polymers. We have particularly developed the design of conjugated polymers as their color of emission can be controlled through a judicious design and they do not use europium whose supply and use can be problematic at high scale, thus leading to expensive lighting systems. Bipyrimidine derivatives are successfully introduced into (D-A)_n polymers as a new developed acceptor unit. Our final goal is to obtain white source of light and thus molecular compounds emitting the three primitive colors (red, blue and green) are targeted. The work presented will focus on the strategy we developed for designing new molecular emitters and novel soft white-emitting materials and investigations of their photophysical properties and photostability.

In this **Chapter I**, we have shown that different luminescent materials have wide different applications, such as home lightings, traffic lightings, lab lightings, sensors, and even become a common source as green and neat energy for chemical reactions and many other research works. In addition, various ways to obtain white light and polymeric materials especially sol-gel materials that can be used to protect the organic luminophor from UV degradation are also introduced. All above construct a good foundation of what we have done for the project.

In the following chapters, details of the materials design, synthesis and full characterization results are shown, as well as the investigation of their possibility to be used as luminophors. The **Chapter II** is focused on the design, synthesis and chemical characterizations of the materials. The **Chapter III** presents details of results of photophysical properties of all the materials both in solution and in solid state. Following the **Chapter IV** shows the results of the materials that investigated as luminophors, including the photophysical properties of the materials in different matrices, the quantum yields determination, photostability and thermostability studies. A general conclusion and perspective of the thesis are presented in the last **Chapter V** as a summary. Finally, a summary of basic information (structure, name, yield, mark) of polymers discussed in the thesis and NMR spectra of selected new compounds are presented in the **Appendix** part.

Chapter II Experimental part

Contents

2.0 General information.....	- 34 -
2.1 Synthesis and chemical characterization of the monomers.....	- 37 -
2.2 Synthesis and chemical characterization of the polymers.....	- 48 -
2.2.1 P1 and P2	- 48 -
2.2.2 P3 , P4 , P5 and P6	- 49 -
2.2.3 P7 and P8	- 53 -
2.2.4 P9	- 54 -
2.2.5 P10	- 54 -
2.2.6 P11 and P12	- 55 -
2.2.7 P13 and P14	- 56 -
2.2.8 P15	- 57 -
2.2.9 P16 , P17 and P18	- 58 -
2.3 Synthesis and chemical characterization of metal complexes.....	- 60 -
2.4 Preparation of the liquid materials.....	- 64 -
2.5 Preparation of thin films.....	- 66 -
2.6 Summary and Perspectives.....	- 68 -

In this chapter, we will describe the experimental procedures for the synthesis of the compounds, the formation of the thin films, and the instruments used. All the structures of the new compounds are summarized in **Appendix I**.

2.0 General information

Conjugated (D-A)_n polymers have gained great attention for their remarkably high performance, such as high solubility, favorable film-forming properties, and facile fabrication technique, using spin-coating and ink-jet printing methods.^{89,116} Such polymers are important light-absorbing systems, due to their in-chain donor-acceptor interactions, as a result, their band gaps are lowered and the emissions are shifted to the red. On the other hand, we are able to modulate the LUMO energy levels of (D-A)_n type conjugated polymers by modifications of both D unit and A unit as building blocks with suitable energy levels, due to the intra-chain charge transfer from the donor to acceptor.⁹¹ Stable and efficient luminescence of three primary colors, *videlicet* red, green, and blue, is essential to achieve a full-color display. Among them, only the red and the green polymer light-emitting diodes (PLEDs) have reached sufficiently high efficiencies and lifetimes for commercial applications. The degradation of commonly used fluorene-based polymeric blue emitting luminescent materials which correspond to the cleavage of the alkyl chains with subsequent formation of fluorenone moieties will lead to undesirable red emission and unsatisfactory lifetimes is still a major issue unsolved.¹¹⁷ (The detail of the photodegradation procedure will be described in part **§4.5 of Chapter IV**). Light-emitting conjugated polymers continue to draw great attention due to their potential display applications.

2,2'-bipyrimidine (BPM) has been reported as a ligand for designing molecular complexes as well as coordination polymeric lanthanide materials.¹¹⁸ In particular, it can adopt a bridging

¹¹⁶ a. Y. Xu, H. Sun, W. Li, Y. Lin, F. Balestra, G. Ghibaudo, and Y.-Y. Noh. *Adv. Mater.*, **2017**, 1702729.

b. K. Müllen and W. Pisula. *J. Am. Chem. Soc.*, **2015**, 137 (30), 9503-9505.

c. D. Hashemi, X. Ma, J. Kim and J. Kieffer. **2017**. arXiv:1707.01564. <https://arxiv.org/abs/1707.01564v1>.

d. X. Long, C. Dou, J. Liu, and L. Wang. *Macromolecules*, **2017**, 50 (21), pp 8521-8528.

e. P. Yang, H. Wu, H. Wen, W. Hung. *SEuropean Polymer Journal*. **2013**, 49, 2303-2315.

¹¹⁷ W. Zhao, T. Cao, J. M. White. *Adv.Funct.Mater.*, **2004**, 14(8), 783-790.

¹¹⁸ a. M. J. Crossley, S. Gorjian, S. Sternhell and K. M. Tansey. *Aust. J. Chem.*, **1994**, 47, 723-738.

b. Q. Liu, R. Wang and S. Wang. *Dalton Trans.*, **2004**, 2073-2079.

c. G. Zucchi, O. Maury, P. Thuery, and M. Ephritikhine. *Inorganic Chemistry*, Vol. 47, No. 22, **2008**.

d. G. Zucchi, O. Maury, P. Thuery, F. Gummy, J.-C.G. Bünzli, M. Ephritikhine, *Chem. Eur. J.*, **2009**, 15, 9686-9696.

e. G. Zucchi, P. Thuery, E. Riviere and M. Ephritikhine. *Chem. Commun.*, **2010**, 46, 9143-9145.

f. G. Zucchi, T. Jeon, D. Tondelier, D. Aldakov, P. Thuery, M. Ephritikhine and B. Geffroy. *J. Mater. Chem.*, **2010**, 20, 2114-2120.

g. G. Zucchi, *International Journal of Inorganic Chemistry*, vol. 2011, Article ID 918435, 13 pages, **2011**.

h. G. Zucchi, X. F. Le Goff. *Inorganica Chimica Acta*. **2012**, 380, 354-357.

i. G. Zucchi, X. F. Le Goff. *Polyhedron*. **2013**, 52, 1262-1267.

j. H. Ozawa, H. Kawaguchi, Y. Okuyama, and H. Arakawa. *Eur. J. Inorg. Chem.*, **2013**, 5187-5195.

k. T. Mukuta, N. Fukazawa, K. Murata, A. Inagaki, M. Akita, S. Tanaka, S. Koshihara, and K. Onda. *Inorg. Chem.*, **2015**, 54 (20),

coordination mode leading to the linkage of two metal ions. Plenty of studies¹¹⁷ reported to date show the great potential that BPM can bring to lanthanide chemistry and physics. They give both highly green and red emissive terbium and europium complexes, respectively. However, to the best of our knowledge, there is no previous report introducing BPM into the bond skeleton of (D-A)_n copolymers.

Interested in the function of BPM as an electron deficient/accepting unit in (D-A)_n conjugated polymers, we herein synthesized and characterized a series of new polymers, **P1-P14** and **P16**, based on the application of BPM as acceptor unit, as well as the abundantly reported polymer, poly(di-hexylfluorene) (**PF**). The four nitrogen atoms render the BPM unit electron-deficient. It is worth to be exploited for designing new highly emissive hybrid materials due to its unique characteristics, such as electron-deficient property and good bridging coordination ability with metal ions to afford a variety of structures. A conjugated polymer, **P15**, composed of benzo-thiadiazole (BTD) as acceptor unit instead of bipyrimidine compared to **P10** was also designed and synthesized. In addition, the effect of the pendant groups in the conjugated polymers were also studied by comparison with the newly designed and synthesized polymers **P16-P18**. To be noted, the side chains of polymers **P16-P18** all contain a moiety with a *N*-heterocyclic aromatic unit that is widely used for metal complexation, such as sensing work, they could be also very interesting in coordination chemistry.

Besides, in this Chapter, the synthesis and chemical characterization of some novel metal complexes with BPM derivatives as ligand are also presented, followed by the demonstration of the preparation of the carbazole-silica (**C-Si**) precursor and the liquid materials.

Lastly, the formation of thin films under different occasions are also demonstrated. Solution-processed film preparation techniques, such as spin-coating or painting methods are applied in this work due to their many advantages, such as better control of the doping level, better homogeneous morphology and easy processibility over large area size that can be readily upgraded to industrial scale.¹¹⁹

9681–9683.

m. G. Beaulieu-Houle, N. G. White, and M. J. MacLachlan. *Cryst. Growth Des.*, **2018**, 18 (4), 2210-2216.

n. C. K. Prier, D. A. Rankic, and D. W. C. MacMillan. *Chem. Rev.*, **2013**, 113, 5322-5363.

¹¹⁹ a. F. Cao, D. Zhao, P. Shen, J. Wu, H. Wang, Q. Wu, F. Wang, and X. Yang. *Adv. Optical Mater.*, **2018**, 1800652.

b. H. Wu, L. Ying, W. Yang and Y. Cao. *Chem. Soc. Rev.*, **2009**, 38, 3391–3400.

Materials and instruments

2-chloropyrimidine, Zinc, Nickel chloride (NiCl_2), Triphenylphosphine (PPh_3), Bromine, 2-isopropoxy-4,4,5,5-tetramethyl-1,3,2-dioxaborolane, n-Butyllithium, 4,4,4',4',5,5,5',5'-octamethyl-2,2'-bi(1,3,2-dioxaborolane), 9H-carbazole, 1-bromohexane, 1-bromooctane, ethyl formate, 4-Toluenesulfonyl chloride, 1,6-dibromohexane, 2-(pyridin-2-yl)-1H-benzo[d]imidazole, Bromobenzene and Phenylboronic acid were purchased from VWR and used as received. 9,9-dihexyl-2,7-dibromofluorene, 4-bromobenzaldehyde, $\text{Eu}(\text{NO}_3)_3 \cdot x\text{H}_2\text{O}$, $\text{EuCl}_3 \cdot 6\text{H}_2\text{O}$, CuI, 4,7-dichloro-1,10-phenanthroline, 4,4,4-trifluoro-1-(thiophen-2-yl)butane-1,3-dione, 1,10-phenanthroline, 9,9-Dihexylfluorene-2,7-bis(trimethyleneborate), 1-(pyridin-2-yl)ethanone, N-Bromosuccinimide (NBS), 2,2'-(9,9-dioctyl-9H-fluorene-2,7-diyl)bis(1,3,2-dioxaborinane) (**M2**), 4,7-bis(4,4,5,5-tetramethyl-1,3,2-dioxaborolan-2-yl)benzo[c][1,2,5]thiadiazole (**M3**) and 3,6-dibromo-9-hexyl-9H-carbazole (**M4**) were purchased from Aldrich. 2,2'-bipyrimidine (**C1**)¹²⁰, 5,5'-dibromo-2,2'-bipyrimidine (**M1**)¹²¹ and 9-(4-([2,2':6',2''-terpyridin]-4'-yl)phenyl)-3,6-dibromo-9H-carbazole (**M12**)¹²² were synthesized from revised approaches according to reported procedures, as well as *Poly(9,9-di-n-hexyl-2,7-fluorene)* (**PF**)¹²³. Dichloromethane (DCM) and Tetrahydrofuran (THF) of GPC grade for spectroscopy from VWR were applied for photoluminescence studies. All other chemicals and reagents were used as received from Aldrich, VWR and Alfa Aesar Chemical Co. unless otherwise specified. All solvents were carefully dried and purified before use. All manipulations involving air-sensitive reagents were performed under a dry argon atmosphere.

NMR spectra have been recorded on a Bruker Avance 300 spectrometer using CDCl_3 as the solvent; chemical shifts are given with respect to TMS ($\delta = 0$). GPC measurements were done with Viscotek equipment using THF as solvent and polystyrene as standard. The UV-Vis absorption spectra were recorded using a JENWAY UV-VIS Spectrophotometer Model UV

¹²⁰ a. N. Plé et al. *Journal of Heterocyclic Chemistry*, **2005**, 42, 1423-1428.

b. T. Mukuta et al. *Inorg. Chem.* **2014**, 53, 2481-2490.

c. S. Wang, et al. *Dalton Trans.*, **2004**, 2073-2079.

d. M. J. Crossley et al. *Aust. J. Chem.*, **1994**, 47, 723-738.

e. H. Hou et al. *J. APPL. POLYM. SCI.* **2014**, 131(24), 40828. f. Schwab, Peter F.H. et al. *J. Org. Chem.*, **2002**, 67(2), 443-449.

¹²¹ a. Schwab et al. *J. Org. Chem.* **2002**, 67, 443-449.

b. R. Ziesel, C. Stroh. *Tetrahedron Letters*, **2004**, 45, 4051-4055.

c. D. I. M. D'Souza, D. A. Leigh, M. Papmeyer & S. L. Woltering. *Nature protocols*, **2012**, 7(11): 2022-2018.

¹²² a. G. W. V. Cave and C. L. Raston. *Chem. Commun.*, **2000**, 2199-2200.

b. J. Wang, G. S. Hanan. *SYNLETT*, **2005**, 8, 1251-1254.

c. G. W. V. Cave and C. L. Raston. *J. Chem. Soc., Perkin Trans.*, **2001**, 1, 3258-3264.

d. N. B. McKeown, S. Badriya, M. Helliwell and M. Shkunov. *J. Mater. Chem.*, **2007**, 17, 2088-2094.

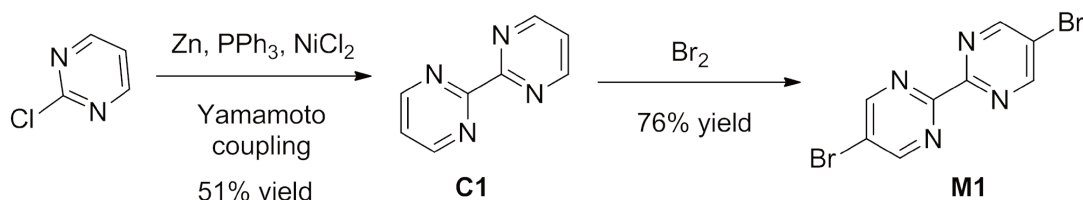
¹²³ a. H. Arakawa et al. *Eur. J. Inorg. Chem.* **2013**, 5187-5195.

b. H. Hou et al. *CrystEngComm*, **2012**, DOI: 10.1039/c2ce25759a.

c. A. Sergent, a. G. Zucchi. et al. *J. Mater. Chem. C*, **2013**, 1, 3207-3216.

6800. THF was used as solvent. The photoluminescence (PL) spectra were obtained using a HORIBA Jobin Yvon Spectrofluorometer Model Fluoromax-4 (S1/R1 was used for all the spectra). Thermogravimetric Analyses (TGA) were made on a Netzsch STA 409 PC Luxx[®] analyser under a N₂ atmosphere at a rate of 10 °C min⁻¹. Thin films were either deposited from Dichlorobenzene (DCB) solution on glass substrates by spin-coating (2000 rpm for 30 s) using a Ossila spin coater, or deposited by painting at room temperature. The film thicknesses were measured through Atomic Force Microscopy (AFM) measurements which were performed using a dimension 3000 microscope from Digital Instruments, and the results were presented at **Chapter III**. The glass substrates were treated in PSD Series-Digital UV Ozone System (Model # PSD-UVC) for 15 mins before film formation. Thin-layer chromatography (TLC) using aluminium-backed TLC plates coated with silica gel 60 F₂₅₄ from Merck KGaA was used to measure every reaction's progress.

2.1 Synthesis and chemical characterization of the monomers



Scheme 2-1 Synthetic pathways to BPM precursor **C1** and monomer **M1**

2,2'-bipyrimidine (C1)

A 100 mL dried round bottom flask was charged with PPh₃ (4.58 g, 17.5 mmol), NiCl₂ (0.57 g, 5.40 mmol) and Zn (0.57 g, 8.70 mmol), and dry DMF (20 mL) under argon. The mixture was vigorously stirred at room temperature for 1 h. 2-chloropyrimidine (2 g, 17.50 mmol) was then added under argon. The solution turned dark slowly. After 1 h, the temperature was increased to 80 °C for 70 h. Then the reaction mixture was cooled to room temperature and filtered through celite. The brown residue was washed with chloroform (CHCl₃) and DMF. After evaporation of the solvent *in vacuo*, an aqueous solution of EDTA-Na⁺ (7.27 g, 17.50 mmol) was added to the residue. After stirring for 3 h, the solution was washed with diethyl ether (3 x 50 mL) and CHCl₃ (8 x 50 mL). The part in diethyl ether was almost pure PPh₃ and the part in CHCl₃ was almost the pure product. CHCl₃ was removed by evaporation and recrystallized from a mixture of diethyl ether and hexane to yield the yellow solid product (1.42 g, 51% yield). This result is

consistent with previous reports.¹²⁴

¹H NMR (300 MHz, CDCl₃) δ 9.02 (d, J = 4.8 Hz, 4H), 7.44 (t, J = 4.8 Hz, 2H).

¹³C NMR (75 MHz, CDCl₃) δ 161.8, 157.6, 121.2.

To be noted, other methods were also tried to synthesize **C1** according to literature reports¹²⁴⁻¹²⁵, shown as following **Figure 2-1**, but unfortunately we didn't get the desired product from this synthetic approaches.

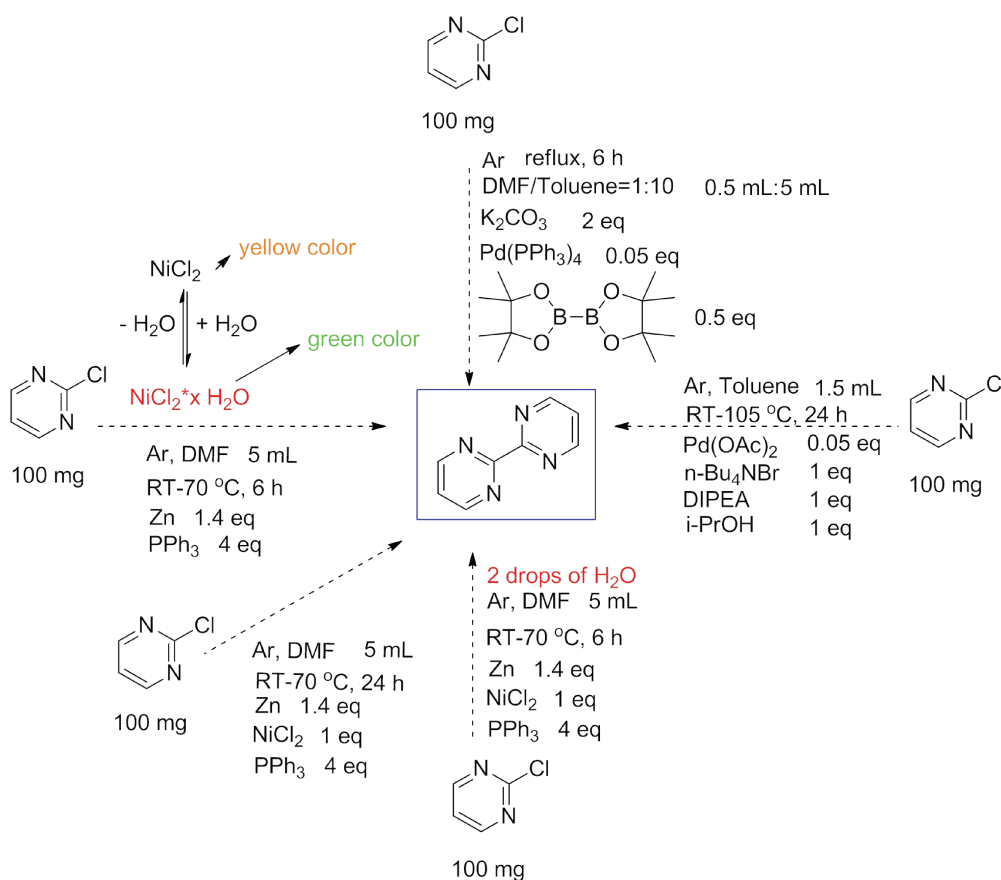


Figure 2-1 Unsuccessful synthetic approaches of **C1**

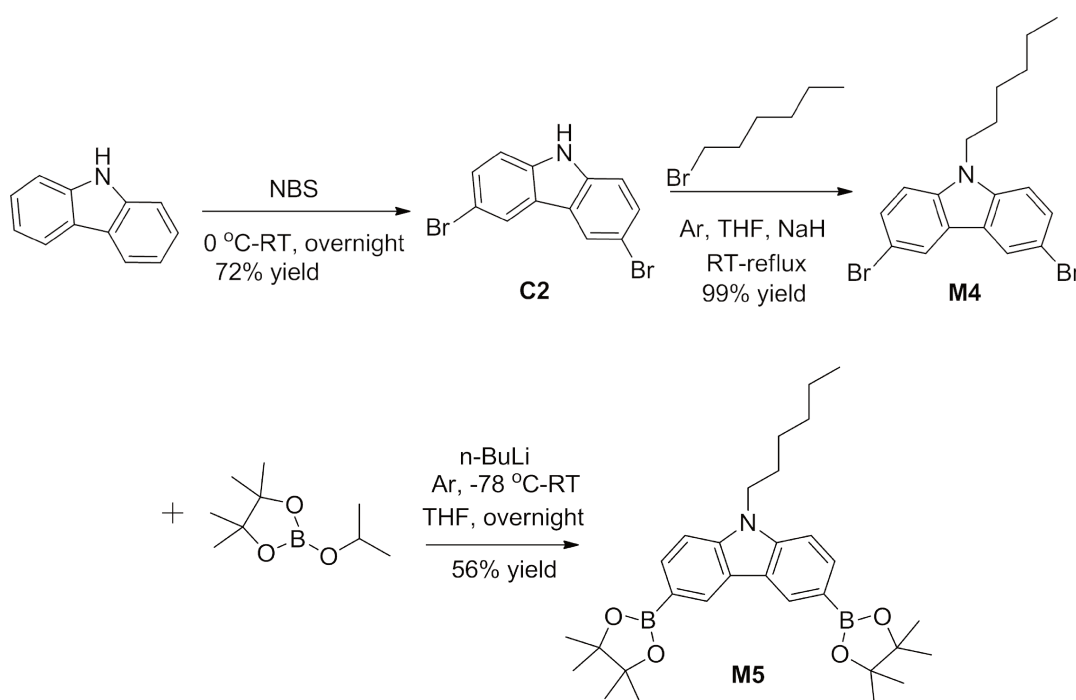
5,5'-dibromo-2,2'-bipyrimidine (**M1**)

- ¹²⁴ a. N. Plé et al. *J. Heterocycl. Chem.*, **2005**, 42, 1423-1428.
 b. T. Mukuta et al. *Inorg. Chem.* **2014**, 53, 2481-2490.
 c. S. Wang, et al. *Dalton Trans.*, **2004**, 2073-2079.
 d. M. J. Crossley et al. *Aust. J. Chem.*, **1994**, 47, 723-738.
 e. H. Hou et al. *J. APPL. POLYM. SCI.* **2014**, 131(24), 40828.
 f. Schwab, Peter F.H. et al. *J. Org. Chem.*, **2002**, 67(2), 443-449.
¹²⁵ a. *Synth. Commun.*, **1991**, 21(7), 901-906.
 b. *Biorg. Med. Chem.*, **2009**, 17: 6651-6658.

2,2'-bipyrimidine (0.55 g, 3.48 mmol) and bromine (1.43 mL, 27.82 mmol) were heated at 150 °C in a pressure tube for 72 h under argon. The mixture was cooled and the hard solid was powdered and treated with a solution of Na₂SO₃ to remove the unreacted bromine. The residue was washed with the minimum amount of THF, and then extracted with CHCl₃ and water. The organic part was concentrated under vacuum and the residue was recrystallized from a mixture of CHCl₃ and hexane to yield the product as a yellow solid (0.83 g, 76% yield). This result is consistent with that reported previously.¹²³

¹H NMR (300 MHz, CDCl₃) δ 9.05 (s, 4H).

¹³C NMR (75 MHz, CDCl₃) δ 159.7, 158.9, 121.9.



Scheme 2-2 Synthetic pathways to monomers **M4** and **M5**

3,6-dibromo-9H-carbazole (C2)

To a three-neck flask was added 9H-carbazole (10 g, 0.06 mol) and a stirring bar under argon. 20 mL of DMF was added to dissolve it. To a dropping funnel was added NBS (23.42 g, 0.13 mol) and DMF (30 mL), which were added dropwise to the reaction mixture over 2 h at 0 °C. The reaction mixture was stirred overnight at room temperature. The mixture was then poured slowly into a beaker containing ice, stirred for 1 h, filtered, and washed with water. After recrystallization from CHCl₃ and hexane, the product was obtained as a grey powder (14.00 g, 72% yield).

^1H NMR (300 MHz, CDCl_3) δ 8.13 (d, J = 1.5 Hz, 3H), 7.53 (d, J = 1.8 Hz, 1H), 7.50 (d, J = 1.8 Hz, 1H), 7.32 (s, 1H), 7.29 (s, 1H).

^{13}C NMR (75 MHz, CDCl_3) δ 138.4, 129.3, 124.1, 123.3, 112.6, 112.2.

This result is consistent with that reported previously.¹²⁶

3,6-dibromo-9-hexyl-9H-carbazole (M4)

To a dried flask was added 3,6-dibromo-9H-carbazole (2.00 g, 6.15 mmol) and 20 mL of anhydrous THF under argon. Sodium hydride (0.49 g, 12.30 mmol) was added into the flask at 0 °C and stirred for 30 min. 1-bromohexane (1.74 mL, 18.50 mmol) was added dropwise and the mixture was refluxed for 12 h. The reactant was cooled to room temperature and water was added. After extraction with ethyl acetate for three times, the organic part was dried under vacuum. The residue was purified by column chromatography (ethyl acetate:hexane = 1:5) to yield a white crystalline product (2.56 g, 99% yield).

^1H NMR (300 MHz, CDCl_3) δ 8.14 (s, 2H), 7.54 (d, J = 8.7 Hz, 2H), 7.26 (d, J = 8.7 Hz, 2H), 4.23 (t, J = 7.2 Hz, 2H), 1.82 (t, J = 6.9 Hz, 2H), 1.30-1.20 (m, 6H), 0.85 (t, J = 6.0 Hz, 3H).

^{13}C NMR (75 MHz, CDCl_3) δ 139.3, 129.0, 123.4, 123.3, 111.9, 110.4, 43.4, 31.5, 28.8, 26.9, 22.5, 14.0.

This result is consistent with that reported previously.^{125,127}

9-hexyl-3,6-bis(4,4,5,5-tetramethyl-1,3,2-dioxaborolan-2-yl)-9H-carbazole (M5)

To a solution of 3,6-dibromo-9-hexyl-9H-carbazole (1.00 g, 2.44 mmol) in THF (30 mL) in a dried flask at -78 °C was added n-BuLi (4.10 mL, 10.25 mmol) dropwise under argon. After stirring for 1 h, 2-isopropoxy-4,4,5,5-tetramethyl-1,3,2-dioxaborolane (2.10 mL, 10.25 mmol) was rapidly added to the solution and the mixture was stirred at -78 °C for another 1 h. Then the reactant medium was warmed to room temperature and stirred overnight. The mixture was poured into water and extracted with diethyl ether. The organic layer was dried over anhydrous MgSO_4 and concentrated under vacuum. The residue was purified by column chromatography (ethyl acetate:hexane = 1:5) and recrystallized from MeOH and acetone (10:1). The product was

¹²⁶ a. M. Majchrzak, M. Grzelak, B. Marciniak. *Org. Biomol. Chem.*, **2016**, *14*, 9406.

b. J. S. Park, S.-H. Jin, Y.-S. Gal, J. H. Lee & J. W. Lee. *Molecular Crystals and Liquid Crystals*, **2012**, *567*:1, 102-109.

c. N. Berton, F. Chandezon, S. Sadki, et al. *J. Phys. Chem. B.*, **2009**, *113*, 14087-14093.

¹²⁷ a. W. Huang, L. Su, and Z. Bo. *J. AM. CHEM. SOC.*, **2009**, *131*, 10348-10349.

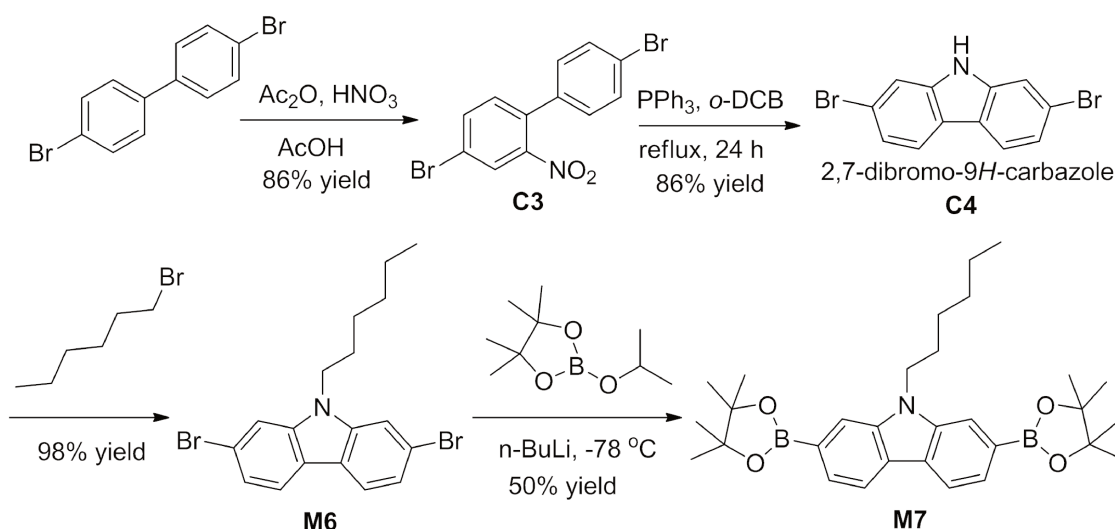
b. S. A. KIM, D. K. LEE, J. H. KIM, et al. *Mol. Cryst. Liq. Cryst.*, **2011**, *551*:, 283-294.

obtained as a white solid (0.69 g, 56% yield).

^1H NMR (300 MHz, CDCl_3) δ 8.70(s, 2H), 7.92(d, $J=8.1$ Hz, 2H), 7.40 (dd, $J=1.5$ Hz, 8.1 Hz, 2H), 4.30 (t, $J=6.3$ Hz, 2H), 1.90-1.80 (m, 2H), 1.50-1.30 (m, 30H), 0.86 (t, $J=1.5$ Hz, 3H).

^{13}C NMR (75 MHz, CDCl_3) δ 142.7, 132.1, 128.1, 122.9, 108.2, 83.6, 77.6, 77.2, 76.8, 43.1, 31.6, 28.9, 26.9, 25.0, 24.9, 22.6, 14.1.

This result is consistent with that reported previously.^{125,128}



Scheme 2-3 Synthetic pathways to monomers **M6** and **M7**

4,4'-dibromo-2-nitro-1,1'-biphenyl (**C3**)

To a 250 mL round-bottom flask charged with 4,4'-dibromo-1,1'-biphenyl (5.00 g, 0.016 mol) and cooled with a water bath, a mixture of HOAc (40 mL) and fuming HNO_3 (24 mL, 0.128 mol) was added dropwise. After completion of the reaction (as followed by TLC), water (100 mL) was added and stirred for 10 min. Then the mixture was extracted with CHCl_3 for three times, and the organic solvent was removed under vacuum. The product was collected as a yellow solid (4.92 g, 86% yield).

^1H NMR (300 MHz, CDCl_3) δ 8.03 (s, 1H), 7.75 (d, $J=8.4$ Hz, 1H), 7.56 (d, $J=7.2$ Hz, 2H), 7.29 (d, $J=8.1$ Hz, 1H), 7.15 (d, $J=8.4$ Hz, 2H).

¹²⁸ a. Y. Bao, Q. Li, R. Bai, et al. *Chem. Commun.*, **2012**, 48, 118–120.

b. N. Blouin, A. Michaud, and M. Leclerc. *Adv. Mater.*, **2007**, 19, 2295–2300.

c. Idzik KR1, Cywinski PJ, Cranfield CG, Mohr GJ, Beckert R. *J. Fluoresc.*, **2011**, 21:1195–1204.

This result is consistent with that reported previously.¹²⁹

2,7-dibromo-9H-carbazole (C4)

To a dried flask was added 4,4'-dibromo-2-nitro-1,1'-biphenyl (1.00 g, 0.003 mol) and *o*-DCB (10 mL) under argon. Triphenylphosphine (1.837 g, 0.075 mol) was added and the mixture was refluxed for 20 h. After cooling to room temperature, the solvent was removed under low pressure and the residue was purified by silica gel chromatography (ethyl acetate:hexane = 1:10). The product was collected as a white solid (0.782 g, 86% yield).

¹H NMR (300 MHz, CDCl₃) δ 8.07 (br, 1H), 7.88 (d, J = 8.4 Hz, 2H), 7.58 (s, 2H), 7.35 (d, J = 8.4 Hz, 2H).

¹³C NMR (75 MHz, CDCl₃) δ 140.3, 123.3, 121.8, 121.5, 119.7, 113.8.

This result is consistent with that reported previously.¹²⁸

2,7-dibromo-9-hexyl-9H-carbazole (M6)

To a dried flask was added 2,7-dibromo-9H-carbazole (0.86 g, 2.646 mmol) and 15 mL of anhydrous THF under argon. Sodium hydride (0.21 g, 5.29 mmol) was added into the flask at 0 °C and the reactant medium was stirred for 30 min. 1-bromohexane (1.11 mL, 7.94 mmol) was added dropwise and the mixture was refluxed for 12 h. The reactant was cooled to room temperature and water was added. After extraction with ethyl acetate for three times, the organic part was dried under vacuum. The residue was purified by column chromatography (ethyl acetate:hexane = 1:5) to yield a white crystalline product (1.06 g, 98% yield).

¹H NMR (300 MHz, CDCl₃) δ 7.78 (d, J = 8.4 Hz, 2H), 7.48 (d, J = 0.9 Hz, 2H), 7.31 (dd, J = 8.1 Hz, 1.2 Hz, 2H), 4.04 (t, J = 7.5 Hz, 2H), 1.77 (t, J = 6.9 Hz, 2H), 1.40-1.20 (m, 6H), 1.00-0.80 (m, 3H).

¹³C NMR (75 MHz, CDCl₃) δ 141.2, 122.5, 121.4, 121.2, 119.7, 111.9, 43.3, 31.6, 28.8, 26.9, 22.7, 14.1.

This result is consistent with that reported previously.¹²⁶⁻¹²⁷

¹²⁹ a. K.-M. Chang, National Sun Yat-sen University, Synthesis and Photoelectric Properties fo Low Bandgap Thiophene Copolymers, *Master Thesis Dissertation*, June **2012**.

b. A. W. Freeman, M. Urvoy, and M. E. Criswell, *J. Org. Chem.*, **2005**, *70* (13), 5014-5019.

c. S. Beaupre and M. Leclerc, *J. Mater. Chem. A.*, **2013**, *1*, 11097-1110.

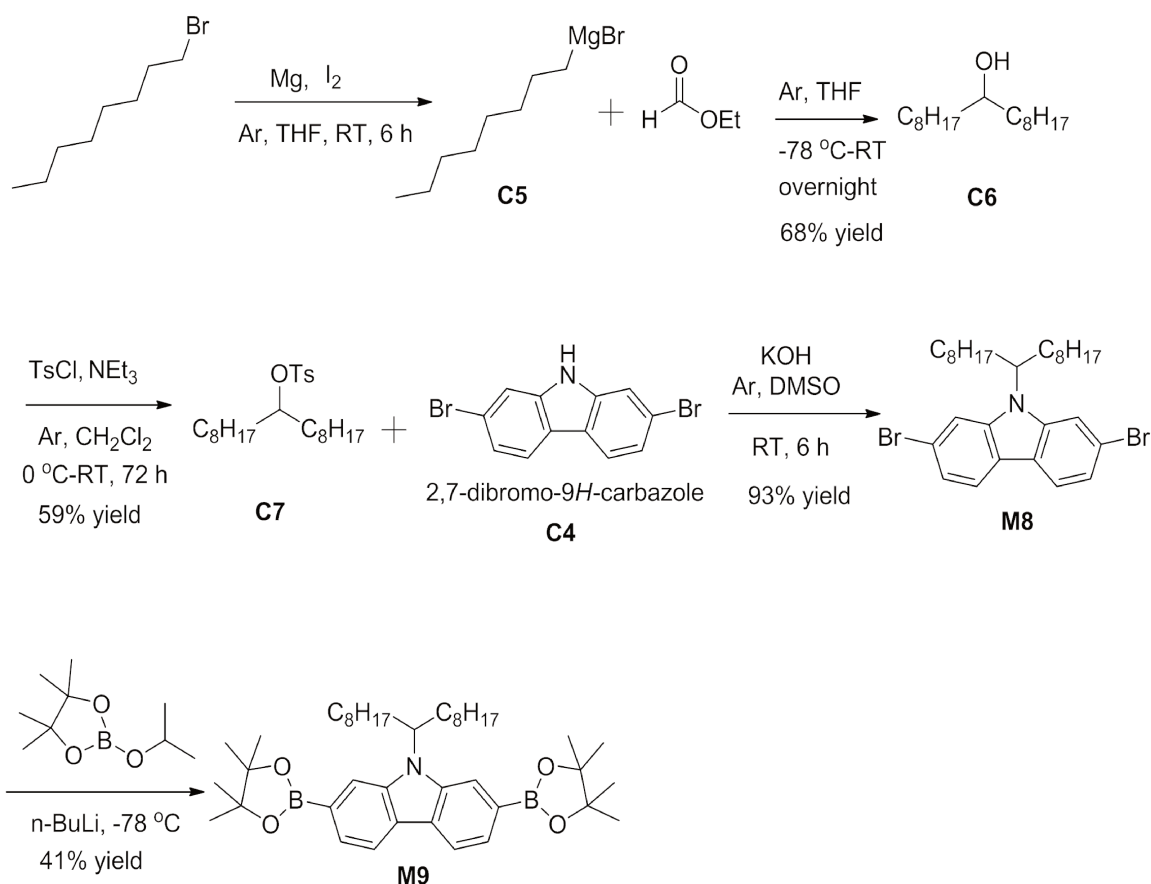
9-hexyl-2,7-bis(4,4,5,5-tetramethyl-1,3,2-dioxaborolan-2-yl)-9H-carbazole (M7)

To a solution of 2,7-dibromo-9-hexyl-9H-carbazole (1.00 g, 2.44 mmol) in THF (30 mL) in a dried flask cooled to -78 °C was added n-BuLi (4.2 eq, 4.1 mL) dropwise under argon. After stirring for 1 h at -78 °C, 2-isopropoxy-4,4,5,5-tetramethyl-1,3,2-dioxaborolane (2.1 mL, 10.25 mmol) was rapidly added to the solution and the mixture was stirred at -78 °C for another 1 h. Then the reactant medium was warmed to room temperature and stirred overnight. The mixture was poured into water and extracted with diethyl ether for three times. The organic layer was dried over anhydrous MgSO₄ and concentrated under vacuum. The residue was purified by column chromatography (ethyl acetate:hexane = 1:5) and recrystallized from MeOH and acetone (10:1). The product was obtained as a white solid (0.62 g, 50% yield)

¹H NMR (300 MHz, CDCl₃) δ 8.13 (d, J = 7.8 Hz, 2H), 7.89 (s, 2H), 7.68 (d, J = 7.8 Hz, 2H), 4.38 (t, J = 7.2 Hz, 2H), 1.88 (t, J = 7.2 Hz, 2H), 1.40 (s, 30H), 0.88 (t, J = 6.9 Hz, 3H).

¹³C NMR (75 MHz, CDCl₃) δ 140.4, 125.1, 124.8, 120.0, 115.3, 83.8, 42.8, 31.6, 29.2, 26.8, 24.9, 22.6, 14.1.

This result is consistent with that reported previously.¹²⁷



Scheme 2-4 Synthetic pathways to monomers **M8** and **M9*****Heptadecan-9-ol (C6)***

A solution of a mixture of 1-bromooctane (7.41 g, 0.1 mol) and dry THF (100 mL) in a dropping funnel was added slowly to a 250 mL dried round bottom flask charged with magnesium (7.20 g, 0.3 mol) and 1 chip of iodine under argon with strong stirring. After stirring for 6 h, the reactant medium was cooled to -78 °C, and a solution of ethyl formate (52.19 mL, 0.3 mol) in 167 mL of THF was added dropwise. The reaction mixture was allowed to stir overnight at room temperature and then quenched by adding MeOH and a saturated aqueous NH₄Cl solution. This mixture was extracted with diethyl ether for three times, and then washed with a saturated aqueous NaCl solution. The organic fractions were dried over MgSO₄. The crude product was further purified by silica gel chromatography (ethyl acetate:hexane = 1:10 and then 1:5 and then 2:1) to obtain 17.37 g of pure product as a white solid (68 % yield).

¹H NMR (300 MHz, CDCl₃) δ 3.58 (s, 1H), 1.42 (s, 4H), 1.35-1.20 (m, 24H), 0.87 (t, J = 6.3 Hz, 6H).

¹³C NMR (75 MHz, CDCl₃) δ 72.0, 37.5, 31.9, 29.7, 29.6, 29.3, 25.7, 22.7, 14.1.

This result is consistent with that reported previously.¹³⁰

Heptadecan-9-yl 4-methylbenzenesulfonate (C7)

To a 100 mL dried round bottom flask charged with Heptadecan-9-ol (8 g, 0.031 mol), Trimethylamine hydrochloride (2.98 g, 0.031 mol) and dry DCM (40 mL) at 0 °C was added Et₃N (13.01 mL, 0.093 mol) under argon. A solution of *p*-Toluenesulfonyl chloride (7.136 g, 0.037 mol) in DCM (20 mL) was added to the system. The mixture was slowly warmed to room temperature and stirred overnight. Water was added and the mixture was extracted three times with CHCl₃, washed with water and brine, dried over Na₂SO₄, and concentrated under reduced pressure. The crude product was purified by silica-gel column chromatography (ethyl acetate:hexane = 1:10 as eluent) to give 14.11 g of a colorless oil (98% yield).

¹H NMR (300 MHz, CDCl₃) δ 7.78 (d, J = 8.1 Hz, 2H), 7.30 (d, J = 8.1 Hz, 2H), 4.52 (t, J = 6.0 Hz, 1H), 2.42 (s, 3H), 1.55-45 (m, 4H), 1.40-1.10 (m, 24H), 0.86 (t, J = 6.6 Hz, 6H).

¹³⁰ A. Saeki, S. Yoshikawa, M. Tsuji, et al. *J. Am. Chem. Soc.*, **2012**, *134*, 19035–19042.

^{13}C NMR (75 MHz, CDCl_3) δ 144.3, 134.8, 129.6, 127.7, 84.7, 34.1, 31.8, 29.4, 29.3, 29.2, 24.7, 22.7, 21.6, 14.1.

This result is consistent with that reported previously.^{128,129}

2,7-dibromo-9-(heptadecan-9-yl)-9H-carbazole (M8)

To a 100 mL dried round bottom flask charged with 2,7-dibromo-9H-carbazole (2.00 g, 6.154 mol) and DMSO (15 mL), was added KOH (1.727 g, 30.77 mol) and the mixture was stirred for 30 min. A solution of Heptadecan-9-yl 4-methylbenzenesulfonate (3.791 g, 9.23 mol) in DMSO (5 mL) was added dropwise at room temperature. After stirring for 6 h, the mixture was poured into distilled water. The aqueous layer was extracted with Hexanes. The organic layer was dried and concentrated under vacuum. The crude product was purified by silica-gel column chromatography (Hexanes as eluent) to give 3.219 g of a colorless oil (93% yield).

^1H NMR (300 MHz, CDCl_3) δ 7.90 (t, $J = 8.4$ Hz, 2H), 7.71 (s, 1H), 7.55 (s, 1H), 7.34 (d, $J = 5.7$ Hz, 2H), 4.46-4.38 (m, 1H), 2.30-2.10 (m 2H), 2.05-1.80 (m, 2H), 1.26-1.10 (m, 22H), 0.90-0.81 (m, 6H).

^{13}C NMR (75 MHz, CDCl_3) δ 143.0, 139.6, 130.5, 122.5, 121.6, 121.4, 121.0, 119.9, 119.3, 114.7, 112.3, 57.1, 33.6, 32.8, 32.1, 31.9, 29.9, 29.8, 29.4, 29.3, 26.9, 22.84, 22.75, 14.3, 14.2.

This result is consistent with that reported previously.^{127,128,129,131}

9-(heptadecan-9-yl)-2,7-bis(4,4,5,5-tetramethyl-1,3,2-dioxaborolan-2-yl)-9H-carbazole (M9)

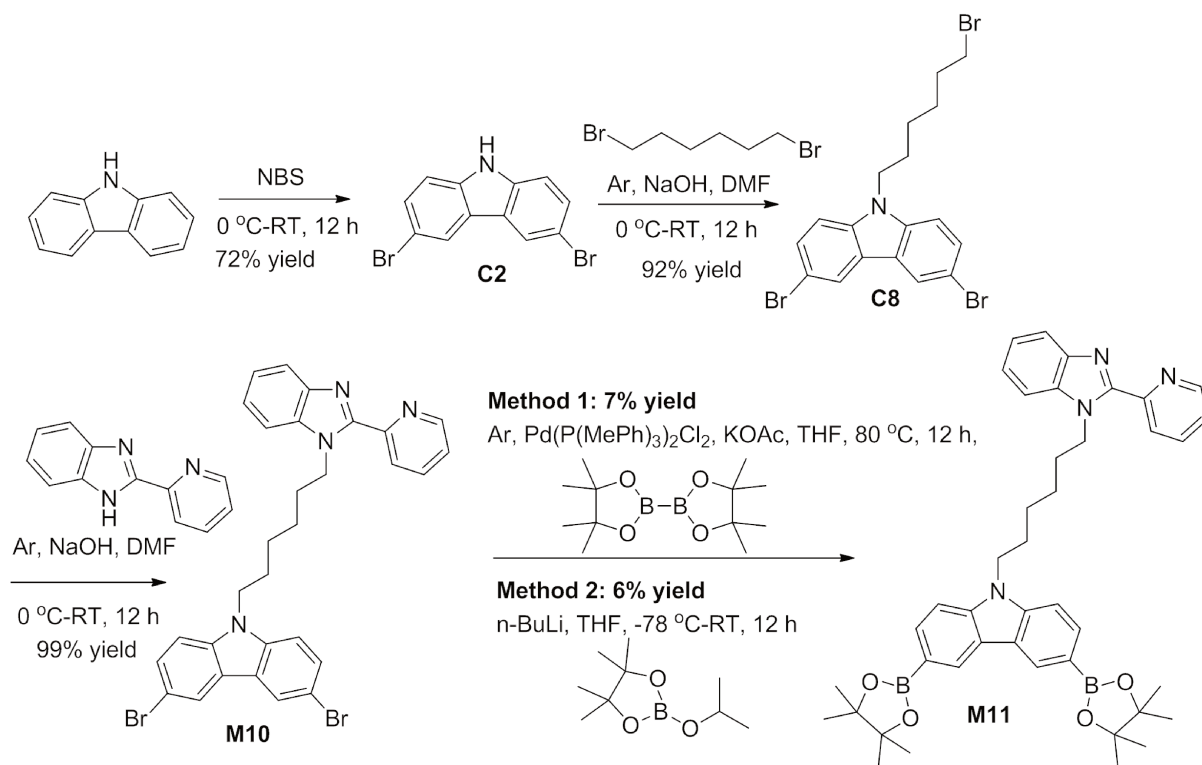
To a solution of 2,7-dibromo-9-(heptadecan-9-yl)-9H-carbazole (1.609 g, 2.86 mmol) in THF (45 mL) in a dried flask at -78°C was added n-BuLi (4.80 mL, 12.01 mmol) dropwise under argon system. After stirring for 1 h in this temperature, 2-isopropoxy-4,4,5,5-tetramethyl-1,3,2-dioxaborolane (2.45 mL, 12.01 mmol) was added rapidly to the solution and the mixture was stirred at -78°C for another 1 h. Then the reactant medium was warmed to room temperature and stirred overnight. The mixture was poured into water and extracted with diethyl ether for three times. The organic layer was dried over anhydrous MgSO_4 and concentrated under vacuum. The residue was purified by column chromatography (ethyl acetate:hexane = 1:5) and recrystallized from MeOH/acetone (10:1). The product was obtained as a white solid (0.778 g, 41% yield).

¹³¹ B. Kim, J. Y. Kim, C. Yang, et al. *Macromolecules*. **2012**, 45, 8658–8664.

^1H NMR (300 MHz, CDCl_3) δ 8.11 (br, 2H), 8.02 (br, 1H), 7.88 (br, 1H), 7.66 (d, $J = 7.2$ Hz, 2H), 4.69 (br, 1H), 2.33 (br, 2H), 1.94 (br, 2H), 1.39 (br, 24H), 1.12 (br, 24H), 0.82 (br, 6H).

^{13}C NMR (75 MHz, CDCl_3) δ 142.0, 138.7, 126.0, 124.6, 120.0, 119.7, 118.1, 115.4, 83.7, 56.4, 33.8, 31.8, 29.5, 29.3, 29.2, 26.8, 24.9, 22.6, 14.0.

This result is consistent with that reported previously.^{127,128,129,132}



Scheme 2-5 Synthetic pathways to monomers **M10** and **M11**

3,6-dibromo-9-(6-bromohexyl)-9H-carbazole (**C8**)

To a dried flask was added 3,6-dibromo-9H-carbazole (5.00 g, 0.015 mol) and 20 mL of anhydrous DMF under argon. Sodium hydroxide (0.7385 g, 0.018 mmol) was added into the flask at 0 °C and the reactant medium was stirred for 30 min. 1,6-dibromohexane (7.10 mL, 0.045 mol) was added dropwise and the mixture was stirred at room temperature for 12 h. Water was added to quench the reaction. After extraction with ethyl acetate for three times, the organic part was dried under vacuum. The residue was purified by column chromatography (ethyl acetate:hexane = 1:10) to yield a white solid product (6.883 g, 92% yield).

¹³² Z.-G. Zhang, Y.-L. Liu, Y. Li, et al. *Macromolecules.*, **2010**, 43, 9376–9383.

^1H NMR (300 MHz, CDCl_3) δ 8.14 (d, J = 2.1 Hz, 2H), 7.56-7.53 (m, 2H), 7.28-7.25 (m, 2H), 4.25 (t, J = 7.2 Hz, 2H), 3.36 (t, J = 6.6 Hz, 2H), 1.85-1.79 (m, 6H), 1.48-1.28 (m, 3H).

^{13}C NMR (75 MHz, CDCl_3) δ 139.3, 129.1, 123.5, 123.3, 112.0, 110.4, 43.1, 33.7, 32.5, 28.7, 27.8, 26.4.

This result is consistent with that reported previously.¹³³

3,6-dibromo-9-(6-(2-(pyridin-2-yl)-1H-benzo[d]imidazol-1-yl)hexyl)-9H-carbazole (M10)

To a dried bottle was added 2-(pyridin-2-yl)-1H-benzo[d]imidazole (0.80 g, 4.10 mmol) and 10 mL of DMF under argon. Sodium hydroxide (0.246 g, 6.15 mmol) was added into the flask at 0 °C and the reactant medium was stirred for 30 min. 3,6-dibromo-9-(5-bromopentyl)-9H-carbazole (2 g, 4.098 mmol) was added and the mixture was stirred at room temperature for 12 h. The reactant medium was poured into ice-cold water and stirred for 1 h. The solid was filtered, dried under vacuum, and recrystallized from THF:Hexane (1:10) to yield a white solid (2.444 g, 99% yield).

^1H NMR (300 MHz, CDCl_3) δ 8.50(d, J = 4.2 Hz, 1H), 8.38(d, J = 7.8 Hz, 1H), 8.13(d, J = 2.1 Hz, 2H), 7.80-7.84(m, 2H), 7.51(dd, J = 1.8 Hz, 8.7 Hz, 2H), 7.35-7.25 (m, 4H), 7.20(s, 1H), 7.17(s, 1H), 4.77 (t, J = 7.2 Hz, 2H), 4.18 (t, J = 7.2 Hz, 2H), 1.86-1.74 (m, 8H).

^{13}C NMR (75 MHz, CDCl_3) δ 150.6, 149.8, 148.5, 142.6, 139.2, 136.8, 136.6, 129.1, 124.7, 123.7, 123.4, 123.3, 122.6, 120.2, 112.0, 110.3, 110.1, 45.2, 43.1, 29.9, 28.7, 26.8, 26.6.

This result is consistent with that reported previously.¹³²

9-(6-(2-(pyridin-2-yl)-1H-benzo[d]imidazol-1-yl)hexyl)-3,6-bis(4,4,5,5-tetramethyl-1,3,2-dioxaborolan-2-yl)-9H-carbazole (M11)

Method 1: To a dried bottle was added 3,6-dibromo-9-(6-(2-(pyridin-2-yl)-1H-benzo[d]imidazol-1-yl)hexyl)-9H-carbazole (200 mg, 0.33 mmol), 4,4,4',4',5,5,5',5'-octamethyl-2,2'-bi(1,3,2-dioxaborolane) (202.4 mg, 0.80 mmol) and anhydrous KOAc (195.52 mg, 1.98 mmol) under argon. 5 mL of THF was added. Dichlorobis(tri-*o*-tolylphosphine)palladium(II) (7.83 mg, 0.01 mmol) was added into the flask. The mixture was stirred at 80 °C for 12 h. The reactant medium was cooled to room temperature and the solvent was removed under reduced

¹³³ B. Du, W. Yang, J. Peng, et al. *polymer*, **2007**, 48, 1245-125.

pressure. The residue was extracted with DCM. The combined organic layer was dried over anhydrous MgSO_4 , filtered and concentrated under vacuum. The residue was further purified by column chromatography (DCM:Hexane = 1:1) to yield a white solid (15 mg, 7% yield).

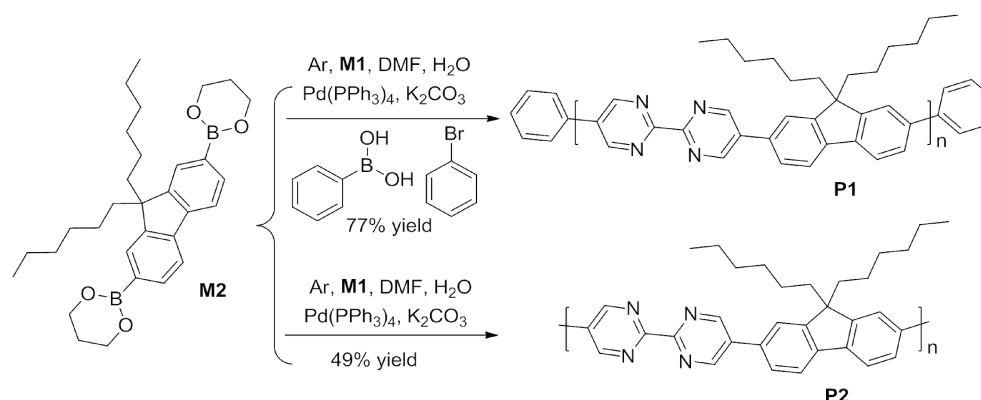
Method 2: **M11** was prepared in 6% yield by a method similar to that used for **M5**.

^1H NMR (300 MHz, CDCl_3) δ 8.60 (s, 1H), 8.13 (d, J = 6.6 Hz, 1H), 7.92 (d, J = 6.6 Hz, 2H), 7.41-7.06 (m, 10H), 6.71 (s, 1H), 4.40-4.30 (m, 2H), 3.40-3.30 (m, 2H), 2.40-2.30 (m, 2H), 2.00-1.80 (m, 2H), 1.55-1.33 (m, 28H).

2.2 Synthesis and chemical characterization of the polymers

General procedure for polymers synthesis. The polymers were obtained from Suzuki-Miyaura coupling reactions following a revised procedure previously reported.¹²⁰

2.2.1 P1 and P2



Scheme 2-6 Synthetic pathways to BPM precursors and polymers **P1** and **P2**

Poly(2,2'-bipyriridine-alt-2,7-(9,9-dihexyl-9H-fluorene)) with endcapping (P1)

5,5'-dibromo-2,2'-bipyriridine (100 mg, 0.317 mmol) and 2,2'-(9,9-dioctyl-9H-fluorene-2,7-diyl)bis(1,3,2-dioxaborinane) (159.0 mg, 0.317 mmol) were added to a 25 mL dried three-neck round bottom flask. 10 mL of DMF were added to fully dissolve the solid and then K_2CO_3 (131.23 mg, 0.950 mmol) was added. 5 min later, water (2 mL) was added and the reactant medium was degassed for 30 min. $\text{Pd}(\text{PPh}_3)_4$ (18.29 mg, 0.0158 mmol) was added. The reaction medium was heated at 140 °C for 72 h. Bromobenzene (19.88 mg, 0.127 mmol) was then added. The reaction was heated at 140 °C for 12 h. Phenylboronic acid (15.44 mg, 0.1266 mmol) was

added and the reaction mixture was again heated at 140 °C for 12 h. The mixture was cooled and MeOH was added dropwise. After a few days at 4 °C, the methanol solution was filtered and the residue was dissolved in CHCl₃. MeOH was again added dropwise, and after a few days at 4 °C, the methanol solution was filtered. The residue was further purified by Soxhlet extraction with acetone for 2 days. A yellow product (120 mg, 77% yield) was collected.

¹H NMR (300 MHz, CDCl₃) δ 9.33 (s, 4H), 7.97 (d, J = 8.4 Hz, 2H), 7.69-7.75 (m, 4H), 1.11 (br, 13H), 0.78 (br, 13H).

¹³C NMR (75 MHz, CDCl₃) δ 160.8, 156.0, 152.7, 141.4, 134.4, 133.3, 126.5, 121.5, 121.3, 55.9, 40.1, 31.4, 29.5, 23.9, 22.5, 14.0.

Not enough soluble for GPC measurement.

The amount of the carbazole unit and bipyrimidine unit in the polymer chain was calculated to be 50% respectively according to the ¹H NMR spectrum.

Poly(2,2'-bipyrimidine-alt-2,7-(9,9-dihexyl-9H-fluorene)) without endcapping (P2)

P2 was prepared by a method similar to that for **P1** with 49% yield, but without the steps of adding Bromobenzene and Phenylboronic acid for endcapping.

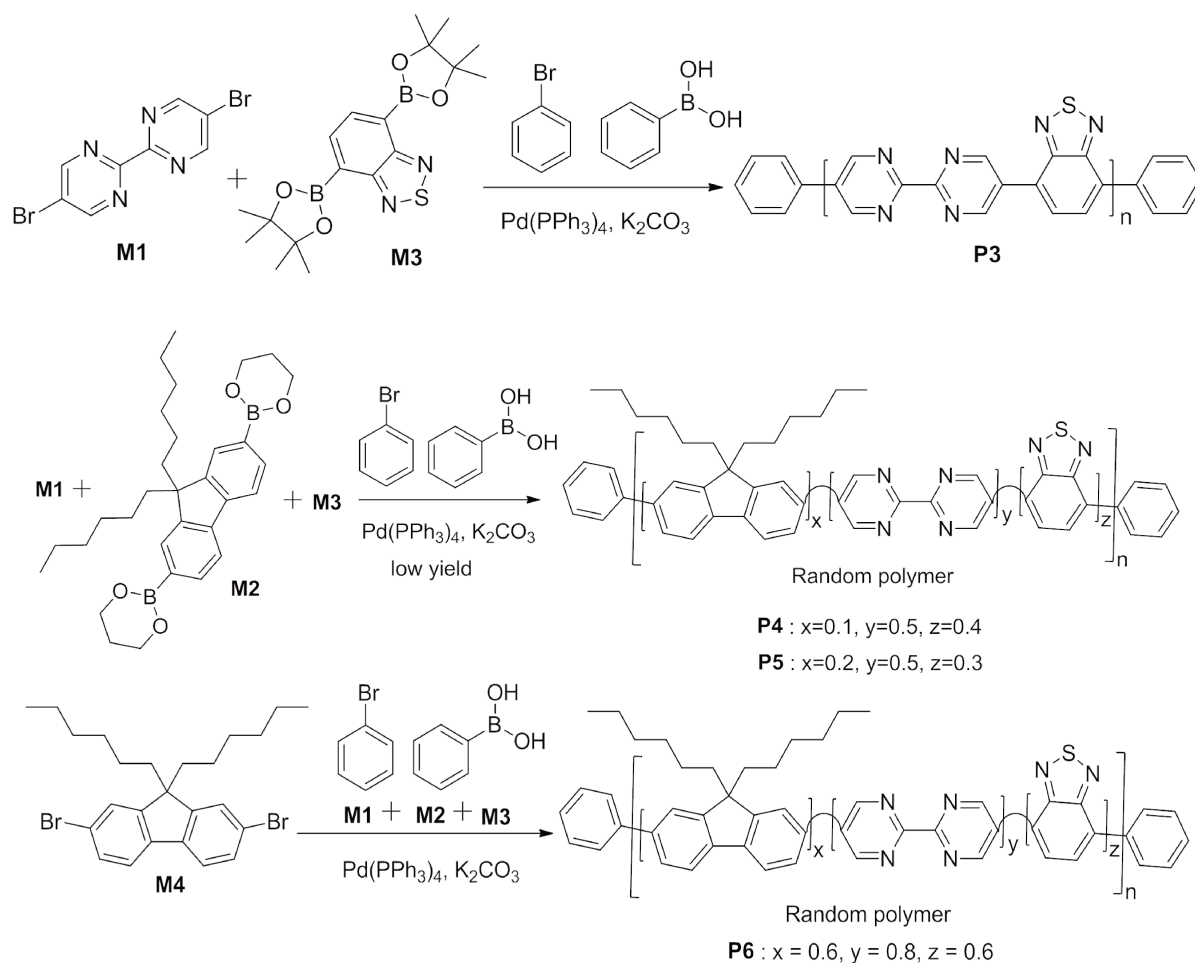
¹H NMR (300 MHz, CDCl₃) δ 9.33 (br, 4H), 7.96 (d, J = 7.2 Hz, 2H), 7.69-7.75 (m, 4H), 7.38 (s, 1H), 1.11 (br, 13H), 0.77 (br, 13H).

¹³C NMR (75 MHz, CDCl₃) δ 160.7, 156.0, 152.7, 141.4, 134.5, 133.2, 126.5, 126.1, 121.5, 121.3, 120.7, 55.9, 55.4, 40.1, 31.4, 29.5, 23.9, 22.5, 14.0.

Not enough soluble for GPC measurement.

The molar ratio of the two monomers in the polymer chain is calculated to be 50 % each as well from the ¹H NMR spectrum.

2.2.2 P3, P4, P5 and P6

Scheme 2-7 Synthetic pathways to polymers **P3**, **P4**, **P5** and **P6*****Poly(2,2'-bipyrimidine-alt-benzo[c][1,2,5]thiadiazole) (P3)***

Following the general procedure for polymers synthesis depicted for **P1**, 5,5'-dibromo-2,2'-bipyrimidine (100 mg, 0.317 mmol) and 4,7-bis(4,4,5,5-tetramethyl-1,3,2-dioxaborolan-2-yl)benzo[c][1,2,5]thiadiazole (122.83 mg, 0.317 mmol) were added to a 25 mL dried three-neck round bottom flask. 10 mL of DMF were added to dissolve the solid and then K_2CO_3 (131.23 mg, 0.950 mmol) was added. 5 min later, water (2 mL) was added and the system was degassed for 30 min. $\text{Pd(PPh}_3)_4$ (18.29 mg, 0.0158 mmol) was added and the reactant medium was further degassed for 15 min. The reaction medium was heated at 140 °C for 72 h. Bromobenzene (19.88 mg, 0.127 mmol) was then added. The reaction was heated at 140 °C for 12 h. Phenylboronic acid (15.44 mg, 0.127 mmol) was added and the reaction mixture was again heated at 140 °C for 12 h. The mixture was cooled and MeOH was added dropwise. After a few days at 4 °C, the methanol solution was filtered and the residue was dissolved in CHCl_3 . To be noted, most of the solid could not dissolve in CHCl_3 and other common solvents such as THF,

MeOH, Ethyl acetate, dichloromethane and H₂O. The CHCl₃ solution was concentrated in vacuum, and a very few amount of solid was isolated, and redissolved in the minimum amount of CHCl₃. MeOH was added dropwise to make the product precipitate. After a few days at 4 °C, the methanol solution was again filtered. Collected the solid part and further purified the product by Soxhlet extraction with acetone. Few product (<10 mg) was collected and even is not enough for more analysis.¹²²

Poly(2,7-(9,9-dihexyl-9H-fluorene)-co-(2,2'-bipyrimidine)-co-(benzo[c][1,2,5]thiadiazole)) in ratio 0.1:0.5:0.4 (**P4**)

Following the general procedure for polymers synthesis depicted for **P1**, 5,5'-dibromo-2,2'-bipyrimidine (100 mg, 0.317 mmol), 2,2'-(9,9-dioctyl-9H-fluorene-2,7-diyl)bis(1,3,2-dioxaborinane) (31.80 mg, 0.063 mmol), 4,7-bis(4,4,5,5-tetramethyl-1,3,2-dioxaborolan-2-yl)benzo[c][1,2,5]thiadiazole (98.27 mg, 0.253 mmol) were added to a 25 mL dried three-neck round bottom flask. 10 mL of DMF were added to dissolve the solid and then K₂CO₃ (131.23 mg, 0.950 mmol) was added. 5 min later, water (2 mL) was added and the system was degassed for 30 min. Pd(PPh₃)₄ (18.29 mg, 0.0158 mmol) was added and the reactant medium was degassed an additional 15 min. The reaction was heated at 140 °C for 72 h. Bromobenzene (19.88 mg, 0.127 mmol) was then added. The reaction was heated at 140 °C for 12 h. Phenylboronic acid (15.44 mg, 0.127 mmol) was added and the reaction mixture was again heated at 140 °C for 12 h. The mixture was cooled and MeOH was added dropwise. After a few days at 4 °C, the methanol solution was filtered and the residue was dissolved in CHCl₃. As for **P3**, most of the solid could not dissolved in CHCl₃ and other common solvents, including THF, MeOH, EA, DCM and H₂O. After filtration, the solvent was evaporated under vacuum, less than 10 mg of a solid were obtained. The minimum amount of CHCl₃ to dissolve the residue was added. MeOH was added again to the chloroform solution and the flask was stored at 4 °C for a few days, after which the solution was filtered. The solid was further purified by Soxhlet extraction with acetone for 2 days. Less than 10 mg of a brown solid were obtained.¹²⁰

¹H NMR (300 MHz, CDCl₃) δ 9.71 (d, *J* = 11.4 Hz, 4H), 9.31 (d, *J* = 6.3 Hz, 1H), 9.09 (d, *J* = 4.8 Hz, 1H), 7.50-8.18 (m, 8H), 1.59 (s, 27H), 1.07-1.11 (m, 5H), 0.74-0.84 (m, 6H).

Not enough soluble for GPC measurement.

Poly(2,7-(9,9-dihexyl-9H-fluorene)-co-(2,2'-bipyrimidine)-co-(benzo[c][1,2,5]thiadiazole) in ratio 0.2:0.5:0.3 (**P5**)

Following the general procedure for polymers synthesis depicted for **P1**, the synthesis of **P5** was run from 5,5'-dibromo-2,2'-bipyrimidine (100 mg, 0.317 mmol), 2,2'-(9,9-dioctyl-9H-fluorene-2,7-diyl)bis(1,3,2-dioxaborinane) (63.59 mg, 0.127 mmol), 4,7-bis(4,4,5,5-tetramethyl-1,3,2-dioxaborolan-2-yl)benzo[c][1,2,5]thiadiazole (73.70 mg, 0.190 mmol) in DMF. A yellow product (10 mg, 8% yield) was collected after purification (precipitation and Soxhlet extraction).¹²⁰

¹H NMR (300 MHz, CDCl₃) δ 9.70 (d, J = 10.5 Hz, 2H), 9.32 (s, 2H), 7.68-8.02 (m, 5H), 1.42-1.84 (m, 2H), 1.11-1.40 (m, 13H), 0.77 (s, 7H).

¹³C NMR (75 MHz, CDCl₃) δ 157.7, 156.0, 152.7, 126.5, 121.5, 55.9, 40.1, 31.4, 29.7, 23.9, 22.5, 14.0.

Not enough soluble for GPC measurement.

Poly(2,7-(9,9-dihexyl-9H-fluorene)-co-(2,2'-bipyrimidine)-co-(benzo[c][1,2,5]thiadiazole) in ratio 0.6:0.8:0.6 (**P6**)

Following the general procedure for polymers synthesis depicted for **P1**, the synthesis of **P6** was run from 5,5'-dibromo-2,2'-bipyrimidine (100 mg, 0.317 mmol, 0.8 eq), 2,2'-(9,9-dioctyl-9H-fluorene-2,7-diyl)bis(1,3,2-dioxaborinane) (79.49 mg, 0.158 mmol), 4,7-bis(4,4,5,5-tetramethyl-1,3,2-dioxaborolan-2-yl)benzo[c][1,2,5]thiadiazole (92.13 mg, 0.237 mmol) and 2,7-dibromo-9,9-dihexyl-9H-fluorene (38.96 mg, 0.079 mmol) in DMF (10 mL). 35 mg (22%) of a yellow solid were obtained after purification.¹²⁰

¹H NMR (300 MHz, CDCl₃) δ 9.71 (dd, J = 2.4, 11.1 Hz, 2H), 9.33 (d, J = 6.0 Hz, 1H), 7.68-8.12 (m, 7H), 1.60 (s, 5H), 1.12-1.25 (m, 14H), 0.77-0.83 (m, 12H).

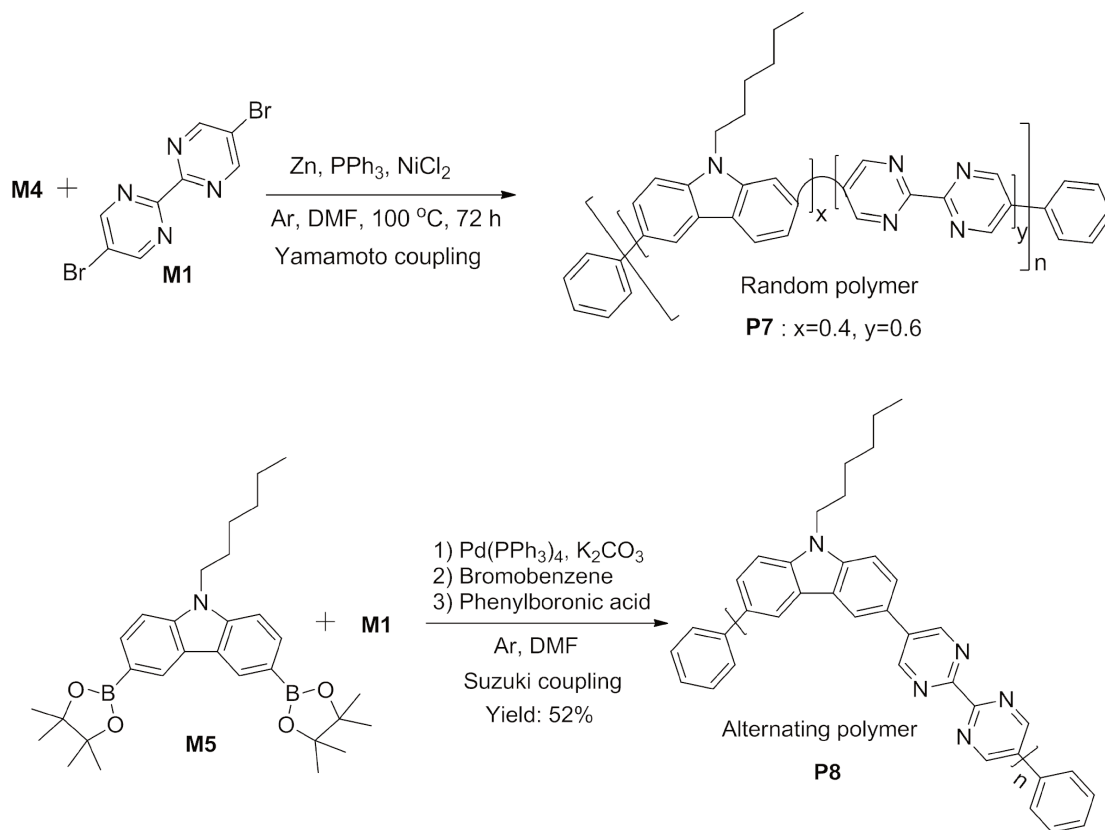
¹³C NMR (75 MHz, CDCl₃) δ 158.9, 158.2, 157.76, 157.75, 156.0, 155.9, 155.5, 153.5, 152.8, 151.8, 131.1, 131.0, 129.5, 128.5, 128.42, 128.38, 127.3, 127.2, 126.5, 126.3, 126.2, 122.8, 121.5, 121.4, 120.0, 55.3, 40.3, 31.5, 29.7, 23.9, 22.6, 14.0.

Not enough soluble for GPC measurement.

The syntheses of **P1** to **P6** show that the π -stacking between the polymer chains greatly influences the solubility of the polymers. Thus, it is important to introduce sufficiently bulky side chains to avoid the strong π -stacking between the polymer chains in order to increase the

solubility.

2.2.3 P7 and P8



Scheme 2-8 Synthetic pathways to the polymers **P7** and **P8**

Poly((2,2'-bipyrimidine)-co-3,6-(9,9-dihexyl-9H-carbazole)) (P7)

Following the Yamamoto synthetic procedure used to obtain 2,2'-bipyrimidine (**C1**), of which 100 mg of **M1** was used in the reaction, a very few amount of the solid product was obtained and that was not enough for further analysis. This may be due to the low chemical reactivity of **M1**.

Poly((2,2'-bipyrimidine)-alt-3,6-(9,9-dihexyl-9H-carbazole)) (P8)

Following the general procedure used for the synthesis of **P1**, **P8** was obtained from 5,5'-dibromo-2,2'-bipyrimidine and 9-hexyl-3,6-bis(4,4,5,5-tetramethyl-1,3,2-dioxaborolan-2-yl)-9H-carbazole as a brown product in 52% yield.

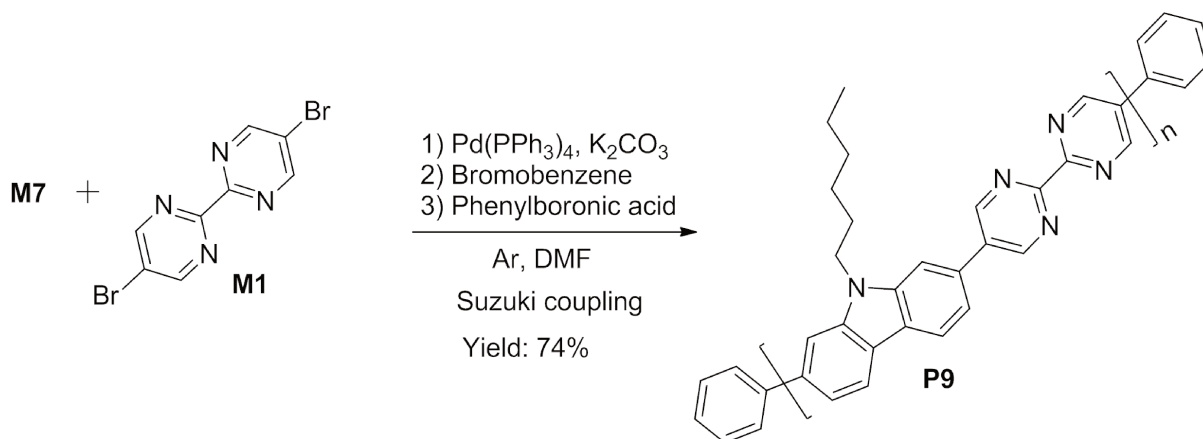
^1H NMR (300 MHz, CDCl_3) δ 9.40 (d, $J = 3.0$ Hz, 4H), 8.55 (d, $J = 3.0$ Hz, 2H), 7.85 (br, 2H),

7.64 (t, $J = 5.1$ Hz, 2H), 2.37 (t, $J = 6.0$ Hz, 2H), 1.95 (br, 2H), 1.33 (m, 6H), 0.88 (br, 3H).

^{13}C NMR (75 MHz, CDCl_3) δ 162.6, 160.3, 155.9, 141.4, 125.3, 123.6, 122.2, 119.6, 119.2, 110.3, 31.6, 29.7, 29.0, 27.0, 22.6, 14.1.

Not enough soluble for GPC measurement.

2.2.4 P9



Scheme 2-9 Synthetic pathway to the polymer **P9**

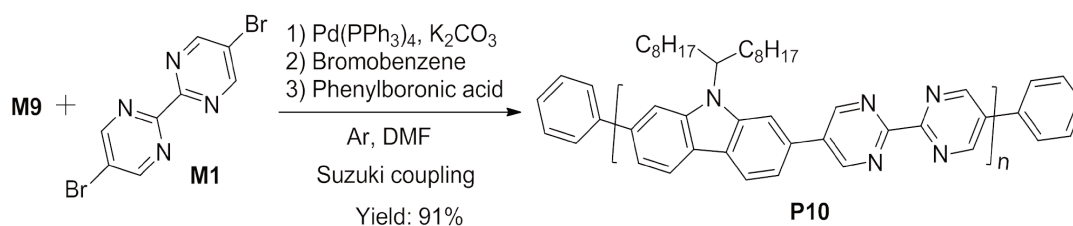
Poly(2,2'-bipyrimidine-alt-2,7-(9,9-dihexyl-9H-carbazole)) (P9)

Following the general procedure described for the synthesis of **P1**, **P9** was synthesized from 5,5'-dibromo-2,2'-bipyrimidine and 9-hexyl-2,7-bis(4,4,5,5-tetramethyl-1,3,2-dioxaborolan-2-yl)-9H-carbazole and obtained as a brown product in 74% yield.

^1H NMR (300 MHz, CDCl_3) δ 9.39 (s, 2H), 9.35 (s, 1H), 9.08(d, $J = 4.8$ Hz, 1H), 8.33 (s, 2H), 7.72-7.48 (m, 4H), 4.52 (t, $J = 2.7$ Hz, 2H), 2.00 (m, 2H), 1.36 (m, 6H), 0.87 (t, $J = 6.9$ Hz, 3H).

Not enough soluble for GPC measurement.

2.2.5 P10

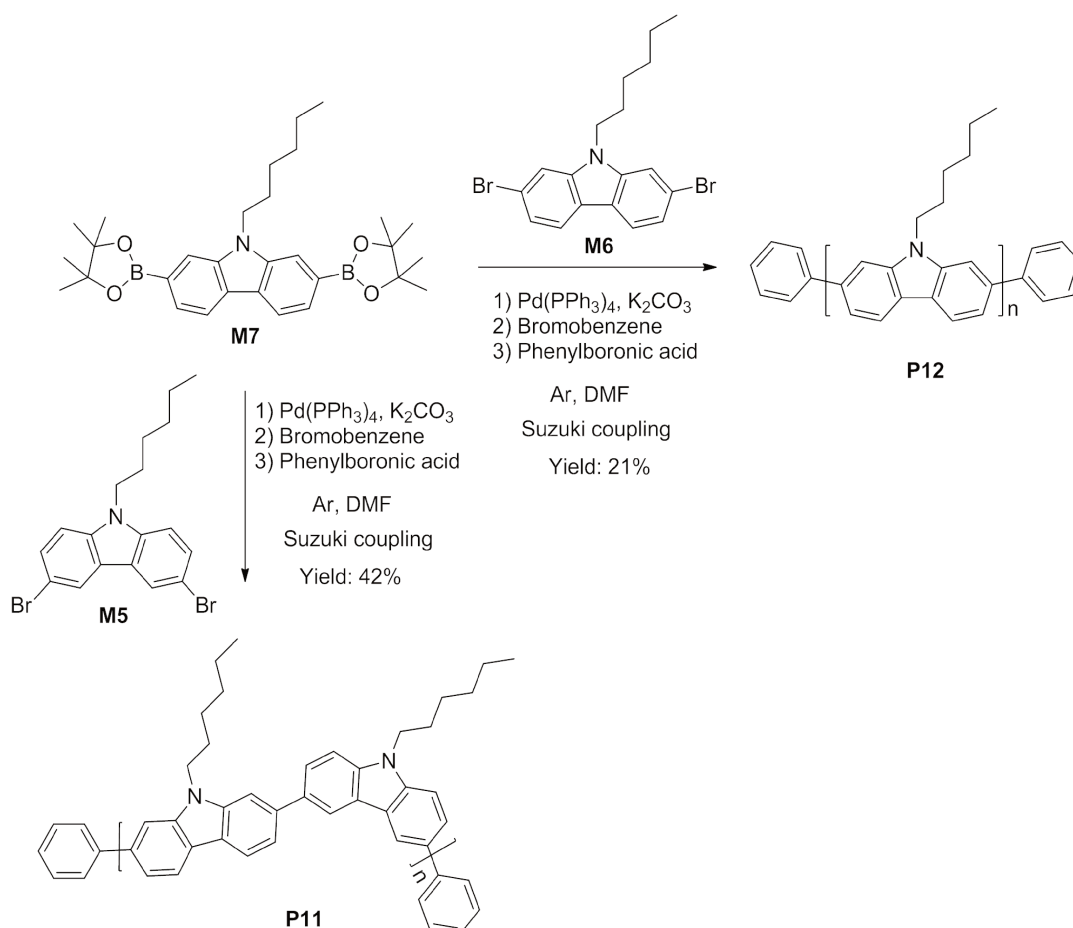


Scheme 2-10 Synthetic pathways to the polymer **P10*****Poly(2,2'-bipyrimidine-alt-2,7-(9-(heptadecan-9-yl)-9H-carbazole)) (P10)***

Following the general procedure described for the synthesis of **P1**, **P10** was synthesized from 5,5'-dibromo-2,2'-bipyrimidine and 9-(heptadecan-9-yl)-2,7-bis(4,4,5,5-tetramethyl-1,3,2-dioxaborolan-2-yl)-9H-carbazole as a brown product in 91% yield.

^1H NMR (300 MHz, CDCl_3) δ 9.37 (s, 4H), 8.35 (s, 2H), 7.89(s, 1H), 7.71 (s, 1H), 7.60 (s, 2H), 4.75 (s, 1H), 2.38 (s, 2H), 2.09(s, 2H), 1.56 (m, 24H), 0.78 (m, 3H).

Not enough soluble for GPC measurement.

2.2.6 P11 and P12**Scheme 2-11** Synthetic pathways to polymers **P11** and **P12*****Poly(3,6-(9-hexyl-9H-carbazole))-alt-2,7-(9-hexyl-9H-carbazole)) (P11)***

Following the general procedure described for the synthesis of **P1**, **P11** was synthesized from 3,6-dibromo-9-hexyl-9H-carbazole and 9-hexyl-2,7-bis(4,4,5,5-tetramethyl-1,3,2-dioxaborolan-2-yl)-9H-carbazole and obtained as a brown product in 42% yield.

^1H NMR (300 MHz, CDCl_3) δ 8.81-8.43 (m, 2H), 8.19 (br, 2H), 7.88-7.50(m, 9H), 4.39 (br, 4H), 1.95 (br, 4H), 1.33 (br, 12H), 0.87 (br, 6H).

^{13}C NMR (75 MHz, CDCl_3) δ 141.7, 140.4, 140.0, 128.8, 127.6, 125.9, 123.6, 121.5, 120.5, 119.4, 119.0, 109.8, 107.3, 43.2, 31.7, 29.1, 27.0, 22.6, 14.1.

$M_n = 3.0$ kDa; $M_w = 7.1$ kDa.

Poly(2,7-(9-hexyl-9H-carbazole)) (P12)

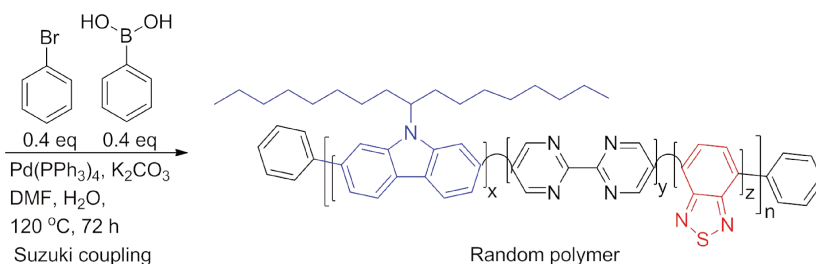
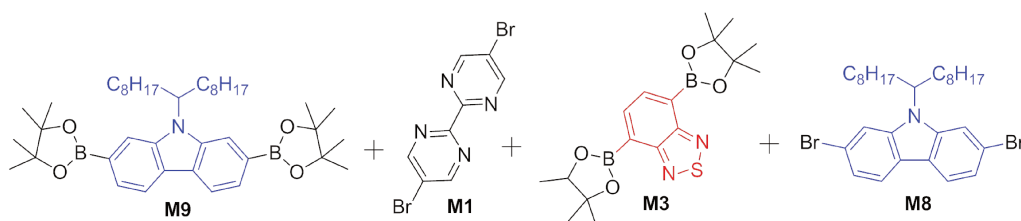
Following the general procedure described for the synthesis of **P1**, **P12** was synthesized from 2,7-dibromo-9-hexyl-9H-carbazole and 9-hexyl-2,7-bis(4,4,5,5-tetramethyl-1,3,2-dioxaborolan-2-yl)-9H-carbazole and obtained as a brown product in 21% yield.

^1H NMR (300 MHz, CDCl_3) δ 8.45-8.20(m, 4H), 7.60-7.30(m, 8H), 4.50 (br, 4H), 2.02 (br, 4H), 1.75-1.20(m, 12H), 0.88 (br, 6H).

^{13}C NMR (75 MHz, CDCl_3) δ 141.6, 140.3, 121.9, 120.6, 119.3, 107.8, 43.3, 31.7, 29.1, 27.2, 22.6, 14.1.

Not enough soluble for GPC measurement.

2.2.7 P13 and P14



P13 : $x = 0.6$, $y = 0.8$, $z = 0.6$, 64% yield

P14 : $x = 0.6$, $y = 0.3$, $z = 0.5$, 21% yield

Scheme 2-12 Synthetic pathways to polymers **P13** and **P14**

Poly(2,7-(9-(heptadecan-9-yl)-9H-carbazole)-co-(2,2'-bipyrimidine)-co-benzo[c][1,2,5]thiadiazole) in ratio 0.6:0.8:0.6 (**P13**)

Following the general procedure for polymers synthesis depicted for **P1**, **P13** was obtained from 5,5'-dibromo-2,2'-bipyrimidine, 9-(heptadecan-9-yl)-2,7-bis(4,4,5,5-tetramethyl-1,3,2-dioxaborolan-2-yl)-9H-carbazole, 4-(4,4,5,5-tetramethyl-1,3,2-dioxaborolan-2-yl)-7-(4,4,5-trimethyl-1,3,2-dioxaborolan-2-yl)benzo[c][1,2,5]thiadiazole and 2,7-dibromo-9-(heptadecan-9-yl)-9H-carbazole as a yellow solid in 64% yield.

¹H NMR (300 MHz, CDCl₃) δ 9.75-9.65 (m, 0.7H), 9.40-9.09 (m, 0.9H), 8.33-8.05 (m, 1H), 7.95-7.49 (m, 1.7H), 4.74 (br, 0.3H), 2.40 (br, 0.6H), 2.05 (br, 0.6H), 1.15 (br, 7.2H), 0.80 (br, 1.8H).

Not enough soluble for GPC measurement.

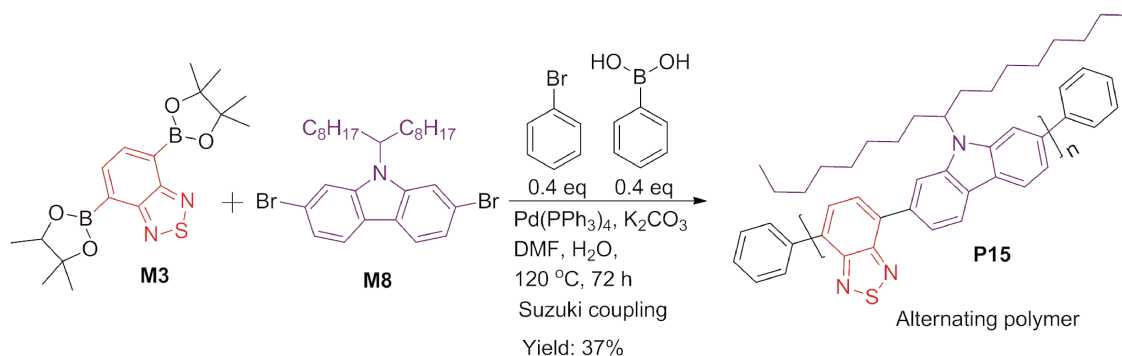
Poly(2,7-(9-(heptadecan-9-yl)-9H-carbazole)-co-(2,2'-bipyrimidine)-co-benzo[c][1,2,5]thiadiazole) in ratio 0.6:0.3:0.5 (**P14**)

Following the general procedure for polymers synthesis depicted for **P1**, **P14** was obtained from 5,5'-dibromo-2,2'-bipyrimidine, 9-(heptadecan-9-yl)-2,7-bis(4,4,5,5-tetramethyl-1,3,2-dioxaborolan-2-yl)-9H-carbazole, 4-(4,4,5,5-tetramethyl-1,3,2-dioxaborolan-2-yl)-7-(4,4,5-trimethyl-1,3,2-dioxaborolan-2-yl)benzo[c][1,2,5]thiadiazole and 2,7-dibromo-9-(heptadecan-9-yl)-9H-carbazole as a yellow solid product in 21% yield.

¹H NMR (300 MHz, CDCl₃) δ 9.75 (br, 0.55H), 9.38 (br, 0.65H), 8.70-7.39 (m, 4.62H), 4.76 (br, 0.6H), 2.44 (br, 1.2H), 2.05 (br, 1.2H), 1.16 (br, 14.4H), 0.80 (br, 3.6H).

Not enough soluble for GPC measurement.

2.2.8 P15

Scheme 2-13 Synthetic pathway to the polymer **P15**

Poly(2,7-(9-(heptadecan-9-yl)-9H-carbazole)-alt-(benzo[c][1,2,5]thiadiazole)) (P15)

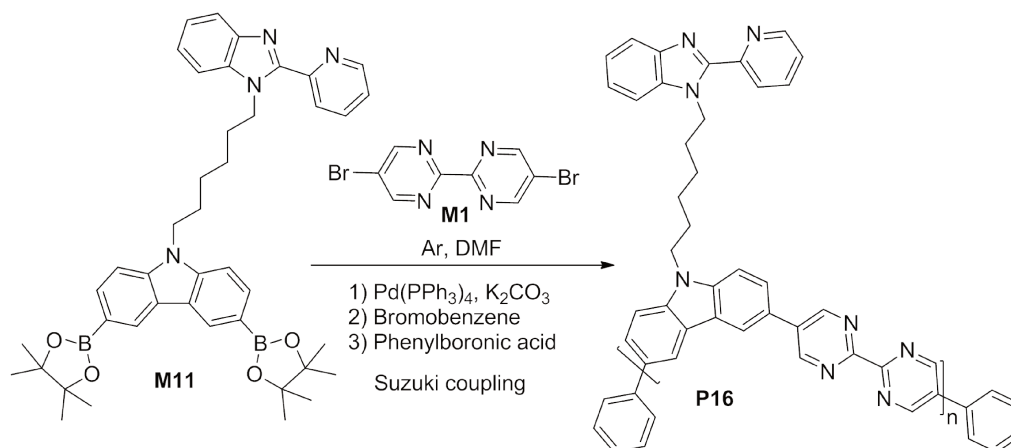
Following the general procedure for polymers synthesis depicted for **P1**, **P15** was obtained from 2,7-dibromo-9-(heptadecan-9-yl)-9H-carbazole and 4-(4,4,5,5-tetramethyl-1,3,2-dioxaborolan-2-yl)-7-(4,4,5-trimethyl-1,3,2-dioxaborolan-2-yl)benzo[c][1,2,5]thiadiazole as a brownish solid in 37% yield.

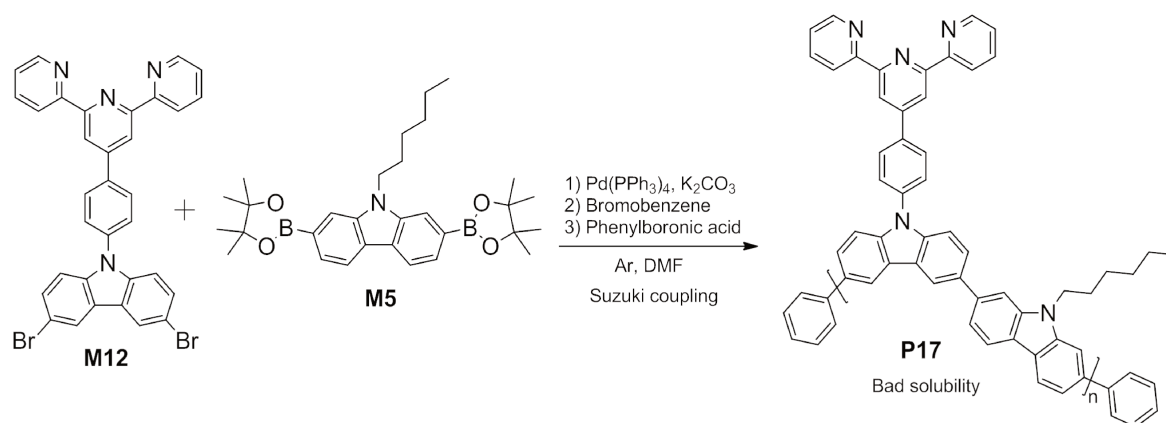
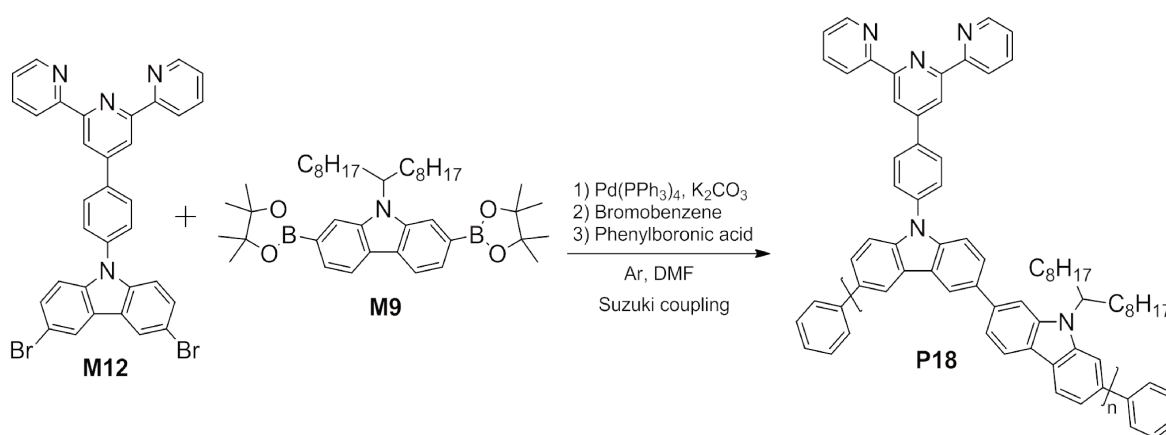
^1H NMR (300 MHz, CDCl_3) δ 8.55-7.74 (m, 8H), 7.50 (br, 1H), 4.80 (s, 1H), 2.49 (br, 2H), 2.04 (br, 2H), 1.16 (br, 24H), 0.79 (br, 6H).

^{13}C NMR (75 MHz, CDCl_3) δ 154.6, 143.0, 139.5, 134.0, 132.2, 128.4, 120.7, 120.4, 120.2, 113.1, 110.2, 56.6, 34.0, 31.8, 29.5, 29.4, 29.3, 26.9, 22.6, 14.1.

Not enough soluble for GPC measurement.

2.2.9 P16, P17 and P18

Scheme 2-14 Synthetic pathway to the polymer **P16**

Scheme 2-15 Synthetic pathway to the polymer **P17**Scheme 2-16 Synthetic pathway to the polymer **P18**

Poly(9-hexyl-9H-carbazole-alt-3,6-(phenyl-terpyridine) carbazole) (P17)

Following the general procedure for polymers synthesis depicted for **P1**, **P17** was obtained from 9-(4-([2,2':6',2'']-terpyridin]-4'-yl)phenyl)-3,6-dibromo-9H-carbazole and 9-hexyl-2,7-bis(4,4,5,5-tetramethyl-1,3,2-dioxaborolan-2-yl)-9H-carbazole as a brown solid (about 5 mg, low yield) was collected.

^1H NMR (300 MHz, CDCl_3) δ 8.92-8.58 (m, 7H), 8.58 (s, 2H), 8.20-7.28 (m, 19H), 4.75-4.30 (m, 2H), 2.16-1.85 (m, 2H), 1.45-1.25 (m, 6H), 0.90-0.75 (m, 3H).

^{13}C NMR (75 MHz, CDCl_3) δ 156.1, 149.2, 141.7, 140.5, 139.7, 138.5, 137.0, 135.1, 129.0, 127.2, 126.4, 124.4, 124.0, 121.6, 121.4, 120.6, 118.9, 110.3, 108.7, 107.4, 31.7, 29.7, 29.1, 27.1, 22.6, 14.1.

Not enough soluble for GPC measurement.

Poly(9,9-dihexyl-9H-fluorene-alt-3,6-(phenyl-terpyridine) carbazole) (P18)

Following the general procedure for polymers synthesis depicted for **P1**, **P18** was obtained from 9-(4-([2,2':6',2''-terpyridin]-4'-yl)phenyl)-3,6-dibromo-9H-carbazole and 9-(heptadecan-9-yl)-2,7-bis(4,4,5,5-tetramethyl-1,3,2-dioxaborolan-2-yl)-9H-carbazole as a brown solid in 36% yield.

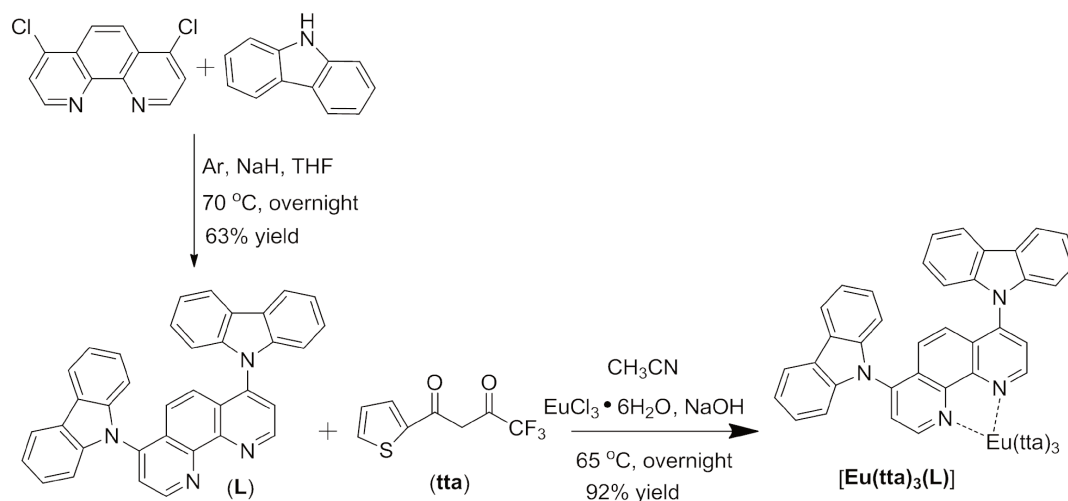
^1H NMR (300 MHz, CDCl_3) δ 8.89 (s, 2H), 8.72-8.78 (m, 3H), 8.58 (s, 2H), 8.20-8.25 (m, 4H), 7.84-7.95 (m, 7H), 7.65 (s, 3H), 7.38-7.43 (m, 4H), 7.22-7.25 (m, 2H), 4.60-4.80 (m, 1H), 2.26-2.52 (m, 2H), 1.85-2.01 (m, 2H), 0.90-1.25 (m, 24H), 0.68-0.81 (m, 6H).

^{13}C NMR (75 MHz, CDCl_3) δ 156.1, 149.2, 140.5, 137.0, 129.0, 127.2, 124.4, 124.0, 121.4, 118.9, 110.7, 107.6, 56.4, 33.8, 31.8, 29.4, 29.2, 26.9, 22.6, 14.1.

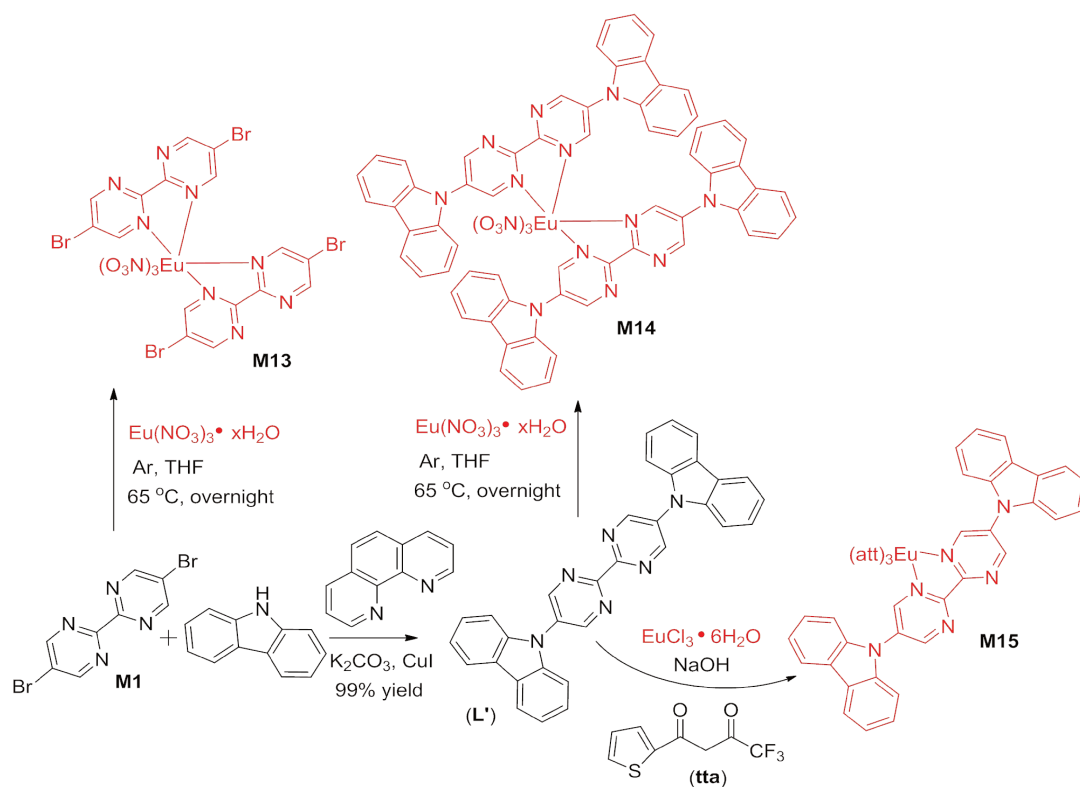
$M_n = 1.6$ kDa; $M_w = 2.6$ kDa.

2.3 Synthesis and chemical characterization of metal complexes

Their syntheses and NMR data are as follows. The europium compounds were chosen as they have long been used in our lab as highly efficient red emitting components and we are familiar with their properties.



Scheme 2-17 Synthetic pathways to the metal complex $\text{Eu}(\text{tta})_3(\text{L})$

Scheme 2-18 Synthetic pathways to metal complexes **M13**, **M14** and **M15**

4,7-di(9H-carbazol-9-yl)-1,10-phenanthroline (**L**)

To a 100 mL dried round bottom flask charged with carbazole (270 mg, 1.61 mol) and dry THF (40 mL) at 0 °C was added NaH (92 mg, 2.29 mmol) under argon. 4,7-dichloro-1,10-phenanthroline (200 mg, 0.80 mmol) was added to the mixture after 1 h and the reaction was stirred at 70 °C overnight. The mixture was filtered and concentrated in vacuum. The residue was dissolved in 20 mL of DCM, filtered, and the DCM was removed by rotary evaporation. Colorless crystals were obtained by recrystallization from THF and pentane (255.2 mg, 63% yield).

1H NMR (300 MHz, $CDCl_3$) δ 9.48 (d, J = 4.8 Hz, 2H), 8.15 (d, J = 7.8 Hz, 4H), 7.86 (d, J = 4.5 Hz, 2H), 7.29-7.37 (m, 10H), 7.07 (d, J = 7.5 Hz, 4H).

^{13}C NMR (75 MHz, $CDCl_3$) δ 96.1, 95.4, 94.1, 93.5, 89.83, 89.81, 89.2, 88.9, 88.43, 88.36, 85.7.

This result is consistent with that reported previously.¹¹⁴

[Eu(tta)₃(L)]: To a 25 mL dried round bottom flask charged with 4,4,4-trifluoro-1-(thiophen-2-yl)butane-1,3-dione (246 mg, 1.11 mol) and dry acetonitrile (5 mL), an aqueous solution of

NaOH (45 mg, 1.12 mmol) was added. After stirring for 15 min at 65 °C, an aqueous solution of $\text{EuCl}_3 \cdot 6\text{H}_2\text{O}$ (135 mg, 0.37 mmol) was added. After stirring for 30 min at 65 °C, L (186 mg, 0.37 mmol) was added, and the reaction mixture was stirred overnight at 65 °C, then cooled to room temperature and poured into water. A yellow precipitate was filtered off, washed with water and dried. Product (449 mg, 92% yield) was obtained after recrystallization by slow diffusion of pentane into a chloroform solution. Red luminescence from Eu^{3+} was seen under 365 nm UV light, which means the energy transfer from the ligand to the Eu^{3+} ion occurred and also means that the coordination of the ligand to the Eu^{3+} ion emerged.

^1H NMR (300 MHz, CDCl_3) δ 11.22 (br, 2H), 9.01 (d, $J = 11.4$ Hz, 4H), 8.58 (d, $J = 3.3$ Hz, 3H), 8.25 (d, $J = 3.9$ Hz, 3H), 7.62-7.67 (m, 7H), 6.99 (d, $J = 1.8$ Hz, 4H), 6.47 (t, $J = 1.2$ Hz, 4H), 6.05 (d, $J = 1.2$ Hz, 4H), 2.85 (m, 3H).

This result is consistent with that reported previously.¹¹⁴

5,5'-di(9H-carbazol-9-yl)-2,2'-bipyrimidine (L')

An oven-dried pressure tube was charged with 5,5'-dibromo-2,2'-bipyrimidine (100 mg, 0.32 mmol), CuI (12.06 mg, 0.6 mmol), K_2CO_3 (91.87 mg, 0.64 mmol), 1,10-phenanthroline (11.41 mg, 0.6 mmol), and carbazole (111.14 mg, 0.64 mmol) under argon. Dry DMF (5 mL) was added and then the tube was sealed and heated overnight at 140 °C. After completion, the reactant medium was poured into ice-water, stirred for 30 min, filtered, washed with water and hexane. Recrystallization from diffusion of hexane into THF gave the product as a white solid (139.16 mg, 99% yield).¹³⁴

^1H NMR (300 MHz, CDCl_3) δ 9.39 (br, 4H), 8.17 (d, $J = 7.8$ Hz, 4H), 7.47-7.55 (m, 8H), 7.37-7.42 (m, 4H).

^{13}C NMR (75 MHz, CDCl_3) δ 155.6, 139.8, 126.9, 124.4, 121.7, 120.9, 109.0.

[Eu(NO₃)₃(M1)₂] (M13)

A dried round bottom flask was added 5,5'-dibromo-2,2'-bipyrimidine (100 mg, 0.21 mmol) and $\text{Eu}(\text{NO}_3)_3 \cdot x\text{H}_2\text{O}$ (53.49 mg, 0.10 mmol) under argon. Dry THF (5 mL) was added and stirred overnight at 65 °C. The reactant medium was cooled to room temperature and the solvent was

¹³⁴ M. S. Park, J. Y. Lee. *Organic Electronics*, **2013**, 14(5), 1291-1296.

removed with a syringe under argon flushing. Recrystallization from THF in a glove box gave the product as a white microcrystalline powder (50% yield).¹³⁵ Red luminescence from Eu^{3+} was seen under 365 nm UV light, which means the energy transfer from the ligand to the Eu^{3+} ion occurred and also means that the coordination of the ligand to the Eu^{3+} ion emerged.

^1H NMR (300 MHz, CDCl_3) δ 9.04-9.12 (m, 8H).

^{13}C NMR (75 MHz, CDCl_3) δ 159.7, 158.9, 121.9.

[Eu(NO₃)₃(L')₂] (M14)

A dried round bottom flask was charged with 5,5'-di(9H-carbazol-9-yl)-2,2'-bipyrimidine (100 mg, 0.205 mmol) and $\text{Eu}(\text{NO}_3)_3 \cdot x\text{H}_2\text{O}$ (34.59 mg, 0.5 eq) under argon. Dry THF (5 mL) was added and the reactant medium was stirred overnight at 65 °C, then cooled to room temperature and the solution was removed use syringe with argon blowing. Recrystallization from THF in glove box gave the product as a white microcrystalline powder (45% yield).¹³⁴ Red luminescence from Eu^{3+} was seen under 365 nm UV light, which means the energy transfer from the ligand to the Eu^{3+} ion occurred and also means that the coordination of the ligand to the Eu^{3+} ion emerged.

^1H NMR (300 MHz, CDCl_3) δ 9.48 (br, 8H), 8.23 (br, 8H), 7.69 (br, 8H), 7.48 (d, J = 23.4 Hz, 16H).

^{13}C NMR (75 MHz, CDCl_3) δ 139.8, 127.1, 124.6, 122.0, 121.0, 109.2.

[Eu(tta)₃(L')] (M15)

A dried round bottom flask was added 4,4,4-trifluoro-1-(thiophen-2-yl)butane-1,3-dione (136.44 mg, 0.61 mmol) and CH_3CN (4 mL) under argon. An aqueous solution of NaOH (24.73 mg, 0.61 mmol) was added and the reactant medium was stirred for 15 min at 65 °C. An aqueous solution of $\text{EuCl}_3 \cdot 6\text{H}_2\text{O}$ (75.00 mg, 0.20 mmol) was then added and the medium was further stirred for 30 min at 65 °C under argon. 5,5'-di(9H-carbazol-9-yl)-2,2'-bipyrimidine (100 mg, 0.21 mmol) was added. After stirring overnight at 65 °C, the reactant medium was cooled to room temperature and poured into ice-water. A yellow precipitate was filtered off, washed with water

¹³⁵ a. G. Zucchi, O. Maury, P. Thuéry, F. Gumy, J.-C.G. Bünzli, M. Ephritikhine, *Chem. Eur. J.*, **2009**, *15*, 9686-9696.

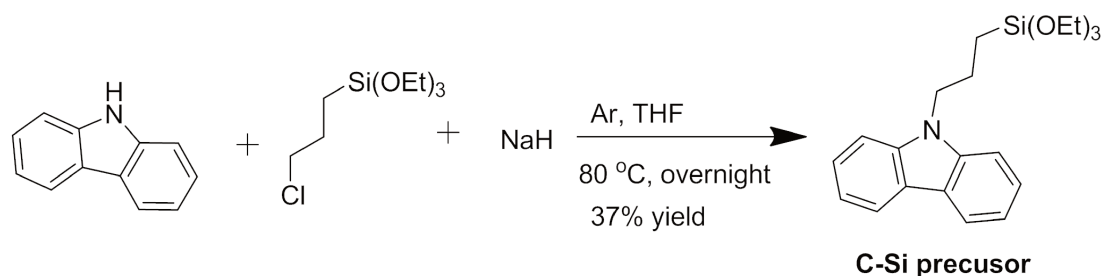
b. ZHAO N., MA R., XU L., WANG S., WANG R., ZHANG J., *JOURNAL OF HEBEI NORMAL UNIVERSITY*, **2008**, *32*:209-212.

and dried. Recrystallization from THF in a glove box gave the product as a white microcrystalline powder (55% yield).¹³⁴⁻¹³⁶

¹H NMR (300 MHz, CDCl₃) δ 8.20 (br, 8H), 7.66 (br, 6H), 7.38 (br, 9H), 6.83 (br, 2H), 6.38 (br, 2H), 6.03 (br, 2H), 2.97 (d, J = 14.7 Hz, 6H).

2.4 Preparation of the liquid materials

Liquid precursor



Scheme 2-19 Synthetic pathways to liquid **C-Si precursor**

9-(3-(triethoxysilyl)propyl)-9H-carbazole (C-Si precursor)

To a 200 mL flame dried round bottom flask charged with carbazole (5.00 g, 0.030 mol) and dry THF (100 mL) at 0 °C was added NaH (1.435 g, 0.036 mol) under argon. (3-chloropropyl)triethoxysilane (7.201 g, 0.030 mol) was added to the mixture after 1 h and the reaction was stirred at 80 °C overnight. The mixture was filtered, concentrated in vacuum, and purified by flash column chromatography with petroleum ether/ethyl acetate (v/v = 15:1) to afford a brown liquid product (4.158 g, 37% yield).

¹H NMR (300 MHz, CDCl₃) δ 8.13 (d, J = 7.8 Hz, 2H), 7.47-7.49 (m, 4H), 7.22-7.28 (m, 2H), 4.34 (t, J = 7.5 Hz, 2H), 3.79-3.86 (m, 6H), 2.00-2.06 (m, 2H), 1.23 (t, J = 7.2 Hz, 9H), 0.71-0.76 (m, 2H).

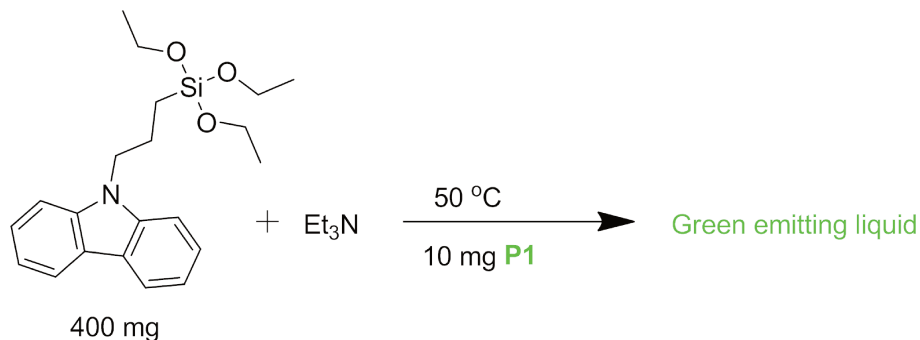
¹³C NMR (75 MHz, CDCl₃) δ 140.5, 125.6, 122.8, 120.3, 118.7, 108.8, 58.5, 45.3, 22.4, 18.3, 7.9.

This result is consistent with that reported previously.¹¹⁴

¹³⁶ G. Zucchi, V. Murugesan, D. Tondelier, D. Aldakov, T. Jeon, F. Yang, P. Thuery, M. Ephritikhine, and B. Geffroy. *Inorg. Chem.*, **2011**, 50: 4851–4856.

General procedure for liquid materials. The liquid materials were obtained by a co-doping method following Xiaoguang Huang's PhD manuscript.¹¹⁴

A typical procedure is shown on **Scheme 2-20** for the synthesis of a liquid material with **P1**.



Scheme 2-20 Synthetic pathways to Green emitting liquid of **P1**

To a 25 mL dried round bottom flask was added the C-Si precursor (400 mg, 1.08 mmol). Four drops of triethylamine were added at 50°C. The reactant medium was stirred for 3 h and then **P1** (10 mg) was added. Mixing all the components overnight yielded the liquid composite as a yellow liquid after removal of the excess of triethylamine under vacuum.

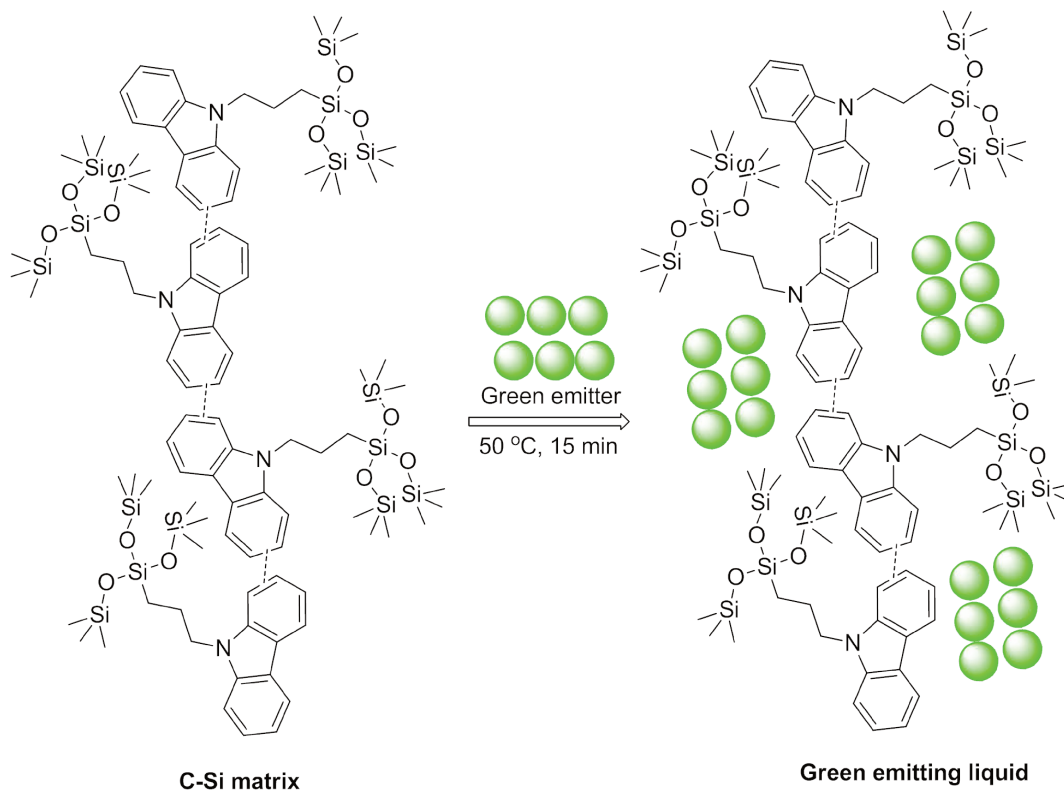


Figure 2-2 Illustration of the formation of the green emitting liquid

An illustration of the formation of a green emitting liquid material is shown in above **Figure 2-2**.

2.5 Preparation of thin films

In comparison with vacuum deposition, solution-processed film preparation techniques, including spin-coating, screen and ink-jet printing, direct- and flexo-printing, slot-die coating and dipping, etc., are more feasible to manufacture large-area films, better compatibility with flexible substrates, and more cost-effective.^{118,137} Moreover, flexible substrates and better control of the doping process can be facily adopted. Among them, the technique of spin-coating has drawn extensive attention in thin-film deposition for several decades due to its numerous advantages, such as a better control of doping level, leading to homogeneous morphology and easy processability over large areas that can be readily upgraded to industrial scale.^{118,138}

The spin-coating process starts with the dilution of the material to be deposited in a solvent. A typical process of spin-coating involves depositing a small puddle of the solution prepared on the center of a glass substrate, which is either spinning at low speed or not spinning at all, set in the middle of the spin-coater, and then the substrate is rotated at high speed (typically around 2000-5000 rpm). The centripetal acceleration will cause the solution to spread to the edge of the substrate, leaving a thin film of the coating material on the surface. A schematic illustration of treatment of films through a spin-coating method is shown in **Figure 2-3**. The final film thickness and other properties will depend on the nature of the solution (the viscosity, drying rate, solid content, surface tension, and the amount, etc.) and the parameters chosen for the spin process. Factors such as the rotational speed, acceleration, and spinning time contribute to how the properties of coated films are defined.^{139,140}

¹³⁷ a. Amruth C, Marco C., Jonathan G., James K., Nicholas S., Beata L., and Jacek U., *Micromachines*, **2019**, 10(1), 53.

b. J. Huang, Z. Xu, Z. Cai, J. Guo, J. Guo, P. Shen, Z. Wang, Z. Zhao, D. Ma and B. Z. Tang. *J. Mater. Chem. C*, **2019**, 7, 330-339.

¹³⁸ Z. Li, T. R. Klein, D. H. Kim, M. Yang, J. J. Berry, M. F. A. M. v. Hest and K. Zhu. *Nature reviews*, **2018**, 3, 18017.

¹³⁹ D. W. Schubert, T. Dunkel. *Mater. Res. Innovations*, **2003**, 7, 314.

¹⁴⁰ N.-T. Nguyen, *Micromixers* (second edition), Imprint: William Andrew, **2012**, Pages 113-161. ISBN: 978-1-4377-3520-8. DOI: <https://doi.org/10.1016/C2011-0-69734-0>.

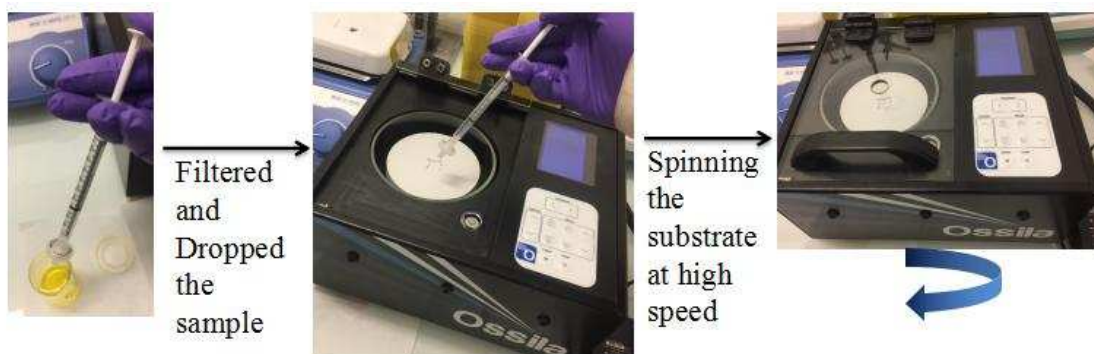


Figure 2-3 Schematic illustration of treatment of films through a spin-coating method

As the thickness, the morphology and the photoluminescent properties of solution-processed thin-film are strongly influenced by the processing parameters, such as the substrate temperature, the solvent, coating speed, spin-time and thermal treatments, the films studied in this work were fabricated in same conditions.^{122,136}

General procedure for the preparation of pure emitters as thin films

The glass substrates were firstly cleaned in ethanol (15 min) and acetone (15 min) in an ultrasonic bath, respectively. After cleaning, substrates were treated by an UV-ozone cleaner for 15 min to increase the surface energy before spin-coating. All the spin-coating processes were performed in ambient atmosphere. The emitters (typically 5 mg) for the films were dissolved in dichlorobenzene (1 mL) and the solutions were stirred overnight at room temperature. The solutions were filtered with 0.45 μm syringe filters prior to deposition.

The materials were spin coated on glass substrates at 2000 rpm for 30 sec from the above filtered solutions, followed by thermal treatment at 80 $^{\circ}\text{C}$ in an oven for 8 h.

Pure films of $[\text{Eu}(\text{tta})_3(\text{L})]$, **PF**, **P1**, **P8**, **P9**, **P10**, **P11**, **P12**, **P13** and **P14** were fabricated and studied according to the introduced general procedure.

General procedure for the preparation of emitters in polymer matrix as thin films

The emitters were dissolved in a mixed solution composed of different polymer matrices (eg. C-Si matrix, PMMA, Polystyrene, Poly(Ethylene-co-vinyl acetate)) and dichlorobenzene in different composition and the solutions were stirred overnight at room temperature. The solutions were filtered through 0.45 μm syringe filters prior to deposition.

The materials were spin coated on glass substrates at 2000 rpm for 30 sec and thermally annealed at 80 °C in an oven for 8 h.

To be note about the calculation, the wt% of polymer in certain concentration of matrix mentioned in this thesis was the comparison of the weight of the polymer and the matrix. For example, 1 % wt of **P1** in 5 mg/mL **PMMA**: it means the weight ratio of **P1/PMMA** is 1%, and the concentration of the precursor is 5 mg/mL.

Films of **PF**, **P1**, **P8**, **P10**, **P13** and **P14** were fabricated and studied according to the introduced general procedure in this work.

General procedure for the preparation of polymers in PMMA as thin films for the measurement of absolute quantum yield

In a first step, we prepared a solution of PMMA in tetrahydrofuran (5 g PMMA in 40 mL THF, 12.35% wt PMMA). An appropriate amount (according to the calculation of the percentage of polymer with PMMA) of this solution was then mixed with the desired amount of phosphor. The solutions were stirred well for 15 h at room temperature.

In a second step, the luminescent composite films based on these luminophores were made using a coating bench. The thickness of the film was 200 µm fixed by the bar-coater knife. The composite films produced were treated at a temperature of 60 °C for 2 hours to allow the polymer to crosslink. The composite films obtained are transparent and homogeneous.

2.6 Summary and Perspectives

In this chapter, we have presented the synthesis and characterization of a variety of monomers and polymers, various metal complexes, precursors and diverse liquid materials, and the film formation as well.

More specifically, a series of novel carbazole copolymers (**P11**, **P12**) with different binding positions were synthesized by Suzuki coupling. A series of novel random or alternating conjugated polymers (**P1-P14** and **P16**) based on 2,2'-bipyrimidine as acceptor and carbazole/fluorene units as donors, with different binding positions were synthesized by Yamamoto or Suzuki coupling. Some multifunctional carbazole-based conjugated polymers (**P17**, **P18**) were designed and synthesized. These compounds will allow to study the structure-

property relationship. From **P1** to **P2**, we aimed at analyzing the influence of the phenyl end-capping. With polymers **P3-P6**, we will evaluate the influence of the size of the pendant groups on the solubility in common solvents, such as DCM, THF and chloroform. **P8-P12** were designed in order to get more photostable materials by suppressing the fluorene unit. Meanwhile, we intend to analyze the impact of the linearity of the polymer chains on their fluorescent properties. Inspired by the white emission from **P6** under near UV irradiation, we then designed and synthesized **P13** and **P14** that also introduced carbazole derivatives instead of fluorene derivatives employed in **P6**, for the sake of obtaining white emission and improving the photostability of the polymers as well. Polymers **P13**, **P14**, and **P15** were designed to take advantage of the use of the BTD unit as an acceptor unit to shift the emission to the red. **P17** and **P18** were designed and anticipated for multifunctional applications.

Various Eu^{3+} complexes, including **Eu(tta)₃(L)** and **M13-M15** for red emission were also designed and synthesized. Besides, different ligands based on BPM were introduced.

The syntheses of the liquid C-Si precursor and different soft materials were demonstrated afterwards, followed by the film formation of different emitters under different conditions. Different polymer matrices (PMMA, polystyrene, Poly(Ethylene-co-vinyl acetate), as well as C-Si matrix were investigated. All the liquid materials and thin films were fabricated under the same conditions for better comparison in their properties studies, considering that their processing parameters may have influence on their photophysical properties.

As above shown, BPM can both serve as a monomer for the design of conjugated polymers and a ligand to the Eu(III) ions. In particular, we have designed and synthesized many new visible-emitting conjugated polymers incorporating BPM as an acceptor unit. Polymers containing BPM could open the way to a new family of luminescent metallopolymers as they can readily coordinate metal ions. Our work may pioneer the application of BPM as a novel acceptor in the design of conjugated polymers and opens the way to a new family of polymers.

Chapter III Photophysical properties of pure polymers

Contents

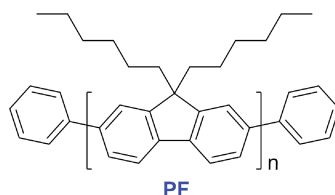
3.1 Polymers in Solution.....	- 71 -
3.1.1 Absorption and PL spectra of PF	- 71 -
3.1.2 Absorption and PL spectra of P1	- 74 -
3.1.3 Absorption and PL spectra of P2	- 78 -
3.1.4 Absorption and PL spectra of P5	- 81 -
3.1.5 Absorption and PL spectra of P6	- 85 -
3.1.6 Absorption and PL spectra of P8	- 87 -
3.1.7 Absorption and PL spectra of P9	- 91 -
3.1.8 Absorption and PL spectra of P10	- 95 -
3.1.9 Absorption and PL spectra of P11	- 98 -
3.1.10 Absorption and PL spectra of P12	- 102 -
3.1.11 Absorption and PL spectra of P13	- 106 -
3.1.12 Absorption and PL spectra of P14	- 110 -
3.1.13 Absorption and PL spectra of P15	- 113 -
3.1.14 Absorption and PL spectra of P18	- 116 -
3.1.15 Comparison of absorption and PL spectra of PF and P1	- 119 -
3.1.16 Comparison of absorption and PL spectra of P1 and P2	- 120 -
3.1.17 Comparison of absorption and PL spectra of P1 , P5 , P6 and P8	- 121 -
3.1.18 Comparison of absorption and PL spectra of P8 and P9	- 123 -
3.1.19 Comparison of absorption and PL spectra of P9 and P10	- 124 -
3.1.20 Comparison of absorption and PL spectra of PF , P11 and P12	- 125 -
3.1.21 Comparison of absorption and PL spectra of P6 , P13 and P14	- 126 -
3.1.22 Comparison of absorption and PL spectra of P13 in different solvents.....	- 127 -
3.1.23 Comparison of absorption and emission spectra of P10 , P13 and P15	- 137 -
3.2 Polymers as pure thin films.....	- 138 -
3.2.1 Absorption.....	- 139 -
3.2.2 Excitation and emission of polymers as thin films.....	- 141 -
3.3 Summary.....	- 155 -

Having obtained various luminescent materials with different chemical compositions, the absorption and photoluminescent (PL) properties of the materials were investigated, either in solution or in solid state. Results are detailed in this chapter. They will help us to determine and confirm the emission color of each material and to know the best experimental conditions that should be used to obtain the highest emission intensity for each of them. By comparison of the results, we will know the influence of the backbone, linearity and side-chain engineering of the polymers to their photophysical properties, which in reverse will help us to better design new molecules with improved properties.

3.1 Polymers in Solution

Firstly, the optical properties of each polymer were measured in solution. We used dichloromethane (DCM) and tetrahydrofuran (THF) as solvent in most case as the polymers we have studied are dissolved better in these solvents.

3.1.1 Absorption and PL spectra of PF



Poly(di-hexylfluorene) (**PF**), was firstly synthesized according to reported procedure as a commonly used blue emitting molecule.¹²² In fact, among plenty of chemical moieties, fluorene has been widely investigated and applied in the PLEDs because it leads to highly efficient photo- and electroluminescent materials, with excellent thermal stability, and good solubility in common organic solvents.¹⁴¹ A further advantage of the fluorene moiety is that the bridge carbon atom can be easily functionalised with two alkyl chains of different length so that good solubility in many organic solvents as well as low melting point can be achieved.¹⁴² Among them, the 2,7-disubstituted fluorene structural unit is a rigid, planar and highly conjugated moiety as reported, which can provide a higher degree of delocalisation.¹⁴³

¹⁴¹ C. Pan, L. Wang, W. Zhou, L. Cai, D. Xie, Z. Chen, and L. Wang. *Polymers*, **2019**, *11*, 278.

¹⁴² M. Sims, D. D. C. Bradley, M. Ariu, M. Koeberg, A. Asimakis, M. Grell, D. G. Lidzey. *Adv.Funct.Mater.*, **2004**, *14*(8), 765-781.

¹⁴³ G. Hu, M. R. Billa, S. P. Kitney and S. M. Kelly. *Liquid Crystals*, **2017**, *45*(7): 965-979.

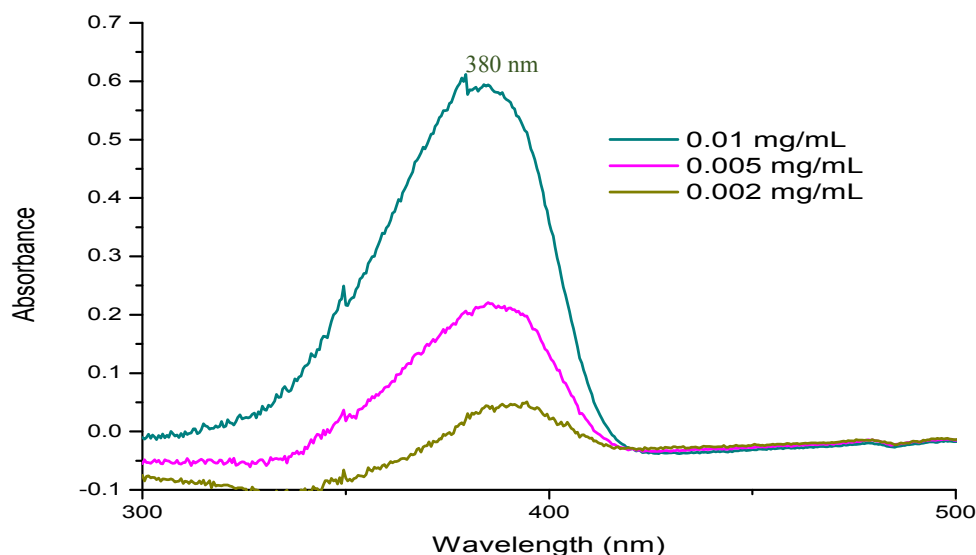


Figure 3-1 Absorption spectra of PF in DCM at different concentrations.

As **Figure 3-1** shown, the polymer PF in DCM has a broad absorption ranging from 300 nm to 420 nm, attributed to the intramolecular charge transfer (ICT) mainly associated with electron transfer from the donor to the acceptor moieties,¹⁴⁴⁻¹⁴⁵ and the maximum is around 380 nm when the concentration is 0.01 mg/mL, which means that the near UV light is a good source of irradiation for the emission. With the increase of the concentration, the absorption intensity is also increasing.

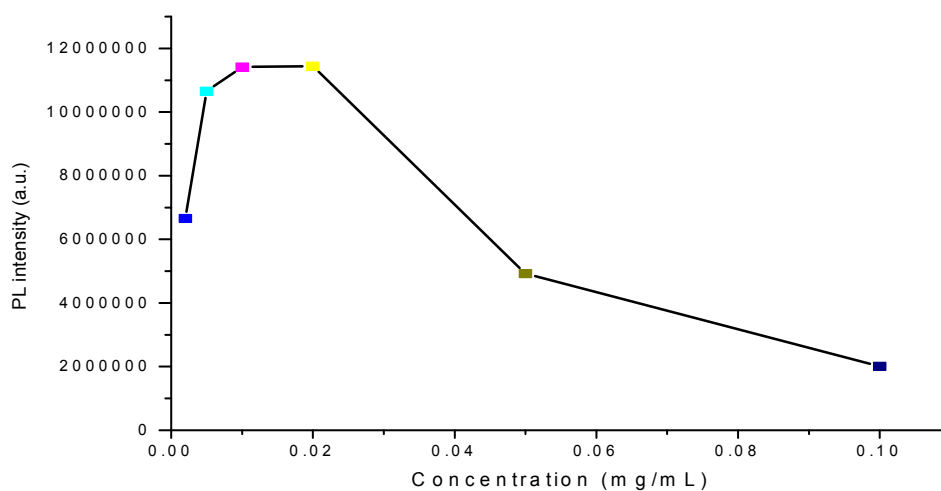


Figure 3-2 Emission intensity of PF versus concentration ($\lambda_{\text{exc}} = 375 \text{ nm}$).

As shown on **Figure 3-2**, the concentration should be no more than 0.01 mg/mL, so that the curve of PL intensity versus concentration is in the linear domain which indicate that there have

¹⁴⁴ C. V. Kumar, L. Cabau, E. N. Koukaras, S. A. Siddiqui, G. D. Sharma and E. Palomares. *Nanoscale*, **2015**, 7, 7692-7703.

¹⁴⁵ J. U. Kima, S. S. Reddy, L.-S. Cui, H. Nomura, S. Hwang, D. H. Kim, H. Nakanotani, S.-H. Jinc, C. Adachi. *Journal of Luminescence*, **2017**, 190, 485-491.

no aggregation formed.

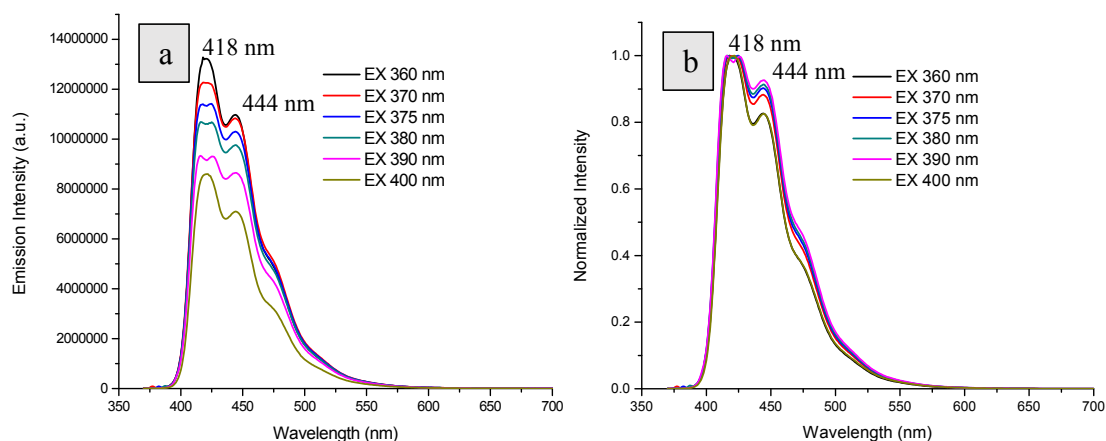
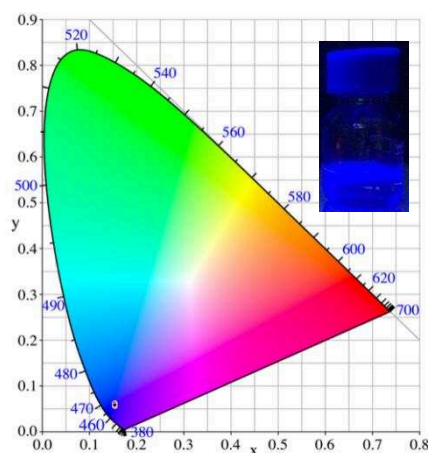


Figure 3-3 a) Emission spectra of **PF** in **DCM**; b) Corresponding normalized emission spectra. (0.01 mg/mL, slits were 2,2 nm)

Above **Figure 3-3** shows that the band of the emission spectrum of **PF** in **DCM** is ranging from 400 nm to 600 nm with two maxima, at 418 nm and 444 nm, respectively, when excited at 360-400 nm. The normalized emission spectra show identical emission profile despite the intensity changes, suggesting that the prompt fluorescence are originated from the same S_1 states.



λ_{exc}	CIE x	CIE y
360 nm	0.154	0.057
370 nm	0.153	0.059
375 nm	0.153	0.060
380 nm	0.153	0.061
390 nm	0.153	0.062
400 nm	0.154	0.058

Figure 3-4 CIE coordinates of **PF** in **DCM** (0.005 mg/mL, slits were 2,2 nm, λ_{exc} = 360-400 nm) (The inserted photo shows the emission of **PF** in **DCM** under a 365 nm UV lamp)

The **CIE coordinates** (0.153, 0.060) show the material emits a **blue light** under excitation at 375 nm.

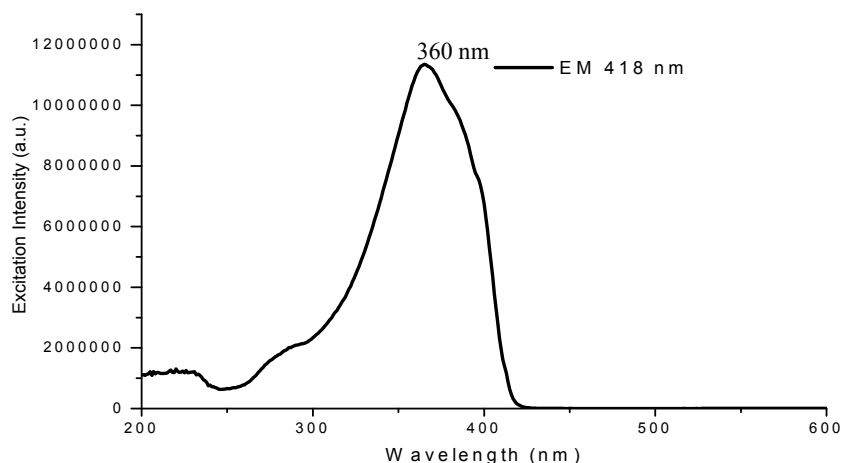


Figure 3-5 Excitation spectra of PF in DCM (0.005 mg/mL, slits were 2,2 nm)

As shown on **Figure 3-5**, the main band of the excitation spectrum is ranging from 250 nm to 450 nm with a maximum at 360 nm, which also means that the near UV light is a good source of irradiation for the emission.

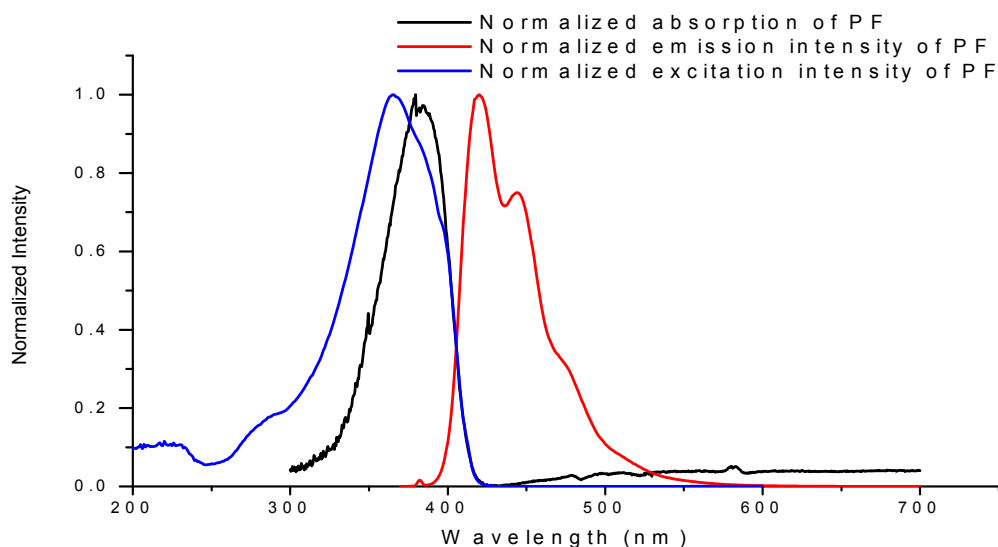
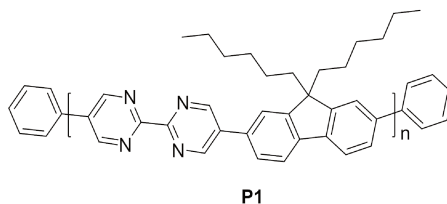


Figure 3-6 Normalized absorption, excitation and emission spectra of PF in DCM

(0.005 mg/mL, slits were 2,2 nm, and for excitation: set $\lambda_{an} = 418$ nm, for emission: set $\lambda_{exc} = 375$ nm)

Above **Figure 3-6** shown that the excitation spectrum (blue) is similar to the absorption spectrum (black) described above, and the main band of the emission spectrum shows two maxima at 418 nm and 444 nm respectively. The maximum of the absorption of **PF** is 380 nm as show above when the concentration is 0.01 mg/mL.

3.1.2 Absorption and PL spectra of P1



We next introduced bipyrimidine (BPM) building blocks for the construction of efficient optical chromophores into conjugated polymers with fluorene derivatives as donor unit. We sought to prepare unsymmetrical electron donor (D) and acceptor (A) moieties. With such type of “push-pull” bichromophoric molecule, we designed and synthesized the novel conjugated polymer by using Suzuki polymerization, labeled **P1**, with alternating D and A groups which we expected to red shifted the emission of polyfluorene.

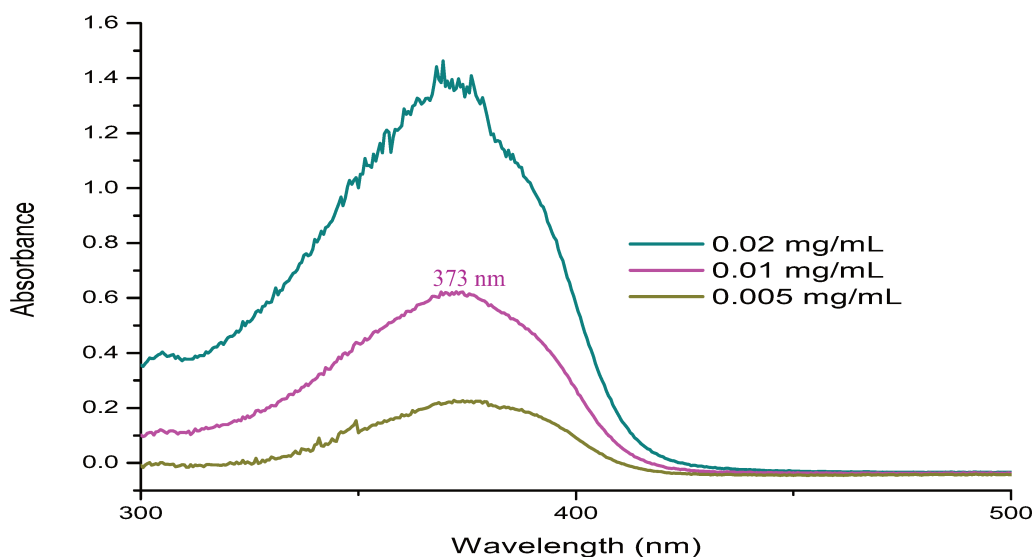


Figure 3-7 Absorption spectra of **P1** in **DCM** in the 0.02-0.005 mg/mL concentration range.

As **Figure 3-7** shows, the polymer **P1** in DCM has a broad absorption ranging from 300 nm to 420 nm and the maximum is around 373 nm attributed to the intramolecular charge transfer (ICT) between the donor and acceptor units,¹⁴⁶ which means that near UV light is a good source of irradiation for the emission. With the increase of the concentration, the absorption intensity is also increasing.

¹⁴⁶ C. V. Kumar, L. Cabau, E. N. Koukaras, S. A. Siddiqui, G. D. Sharma and E. Palomares. *Nanoscale*, **2015**, 7, 7692-7703.

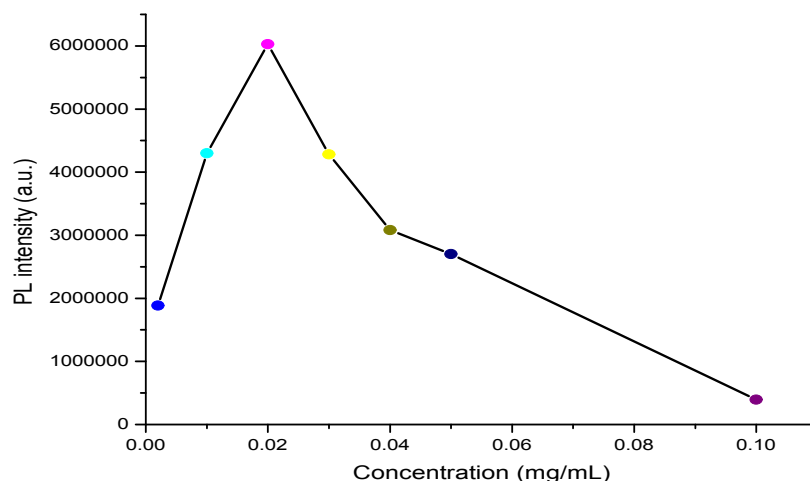


Figure 3-8 Emission intensity of **P1** versus concentration ($\lambda_{\text{exc}} = 375$ nm).

Emission spectra were recorded at different concentration by exciting at the maximum of absorption. The intensity vs concentration is plotted on **Figure 3-8**. It shows that the concentration should be less than 0.02 mg/mL, so that the curve of PL intensity versus concentration is in the linear domain which indicate that there is no aggregation.

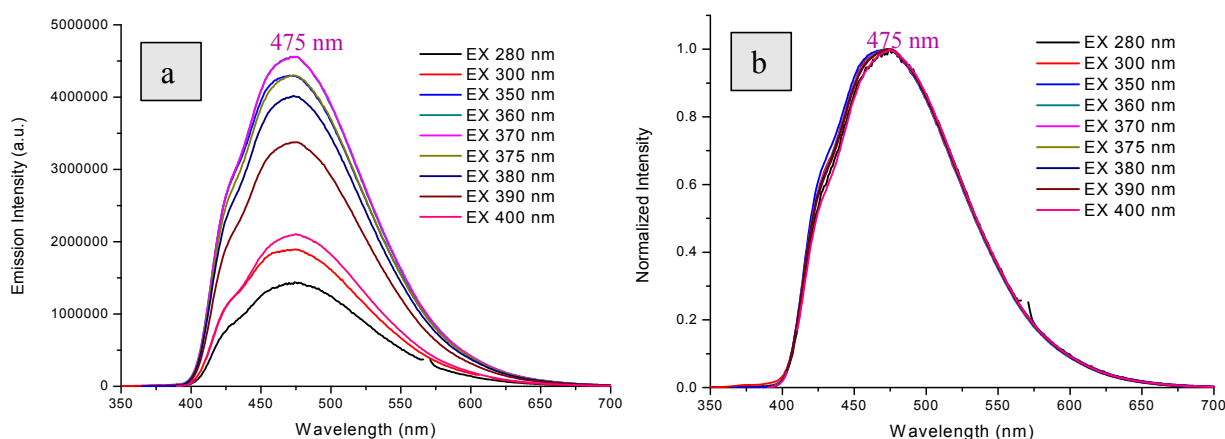


Figure 3-9 a) Emission spectra of **P1** in DCM; b) Corresponding normalized emission spectra. (0.01 mg/mL, slits were 2,2 nm)

The main band of the emission spectrum of **P1** in DCM (0.01 mg/mL) is ranging from 400 nm to 700 nm, and the maximum is 475 nm with different excitations from 280 nm to 400 nm. The normalized emission spectra show identical emission profile despite the intensity changes, suggesting that the prompt fluorescence is originated from the same excited state.¹⁴⁷

¹⁴⁷ P. Li, H. Chan, S.-L. Lai, M. Ng, M.-Y. Chan, and Vivian W. W. Yam. *Angew. Chem. Int. Ed.* **2019**, 10.1002/anie.201903332.

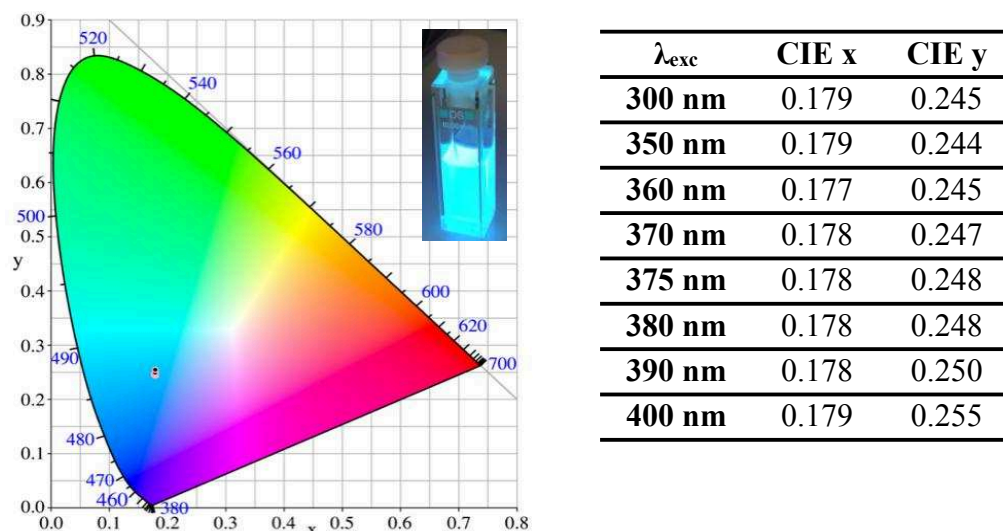


Figure 3-10 CIE coordinates of **P1** in DCM (0.01 mg/mL, slits were 2,2 nm, λ_{exc} = 300-400 nm)

(The inserted photo shows the emission of **P1** in DCM under a 365 nm UV lamp)

The **CIE coordinates** show that the material **emits a greenish blue light** with excitation in the range 300-400 nm.

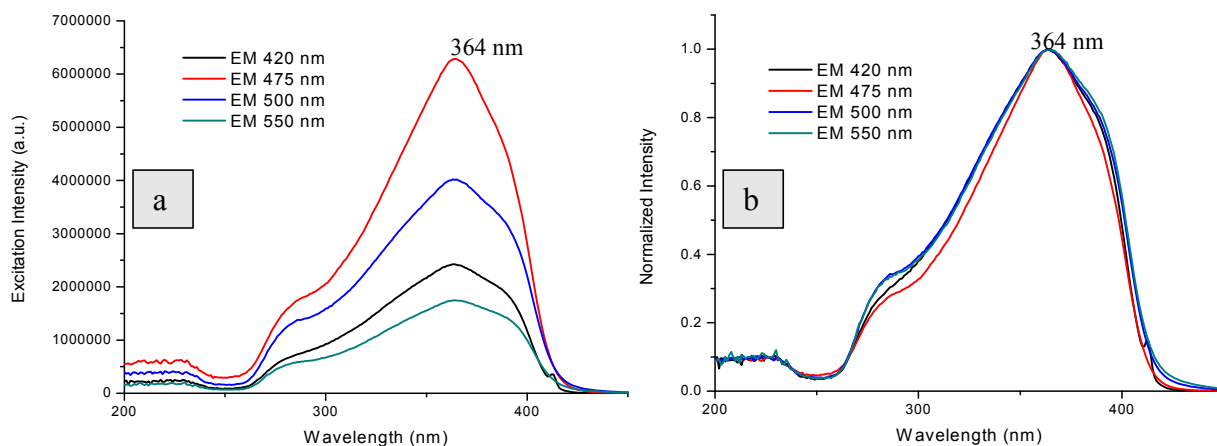


Figure 3-11 a) Excitation spectra of **P1** in DCM; b) Corresponding normalized excitation spectra. (0.01 mg/mL, slits were 2,2 nm)

The main band of the excitation spectrum (**Figure 3-11**) is ranging from 250 nm to 450 nm with a maximum at 364 nm, which also means that the near UV light is a good source of irradiation for the emission. Besides, the excitation bands are the same for different emissions despite the intensity changes.

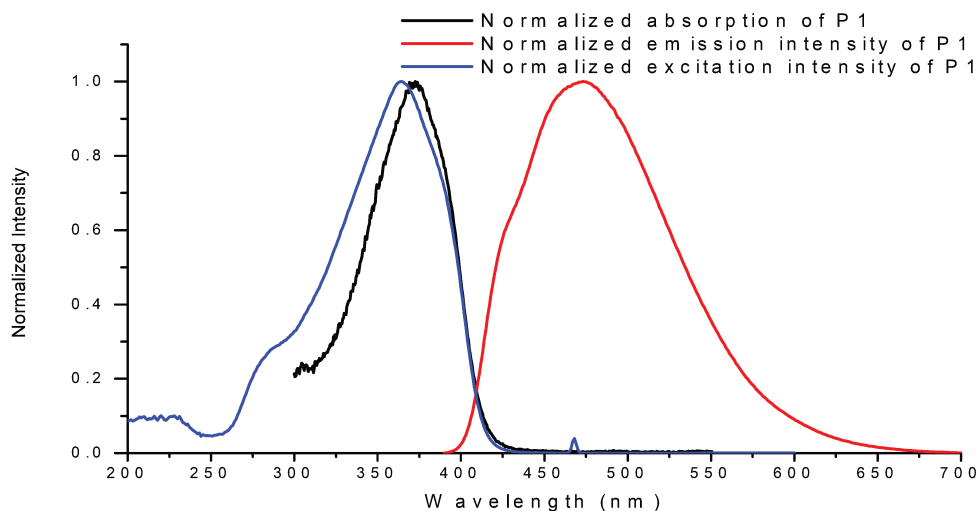
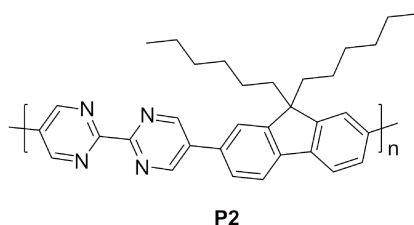


Figure 3-12 Normalized absorption, excitation and emission spectra of **P1** in DCM

(0.01 mg/mL, slits were 2,2 nm, and for excitation: set $\lambda_{an} = 475$ nm, for emission: set $\lambda_{exc} = 375$ nm)

The excitation spectrum (blue) is similar to the absorption spectrum (black) described above, and the main band of the emission spectrum shows a maximum at 475 nm. The maximum of the absorption of **P1** in DCM is 373 nm as shown above when the concentration is 0.01 mg/mL.

3.1.3 Absorption and PL spectra of P2



The non-end-capped polymer, **P2**, was also synthesized, to evaluate if there was any influence of the phenyl end-capping units on the photophysical properties.

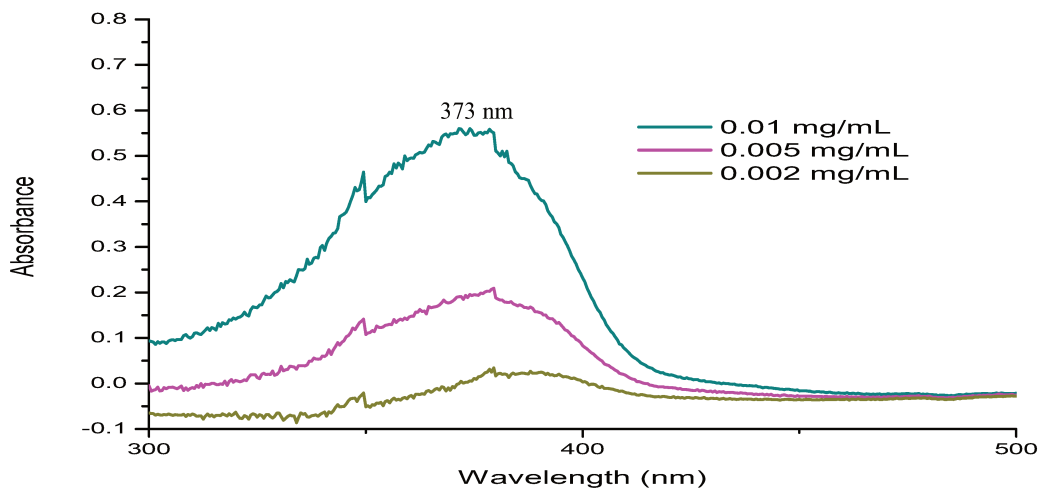
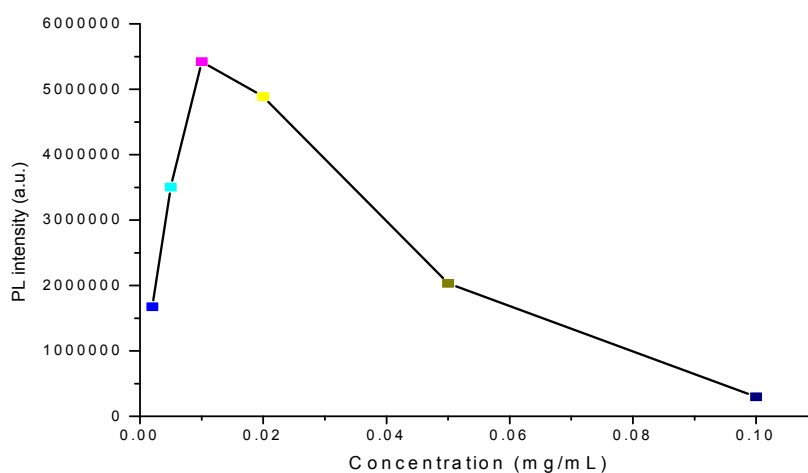
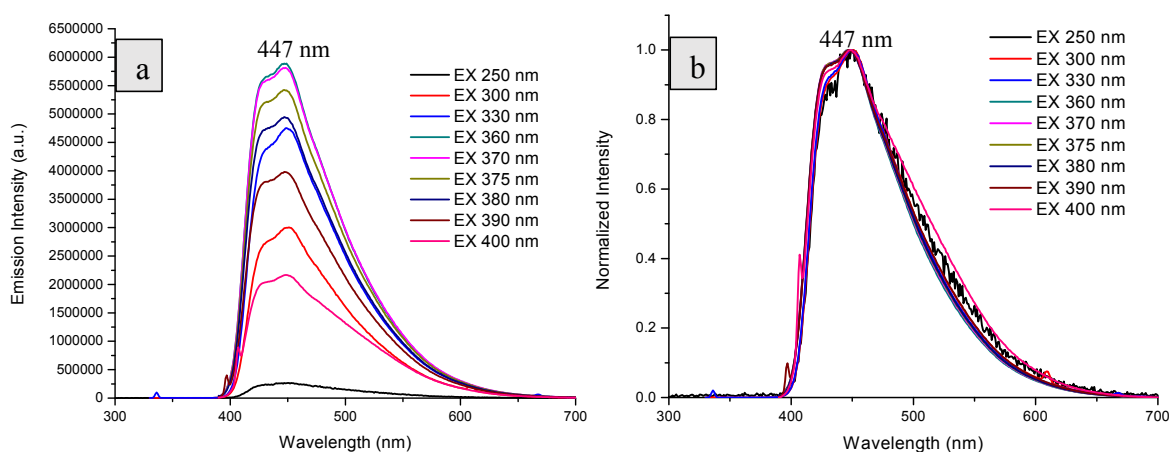


Figure 3-13 Absorption spectra of **P2** in DCM at different concentrations.

As shown on **Figure 3-13**, polymer **P2** in DCM has a broad absorption ranging from 300 nm to 500 nm and the maximum is at 373 nm, which means that the near UV light is a good source of irradiation for the emission. With the increase of the concentration, the absorption intensity is also increasing.

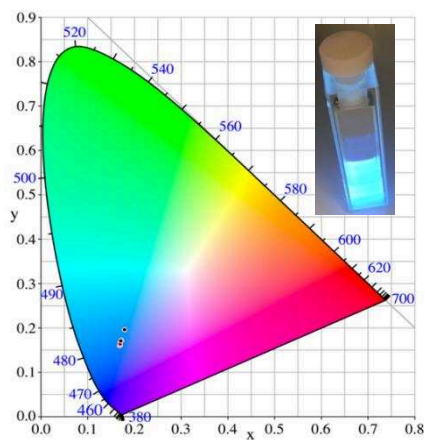
**Figure 3-14** Emission intensity of **P2** versus concentration ($\lambda_{\text{exc}} = 375$ nm).

As **Figure 3-14** shows, for the measurement of this polymer, the concentration should be less than 0.02 mg/mL, so that the curve of PL intensity versus concentration is in the linear domain which indicates that there is no aggregation formed.

**Figure 3-15** a) Emission spectra of **P2** in DCM; b) Corresponding normalized emission spectra. (0.01 mg/mL, slits were 2,2 nm)

The main band of the emission spectrum of **P2** in DCM is ranging from 400 nm to 700 nm, and the maximum is 447 nm with different excitations from 250 nm to 400 nm. The normalized

emission spectra show identical emission profile despite the intensity changes, suggesting that the prompt fluorescence is originated from the same singlet excited state.



λ_{exc}	CIE x	CIE y
300 nm	0.172	0.172
330 nm	0.170	0.168
360 nm	0.168	0.160
370 nm	0.169	0.162
375 nm	0.169	0.163
380 nm	0.170	0.165
390 nm	0.171	0.171
400 nm	0.179	0.196

Figure 3-16 CIE coordinates of **P2** in DCM (0.01 mg/mL, slits were 2,2 nm, $\lambda_{\text{exc}} = 300\text{-}400$ nm) (The inserted photo shows the emission of **P2** in DCM under a 365 nm UV lamp)

The **CIE coordinates** show the material **demonstrated blue light** with excitation at 300-400 nm.

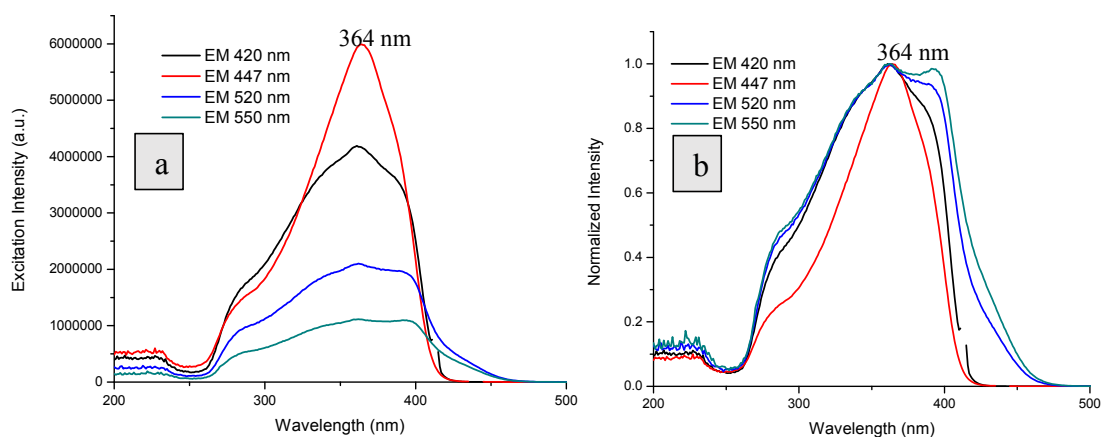


Figure 3-17 a) Excitation spectra of **P2** in DCM; b) Corresponding normalized excitation spectra. (0.01 mg/mL, slits were 2,2 nm)

As shown on **Figure 3-17**, the main band of the excitation spectrum is ranging from 250 nm to 500 nm with a maximum at 364 nm, which also means that the near UV light that we are going to use is a good source of irradiation for the emission. Besides, the excitation bands show similar maxima for different emissions despite the intensity changes.

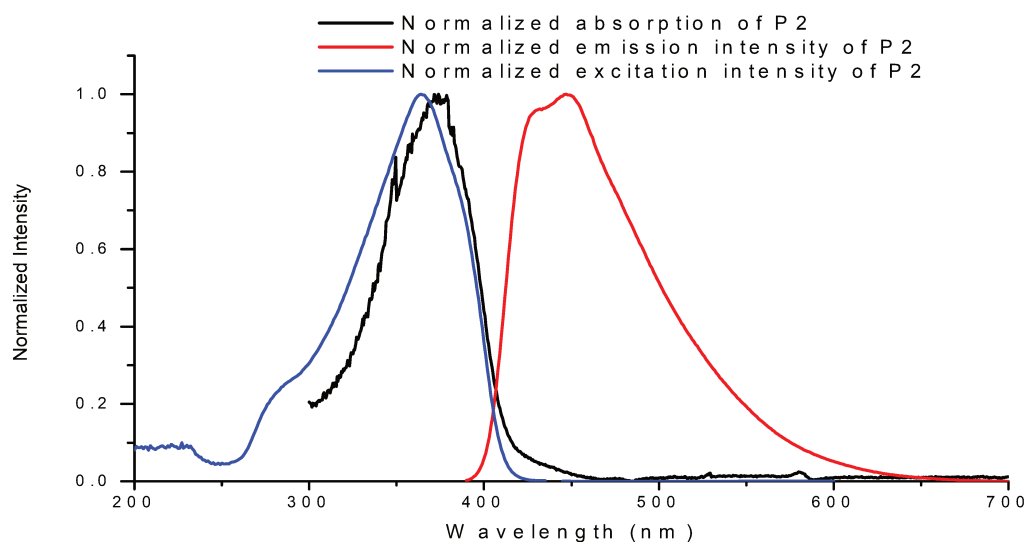
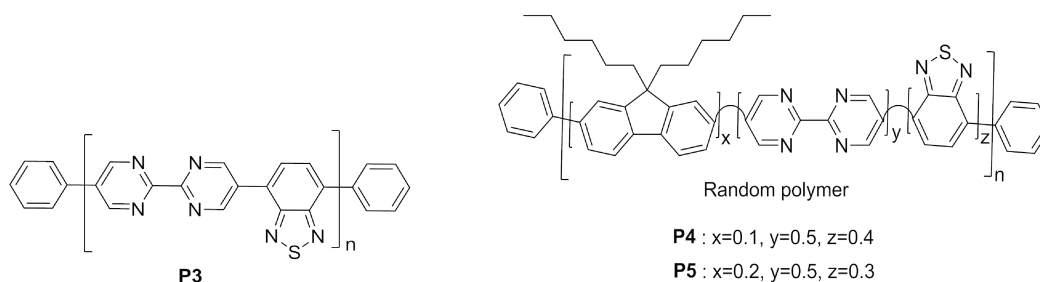


Figure 3-18 Normalized absorption, excitation and emission spectra of **P2** in DCM

(0.01 mg/mL, slits were 2,2 nm, and for excitation: set $\lambda_{an} = 447$ nm, for emission: set $\lambda_{exc} = 375$ nm)

The excitation spectrum (blue) is similar to the absorption spectrum (black) described above, and the main band of the emission spectrum shows a maximum at 447 nm. The maximum of the absorption of **P2** is 373 nm as shown above when the concentration is 0.01 mg/mL.

3.1.4 Absorption and PL spectra of P5



It has been reported that main chain engineering with changing π -conjugated bridges can effectively tune the electronic energy levels of the conjugated polymers.¹⁴⁸ Thus, we synthesized **P3**, which contains the benzo[c][1,2,5]thiadiazole group as donor unit instead of the fluorene derivatives. We expected it to be a new potential green-emitting polymer. Unfortunately, the isolated product was found to have a very low solubility. This may be due to the strong π -stacking between the polymer chains that decreased the solubility. Thus we introduced the fluorene unit with alkyl chains to polymers as bulky substituents to avoid the strong π -stacking between the polymer chains, depicted as **P4**, and we hoped to increase the solubility. The result turned out

¹⁴⁸ T. Yan, H. Bin, Y. Yang, L. Xue, Z. Zhang & Y. Li. *Science China Chemistry*, **2017**, 60(4): 537-544.

that **P4**, in which 10% of 2,2'-(9,9-dioctyl-9H-fluorene-2,7-diyl)bis(1,3,2-dioxaborinane) was introduced into the polymer backbone, was obtained with a low yield. Thus we further increased the proportion of 2,2'-(9,9-dioctyl-9H-fluorene-2,7-diyl)bis(1,3,2-dioxaborinane) up to 20% for the synthesis of **P5** for limiting the strong π -stacking between the polymer chains. Consequently, a yield of 8% was obtained for **P5**.

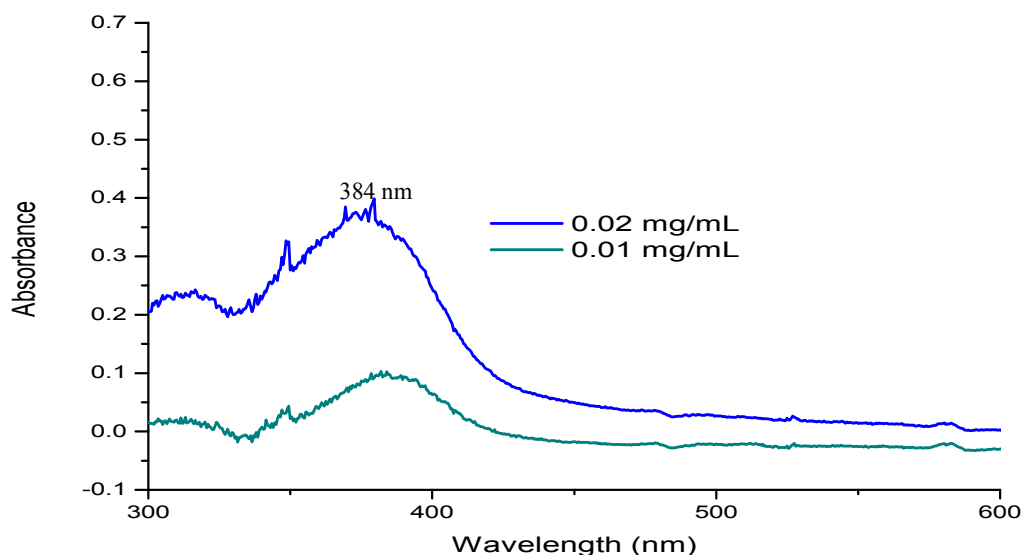


Figure 3-19 Absorption spectra of **P5** in DCM at different concentrations.

As shown on **Figure 3-19**, polymer **P5** in DCM has a broad absorption ranging from 300 nm to 600 nm and the maximum is around 384 nm, which means that the near UV light is a good source of irradiation for the emission. With the increase of the concentration, the absorption intensity is also increasing.

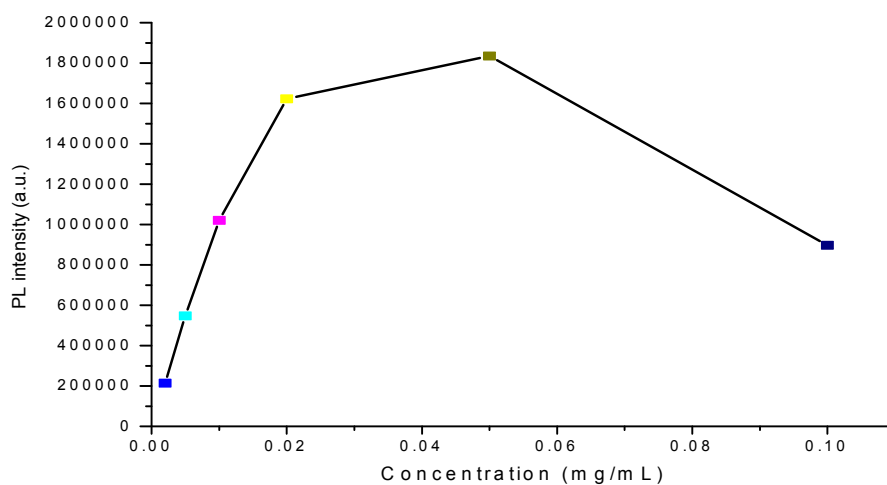


Figure 3-20 Emission intensity of **P5** versus concentration ($\lambda_{\text{exc}} = 375 \text{ nm}$).

As shown in **Figure 3-20**, for the measurement of this polymer, the concentration should also be less than 0.02 mg/mL to avoid any aggregation.

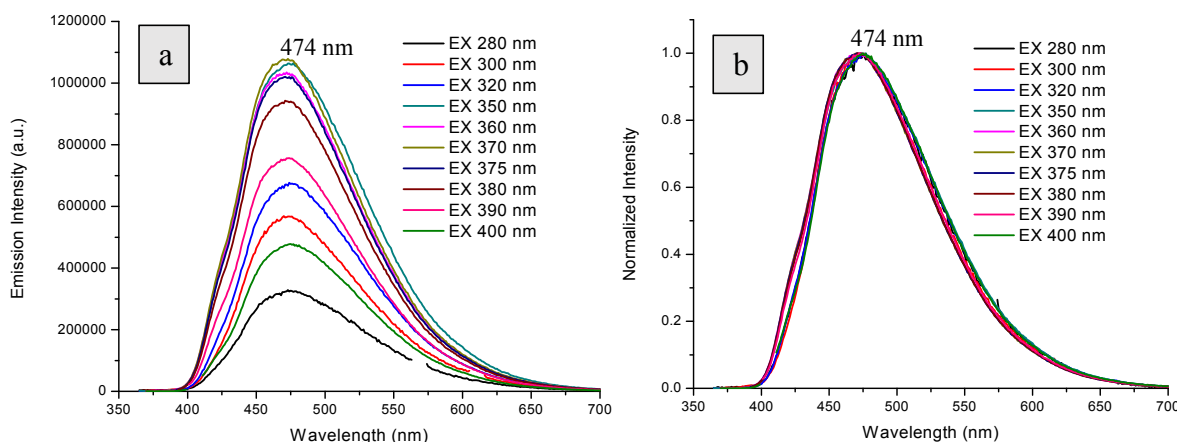
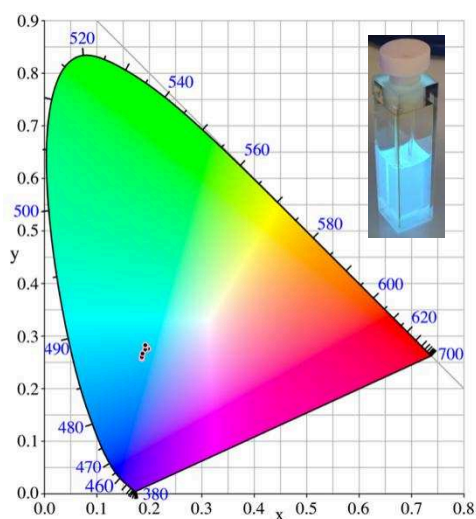


Figure 3-21 a) Emission spectra of **P5** in DCM; b) Corresponding normalized emission spectra. (0.01 mg/mL, slits were 2,2 nm)

The main band of the emission spectrum of **P5** in DCM (**Figure 3-21**) is ranging from 400 nm to 700 nm, and the maximum is 474 nm with different excitations from 280 nm to 400 nm. The normalized emission spectra show identical emission profile despite the intensity changes, suggesting that the prompt fluorescence is originating from the same excited state.



λ_{exc}	CIE x	CIE y
300 nm	0.197	0.276
320 nm	0.194	0.282
350 nm	0.192	0.275
360 nm	0.186	0.259
370 nm	0.185	0.258
375 nm	0.185	0.259
380 nm	0.186	0.260
390 nm	0.187	0.266
400 nm	0.192	0.283

Figure 3-22 CIE coordinates of **P5** in DCM (0.01 mg/mL, slits were 2,2 nm, λ_{exc} = 300-400 nm)

(The inserted photo shows the emission of **P5** in DCM under a 365 nm UV lamp)

The **CIE coordinates** show that the material **emits a greenish blue light** under excitation at 300-400 nm.

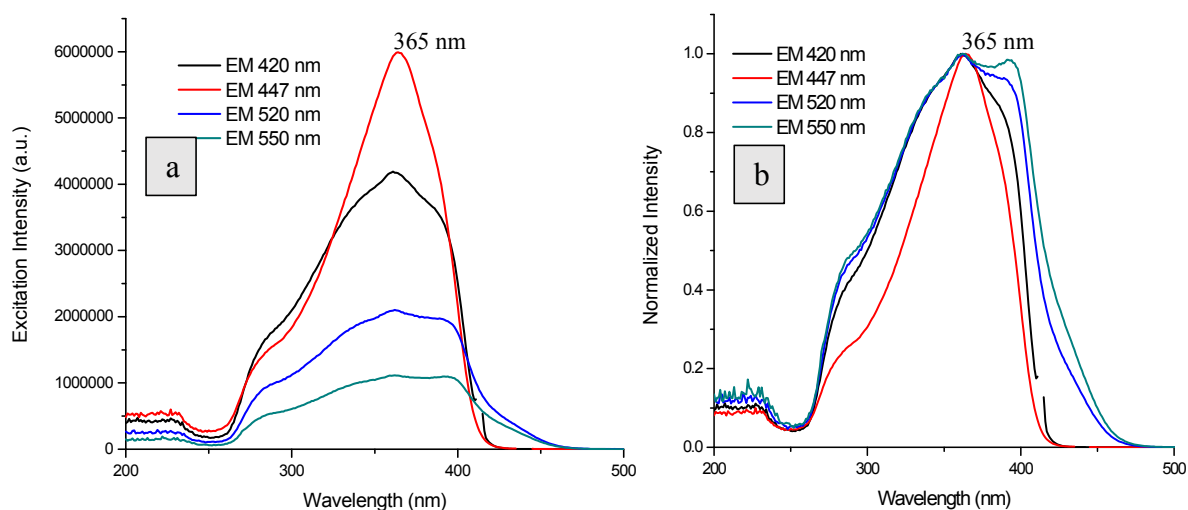


Figure 3-23 a) Excitation spectra of **P5** in **DCM**; b) Corresponding normalized excitation spectra. (0.01 mg/mL, slits were 2,2 nm)

As shown on **Figure 3-23**, the main band of the excitation spectrum is ranging from 250 nm to 500 nm with a maximum at 365 nm and a shoulder at 300 nm, which also means that the near UV light is a good source of irradiation for the emission.

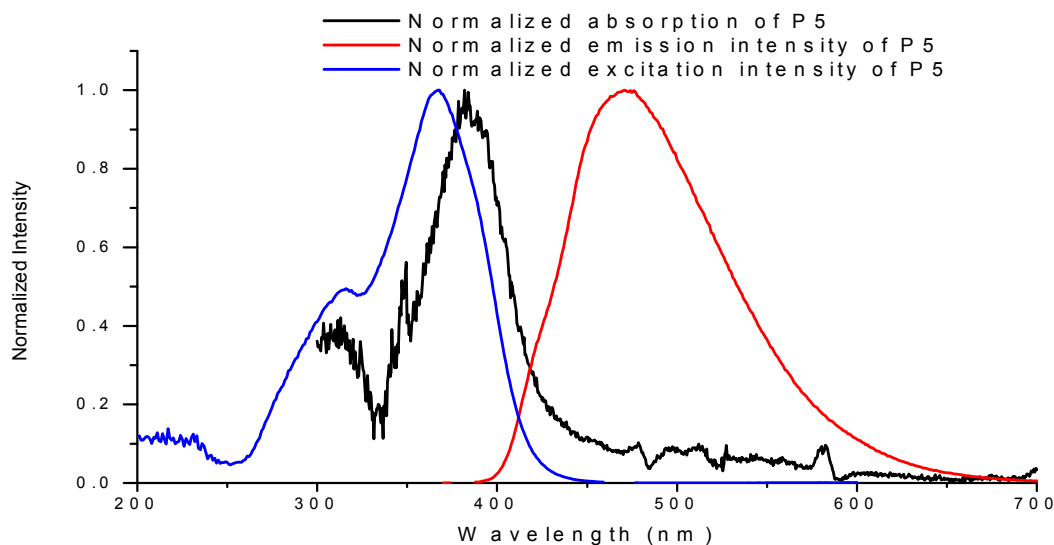
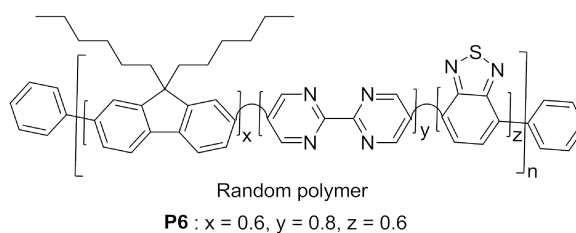


Figure 3-24 Normalized absorption, excitation and emission spectra of **P5** in **DCM**

(0.01 mg/mL, slits were 2,2 nm, and for excitation: set $\lambda_{an} = 474$ nm, for emission: set $\lambda_{exc} = 375$ nm)

The excitation spectrum (blue) is similar to the absorption spectrum (black) described above, and the main band of the emission spectrum shows a maximum at 474 nm. The maximum of the absorption of **P5** is 384 nm as show above when the concentration is 0.01 mg/mL.

3.1.5 Absorption and PL spectra of P6



To further increase the solubility of the polymer and to promote the production efficiency, we designed and synthesized a random copolymer, **P6**, with lower amounts of benzo[c][1,2,5]thiadiazole unit and bipyrimidine. 30% of the 2,2'-(9,9-dioctyl-9H-fluorene-2,7-diyl)bis(1,3,2-dioxaborinane) moiety was introduced into the polymer.

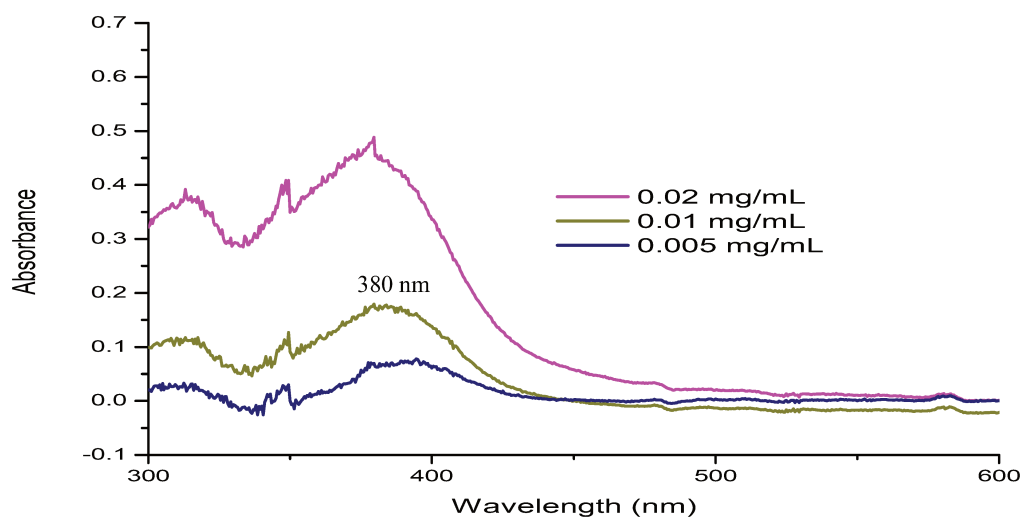


Figure 3-25 Absorption spectra of **P6** in DCM at different concentrations.

As **Figure 3-25** shows, polymer **P6** in DCM has a broad absorption ranging from 300 nm to 600 nm and the maximum is around 380 nm for 0.01 mg/mL, which means that near UV light is an efficient source of irradiation for the emission. With the increase of the concentration, the absorption intensity is also increasing.

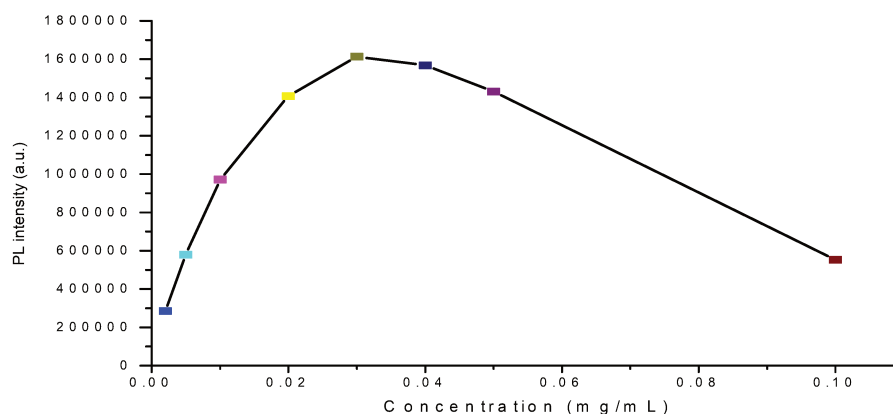


Figure 3-26 Emission intensity of **P6** versus concentration ($\lambda_{\text{exc}} = 375 \text{ nm}$).

As **Figure 3-26** shows, the concentration should be lower than 0.03 mg/mL to be in the linear domain of the PLintensity/concentration curve.

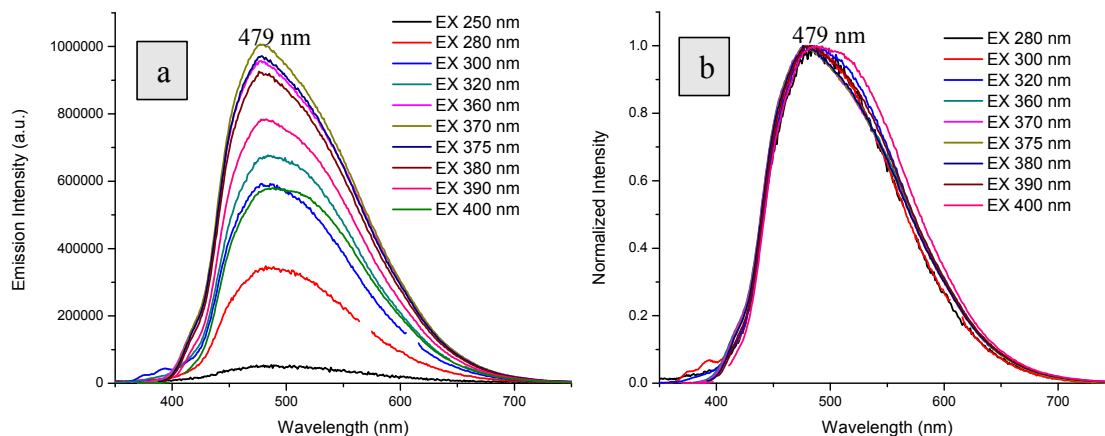
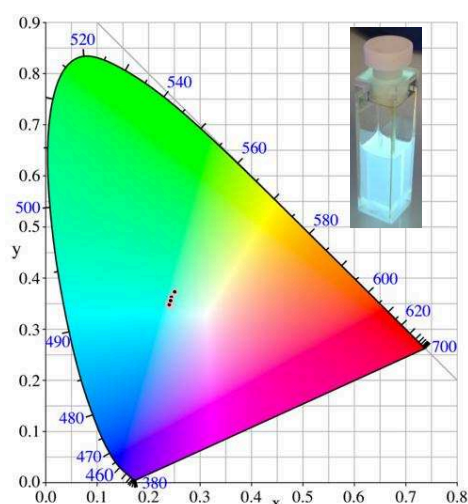


Figure 3-27 a) Emission spectra of **P6** in DCM; b) Corresponding normalized emission spectra. (0.01 mg/mL, slits were 2,2 nm)

The main band of the emission spectrum of **P6** in DCM is ranging from 400 nm to 700 nm, and the maximum is 479 nm with different excitations from 250 nm to 400 nm. The normalized emission spectra show identical emission profile despite the intensity changes, suggesting that the prompt fluorescence is originating from the same excited state.



λ_{exc}	CIE x	CIE y	CCT (Kelvin)
300 nm	0.239	0.351	10614
320 nm	0.244	0.362	9912
360 nm	0.242	0.346	10572
370 nm	0.240	0.345	10763
375 nm	0.240	0.346	10743
380 nm	0.240	0.348	10659
390 nm	0.243	0.356	10158
400 nm	0.251	0.374	9203

Figure 3-28 CIE coordinates of **P6** in DCM (0.01 mg/mL, slits were 2,2 nm, $\lambda_{\text{exc}} = 300\text{-}400 \text{ nm}$) (The inserted photo shows the emission of **P6** in DCM under a 365 nm UV lamp)

The **CIE coordinates** show that the material emits a **green light** under excitation at 300-400 nm.

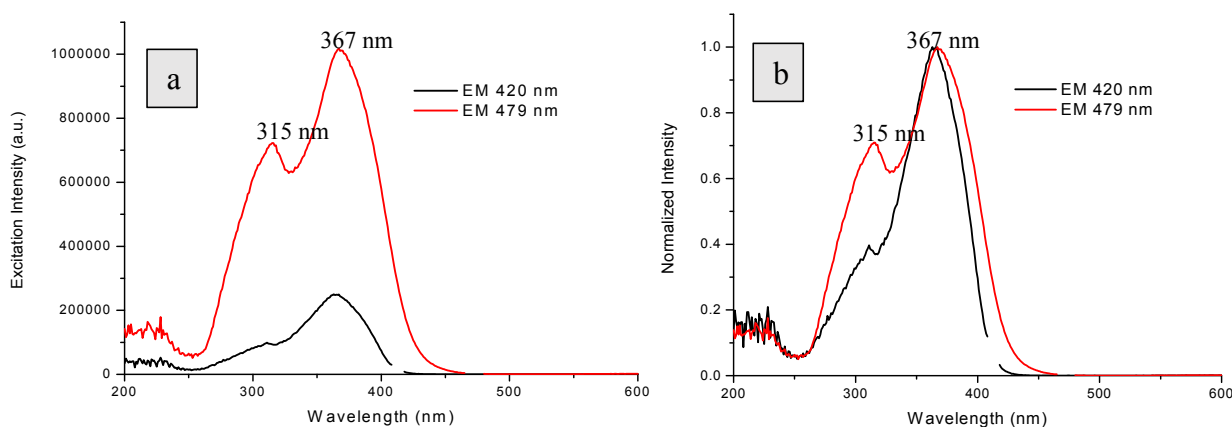


Figure 3-29 a) Excitation spectra of **P6** in DCM; b) Corresponding normalized excitation spectra. (0.01 mg/mL, slits were 2,2 nm)

As shown on **Figure 3-29**, the main band of the excitation spectrum is ranging from 250 nm to 450 nm with two maxima at 315 nm and 367 nm respectively, which also means that the near UV light is a good source of irradiation for the emission. Besides, when the emission wavelength increased, the maximum at 367 nm was decreased comparing with the maximum at 315 nm.

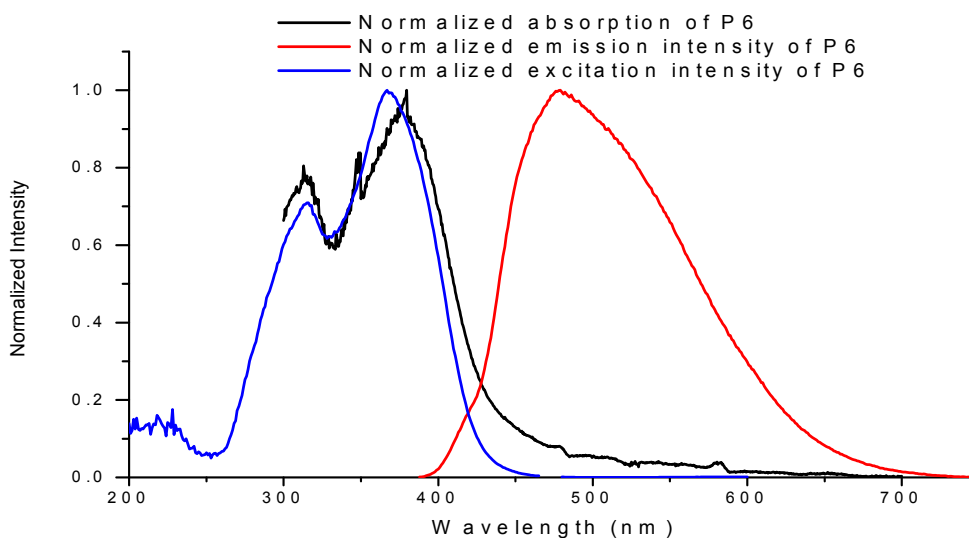
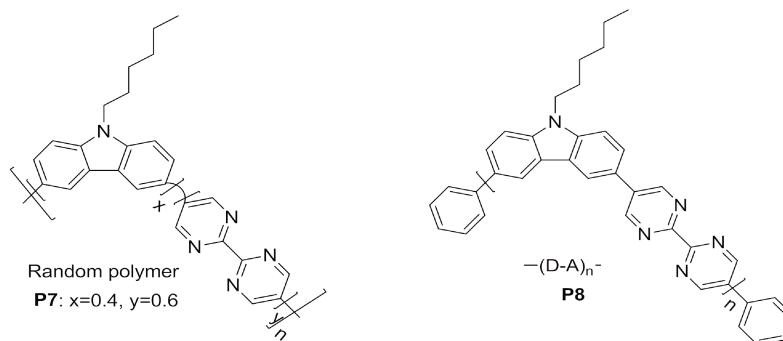


Figure 3-30 Normalized absorption, excitation and emission spectra of **P6** in DCM

(0.01 mg/mL, slits were 2,2 nm, and for excitation: set $\lambda_{an} = 479$ nm, for emission: set $\lambda_{exc} = 375$ nm)

The excitation spectrum (blue) is similar to the absorption spectrum (black) described above, and the main band of the emission spectrum shows a maximum at 479 nm. The maximum of the absorption of **P6** is 380 nm as show above when the concentration is 0.01 mg/mL.

3.1.6 Absorption and PL spectra of P8



Above we have successfully developed a series of conjugated polymers incorporating both the bipyrimidine and the fluorene units in their backbone, either in an alternating form or in a random arrangement. Unfortunately, and as it will be discussed in part §4.2 of Chapter IV, it has been shown at Clermont Ferrand Institute of Chemistry (ICCF) that the polyfluorene derivatives are not stable under UV light. In order to increase the photostability of the polymers, two strategies can be investigated: i) using UV-absorbing molecules to protect the emitters;¹⁴⁹ and ii) synthesizing emitting polymers without fluorene units, instead, introducing units with better photostability.¹⁵⁰ The first strategy mentioned here could result in the decrease of the emission intensity as well as a part of the UV light used to excite the compounds will be absorbed by the UV absorber. Therefore, the way to design other units instead of fluorene has been preferred in this work.

Among many others, carbazole derivatives were reported to possess a better photostability compared to fluorene units and therefore were widely applied as a donor units either in light-emitting diodes and polymeric solar cells. The advantage of carbazole over fluorene or other heterofluorene derivatives is that the nitrogen atom provides a lone electron pair that gives a fully aromatic structure and therefore, a better stability.¹⁵¹

Based on the above result found in the literature, we introduced carbazole as an electron-rich unit in the structure of the polymers. The new random and alternating polymers **P7** and **P8** comprising 3,6-carbazole and BPM units, respectively, were thus synthesized.

¹⁴⁹ G.R. Ferreira, B. Nowacki, A. Magalhães, E.R. deAzevedo, E.L. de Sá, L.C. Akcelrud, R.F. Bianchi, *Mater. Chem. Phys.* **2014**, *146*, 212–217.

¹⁵⁰ M. Manceau, E. Bundgaard, J. E. Carle, O. Hagemann, M. Helgesen, R. Søndergaard, M. Jørgensen, F. C. Krebs, *J. Mater. Chem.*, **2011**, *21*, 4132–4141.

¹⁵¹ a. M. Manceau, E. Bundgaard, F. C. Krebs et al. *J. Mater. Chem.*, **2011**, *21*, 4132.

b. W. ZHUANG. Design, Synthesis and Modelling of Conjugated Polymers for Organic Photovoltaics. THESIS FOR THE DEGREE OF DOCTOR OF PHILOSOPHY. CHALMERS UNIVERSITY OF TECHNOLOGY. **2013**.

c. M. Wang, M. J. Ford, C. Zhou, M. Seifrid, T. Nguyen, and G. C. Bazan. *J. Am. Chem. Soc.*, **2017**, *139* (48), 17624–17631.

d. P.-L. T. Boudreault, S. Beaupre and M. Leclerc. *Polym. Chem.*, **2010**, *1*, 127–136.

e. A. Sergent, G. Zucchi, R. B. Pansu, M. Chaigneau, B. Geffroy, D. Tondelier and M. Ephritikhine. *J. Mater. Chem. C*, **2013**, *1*, 3207–3216.

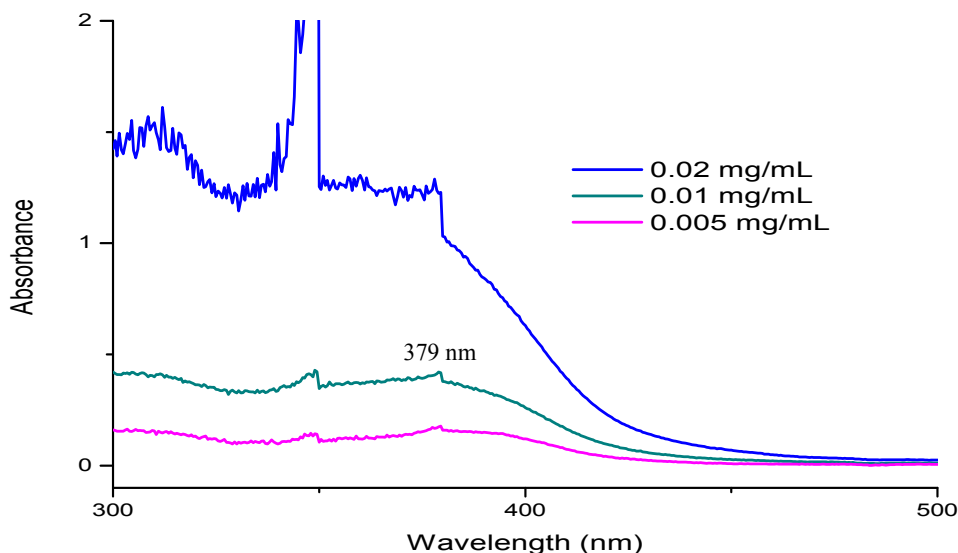


Figure 3-31 Absorption spectra of **P8** in **DCM** at different concentrations.

As **Figure 3-31** shows, polymer **P8** in DCM has a broad absorption ranging from 300 nm to 500 nm and the maximum is around 379 nm when the concentration is 0.01 mg/mL, which means that near UV light is a good source of irradiation for the emission.

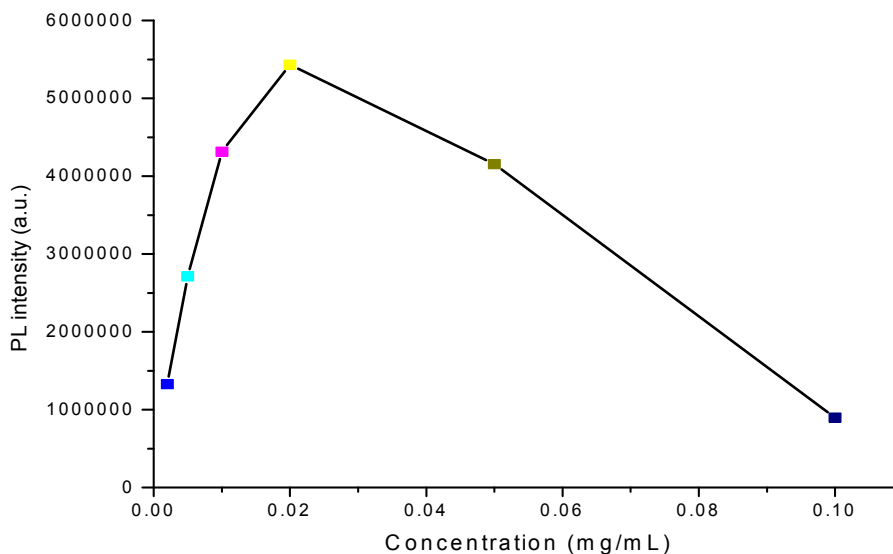


Figure 3-32 Emission intensity of **P8** versus concentration ($\lambda_{\text{exc}} = 375 \text{ nm}$).

Figure 3-32 shows that measurements should be done at a concentration lower than 0.02 mg/mL, so that the curve of PL intensity versus concentration is in the linear domain which indicates that there is no aggregation.

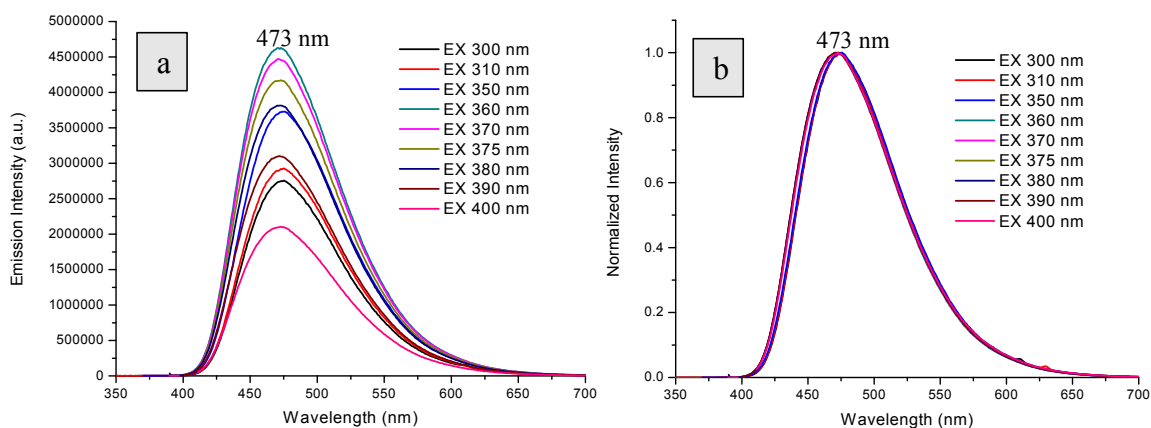
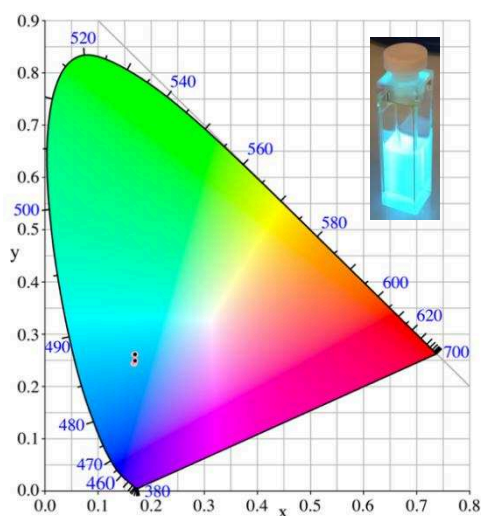


Figure 3-33 a) Emission spectra of **P8** in **DCM**; b) Corresponding normalized emission spectra. (0.01 mg/mL, slits were 2,2 nm)

The main band of the emission spectrum of **P8** in **DCM** is ranging from 400 nm to 700 nm, and the maximum is 473 nm with different excitations from 300 nm to 400 nm. The normalized emission spectra show an identical emission profile despite the intensity changes, suggesting that the prompt fluorescence is originating from the same excited state.



λ_{exc}	CIE x	CIE y
300 nm	0.169	0.261
310 nm	0.169	0.261
350 nm	0.170	0.262
360 nm	0.167	0.244
370 nm	0.168	0.245
375 nm	0.168	0.245
380 nm	0.168	0.246
390 nm	0.168	0.247
400 nm	0.170	0.249

Figure 3-34 CIE coordinates of **P8** in **DCM** (0.01 mg/mL, slits were 2,2 nm, λ_{exc} = 300-400 nm) (The inserted picture shows the emission of **P8** in **DCM** under a 365 nm UV lamp)

The **CIE coordinates** show that the material emits a **greenish blue light** under excitation at 300-400 nm.

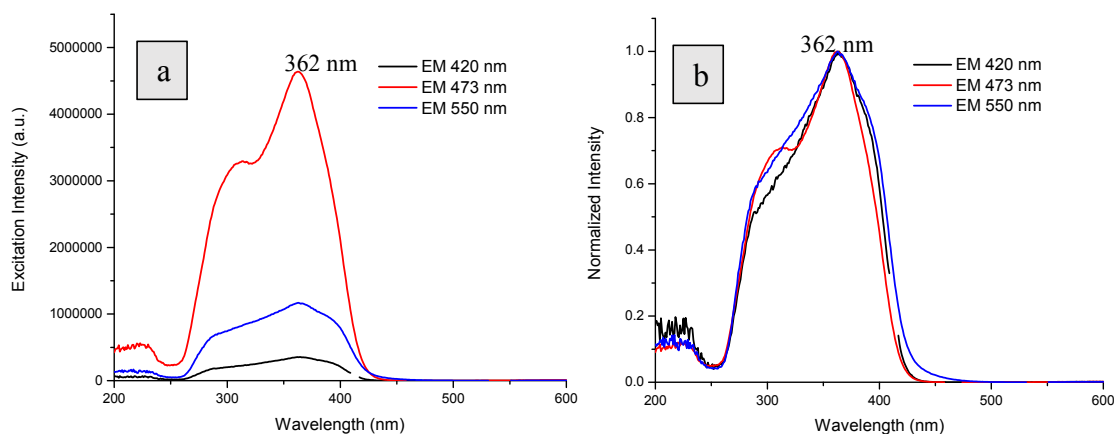


Figure 3-35 a) Excitation spectra of **P8** in DCM; b) Corresponding normalized excitation spectra. (0.01 mg/mL, slits were 2,2 nm)

As shown, the main band of the excitation spectrum is ranging from 250 nm to 500 nm with a maximum at 362 nm, which also means that the near UV light is a good source of irradiation for the emission.

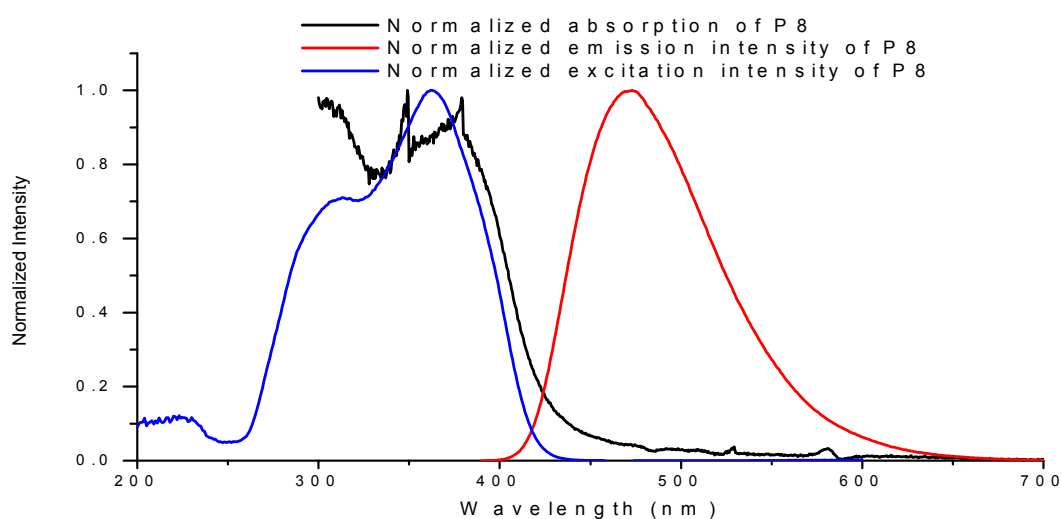
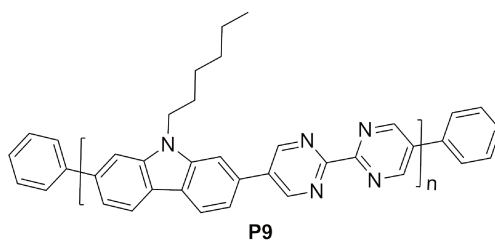


Figure 3-36 Normalized absorption, excitation and emission spectra of **P8** in DCM

(0.01 mg/mL, slits were 2,2 nm, and for excitation: set $\lambda_{an} = 473$ nm, for emission: set $\lambda_{exc} = 375$ nm)

The excitation spectrum (blue) is similar to the absorption spectrum (black) described above, and the main band of the emission spectrum shows a maximum at 473 nm. The maximum of the absorption of **P8** is 379 nm as show above when the concentration is 0.01 mg/mL.

3.1.7 Absorption and PL spectra of P9



In order to probe the influence of the branching points of the carbazole unit on the photophysical properties (see **Chapter IV**), we designed and synthesized the corresponding **P9** polymer with the carbazole unit branched at the 2 and 7 positions. In particular, as reported,¹⁵² 2,7-carbazole units can generate more linear polymers that may lead to a higher conjugation length. (See **Figure 3-37**) Thus, a decrease of the bandgap of the polymers could be expected and thus a red-shift of the emission. As a matter of fact, since the first synthesis of 2,7-functionalized carbazoles was performed in 1951 by Smith and Brown,¹⁵³ both the synthesis and the application of this class of units have been widely investigated for electro-optic devices, such as organic light-emitting diodes (OLEDs)^{142,154} and organic photovoltaics.^{151,155}

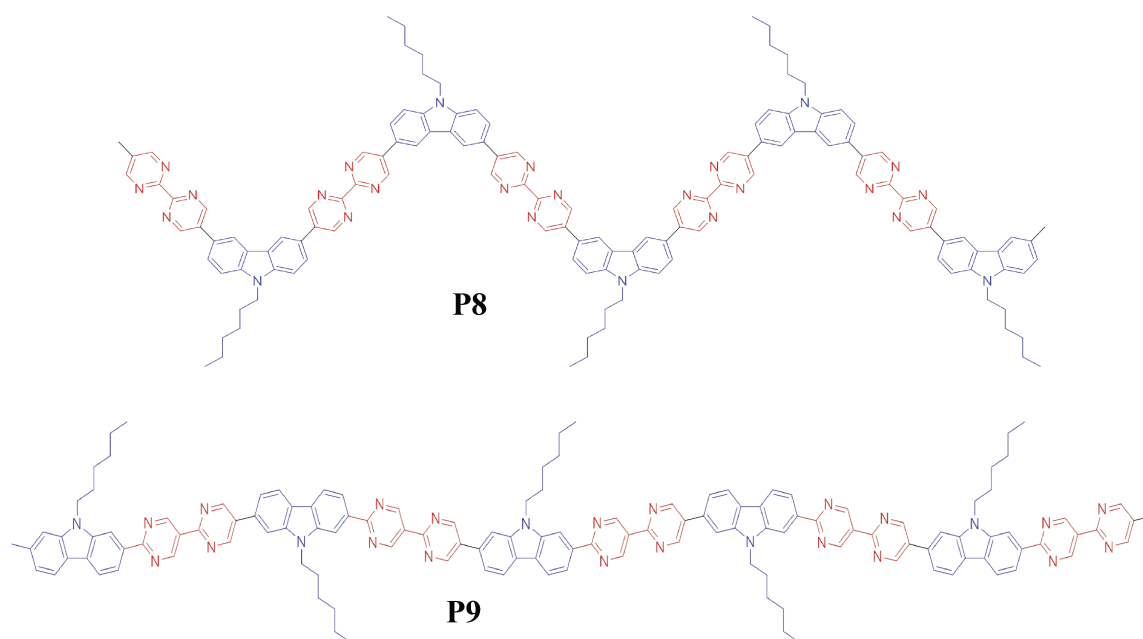


Figure 3-37 The possible conformations of chains of **P8** and **P9**.

¹⁵² P.-L. T. Boudreault, S. Beaupre and M. Leclerc. *Polym. Chem.*, **2010**, 1, 127-136.

¹⁵³ a. P. A. S. Smith, and B. B. Brown. *J. Am. Chem. Soc.*, **1951**, 73(6): 2435-2437.

b. P. A. S. Smith, and B. B. Brown. *J. Am. Chem. Soc.*, **1951**, 73 (6): 2438-2441.

¹⁵⁴ a. G. Hu, S. P. Kitney, S. M. Kelly, W. Harrison & M. O'Neill. *Liquid Crystals*, **2017**, 44 (11): 1632-1645.

b. V. Joseph, K. R. J. Thomas, S. Sahoo, M. Singh, *ACS Omega*, **2018**, 3, 16477-16488.

¹⁵⁵ I. Etxebarria, J. Ajuria, and R. Pacios. *J. of Photonics for Energy*, **2015**, 5(1), 057214.

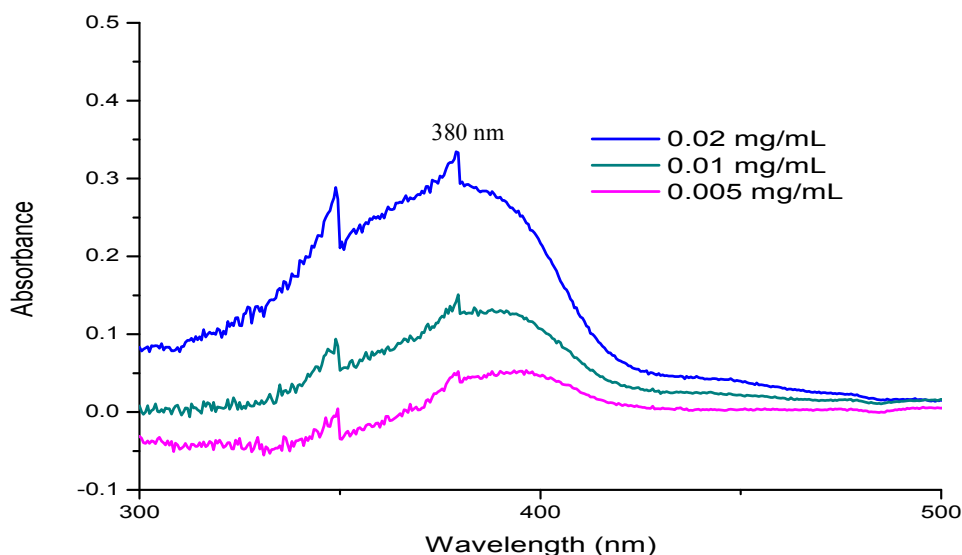


Figure 3-38 Absorption spectra of **P9** in **DCM** at different concentrations.

As **Figure 3-38** shows, the polymer **P9** in DCM has a broad absorption ranging from 300 nm to 600 nm and the maximum is around 380 nm, which means that the near UV light is a convenient source of irradiation for **P9**. With the increase of the concentration, the absorption intensity is also increasing.

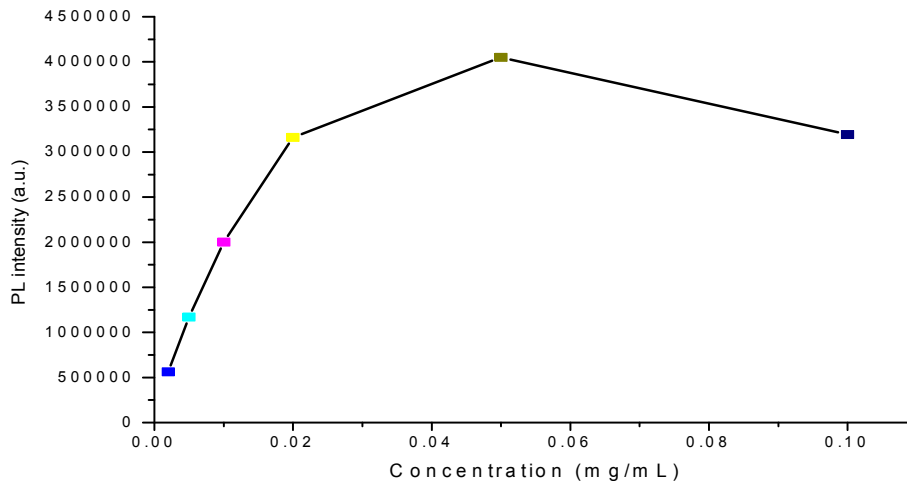


Figure 3-39 Emission intensity of **P9** versus concentration ($\lambda_{\text{exc}} = 375 \text{ nm}$).

Figure 3-39 shows that the concentration should be lower than 0.02 mg/mL, so that the curve of PL intensity versus concentration is in the linear domain which indicates that there is no aggregation.

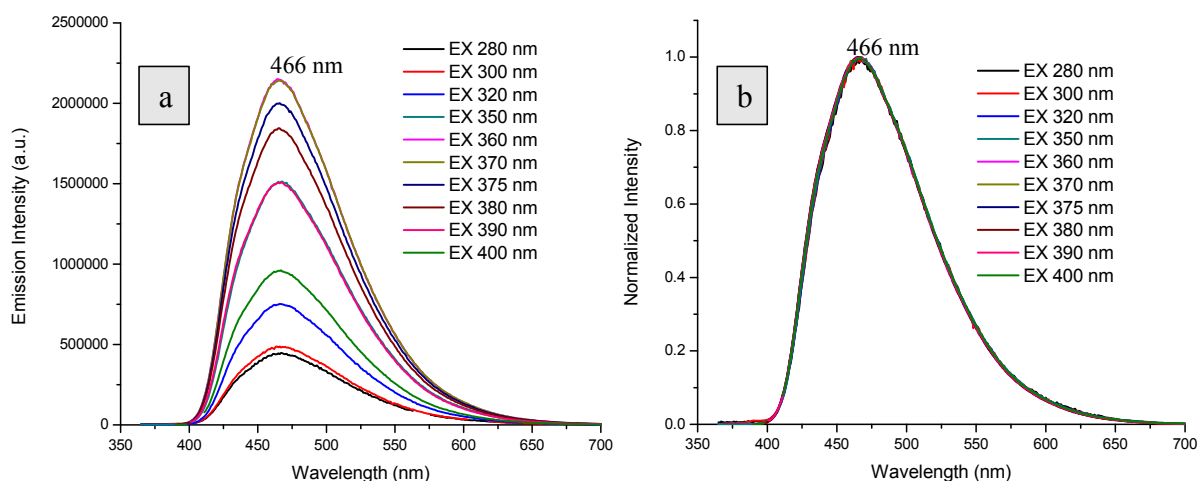
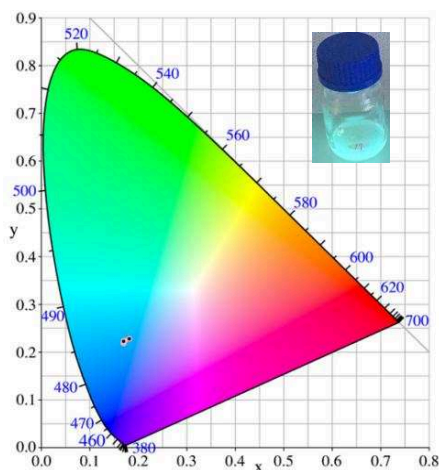


Figure 3-40 a) Emission spectra of **P9** in DCM; b) Corresponding normalized emission spectra. (0.01 mg/mL, slits were 2,2 nm)

The main band of the emission spectrum of **P9** in DCM is ranging from 400 nm to 700 nm, and the maximum is 466 nm with different excitations from 280 nm to 400 nm (**Figure 3-40**). The normalized emission spectra show identical emission profile despite the intensity changes, suggesting that the fluorescence of **P9** is originating from the same excited state whatever the excitation wavelength is used.



λ_{exc}	CIE x	CIE y
300 nm	0.182	0.228
320 nm	0.172	0.225
350 nm	0.170	0.225
360 nm	0.169	0.218
370 nm	0.169	0.219
375 nm	0.169	0.220
380 nm	0.169	0.220
390 nm	0.169	0.220
400 nm	0.170	0.222

Figure 3-41 CIE coordinates of **P9** in DCM (0.01 mg/mL, slits were 2,2 nm, λ_{exc} = 300-400 nm) (The inserted photo shows the emission of **P9** in DCM under a 365 nm UV lamp)

The **CIE coordinates** (**Figure 3-41**) show the material **emits a greenish blue light** under excitation at 300-400 nm.

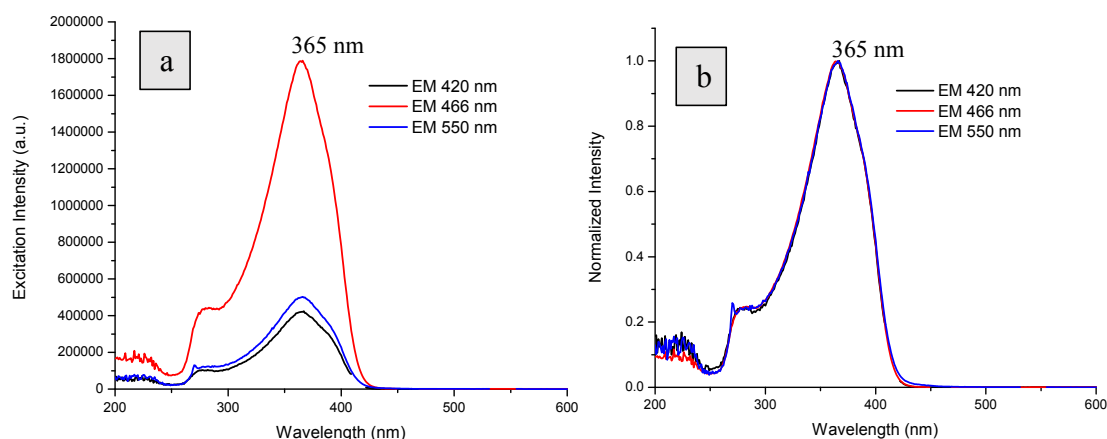


Figure 3-42 a) Excitation spectra of **P9** in DCM; b) Corresponding normalized excitation spectra. (0.01 mg/mL, slits were 2,2 nm).

As shown on **Figure 3-42**, the main band of the excitation spectrum is ranging from 250 nm to 450 nm with a maximum at 365 nm, which also means that the near UV light is a convenient source of irradiation. Besides, the excitation bands are identical for different emissions despite the intensity changes.

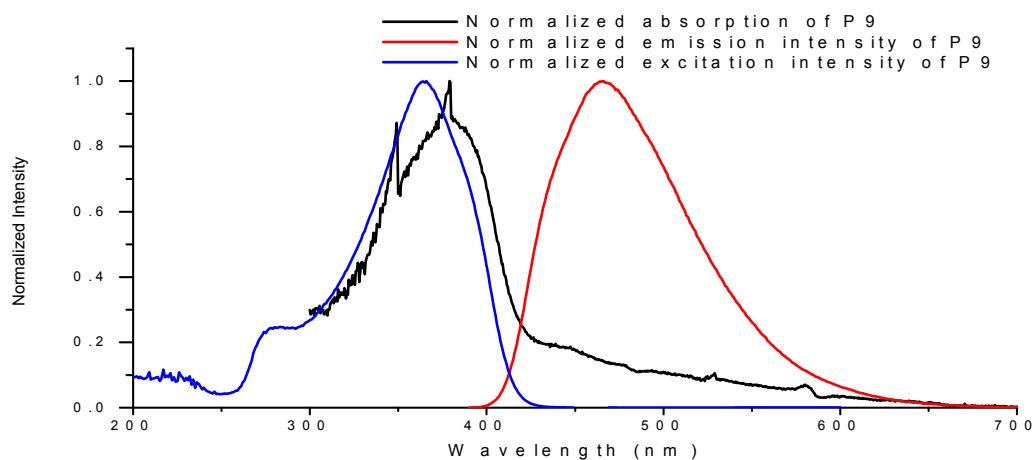
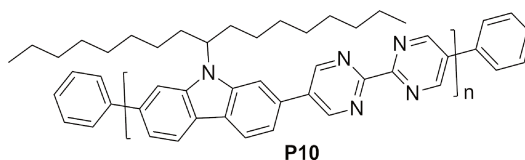


Figure 3-43 Normalized absorption, excitation and emission spectra of **P9** in DCM

(0.01 mg/mL, slits were 2,2 nm, and for excitation: set $\lambda_{an} = 466$ nm, for emission: set $\lambda_{exc} = 375$ nm)

The excitation spectrum (**Figure 3-43**, blue trace) is similar to the absorption spectrum (black trace) described above, and the main band of the emission spectrum shows a maximum at 466 nm. The maximum of the absorption of **P9** is 380 nm as shown above when the concentration is 0.01 mg/mL.

3.1.8 Absorption and PL spectra of P10



For the purpose of improving the solubility of the polymer, we further designed the alternating donor-acceptor conjugated polymer (**P10**) with bulkier side-chains, compared to **P9**.

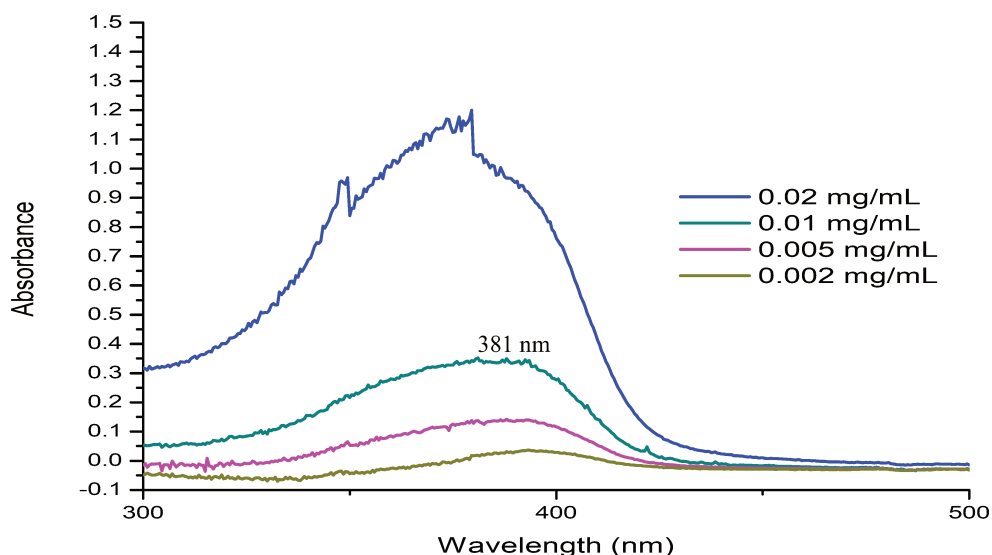


Figure 3-44 Absorption spectra of **P10** in DCM at different concentrations.

As shown on **Figure 3-44**, polymer **P10** in DCM has a broad absorption ranging from 300 nm to 500 nm and the maximum is around 381 nm, which means that the near UV light is appropriate for irradiation. When increasing the concentration, the absorption intensity is also increasing.

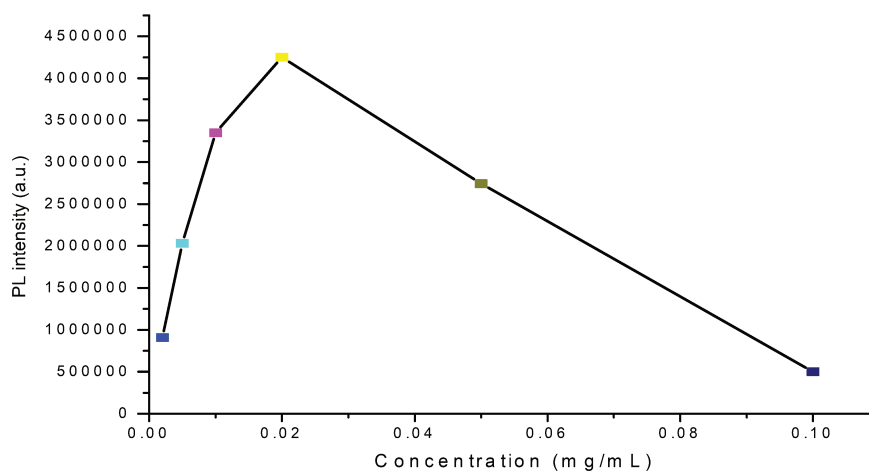


Figure 3-45 Emission intensity of **P10** versus concentration ($\lambda_{\text{exc}} = 375$ nm).

Variation of the emission intensity with the concentration (**Figure 3-45**) shows that the concentration should be lower than 0.02 mg/mL to avoid any intermolecular interaction.

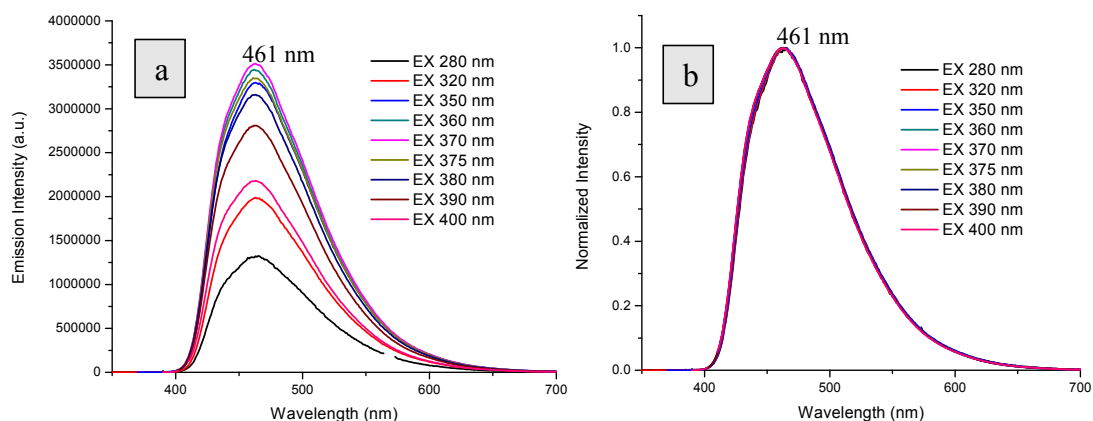
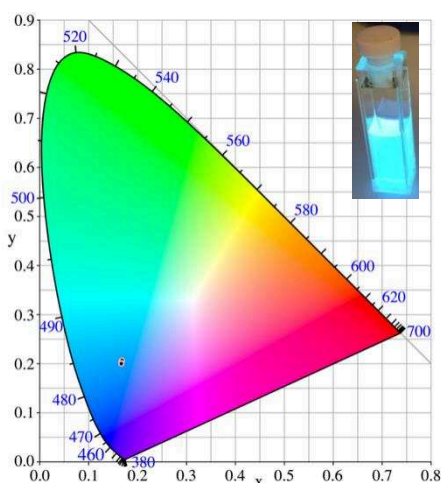


Figure 3-46 a) Emission spectra of **P10** in DCM; b) Corresponding normalized emission spectra. (0.01 mg/mL, slits were 2,2 nm).

The main band of the emission spectrum of **P10** in DCM is ranging from 400 nm to 700 nm, and the maximum is 461 nm with different excitations from 280 nm to 400 nm. The normalized emission spectra show identical emission profile despite the intensity changes, suggesting that the fluorescence is originating from the same excited state.



λ_{exc}	CIE x	CIE y
320 nm	0.167	0.205
350 nm	0.167	0.206
360 nm	0.166	0.201
370 nm	0.166	0.202
375 nm	0.166	0.202
380 nm	0.166	0.202
390 nm	0.166	0.201
400 nm	0.166	0.199

Figure 3-47 CIE coordinates of **P10** in DCM (0.01 mg/mL, slits were 2,2 nm, λ_{exc} = 300-400 nm) (The inserted photo shows the emission of **P10** in DCM under a 365 nm UV lamp)

The **CIE coordinates** show the material emits a **greenish blue light** under excitation at 300-400 nm.

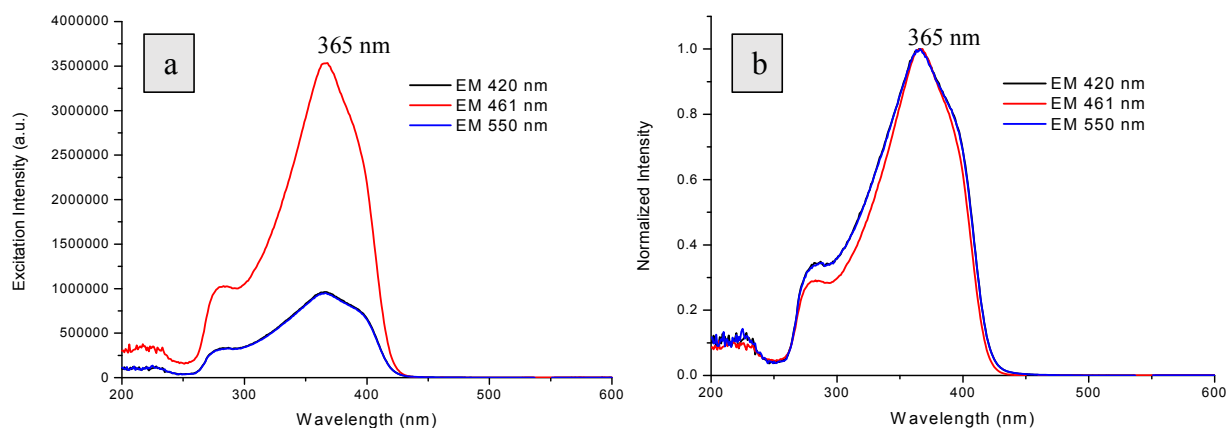


Figure 3-48 a) Excitation spectra of **P10** in **DCM**; b) Corresponding normalized excitation spectra. (0.01 mg/mL, slits were 2,2 nm).

As shown, the main band of the excitation spectrum is ranging from 250 nm to 450 nm with a maximum at 365 nm, which also means that the near UV light is an efficient source of irradiation. Besides, the excitation bands are similar for different emissions despite the intensity changes.

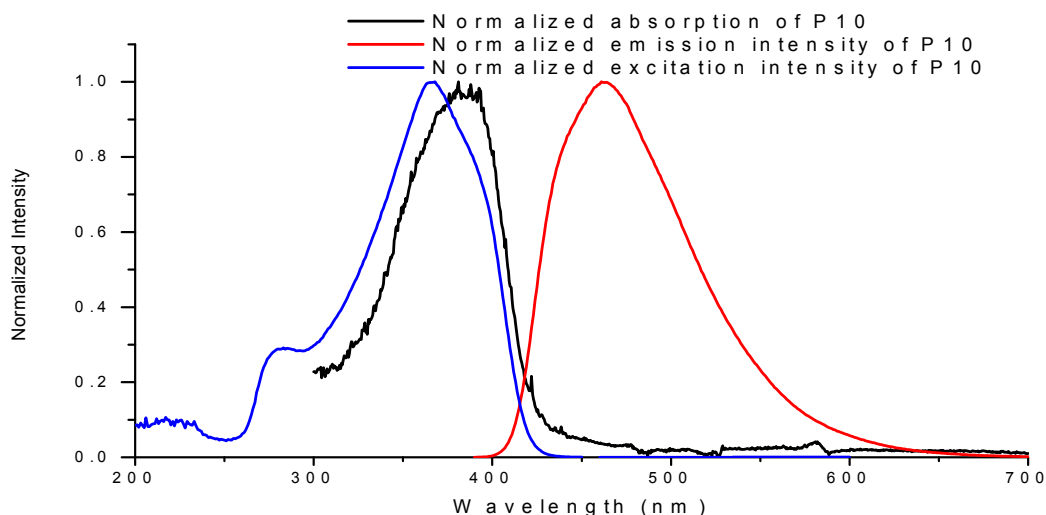
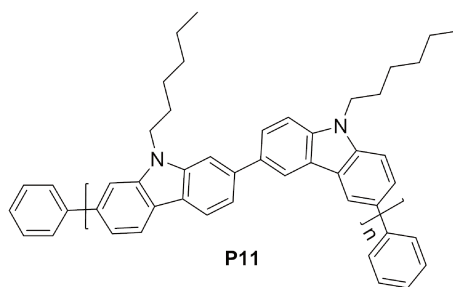


Figure 3-49 Normalized absorption, excitation and emission spectra of **P10** in **DCM**

(0.01 mg/mL, slits were 2,2 nm, and for excitation: set $\lambda_{an} = 461$ nm, for emission: set $\lambda_{exc} = 375$ nm)

The excitation spectrum (blue) is similar to the absorption spectrum (black) described above, and the main band of the emission spectrum shows a maximum at 461 nm. The maximum of the absorption of **P10** is 381 nm as show above when the concentration is 0.01 mg/mL.

3.1.9 Absorption and PL spectra of P11



For improving the photostability of the blue emitting materials, we also designed and synthesized conjugated polymers **P11** that composed poly(*N*-alkyl-3,6-carbazole) derivatives instead of fluorene derivatives. In fact, polycarbazoles have been extensively investigated due to their good film-forming abilities and good solubilities in common organic solvents, such as chloroform, THF, toluene, DCM, and 1,2-dichloroethane, and their hole-transporting properties. They can be easily fabricated into thin films using either spin-coating or simple solvent-casting techniques.¹⁵⁶ Besides, it was also reported that the use of polycarbazoles will permit to construct opto-electronically functional devices and asymmetric recognition devices with better performance as compared with polyfluorenes.¹⁵⁷

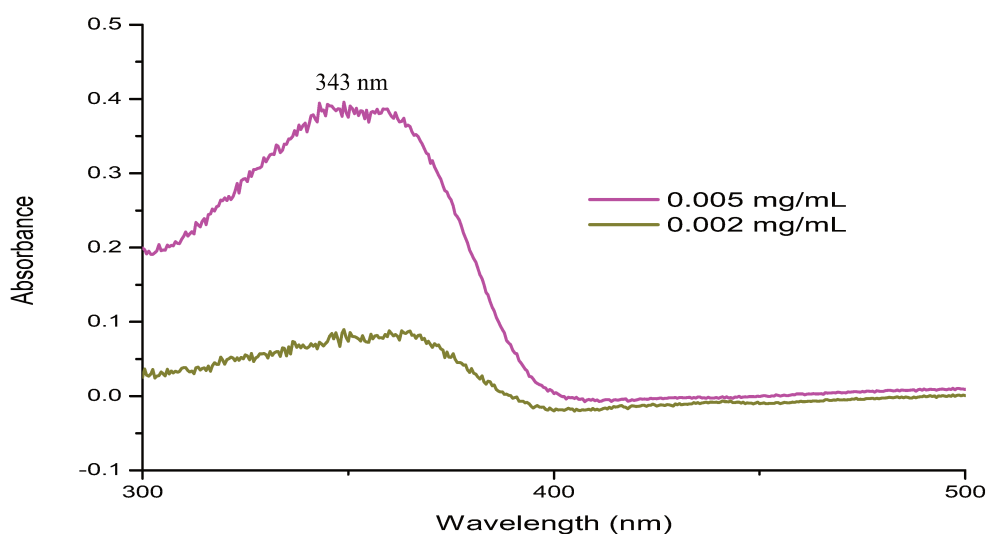


Figure 3-50 Absorption spectra of **P11** in **DCM** at different concentrations.

As shown on **Figure 3-50**, the polymer **P11** in DCM has a broad absorption ranging from 300 nm to 400 nm and the maximum is around 343 nm, which means that near UV light is appropriate for exciting **P11**. With the increase of the concentration, the absorption intensity is also increasing.

¹⁵⁶ Z.-B. Zhang, M. Fujiki, H.-Z. Tang, M. Motonaga, and K. Torimitsu. *Macromolecules*, **2002**, 35, 1988-1990.

¹⁵⁷ M. Fujiki, Ikoma-shi (JP); C. E. Mckenna, Pacific Palisades, CA (US); Z.-B. Zhang, Alhambra, CA (US). **2004**. US 20040087761 A1.

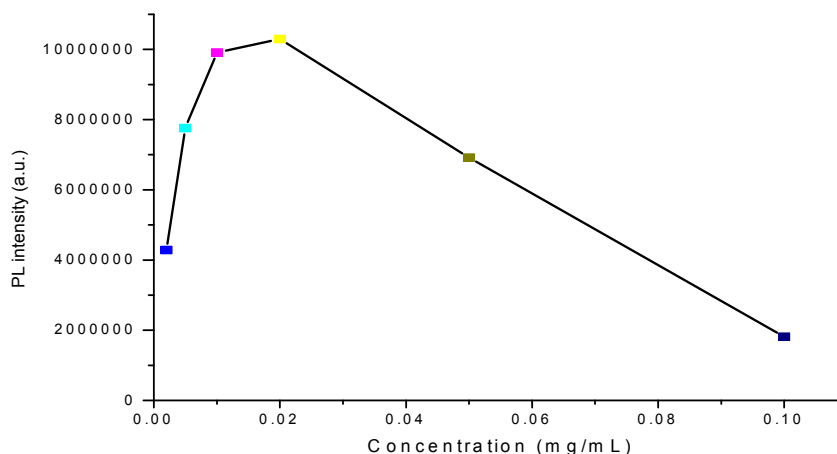


Figure 3-51 Emission intensity of **P11** versus concentration ($\lambda_{\text{exc}} = 375$ nm).

Concentration should be no more than 0.01 mg/mL, so that the curve of PL intensity versus concentration is in the linear domain.

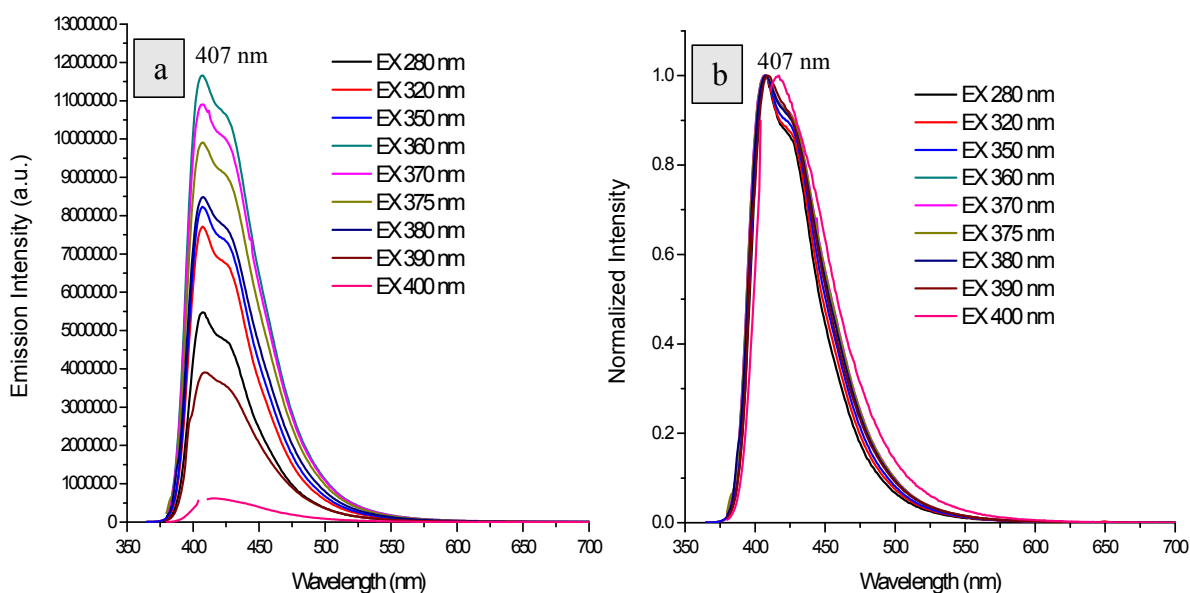
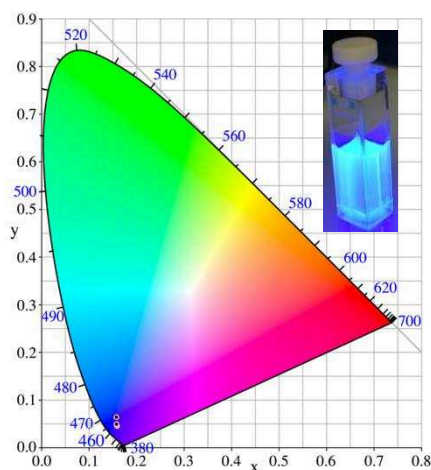


Figure 3-52 a) Emission spectra of **P11** in DCM; b) Corresponding normalized emission spectra. (0.01 mg/mL, slits were 2,2 nm).

The main band of the emission spectrum of **P11** in DCM is ranging from 375 nm to 600 nm, and the maximum is 407 nm with different excitations from 280 nm to 400 nm. The normalized emission spectra show identical emission profile despite the intensity changes, suggesting that the fluorescence is originating from the same excited state.



λ_{exc}	CIE x	CIE y
320 nm	0.158	0.045
350 nm	0.158	0.046
360 nm	0.157	0.049
370 nm	0.157	0.050
375 nm	0.157	0.050
380 nm	0.157	0.049
390 nm	0.158	0.049
400 nm	0.158	0.064

Figure 3-53 CIE coordinates of **P11** in **DCM** (0.01 mg/mL, slits were 2,2 nm, λ_{exc} = 300-400 nm) (The inserted photo shows the emission of **P11** in **DCM** under a 365 nm UV lamp)

The **CIE coordinates** (0.157, 0.050) show that the material emits a **blue light** with excitation at 375 nm.

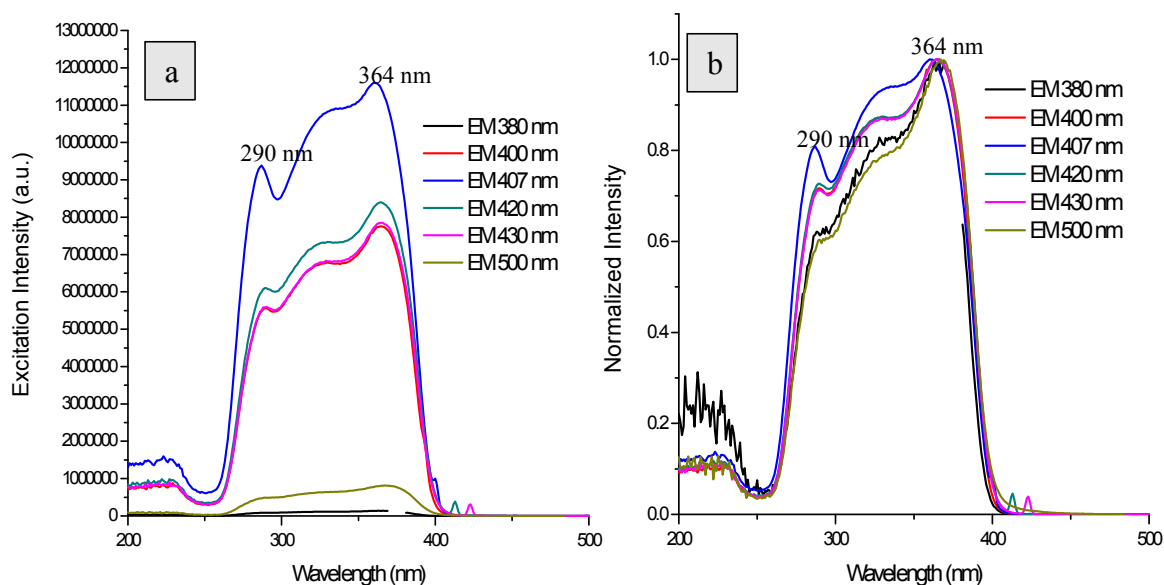


Figure 3-54 a) Excitation spectra of **P11** in **DCM**; b) Corresponding normalized excitation spectra. (0.01 mg/mL, slits were 2,2 nm)

As shown, the main band of the excitation spectrum is ranging from 250 nm to 400 nm with two maxima at 290 nm and 364 nm respectively. Besides, the excitation bands are similar for different emissions despite the intensity changes.

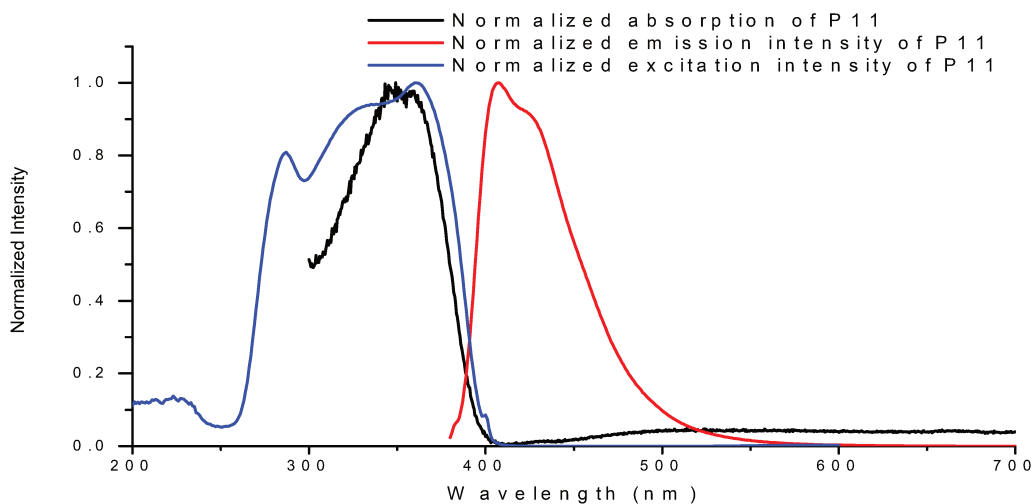
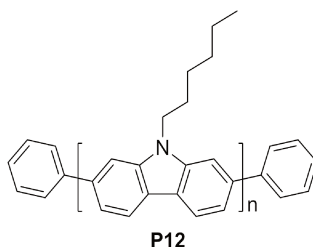


Figure 3-55 Normalized absorption, excitation and emission spectra of **P11** in DCM

(0.01 mg/mL, slits were 2,2 nm, and for excitation: set $\lambda_{an} = 407$ nm, for emission: set $\lambda_{exc} = 375$ nm)

The excitation spectrum (**Figure 3-55**, blue trace) is similar to the absorption spectrum (black trace) described above, and the main band of the emission spectrum shows a maximum at 407 nm. The maximum of the absorption of **P11** is 343 nm as show above when the concentration is 0.01 mg/mL.

3.1.10 Absorption and PL spectra of P12



P12 that is composed of poly(*N*-alkyl-2,7-carbazole) derivatives instead of poly(*N*-alkyl-3,6-carbazole) as donor units was also designed and synthesized. In comparison with **P11**, the polymer **P12** was supposed to be more linear. It was thus expected to show a higher conjugation length (see **Figure 3-56**), and, in consequence, a red-shift of the absorption and emission properties.

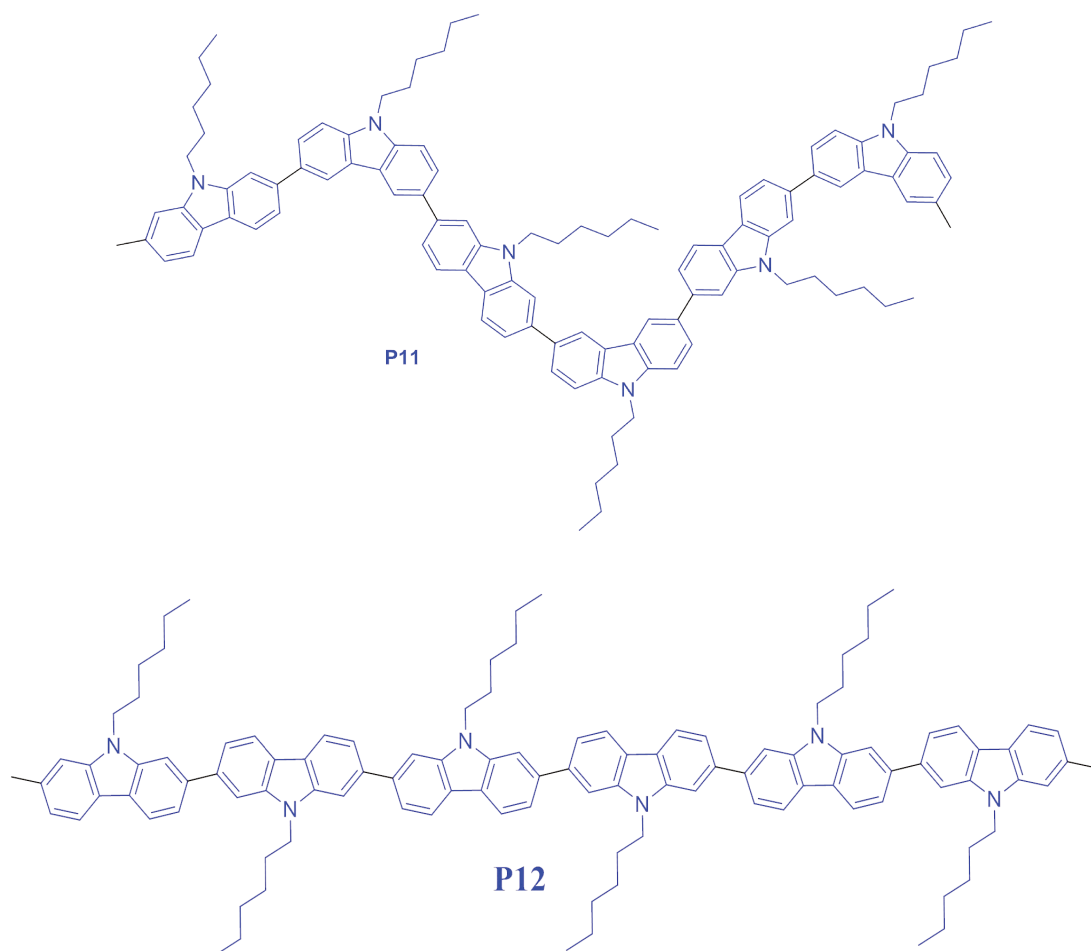


Figure 3-56 The possible conformations of chains of **P11** and **P12**.

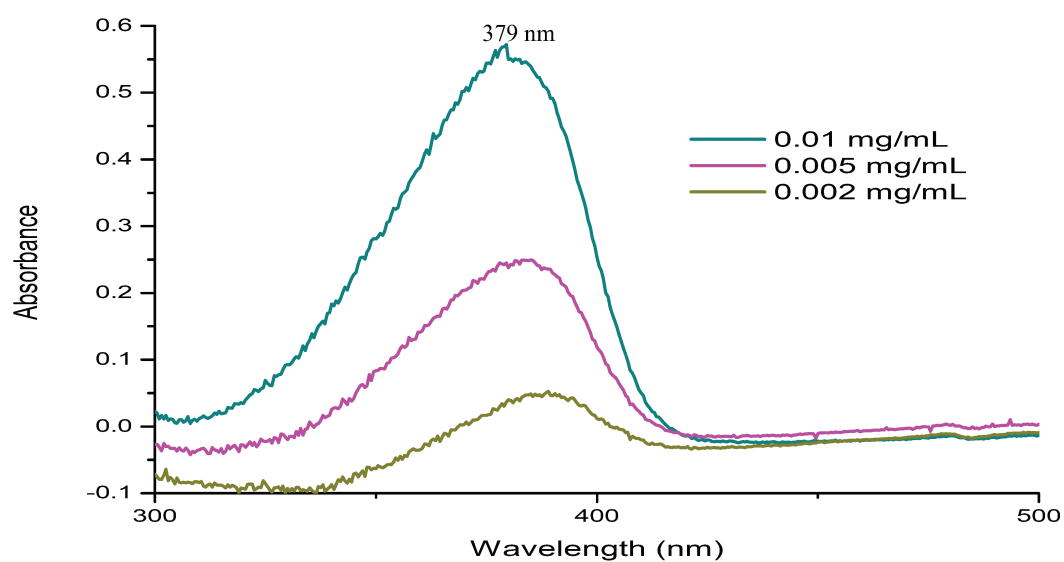


Figure 3-57 Absorption spectra of **P12** in **DCM** at different concentrations.

As shown on **Figure 3-57**, the polymer **P12** dissolved in DCM has a broad absorption ranging from 300 nm to 500 nm and the maximum is around 379 nm, which means that the near UV light

is a good source of irradiation for the emission. With the increase of the concentration, the absorption intensity is also increasing.

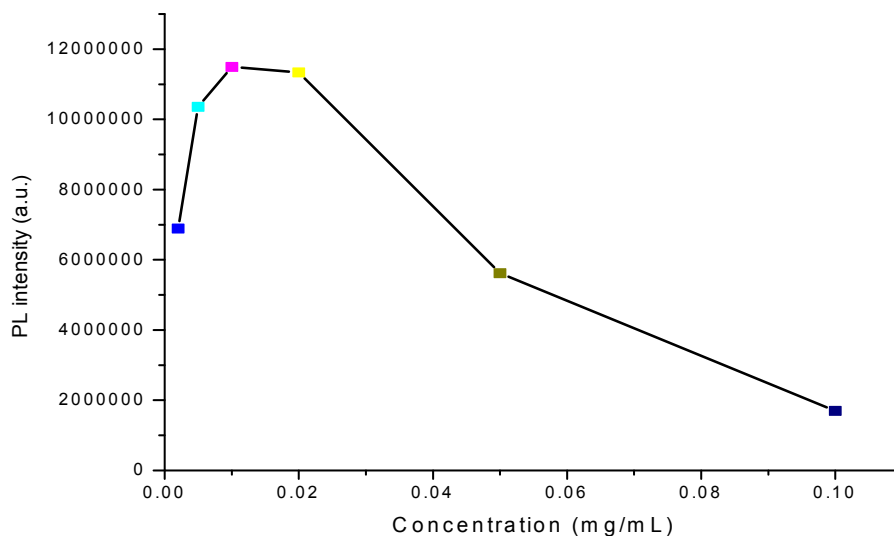


Figure 3-58 Emission intensity of **P12** versus concentration ($\lambda_{\text{exc}} = 375$ nm).

However, concentration should be lower than 0.01 mg/mL, so that the curve representing the PL intensity versus concentration is in the linear domain.

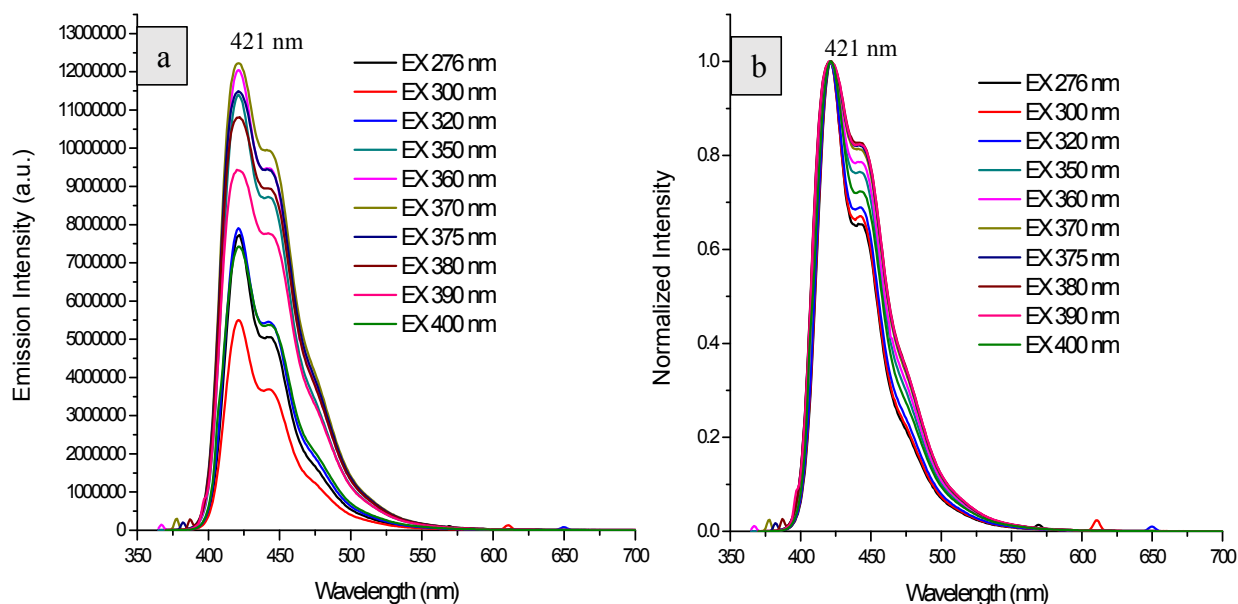
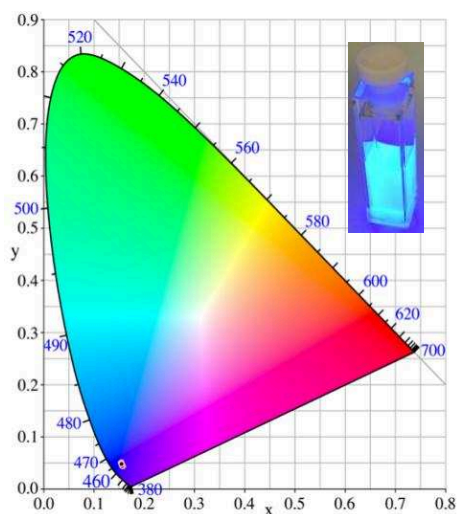


Figure 3-59 a) Emission spectra of **P12** in DCM; b) Corresponding normalized emission spectra. (0.01 mg/mL, slits were 2,2 nm)

The main band of the emission spectrum of **P12** in DCM is ranging from 400 nm to 550 nm, and the maximum is at 421 nm with different excitations from 276 nm to 400 nm. The normalized

emission spectra show identical emission profile despite the intensity changes.



λ_{exc}	CIE x	CIE y
300 nm	0.158	0.044
320 nm	0.156	0.044
350 nm	0.155	0.048
360 nm	0.154	0.049
370 nm	0.154	0.050
375 nm	0.154	0.050
380 nm	0.154	0.051
390 nm	0.154	0.051
400 nm	0.155	0.048

Figure 3-60 CIE coordinates of **P12 in DCM** (0.01 mg/mL, slits were 2,2 nm, λ_{exc} = 300-400 nm) (The inserted photo shows the emission of **P12** in DCM under a 365 nm UV lamp)

The **CIE coordinates** (0.154, 0.050) show that the material emits **blue light** under excitation at 375 nm.

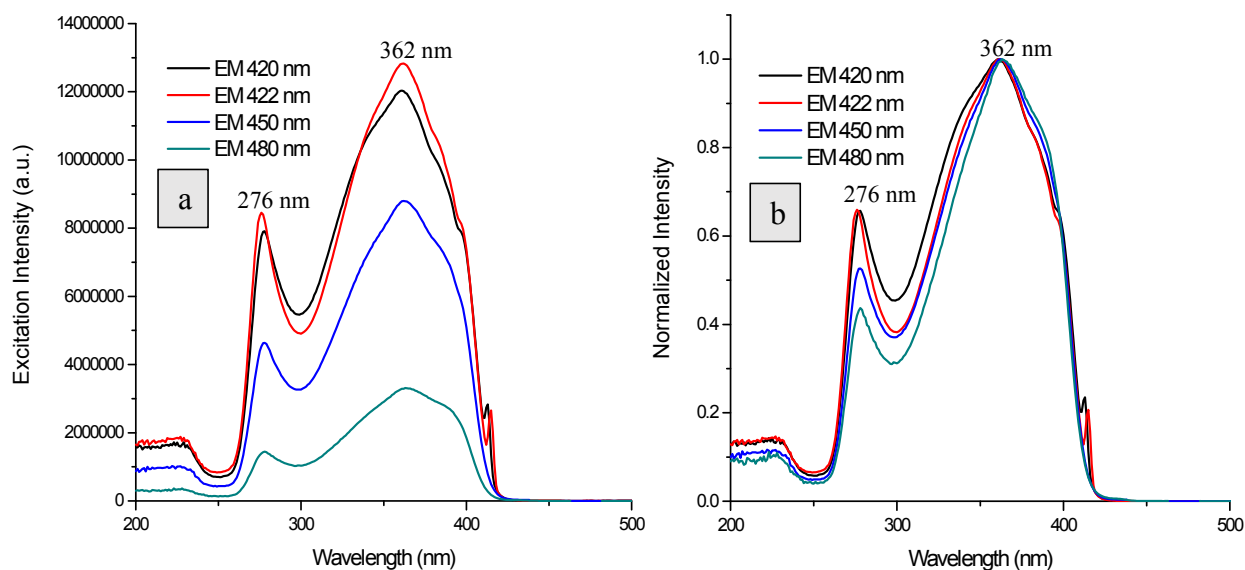


Figure 3-61 a) Excitation spectra of **P12 in DCM**; b) Corresponding normalized excitation spectra. (0.01 mg/mL, slits were 2,2 nm).

As shown on **Figure 3-61**, the main band of the excitation spectrum is ranging from 250 nm to 450 nm with two maxima at 276 nm and 362 nm respectively, which also means that the near UV light is a good source of irradiation for the emission. Besides, the excitation bands are

similar for different emissions despite the intensity changes.

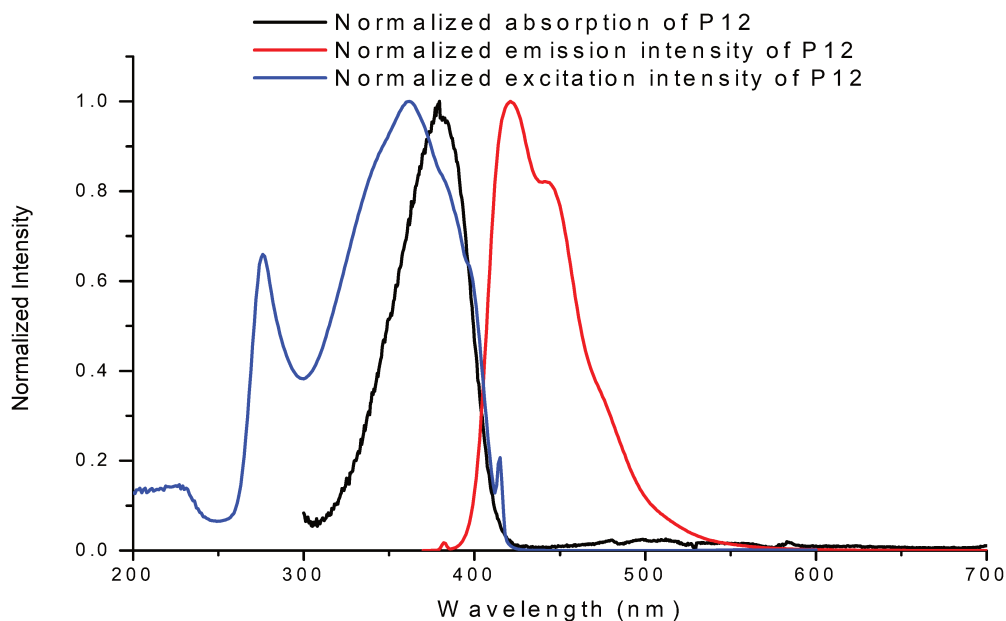
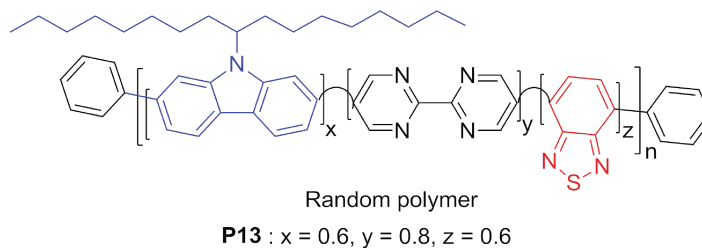


Figure 3-62 Normalized absorption, excitation and emission spectra of **P12** in DCM

(0.01 mg/mL, slits were 2,2 nm, and for excitation: set $\lambda_{an} = 421$ nm, for emission: set $\lambda_{exc} = 375$ nm)

The excitation spectrum (**Figure 3-62**, blue trace) is broader compared with the absorption spectrum (black trace) described above when the concentration is 0.01 mg/mL. The maximum of the absorption of **P12** is 379.5 nm as shown above. The main band of the emission spectrum shows a maximum at 421 nm. The spectra show that for the best emission of this polymer, the excitation wavelength is better in the range of 350-390 nm, which means that the near UV light is suitable for the excitation.

3.1.11 Absorption and PL spectra of P13



Motivated by the photophysical properties of the above polymers (see **Chapter IV**), and in order to tune the emission color, we designed and synthesized more random conjugated polymers with

carbazole as donor and 2,2'-bipyrimidine and benzothiadiazole as electron accepting groups, respectively.

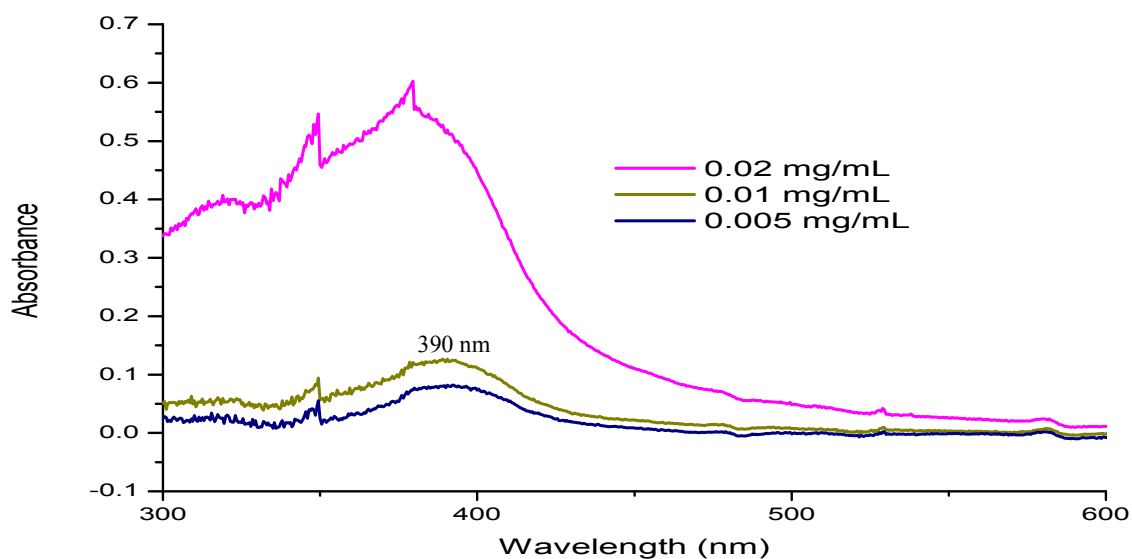


Figure 3-63 Absorption spectra of **P13** in **DCM** at different concentrations.

As **Figure 3-63** shows, polymer **P13** in DCM has a broad absorption ranging from 300 nm to 600 nm and the maximum is around 390 nm, which means that the near UV light is suitable for the excitation. With the increase of the concentration, the absorption intensity is also increasing.

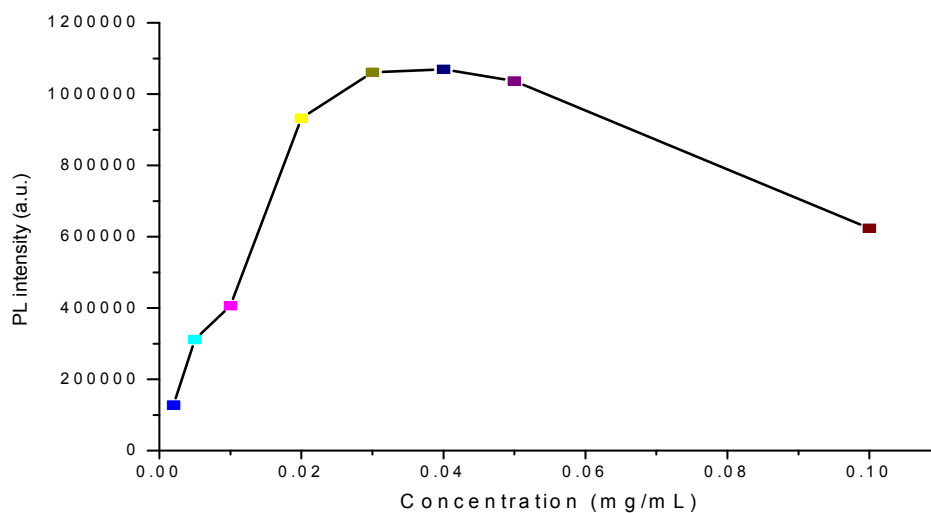


Figure 3-64 Emission intensity of **P13** versus concentration ($\lambda_{\text{exc}} = 375 \text{ nm}$).

Concentration should be less than 0.03 mg/mL, so that the curve of PL intensity versus concentration is in the linear domain which indicate that there have no aggregation formed.

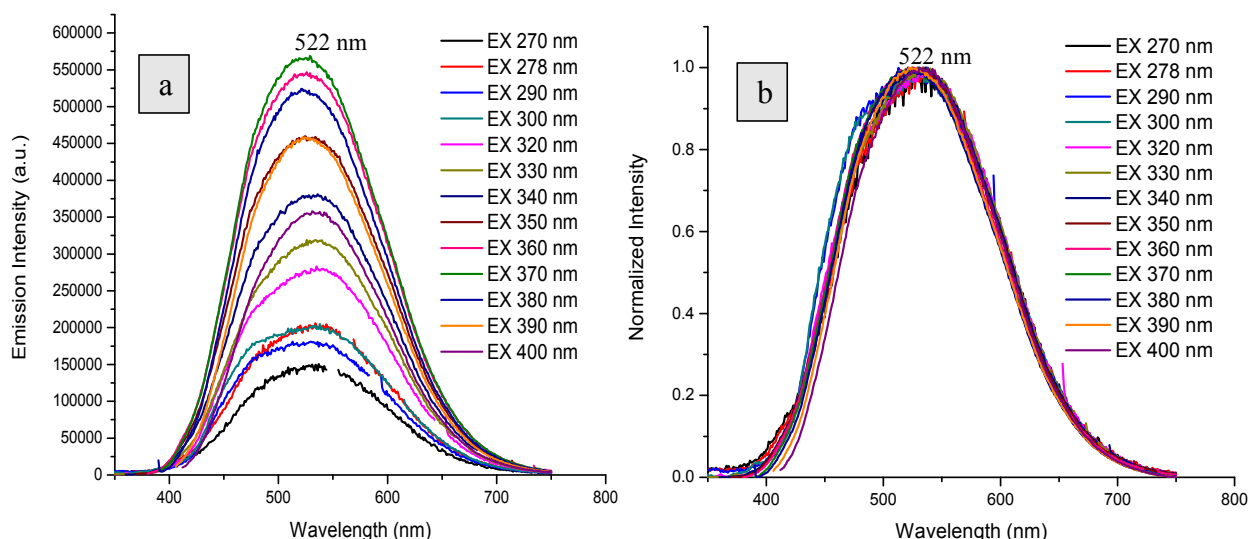
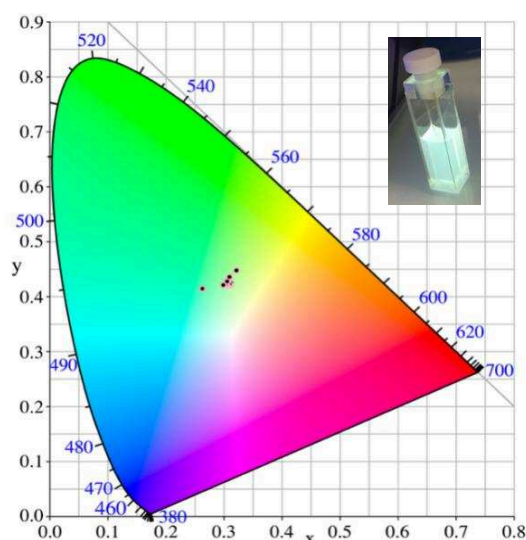


Figure 3-65 a) Emission spectra of **P13** in DCM; b) Corresponding normalized emission spectra. (0.01 mg/mL, slits were 2,2 nm)

The main band of the emission spectrum of **P13** in DCM is ranging from 350 nm to 750 nm, and the maximum is found at 522 nm with different excitations from 270 nm to 400 nm. The normalized emission spectra show identical emission profile despite the intensity changes, suggesting that the prompt fluorescence are originated from the same S_1 states. It is of particular importance that the maximum of emission intensity is obtained after excitation at 370 nm, a wavelength close to the one emitted by the LEDs that will be used for investigating the materials as phosphors.



λ_{exc}	CIE x	CIE y	CCT (K)
300 nm	0.263	0.414	7928
320 nm	0.310	0.422	6175
340 nm	0.312	0.425	6107
350 nm	0.309	0.423	6226
360 nm	0.305	0.422	6337
370 nm	0.304	0.423	6370
375 nm	0.299	0.421	6548
380 nm	0.305	0.428	6329
390 nm	0.310	0.436	6161
400 nm	0.321	0.448	5814

Figure 3-66 CIE coordinates of **P13** in DCM (0.01 mg/mL, slits were 2,2 nm, λ_{exc} = 300-400 nm) (The inserted photo shows the emission of **P13** in DCM under a 365 nm UV lamp).

The CIE coordinates (0.299, 0.421) and the CCT data show that the material emits **cool white light (5000-8300 K CCT)** under excitation at 375 nm.

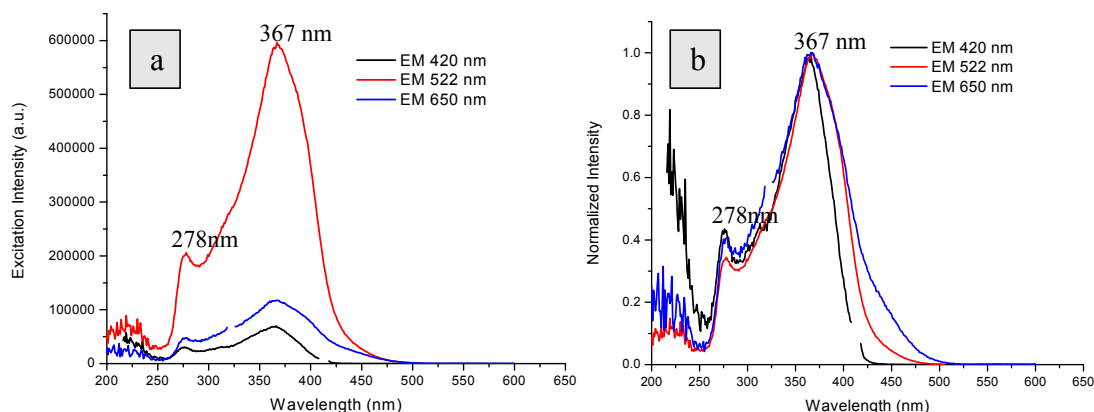


Figure 3-67 a) Excitation spectra of **P13** in DCM; b) Corresponding normalized excitation spectra. (0.01 mg/mL, slits were 2,2 nm).

As shown on **Figure 3-67**, the main band of the excitation spectrum is ranging from 250 nm to 500 nm with two maxima at 278 nm and 367 nm respectively. Besides, the excitation bands are similar for different emissions despite the intensity changes.

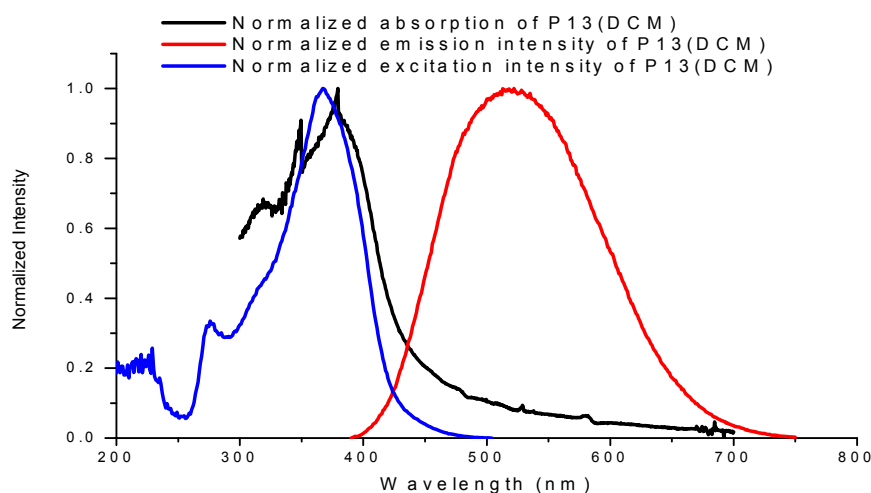
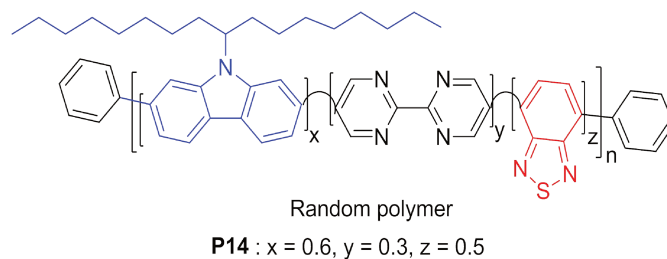


Figure 3-68 Normalized absorption, excitation and emission spectra of **P13** in DCM

(0.01 mg/mL, slits were 2,2 nm, and for excitation: set $\lambda_{an} = 522$ nm, for emission: set $\lambda_{exc} = 375$ nm).

The excitation spectrum (**Figure 3-68**, blue trace) is similar to the absorption spectrum (black trace) described above, and the main band of the emission spectrum shows a maximum at 522 nm. The maximum of the absorption of **P13** in DCM is 390 nm as shown on **Figure 3-60** when the concentration is 0.01 mg/mL.

3.1.12 Absorption and PL spectra of P14



To optimize the quality of the white light, we further designed and synthesized polymer **P14** which contains a lower amount of bipyrimidine as acceptor compared to polymer **P13**.

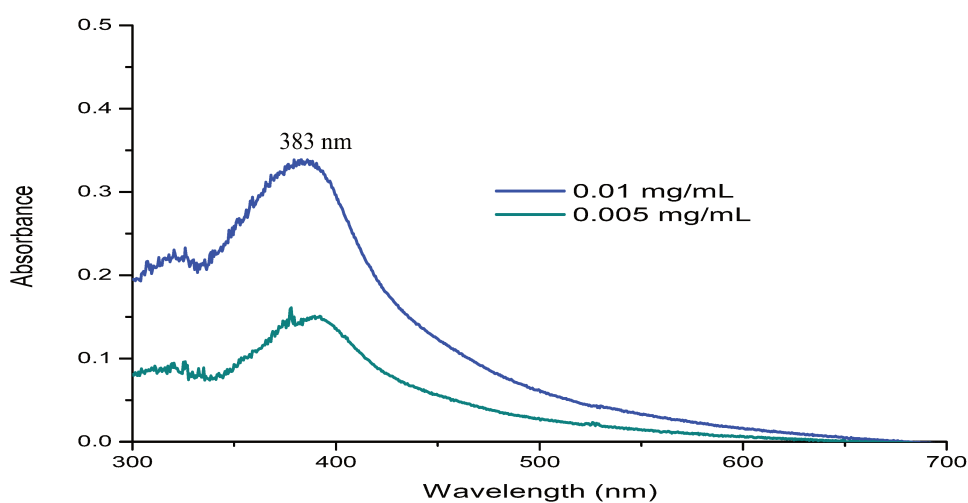


Figure 3-69 Absorption spectra of **P14** in **DCM** at different concentrations.

As shown on **Figure 3-69**, the polymer **P14** in DCM has a broad absorption ranging from 300 nm to 700 nm and the maximum is around 383 nm, which means that the near UV light is a good source of irradiation. With the increase of the concentration, the absorption intensity is also increasing linearly until a concentration of 0.02 mg/mL (**Figure 3-70**).

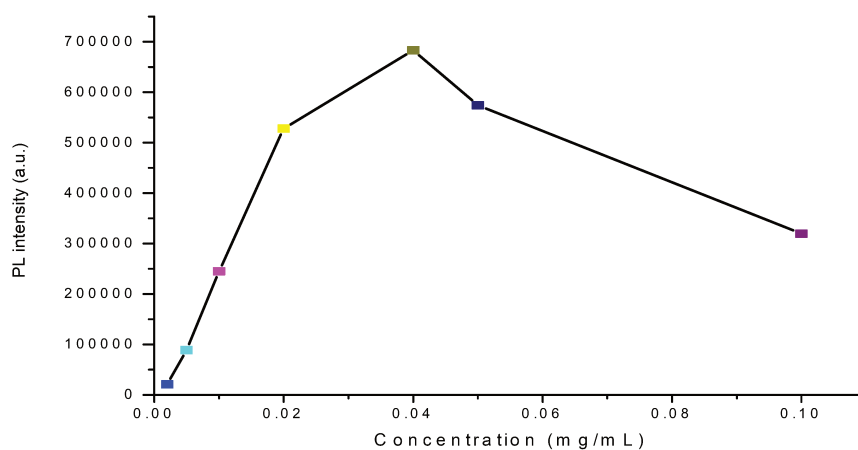
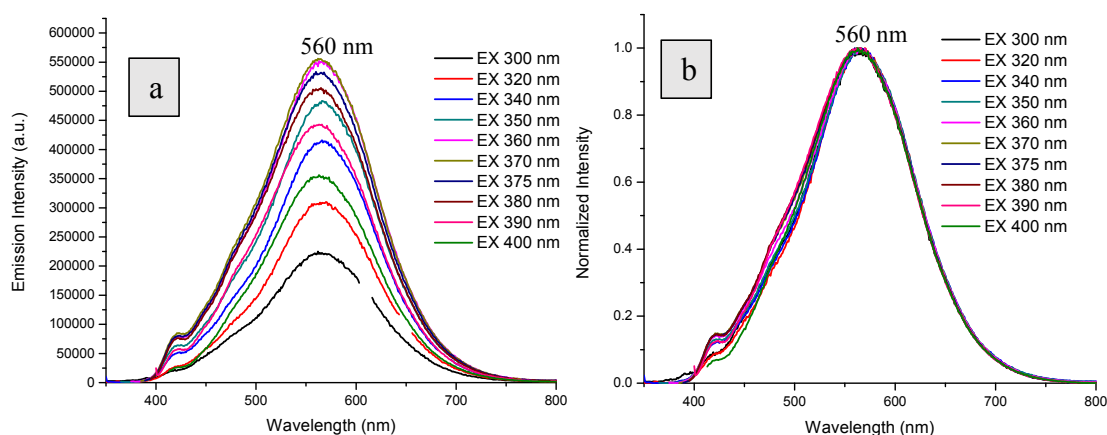
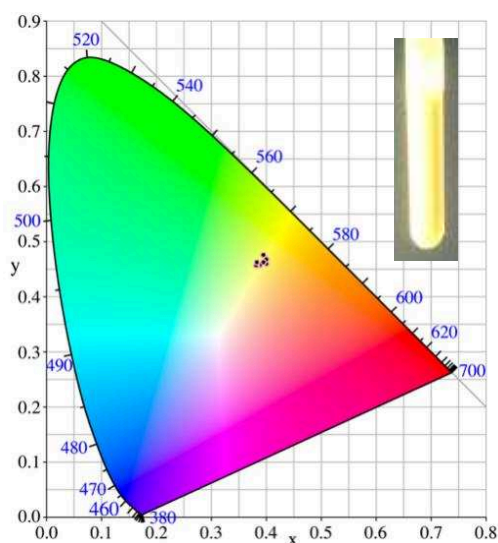


Figure 3-70 Emission intensity of **P14** versus concentration ($\lambda_{\text{exc}} = 375$ nm).**Figure 3-71** a) Emission spectra of **P14** in DCM; b) Corresponding normalized emission spectra. (0.01 mg/mL, slits were 2,2 nm).

The main band shown on the emission spectrum of **P14** in DCM is ranging from 350 nm to 800 nm, and the maximum is 560 nm with different excitations from 300 nm to 400 nm. The normalized emission spectra show identical emission profile despite the intensity changes.



λ_{exc}	CIE x	CIE y	CCT (Kelvin)
300 nm	0.401	0.460	4020
320 nm	0.400	0.468	4064
340 nm	0.395	0.463	4133
360 nm	0.388	0.458	4259
370 nm	0.383	0.457	4345
375 nm	0.382	0.457	4364
380 nm	0.381	0.458	4400
390 nm	0.382	0.463	4390
400 nm	0.394	0.476	4210

Figure 3-72 CIE coordinates of **P14** in DCM (0.01 mg/mL, slits were 2,2 nm, $\lambda_{\text{exc}} = 300$ -400 nm) (The inserted photo shows the emission of **P14** in DCM under a 365 nm UV lamp).

The CIE coordinates (0.382, 0.457) show the material emits a **neutral white light** (3700-5000 K CCT) under excitation at 375 nm.

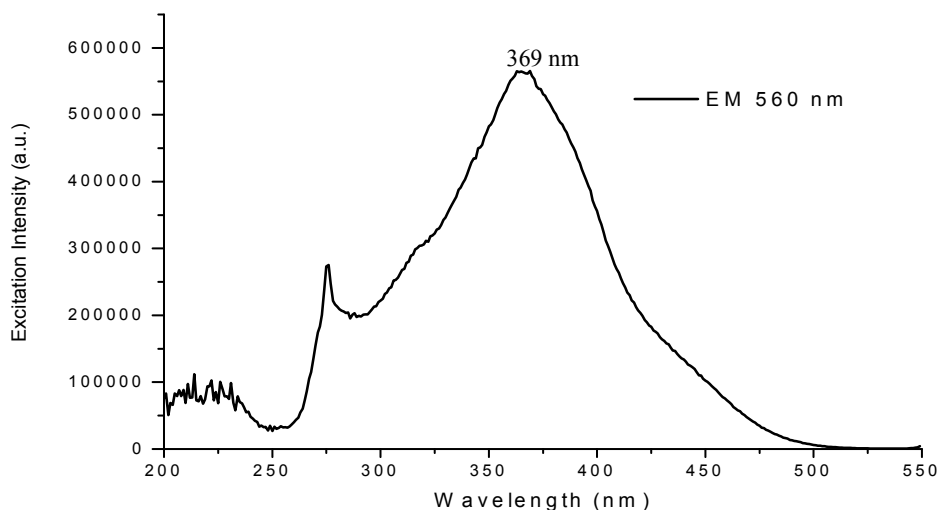


Figure 3-73 Excitation spectra of **P14** in **DCM** (0.01 mg/mL, slits were 2,2 nm)

The main band of the excitation spectrum is ranging from 250 nm to 500 nm with a maximum at 369 nm (**Figure 3-73**).

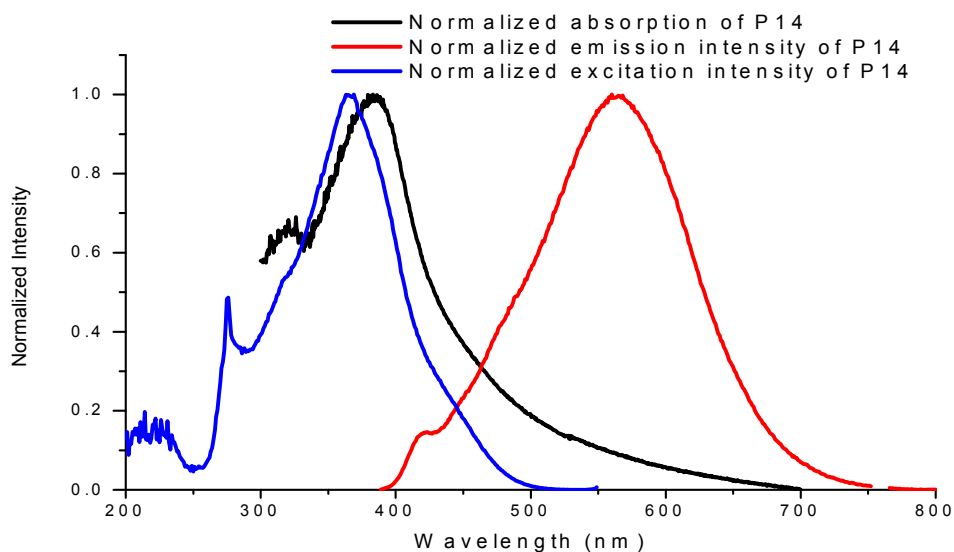
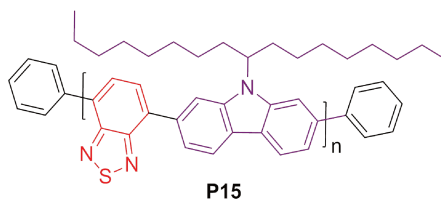


Figure 3-74 Normalized absorption, excitation and emission spectra of **P14** in **DCM**

(0.01 mg/mL, slits were 2,2 nm, and for excitation: set $\lambda_{an} = 560$ nm, for emission: set $\lambda_{exc} = 375$ nm).

The excitation spectrum (**Figure 3-74**, blue trace) is little blue shifted compared to the absorption spectrum (black trace) described above for a concentration of 0.01 mg/mL. The maxima of the absorption and excitation of **P14** are 383 nm and 369 nm, respectively. It indicates that the near UV light that will be used is a good source of irradiation. The main band of the emission spectrum shows a maximum at 560 nm.

3.1.13 Absorption and PL spectra of P15



The PL results of **P10** which uses bipyrimidine as acceptor and carbazole as donor show that this polymer emits a greenish blue light ($\lambda_{em} = 461$ nm) in DCM after excitation at 375 nm. It is much red-shift compared to polyfluorene ($\lambda_{em} = 421$ nm). Further, we have shown that **P13** and **P14**, in which we have introduced benzo-thiadiazole (BTD) as part of acceptor instead of bipyrimidine, show emissions that were more red-shifted and which were even white ($\lambda_{em} = 522$ nm, FWHM = 145 nm and $\lambda_{em} = 560$ nm, FWHM = 143 nm for **P13** and **P14**, respectively). Here we further study the results of **P15** that only uses BTD as acceptor and compare it to **P10**. In this case, we will better confirm whether benzo-thiadiazole will more red shift the emission of the polymers than bipyrimidine.

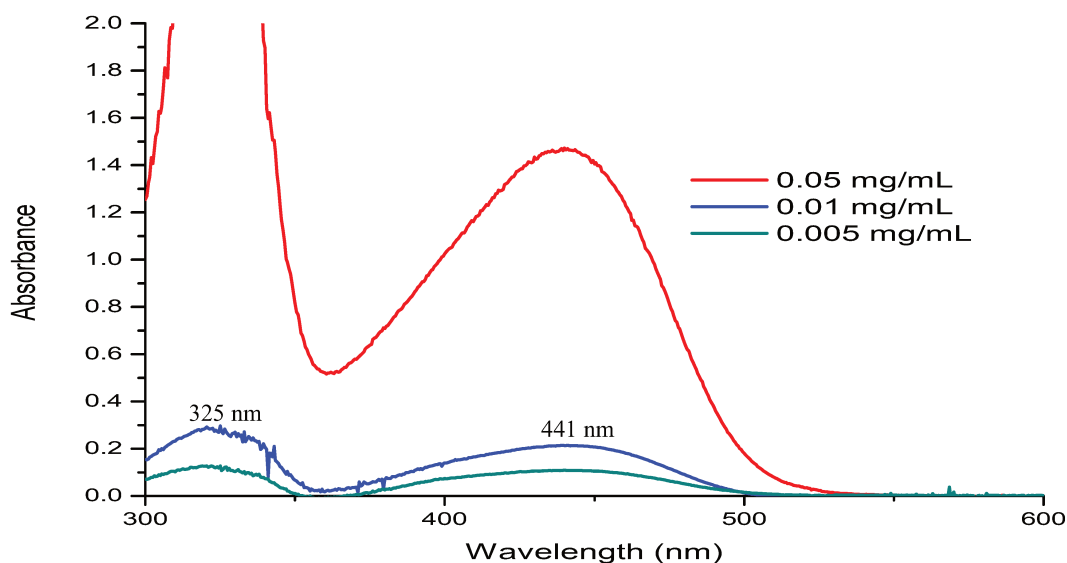


Figure 3-75 Absorption spectra of **P15** in DCM at different concentrations.

Figure 3-75 shows that polymer **P15** dissolved in DCM has a broad absorption ranging from 300 nm to 550 nm with maxima at 325 nm and 441 nm, respectively. When increasing the concentration, the absorption intensity is also increasing linearly until the concentration is 0.02 mg/mL (**Figure 3-76**).

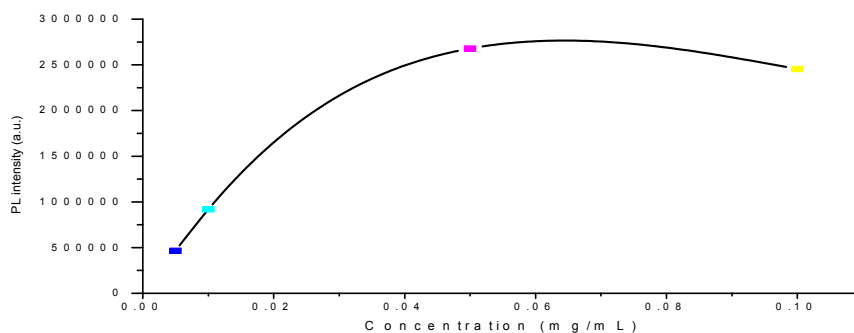


Figure 3-76 Emission intensity of **P15** versus concentration ($\lambda_{\text{exc}} = 375$ nm).

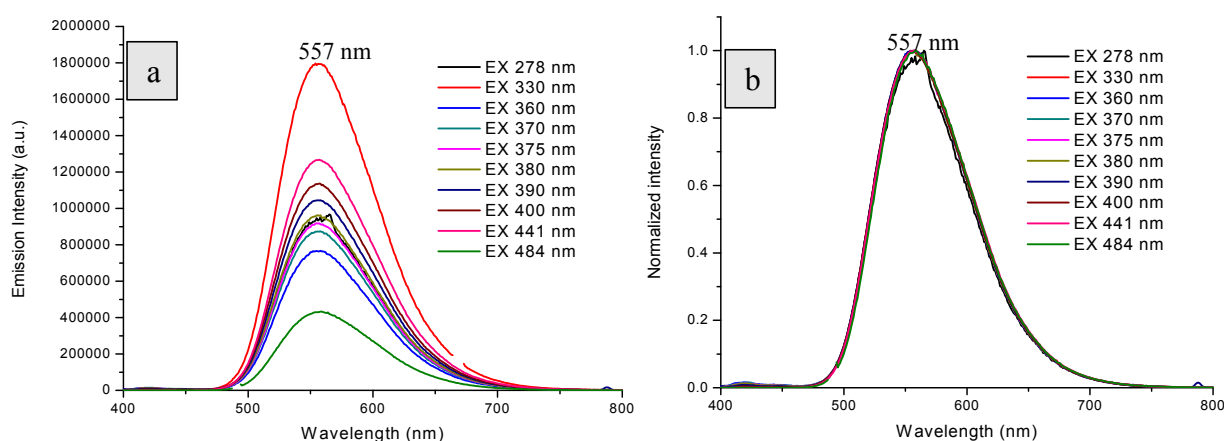
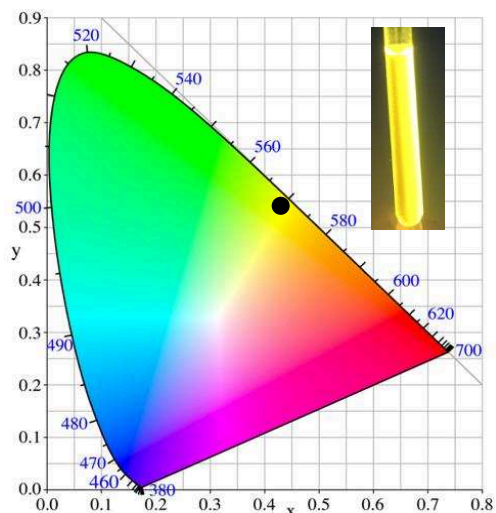


Figure 3-77 a) Emission spectra of **P15** in DCM; b) Corresponding normalized emission spectra. (0.01 mg/mL, slits were 2,2 nm).

The main band of the emission spectrum of **P15** in DCM is ranging from 450 nm to 750 nm, and the maximum is 557 nm with different excitations from 278 nm to 484 nm. The normalized emission spectra show identical emission profile despite the intensity changes.



λ_{exc}	CIE x	CIE y	CCT (Kelvin)
330 nm	0.430	0.552	3934
360 nm	0.428	0.549	3953
370 nm	0.428	0.549	3952
375 nm	0.428	0.550	3945
380 nm	0.428	0.550	3950
390 nm	0.429	0.551	3942
400 nm	0.430	0.551	3932
441 nm	0.431	0.549	3900
484 nm	0.434	0.549	3870

Figure 3-78 CIE coordinates of **P15** in DCM (0.01 mg/mL, slits were 2,2 nm, $\lambda_{\text{exc}} = 330$ -484 nm) (The

inserted photo shows the emission of **P15** in DCM under a 365 nm UV lamp).

The **CIE coordinates** (0.428, 0.550) show that the material emits a **neutral white light (3700-5000 K CCT)** under excitation at 375 nm.

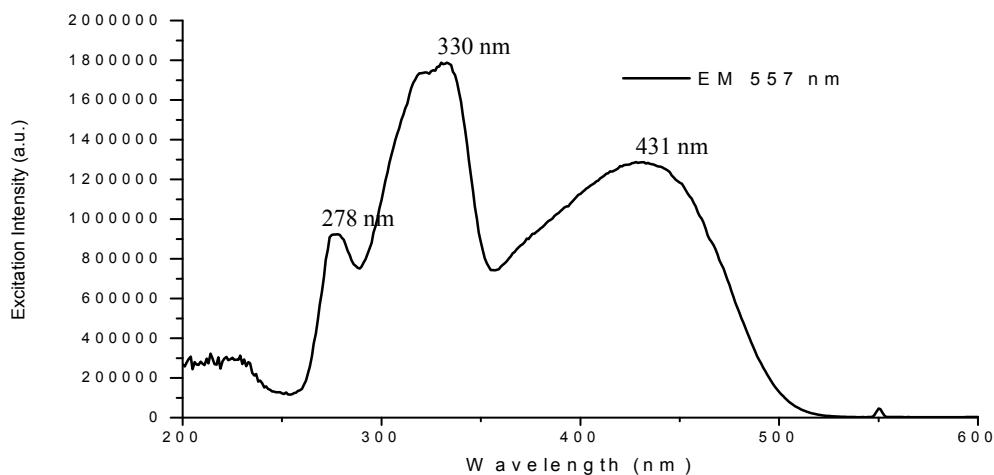


Figure 3-79 Excitation spectra of **P15** in **DCM** (0.01 mg/mL, slits were 2,2 nm).

The excitation spectrum shown on **Figure 3-79** shows three maxima at 278 nm, 330 nm and 431 nm when the emission is set at 557 nm.

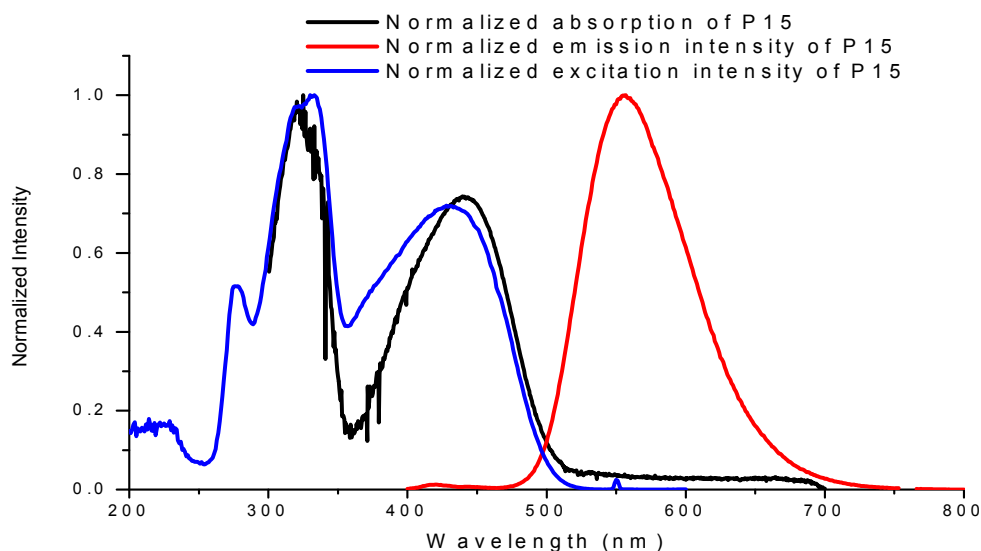


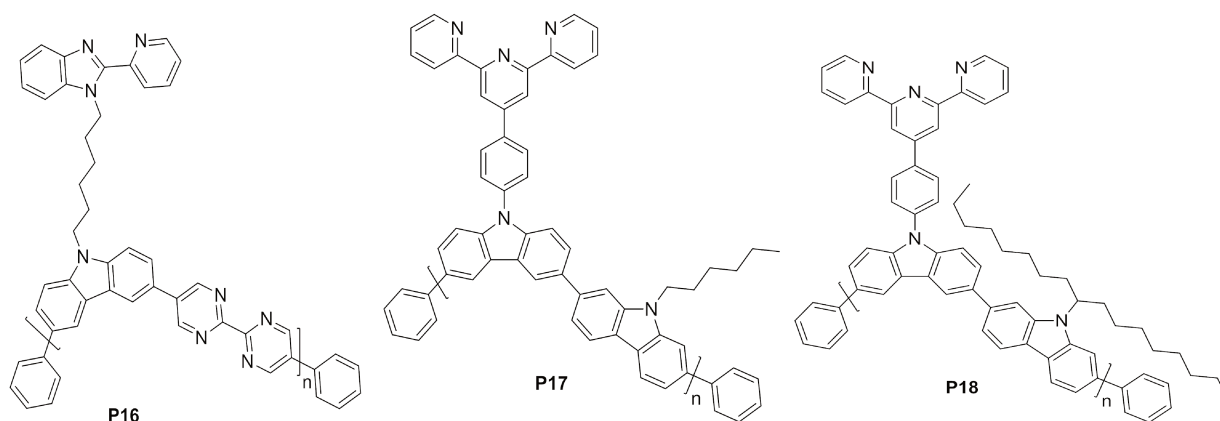
Figure 3-80 Normalized absorption, excitation and emission spectra of **P15** in **DCM**

(0.01 mg/mL, slits were 2,2 nm, and for excitation: set $\lambda_{an} = 557$ nm, for emission: set $\lambda_{exc} = 375$ nm)

The excitation spectrum (**Figure 3-80**, blue trace) is similar to the absorption spectrum (black trace), and the main band of emission shows a maximum at 557 nm. The maxima of absorption

of **P15** are 325 nm and 441 nm respectively as shown above when the concentration is 0.01 mg/mL. This may attributed to the strong intermolecular interactions (delocalized excitonic π - π^* transition in the polymer chains) and intramolecular charge transfer (ICT) effect.

3.1.14 Absorption and PL spectra of P18



It is well known that different side chain of the conjugated polymers can result in very different properties. Particularly, reports¹⁵⁸ shown that side-chain conjugation is an effective strategy for the design of high-performance nonfullerene acceptors. Side-chain conjugation can facilitates intramolecular conjugation and intermolecular interaction, which is beneficial to absorption and charge transport. To be specific, side-chain conjugation can not only extending the intramolecular conjugation, which would extend and enhance the absorption, but also facilitating the intermolecular interaction and π - π overlap, resulting in higher charge carrier mobility. It leads to the redshift of the absorption and emission,¹⁵⁹ and higher electron mobility.

Herein, we designed and synthesized a class of polymers with different side chains. Among them, **P16** composed of a carbazole unit with non-conjugated bulky side chains as donor groups and the BPM unit as acceptor, **P17** and **P18** are polymers with a poly(carbazole) backbone, of which both contain a carbazole unit with a conjugated side chain. It is worth mentioning that these three polymers all possess a side chain containing a moiety of *N*-heterocyclic aromatic unit or scaffold that is widely used in metal complexation field, such as sensing work, either is 2-(pyridin-2-yl)-1H-benzo[d]imidazole¹⁶⁰ or terpyridine moiety.¹⁶¹ Benzimidazole is one of the oldest known

¹⁵⁸ a. J. Wang, W. Wang, X. Wang, Y. Wu, Q. Zhang, C. Yan, W. Ma, W. You, and X. Zhan. *Adv. Mater.*, **2017**, 1702125.

b. J. Wang, J. Zhang, Y. Xiao, T. Xiao, R. Zhu, C. Yan, Y. Fu, G. Lu, X. Lu, S. R. Marder, and X. Zhan. *J. Am. Chem. Soc.*, **2018**, *140*, 9140-9147.

c. Y.-H. Chen, Y.-Y. Lin, Y.-C. Chen, J. T. Lin, R.H. Lee, W.-J. Kuo, R.-J. Jeng. *Polymer*, **2011**, *52*, 976-986.

¹⁵⁹ H. Chen, M. Denis, P.-A. Bouit, Y. Zhang, X. Wei, D. Tondelier, B. Geffroy, Z. Duan, and M. Hissler. *Appl. Sci.*, **2018**, *8*, 812.

¹⁶⁰ G. Xiang, S. Lin, W. Cui, L. Wang, L. Zhou, L. Li, D. Cao. *Sensors and Actuators B*, **2013**, *188*, 540-547.

nitrogen heterocycles, of which the properties have been studied for more than one hundred years. It was reported as ligand for metal complex,¹⁶² receptors for chemosensor and many useful intermediates/subunits¹⁶³ for the development of molecules.¹⁵⁹ Terpyridines are attractive building blocks for the construction of supramolecular assemblies for their remarkably high binding affinity toward most transition metal ions by $d\pi \rightarrow p\pi^*$ bonding, together with their chelation properties, strong and directed metal coordination capacity.¹⁶⁴ Thus these polymers are also interesting in the applications as optical chemosensors in molecular biology, medical diagnostics and the analysis of water contaminants. A new type of promising polymeric fluorescent chemosensor was provided which has potential applications in future optoelectronic devices.

Synthesis of **P16** was firstly performed. As a pity, the yield of monomer **M11** designed for this polymer is low, which may due to the interference of the benzimidazole unit with base during the reaction. Then we tried the synthesis of **P17**, which with a full carbazole back-bone. Unfortunately, most part of the product collected from the polymer have low solubility in common solvents and more analysis can't be done with it. To increase the solubility of the generated functionalized polymer, the monomer **M9** with a much bulky side-chain was selected instead of **M5**, according to our experience of polymer **P10**. To our delight, the resulting polymer **P18** possess a much better yield.

¹⁶¹ a. Y. Hong, S. Chen, C. W. T. Leung, J. W. Y. Lam, J. Liu, N.-W. Tseng, R. T. K. Kwok, Y. Yu, Z. Wang, and B. Z. Tang. *ACS Appl. Mater. Interfaces*, **2011**, 3, 3411–3418.

b. Y. Li, Z. W. Jiang, S. Y. Xiao, C. Z. Huang, and Y. F. Li. *Anal. Chem.*, **2018**, 90, 20, 12191-12197.

c. S. Fang, S. Y.-L. Leung, Y. Li, and V. W.-W. Yam. *Chem. Eur. J.*, **2018**, 24, 1–8.

d. V. W.-W. Yam, K. M.-C. Wong, and N. Zhu. *Angew. Chem. Int. Ed.*, **2003**, 42 (12), 1400-1403.

d. X. Wang, Q. Lin, S. Ramachandran, G. Pembouong, R. B. Pansu, I. Leray, B. Lebental, G. Zucchi. *Sensors & Actuators: B. Chemical*, **2019**, 286, 521–532.

e. S. Yin, J. Zhang, H. Feng, Z. Zhao, L. Xu, H. Qiu, B. Tang. *Dyes and Pigments*, **2012**, 95, 174-179.

¹⁶² a. S. Liu, R. Pan, G. Li, W. Su, and C. Ni. *Journal of Chemistry*, **2017**, doi: org/10.1155/2017/8647419.

b. S.-G. Liu, J.-L. Zuo, Y.-Z. Li, X.-Z. You. *Journal of Molecular Structure*, **2004**, 705, 153-157.

c. S.-G. Liu, J.-L. Zuo, Y. Wang, Y.-Z. Li, X.-Z. You. *Journal of Physics and Chemistry of Solids*, **2005**, 66, 735–740.

d. X.-T. Zhou, H.-B. Ji, S.-G. Liu. *Tetrahedron Letters*, **2013**, 54, 3882–3885.

¹⁶³ S. Takizawa, V. A. Montes and P. Anzenbacher Jr. *Chem. Mater.*, **2009**, 21 (12), 2452–2458.

¹⁶⁴ P. D. VELLIS, J. A. MIKROYANNIDIS, C.-N. LO, C.-S. HSU. *J. Polym. Sci., Part A: Polym. Chem.*, **2008**, 46, 7702–7712.

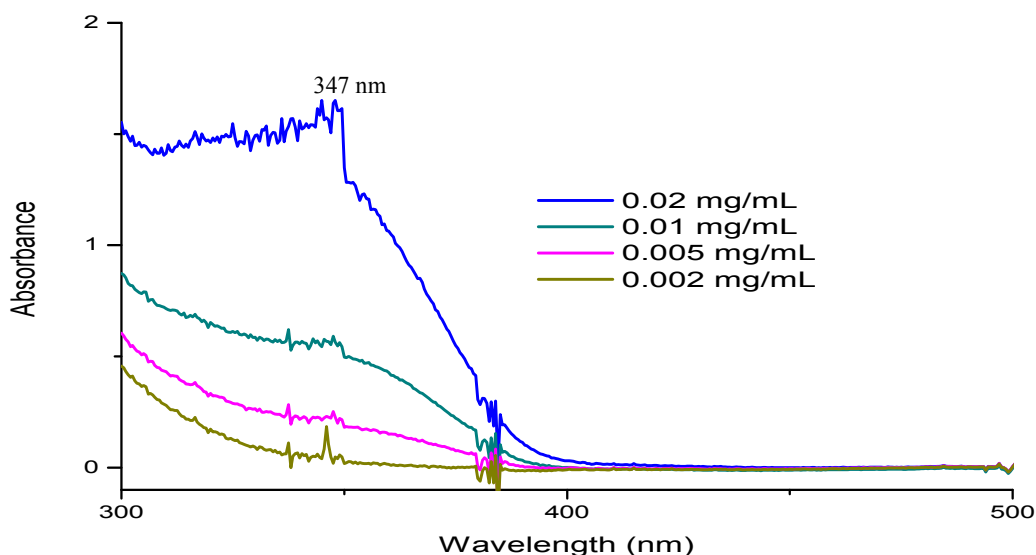


Figure 3-81 Absorption spectra of **P18** in **DCM** at different concentrations.

The absorption spectra recorded with different concentrations are shown on **Figure 3-81**. **P18** has a broad absorption ranging from 300 nm to 500 nm and the maximum is around 347 nm. With the increase of the concentration, the absorption intensity is also increasing.

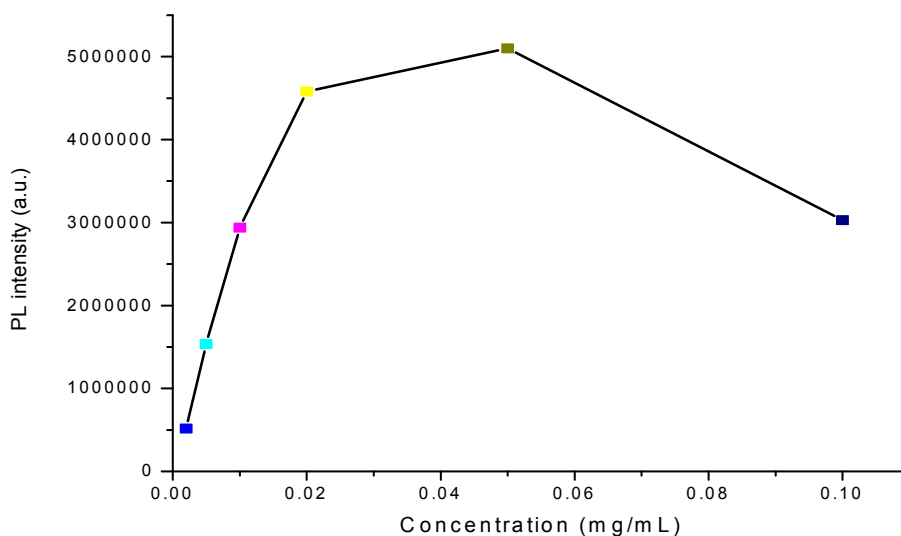


Figure 3-82 Emission intensity of **P18** versus concentration ($\lambda_{\text{exc}} = 375$ nm).

Photoluminescence spectra measured with different concentrations show that measurements should not be done with concentrations higher than 0.02 mg/mL.

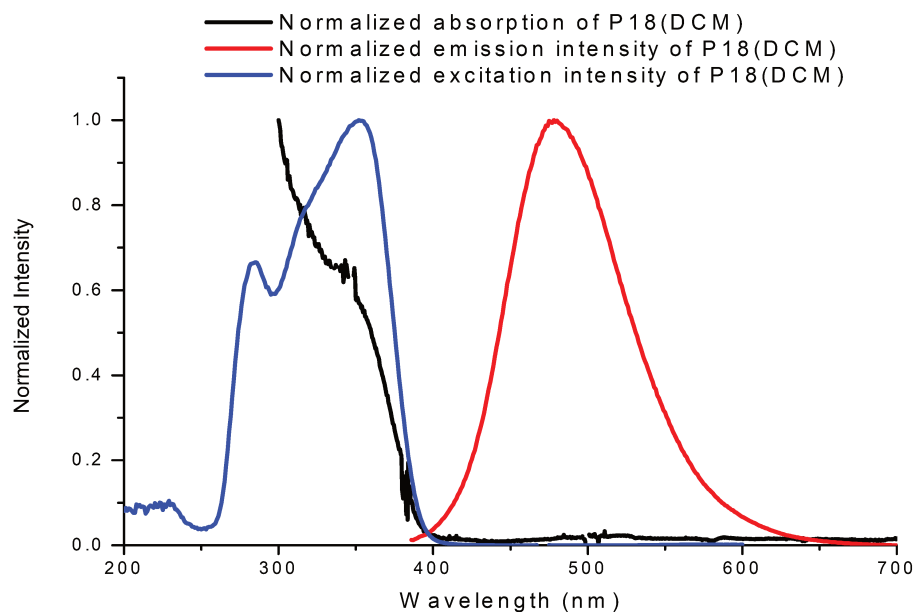


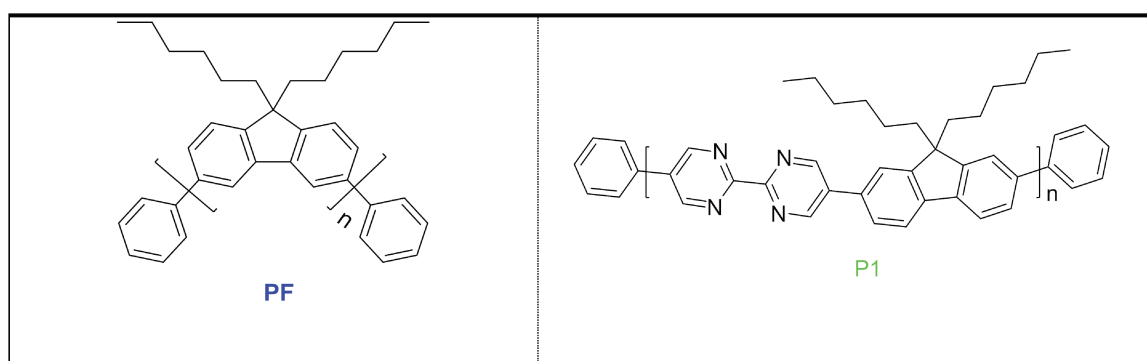
Figure 3-83 Normalized absorption, excitation and emission spectra of **P18 in DCM**

(0.01 mg/mL for absorption, 0.005 mg/mL for excitation and emission, slits were 2,2 nm, and for excitation: set $\lambda_{an} = 478$ nm, for emission: set $\lambda_{exc} = 375$ nm).

The main band of the excitation spectrum (**Figure 3-83**, blue trace) shows a maximum at 352 nm and the main band of the emission spectrum shows a maximum at 478 nm. The figure also shows that this polymer have a wide absorption when the wavelength is lower than 400 nm.

Following we are going to compare above results of the different polymers to evaluate the influence of the design on the photophysical properties.

3.1.15 Comparison of absorption and PL spectra of PF and P1



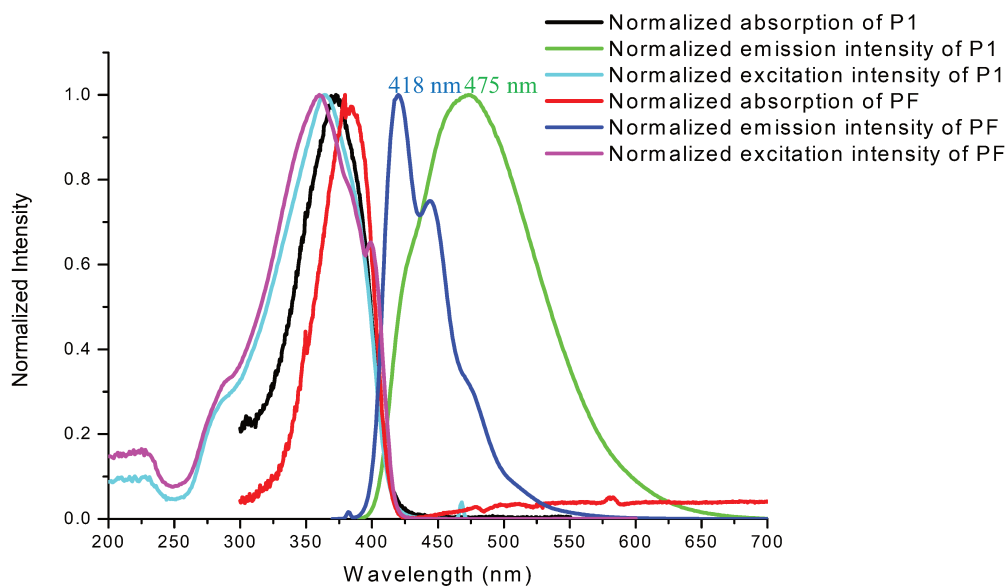


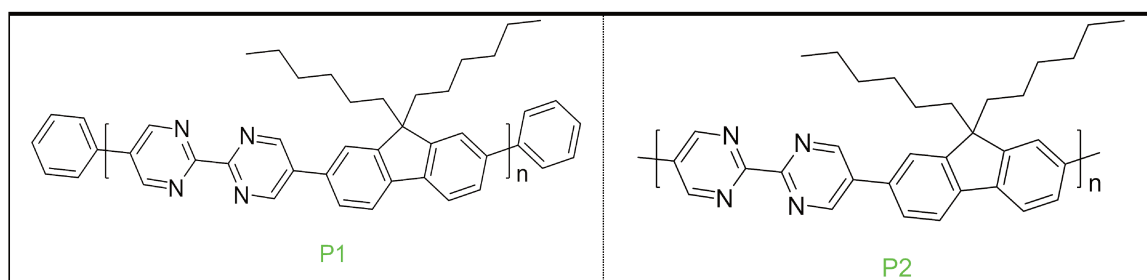
Figure 3-84 Comparison of **PF** and **P1** in DCM (0.01 mg/mL for **P1**, 0.005 mg/mL for **PF**, slits were 2,2 nm, and for emission: set $\lambda_{\text{exc}} = 375$ nm, excitation: set λ_{an} (**PF**) = 418 nm, λ_{an} (**P1**) = 475 nm).

Table 3-1 Summary of the performances of **PF** and **P1** in DCM (0.01 mg/mL for **P1**, 0.005 mg/mL for **PF**, slits were 2,2 nm, and for emission: set $\lambda_{\text{exc}} = 375$ nm, excitation: set λ_{an} (**PF**) = 418 nm, λ_{an} (**P1**) = 475 nm)

Polymer	λ_{abs} (nm)	λ_{exc} (nm)	λ_{em} (nm)	FWHM (nm)	CIE(x, y)
PF	380	360	418, 444	55	(0.153, 0.060)
P1	372	364	475	106	(0.178, 0.248)

As can be seen on **Figure 3-84**, the emission of **P1** is red shifted with respect to that of **PF**. This indicates that by introducing BPM as acceptor unit into the polyfluorene backbone, one can successfully reduce the bandgap. The shift of the emission spectrum is around 57 nm. Meanwhile, the FWHM data indicate that the (D-A)_n alternating polymer **P1** has a much broader emission band than the copolymer **PF**.

3.1.16 Comparison of absorption and PL spectra of P1 and P2



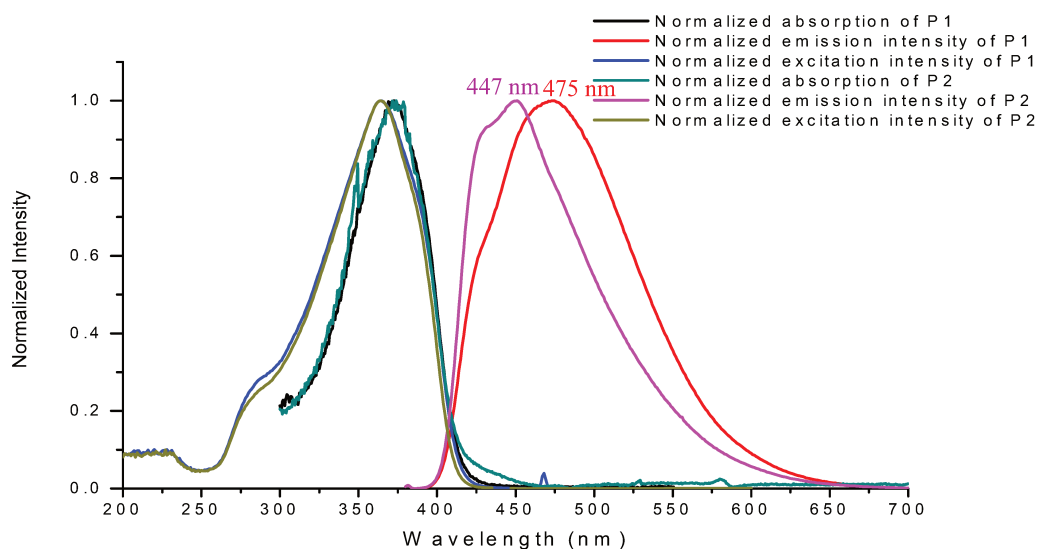


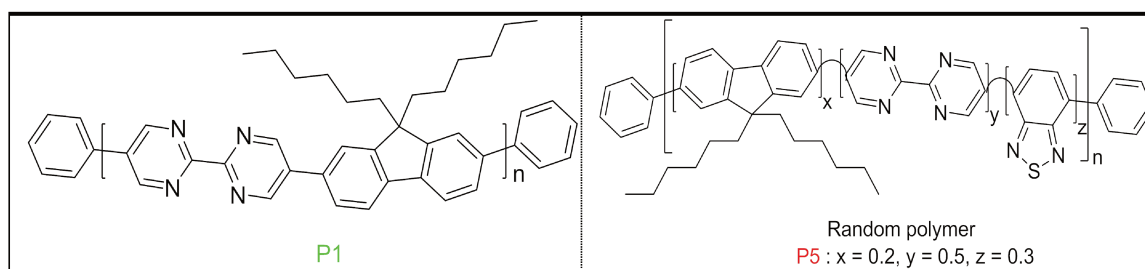
Figure 3-85 Comparison of **P1** and **P2** in DCM (0.01 mg/mL, slits were 2,2 nm, and for emission: set $\lambda_{\text{exc}} = 375$ nm, excitation: set $\lambda_{\text{an}}(\text{P1}) = 475$ nm, $\lambda_{\text{an}}(\text{P2}) = 447$ nm)

Table 3-2 Summary of performances of **P1** and **P2** in DCM (0.01 mg/mL, slits were 2,2 nm, and for emission: set $\lambda_{\text{exc}} = 375$ nm, excitation: set $\lambda_{\text{an}}(\text{P1}) = 475$ nm, $\lambda_{\text{an}}(\text{P2}) = 447$ nm)

Polymer	λ_{abs} (nm)	λ_{exc} (nm)	λ_{em} (nm)	FWHM (nm)	CIE(x, y)
P1	373	364	475	106	(0.178, 0.248)
P2	373	364	447	87	(0.169, 0.163)

P2 possesses the same polymer backbone as **P1** but without end-capping. **Figure 3-85** shows that the absorption and excitation spectra of **P1** and **P2** are very similar. However, it shows that the emission of **P2** is blue-shifted by approximately 28 nm compared to that of **P1**. This indicates that the end-capping can also play an important role in the emission. In the present case, it increases the conjugation. Meanwhile, the FWHM data indicate that the polymer **P1** with end-capping have a broader emission band than the polymer **P2**.

3.1.17 Comparison of absorption and PL spectra of P1, P5, P6 and P8



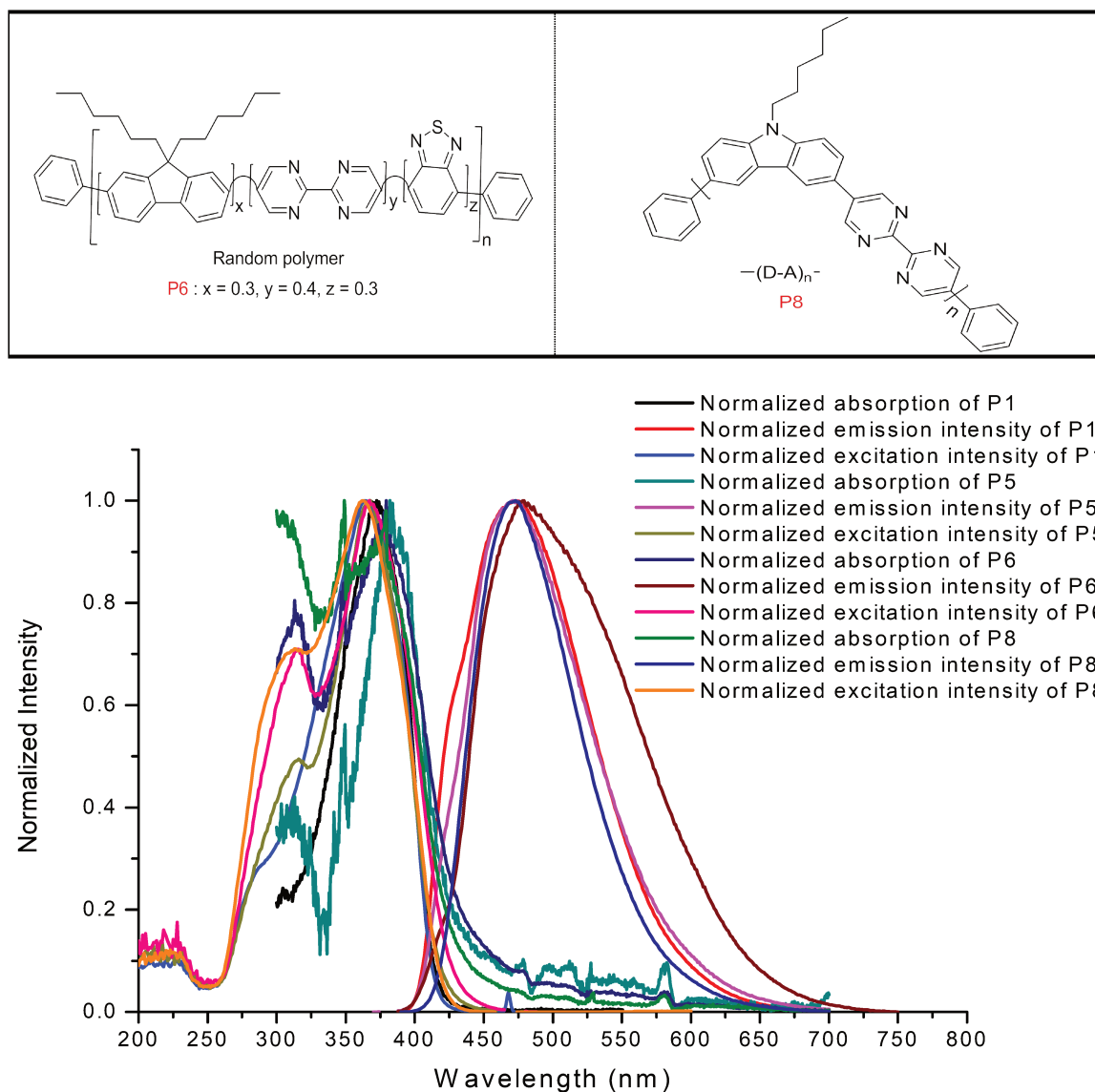


Figure 3-86 Comparison of **P1**, **P5**, **P6** and **P8** in DCM (0.01 mg/mL, slits were 2,2 nm, and for emission: set $\lambda_{exc} = 375$ nm, excitation: set λ_{an} (**P1**) = 475 nm, λ_{an} (**P5**) = 474 nm, λ_{an} (**P6**) = 479 nm, λ_{an} (**P8**) = 473 nm)

Table 3-3 Summary of performances of **P1**, **P5**, **P6** and **P8** in DCM (0.01 mg/mL, slits were 2,2 nm, and for emission: set $\lambda_{exc} = 375$ nm, excitation: set λ_{an} (**P1**) = 475 nm, λ_{an} (**P5**) = 474 nm, λ_{an} (**P6**) = 479 nm, λ_{an} (**P8**) = 473 nm)

Polymer	λ_{abs} (nm)	λ_{exc} (nm)	λ_{em} (nm)	FWHM (nm)	CIE(x, y)
P1	373	364	475	106	(0.178, 0.248)
P5	384	365	474	100	(0.185, 0.259)
P6	380	315, 367	479	128	(0.240, 0.346)
P8	379	362	473	85	(0.168, 0.245)

As shown on **Figure 3-86**, the absorption and excitation spectra of these polymers are similar. Concerning emission spectra, though the maxima are also similar, the random polymer **P6** shows

a much broader band and, as a consequence, its emission is red shifted compared to that of the others. Comparison between **P6** with **P5**, which are both random polymers but the fluorene amount is higher in **P6**, shows that **P6** possesses an increased band width. Regarding **P8** and **P1**, the introduction of 3,6-carbazole instead of 2,7-fluorene as donor unit has no much influence to the absorption and excitation properties, but the FWHM was decreased, which means the emitting color became more pure. These results show that the backbone of the polymers plays an important role in their optical properties.

3.1.18 Comparison of absorption and PL spectra of **P8** and **P9**

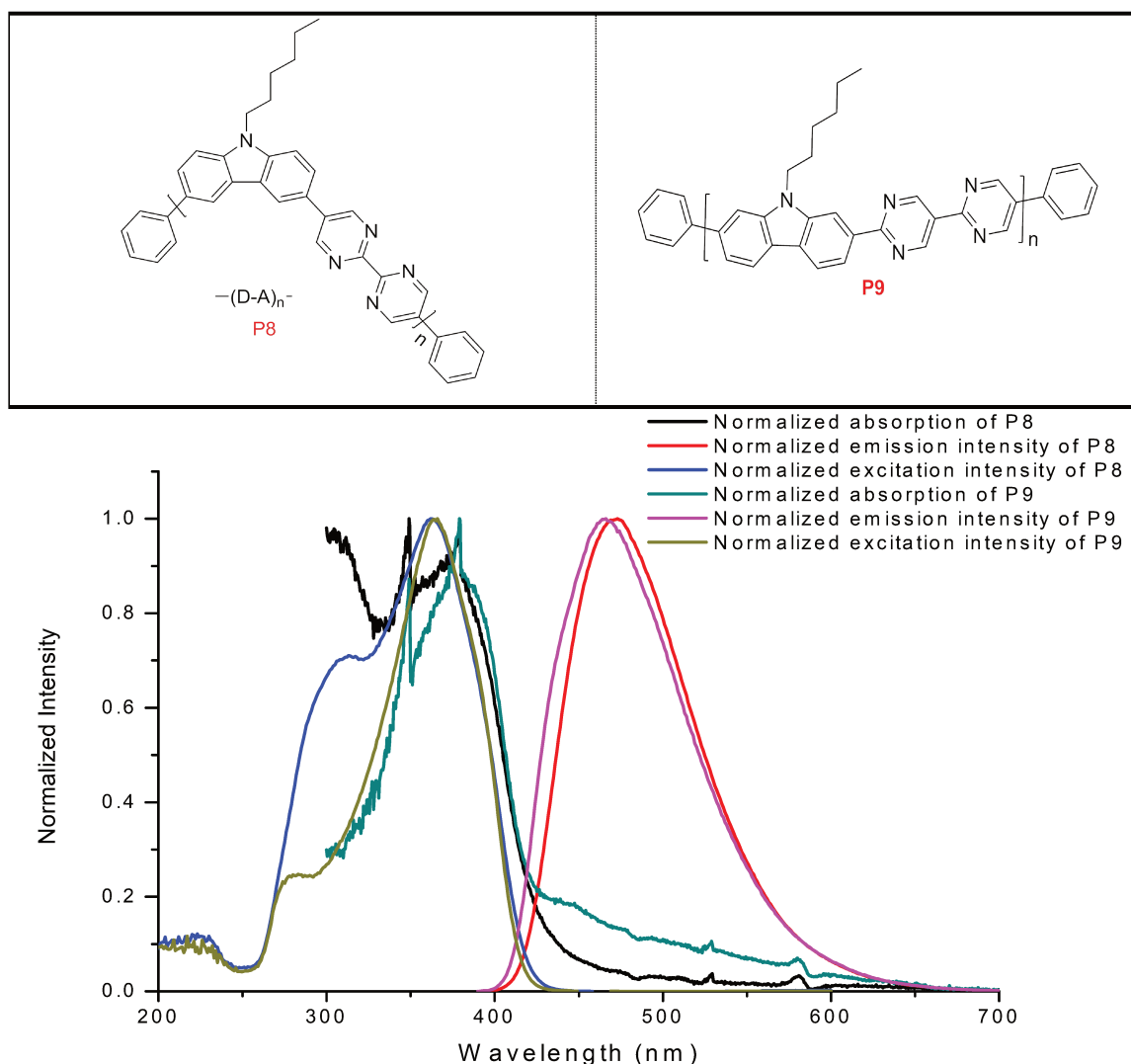


Figure 3-87 Comparison of **P8** and **P9** in DCM (0.01 mg/mL, slits were 2,2 nm, and for emission: set $\lambda_{\text{exc}} = 375$ nm, excitation: set λ_{an} (**P8**) = 473 nm, λ_{an} (**P9**) = 466 nm)

Table 3-4 Summary of performances of **P8** and **P9** in DCM (0.01 mg/mL, slits were 2,2 nm, and for emission: set $\lambda_{\text{exc}} = 375$ nm, excitation: set λ_{an} (**P8**) = 473 nm, λ_{an} (**P9**) = 466 nm)

Polymer	λ_{abs} (nm)	λ_{exc} (nm)	λ_{em} (nm)	FWHM (nm)	CIE(x, y)
P8	379	362	473	85	(0.168, 0.245)
P9	379.5	366	466	90	(0.169, 0.220)

As **Figures 3-87** shows, the data obtained for **P9** and **P8** are quite close, although **P9** used 2,7-carbazole instead of 3,6-carbazole as donor unit and was supposed to be more linear compared to **P8** (see **Figure 3-37**).

3.1.19 Comparison of absorption and PL spectra of P9 and P10

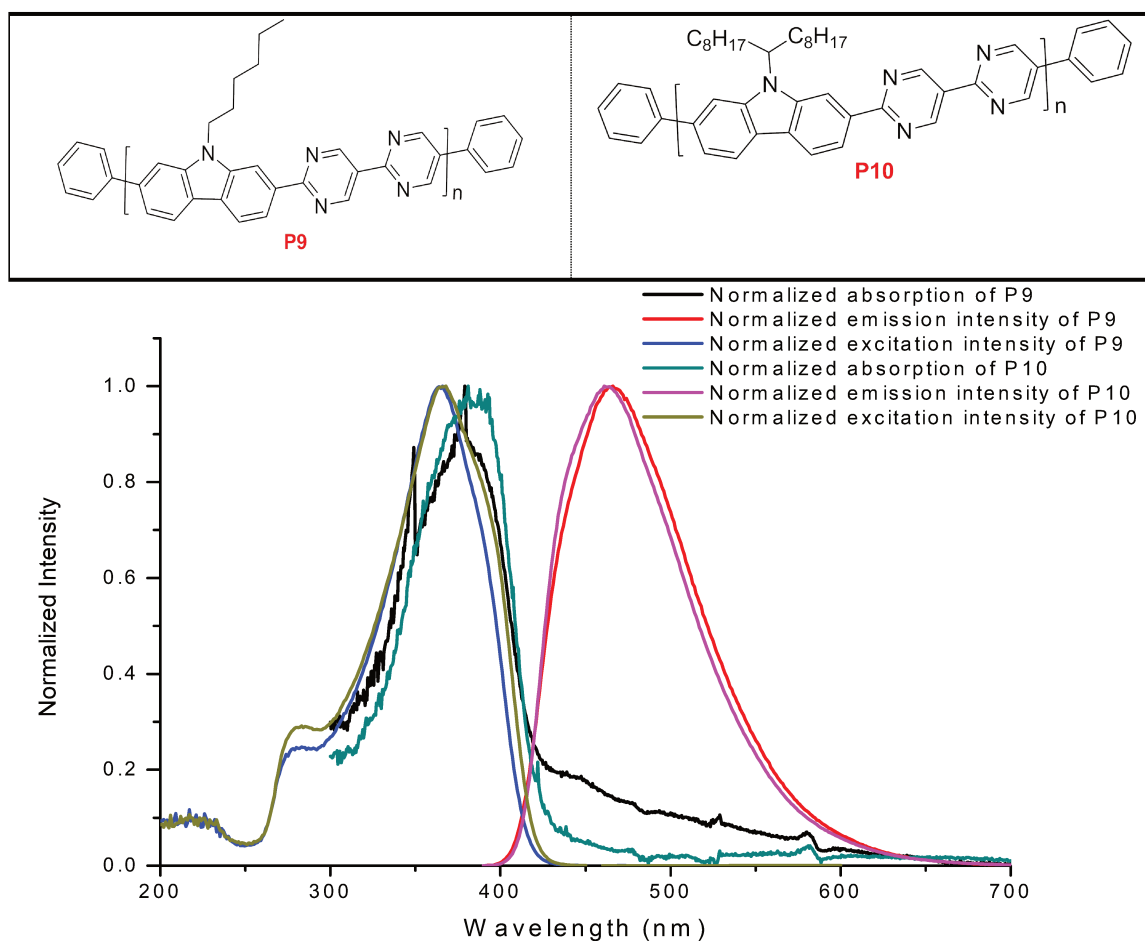


Figure 3-88 Comparison of **P9** and **P10** in DCM (0.01 mg/mL, slits were 2,2 nm, and for emission: set $\lambda_{\text{exc}} = 375$ nm, excitation: set λ_{an} (**P9**) = 466 nm, λ_{an} (**P10**) = 461 nm)

Table 3-5 Summary of performances of **P9** and **P10** in DCM (0.01 mg/mL, slits were 2,2 nm, and for emission: set $\lambda_{\text{exc}} = 375$ nm, excitation: set λ_{an} (**P9**) = 466 nm, λ_{an} (**P10**) = 461 nm)

Polymer	λ_{abs} (nm)	λ_{exc} (nm)	λ_{em} (nm)	FWHM (nm)	CIE(x, y)
P9	380	366	466	90	(0.169, 0.220)
P10	381	366	461	86	(0.166, 0.202)

Figure 3-88 shows the spectra of **P9** and **P10**. The data are relatively similar, as they have a similar linear backbone. It shows that the branched alkyl chains have few influence on the polymer's optical properties. It's worth mentioning that we have studied the solubility of these polymers. We used Dichlorobenzene (DCB) as solvent as it has higher boiling temperature, so that we can avoid the volume change of the solvent during the days under stirring and under sonicator. It shows that the solubility for **P9** is 10-15 mg and **P10** is 20-25 mg, in 1 mL of DCB at 20 °C. For example, 10 mg of **P9** dissolved all in 1 mL DCB. When added another 5 mg **P9** to the mixture, some sediments can be seen at the bottom of the bottle even it was stirred for 24 h. Hence it confirms the better solubility of **P10** compared to **P9**. Therefore, it is a good method to increase the solubility of the polymer by introducing a more bulky lateral chain.

3.1.20 Comparison of absorption and PL spectra of PF, P11 and P12

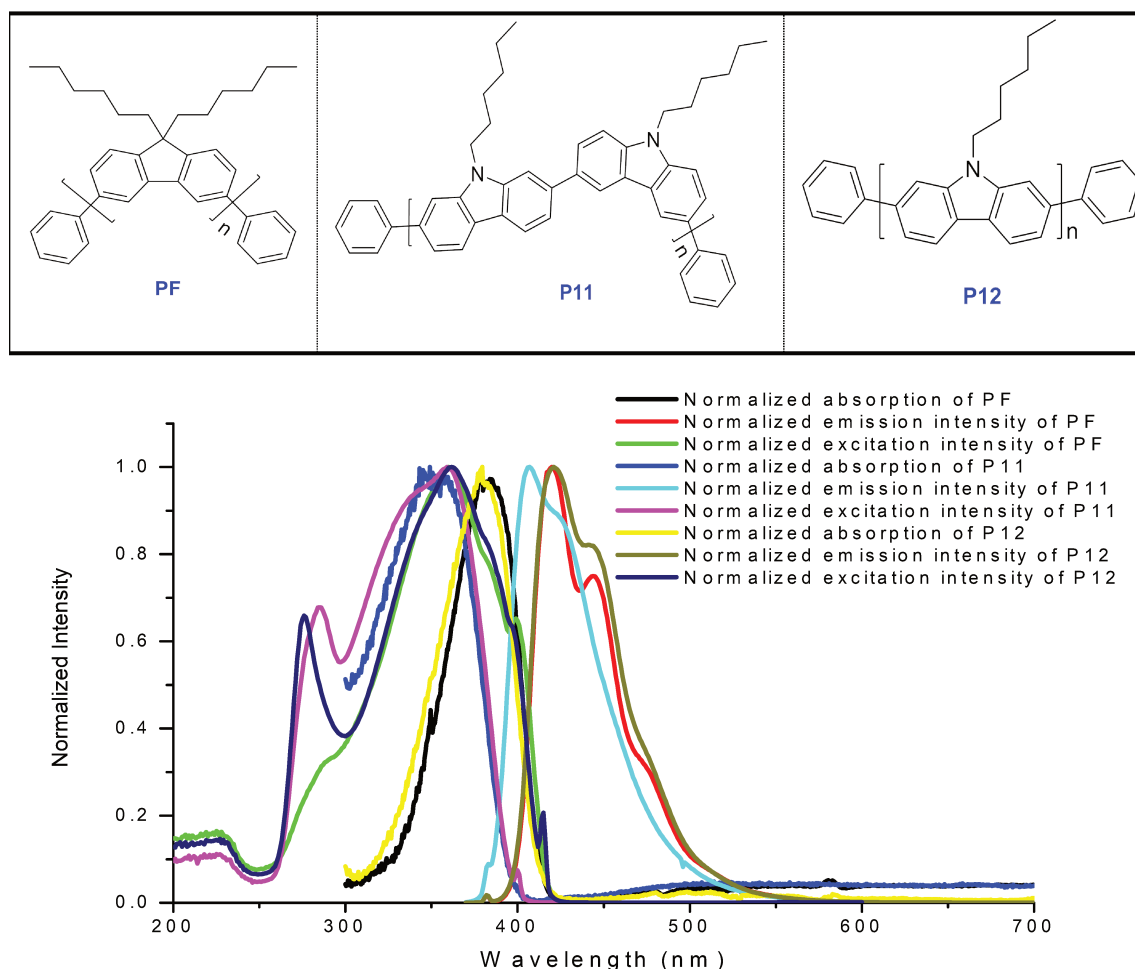


Figure 3-89 Comparison of **PF**, **P11** and **P12** in DCM (0.01 mg/mL for **P1**, 0.005 mg/mL for **PF**, slits were 2,2 nm, and for emission: set $\lambda_{\text{exc}} = 375$ nm, excitation: set $\lambda_{\text{an}}(\text{PF}) = 418$ nm, $\lambda_{\text{an}}(\text{P11}) = 407$ nm, $\lambda_{\text{an}}(\text{P12}) = 421$ nm)

Table 3-6 Summary of performances of **PF**, **P11** and **P12** in **DCM** (0.01 mg/mL for **P1**, 0.005 mg/mL for **PF**, slits were 2,2 nm, and for emission: set $\lambda_{\text{exc}} = 375$ nm, excitation: set λ_{an} (**PF**) = 418 nm, λ_{an} (**P11**) = 407 nm, λ_{an} (**P12**) = 421 nm)

Polymer	λ_{abs} (nm)	λ_{exc} (nm)	λ_{em} (nm)	FWHM (nm)	CIE(x, y)
PF	380	360	418, 444	55	(0.153, 0.060)
P11	343	290, 364	407, 421	57	(0.157, 0.050)
P12	380	276, 362	421, 444	56	(0.154, 0.050)

As above **Figure 3-89** shown, the results of **PF** and **P12** are quite close, probably because of a similar backbone conformation. It shows that the replacement of fluorene by carbazole has few influence on the optical properties. The FWHM of these polymers are similar. Among them, **P11**, which has a more zigzag conformation, is more blue shifted (see **Figure 3-56**).

3.1.21 Comparison of absorption and PL spectra of P6, P13 and P14

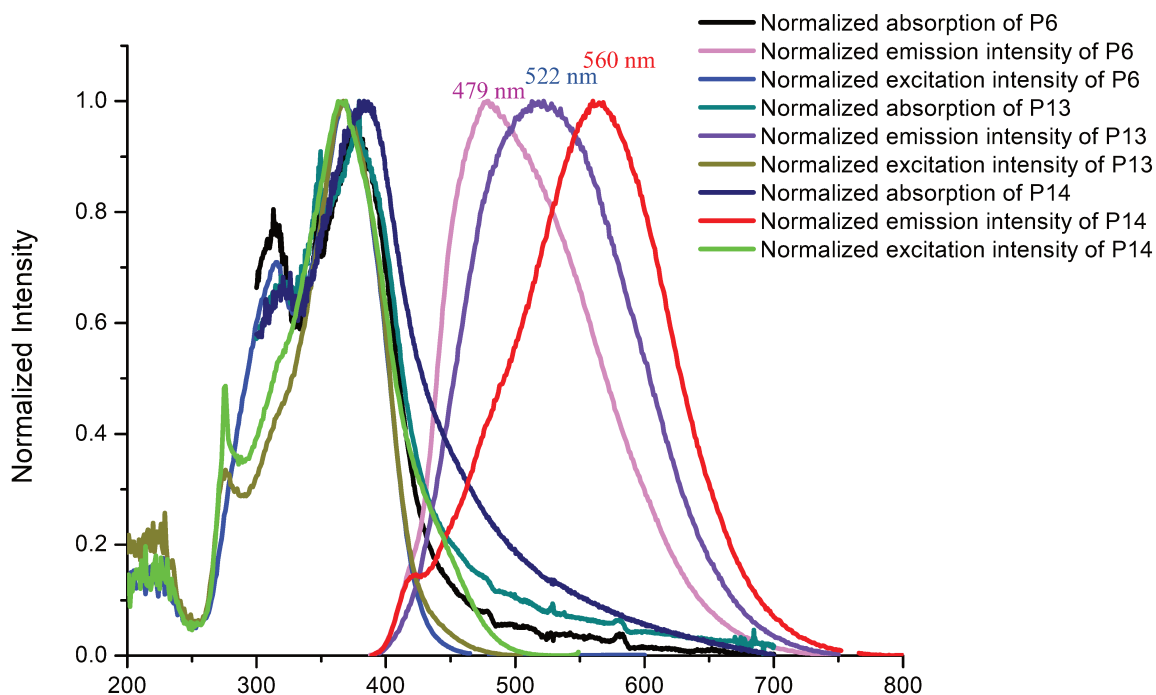
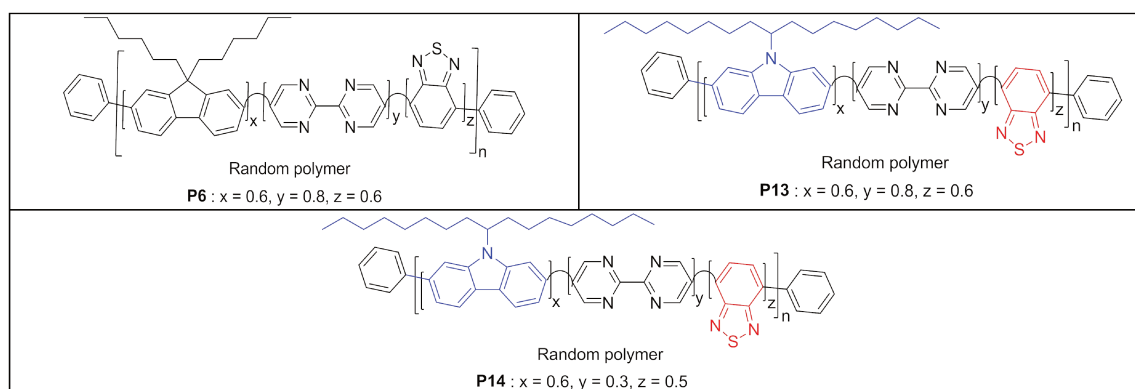


Figure 3-90 Comparison of **P6**, **P13** and **P14** in DCM (0.01 mg/mL, slits were 2,2 nm, and for emission: set $\lambda_{\text{exc}} = 375$ nm, excitation: set λ_{an} (**P6**) = 479 nm, λ_{an} (**P13**) = 522 nm, λ_{an} (**P14**) = 560 nm)

Table 3-7 Summary of performances of **P6**, **P13** and **P14** in DCM (0.01 mg/mL, slits were 2,2 nm, and for emission: set $\lambda_{\text{exc}} = 375$ nm, excitation: set λ_{an} (**P6**) = 479 nm, λ_{an} (**P13**) = 522 nm, λ_{an} (**P14**) = 560 nm)

Polymer	λ_{abs} (nm)	λ_{exc} (nm)	λ_{em} (nm)	FWHM (nm)	CIE(x, y)
P6	380	315, 367	479	128	(0.240, 0.346)
P13	391	278, 367	522	145	(0.299, 0.421)
P14	383	276, 369	560	143	(0.382, 0.457)

The spectra reported on **Figure 3-90** show that these random copolymers have a broad emission band; Replacing fluorene (**P6**) by carbazole (**P13**) as a donor unit not only red shifted the emission, but also broadened the emission band. When going from **P13** to **P14**, the increasing amount of benzo-thiadiazole as acceptor induces a red shift of the emission. To be noted, the FWHM of all these three random polymers are much higher than the alternating polymers we have designed and synthesized. Therefore, we may also reasonably come to the conclusion that one can improve the emission bandwidth by making random polymer instead of alternating polymer.

3.1.22 Comparison of absorption and PL spectra of P13 in different solvents

Previously, we have shown results of **P13** in Methylene chloride (DCM, polarity 3.40) which demonstrate cool white light [CIE (0.30, 0.42), CCT 6548 Kelvin] when excited at 375 nm. We further detected the luminescent property of **P13** in some other solvents that either have higher or lower polarity than DCM, including toluene (polarity 2.40), o-dichlorobenzene (DCB, polarity 2.70) and tetrahydrofuran (THF, polarity 4.20). The results obtained are discussed below.

(1) P13 in toluene

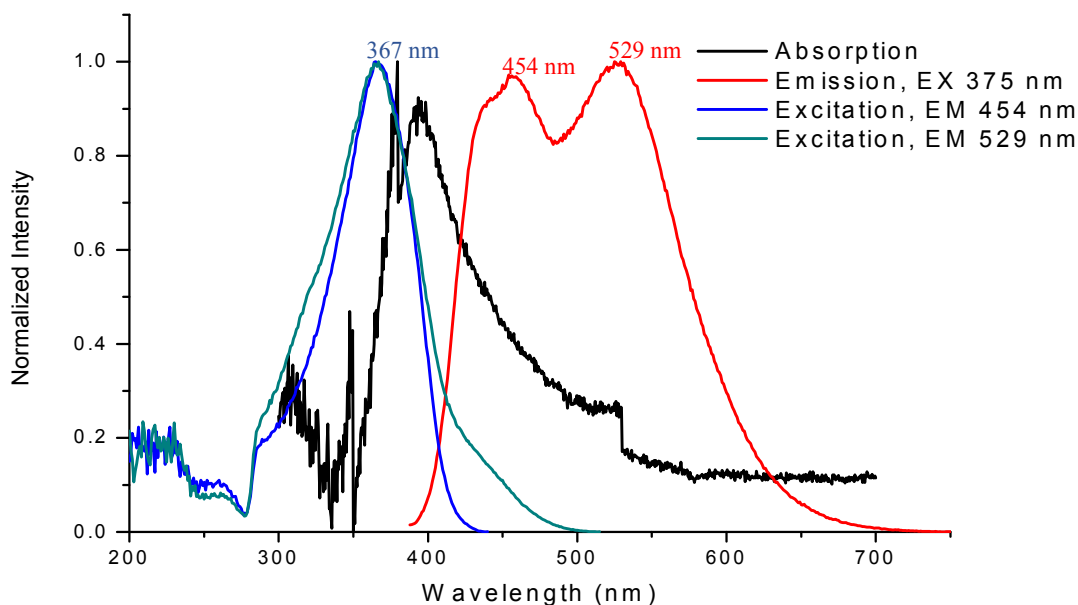


Figure 3-91 Normalized absorption, excitation and emission spectra of **P13 in toluene**

(0.01 mg/mL, slits were 2,2 nm, and for excitation: set $\lambda_{an} = 454$ and 529 nm, for emission: set $\lambda_{exc} = 375$ nm).

For the excitation spectra (blue and green), both $\lambda_{max} = 367$ nm. The absorption spectrum (black, $\lambda_{max} = 380$ nm and 397 nm) shows a broad band from 320 nm to 600 nm. The main bands of the emission spectrum show two maxima, at 454 nm and 529 nm, respectively.

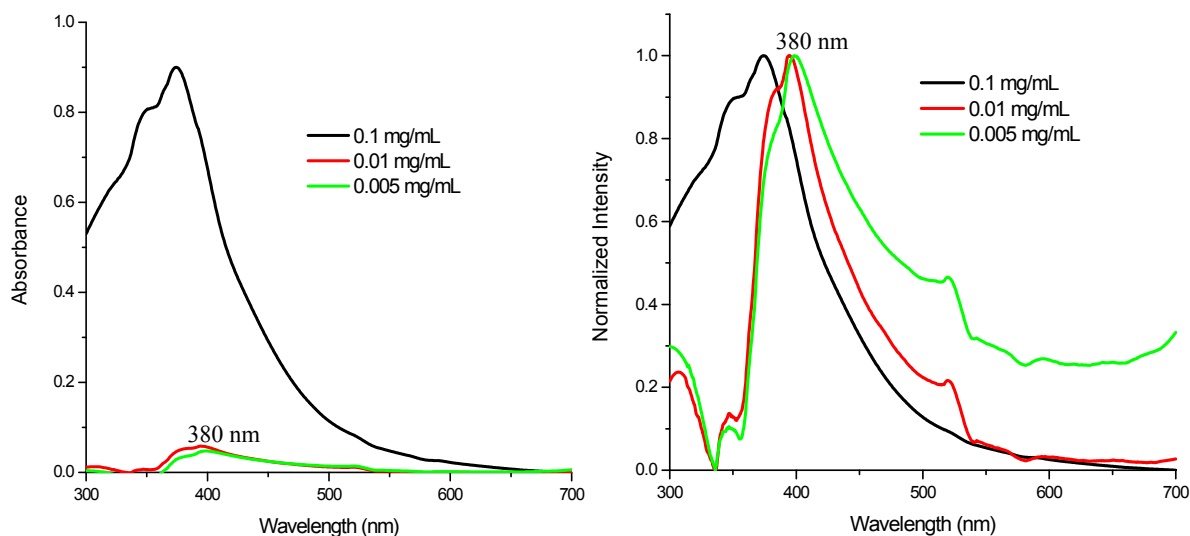


Figure 3-92 Absorption (the left) and Normalized absorption (the right) spectra of **P13 in toluene** at different concentration (slits were 2,2 nm)

The absorption spectra recorded at different concentrations all show a broad band from 300 nm to 700 nm. While the maximum is found at $\lambda_{max} = 380$ nm when the concentration is 0.1 mg/mL, when the solution was more and more diluted, the absorption spectrum showed a slight red-shift.

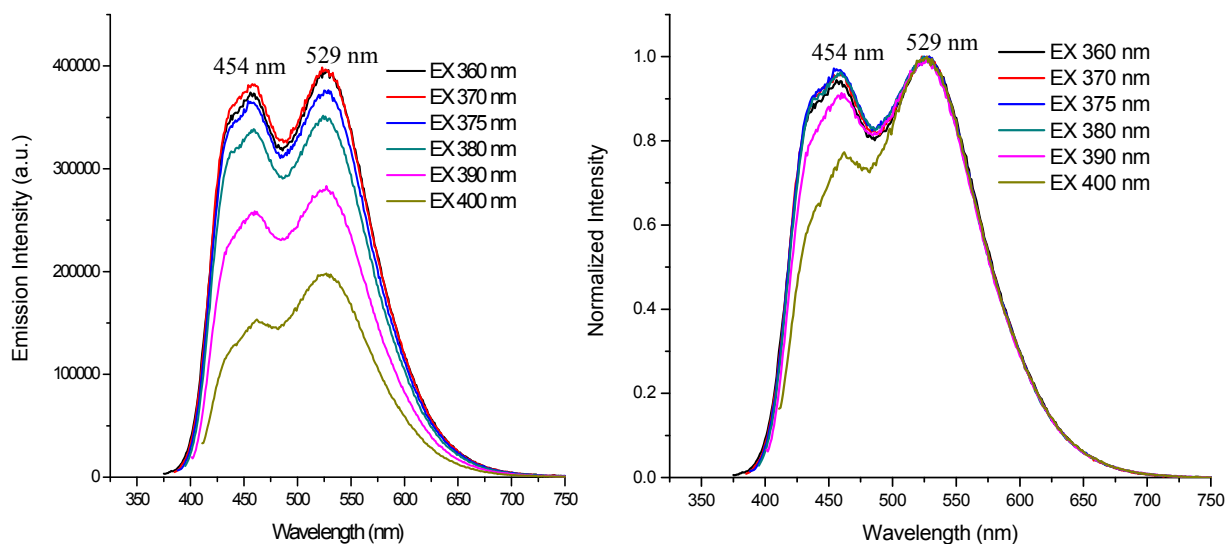
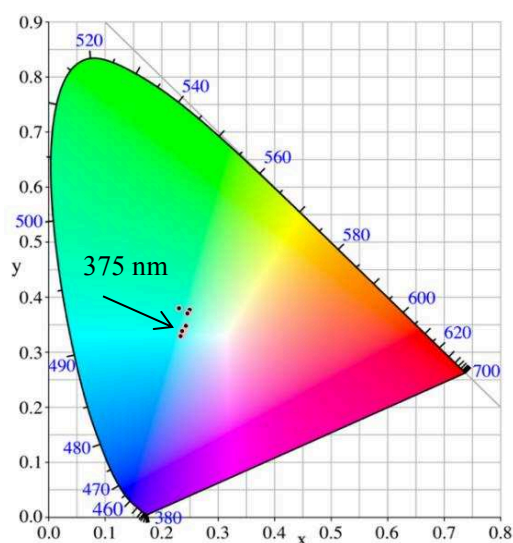


Figure 3-93 Emission (left) and normalized emission (right) spectra of **P13 in toluene** with different excitations (slits were 2,2 nm)

All emission spectra depicted on **Figure 3-93** show two maxima, at 454 nm and 529 nm, respectively, when the solution was excited at 375 nm.



λ_{exc}	CIE x	CIE y	CCT (K)
300 nm	0.230	0.380	10158
320 nm	0.250	0.377	9167
340 nm	0.243	0.348	10462
350 nm	0.239	0.339	11070
360 nm	0.236	0.333	11617
370 nm	0.235	0.330	11966
375 nm	0.234	0.329	12062
380 nm	0.233	0.330	12049
390 nm	0.236	0.339	11358
400 nm	0.246	0.371	9529

Figure 3-94 CIE coordinates of **P13 in toluene** (λ_{exc} = 300-400 nm, slits were 2,2 nm)

The **CIE coordinates** show that the material emits a bluish green emission under different excitations.

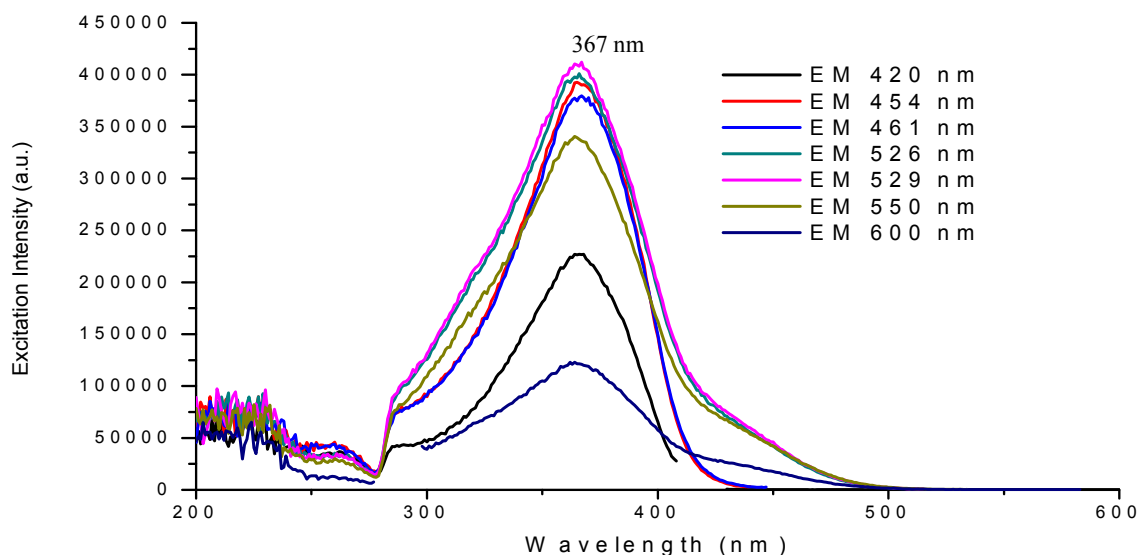


Figure 3-95 Excitation spectra of **P13** in **toluene** with different emissions (slits were 2,2 nm)

Above **Figure 3-95** shows the excitation spectra have a maximum at 367 nm when set with different emission wavelength.

(2) P13 in DCB

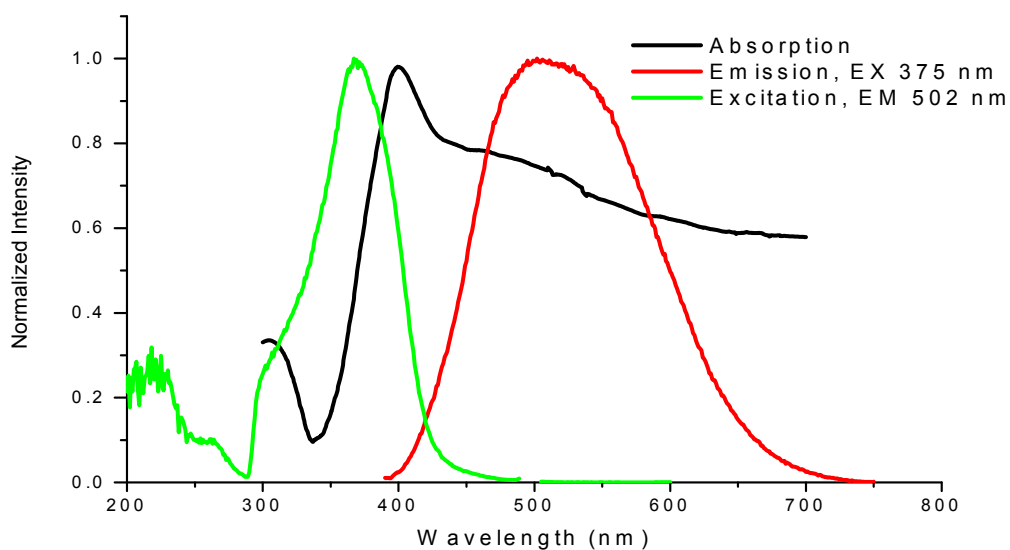


Figure 3-96 Normalized absorption, excitation and emission spectra of **P13** in **DCB**

(0.01 mg/mL, slits were 2,2 nm, and for excitation: set $\lambda_{an} = 502$ nm, for emission: set $\lambda_{exc} = 375$ nm)

As shown on **Figure 3-96**, for the excitation spectra (green), $\lambda_{max} = 365$ nm. The absorption spectrum (black, $\lambda_{max} = 404$ nm) shows a broad band from 300 nm to 700 nm. The main band of the emission spectrum show a maxima at 502 nm.

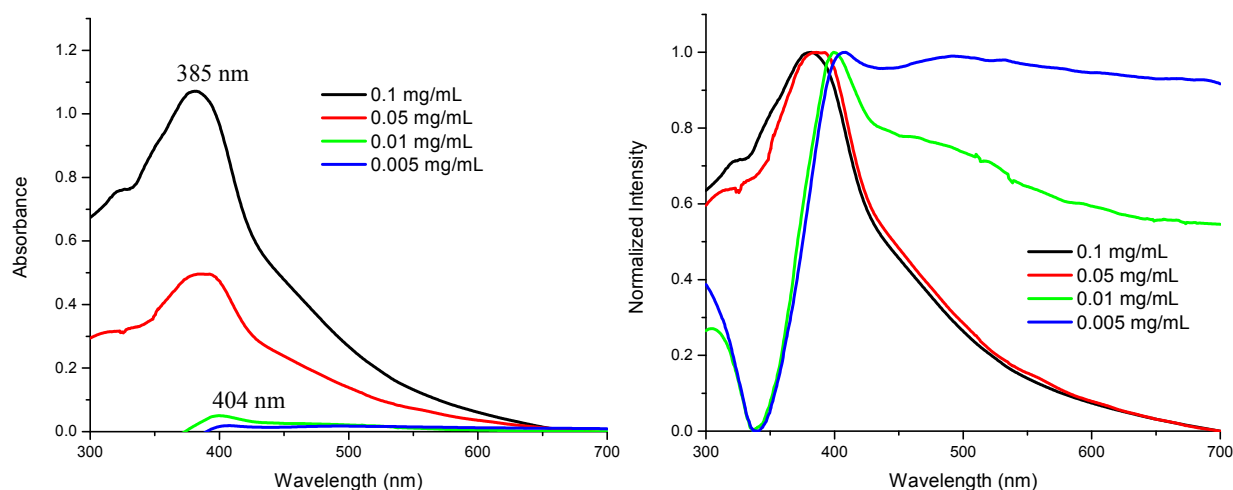


Figure 3-97 Absorption (the left) and Normalized absorption (the right) spectra of **P13 in DCB** at different concentration (slits were 2,2 nm)

The absorption spectra at different concentrations all show a broad band from 300 nm to 700 nm. The maxima are found from 385 nm to 404 nm when the concentration of the solution was decreased from 0.1 mg/mL to 0.005 mg/mL, which also shows a red-shift tendency.

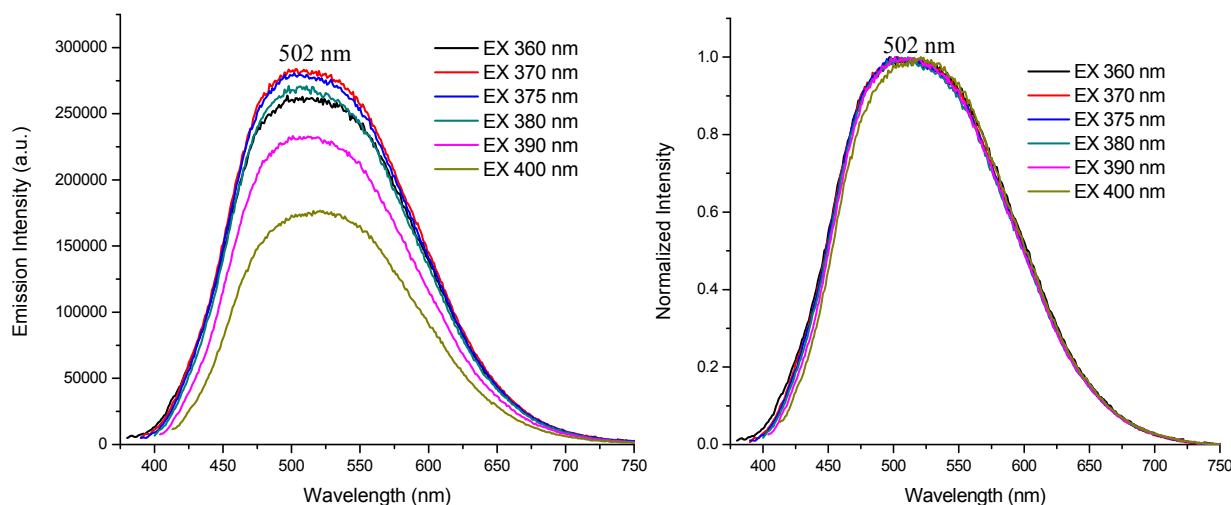
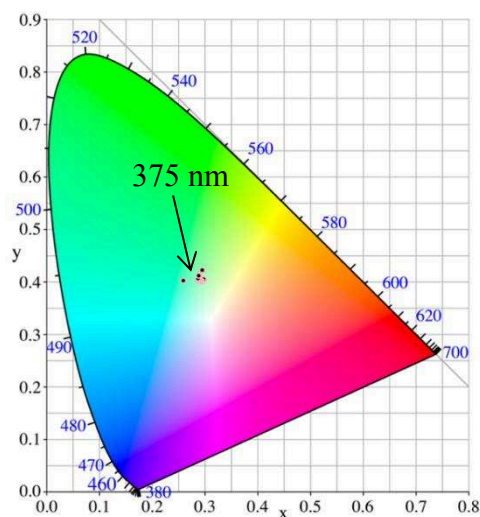


Figure 3-98 Emission (left) and normalized emission (right) spectra of **P13 in DCB** with different excitations (slits were 2,2 nm)

Figure 3-98 shows a broad emission spectrum from 400 nm to 750 nm with a maximum at around 502 nm when the excitation wavelength was between 360 nm to 400 nm. The normalized emission spectra show identical emission profile despite the intensity changes.



λ_{exc}	CIE x	CIE y	CCT (K)
300 nm	0.259	0.403	8242
320 nm	0.297	0.405	6691
340 nm	0.294	0.401	6837
350 nm	0.292	0.402	6915
360 nm	0.289	0.403	7014
370 nm	0.288	0.404	7067
375 nm	0.287	0.405	7087
380 nm	0.286	0.407	7087
390 nm	0.288	0.412	6977
400 nm	0.295	0.423	6672

Figure 3-99 CIE coordinates of **P13 in DCB** with different emissions ($\lambda_{\text{exc}} = 300\text{-}400$ nm, slits were 2,2 nm)

The **CIE coordinates** show the material emits **cool white light (5000-8300 K CCT)** under different excitations from 300-400 nm.

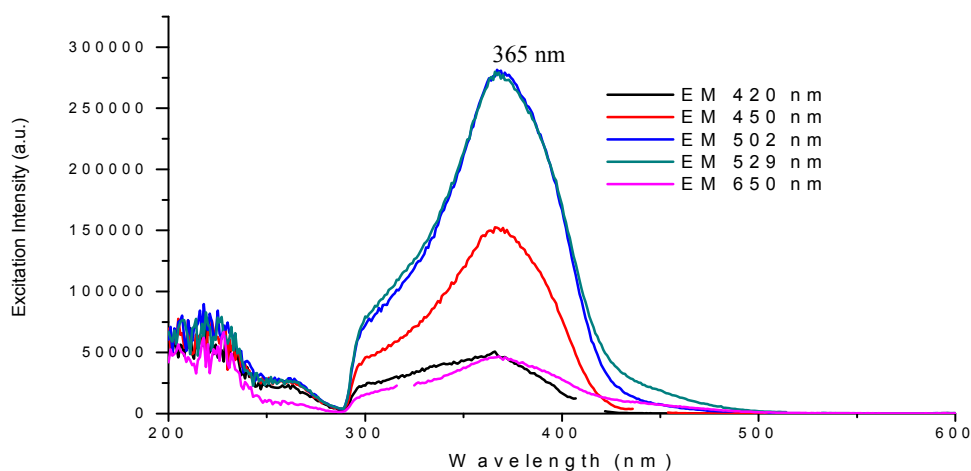


Figure 3-100 Excitation spectra of **P18 in DCB** with different emissions (slits were 2,2 nm)

Above figure shows that the excitation spectra have a maximum at around 365 nm with different excitation wavelength.

(3) P13 in THF

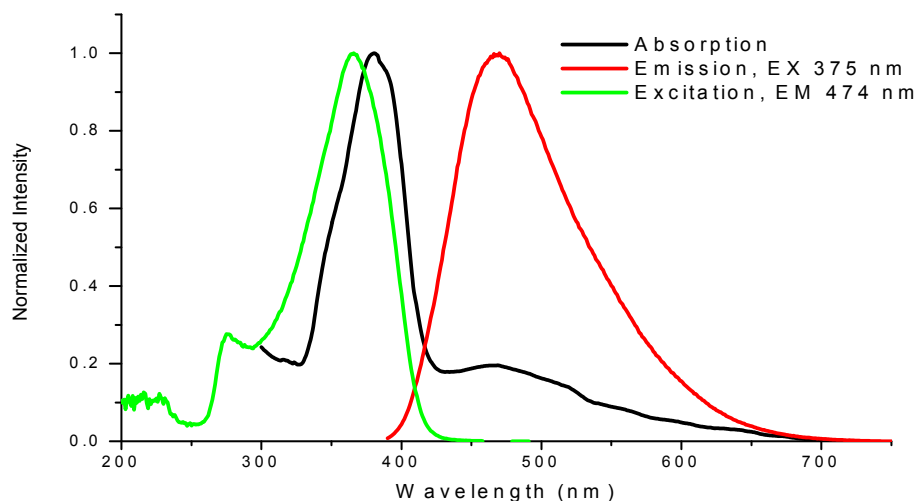


Figure 3-101 Normalized absorption, excitation and emission spectra of **P13 in THF**

(0.01 mg/mL, slits were 2,2 nm, and for excitation: set $\lambda_{an} = 474$ nm, for emission: set $\lambda_{exc} = 375$ nm)

For the excitation spectra (**Figure 3-101**, green trace), two maxima at 275 nm and 365 nm respectively were shown. The absorption spectrum (black trace, $\lambda_{max} = 380$ nm) shows a broad band from 300 nm to 700 nm. The main band of the emission spectrum shows a maximum at 474 nm.

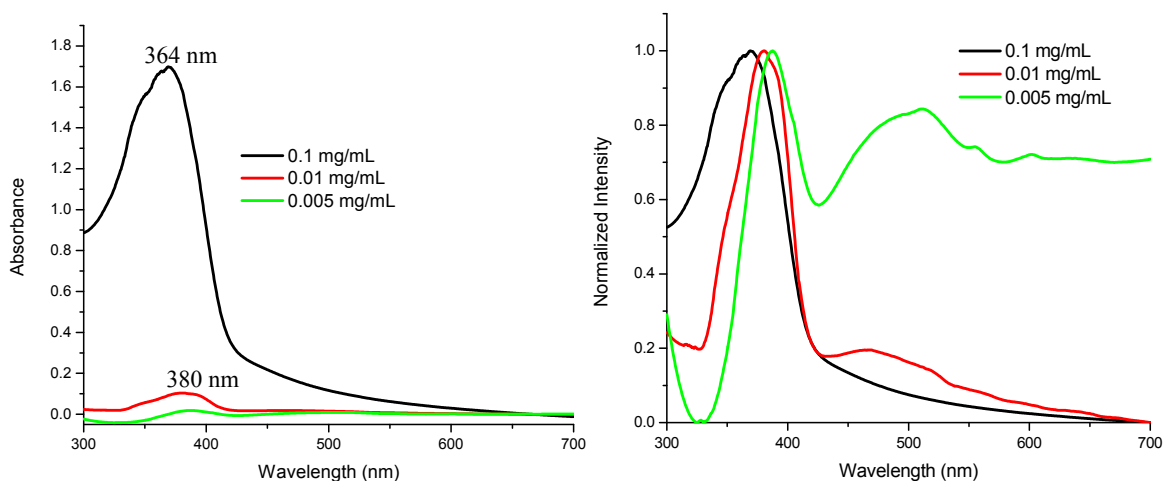


Figure 3-102 Absorption (left) and Normalized absorption (right) spectra of **P13 in THF** at different concentrations (slits were 2,2 nm)

The absorption spectra at different concentration all show a broad band from 300 nm to 700 nm. The maxima are at 364 nm to 380 nm when the concentration of the solution is diluted from 0.1 mg/mL to 0.005 mg/mL, which also shows a red-shift tendency.

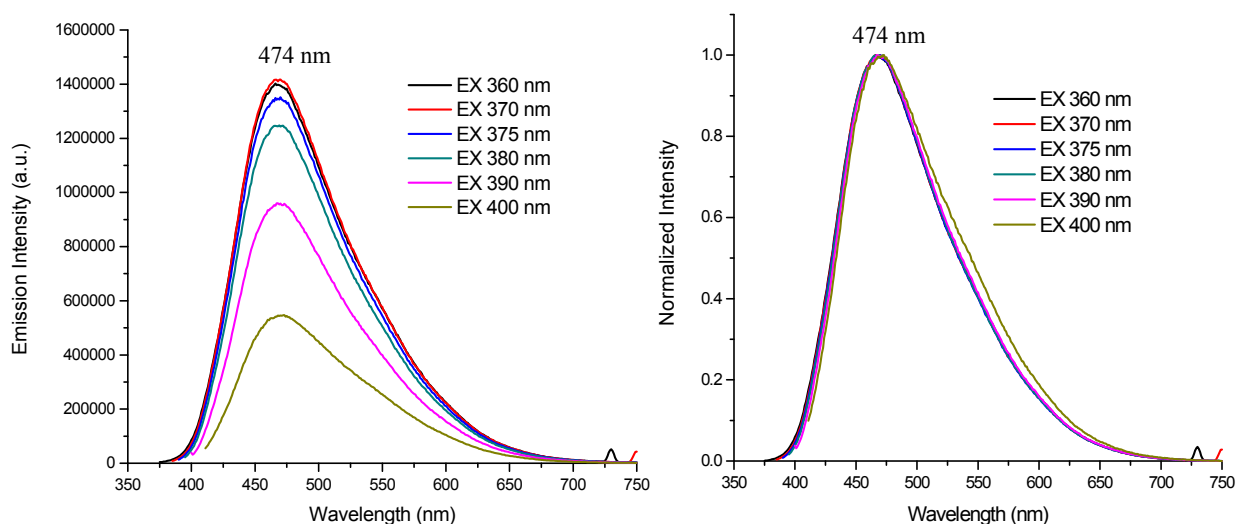
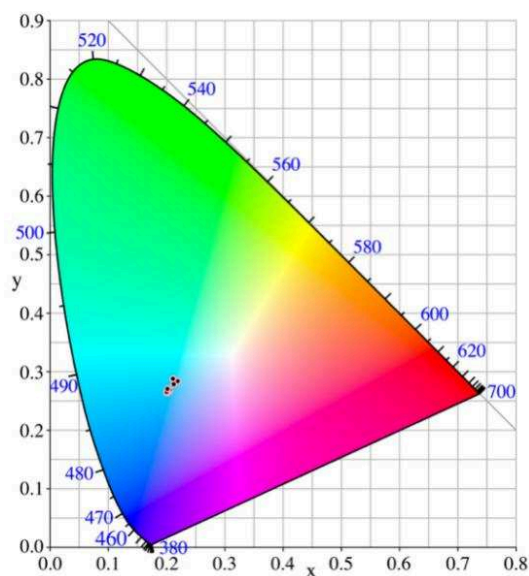


Figure 3-103 Emission (left) and normalized emission (right) spectra of **P13 in THF** with different excitations (slits were 2,2 nm)

Emission spectra obtained after excitation with different wavelengths in the range 360-400 nm are similar (**Figure 3-103**) show a broad band ranging from 375 nm to 725 nm with a maximum at around 474 nm when the excitation wavelength was set between 360 nm to 400 nm. The normalized emission spectra show identical emission profile despite the intensity changes.



λ_{exc}	CIE x	CIE y
300 nm	0.219	0.283
320 nm	0.212	0.279
340 nm	0.205	0.268
350 nm	0.203	0.265
360 nm	0.201	0.264
370 nm	0.200	0.264
375 nm	0.200	0.264
380 nm	0.200	0.265
390 nm	0.202	0.271
400 nm	0.211	0.288

Figure 3-104 CIE coordinates of **P13 in THF** (λ_{exc} = 300-400 nm, slits were 2,2 nm)

The **CIE coordinates** show that the material emits a greenish blue light under excitation in the range of 300-400 nm.

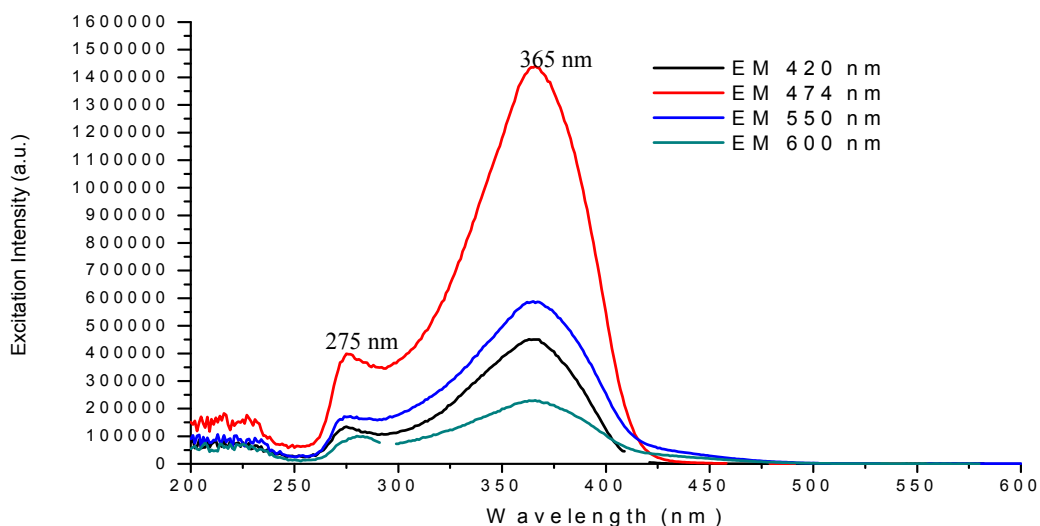


Figure 3-105 Excitation spectra of **P13** in **THF** with different emissions (slits were 2,2 nm)

Figure 3-105 shows that the excitation spectrum has two bands with maxima at around 275 nm and 365 nm, respectively, whatever the emission wavelength is.

(4) Comparison of P13 in different solvents

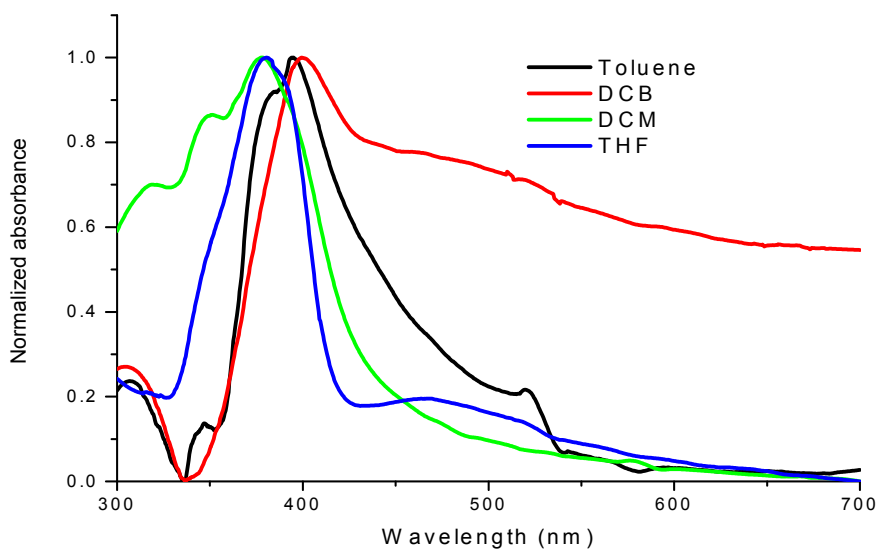


Figure 3-106 Normalized absorption spectra of **P13** in different solvents ($\lambda_{\text{exc}} = 375$ nm, slits were 2,2 nm)

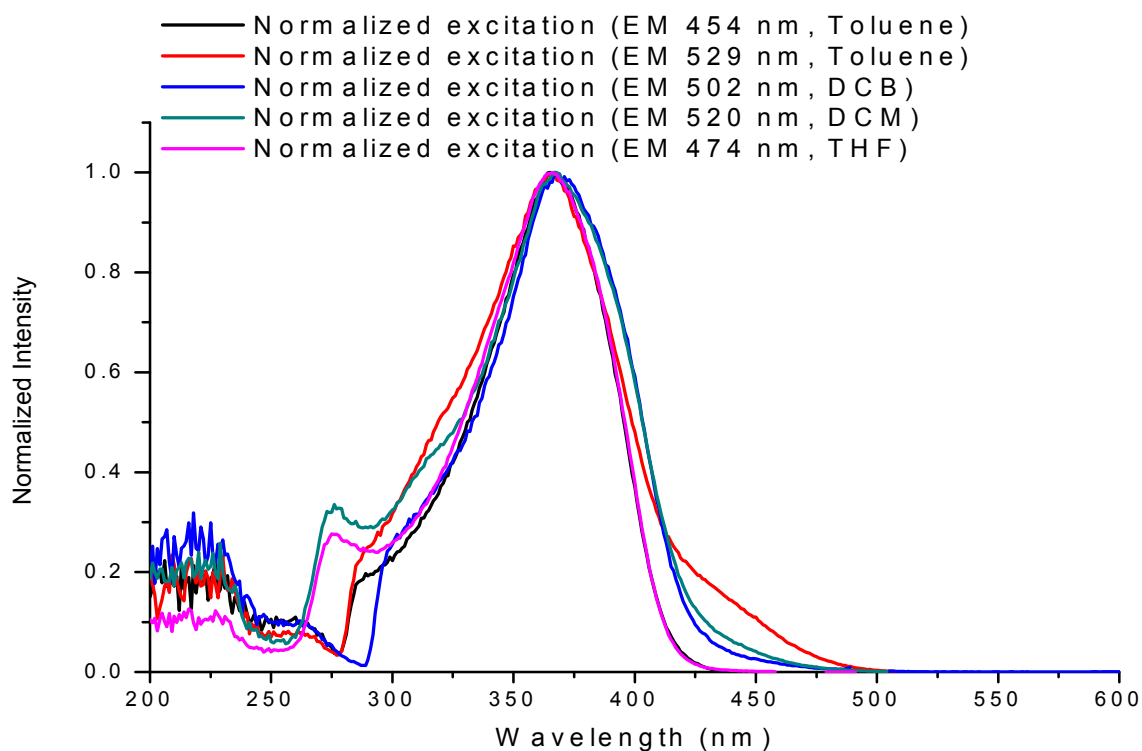


Figure 3-107 Normalized excitation spectra of **P13** in different solvents (slits were 2,2 nm)

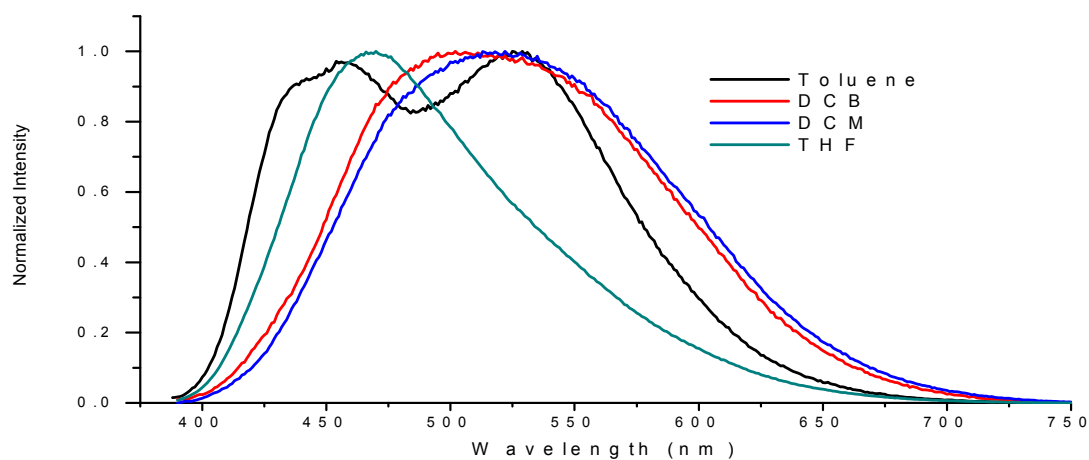


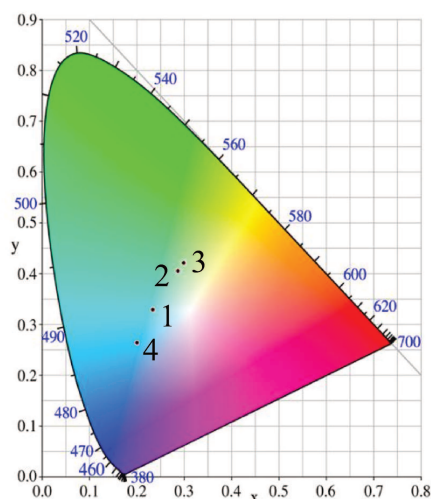
Figure 3-108 Normalized emission spectra of **P13** in different solvents ($\lambda_{exc} = 375$ nm, slits were 2,2 nm)

Table 3-8 Summary of photophysical data of **P13** in different solvents (slits were 2,2 nm)

Solvents	Polarity	$\lambda_{max,absorption}$	$\lambda_{max,emission}$ ($\lambda_{exc} = 375$ nm)	$\lambda_{max,excitation}$ (λ_{an}) [*]
Toluene	2.40	380 nm, 397 nm	454 nm, 529 nm	367 nm
DCB	2.70	404 nm	502 nm	365 nm
DCM	3.40	380 nm	520 nm	367 nm
THF	4.20	380 nm	474 nm	275 nm, 365 nm

* λ_{an} is correspond to the wavelength in emission spectrum that gives maximum intensity

Comparison of spectra of **P13** in different solvents are reported in **Figure 3-106, 3-107, and 3-108**. They show that the solvent influences the photophysical properties of the material. The solvatochromic effect was displayed from the emission spectra. While they all show a broad band between 400-750 nm, the maximum emissions have big difference. Especially, two bands are shown in the emission spectrum measured in toluene.

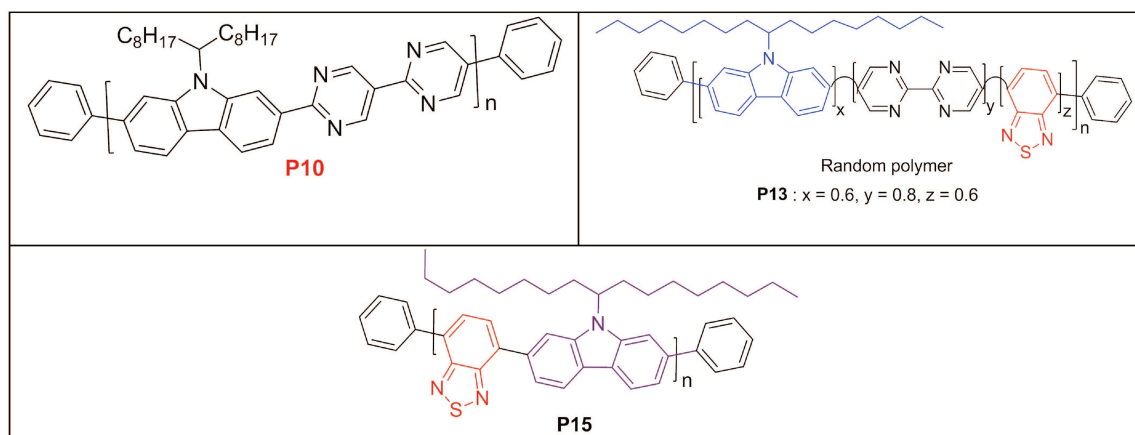


No.	Solvent	CIE x	CIE y	CCT (K)
1	Toluene	0.234	0.329	12062
2	DCB	0.287	0.405	7087
3	DCM	0.299	0.421	6548
4	THF	0.200	0.264	29294

Figure 3-109 CIE coordinates of **P13** in different solvents ($\lambda_{exc} = 375$ nm, slits were 2,2 nm)

The **CIE coordinate diagram** shows that **P13** emits **cool white light (5000-8300 K CCT)** when excited at 375 nm both in DCB and DCM, while the blue component is too important in THF and Toluene to get white light.

3.1.23 Comparison of absorption and emission spectra of P10, P13 and P15



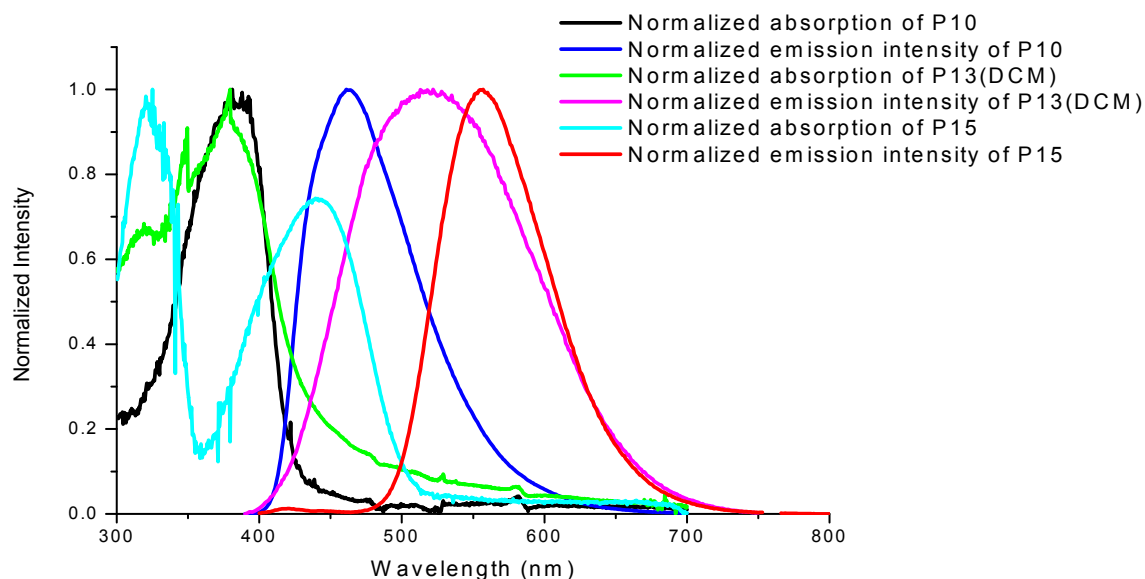


Figure 3-110 Comparison of **P10**, **P13** and **P15** in DCM (0.01 mg/mL, slits were 2,2 nm, and for emission: set $\lambda_{\text{exc}} = 375$ nm)

Table 3-9 Summary of performances of **P10**, **P13** and **P15** in DCM (0.01 mg/mL, slits were 2,2 nm, and for emission: set $\lambda_{\text{exc}} = 375$ nm, excitation: set λ_{an} (**P10**) = 461 nm, λ_{an} (**P13**) = 522 nm, λ_{an} (**P15**) = 557 nm)

Polymer	λ_{abs} (nm)	λ_{exc} (nm)	λ_{em} (nm)	FWHM (nm)	CIE(x, y)
P10	381	366	461	86	(0.166, 0.202)
P13	391	278, 367	522	145	(0.299, 0.421)
P15	325, 441	278, 330, 431	557	89	(0.428, 0.550)

In comparison with the alternating polymers **P10** and **P15**, the emission spectrum of the random polymer **P13** shows a much broader band. Meanwhile, it again confirms that the polymer with more benzo-thiadiazole as acceptor shows the most red shifted emission. Especially in the case of **P15**, which only contains benzo-thiadiazole as acceptor, for which the spectrum is the most red-shifted.

3.2 Polymers as pure thin films

The optical properties of the polymers spin-coated as pure thin films will now be presented. Films were prepared according to the method previously described in §2.4 of Chapter II. Some polymers (**P3**, **P4**, **P5** and **P8**) were not fully studied because of their poor solubility and processability. A pure film of **PF** was used as an example to evaluate the thickness of films made by spin-coating. The measurement reported on **Figure 3-111** shows that the thickness is around 50 nm.

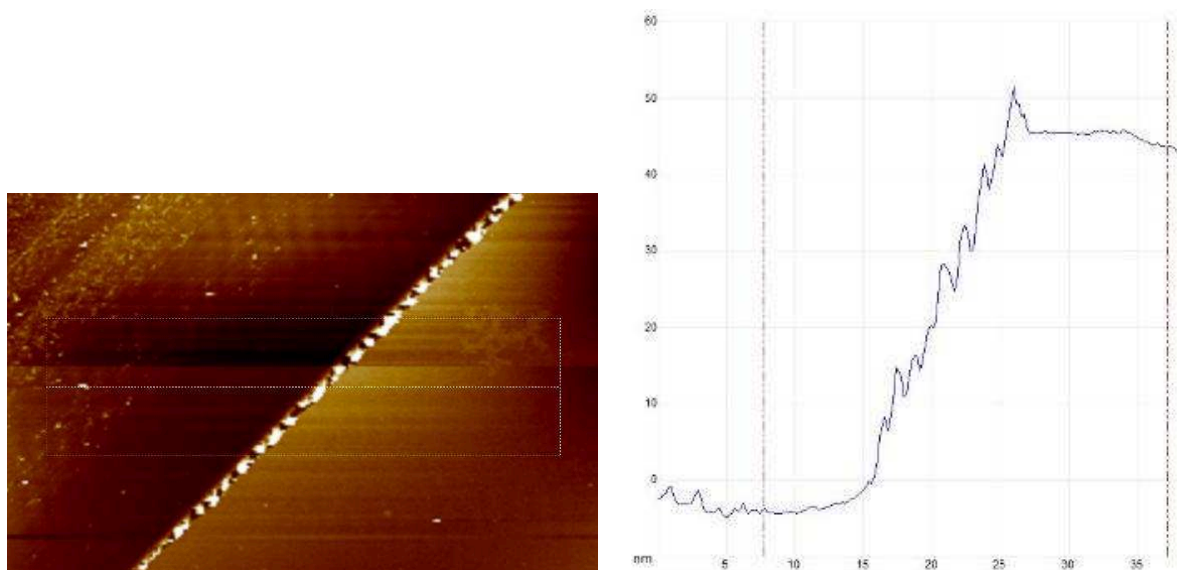


Figure 3-111 The thickness of PF film obtained by spin-coating

3.2.1 Absorption

Figure 3-112 shows the absorption spectra of **PF**, **P1**, **P8**, **P9**, **P10**, **P11**, **P12**, **P13**, **P14** and **P15** as pure thin films. The first figure shows the absorption of three blue emitting polymers. The maxima of the main bands are found at 381 nm, 355 nm and 375 nm, for **PF**, **P11**, and **P12**, respectively, corresponding to the intramolecular charge transfer (ICT) transition in the polymer chains. A weak absorption with maximum at 536 nm is also seen for **P12** which is corresponding to the delocalized excitonic π - π^* transition.¹⁶⁵ The second figure shows the absorption of four green emitting polymers. The maxima for **P1**, **P8**, **P9**, **P10** are found at 371 nm, 374 nm, 374 nm and 371 nm, respectively. These results are close. The third figure shows the absorption of three white emitting polymers. The maximum of emission is found at 370 and 372 nm for **P13** and **P14**, respectively, which is quite close as well. This can be explained by the presence of the three same monomers in these two polymers. The absorption spectrum of **P15** shows a band with two maxima at 346 and 479 nm, respectively. The first band may ascribed to the carbazole unit, while the second one may due to the benzo-thiadiazole unit.

¹⁶⁵ a. J. U. Kima, S. S. Reddy, L.-S. Cui, H. Nomura, S. Hwang, D. H. Kim, H. Nakanotani, S.-H. Jinc, C. Adachi. *Journal of Luminescence*, **2017**, 190, 485-491.

b. J. Kima, S. Chaeb, A. Yib, S. Hongb, H. J. Kimb, H. Suh. *Synthetic Metals*, **2018**, 245, 267-275.

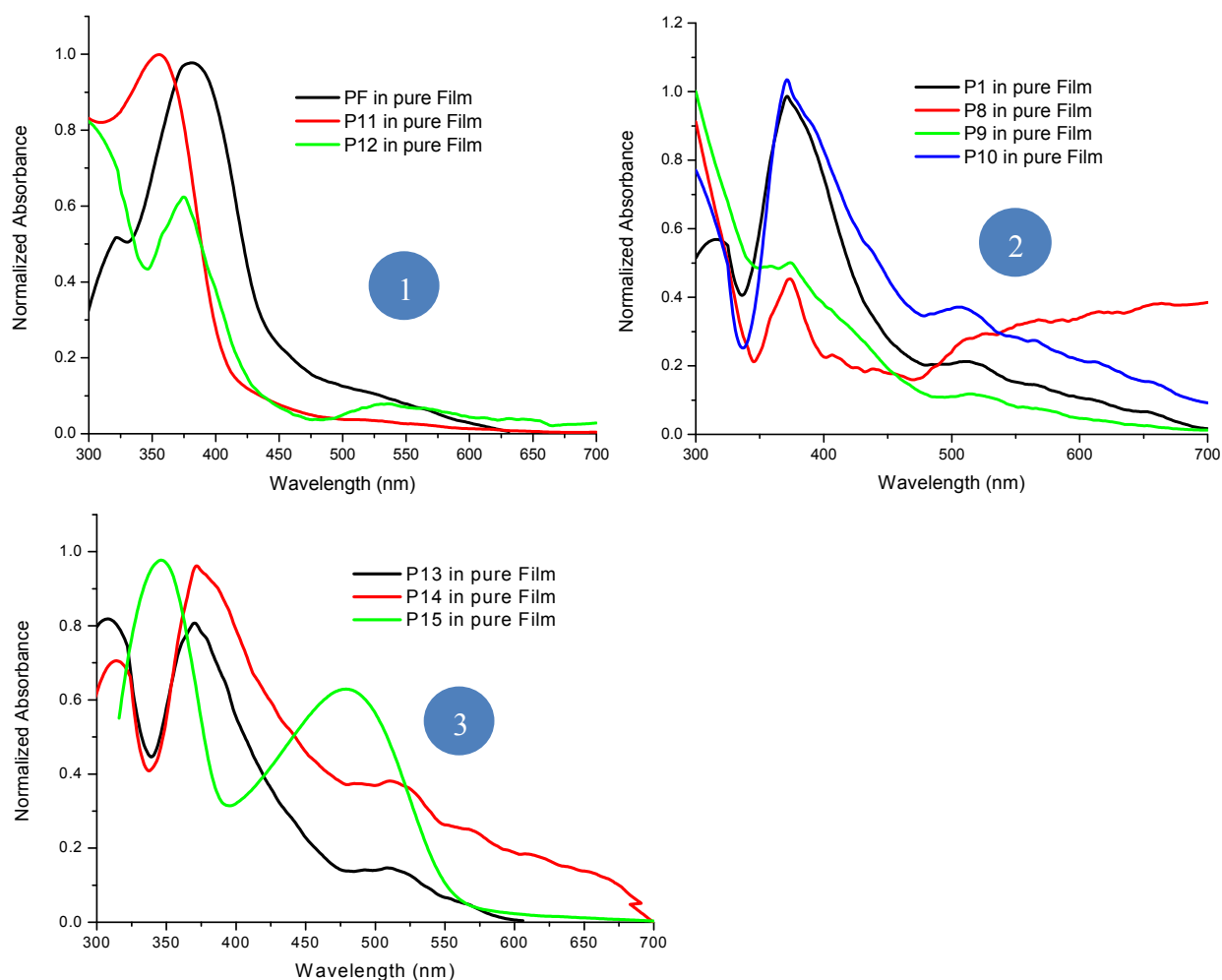


Figure 3-112 Absorption spectra of polymers in pure film.

Table 3-9 Absorption data of polymers in pure film (5 mg/mL, slits were 5,5 nm) and in DCM (0.01 mg/mL, slits were 2,2 nm)

Polymer	Solution (DCM)		Film
	$\lambda_{\text{abs, max}}$ (nm)	$\lambda_{\text{exc, max}}^*$ (nm)	$\lambda_{\text{abs, max}}$ (nm)
PF	380	360	322, 381
P1	373	364	315, 371, 512
P2	373	364	-
P5	384	365	-
P6	315, 380	315, 367	-
P8	379	362	374
P9	379.5	366	374, 516
P10	381	366	371, 507
P11	343	290, 364	355
P12	380	276, 362	375, 536
P13	391	278, 367	308, 370, 508

P14	383	276, 369	314, 372, 511
P15	325, 441	278, 330, 431	346, 479

* For all excitations were set λ_{an} at their maximum emissions except other mentions.

Table 3-9 summarizes the maxima of absorption of the polymers in solution and in pure film. It shows a red-shift of the absorption bands in the solid state compared to the solution. This is attributed to the constrained planar conformation and intermolecular π -electronic interactions induced by the packing of the molecules¹⁶⁶. Furthermore, some additional maxima are observed in films at longer wavelengths in most cases compared with that in solution, suggesting the strong intermolecular interactions and possible partial crystallinity in films.¹⁶⁷

3.2.2 Excitation and emission of polymers as thin films

(1) 5 mg/mL **PF** in DCB spin-coated as thin film, dried in oven at 80 °C

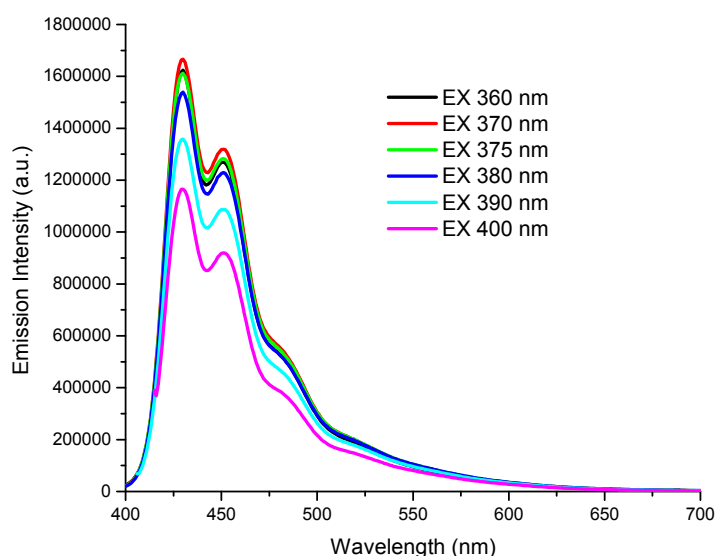


Figure 3-113 Emission spectra of **5 mg/mL of PF in DCB in film** with different excitations (slits were 5,5 nm)

Figure 3-113 shows the emission spectrum of a thin film of **PF** under different excitations. Three maxima are found at around 430 nm, 451 nm and 480 nm respectively.

¹⁶⁶ S. Hayashi, S. Yamamoto, D. Takeuchi, Y. Ie and K. Takagi. *Angew Chem Int Ed Engl.*, **2018**, 57(52):17002-17008.

¹⁶⁷ A. Yassin, G. Savitha, P. Leriche, P. Frere and J. Roncali. *New J. Chem.*, **2012**, 36, 2412–2416.

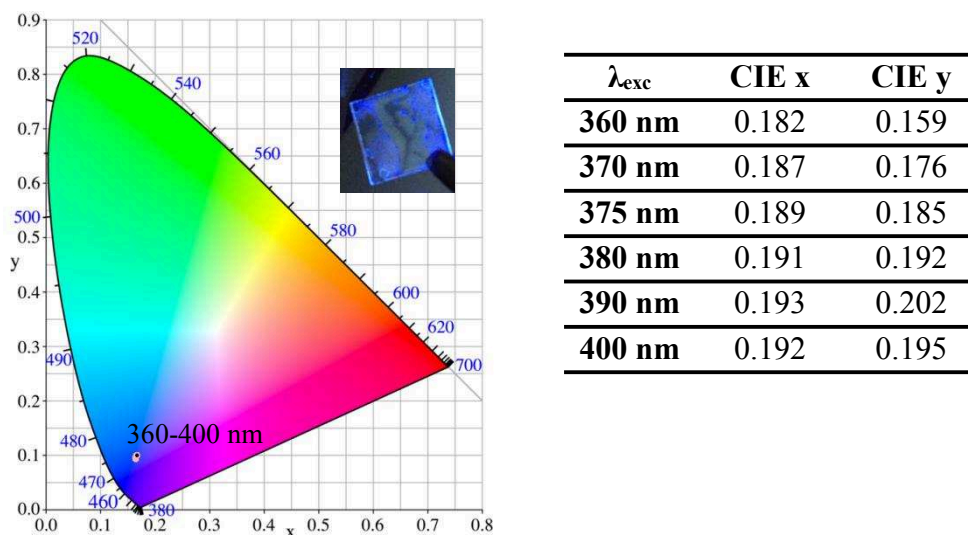


Figure 3-114 CIE coordinates of **5 mg/mL of PF in DCB in film** ($\lambda_{\text{exc}} = 360\text{-}400$ nm, slits were 5,5 nm) (The insert shows the emission of the film under a 365 nm UV lamp)

The **CIE coordinates** (0.189, 0.185) show that the film emits blue light under excitation at 375 nm.

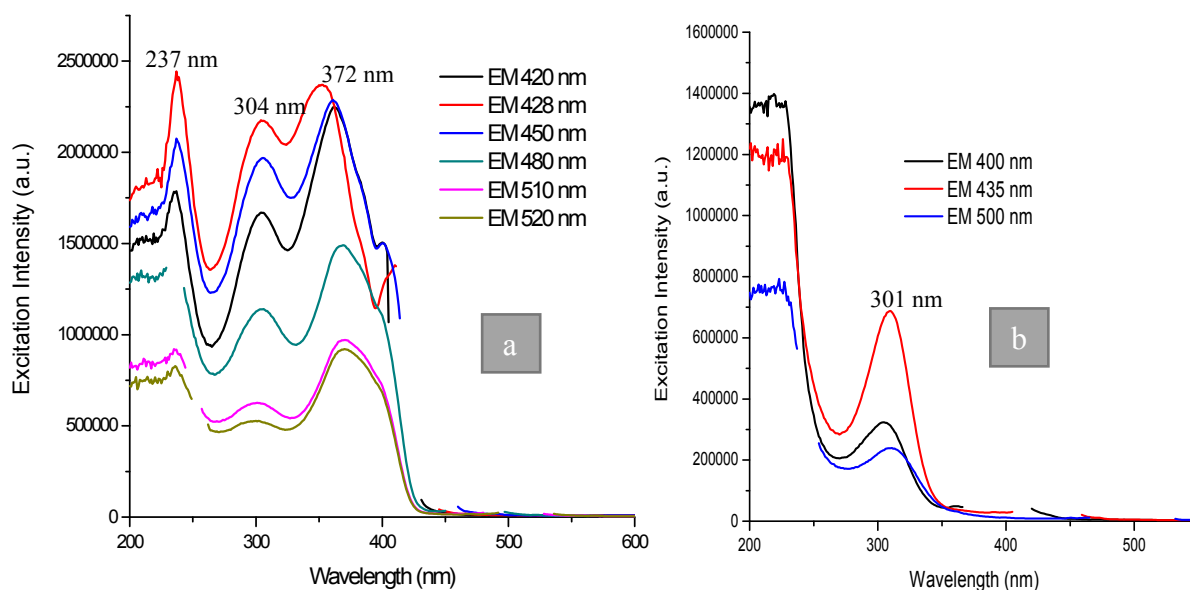


Figure 3-115 Excitation spectra of a) **5 mg/mL of PF in DCB in film** with different emissions (slits were 5,5 nm). b) only glass substrate.

The excitation spectra recorded with different analyzing wavelengths are reported on **Figure 3-115**. They show three maxima at around 237 nm, 304 nm and 372 nm, respectively when the emission wavelength is 420 nm. The former two bands may be ascribed to the excitation of the glass substrate, as shown in **Figure 3-115 (b)**. The last band centered at 372 nm is similar with the

absorption band (centered at 381 nm).

(2) 5 mg/mL **P1** in DCB spin-coated in film, dried in an oven at 80 °C.

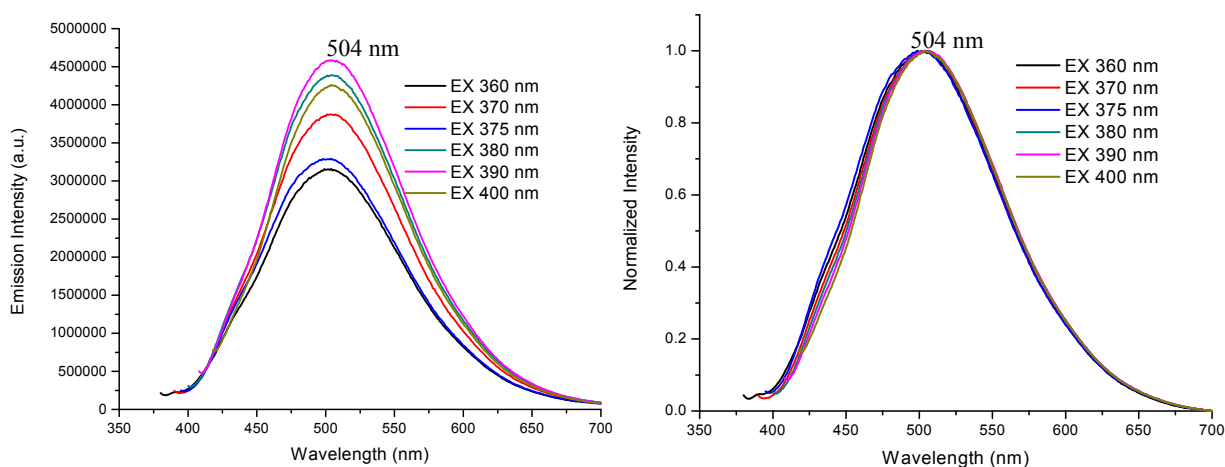
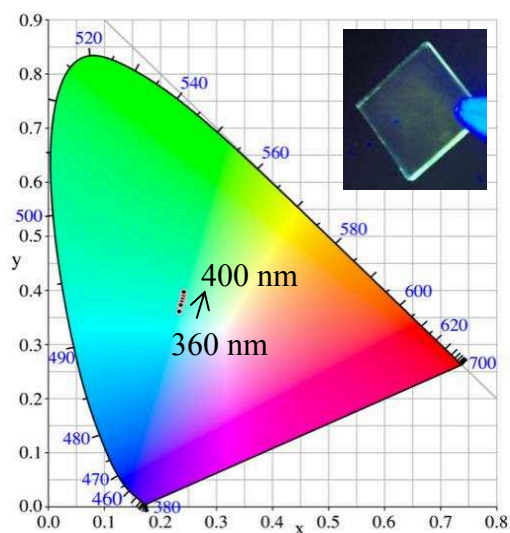


Figure 3-116 Emission spectra (left) and normalized emission spectra (right) of 5 mg/mL **P1** in film with different excitations (slits were 5,5 nm)

Figure 3-116 shows the emission spectrum of a film of **P1** recorded at different excitation wavelengths. The same emission band ranging from 400 nm to 700 nm with a maximum at 504 nm is seen, whatever the excitation used. The normalized emission spectra show identical emission profile.



λ_{exc}	CIE x	CIE y
360 nm	0.236	0.374
370 nm	0.239	0.381
375 nm	0.234	0.367
380 nm	0.240	0.387
390 nm	0.241	0.392
400 nm	0.242	0.397

Figure 3-117 CIE coordinates of 5 mg/mL **P1** in film (λ_{exc} = 360-400 nm, slits were 5,5 nm) (The insert shows the emission of the film under a 365 nm UV lamp).

The **CIE coordinates** (0.234, 0.367) show that **P1** emits **green light** when excited at 375 nm.

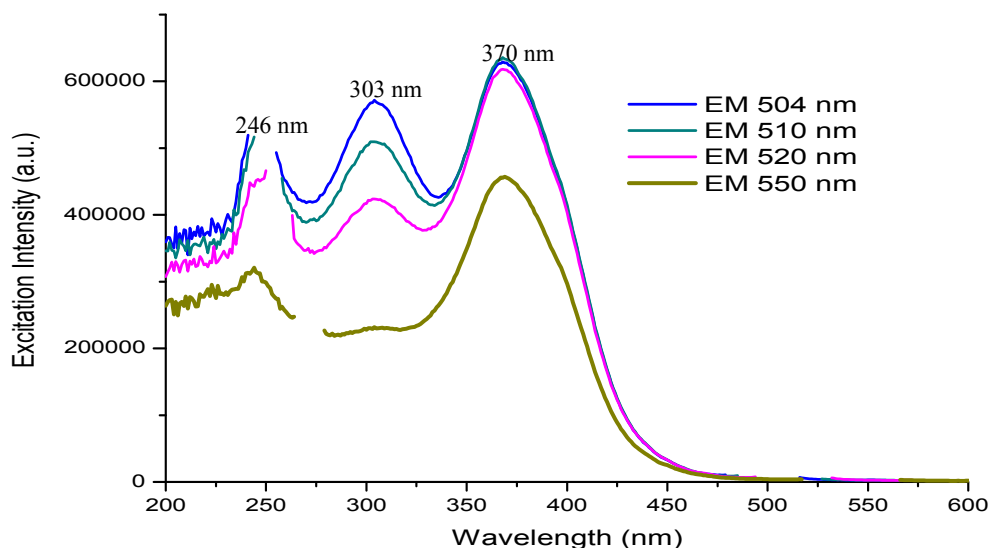


Figure 3-118 Excitation spectra of **5 mg/mL P1 in film** with different emissions (slits were 5,5 nm).

The excitation spectra recorded with different emission wavelengths are reported on **Figure 3-118** which three maxima were seen, at 246 nm, 303 nm and 368 nm, respectively. With the increase of the emission wavelength, the maxima of the excitation spectrum at 246 nm and 370 nm are increasing relatively to the maximum at 299 nm. The bands centered at 246 nm and 303 nm may also ascribed to the glass substrate, as comparison with **Figure 3-115 (b)**.

(3) 5 mg/mL P9 in DCB spin-coated in film, dried in oven at 80 °C

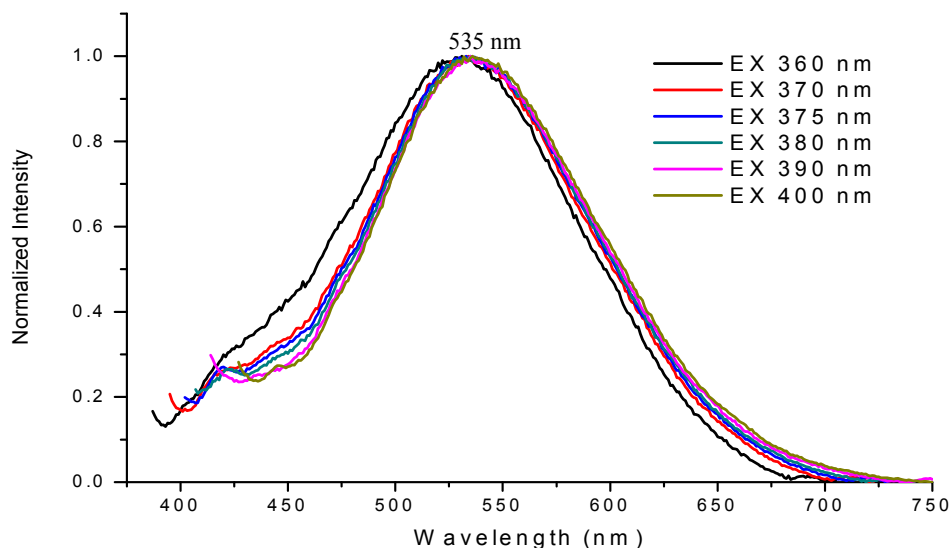


Figure 3-119 Emission spectra of **5 mg/mL P9 in film** with different excitations (slits were 5,5 nm)

Figure 3-119 shows that a film of **P9** emits between 400 nm and 750 nm with a maximum at 535 nm when excited between 360 nm and 400 nm.

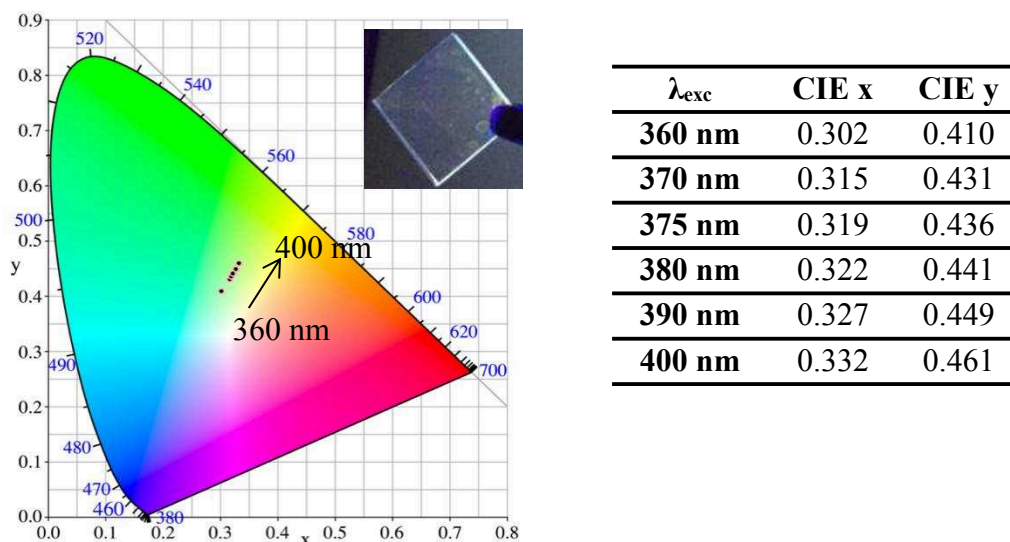


Figure 3-120 CIE coordinates of **5 mg/mL P9** in film (λ_{exc} = 360-400 nm, slits were 5,5 nm) (The insert shows the emission of the film under a 365 nm UV lamp)

The **CIE coordinates** show that **P9** emits a **green light** (Figure 3-120).

(4) **5 mg/mL P10** in DCB spin-coated in film, dried in oven at 80 °C

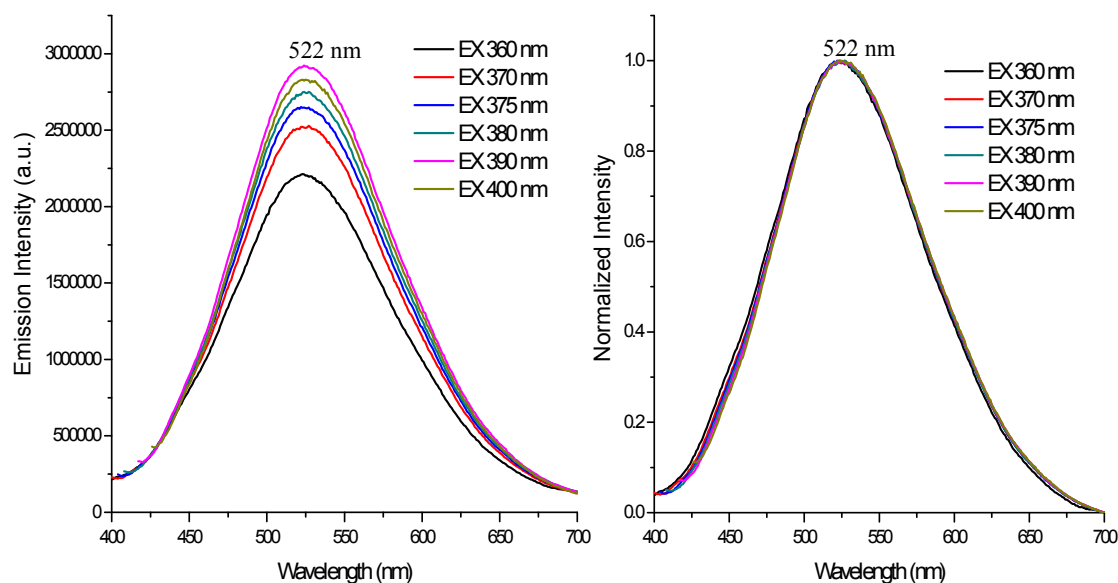
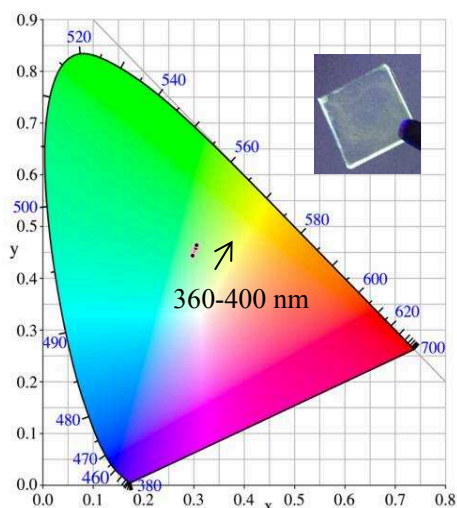


Figure 3-121 Emission spectra (left) and normalized emission spectra (right) of **P10** in film with different excitations (slits were 5,5 nm)

Figure 3-121 shows that a film of **P10** emits between 400 nm and 700 nm with a maximum at 522 nm when excited between 360 nm and 400 nm. The normalized emission spectra show an identical emission profile.



λ_{exc}	CIE x	CIE y	CCT(Kelvin)
360 nm	0.297	0.444	6513
370 nm	0.301	0.452	6364
375 nm	0.302	0.454	6334
380 nm	0.303	0.455	6306
390 nm	0.304	0.459	6249
400 nm	0.306	0.464	6193

Figure 3-122 CIE coordinates of **P10 in film** ($\lambda_{\text{exc}} = 360\text{-}400\text{ nm}$, slits were 5,5 nm) (The insert shows the emission of the film under a 365 nm UV lamp)

The **CIE coordinates and the CCT data** show that **P10** emits **cool white light (5000-8300 K CCT)** after excitation in the range 360-400 nm.

(5) 5 mg/mL P11 in DCB spin-coated in film, dried in oven at 80 °C

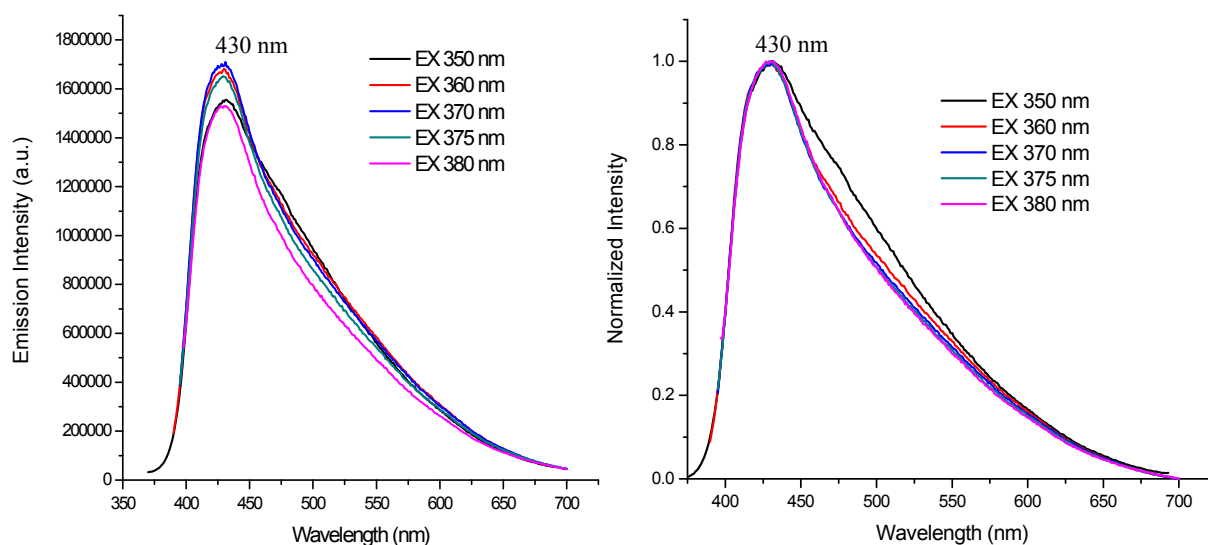
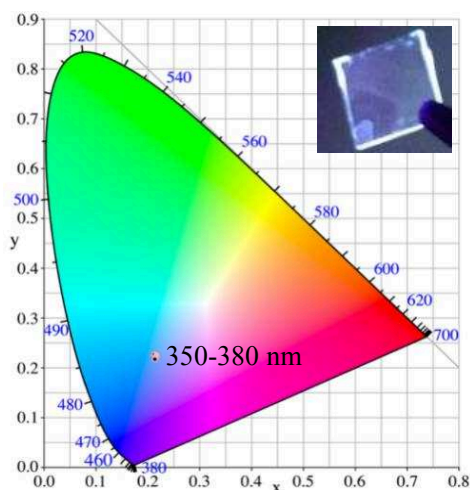


Figure 3-123 Emission spectra (left) and normalized emission spectra (right) of **5mg/mL of P11 in DCB in film** with different excitations (slits were 5,5 nm).

Figure 3-123 shows that the emission of a film of **P11** comprises a band between 375 nm to 700 nm with a maximum at around 430 nm. The normalized emission spectra show identical emission profile.



λ_{exc}	CIE x	CIE y	CCT(Kelvin)
350 nm	0.210	0.230	12568
360 nm	0.220	0.230	12568
370 nm	0.220	0.220	12568
375 nm	0.214	0.220	12011
380 nm	0.210	0.220	12011

Figure 3-124 CIE coordinates of **5mg/mL of P11 in DCB in film** ($\lambda_{\text{exc}} = 350\text{-}380\text{ nm}$, slits were 5,5 nm) (The insert shows the emission of the film under a 365 nm UV lamp).

The blue emission of **P11** is indicated by the **CIE coordinates** of (0.214, 0.220) under excitation at 375 nm.

(6) 5 mg/mL P12 in DCB spin-coated in film, dried in oven at 80 °C

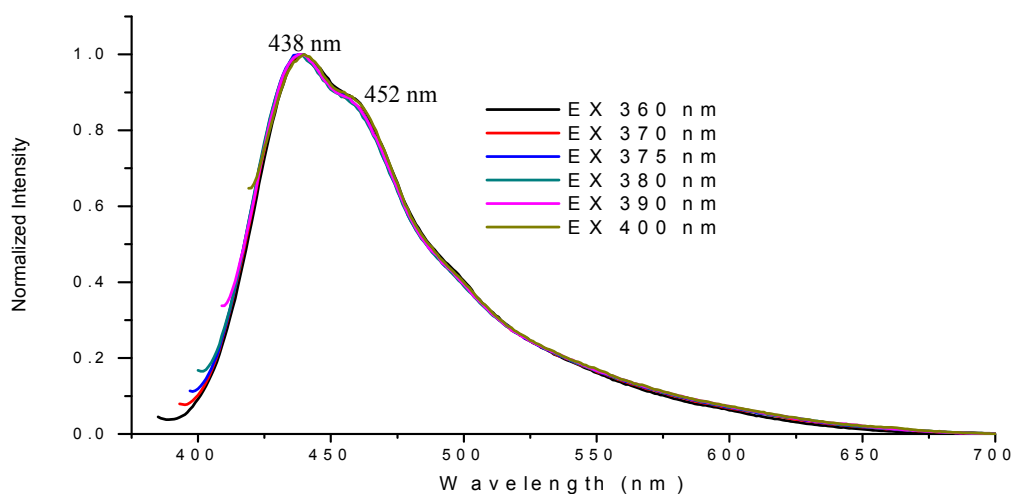
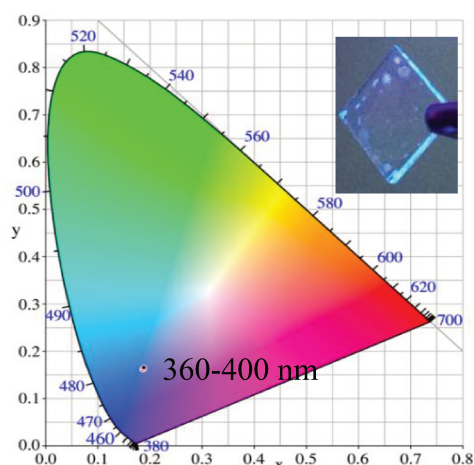


Figure 3-125 Emission spectra of **5 mg/mL P12 in film** with different excitations (slits were 5,5 nm)

As shown in **Figure 3-125**, the emission spectrum of the film of **P12** does not depend on the excitation wavelength. It shows a band between 400 nm and 700 nm with a maximum at 438 nm when excited in the 360-400 nm range. A shoulder peak at around 452 nm also appears, it is probably due to π - π stacking between molecules.



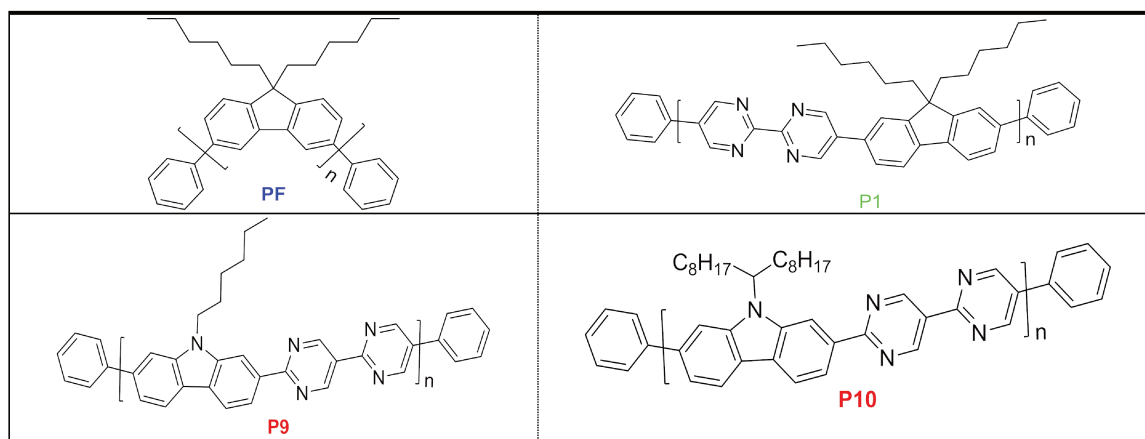
λ_{exc}	CIE x	CIE y
360 nm	0.185	0.162
370 nm	0.186	0.162
375 nm	0.187	0.162
380 nm	0.187	0.162
390 nm	0.187	0.163
400 nm	0.188	0.166

Figure 3-126 CIE coordinates of **5 mg/mL P12 in film** ($\lambda_{\text{exc}} = 360\text{-}400\text{ nm}$, slits were 5,5 nm) (The insert shows the emission of the film under a 365 nm UV lamp)

The **CIE coordinates** of (0,190, 0,162) obtained after excitation at 375 nm shows that a film of **P12** emits blue light.

Following we are going to compare above results of the different polymers to evaluate the influence of the design on the photophysical properties.

(7) Comparison of **PF**, **P1**, **P9** and **P10** in film (5 mg/mL of the polymer in DCB spin-coated and dried in an oven at 80 °C)



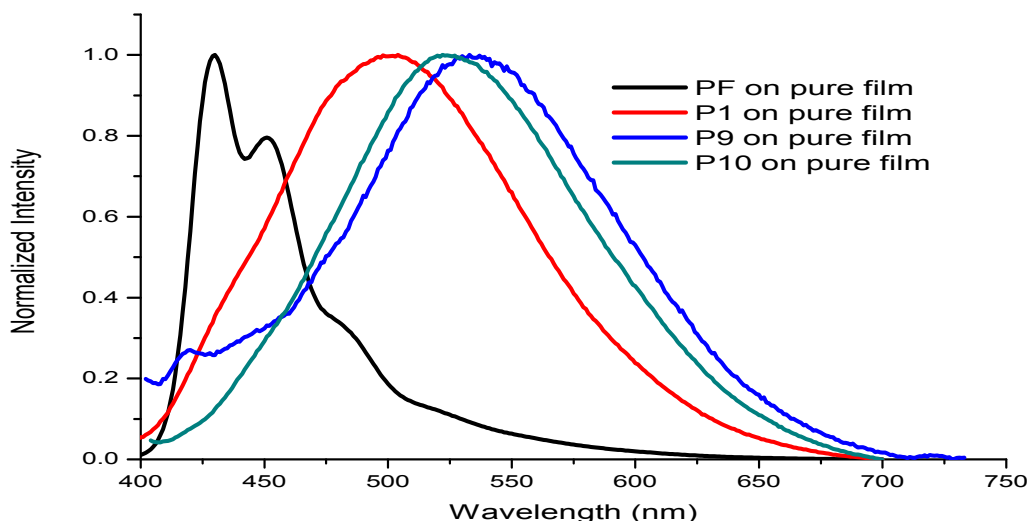


Figure 3-127 Emission spectra of 5 mg/mL PF, P1, P9 and P10 in DCB spin-coated as thin films

(slits were 5,5 nm, for emission: set λ_{exc} = 375 nm, excitation: set λ_{an} (PF) = 420 nm, λ_{an} (P1) = 504 nm)

Table 3-10 Summary of performances of 5 mg/mL PF, P1, P9 and P10 in DCB spin-coated as thin films (slits were 5,5 nm, for emission: set λ_{exc} = 375 nm, excitation: set λ_{an} (PF) = 420 nm, λ_{an} (P1) = 504 nm)

Polymer	λ_{exc} (nm)	λ_{em} (nm)	FWHM (nm)	CIE(x, y)
PF	237, 304, 361	430, 451, 480	52	(0.165, 0.097)
P1	246, 303, 368	504	120	(0.234, 0.367)
P9	305, 368	533	133	(0.327, 0.449)
P10	243, 301, 371	522	122	(0.301, 0.454)

Figure 3-127 depicted the emission spectra of films of the four polymers, and the data are summarized in **Table 3-10**. It can be concluded that:

- 1) by comparison of PF and P1: introducing 2,2'-bipyrimidine as acceptor unit into the polymer backbone results in a red-shifted emission. This indicates the reduction of the bandgap of the polymer by increasing the conjugation length.
- 2) by comparison of P1 and P9: using carbazole instead of fluorene as donor unit resulted in a red-shift of the emission. This indicates that the bandgap of the polymer was reduced by a stronger (D-A)_n interaction between carbazole and BPM.
- 3) by comparison of P9 and P10: when using bulkier lateral chains, the emission of the polymer is slightly blue shifted. This may be due to lower intermolecular π -electronic interactions of chains of P10. As the influence on the emission is relatively low, it remains an adoptable method that can be used to improve the solubility of the polymers.

(8) Comparison of **PF**, **P11** and **P12** in film (5 mg/mL polymer in DCB spin-coated in film, dried in oven at 80 °C)

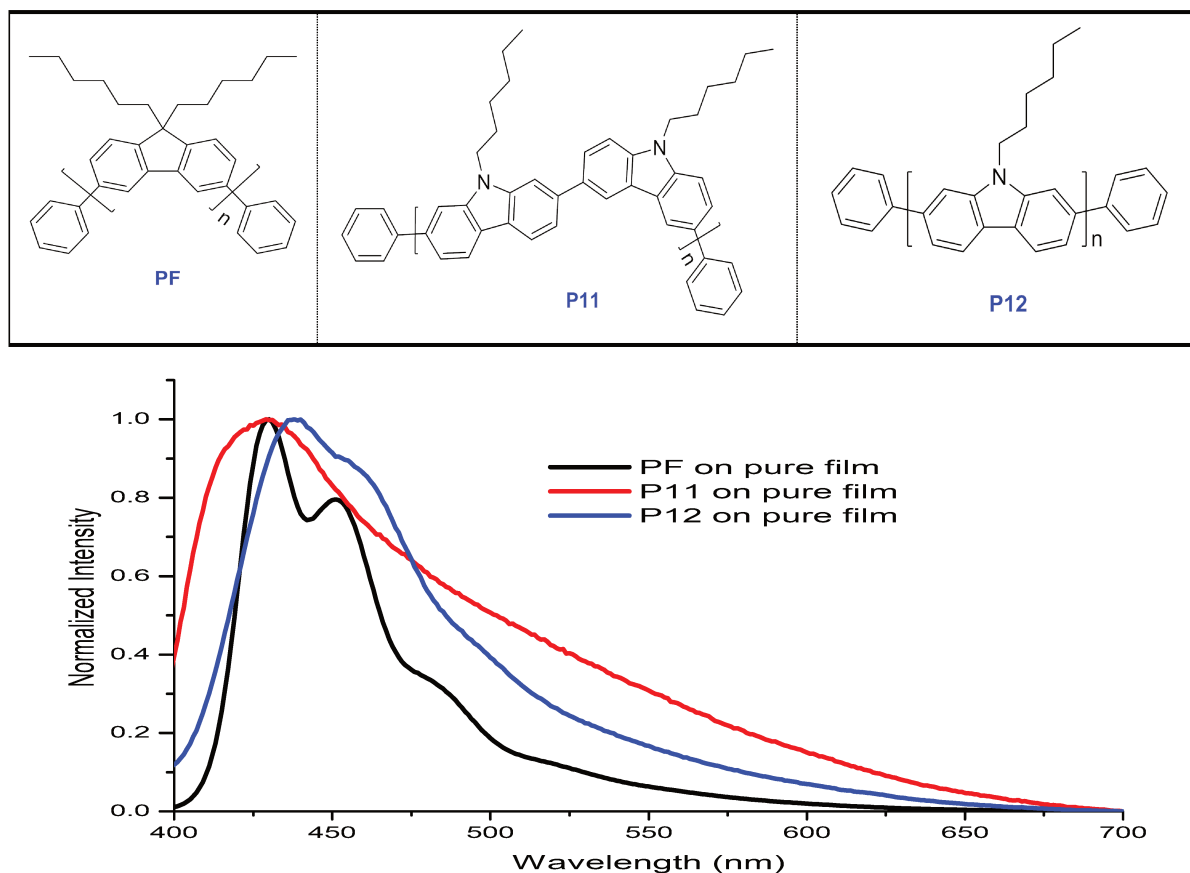


Figure 3-128 Emission spectra of 5 mg/mL **PF**, **P11** and **P12** in DCB in films (set $\lambda_{\text{exc}} = 375$ nm, slits were 5,5 nm)

Table 3-11 Summary of performances of 5 mg/mL **PF**, **P11** and **P12** in DCB spin-coated as thin films (set $\lambda_{\text{exc}} = 375$ nm, slits were 5,5 nm)

Polymer	λ_{exc} (nm)	λ_{em} (nm)	FWHM (nm)	CIE(x, y)
PF	237, 304, 361	430, 451, 480	52	(0.165, 0.097)
P11	243, 305, 362	430	157	(0.214, 0.220)
P12	240, 304, 367	438, 452	73	(0.187, 0.162)

The emission spectra of the three blue-emitting polymers are reported on **Figure 3-128** and the corresponding data are summarized in **Table 3-11**. They show that:

1) comparing **PF** and **P12**: it confirmed that introducing 2,7-carbazole instead of 3,6-fluorene as donor unit has a low influence on the emission and excitation properties, but the FWHM is increased, which means that the emitting color became less purer.

2) comparing **P11** and **P12**: **P12**, which is expected to have a more linear backbone thanks to the polymerization at the 2,7 positions, possesses a lowest bandgap. This is due to the increase of the conjugation along the linear axis of carbazole¹⁶⁸ and the linear polymer has more interchain interaction and higher integration,¹⁶⁹ which leads to higher mobilities of charge carrier¹⁷⁰ which reduces the bandgap of the polymer. Furthermore, the expected zigzag structure of polymer **P11** (see **Figure 3-56**) also possess a much higher FWHM relatively to **P12**.

(9) 5 mg/mL **P13** in DCB spin-coated in film, dried in an oven at 80 °C

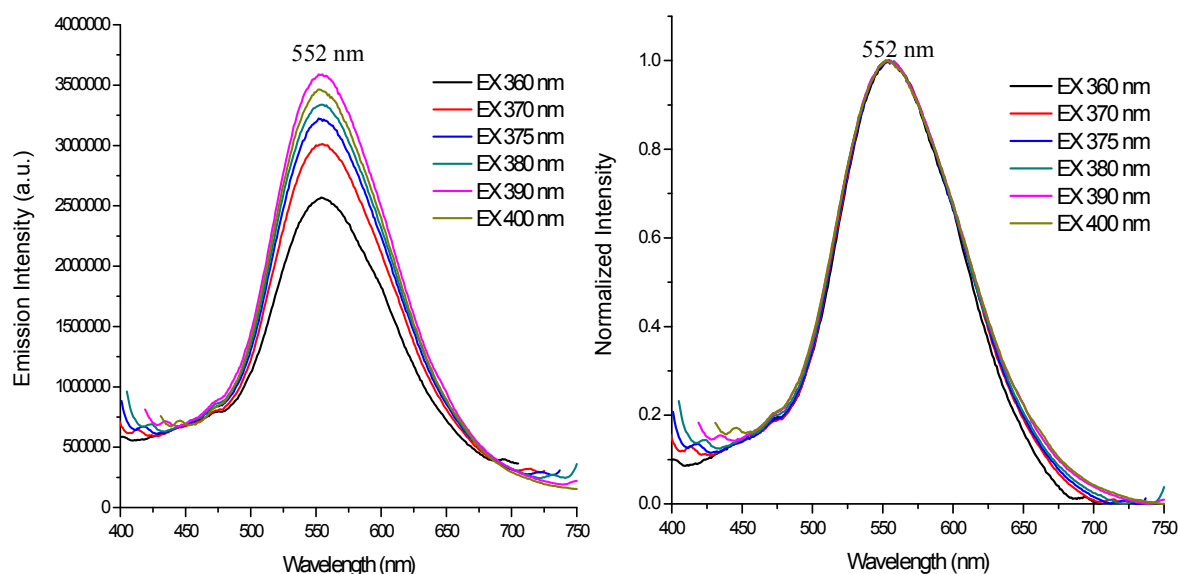


Figure 3-129 Emission (left) and normalized emission (right) spectra of **P13 in film** with different excitations (slits were 5,5 nm)

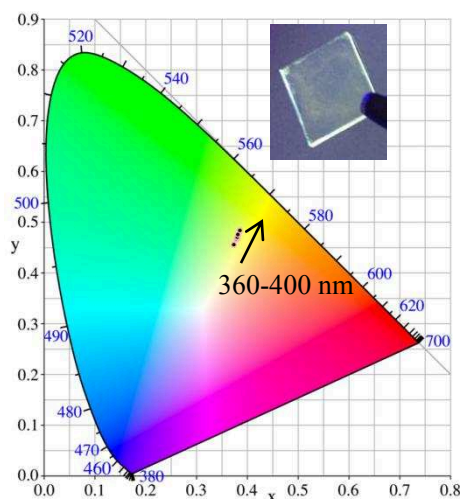
Figure 3-129 and **Figure 3-130** show that a film of **P13** emits **neutral white light** under 360 to 400 nm excitation. The emission spectrum shows a band from 400 nm to 750 nm with a maximum at 552 nm which does not depend on the excitation wavelength when excited in the range 360-400 nm.

¹⁶⁸ a. V. Joseph, K. R. J. Thomas, S. Sahoo, M. Singh, D. K. Dubey, and J.-H. Jou. *ACS Omega*, **2018**, 3, 16477-16488.

b. B. E. Kohler and J. C. Woehl. *Synthetic Metals*, **1997**, 84, 851-852.

¹⁶⁹ H. Wang, P. Cheng, Y. Liu, J. Chen, X. Zhan, W. Hu, Z. Shuai, Y. Li and D. Zhu. *J. Mater. Chem.*, **2012**, 22, 3432-3439.

¹⁷⁰ M. Wang, M. J. Ford, C. Zhou, M. Seifrid, T.-Q. Nguyen, and G. C. Bazan. *J. Am. Chem. Soc.*, **2017**, 139 (48), 17624-17631.



λ_{exc}	CIE x	CIE y	CCT (K)
360 nm	0.373	0.456	4560
370 nm	0.379	0.467	4468
375 nm	0.380	0.470	4460
380 nm	0.380	0.471	4464
390 nm	0.382	0.476	4437
400 nm	0.385	0.484	4404

Figure 3-130 CIE coordinates of **P13 in film** ($\lambda_{\text{exc}} = 340\text{-}400\text{ nm}$, slits were 5,5 nm) (The insert shows the emission of the film under a 365 nm UV lamp)

(10) 5 mg/mL **P14** in DCB spin-coated in film, dried in an oven at 80 °C

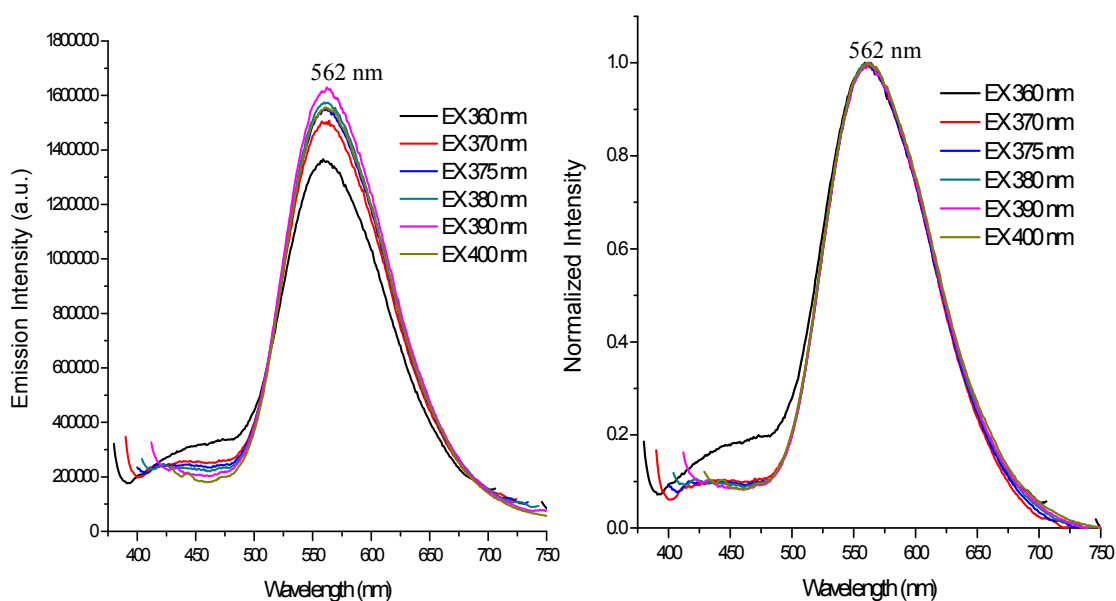
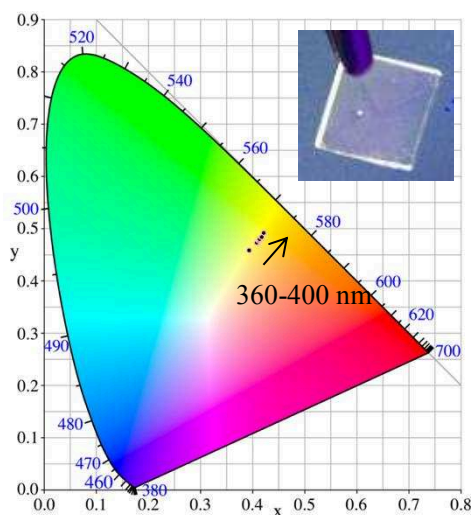


Figure 3-131 Emission spectra (left) and normalized emission spectra (right) of **P14 in film** with excitations at 360-400 nm (slits were 5,5 nm)

Figure 3-131 shows that the emission spectrum of **P14** comprises a broad band ranging from 400 nm to 750 nm with a maximum at 562 nm when the excitation wavelength is set between 360 nm and 400 nm. The normalized emission spectra show identical emission profile.



λ_{exc}	CIE x	CIE y	CCT(Kelvin)
360 nm	0.394	0.458	4143
370 nm	0.408	0.473	3944
375 nm	0.412	0.477	3902
380 nm	0.414	0.480	3876
390 nm	0.417	0.484	3840
400 nm	0.422	0.492	3800

Figure 3-132 CIE coordinates of **P14 in film** ($\lambda_{\text{exc}} = 360\text{-}400\text{ nm}$, slits were 5,5 nm) (The insert shows the emission of the film under a 365 nm UV lamp)

The **CIE coordinates and the CCT data** show that the material emits a **neutral white light (3700-5000 K CCT)** under excitation at 360-400 nm.

(11) 5 mg/mL P15 in DCB spin-coated in film, dried in oven at 80 °C

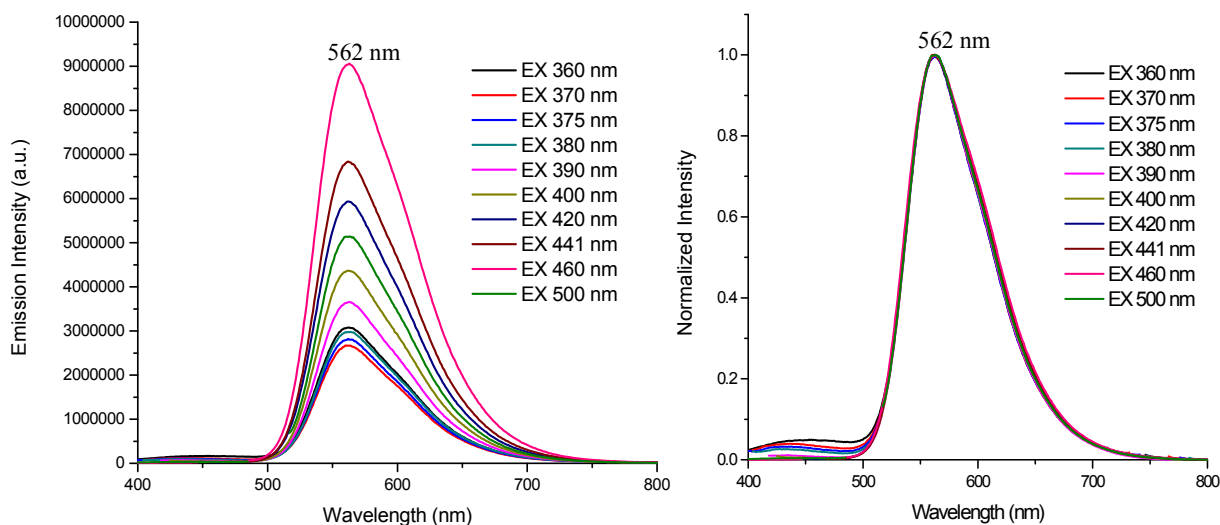
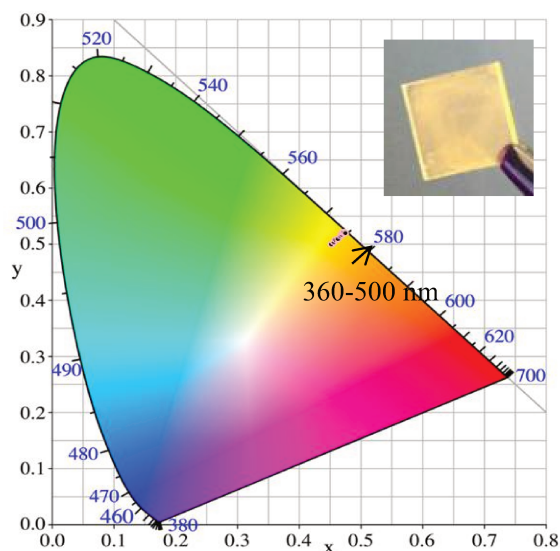


Figure 3-133 Emission spectra (left) and normalized emission spectra (right) of **P15 in film** with excitations at 360-500 nm (slits were 5,5 nm)

Above **Figure 3-133** shows that the emission spectra are ranging from 500 nm to 750 nm with a maximum at 562 nm when the excitation wavelength is in the range of 360-500 nm. The normalized emission spectra show identical emission profile despite the intensity changes, suggesting that the fluorescence is originating from the same S_1 states.



λ_{exc}	CIE x	CIE y	CCT(Kelvin)
360 nm	0.452	0.500	3400
370 nm	0.456	0.505	3363
375 nm	0.459	0.508	3345
380 nm	0.462	0.509	3310
390 nm	0.466	0.515	3285
400 nm	0.469	0.518	3269
420 nm	0.470	0.521	3273
441 nm	0.472	0.521	3242
460 nm	0.472	0.521	3248
500 nm	0.475	0.521	3211

Figure 3-134 CIE coordinates of **P15** in film ($\lambda_{\text{exc}} = 360\text{-}500\text{ nm}$, slits were 5,5 nm) (The insert shows the emission of the film under a 365 nm UV lamp)

The **CIE coordinates** and the **CCT data** show the material emits a **warm white light (2600-3700 K CCT)** under excitation at 360-500 nm.

(12) Comparison of **P10**, **P13**, **P14** and **P15** in film (5 mg/mL polymer in DCB spin-coated in film, dried in oven at 80 °C)

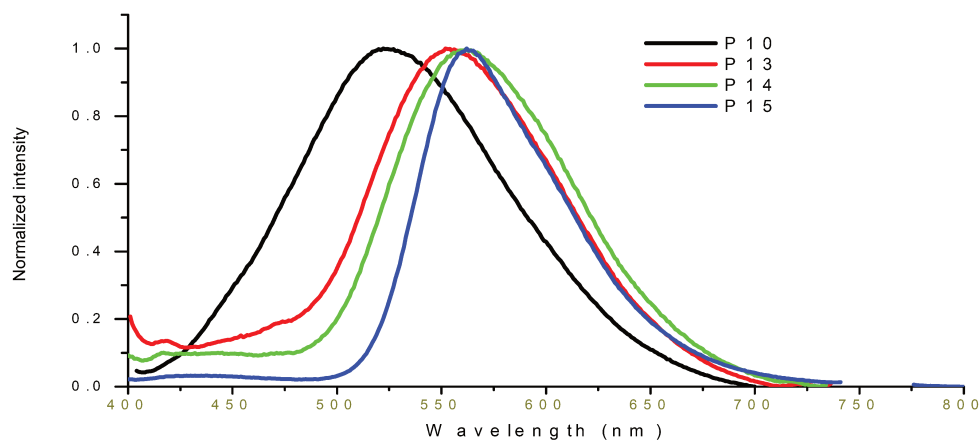
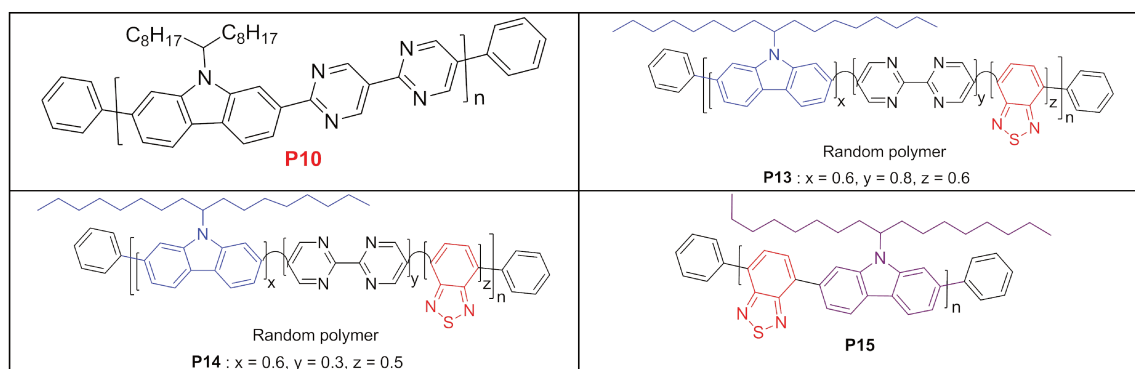


Figure 3-135 Emission spectra of **5 mg/mL P10, P13, P14 and P15** in DCB in films (set $\lambda_{\text{exc}} = 375$ nm, slits were 5,5 nm)

Table 3-12 Summary of performances of **5 mg/mL P10, P13, P14 and P15** in DCB spin-coated as thin films (set $\lambda_{\text{exc}} = 375$ nm, slits were 5,5 nm)

Polymer	λ_{exc} (nm)	λ_{em} (nm)	FWHM (nm)	CIE(x, y)
P10	243, 301, 371	522	122	(0.301, 0.454)
P13	366	552	102	(0.380, 0.470)
P14	242, 368	562	97	(0.412, 0.477)
P15	246, 338, 454	562	79	(0.459, 0.508)

Figure 3-135 and **Table 3-12** again show that the red-shift is directly related to the quantity of benzo-thiadiazole introduced in the polymer backbone as acceptor. The FWHM of the random polymers **P13** and **P14** are also broad.

3.3 Summary

In this Chapter, we have investigated the photophysical properties of the polymers synthesized in Chapter II both in solution and deposited as thin films. **Table 3-13** summarizes the results. They particularly highlight the role of BPM as a new acceptor in designing conjugated polymers.

It shows that all polymers absorb in the near-UV as expected, which is of importance for applications as emitters with near-UV LEDs that will be used (375 nm) (see **Chapter IV**). The emission spectra of thin films of most polymers displayed red-shifted emission compared to their corresponding spectra recorded in DCM. This is frequently observed as this is due to the intermolecular interactions and the formation of aggregation of the polymer chains in the solid state that facilitated the energy migration between the molecules.^{165,167a,171} Besides, the table reveals that the maxima of absorption and excitation of the polymers are similar in most cases as we expected and desired, which indicates that the absorbing level is also the emissive state.

Table 3-13 Summary of performances of polymers deposited as film (5 mg/mL, slits were 5,5 nm) and in DCM (0.01 mg/mL, slits were 2,2 nm)

Polymer	Solution (DCM)			Film		
	λ_{abs} (nm)	λ_{exc}^* (nm)	λ_{em}^{**} (nm)	λ_{abs} (nm)	λ_{exc}^*	λ_{em}^{**} (nm)
PF	380	360	418, 444	381	361	430, 451, 480

¹⁷¹ G. Li, C. Kang, X. Gong, J. Zhang, C. Li, Y. Chen, H. Dong, W. Hu, F. Li, and Z. Bo. *Macromolecules*, **2014**, 47 (14), 4645–4652. DOI: 10.1021/ma500417r.

P1	373	364	475	371	368	504
P2	373	364	447	-	-	-
P5	384	365	474	-	-	-
P6	380	367	479	-	-	-
P8	379	362	473	374		
P9	380	366	466	374	368	533
P10	381	366	461	371	371	522
P11	343	364	407	355	362	430
P12	380	362	421	375	367	438, 452
P13	391	367	522	370	366	552
P14	383	369	560	372	368	562
P15	325, 441	330, 431	557	346, 479	338, 454	562

* For all excitations, λ_{an} were set at their maximum emissions except other mentions.

** For all emissions λ_{exc} were set at 375 nm except other mentions.

Polymers **PF**, **P11** and **P12** all demonstrated emission in the blue, while **P1**, **P8**, **P9** and **P10** all showed a green emission. Very important results were obtained with polymers **P13**, **P14** and **P15** which were found to emit white light both in solution and in thin films. This is of great interest as they can be used as single emitters, thus avoiding mixing different emitters that usually leads to phase separation.

Measurements performed on the polymers in different conditions showed that the geometry, the side-chains, the solvent, and, obviously, the chemical structure of the backbone, all play a significant role in the luminescent properties of the materials.

More precisely, when BPM is introduced in an alternative way in a polyfluorene backbone (from **PF** to **P1**), the emission is shifted to the red, showing that BPM acts as an electron acceptor (the fluorene unit being the donor). In the design of (D-A)_n polymers, it was shown that the interaction was stronger when the carbazole group was used instead of fluorene (comparison between **P1** and **P9**). When going from **P11** to **P12**, we showed that polymerizing the carbazole moiety at the 2 and 7 positions resulted in a red-shift of the emission which was explained by a more linear structure of the backbone, and thus a better overlap between the π orbitals which lead to a higher conjugation.

Introduction of the benzothiadiazole unit resulted in a more pronounced shift to the red, which

means that it is a better electron acceptor than BPM. The simultaneous use of BPM and BTB could lead to white emitting polymers (**P13** and **P14**). These results showed that the chemical engineering strategy we applied is effective and feasible for tuning the photophysical properties of the polymers.

Chapter IV Investigations as luminophors

Contents

4.1 Polymers in different matrices.....	- 159 -
4.1.1 P1 in different matrices.....	- 159 -
4.1.2 P10 in different matrices.....	- 163 -
4.1.3 P13 in different matrices.....	- 169 -
4.1.4 P14 in different matrices.....	- 182 -
4.1.5 P15 in different matrices.....	- 188 -
4.1.6 Summary of the influence of the matrix on the photophysical properties.....	- 195 -
4.2 Investigations on the possibility of Aggregation Induced Emission.....	- 195 -
4.2.1 Introduction.....	- 195 -
4.2.2 Preparation of the samples.....	- 196 -
4.2.3 Absorption and PL results.....	- 197 -
4.2.4 Conclusions.....	- 199 -
4.3 Blends with different emitters for white light emission.....	- 199 -
4.3.1 Blends for white light in solution.....	- 200 -
4.3.2 Blending the emitters in thin films.....	- 205 -
4.4 Quantum yields determination.....	- 206 -
4.4.1 Quantum yields measured in DCM.....	- 207 -
4.4.2 Quantum yields measured in thin film.....	- 208 -
4.5 Photostability studies.....	- 208 -
4.5.1 PF	- 209 -
4.5.2 P1	- 210 -
4.5.3 P8	- 211 -
4.5.4 Influence of the liquid matrix.....	- 213 -
4.5.5 [Eu(tta)₃(L)]	- 214 -
4.6 Thermostability studies.....	- 214 -
4.7 Summary.....	- 216 -

In the previous chapter, we have shown that all polymers were strongly absorbing in the 350-400 nm region and emitted light in the visible. This made them of interest to be investigated as emitters in lighting systems based on near-UV LEDs. In this chapter, we will further investigate the emission properties of these emitters when integrated into matrices used to elaborate phosphors. The quantum yield (QY), photostability and thermostability studies will also be described in order to evaluate the potential of these materials as luminophores. All those are key factors needed to be taken into consideration for their possible further commercial application.

4.1 Polymers in different matrices

As described in **Chapter I**, polymer matrices play a very important role in protecting the materials from light photodegradation. Meanwhile, they also served as solid “solvent” to disperse the luminescent materials in the films. Here we show results of films of polymers in different matrices, such as C-Si matrix, PMMA, polystyrene and so on, prepared accordingly to **§2.4 & §2.5, Chapter II**.

4.1.1 P1 in different matrices

(1) Absorption result

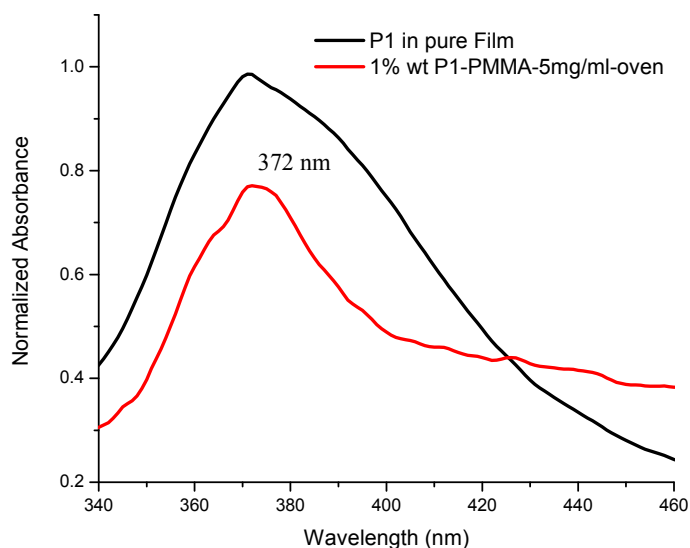


Figure 4-1 Absorption spectra of **P1** in pure film and in PMMA in film (5 mg/mL, slits were 5,5 nm)

As shown above, the main band of the absorption spectrum of **P1** in PMMA (1% wt) is similar with that in pure film, centered at 372 nm.

(2) PL result

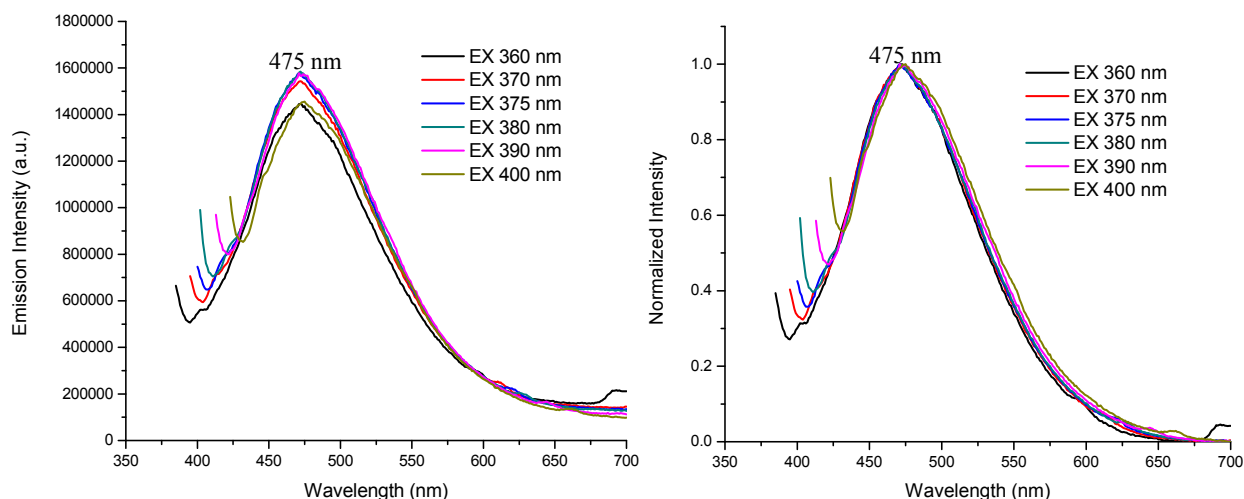
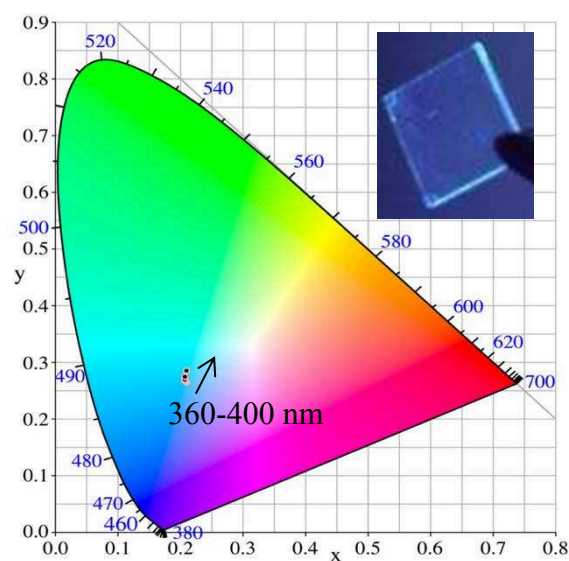


Figure 4-2 Emission spectra (left) and normalized emission spectra (right) of **1% wt P1 in PMMA in film** with different excitations (slits were 5,5 nm).

Figure 4-2 shows that the emission spectrum comprises a broad band ranging from 400 to 700 nm with a maximum at around 475 nm when the excitation wavelength is set from 360 nm to 400 nm. The normalized emission spectra show identical emission profile.



λ_{exc}	CIE x	CIE y
360 nm	0.210	0.266
370 nm	0.207	0.267
375 nm	0.207	0.268
380 nm	0.206	0.269
390 nm	0.206	0.275
400 nm	0.209	0.285

Figure 4-3 CIE coordinates of **1% wt P1 in PMMA in film** ($\lambda_{\text{exc}} = 360\text{-}400$ nm, slits were 5,5 nm) (The insert shows the emission of the film under a 365 nm UV lamp)

The **CIE coordinates** (0.206, 0.268) show that the material emits a **greenish blue light** under excitation at 375 nm.

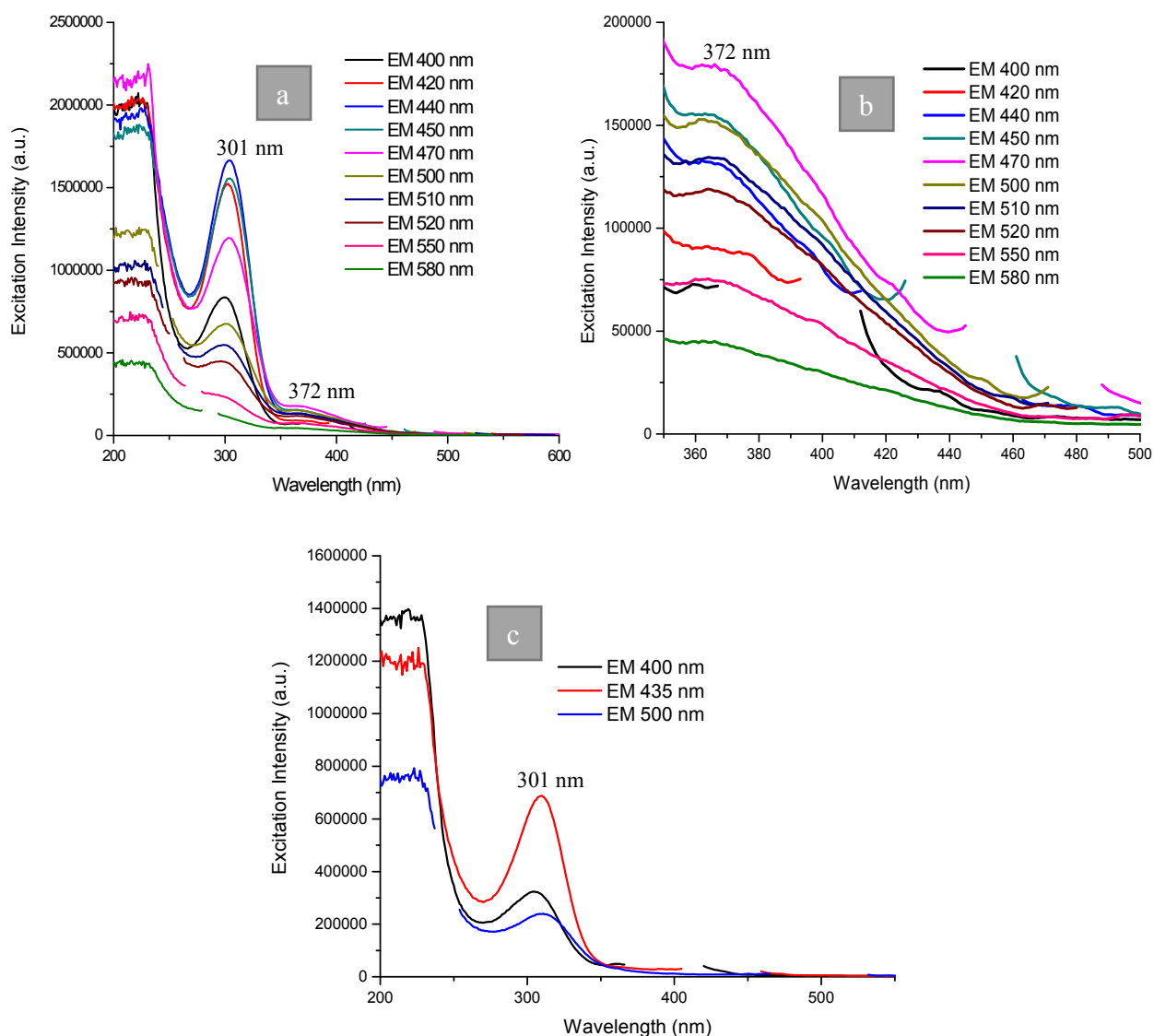


Figure 4-4 Excitation spectra of a) & b) **1% wt P1 in PMMA in film** with different emissions; c) only glass substrate (slits were 5,5 nm).

Figure 4-4 a) & b) shows that the excitation spectrum of 1% wt **P1** in **PMMA** in film with different emission wavelengths has two maxima at 301 nm and 372 nm, respectively. By comparison with **Figure 4-4** c), the band centered at 301 nm may due to the glass substrate used. As a consequence, the best excitation wavelength for the sample of 1% wt **P1** in **PMMA** in film is still in the near UV zone which is close to the LED light that we plan to use.

Table 4-1 Absorption and PL data of **P1** in different conditions in film (slits were 5,5 nm)

Sample	P1 in pure Film	1% wt P1-PMMA-5mg/ml-oven
λ_{abs} (nm)	315, 371, 512	372
λ_{exc}^* (nm)	246, 303, 368	301, 372

λ_{em}^{**} (nm)	504	475
--------------------------	-----	-----

* For all excitations were set λ_{an} at their maximum emissions except other mentions.

** For all emissions were set λ_{exc} at 375 nm except other mentions.

Table 4-1 summarises the results of absorption and PL properties of **P1** in films. The emission of **P1** in PMMA is blue-shifted with respect to that of a pure film of **P1**, as previously observed when PMMA was used as matrix.¹⁷² The polymer chains that have been diluted into PMMA matrices are more or less isolated, the blue shift is due to the absence of interactions among molecules that are isolated in the films, as illustrated in **Figure 4-5 a)**. This also indicates that the PMMA prevents effectively polymer molecules from aggregation. Polymers with lower concentration present shorter emission wavelength due to the weaker molecular interactions among polymer molecules.¹⁷³

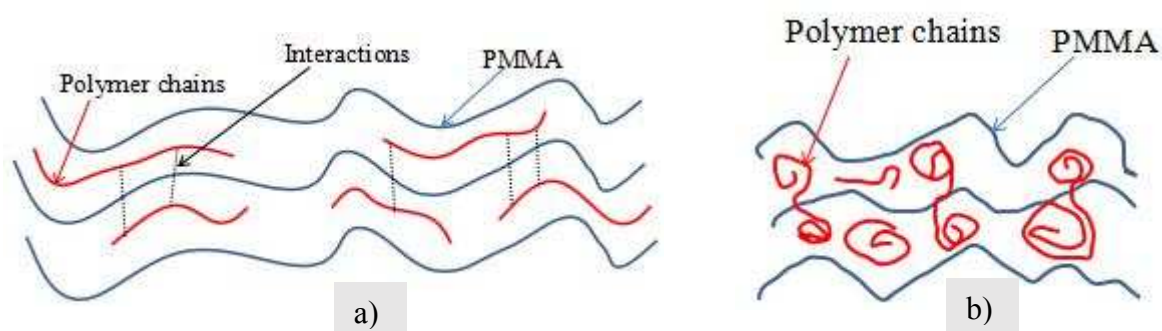


Figure 4-5 Illustration of the interruption of the polymer chains by PMMA: a) the interactions among polymer chains are weakened due to PMMA; b) the intra-chain interactions are interrupted by PMMA.

As a second explanation, the possible mechanism for producing such blue shift is the interruption of the conjugated polymer intra-chains by PMMA, as illustrated in **Figure 4-5 b)**. In the PMMA rich regions, the PMMA interrupts the intra-chain interaction and causes them to be localized in short region (similar to the case of oligomer).¹⁷⁴

The results also demonstrate that the presence of different molecular packings play a basic and critical role for the optical properties of the molecules.

¹⁷² J G MAHAKHODE, S J DHOBLE,, C P JOSHI and S V MOHARIL. *Bull. Mater. Sci.*, **2011**, 34(7), 1649–1651.

¹⁷³ TONG K., XU C., WANG Q., GU B., ZHENG K., YE L., LI X. *CHIN.PHYS.LETT.*, **2008**, 25 (12), 4453.

¹⁷⁴ Shen-Yi Hsy Hsieh-Li Choy and Pei-KuenWei. LIGHT EMISSION IN PHASE SEPARATED CONJUGATED AND NON-CONJUGATED POLYMER BLENDS. CLEOPacific Rim **2003**. The 5th Pacific Rim Conference on Lasers and Electro-Optics (IEEE Cat. No.03TH8671).

4.1.2 P10 in different matrices

4.1.2.1 Absorption result

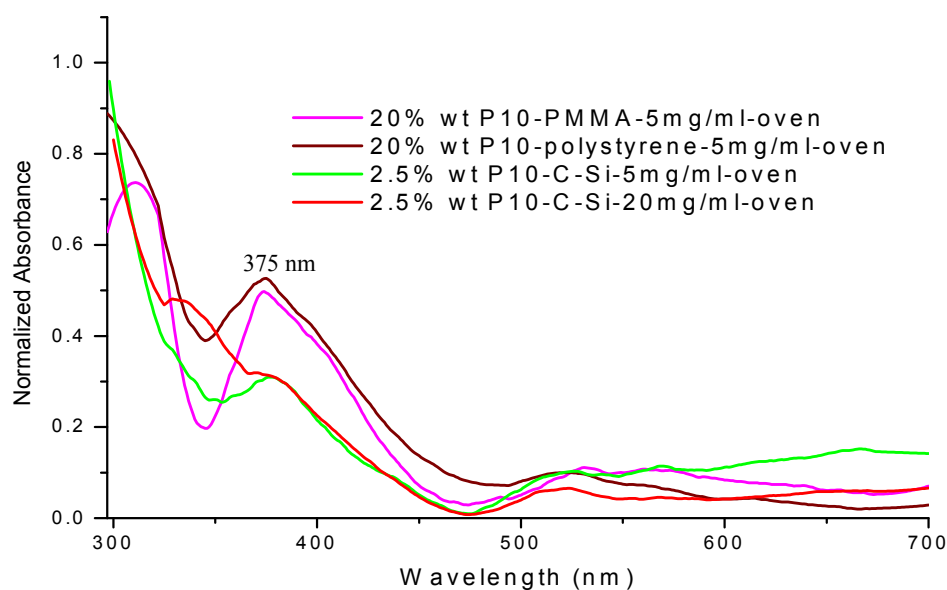


Figure 4-6 Absorption spectra of **P10** in different matrix in film (5 mg/mL, slits were 5,5 nm)

Figure 4-6 shows the absorption spectrum of **P10** in PMMA, polystyrene and the C-Si matrix at different contents. They all show a maximum at 375 nm. No obvious change could be detected depending on the concentration and the matrix.

4.1.2.2 PL results

(1) 20% wt of **P10** in PMMA (5 mg/mL) in film

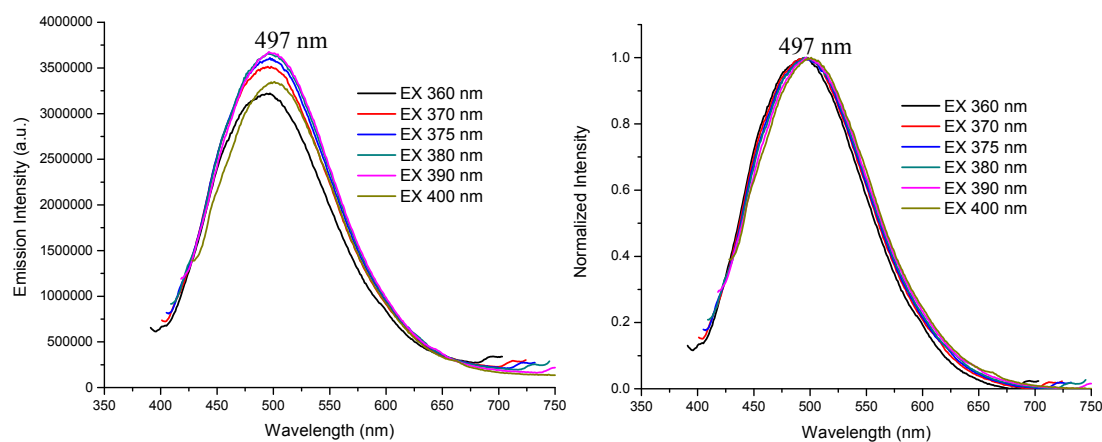


Figure 4-7 Emission spectra (left) and normalized emission spectra (right) of 20% wt of **P10** in PMMA in film with different excitations (slits were 5,5 nm).

The emission spectrum recorded with different excitation wavelengths ranging from 360 to 400 nm is reported on **Figure 4-7**. It shows a broad band between 400 and 700 nm with a maximum at 497 nm. The normalized emission spectrum shows an identical emission profile whatever the excitation wavelength is.

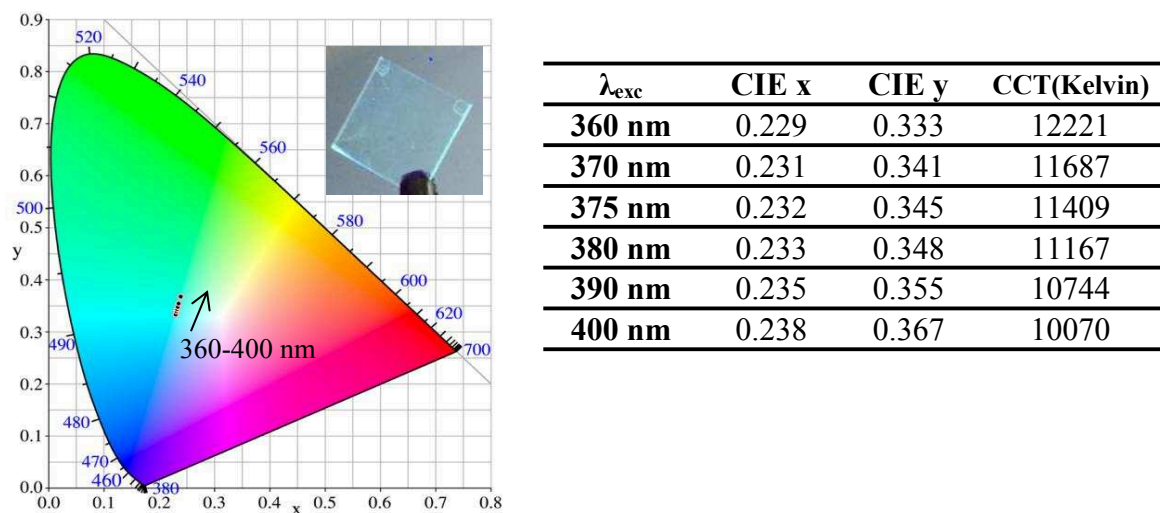


Figure 4-8 CIE coordinates of 20% wt of **P10** in PMMA in film (λ_{exc} = 360-400 nm, slits were 5,5 nm) (The insert shows the emission of the film under a 365 nm UV lamp)

The **CIE coordinates and the CCT data** show that the material emits a **bluish green light** under excitation at 360-400 nm.

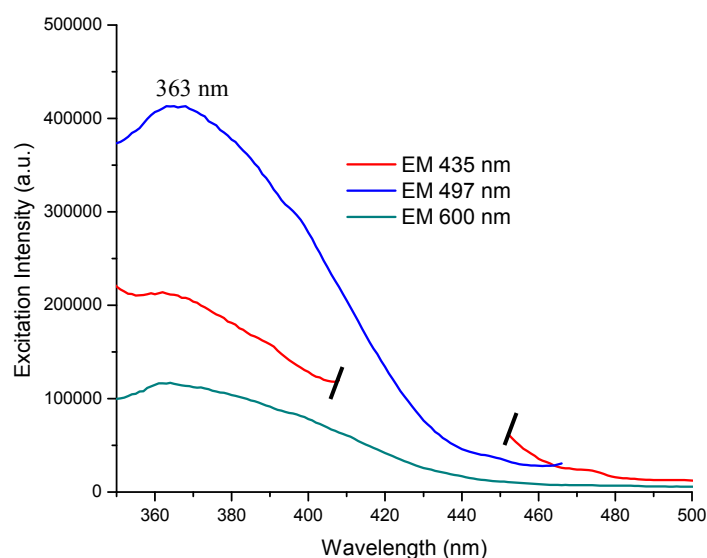


Figure 4-9 Excitation spectra of 20% wt of **P10** in PMMA in film with different emissions (slits were 5,5 nm).

Figure 4-9 shows the excitation spectrum recorded at different emission wavelengths. A maximum at 363 nm can be seen. Part of some spectra were cut to remove the band resulted

from the Rayleigh light scattering.

(2) 20% wt of **P10** in Polystyrene (5 mg/mL) in film

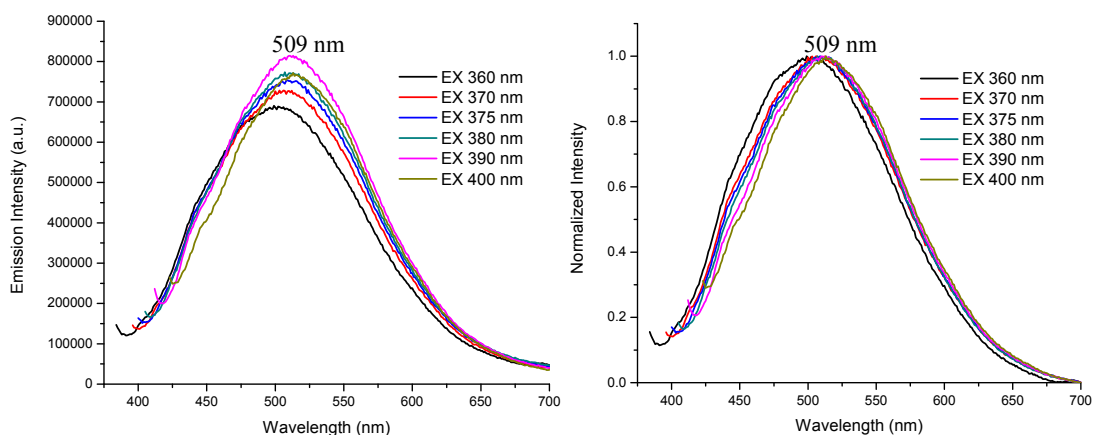
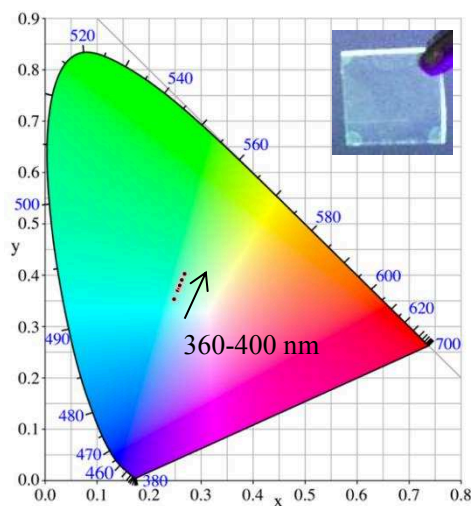


Figure 4-10 Emission spectra (left) and normalized emission spectra (right) of 20% wt of **P10** in polystyrene in film with different excitations (slits were 5,5 nm)

Figure 4-10 shows the emission spectrum of **P10** dissolved into polystyrene (20 wt%). The emission band is broad from 400 to 700 nm, with a maximum at 509 nm when excited at 375 nm. The maximum slightly shifts to the red when the excitation wavelength is increased.



λ_{exc}	CIE x	CIE y	CCT(Kelvin)
360 nm	0.247	0.354	9944
370 nm	0.255	0.371	9018
375 nm	0.258	0.375	8795
380 nm	0.259	0.380	8609
390 nm	0.263	0.391	8263
400 nm	0.268	0.403	7865

Figure 4-11 CIE coordinates of 20% wt of **P10** in polystyrene in film (λ_{exc} = 360-400 nm, slits were 5,5 nm)
(The insert shows the emission of the film under a 365 nm UV lamp)

The **CIE coordinates** and the **CCT data** show that the material emits a **bluish green light** when excited at 360-380 nm and **cool white light (5000-8300 K CCT)** upon excitation at 390-400 nm.

(3) 2.5% wt of P10 in C-Si matrix (5 mg/mL) in film

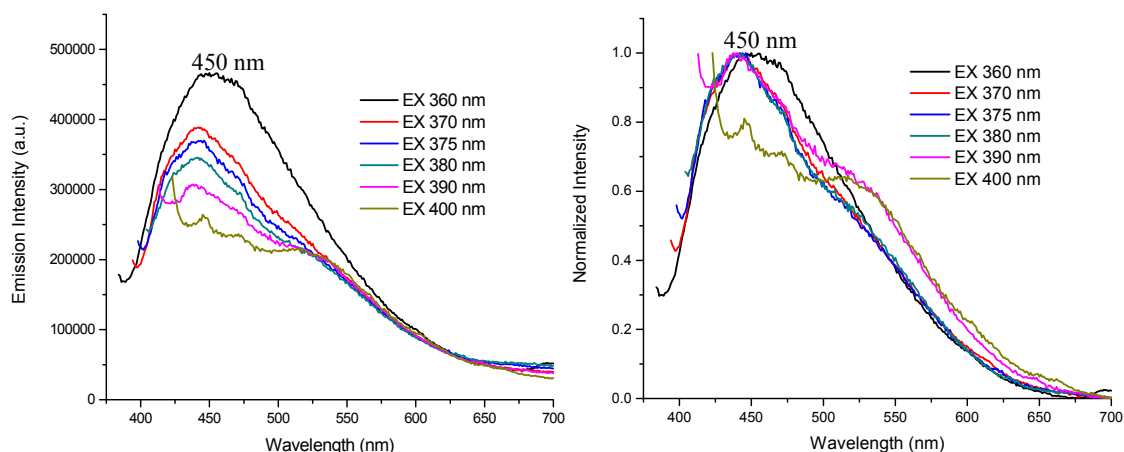


Figure 4-12 Emission spectra (left) and normalized emission spectra (right) of 2.5% wt of P10 in 5 mg/mL C-Si matrix in film with different excitations (slits were 5,5 nm).

Figure 4-12 shows that the emission band has a maximum at around 450 nm when the excitation wavelength is 360 nm, and the band is gradually blue-shifted when the excitation wavelength is increased to 400 nm. This may due to the low intensity of the emission of the film with high influence from the Rayleigh scattering. Besides, the emission may also be influenced by the glass substrate according to our previous results.

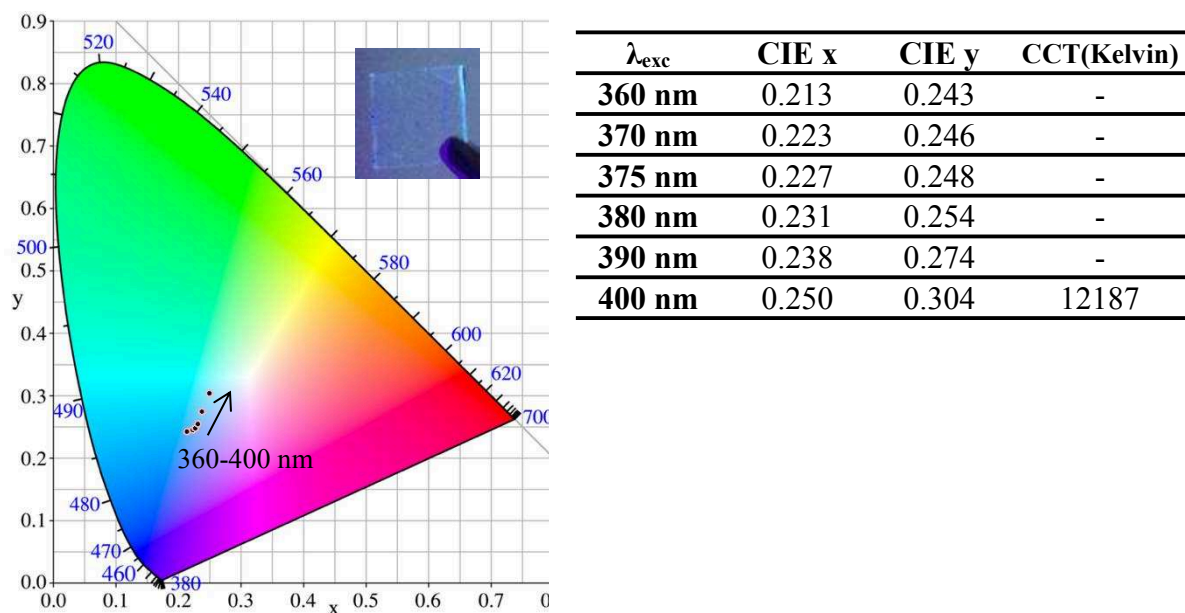


Figure 4-13 CIE coordinates of 2.5% wt of P10 in 5 mg/mL C-Si matrix in film ($\lambda_{exc} = 360-400$ nm, slits were 5,5 nm) (The insert shows the emission of the film under a 365 nm UV lamp)

The CIE coordinates and the CCT data (Figure 4-13) show that the material emits a **greenish**

blue light upon excitation at 360-400 nm.

(4) 2.5% wt of **P10** in C-Si matrix (20 mg/mL) in film

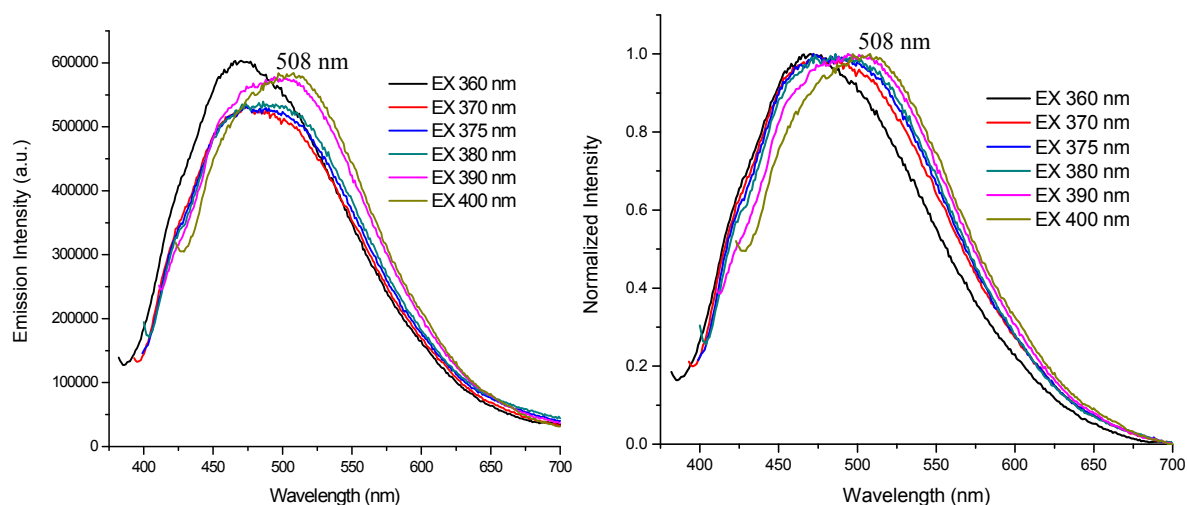


Figure 4-14 Emission spectra (left) and normalized emission spectra (right) of 2.5% wt of **P10** in 20 mg/mL C-Si matrix in film with different excitations (slits were 5,5 nm).

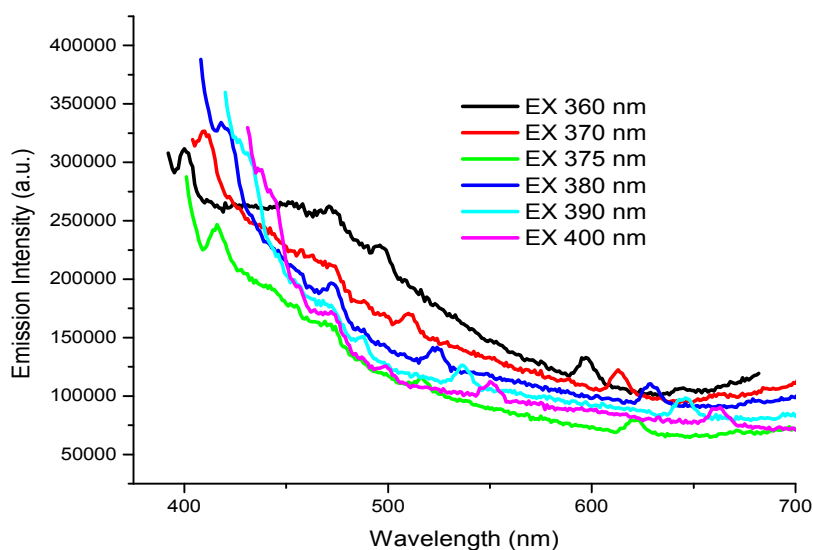


Figure 4-15 Emission spectra of the glass substrate with different excitations (slits were 5,5 nm).

The emission spectra reported on **Figure 4-14** of 2.5% wt of **P10** in C-Si matrix (20 mg/mL) in film with different excitation wavelengths show a broad emission band between 400 and 700 nm with an excitation wavelength from 360 nm to 400 nm. The maxima are similar for excitation between 370 and 390 nm (λ_{max} is around 490 nm), but it is slightly different with excitation at 360 nm (λ_{max} is 470 nm) and 400 nm (λ_{max} is 508 nm). On the whole, it shows some red-shift when the excitation wavelength increases, which may be due to a lower influence of the

emission of the glass substrate, as shown in **Figure 4-15**.

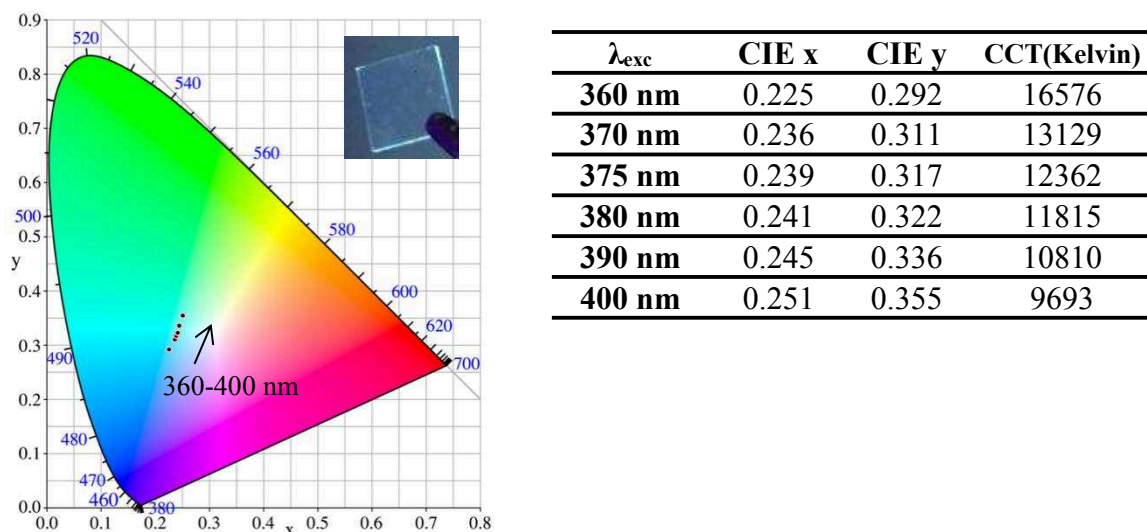


Figure 4-16 CIE coordinates of 2.5% wt of P10 in 20 mg/mL C-Si matrix in film ($\lambda_{exc} = 360-400$ nm, slits were 5,5 nm) (The insert shows the emission of the film under a 365 nm UV lamp)

The CIE coordinates reported in **Figure 4-16** show that the material emits a **bluish green to grenish blue emission** light when excited at 360-400 nm.

4.1.2.3 Comparison of results of P10 in different conditions in films

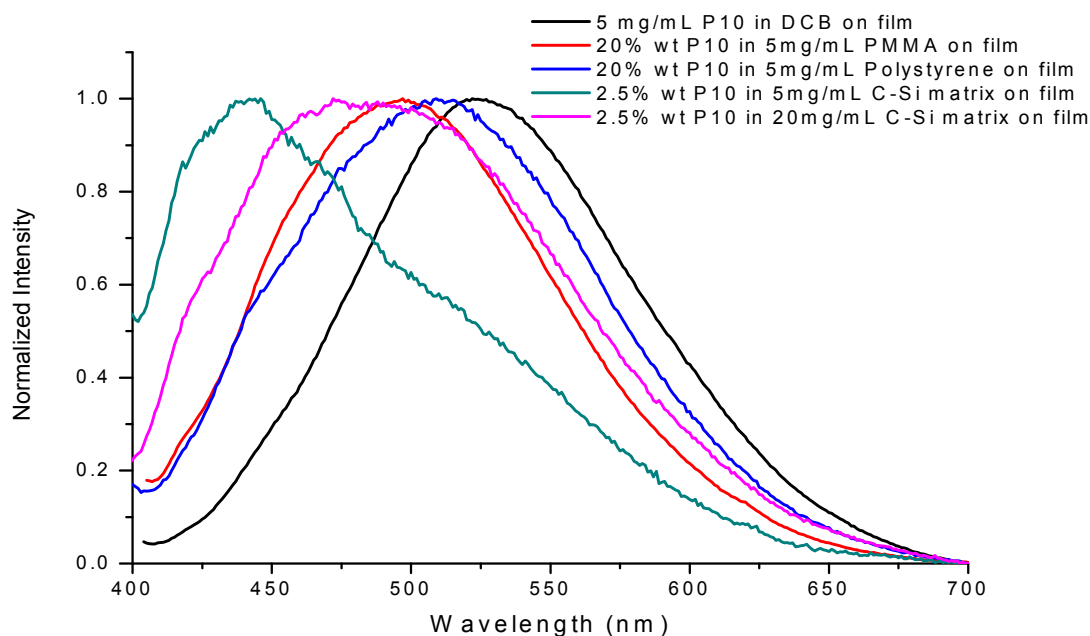


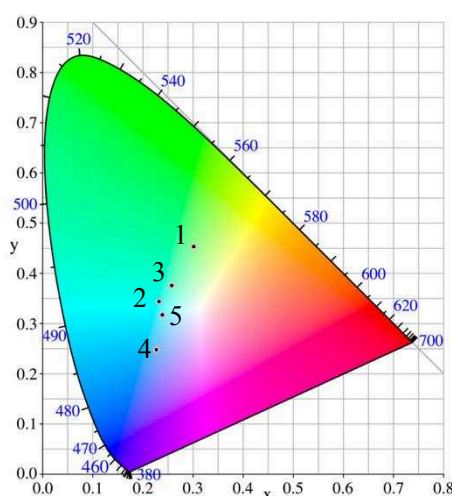
Figure 4-17 Emission spectra of P10 in different conditions in film ($\lambda_{exc} = 375$ nm, slits were 5,5 nm)

Table 4-2 Absorption and PL data of **P10** in different conditions in film (slits were 5,5 nm)

No.	1	2	3	4	5
Sample	P10 in pure film-5mg/ml-oven	20% wt P10-PMMA-5mg/ml-oven	20% wt P10-polystyrene-5mg/ml-oven	2.5% wt P10-C-Si-5mg/ml-oven	2.5% wt P10-C-Si-20mg/ml-oven
λ_{abs} (nm)	371, 507	311, 374, 531	375, 524	377, 527	329, 370, 524
λ_{exc}^* (nm)	243, 301, 371	301, 363	249, 301	244, 304	244, 307
λ_{em}^{**} (nm)	522	497	509	450	508
FWHM	122	124	137	169	150

* For all excitations were set λ_{an} at their maximum emissions except other mentions.

** For all emissions were set λ_{exc} at 375 nm except other mentions.



No.	CIE x	CIE y	CCT(Kelvin)
1	0.302	0.454	6334
2	0.232	0.345	11409
3	0.258	0.375	8795
4	0.227	0.248	29182
5	0.239	0.317	12362

Figure 4-18 CIE coordinates of **P10** in different conditions in film ($\lambda_{exc} = 375$ nm, slits were 5,5 nm)

As shown on **Figure 4-17** and **Figure 4-18**, **P10** deposited as pure film demonstrated cool white light (5000-8300 K CCT) with excitation at 375 nm. When it was doped into different matrices, the latter all demonstrated greenish blue to bluish green light under excitation at 375 nm. Therefore, when doped into a matrix, the emission of **P10** was blue-shifted. This could be explained similarly to what was observed for **P1** (see § 4.1.1). By comparison of case **No.4** and **5** in **Table 4-2**, it shows that films prepared from higher concentration of the liquid precursor before spin-coating also lead to a red-shift of the emission. Besides, the FWHM data in **Table 4-2** indicate that emissions of these films are broad.

4.1.3 P13 in different matrices

4.1.3.1 Absorption results

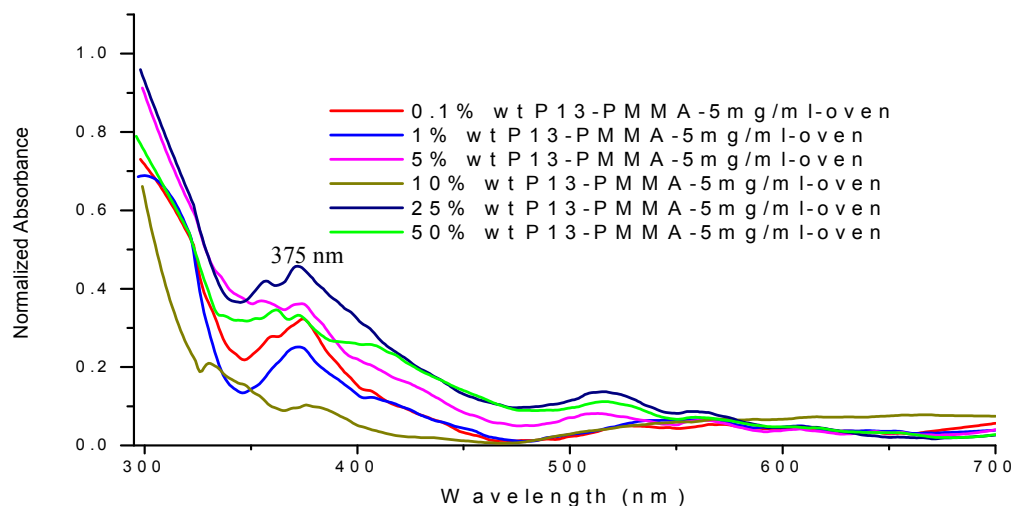
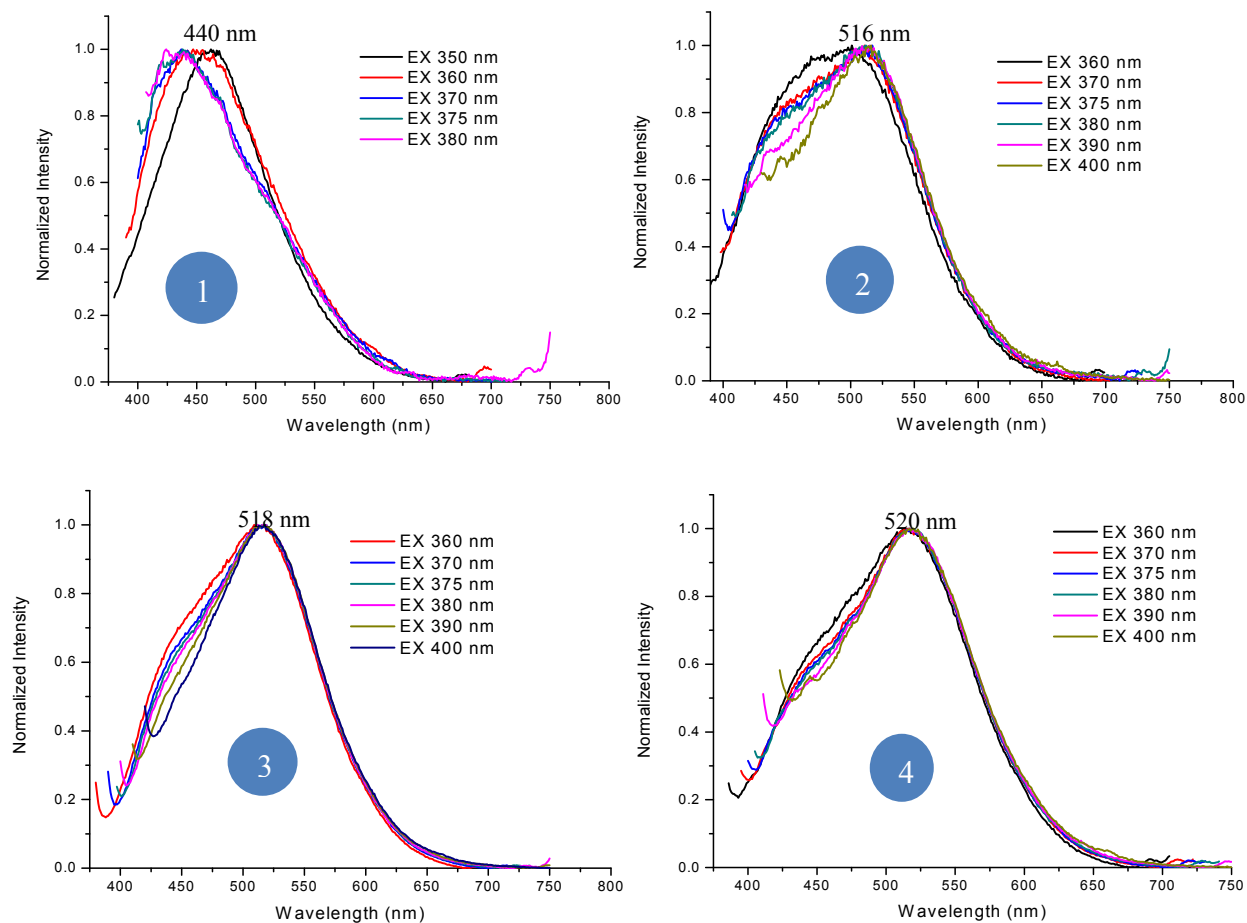


Figure 4-19 Absorption spectra of different amounts of **P13** in PMMA films (5 mg/mL, slits were 5,5 nm)

As shown on **Figure 4-19**, one absorption band with a maximum at 375 nm is observed in the near UV between 350 and 400 nm.

4.1.3.2 PL results

(1) 0.1-50% wt of **P13** in PMMA (5 mg/mL) in film



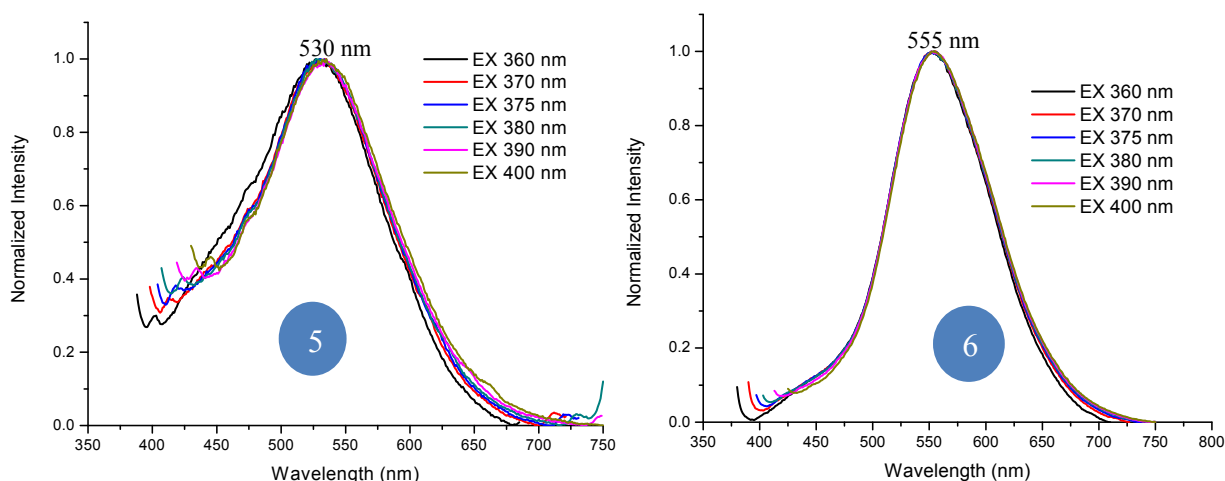


Figure 4-20 Emission spectra of films of **P13** in PMMA with different loadings under different 360-400 nm excitation, 1) 0.1% wt, 2) 1% wt, 3) 5% wt, 4) 10% wt, 5) 25% wt, 6) 50% wt. (5 mg/mL, slits were 5,5 nm).

Figure 4-20 shows the emission spectra of films of **P13** in PMMA with different amounts of **P13** under excitation comprised between 360 and 400 nm. By comparison with **Figure 4-15**, it shows that a higher amount of **P13** in PMMA lead to a lower influence of the emission of the glass substrate. These data are summarized in **Figure 4-21** and **Table 4-3**.

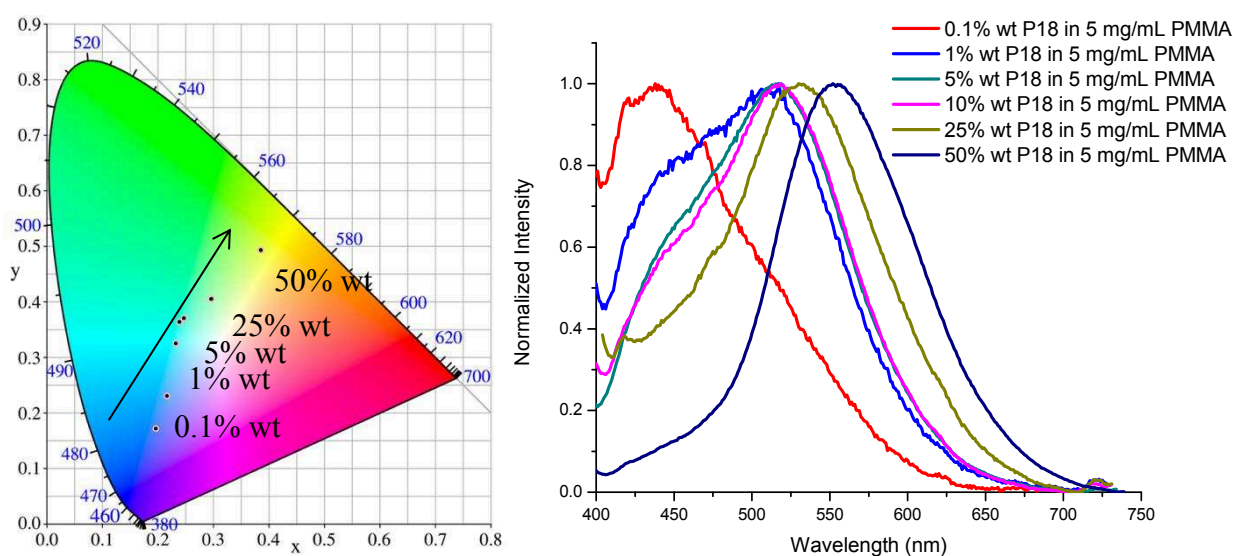
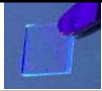



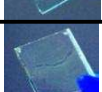



Figure 4-21 Comparison of CIE coordinates and emission spectra of **P13** in PMMA in film ($\lambda_{\text{exc}} = 375 \text{ nm}$, slits were 5,5 nm)

Table 4-3 Summary of PL data for films of **P13** in PMMA with different loadings (slits were 5,5 nm)

Ratio	CIE x	CIE y	CCT (K)	FWHM (nm)	λ_{abs}^* (nm)	λ_{em}^{**} (nm)	Emission [#]
0.1% wt	0.216	0.230	56412	-	375	440	
1% wt	0.231	0.325	12534	158	372	516	
5% wt	0.238	0.365	10170	141	375	518	
10% wt	0.247	0.370	9516	144	378	520	
25% wt	0.296	0.406	6730	145	370	530	
50% wt	0.385	0.493	4441	106	375	555	

* For all excitations were set λ_{an} at their maximum emissions except other mentions.

** For all emissions were set λ_{exc} at 375 nm except other mentions.

The emission of the film under a 365 nm UV lamp.

As shown, with the increase of the amount of **P13**, blue to neutral white emission can be obtained. In the case where the film contains 25% wt of **P13** in PMMA, **cool white emission** was obtained under excitation in the range of 360-400 nm. When the film contains 50% wt of **P13**, **neutral white emission** was obtained in the same conditions. The red-shift of the emission with a higher concentration of **P13** may also be due to the increase of interactions and aggregation among the polymer chains, as well as the formation of exciplexes that resulted in a lower bandgap, apart from the influence of the emission of the glass substrate.

*To find a condition for **P13** to obtain better white emission, more else matrices were further investigated. Following are results of the polymer in Poly(Ethylene-co-vinyl acetate) and polystyrene, which are widely used. PMMA with higher molecular weight was also investigated to know the influence of the molecular weight of the matrix to the emission.*

(2) 5% wt of **P13** in Poly(Ethylene-co-vinyl acetate) (5 mg/mL) in film

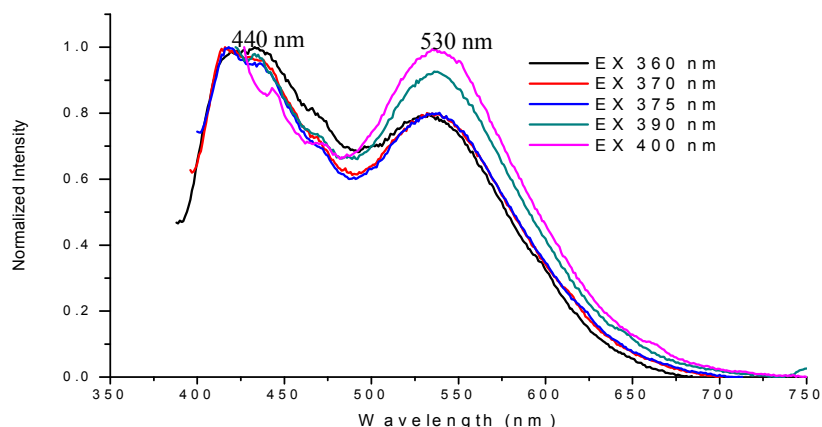
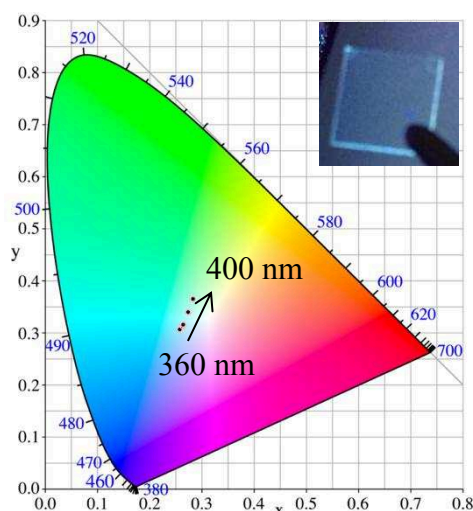


Figure 4-22 Emission spectrum of **5% wt of P13 in Poly(Ethylene-co-vinyl acetate)** in film (5 mg/mL, slits were 5,5 nm)

The emission spectra of **P13** loaded at **5% wt** in Poly(Ethylene-co-vinyl acetate) recorded with different excitation wavelengths in the near-UV are shown on **Figure 4-22**. Two maxima are observed at 440 nm and 530 nm, respectively. The band centered at 440 nm may be ascribed to the emission of the glass substrate, as shown in **Figure 4-15**.



λ_{exc}	CIE x	CIE y	CCT (K)
360 nm	0.258	0.307	11207
370 nm	0.263	0.313	10346
375 nm	0.265	0.315	10129
390 nm	0.274	0.341	8650
400 nm	0.283	0.365	7661

Figure 4-23 CIE coordinates of **5% wt P13 in Poly(Ethylene-co-vinyl acetate)** in film (λ_{exc} = 360-400 nm, slits were 5,5 nm) (The insert shows the emission of the film under a 365 nm UV lamp)

The **CIE coordinates** show that the material gives near white emission with different excitations from 360-400 nm, particularly, it demonstrates cool white light (5000-8300 K CCT) when excited at 400 nm.

(3) 5% wt of P13 in PMMA-2 (5 mg/mL) in film

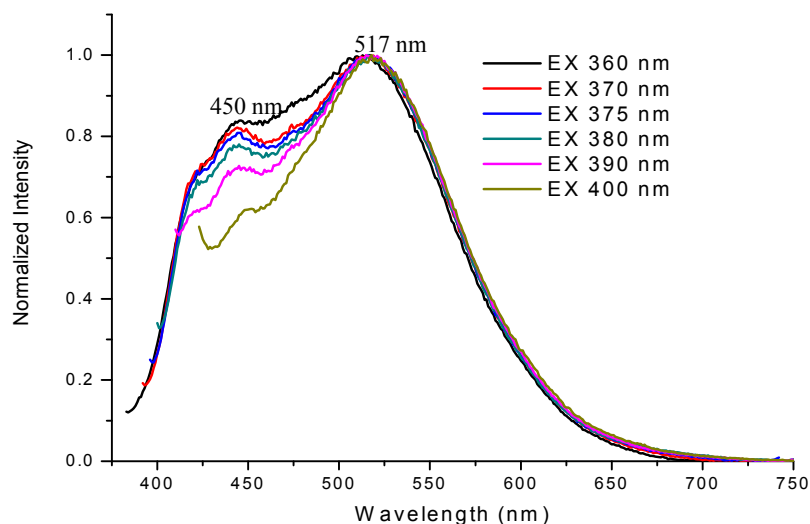
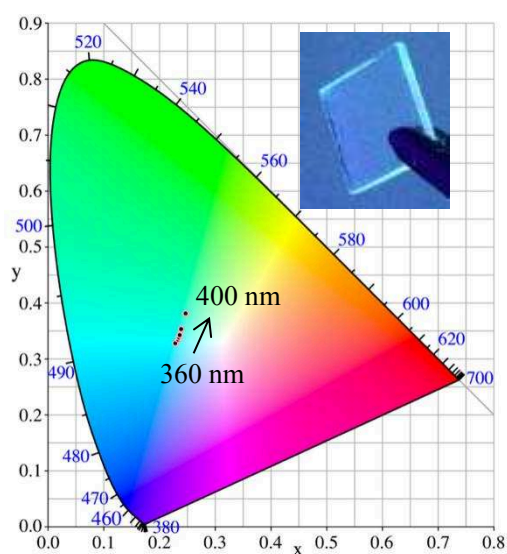


Figure 4-24 Emission spectra of **5% wt of P13 in PMMA-2** in film (5 mg/mL, slits were 5,5 nm)

Figure 4-24 shows that the emission spectrum of a film comprising 5% wt of **P13** in PMMA-2 (the latter having a molecular weight of 996000, higher than the previously used PMMA, whose M_w was 120000). A main band centered at 517 nm with a shoulder peak at 450 nm were observed when the film was excited at 360-400 nm.



λ_{exc}	CIE x	CIE y	CCT (K)
360 nm	0.229	0.328	12591
370 nm	0.233	0.335	11750
375 nm	0.235	0.338	11490
380 nm	0.236	0.342	11233
390 nm	0.238	0.353	10558
400 nm	0.247	0.381	9243

Figure 4-25 CIE coordinates of **5% wt P13 in PMMA-2** in film (λ_{exc} = 360-400 nm, slits were 5,5 nm) (The insert shows the emission of the film under a 365 nm UV lamp)

The **CIE coordinates** are representative of a bluish green emission under excitation at 360-400 nm.

(4) 5% wt of **P13** in Polystyrene (5 mg/mL) in film

552 nm

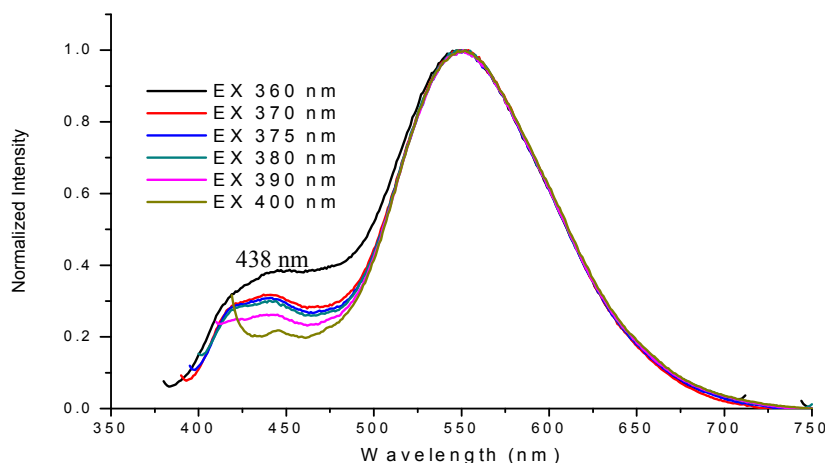
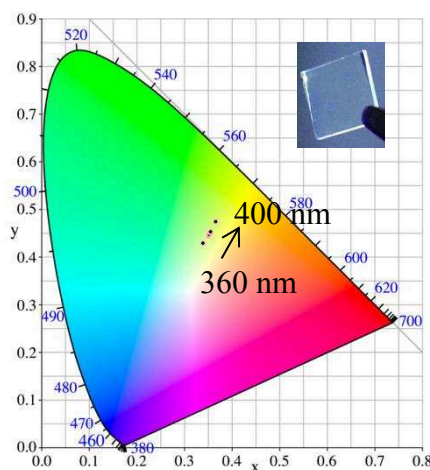


Figure 4-26 Emission spectrum of **5% wt P13 in Polystyrene in film** (5 mg/mL, slits were 5,5 nm)

Figure 4-26 shows that the emission spectrum of a film of **5% wt P13 in Polystyrene** comprises a band centered at 552 nm with a shoulder at 438 nm. The latter may due to the impact of the emission of the glass substrate.



λ_{exc}	CIE x	CIE y	CCT (K)
360 nm	0.338	0.430	5339
370 nm	0.351	0.446	5044
375 nm	0.352	0.449	5013
380 nm	0.354	0.452	4984
390 nm	0.355	0.453	4952
400 nm	0.366	0.475	4764

Figure 4-27 CIE coordinates of **5% wt P13 in Polystyrene in film** (λ_{exc} = 360-400 nm, slits were 5,5 nm)

(The insert shows the emission of the film under a 365 nm UV lamp)

The **CIE coordinates and the CCT data** show that the material emits **cool white light (5000-8300 K CCT)** under 360-375 nm excitation and **neutral white emission (3700-5000 K CCT)** when excited in the range of 380-400 nm.

(5) 20% wt of **P13 in Polystyrene (5 mg/mL)**

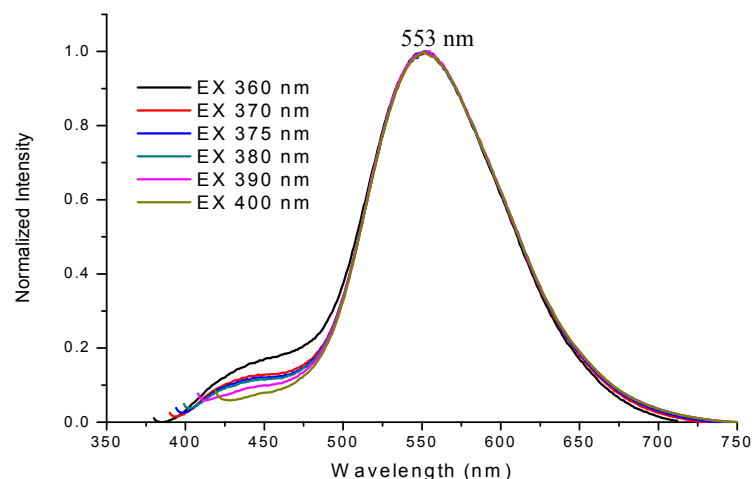
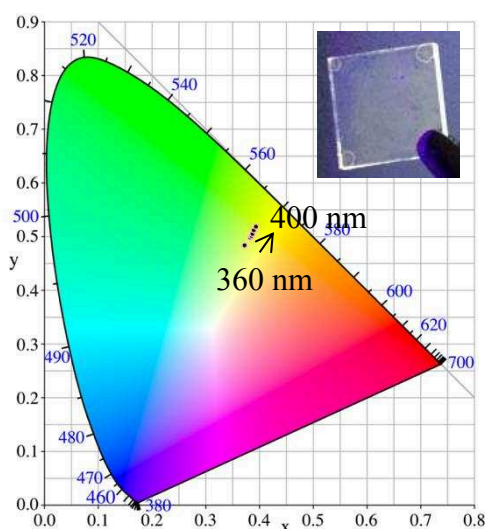


Figure 4-28 Emission spectrum of a film of **20% wt P13 in Polystyrene** (5 mg/mL, slits were 5,5 nm)

The emission spectrum depicted in **Figure 4-28** shows a main band centered at 553 nm with a shoulder peak at 445 nm may ascribed to the emission of the glass substrate.



λ_{exc}	CIE x	CIE y	CCT (K)
360 nm	0.372	0.484	4655
370 nm	0.383	0.499	4496
375 nm	0.385	0.502	4472
380 nm	0.386	0.505	4456
390 nm	0.389	0.512	4418
400 nm	0.394	0.519	4367

Figure 4-29 CIE coordinates of a film of **20% wt P13 in Polystyrene** ($\lambda_{\text{exc}} = 360\text{-}400$ nm, slits were 5,5 nm)

(The insert shows the emission of the film under a 365 nm UV lamp)

The **CIE coordinates and the CCT data** are typical of a **neutral white emission (3700-5000 K CCT)** under excitation between 360 nm and 400 nm.

(6) Film comprising 1% wt of **P13 in C-Si matrix (5 mg/mL)**

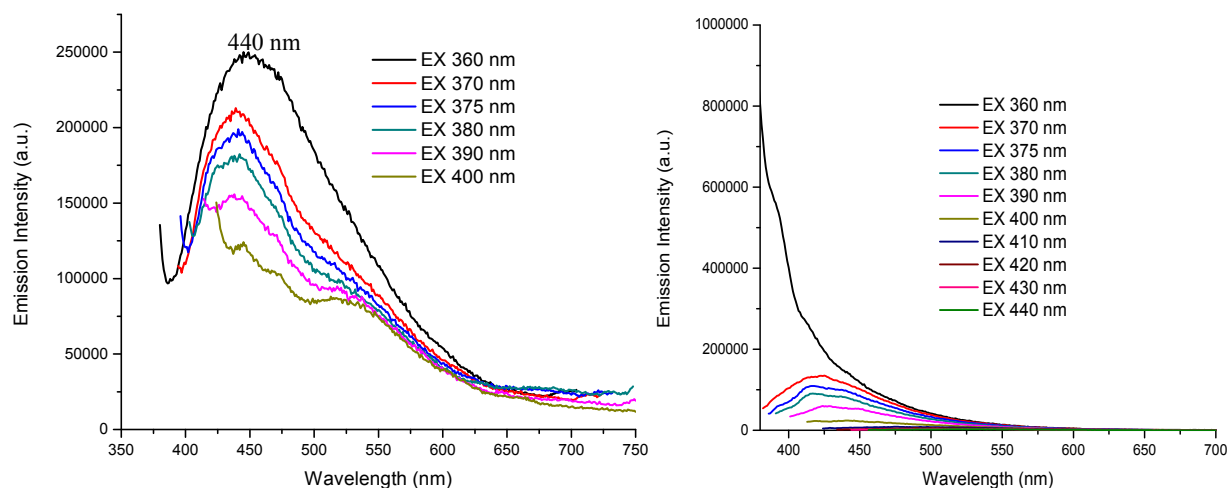
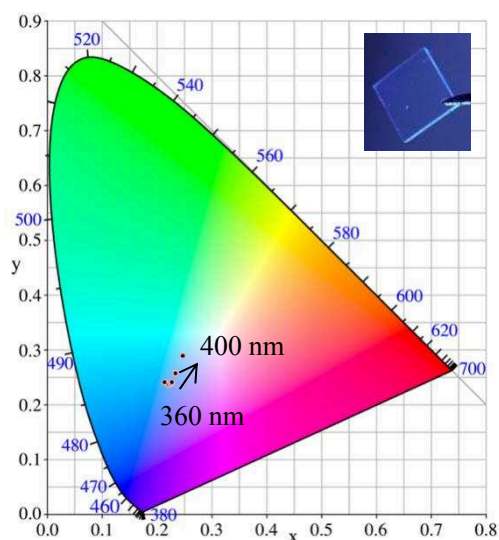


Figure 4-30 Emission spectrum of a) 1% wt P13 in C-Si matrix in film; b) C-Si matrix in DCM at different excitation wavelength (5 mg/mL, slits were 5,5 nm).

Figure 4-30 (a) shows that the emission band of a film of **1% wt P13 in C-Si matrix** is centered at 440 nm. It was much blue shifted compared with other matrices, which may due to the blue emission from the C-Si matrix, as shown in **Figure 4-30 (b)**.



λ_{exc}	CIE x	CIE y	CCT (K)
360 nm	0.214	0.242	39843
370 nm	0.222	0.238	40443
375 nm	0.225	0.238	37139
380 nm	0.227	0.241	34554
390 nm	0.233	0.257	23054
400 nm	0.246	0.289	13948

Figure 4-31 CIE coordinates of **1% wt P13 in C-Si matrix in film** (λ_{exc} = 360-400 nm, slits were 5,5 nm)
(The insert shows the emission of the film under a 365 nm UV lamp)

The **CIE coordinates** show that the material emits blue to near white light when excited in the range of 360 nm and 400 nm.

(7) Film comprising 2.5% wt of **P13 in C-Si matrix (5 mg/mL)**

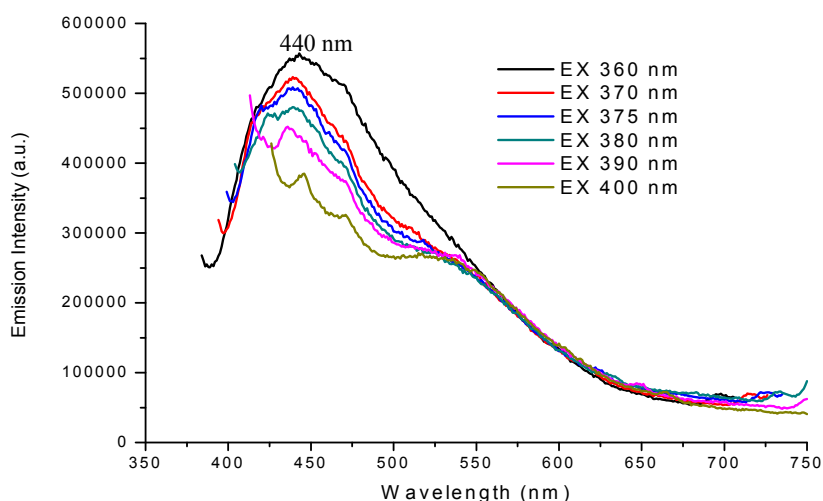
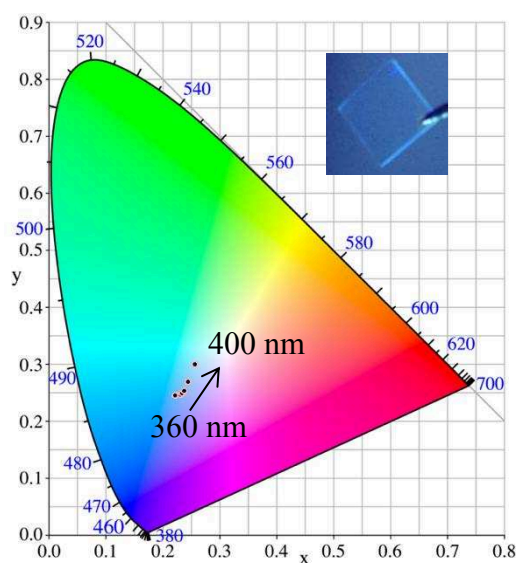


Figure 4-32 Emission spectrum of 2.5% wt P13 in C-Si matrix in film (5 mg/mL, slits were 5,5 nm)

Figure 4-32 shows that the emission spectrum is ranging from 400 nm to 750 nm with a maximum at 440 nm. It was also much blue shifted compared with other matrices, which may also due to the addition of the blue emission from the C-Si matrix.



λ_{exc}	CIE x	CIE y	CCT (K)
360 nm	0.222	0.245	33472
370 nm	0.231	0.246	29227
375 nm	0.234	0.249	26582
380 nm	0.237	0.254	23168
390 nm	0.244	0.269	17438
400 nm	0.257	0.300	11760

Figure 4-33 CIE coordinates of 2.5% wt P13 in C-Si matrix in film (λ_{exc} = 360-400 nm, slits were 5,5 nm)

(The insert shows the emission of the film under a 365 nm UV lamp)

The **CIE coordinates** show that the material emits blue to near white emission under different excitations from 360 to 400 nm.

(8) Film comprising 2.5% wt of **P13 in C-Si matrix (5 mg/mL)** prepared by painting

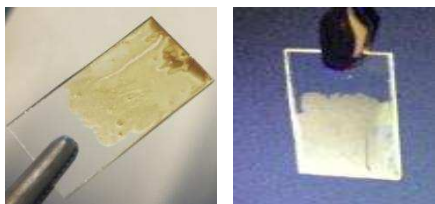


Figure 4-34 Thin film prepared by painting without UV (left) and under a 365 nm UV lamp (right)

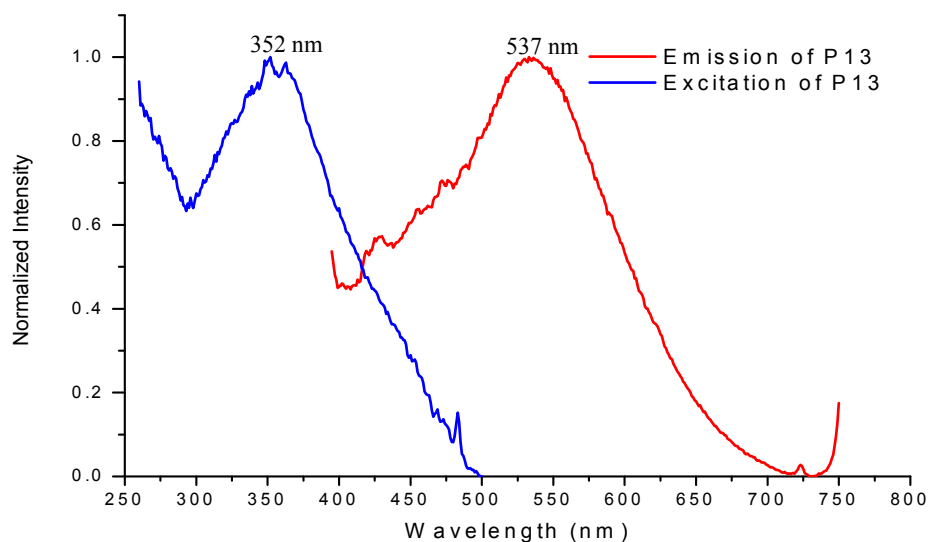
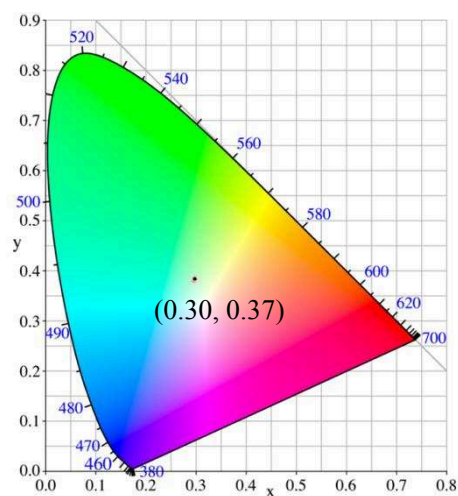


Figure 4-35 Excitation and emission spectra of **P13** in C-Si matrix **in film prepared by painting** (Setting: excitation ($\lambda_{an} = 537$ nm) and emission ($\lambda_{exc} = 375$ nm), slits were 2,2 nm)

As shown on **Figure 4-35**, the excitation spectrum (blue trace) of this material is centered at 352 nm, and the emission spectrum (red trace) shows a broad band from 400 nm to 750 nm with a maximum at 537 nm.



λ_{exc}	CIE x	CIE y	CCT (K)
375 nm	0.300	0.373	6796

Figure 4-36 CIE coordinates of **P13** in film prepared by painting ($\lambda_{exc} = 375$ nm, slit 2,2)

The **CIE coordinates** (0.30, 0.37) indicate that the film emits cool white light (5000-8300 K CCT) when excited at 375 nm.

(9) Comparison of the emission of films of **P13** in different matrices (5 mg/mL)

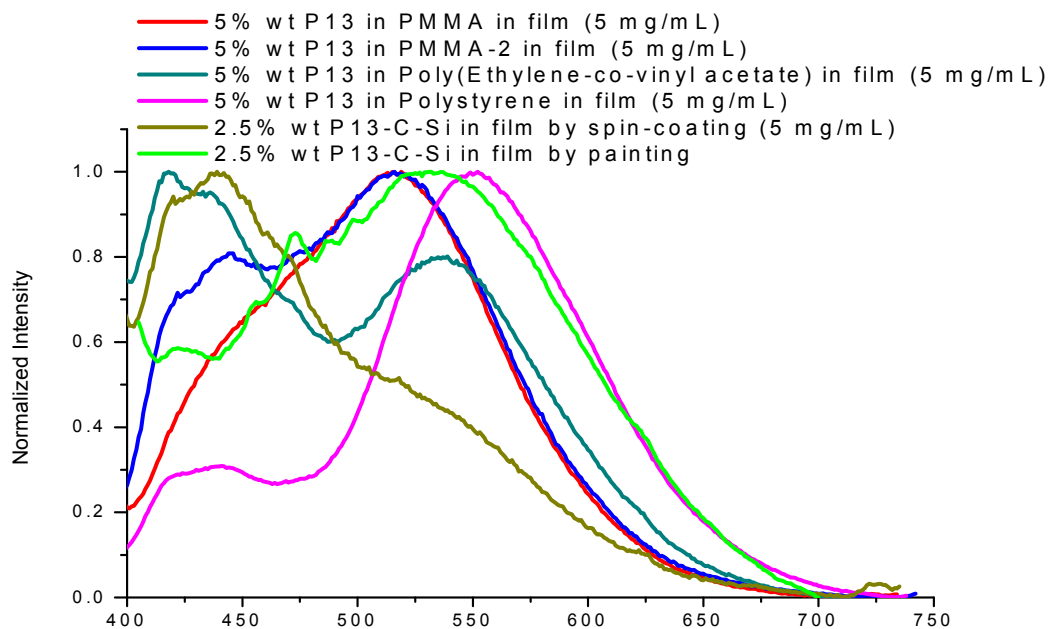


Figure 4-37 Comparison of emission spectra of **P13** in different matrices in film (slits were 5,5 nm)

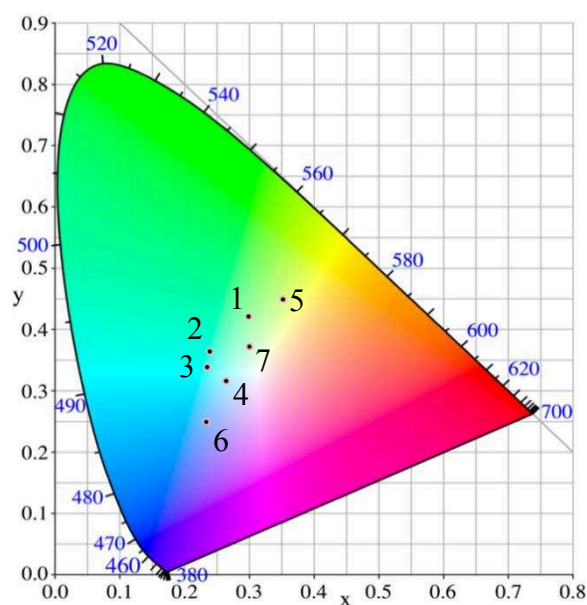
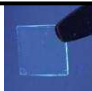
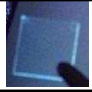
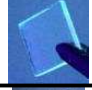
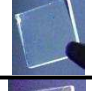
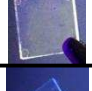
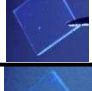
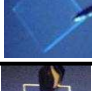
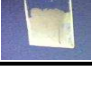


Figure 4-38 CIE coordinates of **P13** in different conditions, 1) **P13** in DCM (0.01 mg/mL), 2) 5% wt **P13** in PMMA in film (5 mg/mL), 3) 5% wt **P13** in PMMA-2 in film (5 mg/mL), 4) 5% wt **P13** in Poly(Ethylene-co-

vinyl acetate) in film (5 mg/mL), 5) 5% wt **P13** in Polystyrene in film (5 mg/mL), 6) 2.5% wt **P13** in C-Si matrix in film by spin-coating (5 mg/mL), 7) 2.5% wt **P13** in C-Si matrix in film by painting. ($\lambda_{\text{exc}} = 375$ nm, for DCM sample: 0.01 mg/mL, slits are 2,2 nm; for films: slits are 5,5 nm)

The emission spectra and CIE coordinates of films of **P13** in different matrices (5 mg/mL) are shown on **Figure 4-37** and **Figure 4-38**, respectively. These data are summarized in **Table 4-4**.

Table 4-4 PL data of **P13** in different matrices in film (5 mg/mL, slits were 5,5 nm)

Conditions	CIE x	CIE y	CCT (K)	FWHM (nm)	λ_{em}^* (nm)	Emission ⁺
5% wt P13 -PMMA	0.238	0.365	10170	141	518	
5% wt P13 -PEA ^o	0.265	0.315	10129	455	440, 530	
5% wt P13 -(PMMA-2) [#]	0.235	0.338	11490	167	517	
5% wt P13 -Polystyrene	0.352	0.449	5013	101	552	
20% wt P13 -Polystyrene	0.385	0.502	4472	99	553	
1% wt P13 -C-Si matrix	0.225	0.238	37139	166	440	
2.5% wt P13 -C-Si matrix	0.234	0.249	26582	204	440	
2.5% wt P13 -C-Si matrix (painted)	0.300	0.373	6796	222	537	

* For all emissions were set λ_{exc} at 375 nm except other mentions.

^o PEA: Poly(Ethylene-co-vinyl acetate).

[#] PMMA and PMMA-2: PMMA is the one from Orgatech, which the molecular weight is 120000, PMMA-2 is another size of PMMA that have bigger molecular weight, which from Chimiorga lab. The molecular weight of PMMA-2 is 996000.

⁺ Under a 365 nm UV lamp.

From the above results, the following conclusions can be drawn:

1) Films of **P13** using different matrices all show a broad emission band from 400 nm to 750 nm. In most cases, emission from blue to near white was obtained, according to the excitation

wavelength and the ratio between the polymer and the matrix.

2) Polystyrene is a better matrix for white emission among all the matrices investigated. Both 5% wt and 20% wt of **P13** in polystyrene demonstrated cool to neutral white light under excitation at 360-400 nm.

3) A higher concentration of polymer is better for red-shifting the emission.

4) The blue emission from C-Si matrix should be taken into consideration when designing luminescent materials.

5) Comparing the results obtained with PMMA and PMMA-2, it shows that PMMA with the smaller molecular weight afforded more redshifted light with lower FWHM.

4.1.4 P14 in different matrices

4.1.4.1 Absorption result

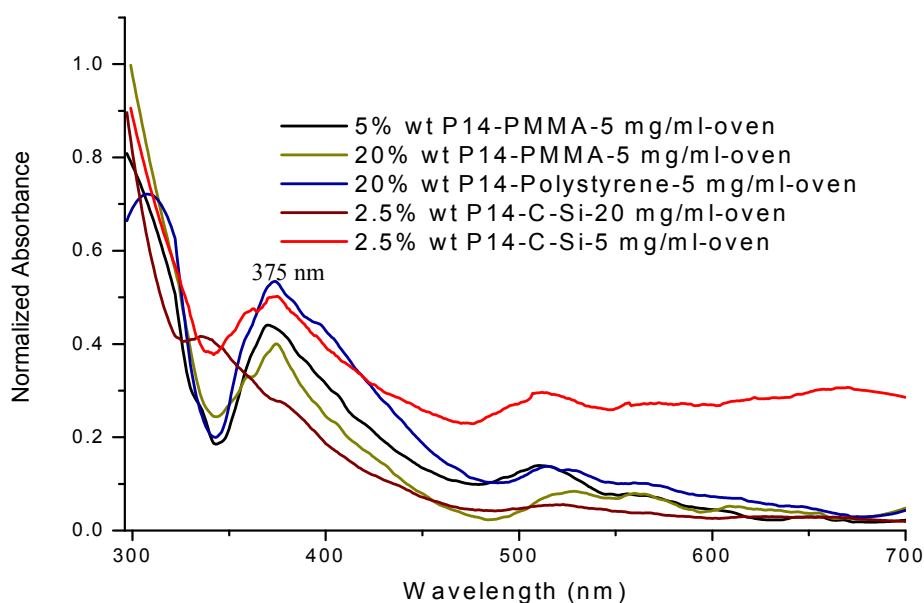


Figure 4-39 Absorption spectra of **P14** in different matrix in film (5 mg/mL, slits were 5,5 nm)

As shown in **Figure 4-39**, the main band of the absorption spectra of **P14** in different matrices (with 0.1-20% wt of **P14**) shows a similar maximum at around 375 nm.

4.1.4.2 PL result

(1) Film of 20% wt of P14 in PMMA (5 mg/mL)

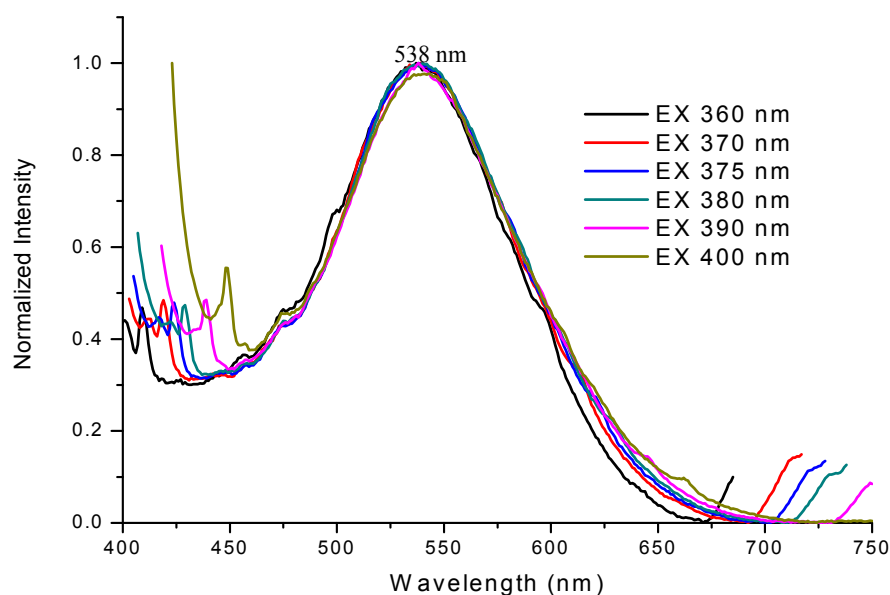
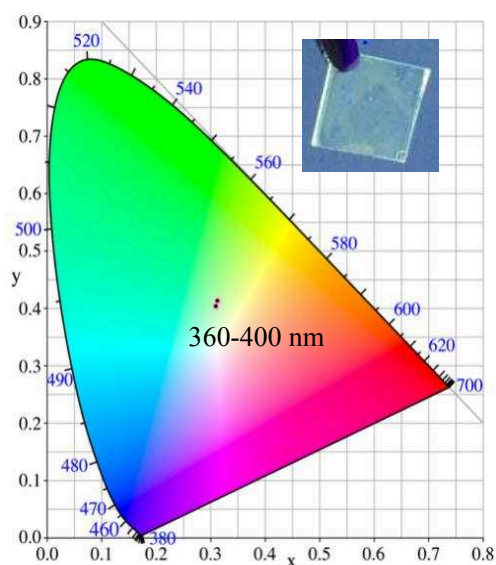


Figure 4-40 Emission spectrum of films of 20% wt P14 in PMMA recorded with different excitations (5 mg/mL, slits were 5,5 nm)

As shown in **Figure 4-40**, the emission spectrum shows a band centered at around 538 nm.



λ_{exc}	CIE x	CIE y	CCT(Kelvin)
360 nm	0.310	0.403	6263
370 nm	0.314	0.412	6103
375 nm	0.314	0.414	6084
380 nm	0.314	0.415	6086
390 nm	0.313	0.415	6108
400 nm	0.313	0.413	6129

Figure 4-41 CIE coordinates of 20% wt of P14 in PMMA in film (λ_{exc} = 360-400 nm, slits were 5,5 nm)
(The insert shows the emission of the film under a 365 nm UV lamp)

The **CIE coordinates** and the **CCT data** are representative of a **cool white emission (5000-8300 K CCT)** under excitation between 360 nm and 400 nm.

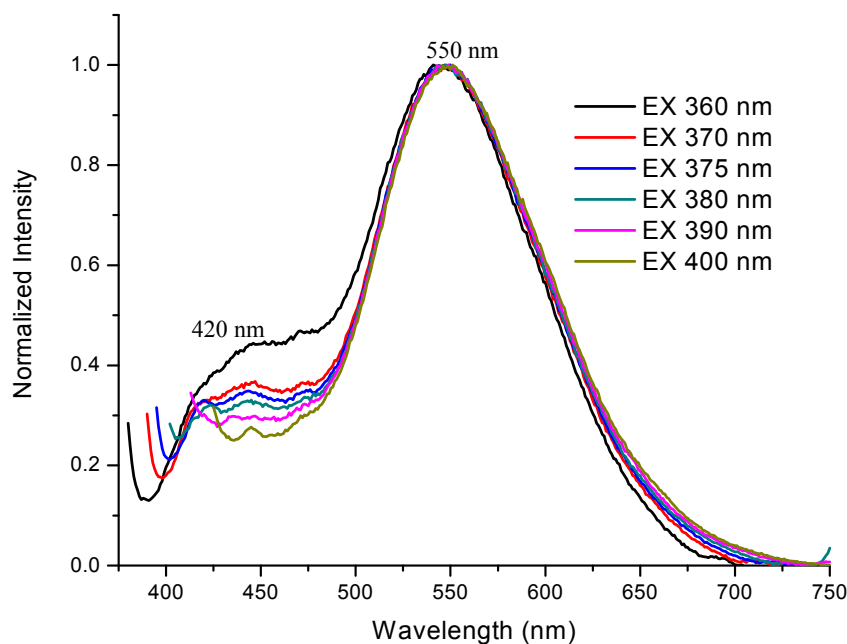
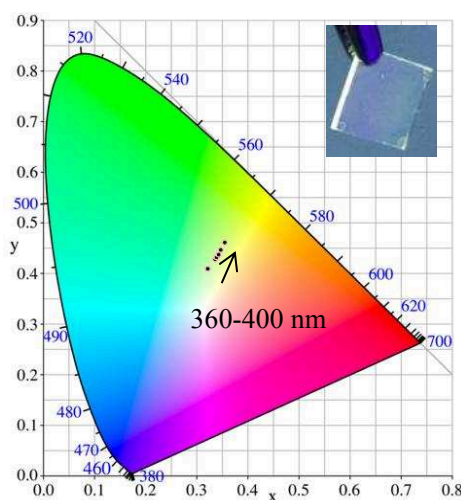
(2) Film of 20% wt of **P14 in Polystyrene (5 mg/mL)**

Figure 4-42 Emission spectrum of a film of **20% wt of P14 in Polystyrene** (5 mg/mL, slits were 5,5 nm)

The emission spectrum reported on **Figure 4-42** shows a main band centered at around 550 nm with a shoulder at 420 nm, which may ascribed to the blue emission of the glass substrate.



λ_{exc}	CIE x	CIE y	CCT(Kelvin)
360 nm	0.322	0.409	5848
370 nm	0.336	0.428	5407
375 nm	0.339	0.433	5320
380 nm	0.342	0.437	5250
390 nm	0.347	0.447	5137
400 nm	0.355	0.461	4962

Figure 4-43 CIE coordinates of a film of **20% wt of P14 in polystyrene** ($\lambda_{\text{exc}} = 360\text{-}400$ nm, slits were 5,5 nm)
(The insert shows the emission of the film under a 365 nm UV lamp)

The **CIE coordinates and the CCT data** indicate a **cool white light (5000-8300 K CCT)** under excitation at 360-390 nm and **neutral white emission (3700-5000 K CCT)** under excitation at 400 nm.

(3) Film of 2.5% wt of P14 in C-Si matrix (5 mg/mL)

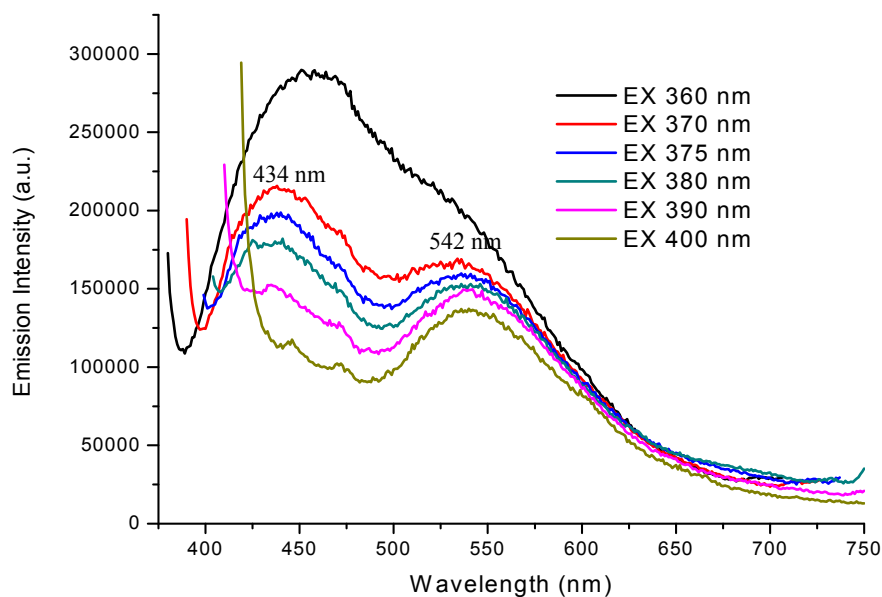
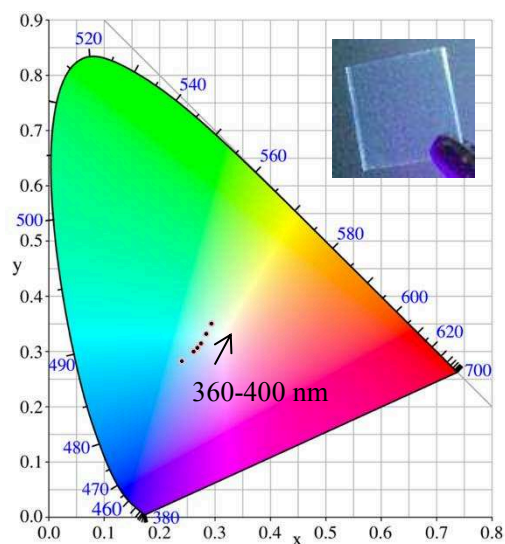


Figure 4-44 Emission spectrum of a film of **2.5% wt of P14 in C-Si matrix** (5 mg/mL, slits were 5,5 nm)

The emission spectrum reported on **Figure 4-44** shows two main bands centered at around 434 nm and 542 nm respectively. The band at lower wavelength is due to the Rayleigh scattering and the emission of the glass substrate according to our previous results.



λ_{exc}	CIE x	CIE y	CCT(Kelvin)
360 nm	0.240	0.283	15699
370 nm	0.261	0.300	11250
375 nm	0.269	0.307	10158
380 nm	0.275	0.315	9340
390 nm	0.284	0.333	8180
400 nm	0.293	0.351	7342

Figure 4-45 CIE coordinates of a film of **2.5% wt of P14 in C-Si matrix** (5 mg/mL, λ_{exc} = 360-400 nm, slits were 5,5 nm) (The insert shows the emission of the film under a 365 nm UV lamp)

The **CIE coordinates and the CCT data** show that the material emits a **greenish blue light** under excitation at 360-380 nm and **cool white light (5000-8300 K CCT)** under excitation at

390-400 nm.

(4) Film of 2.5% wt of P14 in C-Si matrix (20 mg/mL)

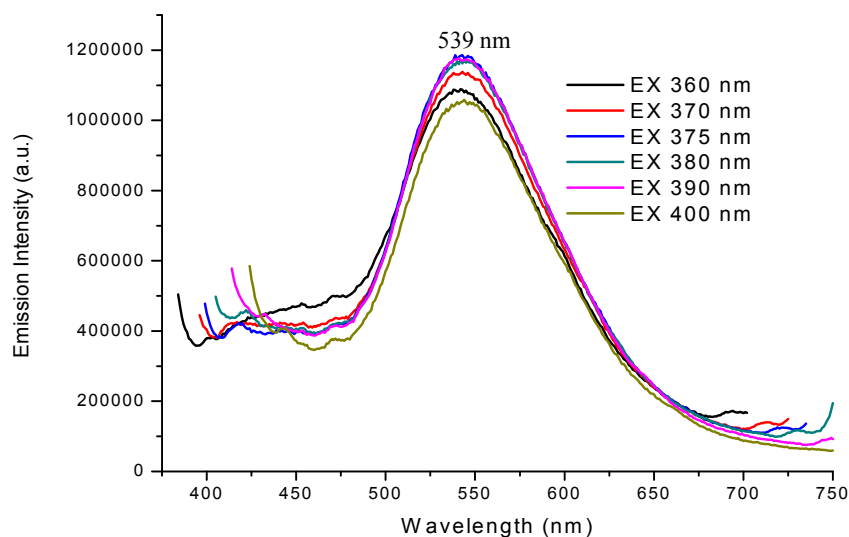
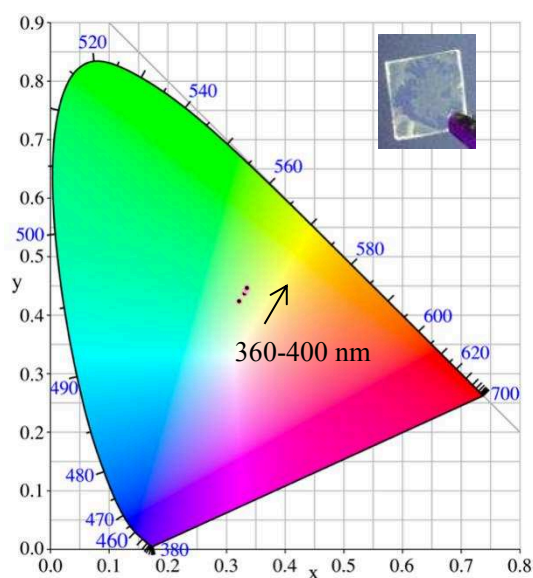


Figure 4-46 Emission (left) and Excitation (right) spectra of a film of **2.5% wt of P14 in C-Si matrix** (20 mg/mL, slits were 5,5 nm)

The emission spectrum reported on **Figure 4-46** shows a wide band ranging from 400 nm to 750 nm centered at 539 nm.



λ_{exc}	CIE x	CIE y	CCT(Kelvin)
360 nm	0.321	0.424	5830
370 nm	0.331	0.438	5558
375 nm	0.334	0.446	5465
380 nm	0.333	0.443	5485
390 nm	0.334	0.444	5472
400 nm	0.335	0.446	5444

Figure 4-47 CIE coordinates of a film comprising **2.5% wt of P14 in C-Si matrix** (20 mg/mL, λ_{exc} = 360-400 nm, slits were 5,5 nm) (The insert shows the emission of the film under a 365 nm UV lamp)

The **CIE coordinates and the CCT data** are representative of a **cool white light (5000-8300 K**

CCT) under excitation at 360-400 nm.

(5) Comparison of the emission of films of **P14** in different matrices

Figure 4-48 shows the emission spectra of different amounts of **P14** in different matrices. These data are summarized in **Table 4-5** and the corresponding CIE coordinates are shown on **Figure 4-49**.

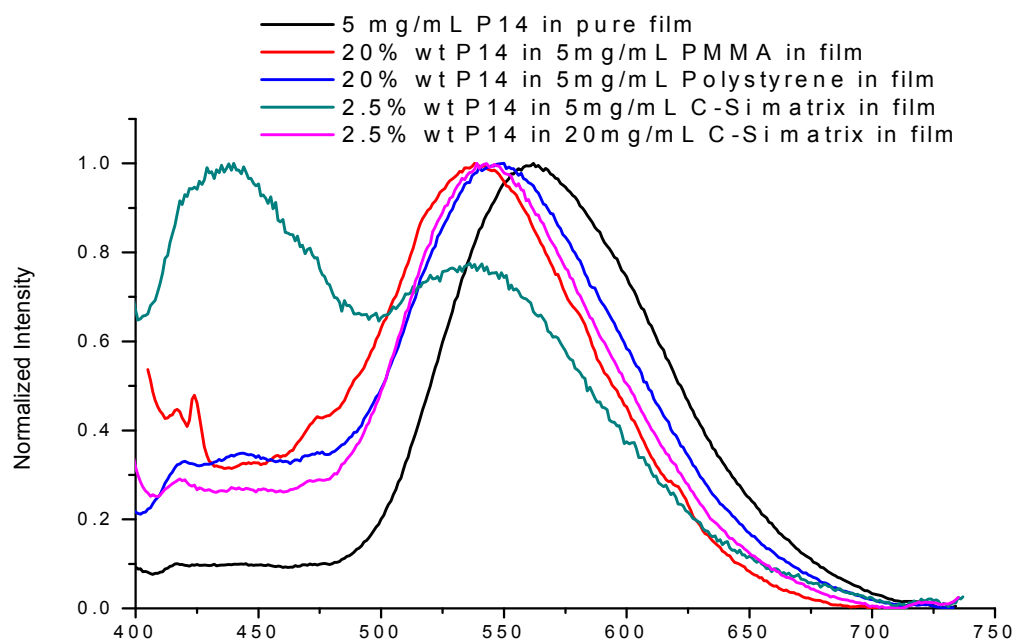
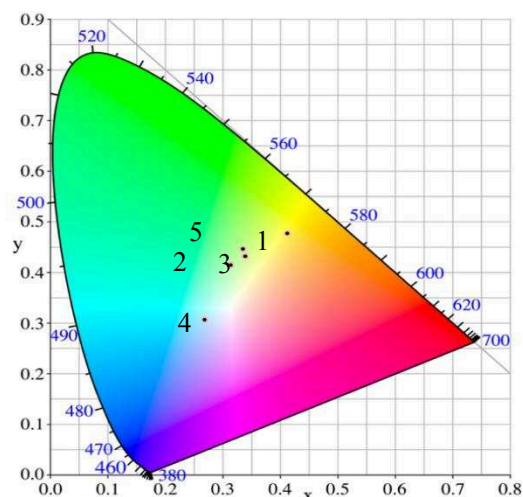


Figure 4-48 Emission spectra of films of **P14** in different conditions ($\lambda_{\text{exc}} = 375$ nm, slits were 5,5 nm)

Table 4-5 Summary of Absorption and PL data of **P14** in different conditions in film (slits were 5,5 nm)

No.	1	2	3	4	5
Sample	P14-5mg/ml- pure film- oven	20% wt P14- PMMA-5mg/ml- oven	20% wt P14- Polystyrene- 5mg/ml-oven	2.5% wt P14- C-Si-5mg/ml- oven	2.5% wt P14- C-Si-20mg/ml- oven
λ_{abs} (nm)	314, 372, 511	374, 529	308, 374, 514	375, 512	335, 523
λ_{em}^* (nm)	562	538	550	451, 542	539
FWHM	97	102	107	298	97

* For all emissions were set λ_{exc} at 375 nm except other mentions.



No.	CIE x	CIE y	CCT(Kelvin)
1	0.412	0.477	3902
2	0.314	0.414	6084
3	0.339	0.433	5320
4	0.269	0.307	10158
5	0.334	0.446	5465

Figure 4-49 CIE coordinates of films comprising **P14** in different conditions ($\lambda_{\text{exc}} = 375$ nm, slits were 5,5 nm)

Doping **P14** into different matrices afforded materials that emit **cool white light (5000-8300 K CCT)** when excited at 375 nm. However, when the matrix was the C-Si matrix and the **P14** loading was low, a greenish blue light was obtained, possibly due to the low content of the polymer in the film that could be highly influenced by the blue emission of the C-Si matrix and the glass substrate, along with an additional influence of the Rayleigh scattering. These results also show that the emission of films of **P14** dissolved in different matrices was blue-shifted with respect to a pure film which emits a neutral white light (3700-5000 K CCT). Further, they showed that the emission was red-shifted in polystyrene, as previously observed.

4.1.5 P15 in different matrices

4.1.5.1 Absorption result

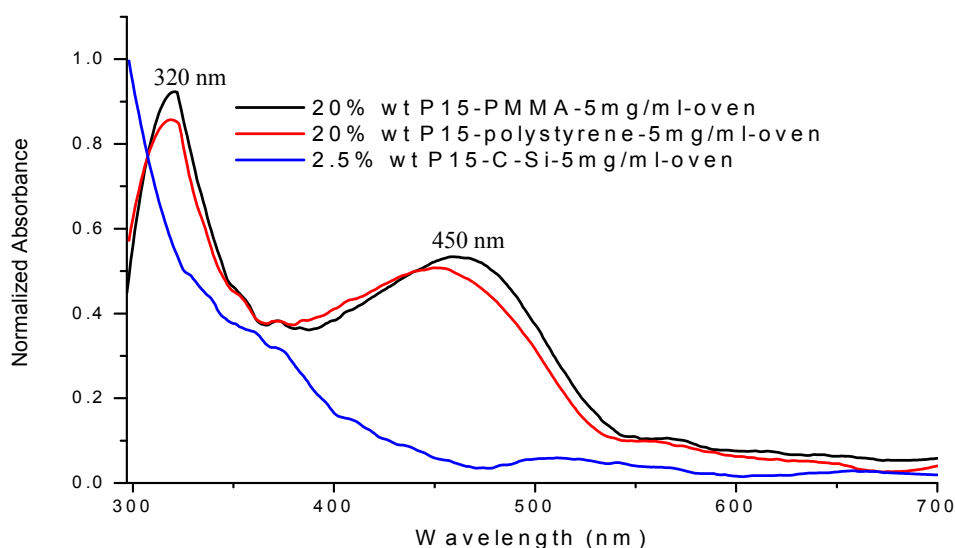


Figure 4-50 Absorption spectra of films of **P15** in different matrices (5 mg/mL, slits were 5,5 nm)

As shown in **Figure 4-50**, the absorption spectra of **P15** in PMMA and polystyrene (20% wt) show two main bands centered at around 320 nm and 450 nm respectively. The band at the lower wavelength may be caused by the glass substrate. While for 2.5% wt of **P15** in C-Si matrix, the absorption spectrum kept decreasing from 300 nm, which may be due to the low composition of the polymer in the precursor of the film and the influence of the blue emission of both the C-Si matrix and the glass substrate.

4.1.5.2 PL results

(1) Film comprising 20% wt of **P15** in PMMA (5 mg/mL)

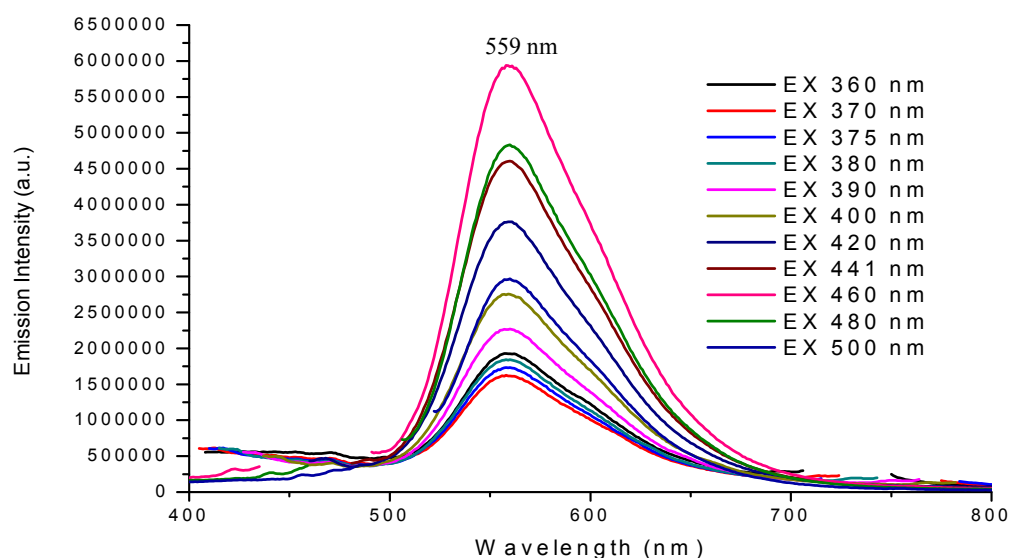
**Figure 4-51** Emission spectrum of a film containing **20% wt of P15 in PMMA** (5 mg/mL, slits were 5,5 nm)

Figure 4-51 shows the emission spectrum of a film comprising 20% wt of **P15** in PMMA recorded with different excitation wavelengths. It consists in a wide band ranging from 400 nm to 800 nm centered at around 559 nm.

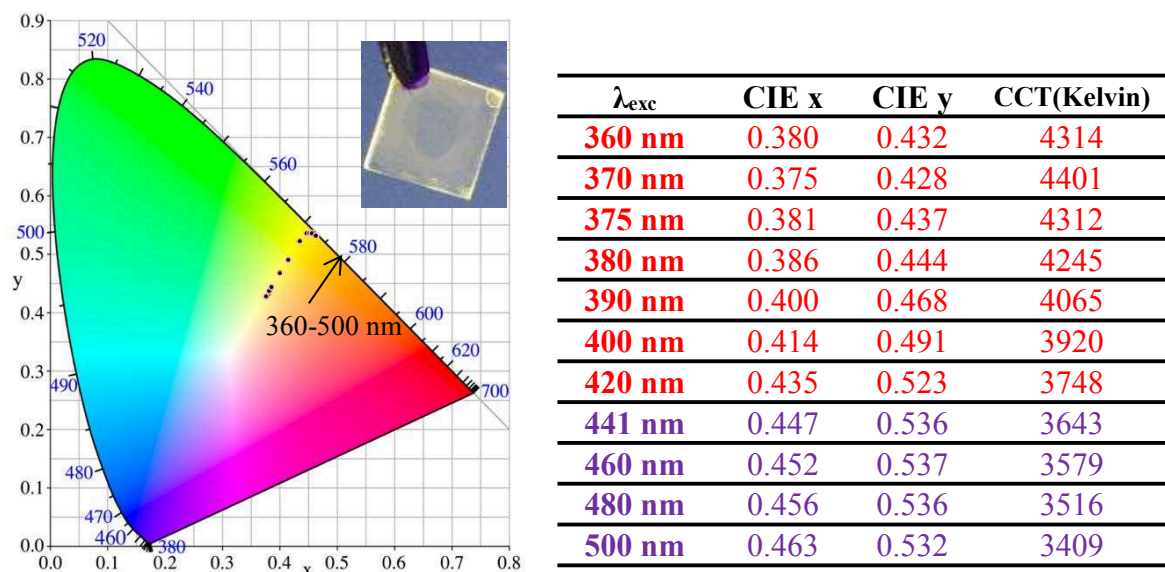


Figure 4-52 CIE coordinates of a film of **20% wt of P15 in PMMA** (λ_{exc} = 360-500 nm, slits were 5,5 nm)
(The insert shows the emission of the film under a 365 nm UV lamp)

The **CIE coordinates and the CCT data** show that the material emits a **neutral white light (3700-5000 K CCT)** when excited at 360-420 nm and a **warm white light (2600-3700 K CCT)** under excitation at 441-500 nm.

(2) Film comprising 20% wt of **P15 in polystyrene (5 mg/mL)**

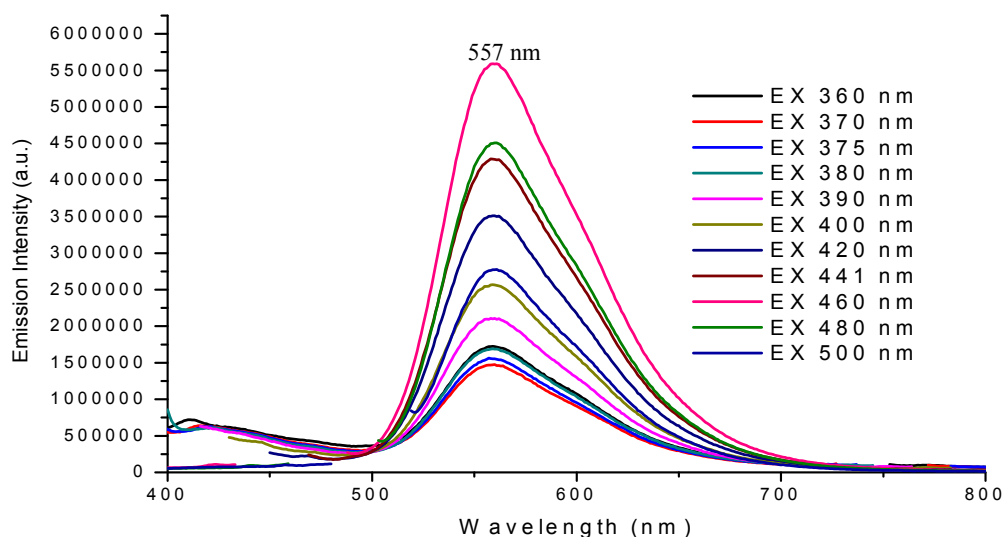


Figure 4-53 Emission spectrum of a film comprising **20% wt of P15 in polystyrene (5 mg/mL, slits were 5,5 nm)**

The emission spectrum of a film comprising 20% wt of **P15 in polystyrene (Figure 4-53)** shows a band centered at around 557 nm. The corresponding CIE coordinates are reported on **Figure 4-**

54. They show that the material emits a **neutral white light** (3700-5000 K CCT) under excitation at 360-400 nm and a **warm white light** (2600-3700 K CCT) when excited at 420-500 nm.

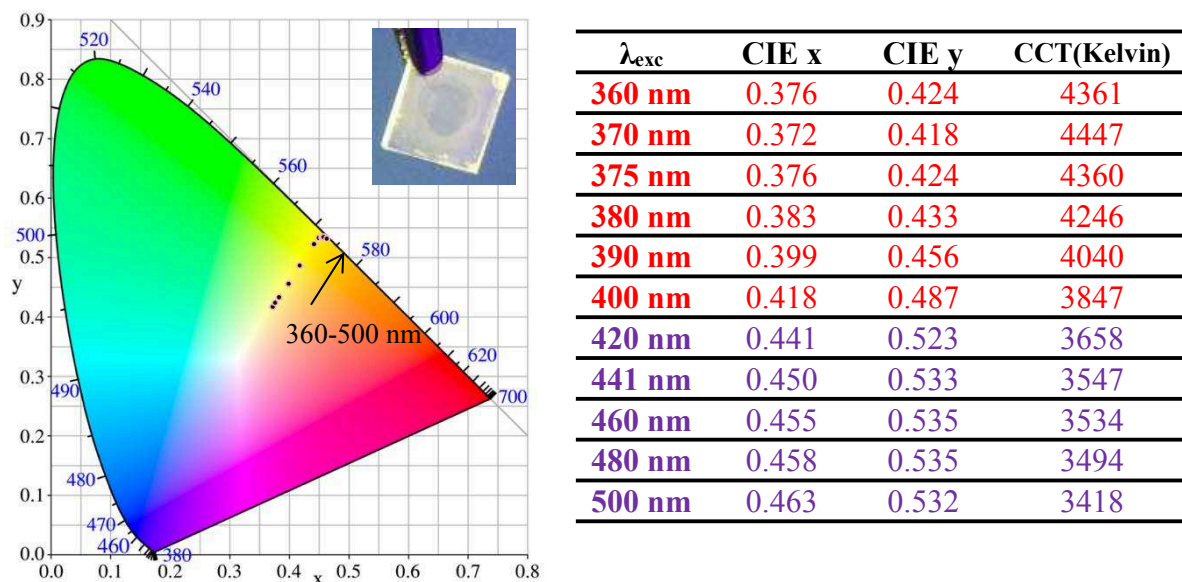


Figure 4-54 CIE coordinates of 20% wt of P15 in polystyrene in film (λ_{exc} = 360-500 nm, slits were 5,5 nm)
(The insert shows the emission of the film under a 365 nm UV lamp)

(3) Film comprising 2.5% wt of P15 in the C-Si matrix (5 mg/mL)

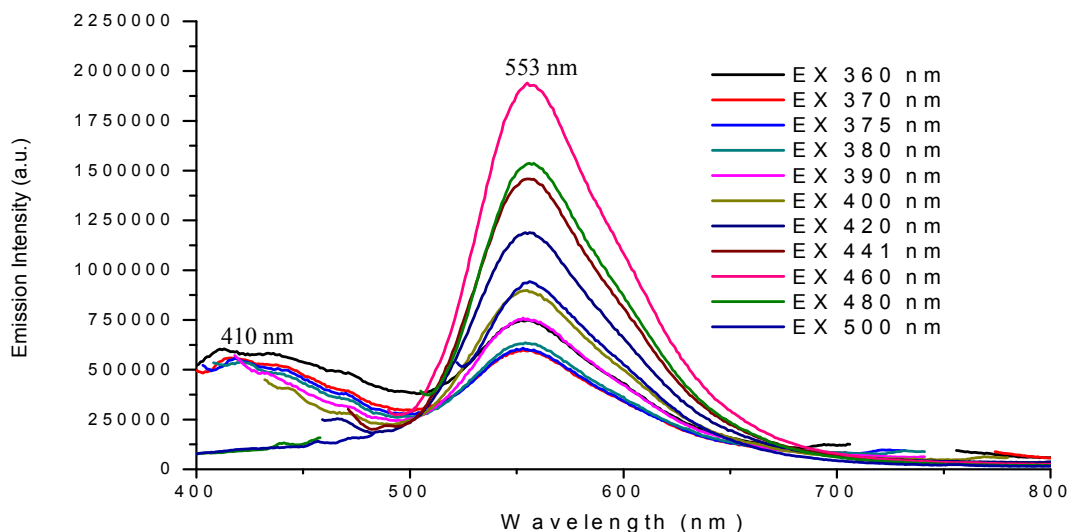


Figure 4-55 Emission spectrum of a film comprising 2.5% wt P15 in the C-Si matrix (5 mg/mL, slits were 5,5 nm)

The emission spectra of a film comprising 2.5% wt of P15 in the C-Si matrix under various excitations are reported on **Figure 4-55**. They all show a main band centered at around 553 nm.

Besides, a small band centered at 410 nm was seen which may be ascribed to the blue emission of the C-Si matrix and the glass substrate.

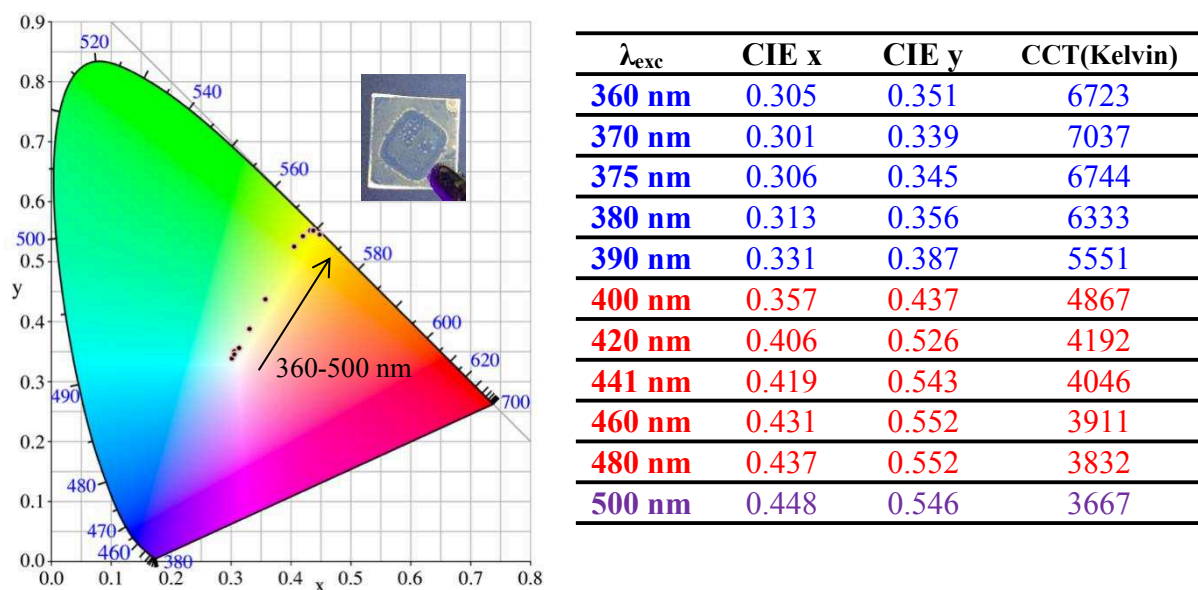


Figure 4-56 CIE coordinates of a film of **2.5% wt of P15** in 5 mg/mL C-Si matrix ($\lambda_{\text{exc}} = 360\text{-}500$ nm, slits were 5,5 nm) (The insert shows the emission of the film under a 365 nm UV lamp)

The **CIE coordinates and the CCT data** show that the film emits a **cool white light (5000-8300 K CCT)** under excitation at 360-390 nm, and a **neutral white light (3700-5000 K CCT)** under excitation at 400-480 nm and a **warm white light (2600-3700 K CCT)** under excitation at 500 nm.

(4) Film of 2.5% wt of P15 in C-Si matrix (20 mg/mL)

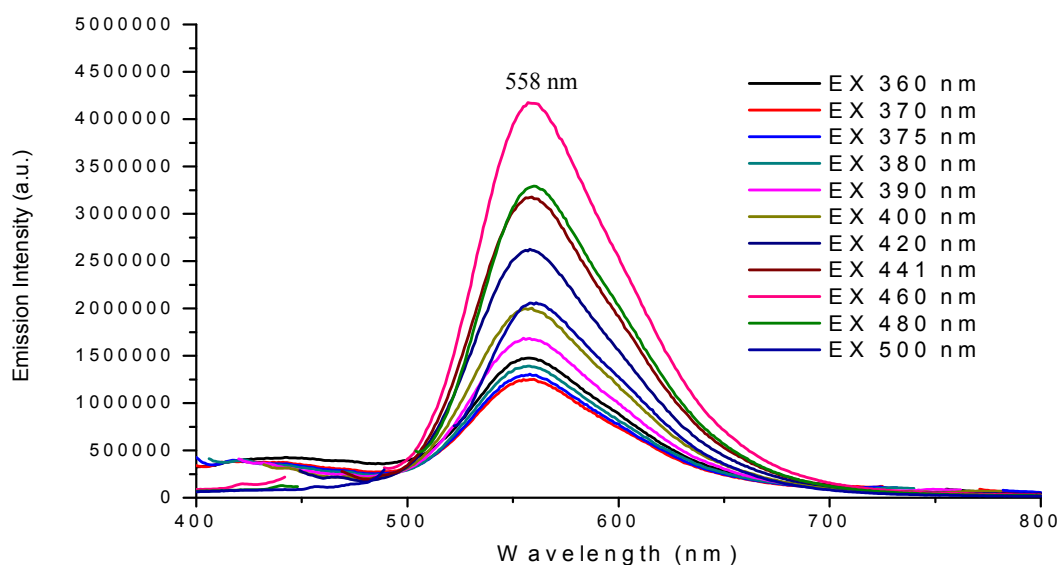
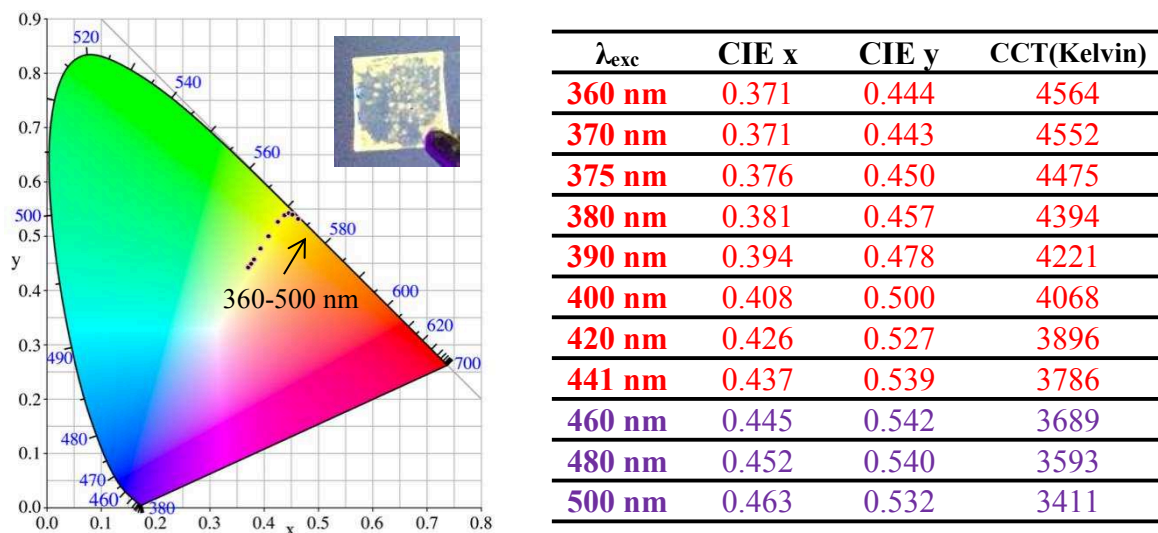


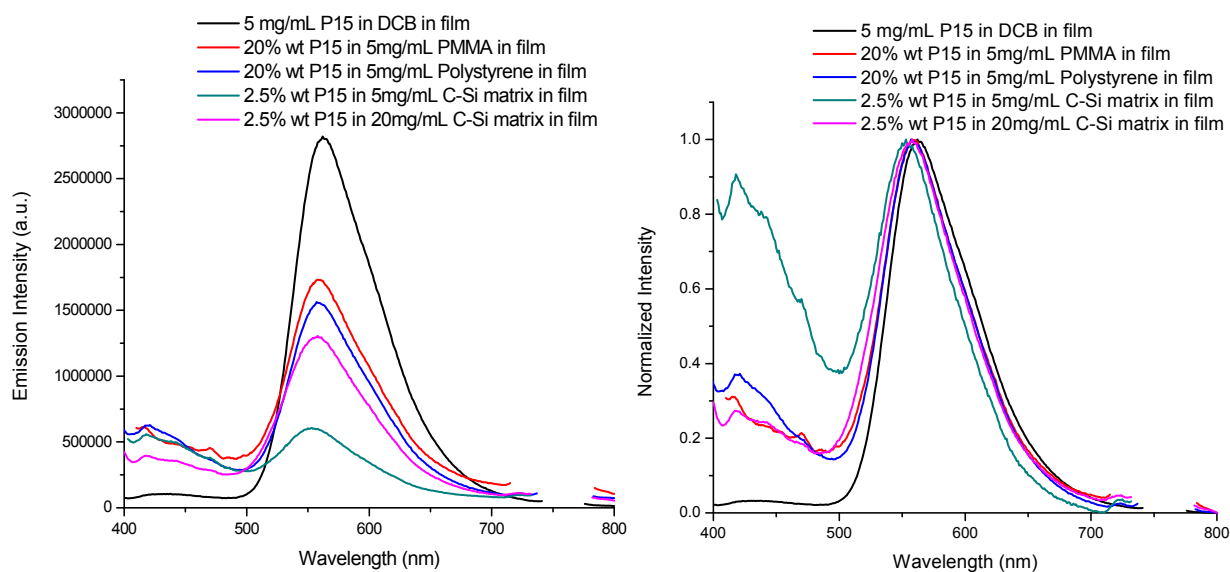
Figure 4-57 Emission spectrum of a film of **2.5% wt of P15 in the C-Si matrix** (20 mg/mL, slits were 5,5 nm)

The emission spectrum of a film of **2.5% wt of P15 in the C-Si matrix** is reported on **Figure 4-57**. An unsymmetrical band with a maximum at about 558 nm was observed.

**Figure 4-58** CIE coordinates of a film of **2.5% wt of P15 in the C-Si matrix** (20 mg/mL, λ_{exc} = 360-500 nm, slits were 5,5 nm) (The insert shows the emission of the film under a 365 nm UV lamp)

The **CIE coordinates and the CCT data** show that the material emits a **neutral white light** (3700-5000 K CCT) under excitation at 360-441 nm and a **warm white light** (2600-3700 K CCT) under excitation at 460-500 nm.

(5) Comparison of **P15** in different matrices

**Figure 4-59** Emission (left) and normalized emission (right) spectra of films of **P15 in different matrices**

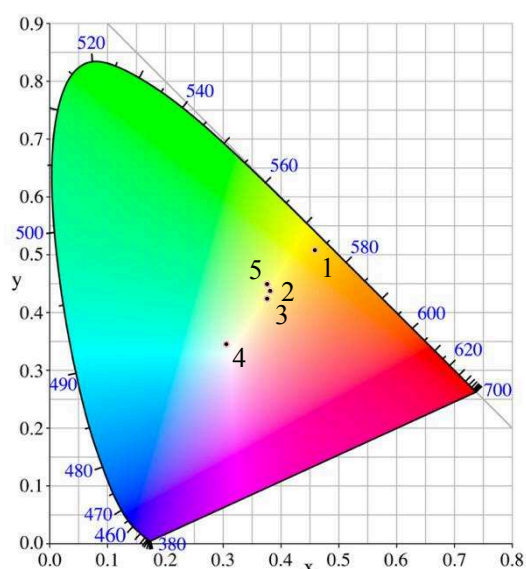
(slits were 5,5 nm)

The emission spectra of films of **P15** dissolved in different matrices are reported on **Figure 4-59**. These data are summarized in **Table 4-6** and **Figure 4-60**.

Table 4-6 Summary of PL data of **P15** in different conditions in films (slits were 5,5 nm)

No.	Conditions	FWHM (nm)	λ_{abs} (nm)	λ_{em} (nm)*
1	5 mg/mL P15 in DCB in film	79	454	562
2	20% wt P15 in 5 mg/mL PMMA in film	72	450	559
3	20% wt P15 in 5 mg/mL Polystyrene in film	69	450	557
4	2.5% wt of P15 in 5 mg/mL C-Si matrix in film	56	-	553
5	2.5% wt of P15 in 20 mg/mL C-Si matrix in film	76	-	558

* For all emissions were set λ_{exc} at 375 nm except other mentions.



No.	CIE x	CIE y	CCT(Kelvin)
1	0.459	0.508	3345
2	0.381	0.437	4312
3	0.376	0.424	4360
4	0.306	0.345	6744
5	0.376	0.450	4475

Figure 4-60 CIE coordinates of **P15** in different conditions in films (λ_{exc} = 375 nm, slits were 5,5 nm)

As shown, the emission spectra of films of **P15** in different conditions are similar and all emit white light. More specifically,

1) comparison of the emissions of **P15** dissolved in different matrices at the same concentration (5 mg/mL) shows that a blue shift is more pronounced in the C-Si matrix than in the other matrices. This may be due to an additional blue emission from the carbazole unit of the matrix, or because of the lower amount of polymer in the matrix.

2) comparison of the emissions of **P15** dissolved in different matrices at different concentrations

(case 4 with 5 mg/mL, case 5 with 20 mg/mL) shows a red shift with the lowest amount of polymer. This could be due to the relatively low influence of the glass substrate when higher concentrations of the matrix were introduced.

*3) the emission of **P15** is more red shifted in pure film.*

Besides, the FWHM data are among 56-80 nm as shown in **Table 4-6**.

4.1.6 Summary of the influence of the matrix on the photophysical properties

As a general feature, the emission of the polymers dissolved in matrices is more blue-shifted compared to that in pure films. This phenomenon is more pronounced in the C-Si matrix which contains an additional blue emission from the carbazole unit. This blue-shift can be reduced by increasing the amount of the polymer in the precursor, which results in a higher intensity of the emission from the polymer and, hence, covered the emission from the matrix. Besides, the blue emission of the glass substrate also affects the results when the polymer amount is too low. According to **Figure 4-20** and **4-21**, the amount of polymer should be no less than 10%, so that we can get a good spectrum. These parameters must be taken into consideration in material's design.

Following, two suggestions are proposed to avoid their impact. Firstly, one can use a higher amount of polymer in the precursor, so that the emission of the glass substrate and the matrix will be negligible. Secondly, using quartz substrates instead of glass substrates should avoid emission from the substrate.

4.2 Investigations on the possibility of Aggregation Induced Emission

4.2.1 Introduction

Most traditionally, organic luminogens are hydrophobic aromatic compounds and their fluorescence is weakened when aggregated because of the aggregation-caused quenching (ACQ) effect resulting from the strong π - π stacking interaction.⁵¹ This prevents their application in

concentrated or pure state or in aqueous media due to the aggregation.¹⁷⁵ In the contrary, some fluorogens show non- or very weak emission in molecularly dissolved state in good solvents, but turn into strong fluorescence when molecular aggregation occurs.¹⁷⁶ This is the aggregation-induced emission (AIE) effect. The restriction of intramolecular rotation (RIR) is the main reason.^{43,50}

In our case, as shown by the spectra reported on **Figure 4-61**, when high amounts of **P13** in polystyrene and PMMA are used, the emission intensity is increased, in accordance with AIE. To verify the AIE property of **P13**, a typical AIE behavior checking method was applied using THF and water as good solvent and poor solvent, respectively.^{174,177} The procedure of the sample preparation is shown on §4.2.2 and the results are shown on §4.2.3.

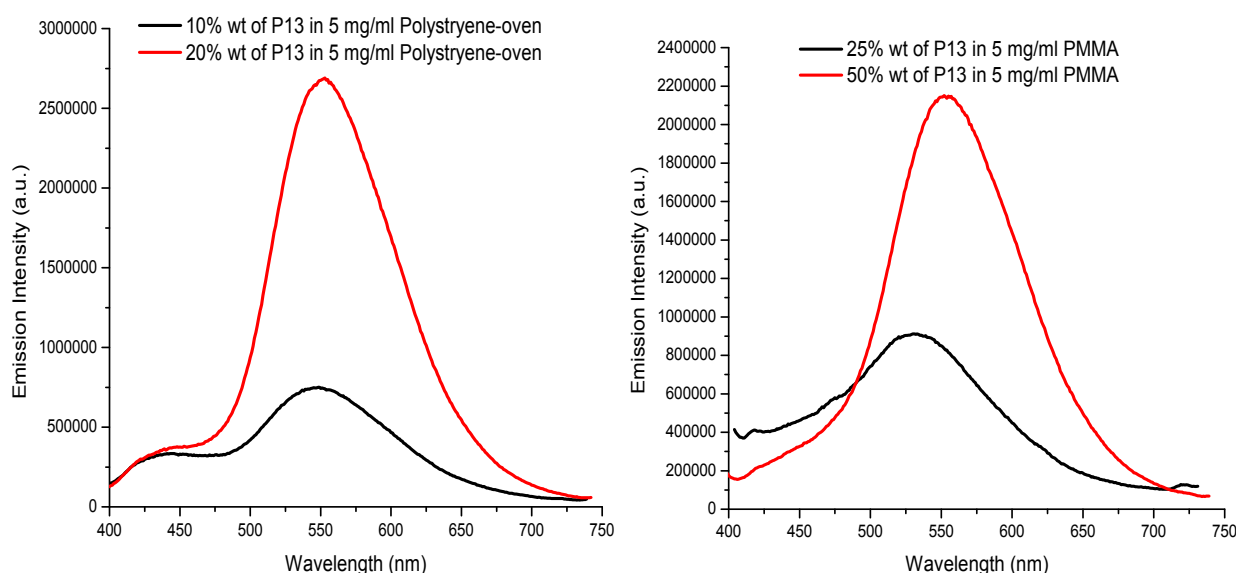


Figure 4-61 Emission spectra of different concentration of **P13** in a) Polystyrene and b) PMMA

4.2.2 Preparation of the samples

- 1) A 0.1 mg/mL THF solution of **P13** was prepared.
- 2) Samples with different fractions of water were added to the above solution, THF and water in the ratio as given in **Table 4-7**. The mixture was shaken for 1-2 mins before UV-vis and PL

¹⁷⁵ G. Huang, Y. Jiang, S. Yang, B. S. Li, and B. Z. Tang. *Adv. Funct. Mater.*, **2019**, 1900516.

¹⁷⁶ N. Li, H. Feng, Q. Gong, C. Wu, H. Zhou, Z. Huang, J. Yang, X. Chen, and N. Zhao. *J. Mater. Chem. C*, **2015**, 3, 11458-11463.

¹⁷⁷ S. Zhou, H. Wan, F. Zhou, P. Gu, Q. Xu, and J. Lu. *Chinese J. Polym. Sci.*, **2019**, 37 (4), 302-326.

measurements.

Table 4-7 Solutions prepared for evaluating the AIE effect with **P13**.

Sample with Water fraction (vol%)	0	10	20	30	40	50	60	70	80	90
0.1 mg/mL of P13 in THF (ml)	0.2	0.2	0.2	0.2	0.2	0.2	0.2	0.2	0.2	0.2
Water (ml)	0	0.2	0.4	0.6	0.8	1.0	1.2	1.4	1.6	1.8
THF (ml)	1.8	1.6	1.4	1.2	1.0	0.8	0.6	0.4	0.2	0

4.2.3 Absorption and PL results

1) Absorption spectra of P13 in THF-water mixtures

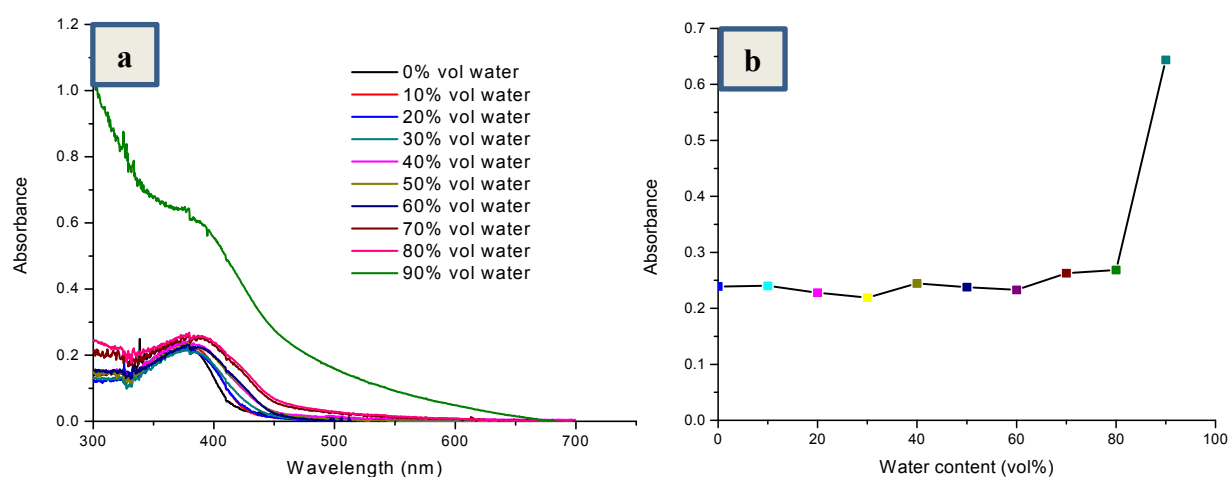


Figure 4-62 a) Absorption spectra of **P13** in **THF-water mixtures** with different water contents b) The maximum of the absorption spectra of **P13** in **THF-water mixtures** versus water contents (0.01 mg/mL)

As shown in **Figure 4-62**, when the water fraction is lower than 80% vol, the addition of water has a little influence on the absorption of each sample. When 90% vol of water was contained, the intensity of the absorption was sharply increased, possibly due to the formation of excimers.

2) Emission spectra of P13 in THF-water mixtures

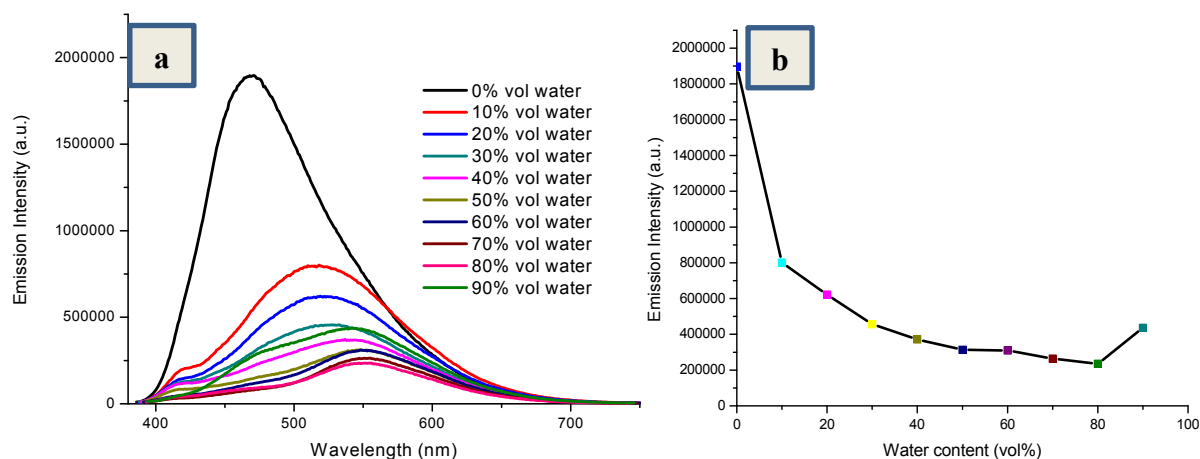


Figure 4-63 a) Emission spectra of **P13** in **THF-water mixtures** with different water fractions b) The maximum of the emission intensity of **P13** in **THF-water mixtures** versus water contents (0.01 mg/mL, slits were 2,2 nm, set $\lambda_{\text{exc}} = 375$ nm)

As **Figure 4-63** shows, the emission intensity was decreased with the increase of the water amount in the mixture. Especially, when the water content was only 10%, the intensity was dramatically decreased. But when the water fraction was increased to 90%, the intensity of the emission was little increased.

Increasing amounts of water up to 90% lead to a red-shift of the emission band, and when the water fraction was more than 90%, the band seemed to be slightly blue-shifted. These results show that water could red-shift the emission of the sample with a decrease in intensity with respect to a pure THF solution.

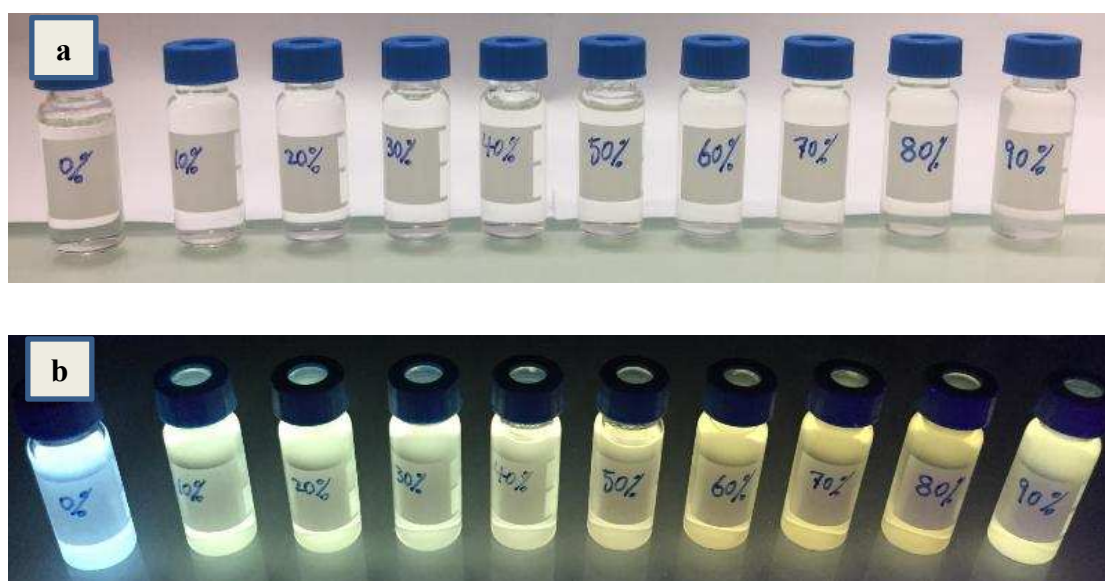


Figure 4-64 Photographs of **P13** in **THF-water mixtures** with different water fractions under a) day light; b)

365 nm UV irradiation.

Figure 4-64 visually shows the bathochromic-shift of the emission with the addition of water in a THF solution of **P13**.

4.2.4 Conclusions

Table 4-8 Absorption and PL results of **P13** in THF-water mixtures with different water fractions

Water fraction (vol%)	0	10	20	30	40	50	60	70	80	90
λ_{abs} (nm)	373.5	373.5	376.5	378	379.5	379.5	377.5	379	379.5	379
I_{abs} (max)	0.2389	0.2401	0.2281	0.219	0.2446	0.2379	0.2329	0.2628	0.2684	0.6439
λ_{em} (nm)	471	518	519	527	537	548	548	555	556	542
I_{em} (max)	1897070	801557	621940	456323	372258	313023	309676	264472	235739	436599
λ_{exc} (nm)	366	367	365	368	368	366	365	367	366	367
I_{exc} (max)	1935900	837460	652826	484938	375396	320040	337720	286933	249378	369114

In summary, polymer **P13** shows ACQ effect instead of AIE effect. But when the water fraction was increased to more than 90%, both the UV-vis and PL intensities are unexpectedly increased which may due to the formation of excimers.

At the same time, the emission band also shows the red-shift effect when water was added, which may be caused by the increase of the polarity of the solvent. The bathochromic shift of these polymer solutions is attributed to the interaction of polymer with the surrounding solvent environment. The better stabilization of the excited state relative to the ground state with increasing solvent polarity results in the bathochromic shift (positive solvatochromism).¹⁷⁸ However, the absorption and the excitation bands were almost no shifted.

4.3 Blends with different emitters for white light emission

As the final goal of this project was to obtain new white emitting materials, in addition to the single white emitting materials, we further investigated blends of different emitters. It has been widely reported that proper blends of materials with three primary colors will lead to white light. Blending different luminescent materials is an attractive approach to finely tune the emission color of a material.

Hereafter are presented the results obtained on blends of polymers and a europium complex

¹⁷⁸ M. N. Kumbar, M. S. Sannaikar, S. K. J. Shaikh, A. A. Kamble, M. N. Wari, S. R. Inamdar, Q. Qiao, Bhavya N. R. Mahendra M., Jagadeesh Prasad D. and Ravindra R. Kamble. *PHOTOCHEM PHOTOBIOLOG*, **2018**, 94 (2), 261-276.

investigated in view of designing white-emitting materials.

4.3.1 Blends for white light in solution

4.3.1.1 Blend of PF, P1 and $\text{Eu}(\text{tta})_3(\text{L})$ in DCM

PF, **P1** and **$\text{Eu}(\text{tta})_3(\text{L})$** were firstly selected as blue, green and red emitters, respectively, and DCM was used as solvent as it can dissolve the three components.

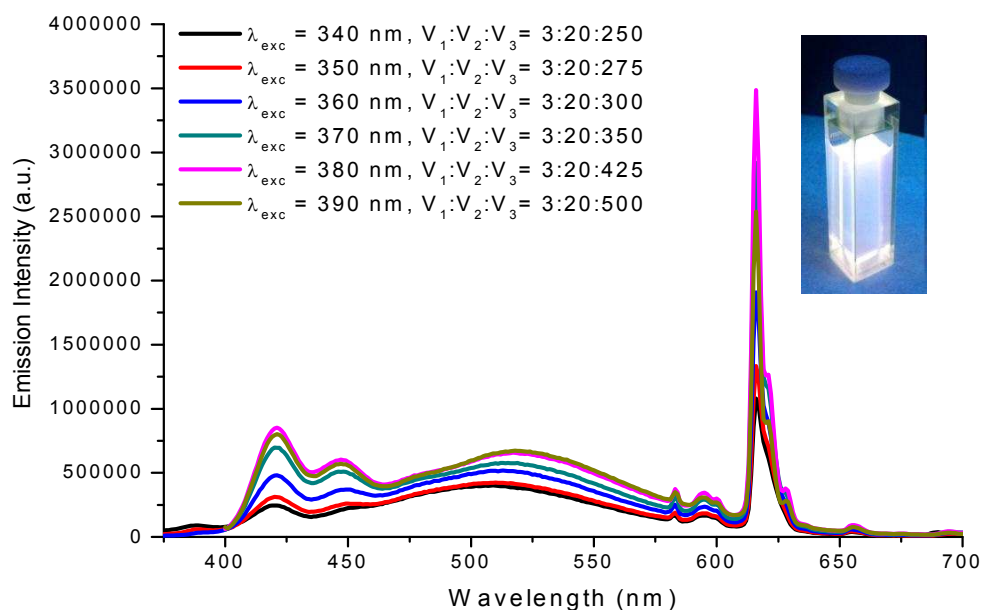
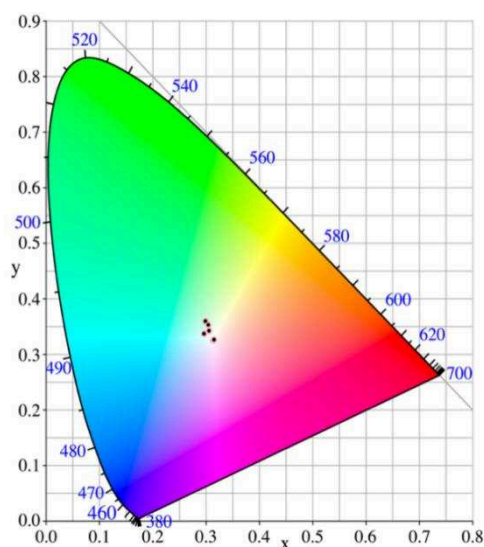


Figure 4-65 Emission spectra of blend of **PF**, **P1** and **$\text{Eu}(\text{tta})_3(\text{L})$** in DCM under corresponding excitation and composition for white light emission (0.01 mg/mL, slits were 2,2 nm, V1: volume of **PF**, V2: volume of **P1**, V3: volume of **$\text{Eu}(\text{tta})_3(\text{L})$**) (The inserted photo shows the emission of the mixture (V1:V2:V3 = 3:20:350) in DCM under a 365 nm UV lamp)



No.	Composition (V1:V2:V3)	λ_{exc} (nm)	CIE x	CIE y	CCT (Kelvin)
1	3:20:250	340	0.30	0.36	6965
2	3:20:275	350	0.30	0.35	6783
3	3:20:300	360	0.31	0.34	6805
4	3:20:350	370	0.31	0.33	6511
5	3:20:425	380	0.31	0.33	6438
6	3:20:500	390	0.30	0.34	7324

Figure 4-66 CIE coordinates of different blends of **PF**, **P1** and **Eu(tta)₃(L)** in DCM for white light emission (0.01 mg/mL, slits were 2,2 nm, V1: volume of **PF**, V2: volume of **P1**, V3: volume of **Eu(tta)₃(L)**)

Figure 4-65 shows the emission spectra of DCM solutions comprising the three emitters in various ratio and recorded with different excitation wavelengths. They all show emission of the three emitters. This is an interesting point as the blue emission can sometime be partially or fully absorbed by the red emitter, leading to a light that misses a blue component, thus making impossible to obtain white light. The picture of the cuvette containing one of these solutions clearly shows that white light was obtained. This is confirmed by the CIE coordinates reported on **Figure 4-66** and the corresponding color temperatures which are in the range of 5000-8300 K CCT.⁶⁵

4.3.1.2 Blend of P10 and P15 in DCM

As shown previously, **P10** and **P15** dissolved in DCM emit bluish green and yellow light, respectively. It looks thus possible to get white light by mixing them in a proper ratio.

(1) $V(\text{P10})/V(\text{P15}) = 1/2$

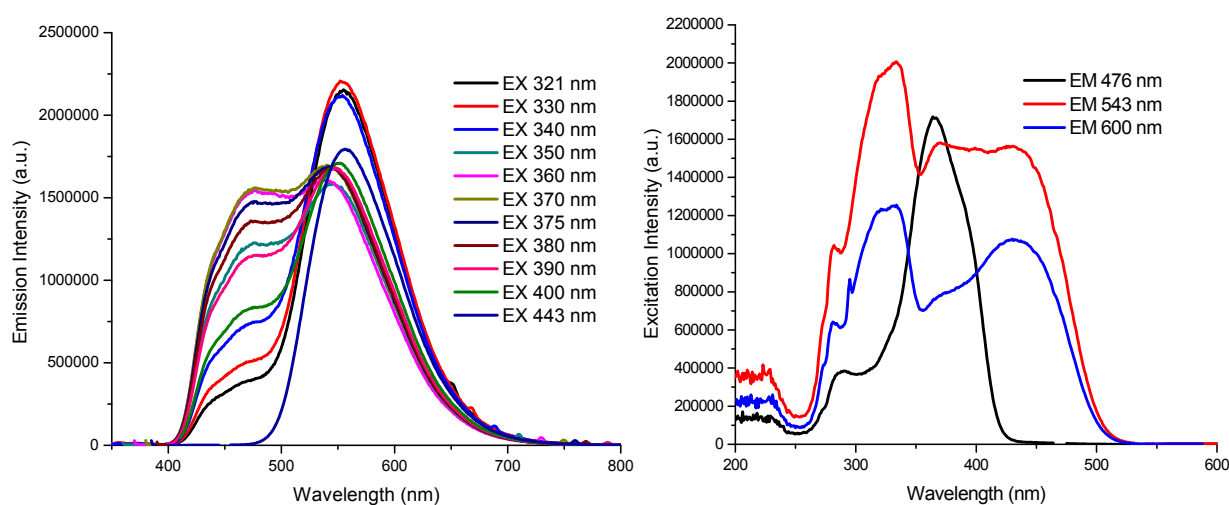
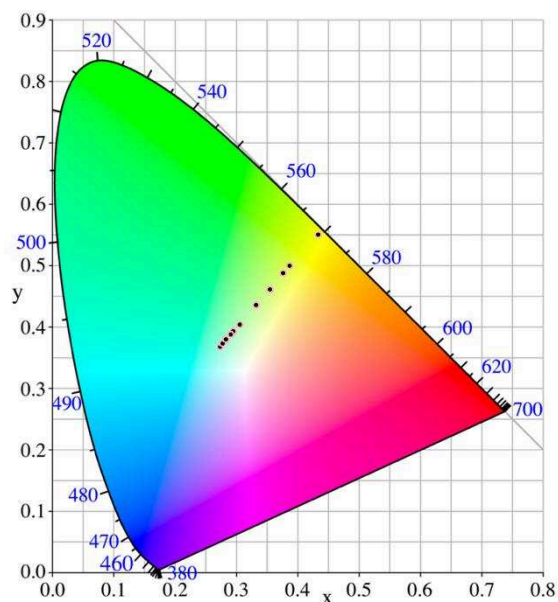


Figure 4-67 Emission (left) and Excitation (right) spectra of blend of $V(\text{P10})/V(\text{P15}) = 1/2$ in DCM (0.01 mg/mL, slits were 2,2 nm)

Figure 4-67 shows the emission (left) and excitation (right) spectra of DCM solutions of **P10** and **P15**. The emission spectra mainly show a broad band (400-750 nm) under excitation at 321-400 nm which is a combination of the emission spectrum of each polymer. When the excitation wavelength increased from 321 nm to 400 nm, the emission band at 400-500 nm was firstly increased and then declined, reaching a maximum in intensity when excited at 370 nm. This

result is consistent with **P10** which absorbs at 377 nm and emits at 461 nm. The excitation spectrum shows three maxima, at 334 nm, 370 nm and 430 nm respectively, with a shoulder peak at 278 nm when the emission analysis is set at 543 nm.



λ_{exc}	CIE x	CIE y	CCT (K)
321 nm	0.387	0.500	4427
330 nm	0.376	0.488	4586
340 nm	0.354	0.462	4986
350 nm	0.295	0.393	6869
360 nm	0.273	0.368	8121
370 nm	0.278	0.373	7823
375 nm	0.283	0.380	7490
380 nm	0.290	0.388	7097
390 nm	0.305	0.405	6409
400 nm	0.332	0.436	5509
443 nm	0.433	0.551	3884

Figure 4-68 CIE coordinates of a solution containing $V(\text{P10})/V(\text{P15}) = 1/2$ in DCM (0.01 mg/mL, slits were 2,2 nm)

The **CIE coordinates** are representative of a **neutral white light (3700-5000 K CCT)** under excitation at 321-340 nm and 443 nm, and a **cool white light (5000-8300 K CCT)** under excitation at 360-390 nm.

(2) $V(\text{P10})/V(\text{P15}) = 3/4$

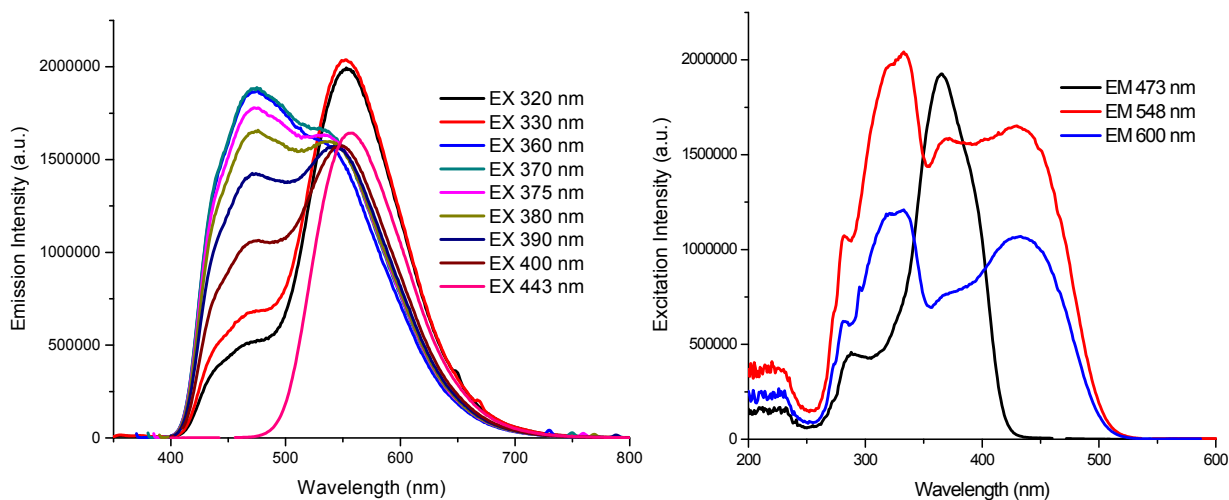


Figure 4-69 Emission (left) and Excitation (right) spectra of a DCM solution containing $V(\text{P10})/V(\text{P15}) = 3/4$

(0.01 mg/mL, slits were 2,2 nm)

The emission and excitation spectra of a DCM solution containing $V(\text{P10})/V(\text{P15}) = 3/4$ are reported on **Figure 4-69**. They show similar results as those obtained with the $V(\text{P10})/V(\text{P15}) = 1/2$ solution.

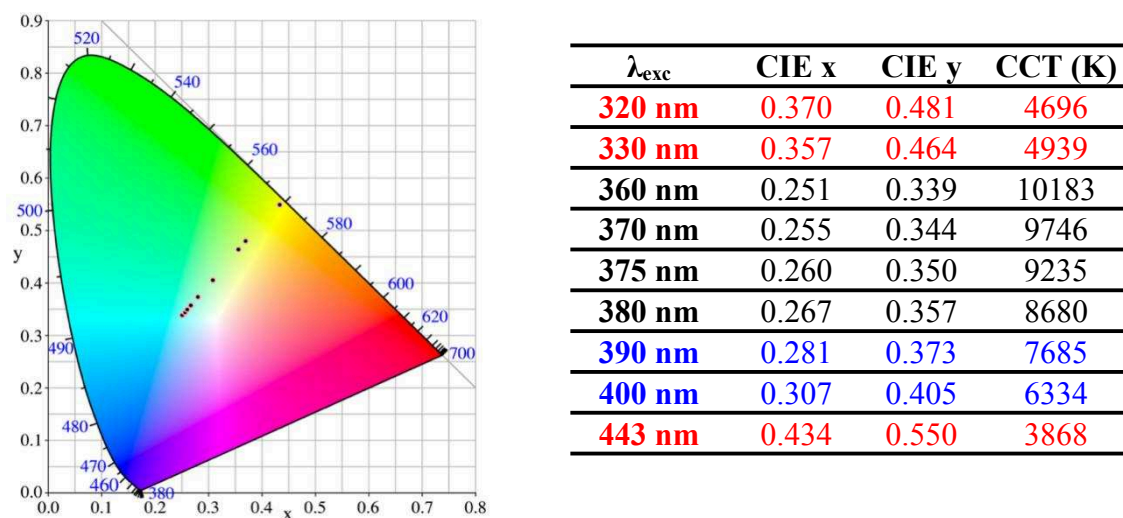


Figure 4-70 CIE coordinates of a DCM solution of $V(\text{P10})/V(\text{P15}) = 3/4$ (0.01 mg/mL, slits were 2,2 nm)

The CIE coordinates show that the material emits a **neutral white light** (3700-5000 K CCT) under excitation at 320-330 nm and 443 nm, and a **cool white light** (5000-8300 K CCT) under excitation at 390-400 nm.

(3) $V(\text{P10})/V(\text{P15}) = 1/1$

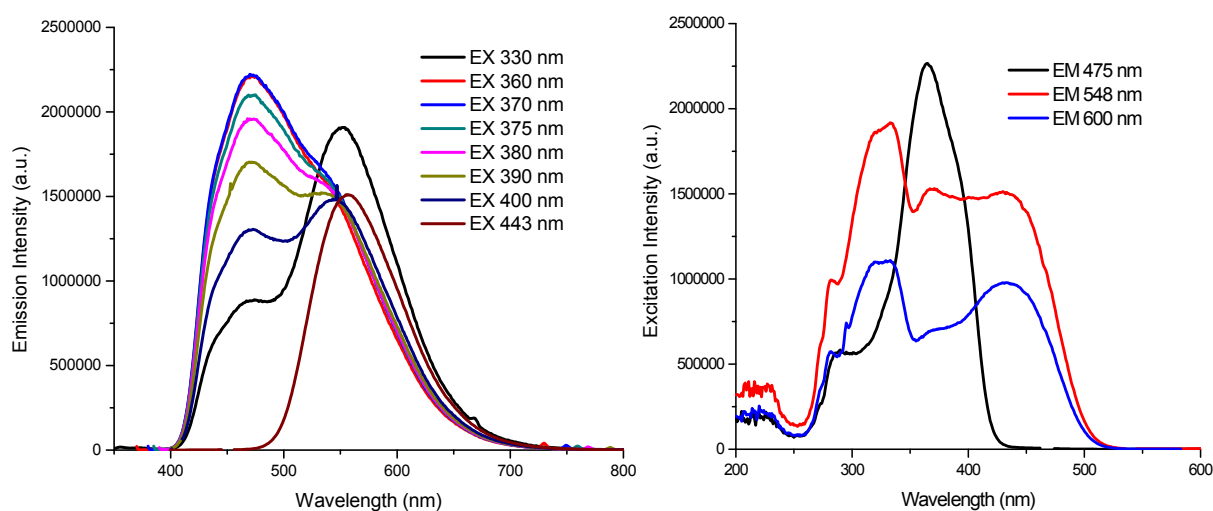


Figure 4-71 Emission (left) and Excitation (right) spectra of a DCM solution comprising $V(\text{P10})/V(\text{P15}) = 1/1$ (0.01 mg/mL, slits were 2,2 nm)

The emission and excitation spectra reported on **Figure 4-71** have been obtained for a DCM solution comprising a V(P10)/V(P15) ratio of 1/1. Results are similar to the V(P10)/V(P15) = 3/4 solution described above.

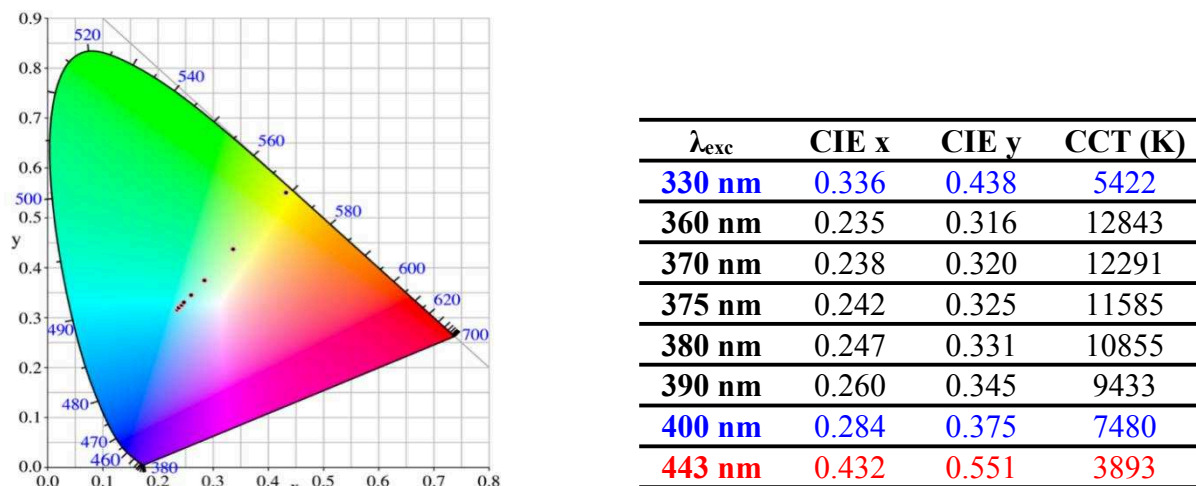


Figure 4-72 CIE coordinates of blend of V(P10)/V(P15) = 1/1 in DCM (0.01 mg/mL, slits were 2,2 nm)

The **CIE coordinates** of this solution are depicted on **Figure 4-72**. They show that the material emits a **neutral white light** (3700-5000 K CCT) under excitation at 443 nm, and a **cool white light** (5000-8300 K CCT) under excitation at 330 and 400 nm.

Above all, by comparison, it shows that the solution with the V(P10)/V(P15) = 1/2 ratio gave the white emission having the best quality. The corresponding CIE coordinates are between (0.27,0.37) and (0.33, 0.43).

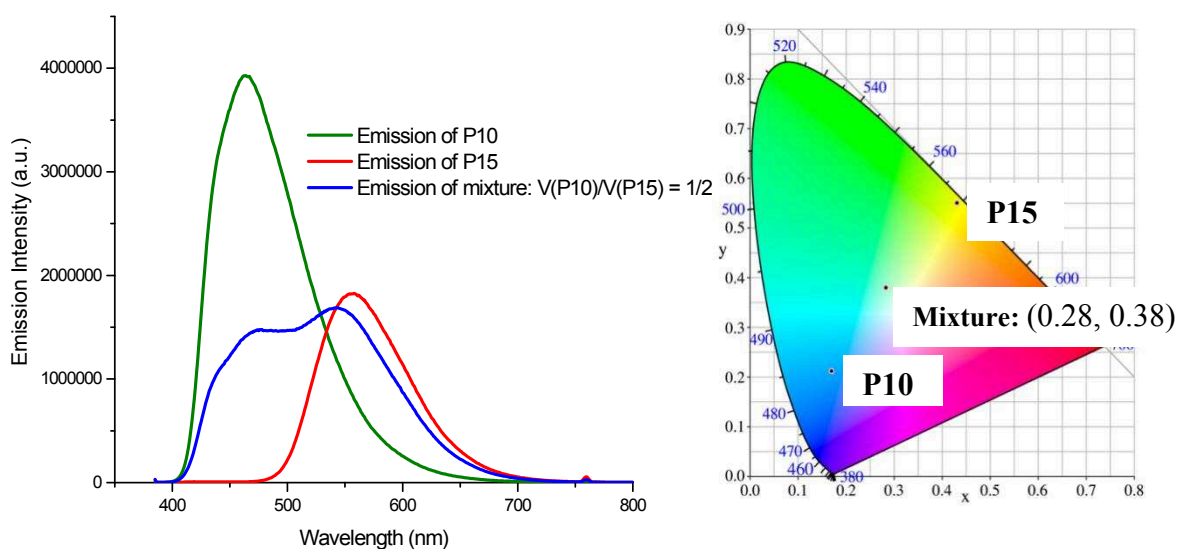


Figure 4-73 Emission spectra and CIE coordinates of P10, P15, and the blend of P10 and P15 in DCM

$$(V(\mathbf{P10})/V(\mathbf{P15}) = 1/2, 0.01 \text{ mg/mL, slits were } 2,2 \text{ nm, } \lambda_{\text{exc}} = 375 \text{ nm})$$

The emission spectra (excitation at 375 nm) and CIE coordinates of **P10**, **P15**, and their **DCM** mixture in a $V(\mathbf{P10})/V(\mathbf{P15}) = 1/2$ ratio are shown on **Figure 4-73**. The CIE coordinates of this blend were found to be (0.28, 0.38), known as **cool white light**.

4.3.2 Blending the emitters in thin films

A blend of 13 mg of **P1** with 27 mg of $[\mathbf{Eu(tta)_3(L)}]$ in the liquid silica matrix (500 mg of the liquid precursor), as shown on **Figure 4-74**, was made by painting on glass substrates. It showed white emission. The excitation and emission spectra are reported on **Figure 4-75**.

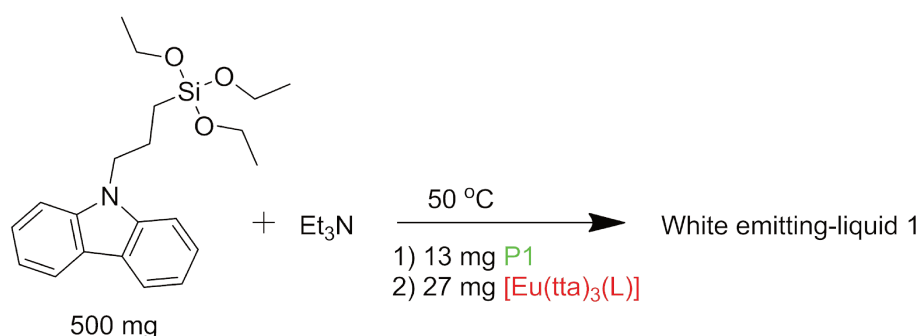


Figure 4-74 Formula shows the mixture of 13 mg **P1** and 27 mg $[\mathbf{Eu(tta)_3(L)}]$ in C-Si matrix leading to a white emitting liquid

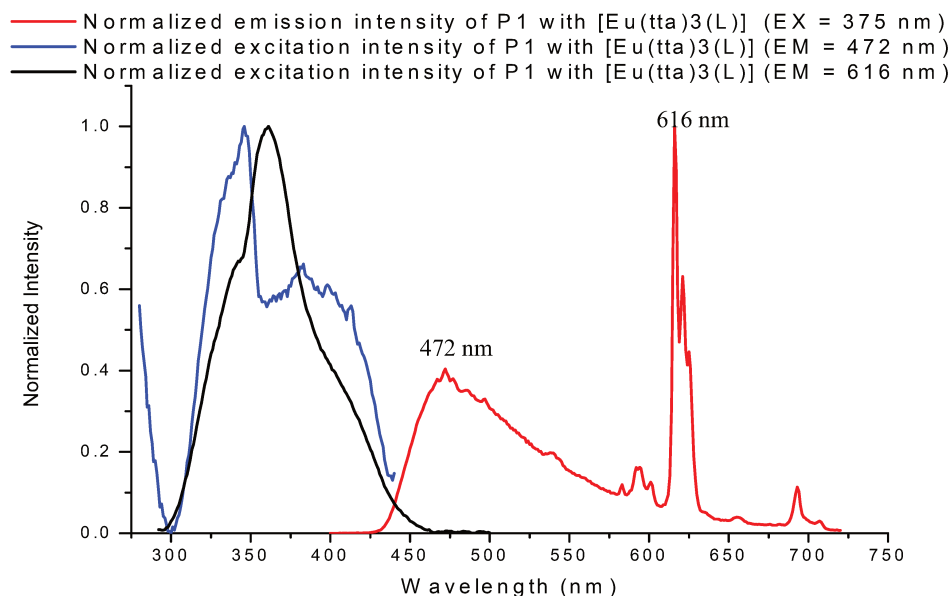
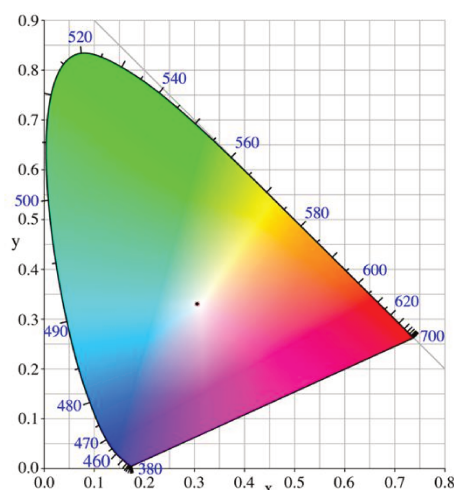


Figure 4-75 Normalized excitation and emission spectra of the blend with 13 mg **P1** and 27 mg $[\mathbf{Eu(tta)_3(L)}]$ in C-Si matrix in film (Setting: excitation ($\lambda_{\text{an}} = 472 \text{ nm}$ and 616 nm) and emission ($\lambda_{\text{exc}} = 375 \text{ nm}$), slits were 2,2 nm)

The excitation spectra ($\lambda_{\text{an}} = 472$ nm for the blue trace and $\lambda_{\text{an}} = 616$ nm for the black trace) of this material show a broad band from 300 nm to 475 nm. When $\lambda_{\text{an}} = 472$ nm, two maxima at 346 nm and 380 nm were seen. When $\lambda_{\text{an}} = 616$ nm, only a maximum at around 365 nm was shown. These bands are similar to the excitation bands of **P1** and **[Eu(tta)₃(L)]**. The emission spectrum shows two maxima at 472 nm and 616 nm, respectively, corresponding to the emission band of **P1** and **[Eu(tta)₃(L)]**, respectively.



CIE x	CIE y	CCT (Kelvin)
0.305	0.331	6914

Figure 4-76 CIE coordinates (0.31, 0.33) of the blend with 13 mg **P1** and 27 mg **[Eu(tta)₃(L)]** in C-Si matrix as thin film ($\lambda_{\text{exc}} = 375$ nm, slits 2,2 nm)

The CIE coordinates shown on **Figure 4-76** are representative of a **cool white light** (5000-8300 K CCT).⁶⁵

4.4 Quantum yields determination

The efficiency of a phosphor is expressed by its quantum yield, which is intrinsic to the materials and corresponds to the ratio of the number of photons emitted to the number of photons absorbed per unit of time by a sample (as formula **4-1**)¹⁷⁹.

$$\text{QY} = \frac{\text{Number of photons emitted per unit of time}}{\text{Number of photons absorbed per unit of time}} \quad (4-1)$$

For any photoluminescent materials, the luminescence QY is a basic property. There are two common methods for measuring it, the absolute method and the relative method. The absolute method directly acquires the QY by detecting all sample fluorescence by using an integrating

¹⁷⁹ Albert M. B., *Pure Appl. Chem.*, **2011**, 83(12), 2213–2228.

sphere. The relative method compares the fluorescence intensity of a standard sample with the fluorescence intensity of the unknown sample to calculate the QY of the unknown sample.¹⁸⁰

In this work, the photoluminescence absolute quantum yield (QY_{abs}) of the luminophores (polymers or Eu-complex in C-Si based matrix prepared as previously described in **Chapter II**), which is the direct measure for the efficiency of the conversion of absorbed light into emitted light, were measured in DCM and PMMA respectively, as it is one of the key parameters for a fluorophore¹⁸¹. This was performed at the University of Clermont-Ferrand.¹⁸² The results are summarized as follows.

4.4.1 Quantum yields measured in DCM

It was determined in **Chapter III** (§3.1.1) that measurements in solution on **PF** should be performed at concentrations lower than 0,01 mg/mL to avoid any interaction between the polymer molecules. This was confirmed by measurements of the absolute quantum yield of **PF** at 1 mg/mL and 0.01 mg/mL. Values of 45.4% and 80.8% were obtained, respectively after excitation at 340 nm. The 0.01 mg/mL solution even showed an absolute quantum yield of 89.7% after excitation at 365 nm.

As will be reported later in this chapter, the bis-alkyl-fluorene groups do not show a satisfying photostability. This means that it is not possible to consider materials with these groups in the design of phosphor for lighting. We thus synthesized the polycarbazoles **P11** and **P12** with the aim of finding blue-emitting polymers that would be more photostable. Measurements of the quantum yields of these two polymers gave values of 55.1% ($\lambda_{exc} = 340$ nm), and 73.9% ($\lambda_{exc} = 370$ nm) for **P11** and **P12**, respectively. These values show that these polymers, and especially **P12**, are very interesting as potential blue emitters. They could be considered to replace **PF**. These values are summarized in **Table 4-9**.

Table 4-9 Absolute QY of polymers in DCM (T = 300 K)

¹⁸⁰ Jan V., *Nanoscience Methods*, **2014**, 3(1), 11-27.

¹⁸¹ F. H. L. Koppensl, T. Mueller, Ph. Avouris, A. C. Ferrari, M. S. Vitiello and M. Polini. *Nature Nanotechnology*, **2014**, 9, 780-793.

¹⁸² a. Rachod B., Résultats des expérimentations faites sur les luminophores. *Rapport de stage Chimie*, institut de chimie de clermont-ferrand, **2017**.

b. K. Yasmine, Etudes des performances optiques de luminophores organiques et/ou hybrides pour une application dans des dispositifs de visualisation ou d'affichage à base de diodes électroluminescentes bleues et/ou UV. *Rapport de stage M1 Chimie*, Groupe thématique Matériaux luminescents, Equipe Matériaux inorganique, **2018**.

c. J. P. Roblin, Résultats des expérimentations faites sur les luminophores. *Rapport de stage Chimie*, Université Clermont Auvergne, CNRS, SIGMA Clermont, **2019**.

Polymers	λ_{exc}	Concentration	QY _{abs}
PF	340 nm	1 mg/mL	45.4%
	340 nm	0.01 mg/mL	80.8%
	365 nm	0.01 mg/mL	89.7%
P11	340 nm	0.01 mg/mL	55.1%
P12	370 nm	0.005 mg/mL	73.9%

Encouraged by these promising results, we have used some of these polymers as emitters to design phosphors.

4.4.2 Quantum yields measured in thin film

Polymers in PMMA as thin films for the measurement of absolute quantum efficiency were prepared as described in **Chapter II (§2.5)**. The absolute quantum yields of these deposits were found to be 10.0%, 6%, 2.7% and 18.7% for the **PF**, **P1**, **P8** and the **Eu complex** emitting material, respectively, as shown on **Table 4-10**.

Table 4-10 Absolute QY of polymers in PMMA (T = 300 K)

Conditions	Eu(tta) ₃ (L) in PMMA	PF in PMMA	P1 in PMMA (λ_{exc} = 330 nm, 3.8 wt%)	P8 in PMMA (λ_{exc} = 295 nm, 4.8 wt%)
QY _{abs}	18.7%	10%	6%	2.7%

4.5 Photostability studies

The stability of LEDs is of critical importance for their application in display and lighting devices.¹⁸³ In this work, preliminary investigations on the photostability of materials containing **PF**, **P1**, **P8** and the **Eu complex** to be used as luminophores were performed at the University of Clermont-Ferrand.¹⁸⁷ The emission of the coated LEDs was monitored as a function of time exposure. A power of 48 W/m² was applied for **PF** and the **Eu complex**, while a power of 61.22 W/m² was applied for the compistes comprising **P1** and **P8**.

It should be noted that the value in W/m² corresponds to the photonic power that arrives on the surface of the sample. In our case, we used a bandpass filter at 460 nm in front of the LED source in order to overcome the excitation LED signal and to select the emission of the phosphor.

¹⁸³ T. Chiba, Y. Hayashi, H. Ebe, K. Hoshi, J. Sato, S. Sato, Y. Pu, S. Ohisa, and J. Kido. *Nature Photonics*, **2018**, 12, 681-687.
b. C. Wurth, M. Grabolle, J. Pauli, M. Spieles & U. Resch-Genger. *Nature Protocols*, **2013**, 8, 1535-1550.

This filter has a transmission close to 100% which has the effect of not disturbing our measurements.

4.5.1 PF

PF was embedded into PMMA and a resin (as described in **Chapter II**) and coated on a 375nm-LED. The emission of this device was then followed over time under a power of 45 W/m². The emission spectrum and the corresponding curve showing the decrease in intensity are reported on **Figure 4-77**. It clearly shows that the material degrades rapidly, as only about 5% of the initial intensity remains after 40 h. This indicates that **PF** is not photostable under these conditions.

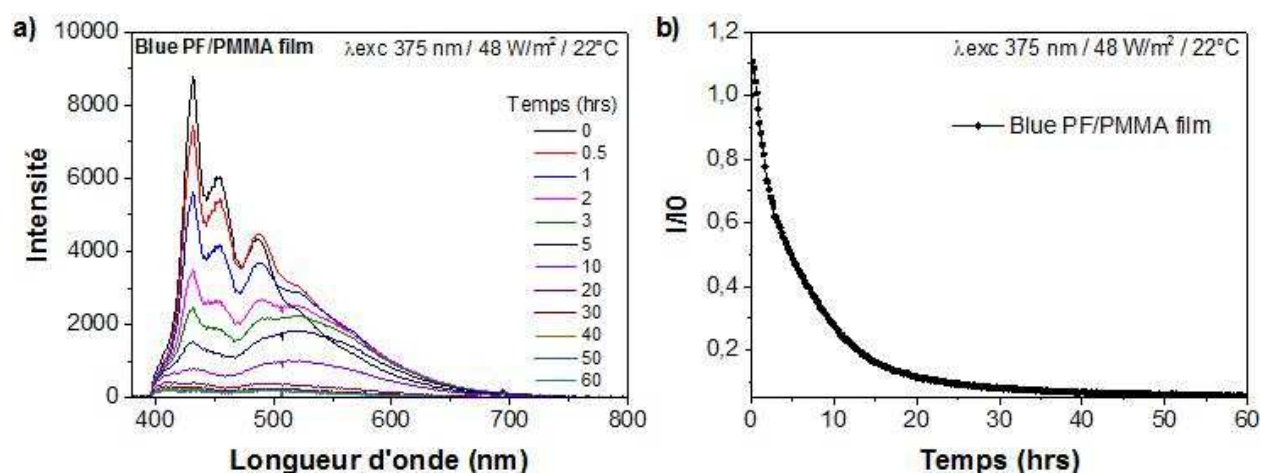


Figure 4-77. Emission spectrum (left, $\lambda_{exc} = 375$ nm, power 45 W/m²); and decay curve (right) of a 375-nm LED covered with a phosphor containing **PF**.

The emission of the **PF**-containing blue-emitting material rapidly decreased (of about half of the initial intensity after 2 h of exposure) with apparition of a broad band at lower energy. This new band could correspond to the cleavage of the alkyle chains with subsequent formation of fluorenone moieties which lead to the quenching of the luminescence. Photo-oxidation of polyfluorenes chains results in ketonic defects (fluorenone groups) which quenches the fluorescence.¹⁸⁴ Possible oxidation and photodegradation processes for fluorenone formation of

¹⁸⁴ a. G.R. Ferreira, B. Nowacki, A. Magalhães, E.R. deAzevedo, E.L. de Sá, L.C. Akcelrud, R.F. Bianchi. *Materials Chemistry and Physics*. **2014**, 146, 212-217.

b. M. Manceau, E. Bundgaard, J. E. Carle, O. Hagemann, M. Helgesen, R. Søndergaard, M. Jørgensen and F. C. Krebs. *J. Mater. Chem.*, **2011**, 21, 4132.

c. V. N. Bliznyuk, S. A. Carter, C. Scott, G. Klärner, R. D. Miller, D. C. Miller, *Macromolecules*. **1999**, 32, 361-369.

d. M. Sims D. D. C. Bradley, M. Ariu, M. Koeberg, A. Asimakis, M. Grell, D. G. Lidzey. *Adv. Funct. Mater.*, **2004**, 14(8): 765-781.

fluorene unit in the polymer chain is shown in the following **Figure 4-78**. Thus, the photostability of polyfulorene is unsatisfactory though with highly efficient blue emission in photoluminescence (PL) and electroluminescence (EL).¹⁵⁷

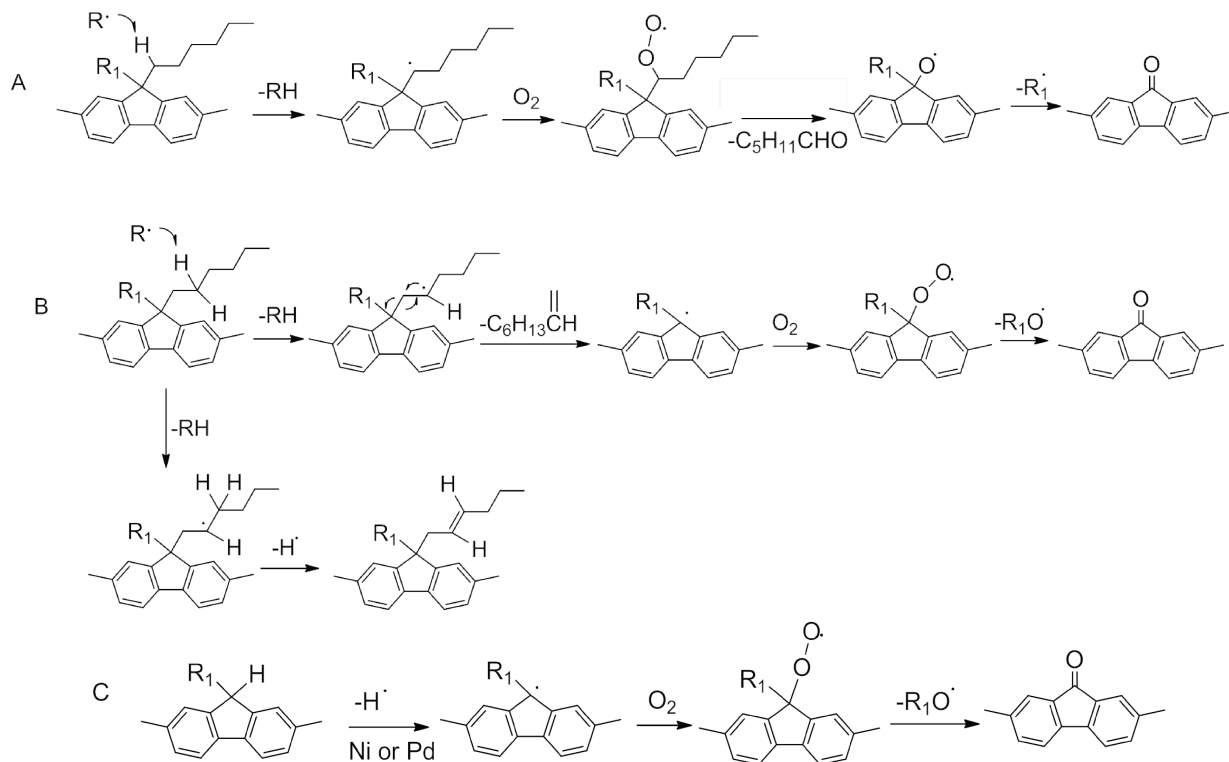


Figure 4-78 Possible oxidation and photodegradation processes for fluorenone formation of fluorene unit in the polymer chain

4.5.2 P1

As shown on **Figure 4-79**, the PL intensity of a phosphor comprising **P1** dropped down dramatically in the first 20 h, especially in the first 10 h, when it was excited continuously at 375 nm. After 20 h, it began to stabilize at around 30% of the initial intensity. This indicates that **P1**

- e. W. Zhao, T. Cao, J. M. White. *Adv. Funct. Mater.*, **2004**, 14(8): 783-790.
- f. Roberto G., Gian Paolo S., Piero M., and Cosimo F. N., *Adv. Funct. Mater.*, **2007**, 17, 538–548.
- g. Robert A., Martin W., Ralf A. A. B., Joost L. J. van D., X. Lou, Oliver H., W. James Feast, E. W. Meijer, and Albertus P. H. J. Schenning. *Adv. Mater.*, **2009**, 21, 597–602.
- h. Y. H. Kim · David A. V. B., *Appl Phys A*, **2009**, 95: 241–247.
- i. L. Romaner, G. Heimel, H. Wiesenhofer, P. Scanducci de Freitas, U. Scherf, J.-L. Bredas, E. Zojer, and E. J. W. *Chem. Mater.*, **2004**, 16, 4667-4674.
- j. Matthew R. Sirtanski, Shaune L. McFarlane and Jonathan G. C. Veinot. *J. Mater. Chem.*, **2010**, 20, 8147–8152.
- k. L. Liu, S. Tang, M. Liu, Z. Xie, W. Zhang, P. Lu, M. Hanif, and Y. Ma. *J. Phys. Chem. B*, **2006**, 110, 13734-13740.
- l. K. A. Luck, H. N. Arnold, T. A. Shastry, T. J. Marks, and M. C. Hersam. *J. Phys. Chem. Lett.*, **2016**, 7, 4223–4229.
- m. V. N. Bliznyuk, S. A. Carter, J. C. Scott, G. Klärner, R. D. Miller, and D. C. Miller. *Macromolecules*, **1999**, 32, 361-369.

was photodegraded sharply during the first 20 h and then became stable. This might also be ascribed to the photodegradation of the fluorene group.¹⁸² As a consequence, the introduction of BPM unit as acceptor to the conjugated polymers has improved the photostability of the material to some degree, but there is still some molecular engineering to perform to design materials with a satisfactory behavior under light exposure.

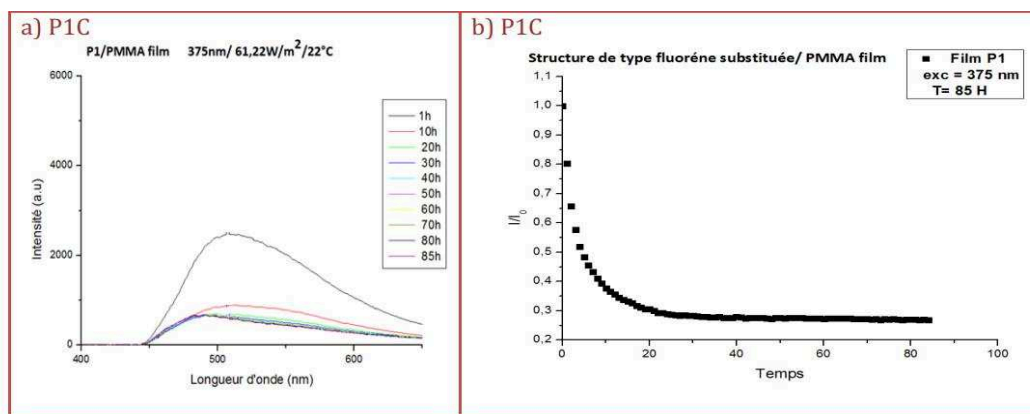


Figure 4-79 a) Evolution of the emission spectrum of the composite comprising **P1** under excitation at 375 nm as a function of time exposure b) Evolution of the PL intensity over time

4.5.3 P8

Figure 4-80 shows the data obtained for a composite comprising **P8**. It can be seen that in the first 10 hours, the PL intensity of **P8** decreased rapidly to around 65% of the initial intensity, and then it tends to become stable. After 40 h, the intensity almost stabilized at around 60% of the initial intensity. This also implies that **P8** was quickly photodegraded in the first 10 hours and then tends to be steady. This could be due to the crack of the side-chains as a carbazoyl radical can be generated, that can further react with oxygen. This ends up in the degradation of the carbazole group, and thus in the interruption of the π -conjugated system. Pfister and Williams also suggested that irradiation of the carbazole group leads to the formation of quinonic oxidized structures after reaction with the superoxide anion $O_2^{\bullet-}$. This second pathway can also contribute to the photodegradation of the sample.¹⁸⁵ (see **Figure 4-81**)

¹⁸⁵ a. A. Rivaton, B. Mailhot, G. Derderian, P. O. Bussiere, and J.-L. Gardette. Investigation of the Photophysical Processes and Photochemical Reactions Involved in PVK Films Irradiated at $\lambda > 300$ nm. *Macromolecules*, **2003**, 36, 5815-5824.

b. A. G. Pfister and D. J. Williams. Photogeneration processes in poly (N - vinylcarbazole). *J. Chem. Phys.*, **1974**, 61, 2416-2426.

c. Pierre-Luc T. Boudreault, Serge Beaupre and Mario Leclerc. Polycarbazoles for plastic electronics. *Polym. Chem.*, **2010**, 1, 127-136.

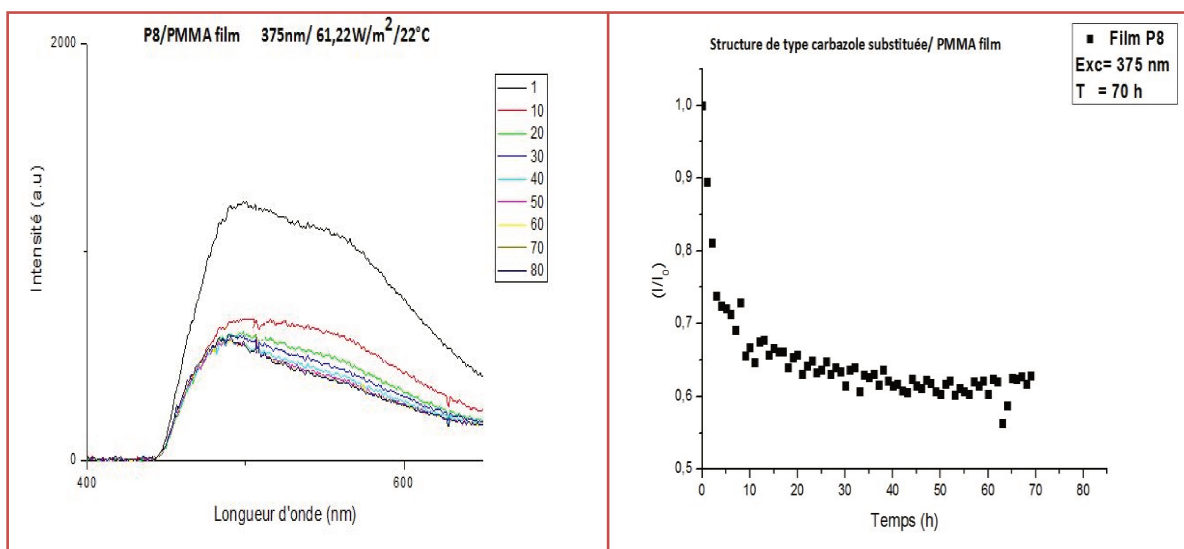


Figure 4-80 a) Evolution of the emission spectrum of the composite comprising **P8** under excitation at 375 nm as a function of time exposure b) Evolution of the PL intensity over time.

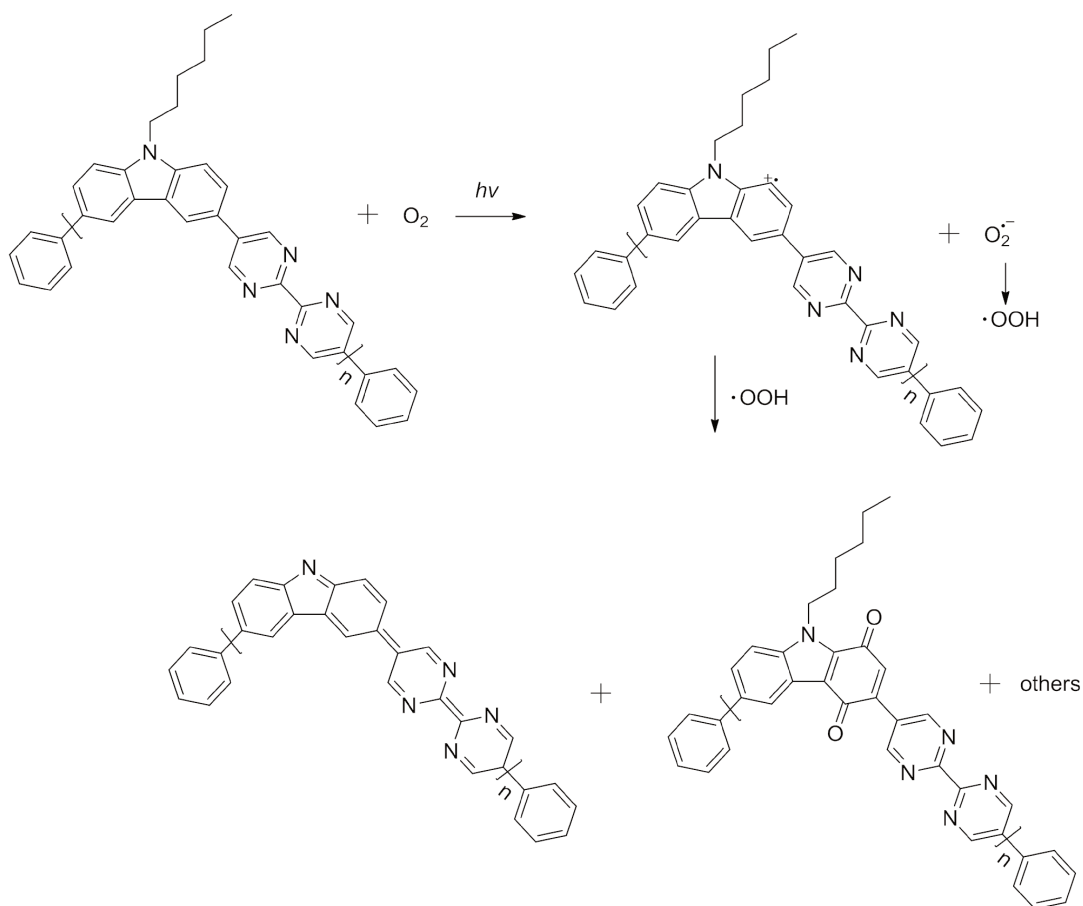


Figure 4-81 Possible oxidation and photodegradation processes of **P8**

In conclusion, **P8** is much more photostable with respect to **P1**. This shows that the carbazole

unit is more photostable than fluorene. This result is consistent with a previous literature report. The advantage of carbazole over fluorene or other hetero-fluorene derivatives is that the nitrogen atom provides a lone electron pair that gives a fully aromatic structure and, therefore, a better stability.¹⁴⁹

4.5.4 Influence of the liquid matrix

Sol-gel matrices are usually used, as they can afford materials with excellent optical transparency, and they can also protect the emitters from UV degradation. We show on **Figure 4-82** the positive influence of the liquid matrix on the photostability of the materials. The remaining intensity of the composite comprising **P1** without the liquid matrix is about 9% of its initial intensity after 50 h of irradiation, while 30% of the initial intensity was left when the liquid matrix was applied. The composite comprising **P8** without the liquid matrix shows a stabilized intensity of 15% of the initial intensity after 50 h, while the remaining intensity is more than 50% when the liquid matrix is used. These results confirm the beneficial impact of the liquid matrix on the photostability of the materials.

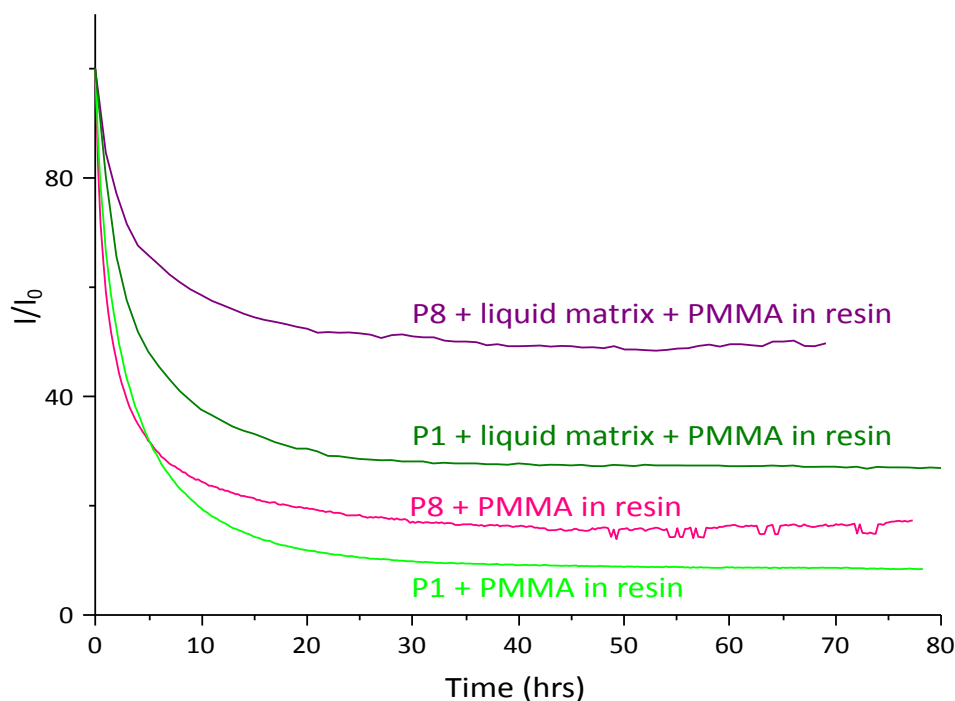


Figure 4-82 Evolution of the intensity of composites comprising **P1** and **P8**, with and without the carbazole-Si matrix.

4.5.5 [Eu(tta)₃(L)]

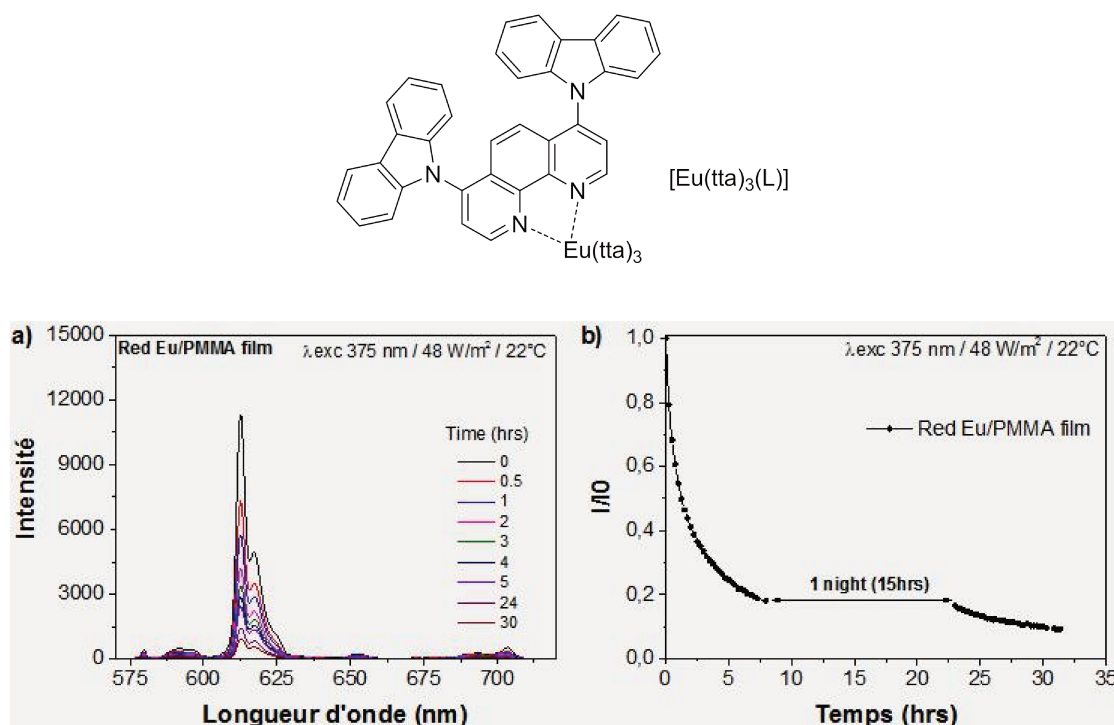


Figure 4-83 a) Evolution of the emission spectra of the composite comprising [Eu(tta)₃(L)] under excitation at 375 nm as a function of time exposure b) Evolution of the PL intensity of this composite under continuous excitation at 375 nm for 32 hours.

Investigations on a composite comprising [Eu(tta)₃(L)] are reported on **Figure 4-83**. They show that the intensity of the Eu³⁺ ion decreased rapidly. It remained only about 10% of the initial intensity after 30 h of irradiation. This result indicates that the photostability of the Eu-metal complex is also not ideal. It may be caused by the break of the coordinated network between europium and the ligands or the decomposition of the ligands under UV.

4.6 Thermostability studies

As heat production is undeniable and unavoidable when the devices are operating, it is of crucial importance to have a clue on the behavior of the materials when heated. We show hereafter the Thermal Gravity Analysis (TGA).

Thermogravimetric analysis (TGA) is one of the most widely used techniques for thermal analysis of various materials due to its simplicity and the information afforded by a simple

thermogram.¹⁸⁶ TGA measures the amount and rate/velocity of variation in the mass of a sample as a function of temperature or time in a certain atmosphere. The measurements are used primarily to determine the thermal or oxidative stabilities of materials, as well as their compositional properties. The technique can be used to analyze materials that either mass loss or gain due to decomposition, oxidation or loss of volatiles (such as moisture). It is particularly useful for the investigation of polymeric materials. The technique is especially employed to characterize the thermal stabilities¹⁸⁷, compositional analysis of multi-component materials or blends¹⁸⁸, the oxidation kinetics and the phase transition¹⁸⁹ and so forth.

In this work, TGA was performed to probe their thermostability over the temperature in the range of 30-600 °C under an atmosphere of argon. The curves are shown in **Figure 4-84**. Main mass losses are observed between 400 and 600 °C, which are attributed to the degradation of polymers. For most polymers studied, the mass loss observed at 400-500 °C is due to the loss of the alkyl chains. All of the compounds show high onset temperature corresponding to 10% weight loss in the range 320–450 °C, indicating their excellent thermostability, which is a good point for their applications.

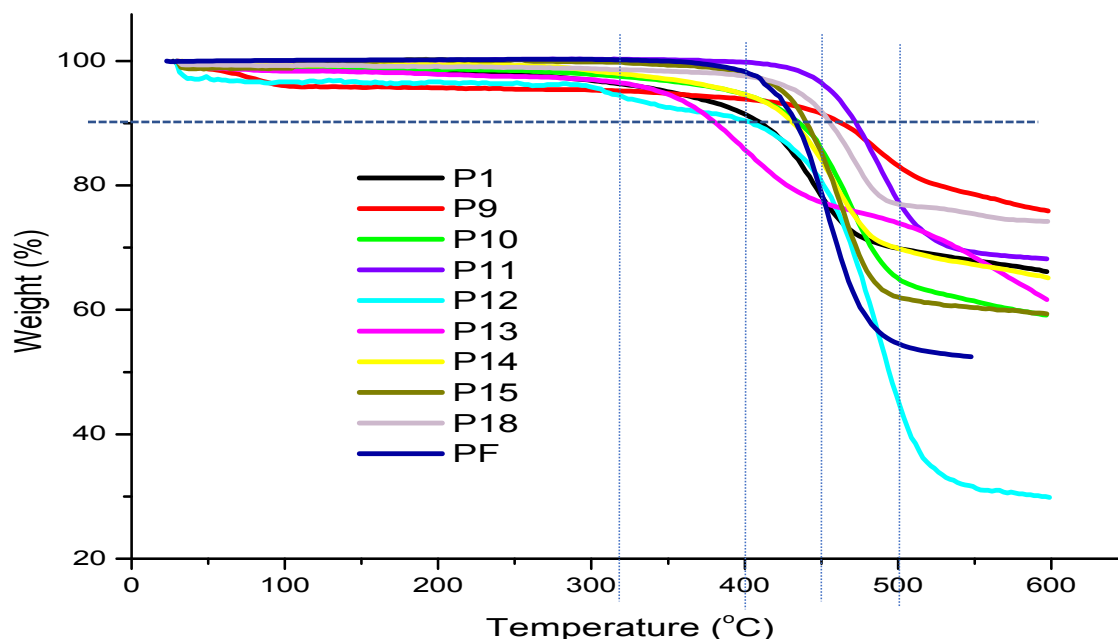


Figure 4-84 TGA curves of the compounds

¹⁸⁶ A. Zeino, A. Abulkibash, M. Khaled, and M. Atieh. *Journal of Nanomaterials*. Volume **2014**, Article ID 561920, 9 pages. <http://dx.doi.org/10.1155/2014/561920>.

¹⁸⁷ Andrey A. Tregubov, D. Barney Walker, Khuong Q. Vuong, J. Justin Gooding, and Barbara A. Messerle. *Dalton Trans.*, **2015**, 44, 7917-7926.

¹⁸⁸ a. Q. Lu, R. Alves de Toledo, F. Xie, J. Li, H. Shim. *Science of the Total Environment*, **2017**, 583, 88–96.

b. K. Johnson, G. Purvis, E. Lopez-Capel, C. Peacock, N. Gray, T. Wagner, C. Marz, L. Bowen, J. Ojeda, N. Finlay, S. Robertson, F. Worrall & C. Greenwell. *Nature Communications*, **2015**, 6, 7628.

¹⁸⁹ F. Noor, H. Zhang, T. Orakianitis and D. Wen. *Phys.Chem.Chem.Phys.*, **2013**, 15, 20176-20188.

4.7 Summary

In this Chapter, we have investigated the possibility to use some of the newly synthesized emitters as luminophors for 375 nm-LEDs. We have presented the photophysical properties of materials made of different polymers in different matrices. We have investigated the influence of the polymer matrices and found out that they also affect the luminescence of the polymers. Generally, matrices were found to blue-shift the emission of the materials, especially the C-Si matrix, as the carbazole unit of the matrix shows some blue emission.

Meanwhile, the polymer **P13** was confirmed to show ACQ property instead of AIE property. At the same time, the emission band of **P13** was red-shifted when water was added, which may be caused by the increase of the polarity of the solvent.

White light was successfully obtained from different blends composed of different emitters both in solution and in film. By controlling the excitation wavelength and the ratio of different component, we were able to control the emission of the luminescent materials.

Last but not the least, we have presented some important characteristics of the materials, including their quantum yield, photostability and thermostability properties, all are of critical importance for their practical application.

Because of the lack of time, only four emitters, **PF**, **P1**, **P8** and the **Eu complex** were investigated for the design of luminophors. We have particularly shown that **PF**, and, in general, polymers containing the alkyl-fluorene unit, could not be viable as emitters for such applications. They degrade very rapidly. The photostability of our newly designed conjugated polymers was successfully improved through a rational chemical engineering strategy. The carbazole derivatives are preferable for future investigations considering their better photostability compared to fluorene units. Some polymers such as **P11** and **P12** are found to have high quantum yields and are promising to replace the commonly used **PF** as blue emitter, since their quantum yields are comparable while their photostability is much improved.

Chapter V Conclusion and perspectives

Contents

5.1 Conclusion.....	- 218 -
5.2 Perspectives.....	- 219 -
5.2.1 Further improvement of the photostability through chemical design.....	- 219 -
5.2.2 Design and synthesis of new BPM-based metal complexes.....	- 219 -
5.2.3 Design and synthesis of new conjugated polymers with red emission.....	- 221 -
5.2.4 Others.....	- 222 -

5.1 Conclusion

In this work, we have designed and synthesized different luminescent materials with a partial control of their luminescence and their physicochemical and photophysical properties. Particularly, this work was focused on the investigation of an interesting multifunctional molecule, BPM, with which we made different conjugated polymers that were obtained by Suzuki coupling reaction in order to design materials with different emission colors in the visible. Consequently, to our delight, we have succeeded in obtaining a variety of materials with different luminescence, such as blue: **PF**, **P11**, **P12** and green: **P1**, **P8**, **P9**, **P10**, and we have successfully got several interesting white emitting materials as well. Two of the white emitting materials were made with two luminescent molecules (**P1** and an **Eu-complex**, or **P10** and **P26**, both contained two emitters only), which avoided the use of polyfluorene as blue emitting component, which is sensitive to UV light and easy to be photo-oxidated and degraded. Three polymers (**P13**, **P14**, **P15**) were even more interesting and special, as they emit white light, thus offering the possibility to avoid blending different emitters. Rare reports can be found in the literature on such white-emitting polymers. Among all the polymers, we have investigated the effect of different elements, including the backbone, side chain, linearity and different matrices such as PMMA, polystyrene, on the stability, photoluminescence (PL) properties and solubility. We concluded that the carbazole unit possesses a better photostability over fluorene or other heterofluorene derivatives due to the nitrogen atom providing a lone electron pair that gives a fully aromatic structure. The solubility and the processability of the polymers clearly depend on the nature and length of the side chains on the nitrogen atom. Long and bulky side chains are increasing the solubility. Concerning the study of the influence of the linearity to the polymer PL properties, we have compared the result of polymers with 2,7-carbazole derivatives and 3,6-carbazole derivatives as donor group respectively with the same acceptor moiety. It shows that increasing the linearity of the polymer chains is also favorable to decrease their energy bandgaps.

To sum up, not only all the synthetic procedures and chemical characterizations of different compounds, including monomers, polymers and metal complexes were studied in this work, but also the photophysical properties of all polymers, either in solutions or in thin films, are presented. Besides, results on photochemical and physico-chemical characterizations of compounds were also summarized. These studies showed that a good control of the structure-property relationships through chemical engineering can lead to identify the limiting factors that could hamper the use of the materials, and solutions have been proposed to improve the

materials performance. Especially, new (D-A)_n polymers containing 2,2'-bipyrimidine could open the way to a new family of luminescent metallopolymer as they can coordinate metal ions. This work will valorize the use of 2,2'-bipyrimidine, as it can both be used as an acceptor moiety to design donor-acceptor polymers and it can act as a sensitizer for the Eu(III) and Tb(III) luminescence. BPM could thus allow the use of very limited quantities of Rare Earths as emitters to tune the emission color. After more chemical structural modifications and developments based on our work, a promising prospect of their improvement and application can be expected.

5.2 Perspectives

Despite the work done in this project, there is still plenty of work that can be done. Following are some promising suggestions that can be anticipated in the field based on our work.

5.2.1 Further improvement of the photostability through chemical design

It has been shown that there are other moieties which are more photostable than carbazole. For instance, the Si-Cyclopentadithiophene moiety reported in Frederik's work was described to be more photostable than carbazole, probably due to the presence of the silicon atom that is known to be less easily oxidized compared with carbon.¹⁴⁹ Consequently, conjugated polymers using this kind of monomer as donor group instead of carbazole and fluorene derivatives may be a feasible and viable way to further improve the photostability of the consequential materials. Following polymer **P19** for example (**Figure 5-1**). We can reasonably expect that the photostability of **P19** may be better compared to polymers studied in this thesis and so it is worth to be studied in a near future.

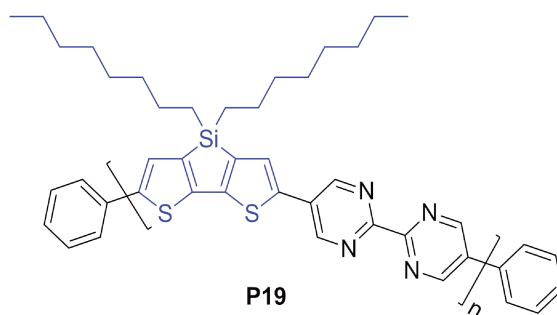


Figure 5-1 Structure of **P19**

5.2.2 Design and synthesis of new BPM-based metal complexes

The choice of ligands plays a critical role in the structure, function and application of metal

complexes.¹⁹⁰ Though some investigations of BPM derivatives have been done, either as ligands for metal complexes¹¹⁷ or as conjugated segments for (D-A)_n conjugation systems,¹⁰³ there is still much exploration to be done and many challenges to be overcome. In fact, at present there have been much more reports on the bipyridine derivatives, which structures are quite close to BPM derivatives.

It is well known that bipyridine derivatives have been widely reported in the application of functionalized metal complexes served mainly as photocatalyst¹⁹¹ or photoelectrochemical probes with high sensitivity and the great potential for in situ analysis.¹⁹² In recent years, some functionalized platinum(II) bipyridine complexes have also been reported to possess tunable aggregation abilities and photophysical properties and thus they are widely explored for applications in nonlinear optics¹⁹³, luminescent materials, optoelectronic devices, and so forth.^{195,196,197} Representatives of reported bipyridine-based metal complexes are shown in **Figure 5-2**. Electrocatalytic and Solar-Driven CO₂ Reduction to CO was achieved with a Manganese Catalyst **5-M1** immobilized on a mesoporous TiO₂ electrode.¹⁹² Phosphonate substituted ruthenium(II) bipyridyl derivatives **5-M2** to **5-M4** were served as photoelectrochemical probes for sensitive and selective detection of mercury(II) in biofluids.¹⁹³ **5-M5**¹⁹⁶ and **5-M6**¹⁹⁷ were reported to be color-tunable by controlling the temperature or solvent, due to their morphologies change upon solvent or temperature variations.

¹⁹⁰ A. Heuer-Jungemann, N. Feliu, I. Bakaimi, M. Hamaly, A. Alkilany, I. Chakraborty, A. Masood, M. F. Casula, A. Kostopoulou, E. Oh, K. Susumu, M. H. Stewart, I. L. Medintz, E. Stratakis, W. J. Parak, and A. G. Kanaras. *Chem. Rev.*, **2019**, *119* (8), 4819-4880.

¹⁹¹ Timothy E. Rosser, Christopher D. Windle, and Erwin Reisner. *Angew. Chem. Int. Ed.*, **2016**, *55*, 7388–7392.

¹⁹² Shuo Wu, Wenjuan Tu, Yanqiu Zhao, Xiuyun Wang, Jie Song, and Xinlan Yang. *Anal. Chem.*, **2018**, *90* (24), 14423–14432.

¹⁹³ a. A. Hilton, T. Renouard, O. Maury, H. Le Bozec, I. Ledoux and J. Zyss. *Chem. Commun.*, **1999**, 2521–2522.

b. O. Maury, J.-P. Guegan, T. Renouard, A. Hilton, P. Dupau, N. Sardon, L. Toupet and H. L. Bozec. *New J. Chem.*, **2001**, *25*, 1553–1566.

¹⁹⁵ Y. Ai, Y. Li, H. Li-Ki Fu, A. Kwun-Wa Chan, V. W.-W. Yam. *Chem. Eur. J.*, **2019**, *25* (20), 5251-5258.

¹⁹⁶ Y. Ai, M. Ng, E. Y.-H. Hong, A. K.-W. Chan, Z.-W. Wei, Y. Li, and V. W.-W. Yam. *Chem. Eur. J.*, **2018**, *24*, 1–9.

¹⁹⁷ a. F.-W. Liu, L. Y. Niu, Y. Chen, V. Ramamurthy, L.-Z. Wu, C.-H. Tung, Y.-Z. Chen, Q.-Z. Yang, *Chem. Eur. J.*, **2016**, *22*, 18132-18139.

b. H. L.-K. Fu, C. Po, H. He, S. Y.-L. Leung, K. S. Wong, V. W.-W. Yam, *Chem. Eur. J.*, **2016**, *22*, 11826-11836.

c. K.-C. Chang, J.-L. Lin, Y.-T. Shen, C.-Y. Hung, C. Y. Chen, S.-S. Sun, *Chem. Eur. J.*, **2012**, *18*, 1312-1321.

d. R. Liu, D. Zhou, A. Azenkeng, Z. Li, Y. Li, K. D. Glusac, W. Sun, *Chem. Eur. J.*, **2012**, *18*, 11440-11448.

e. Z. Li, E. Badaeva, D. Zhou, J. Bjorgaard, K. D. Glusac, S. Killina, W. Sun, *J. Phys. Chem. A*, **2012**, *116*, 4878-4889.

f. Chan, S.-C.; Chan, M. C. W.; Wang, Y.; Che, C.-M.; Cheung, K.-K.; Zhu, N. *Chem. Eur. J.*, **2001**, *7*, 4180.

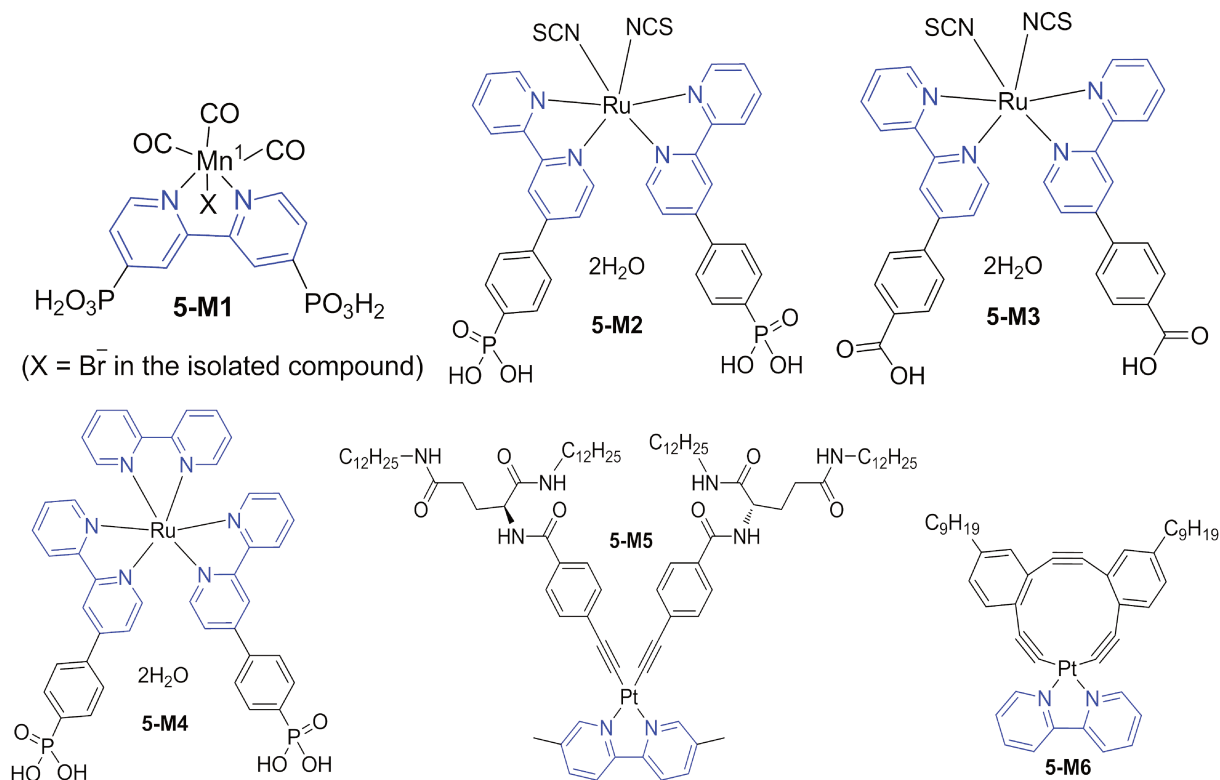


Figure 5-2 Representatives of reported bipyrindine-based metal complexes

One can imagine that bipyrimidine derivatives are even more promising candidates for such applications, as they are more electron deficient than bipyridine derivatives¹⁰⁶ and can also form coordination complexes with various bonding modes. In fact, BPM can act as a bridging unit between metal ions thus leading to an infinity of supramolecular assemblies¹¹⁷ To date, still rare work has been done at this point. Therefore, the design and synthesis of new BPM-based metal complexes for diverse applications are still of great interest.

5.2.3 Design and synthesis of new conjugated polymers with red emission

Another possible work that can be done is to introduce BPM-based monomer into more conjugated polymers, especially in the next exploration of red-emitting conjugated polymers. For instance, **P20** and **P21** (**Figure 5-3**) contain 4,4'-bipyrimidine which has been reported to be more π -electron deficient as it has lower π^* -level compared with 2,2'-bipyrimidine derivatives.¹⁹⁸ Thus 4,4'-bipyrimidine derivatives could be better acceptors, than polymers with stronger D-A interactions that emit red light can possibly be designed. Consequently, **P20** and **P21** could be expected to demonstrate a more pronounced red light compared to **P10**, which shows green

¹⁹⁸ a. Sylvia Ernst and Wolfgang Kaim. *Angew. Chem. Int. Ed. Engl.*, **1985**, 24, 430-431.

b. Elena Ioachim, Elaine A. Medlycott, Matthew I. J. Polson, and Garry S. Hanan. *Eur. J. Org. Chem.*, **2005**, 3775-3780.

emission.

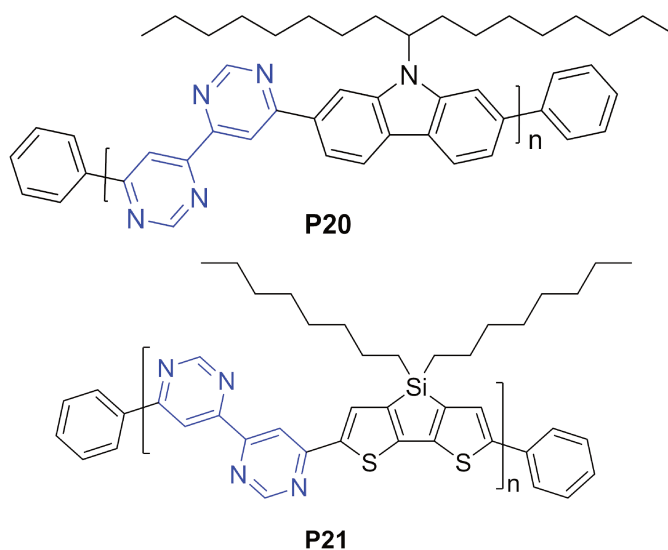
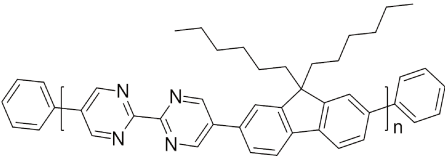
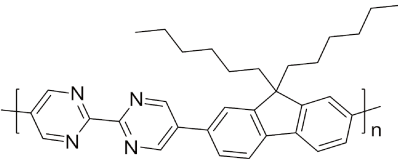
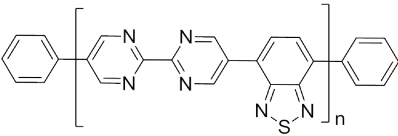
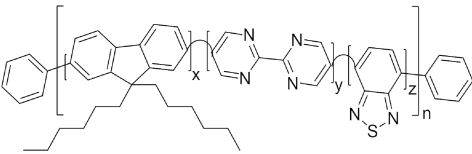
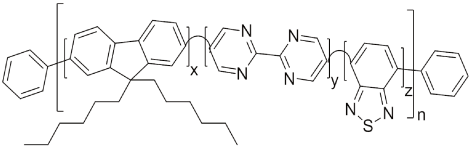


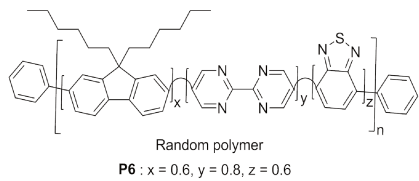
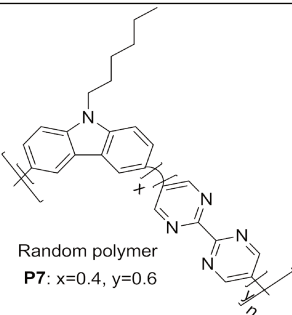
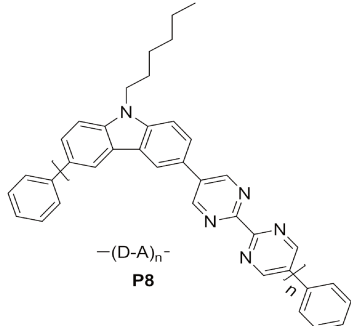
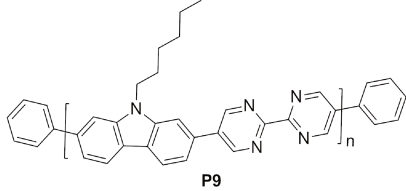
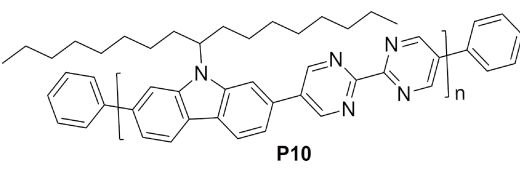
Figure 5-3 Structure of **P20** and **P21**

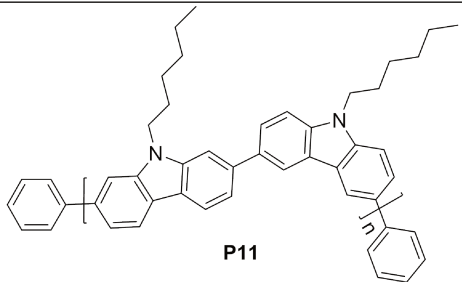
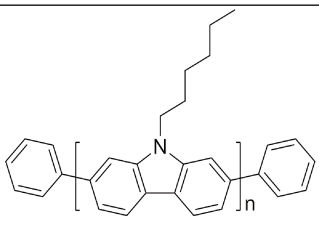
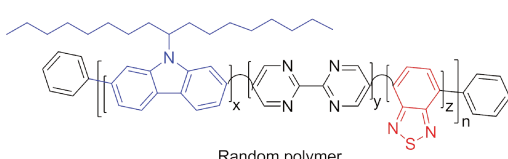
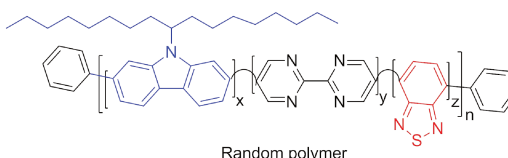
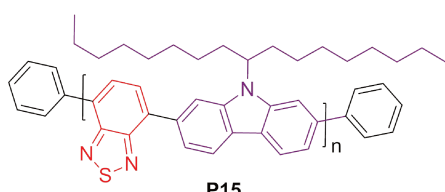
5.2.4 Others

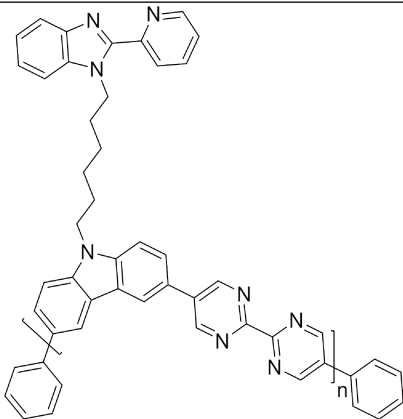
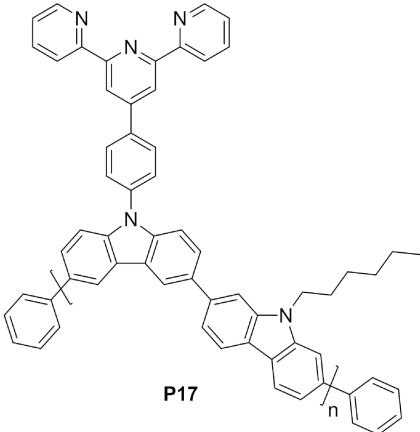
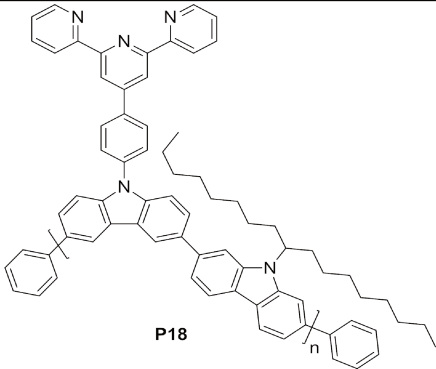
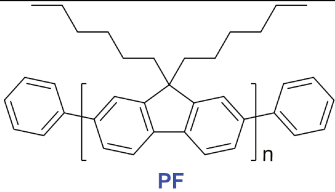
In addition to the above mentioned work, there is no doubt that still much work can be done, such as the development of new soft materials to be used in the film formation, especially BPM-based class II sol-gel materials which are known to be more photostable.¹¹⁴ Besides, more applications of investigated polymers and metal complexes yet remain to be explored. There is still a long way to go before the materials achieved commercial applications.

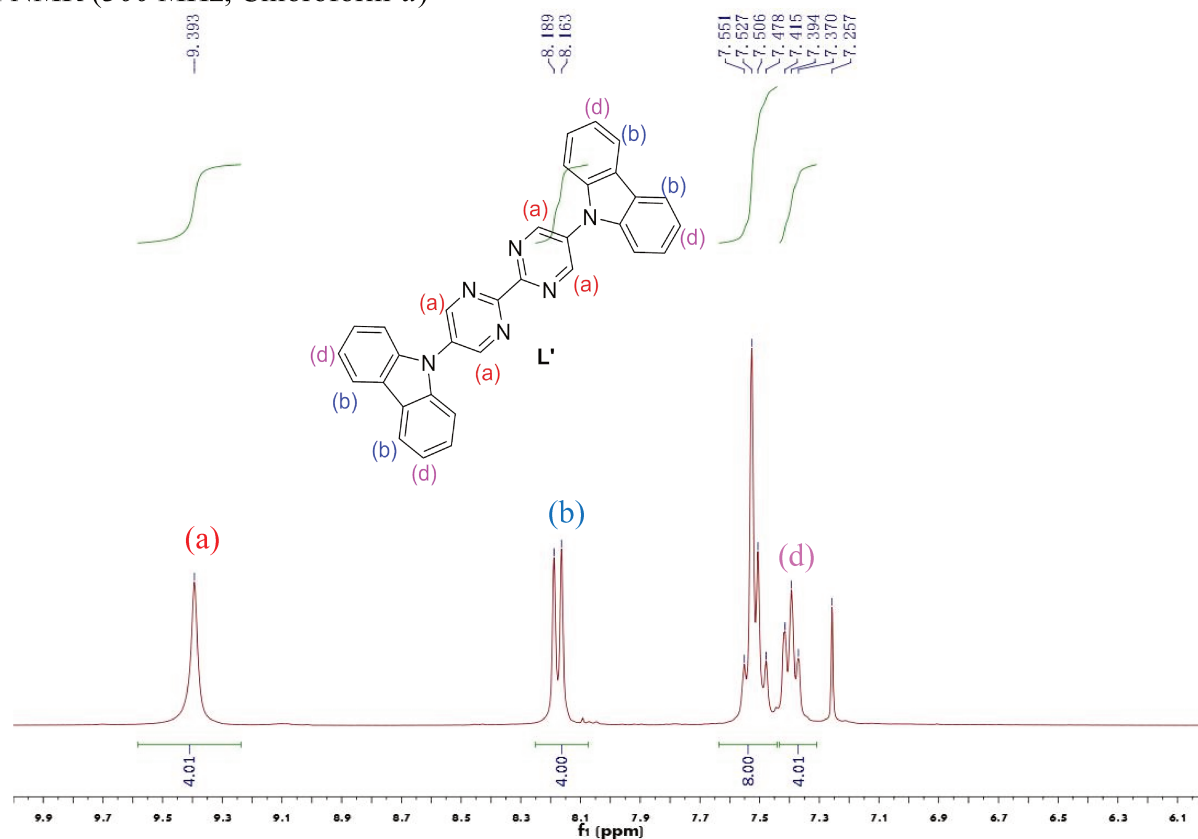
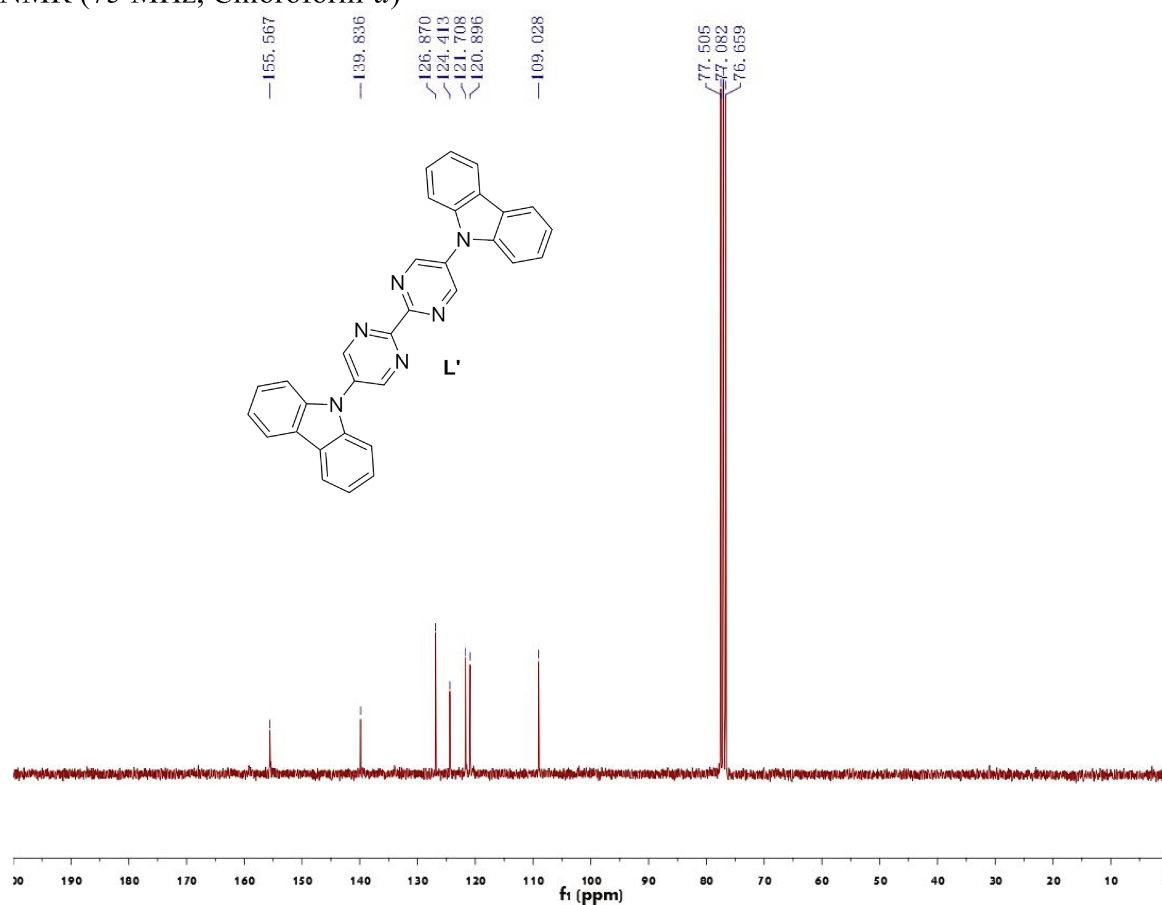
Appendix I Polymers discussed in the thesis

No.	Fomula/Note	Structure
1	<p>P1</p> <p><i>Poly(2,2'-bipyrimidine-alt-2,7-(9,9-dihexyl-9H-fluorene))</i></p> <p>77% yield</p>	 <p>P1</p>
2	<p>P2</p> <p><i>Poly(2,2'-bipyrimidine-alt-2,7-(9,9-dihexyl-9H-fluorene))</i></p> <p><i>without endcapping</i></p> <p>49% yield</p>	 <p>P2</p>
3	<p>P3</p> <p><i>Poly(2,2'-bipyrimidine-alt-benzo[c][1,2,5]thiadiazole)</i></p> <p>Insoluble</p>	 <p>P3</p>
4	<p>P4</p> <p><i>Poly(2,7-(9,9-dihexyl-9H-fluorene)-co-(2,2'-bipyrimidine)-co-(benzo[c][1,2,5]thiadiazole)) in</i></p> <p><i>ratio 0.1:0.5:0.4</i></p> <p>Bad solubility</p>	 <p>Random polymer P4 : x=0.1, y=0.5, z=0.4</p>
5	<p>P5</p> <p><i>Poly(2,7-(9,9-dihexyl-9H-fluorene)-co-(2,2'-bipyrimidine)-co-(benzo[c][1,2,5]thiadiazole)) in</i></p> <p><i>ratio 0.2:0.5:0.3</i></p> <p>8% yield</p>	 <p>Random polymer P5 : x = 0.2, y = 0.5, z = 0.3</p>

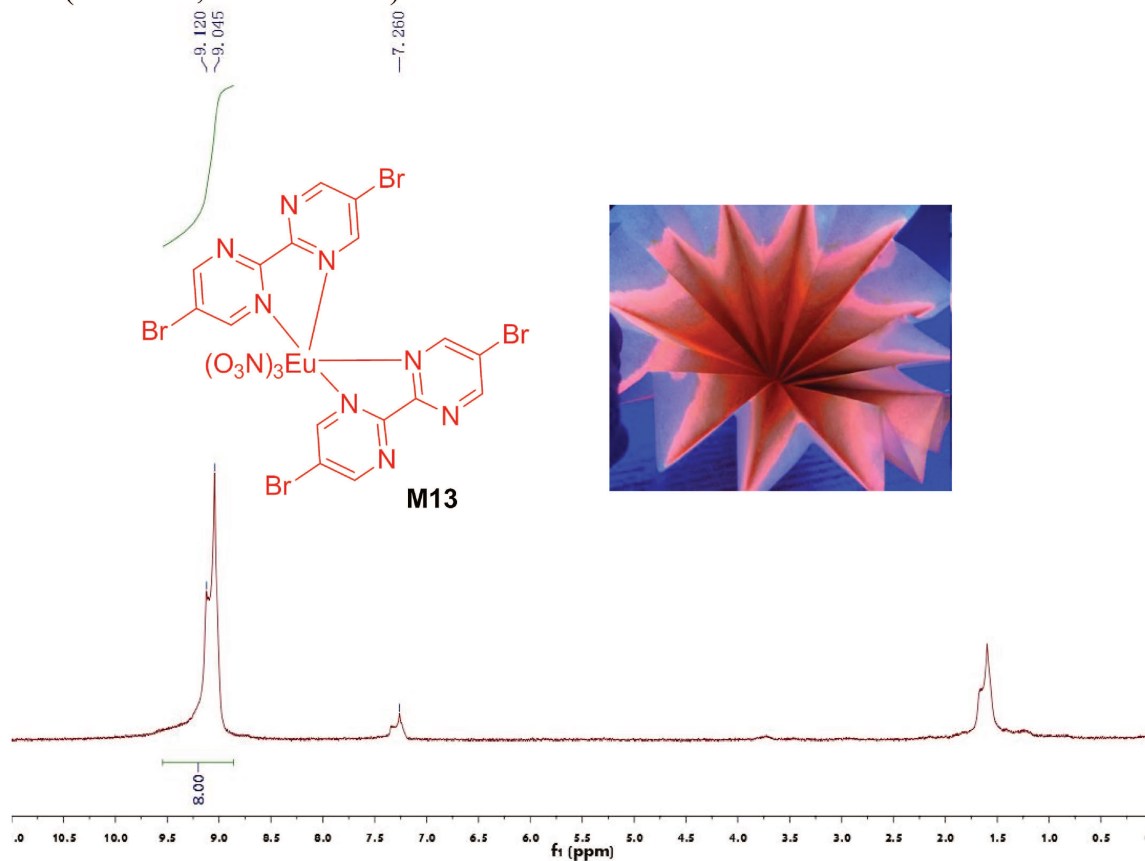
6	<p>P6</p> <p><i>Poly(2,7-(9,9-dihexyl-9H-fluorene)-co-(2,2'-bipyrimidine)-co-(benzo[c][1,2,5]thiadiazole)) in ratio 0.6:0.8:0.6</i></p> <p>22% yield</p>	 <p>Random polymer P6: $x = 0.6$, $y = 0.8$, $z = 0.6$</p>
7	<p>P7</p> <p><i>Poly((2,2'-bipyrimidine)-co-3,6-(9,9-dihexyl-9H-carbazole))</i></p> <p>Low yield</p>	 <p>Random polymer P7: $x=0.4$, $y=0.6$</p>
8	<p>P8</p> <p><i>Poly((2,2'-bipyrimidine)-alt-3,6-(9,9-dihexyl-9H-carbazole))</i></p> <p>52% yield</p>	 <p>-(D-A)_n- P8</p>
9	<p>P9</p> <p><i>Poly(2,2'-bipyrimidine-alt-2,7-(9,9-dihexyl-9H-carbazole))</i></p> <p>74% yield</p>	 <p>P9</p>
10	<p>P10</p> <p><i>Poly(2,2'-bipyrimidine-alt-2,7-(9-(heptadecan-9-yl)-9H-carbazole))</i></p> <p>91% yield</p>	 <p>P10</p>

11	<p>P11</p> <p><i>Poly(3,6-(9-hexyl-9H-carbazole))-alt-2,7-(9-hexyl-9H-carbazole))</i></p> <p>42% yield</p>	 <p>P11</p>
12	<p>P12</p> <p><i>Poly(2,7-(9-hexyl-9H-carbazole))</i></p> <p>21% yield</p>	 <p>P12</p>
13	<p>P13</p> <p><i>Poly(2,7-(9-(heptadecan-9-yl)-9H-carbazole)-co-(2,2'-(benzo[c][1,2,5]thiadiazole)) in ratio 0.6:0.8:0.6</i></p> <p>64% yield</p>	 <p>Random polymer P13 : x = 0.6, y = 0.8, z = 0.6</p>
14	<p>P14</p> <p><i>Poly(2,7-(9-(heptadecan-9-yl)-9H-carbazole)-co-(2,2'-(benzo[c][1,2,5]thiadiazole)) in ratio 0.6:0.3:0.5</i></p> <p>21% yield</p>	 <p>Random polymer P14 : x = 0.6, y = 0.3, z = 0.5</p>
15	<p>P15</p> <p><i>Poly(2,7-(9-(heptadecan-9-yl)-9H-carbazole)-alt-(benzo[c][1,2,5]thiadiazole))</i></p> <p>37% yield</p>	 <p>P15</p>

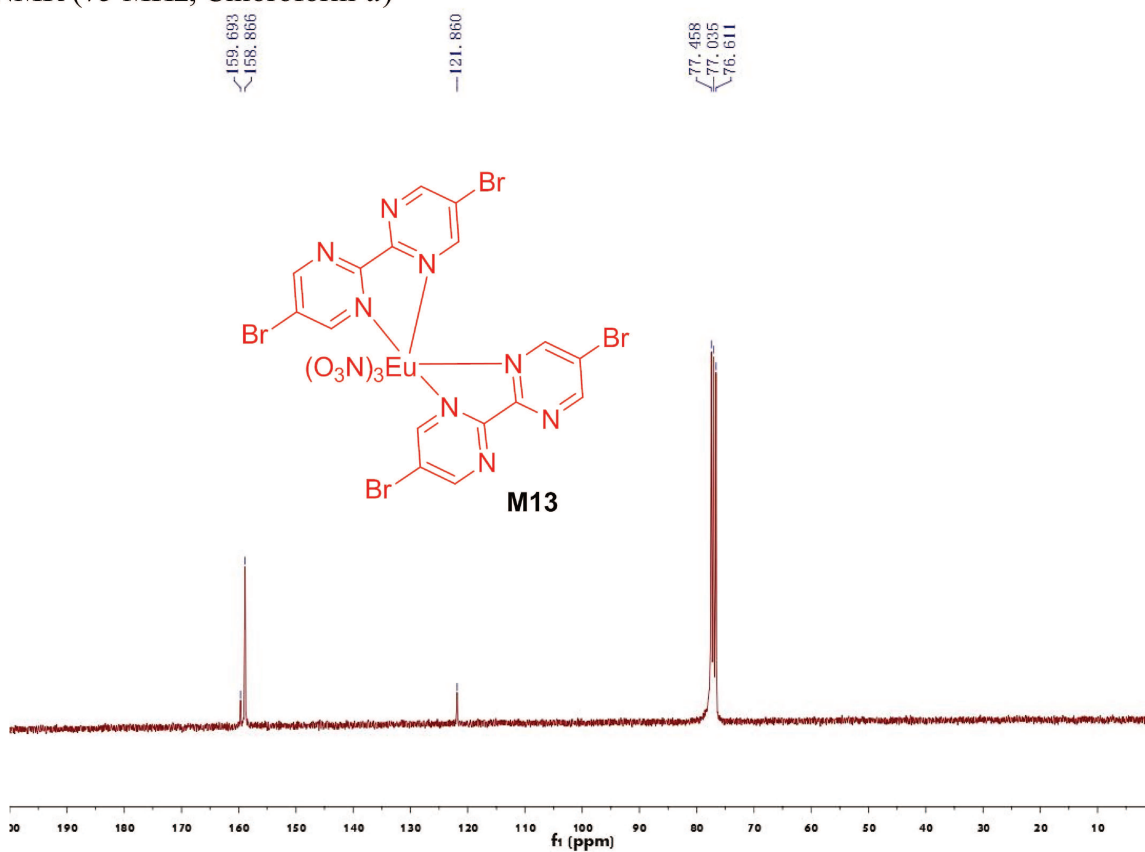
16	P16 <i>Poly(2,2'-bipyrimidine-alt-3,6-(pyridine-benzo-imidazole)carbazole)</i> Low yield	
17	P17 <i>Poly(9-hexyl-9H-carbazole-alt-3,6-(phenyl-terpyridine)carbazole)</i> Bad solubility	
18	P18 <i>Poly(9,9-dihexyl-9H-fluorene-alt-3,6-(phenyl-terpyridine)carbazole)</i> 36% yield	
19	PF <i>Poly(9,9-dihexyl-9H-fluorene)</i> 52% yield	

Appendix II NMR spectra of selected new compounds ^1H NMR (300 MHz, Chloroform-*d*) ^{13}C NMR (75 MHz, Chloroform-*d*)

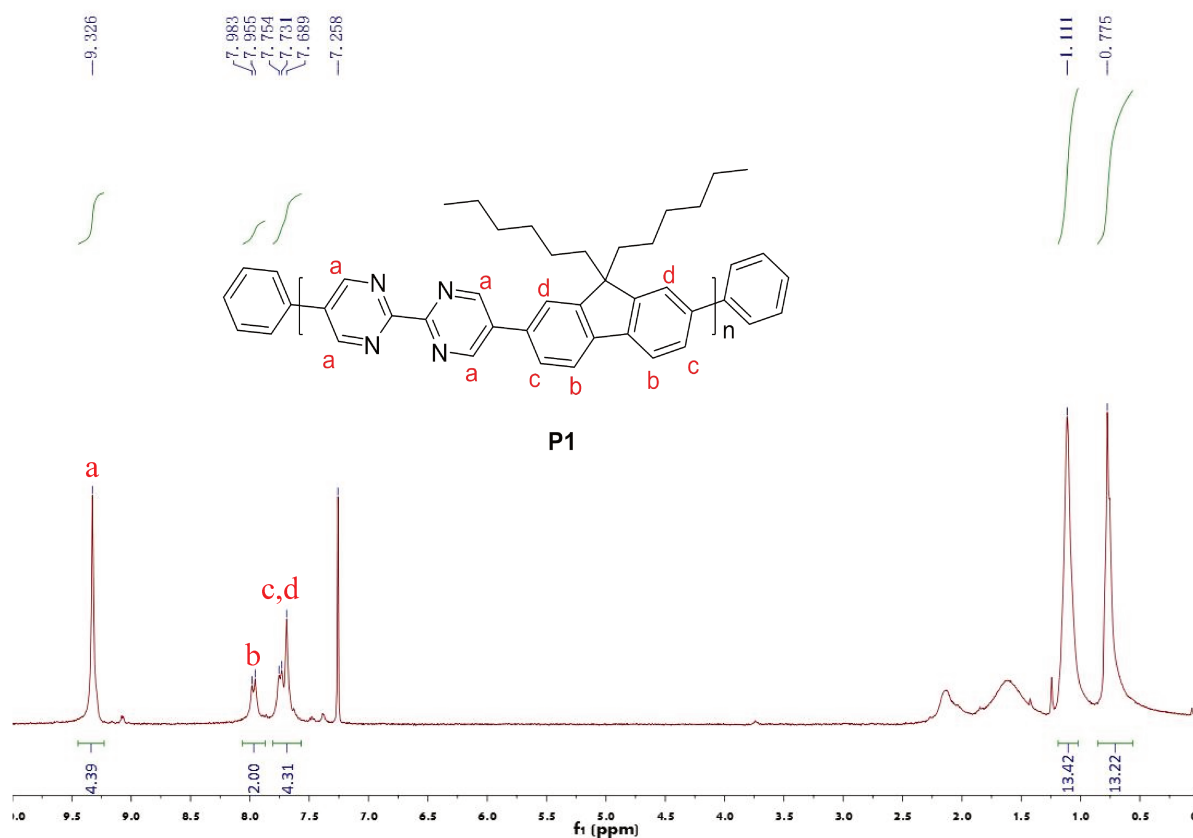
^1H NMR (300 MHz, Chloroform-*d*)



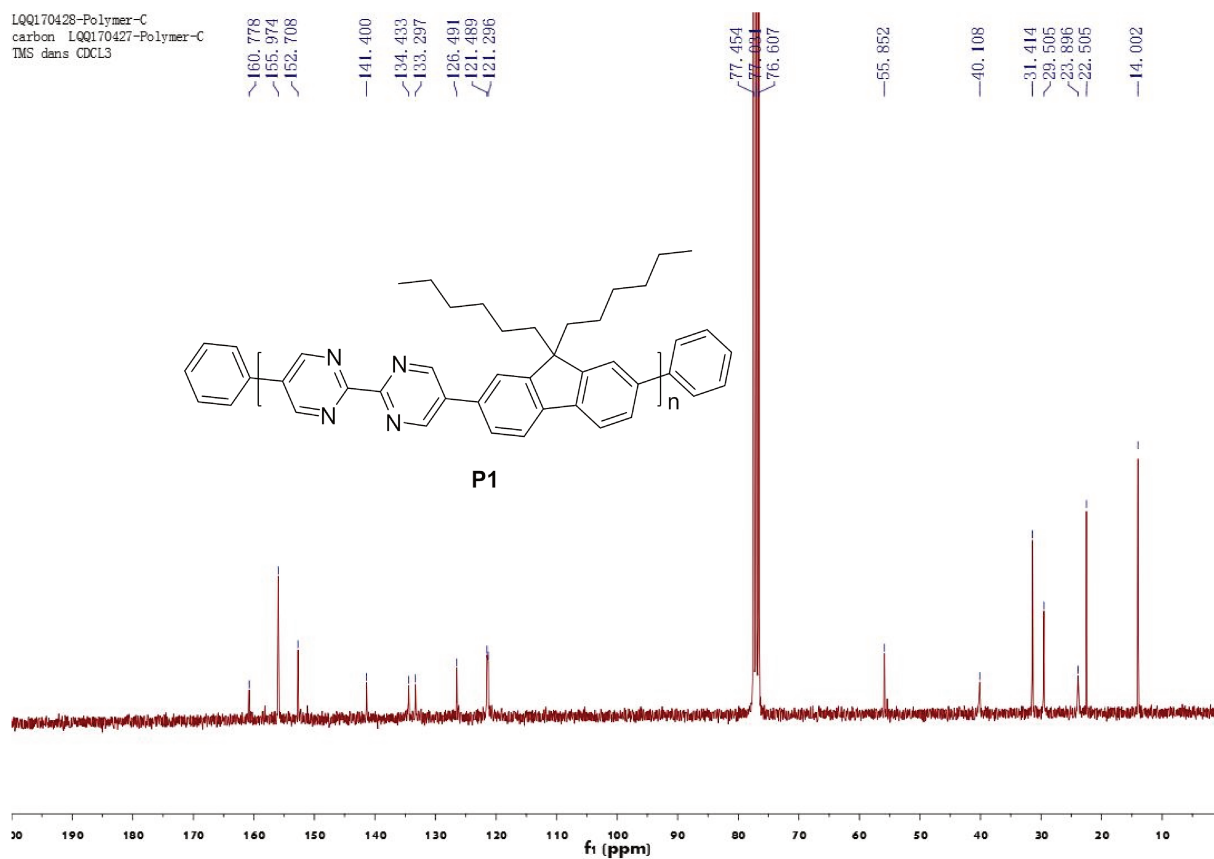
^{13}C NMR (75 MHz, Chloroform-*d*)

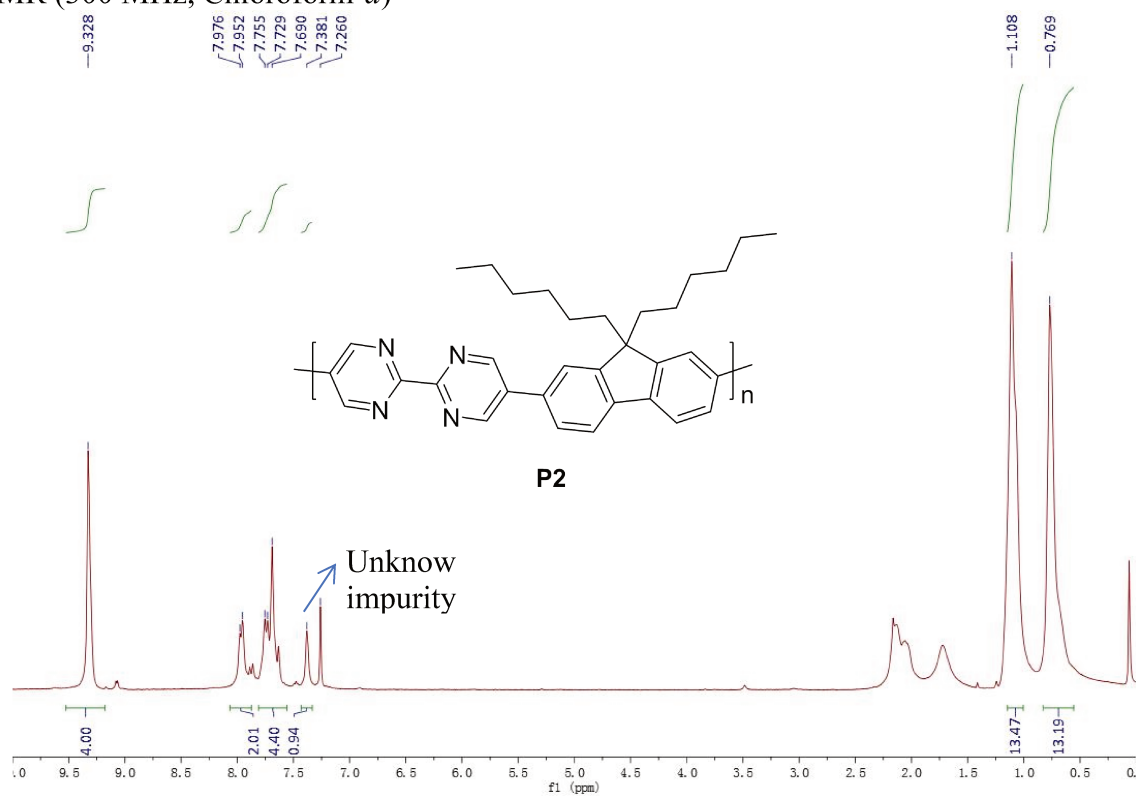
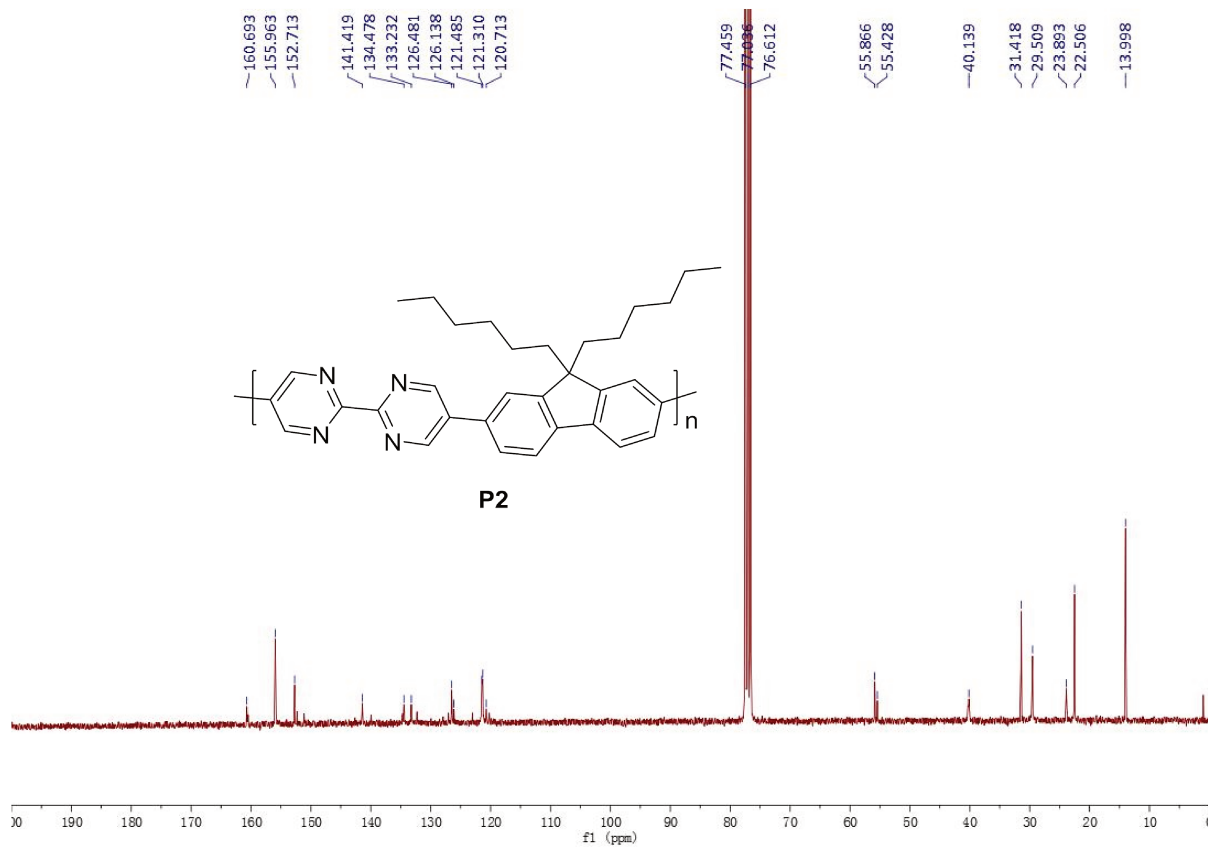


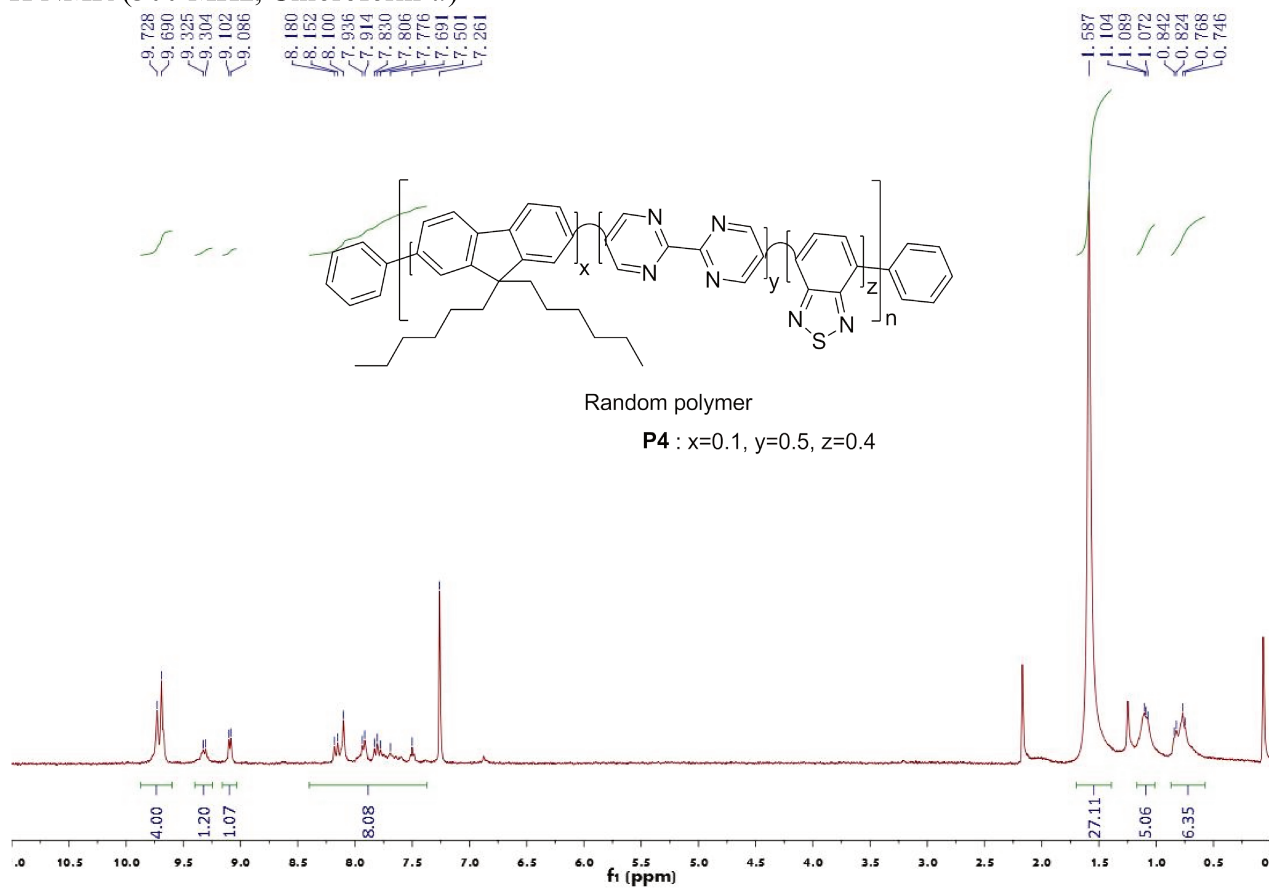
^1H NMR (300 MHz, Chloroform-*d*)

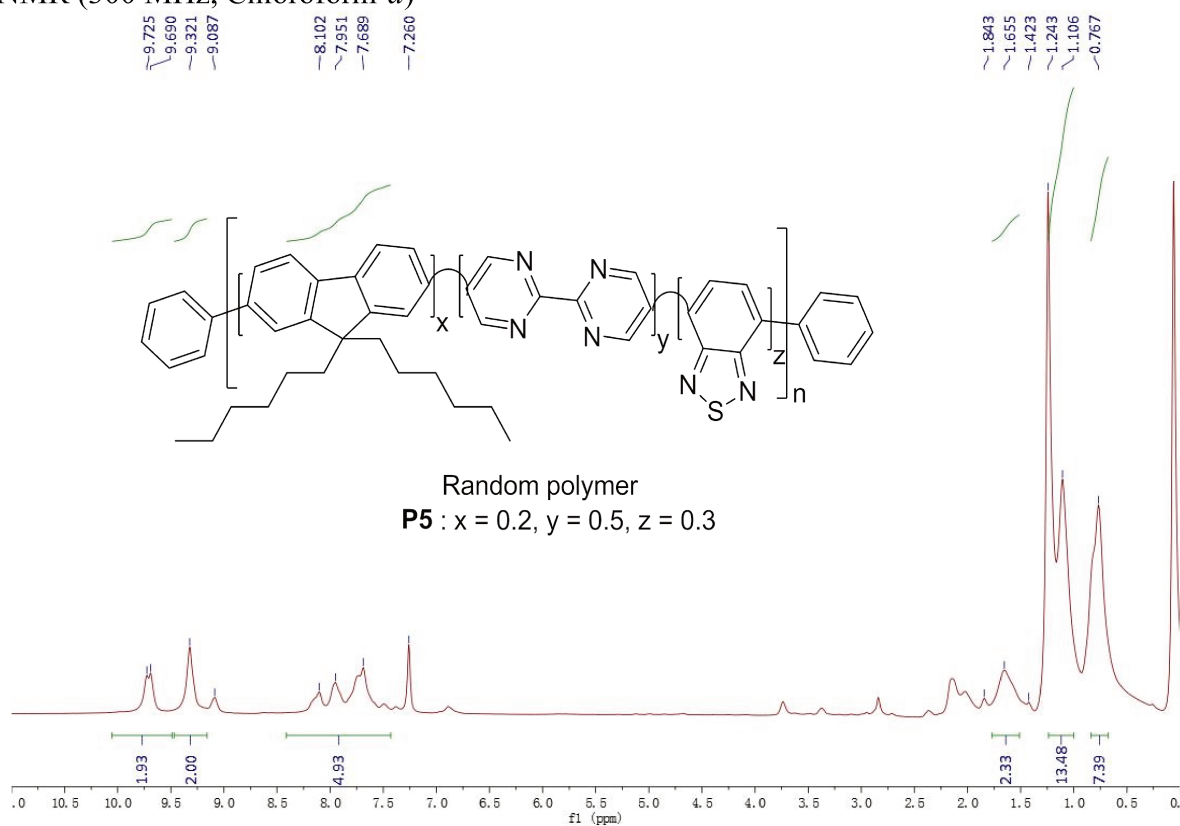
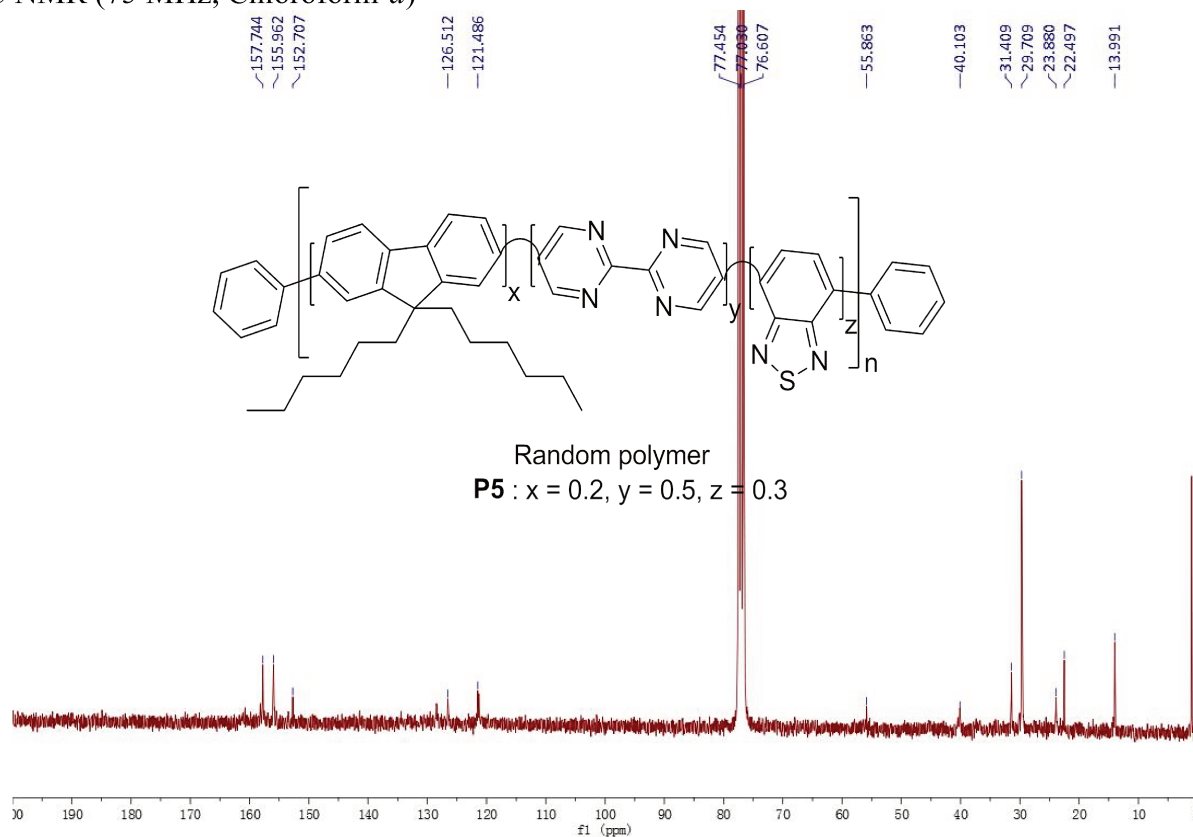


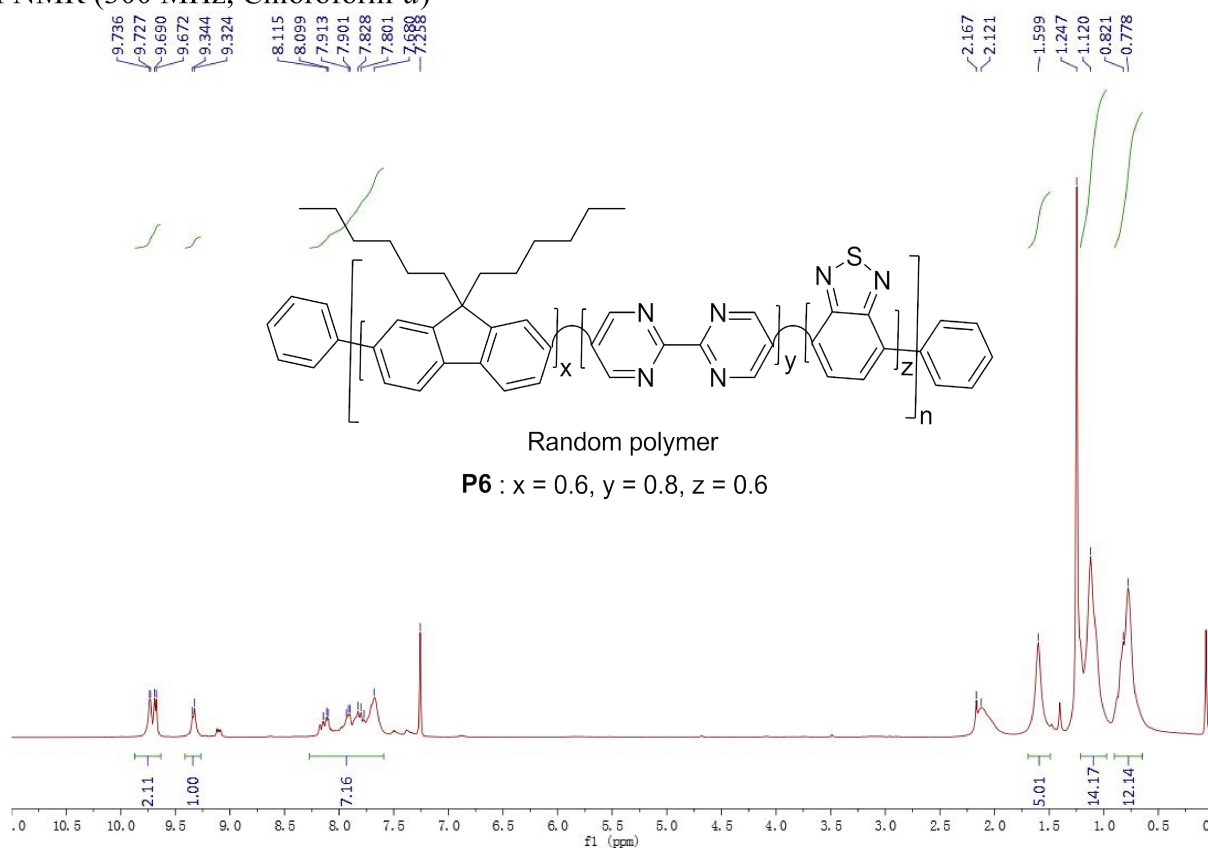
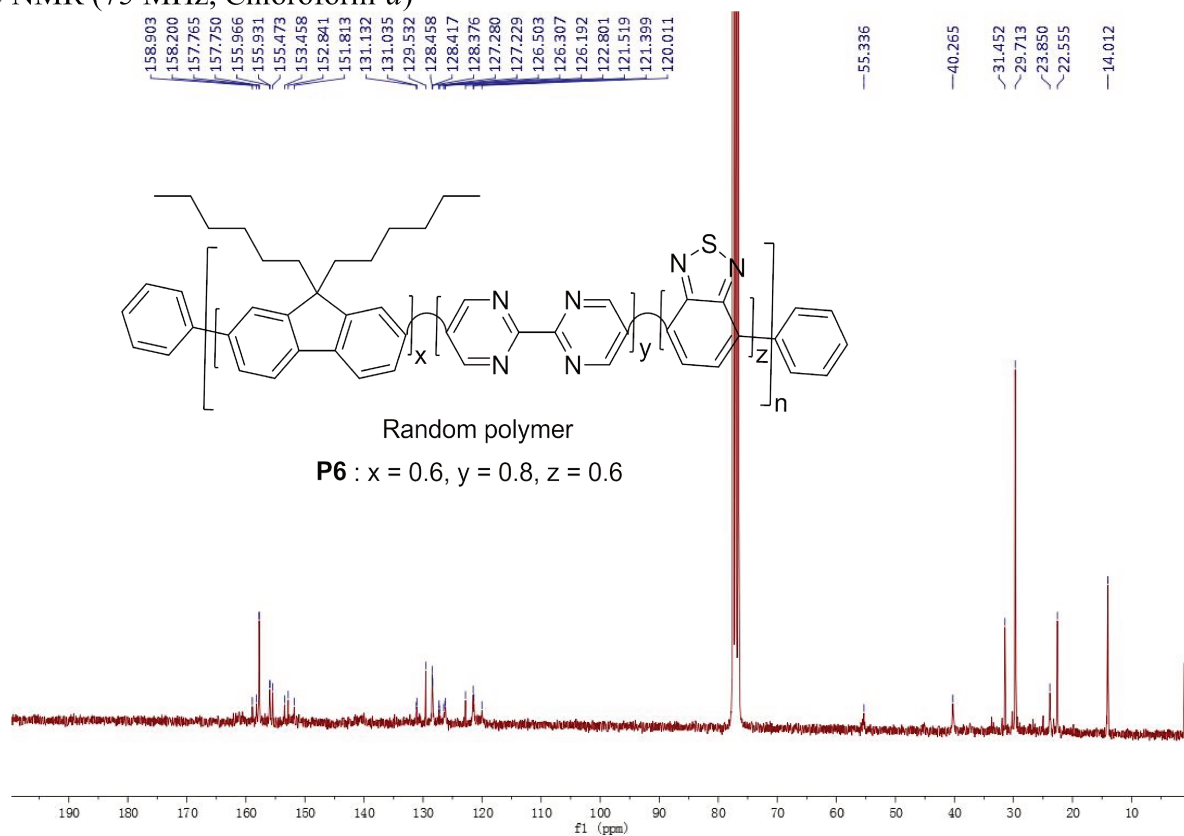
^{13}C NMR (75 MHz, Chloroform-*d*)

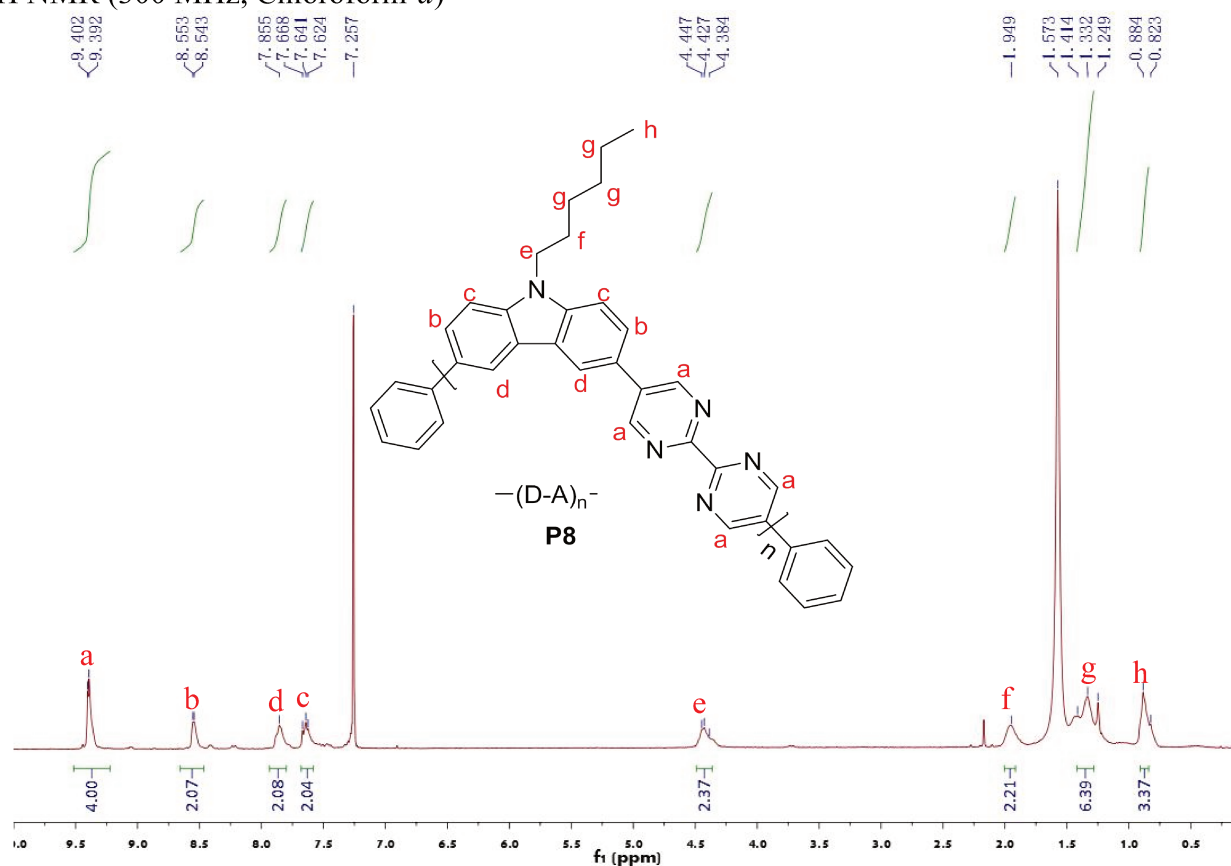
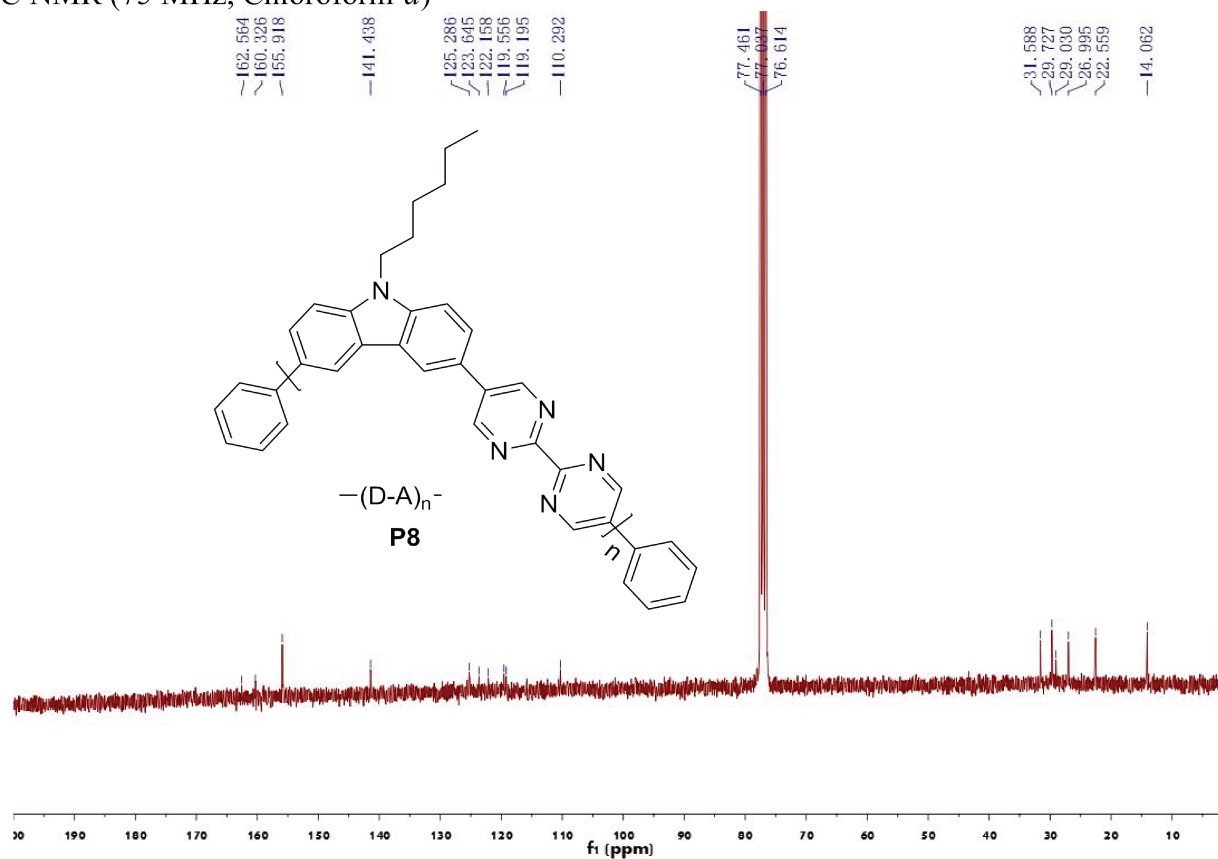


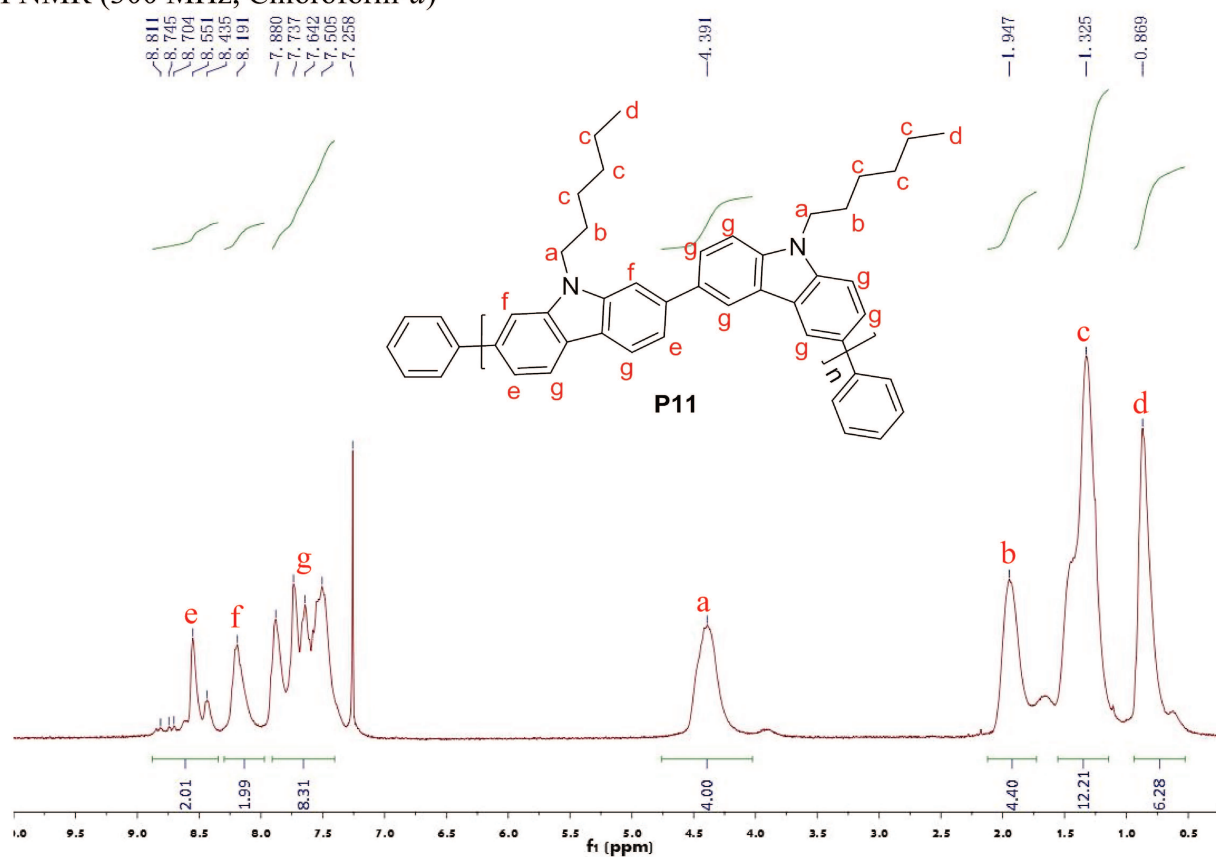
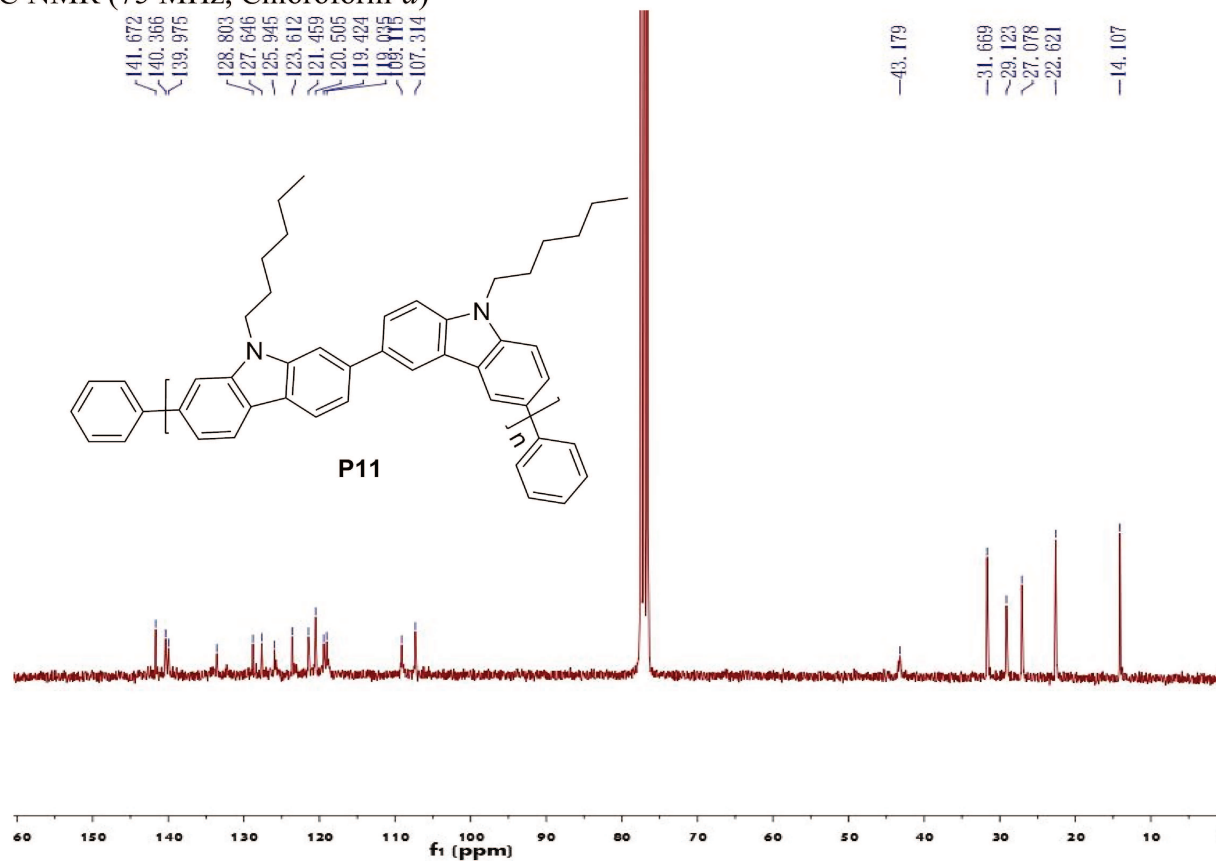
^1H NMR (300 MHz, Chloroform-*d*) ^{13}C NMR (75 MHz, Chloroform-*d*)

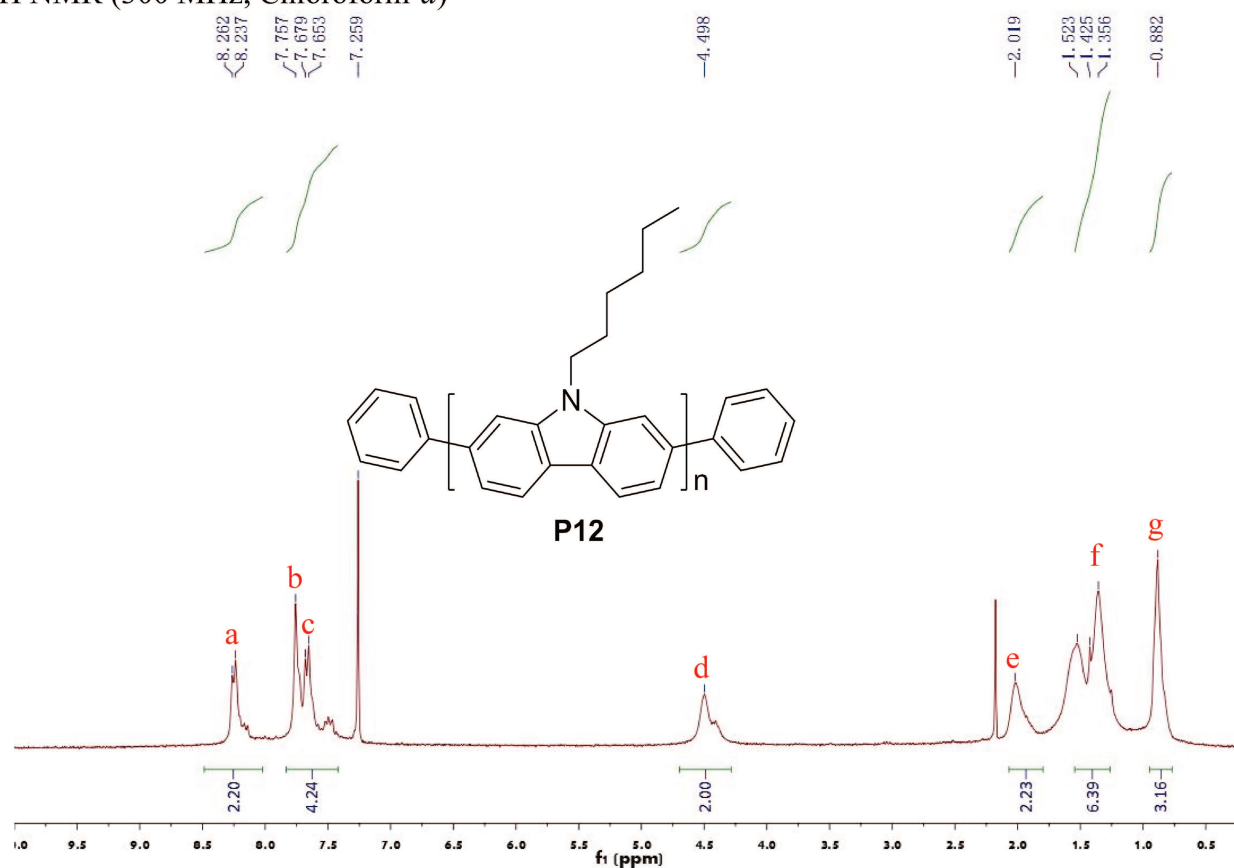
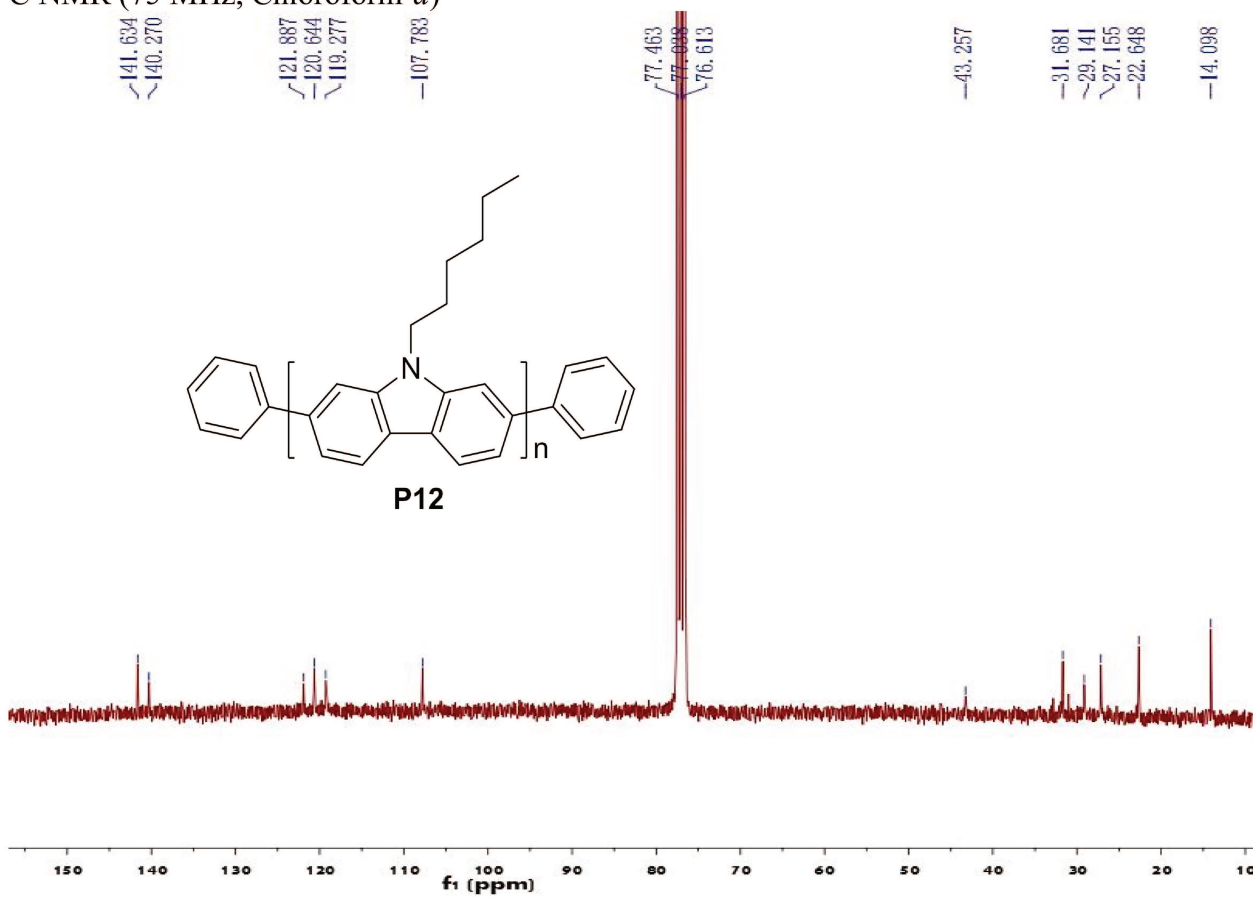
¹H NMR (300 MHz, Chloroform-*d*)

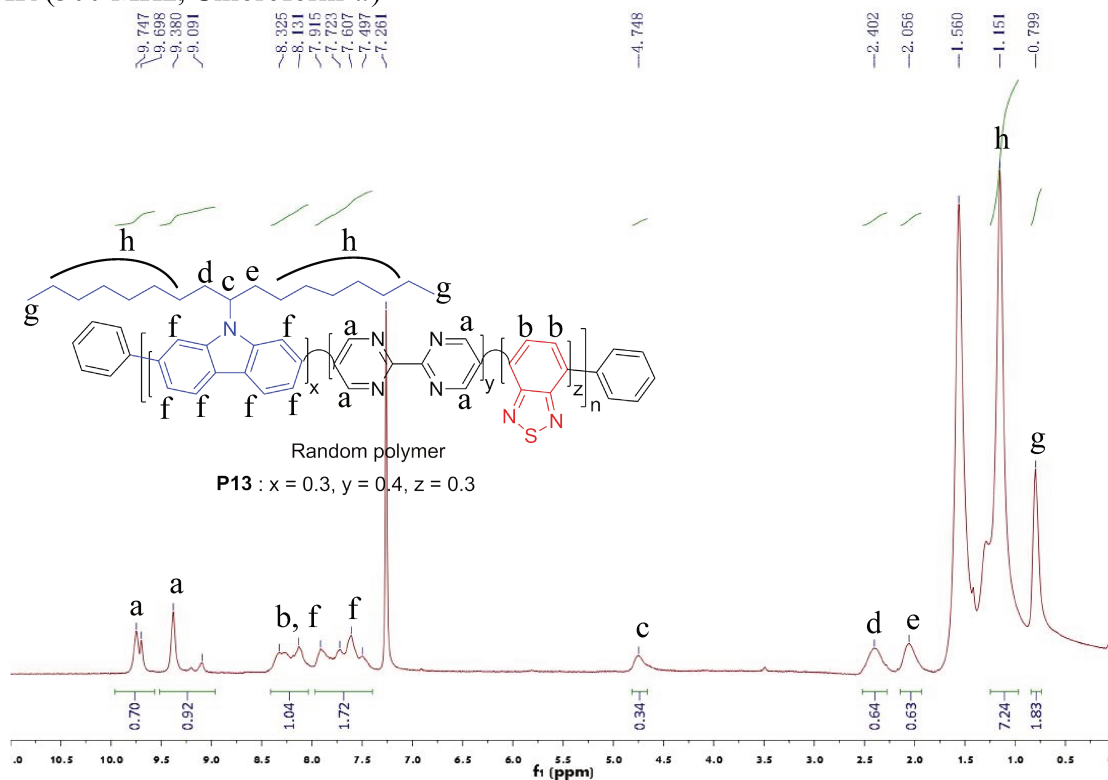
^1H NMR (300 MHz, Chloroform-*d*) ^{13}C NMR (75 MHz, Chloroform-*d*)

^1H NMR (300 MHz, Chloroform- d) ^{13}C NMR (75 MHz, Chloroform- d)

^1H NMR (300 MHz, Chloroform-*d*) ^{13}C NMR (75 MHz, Chloroform-*d*)

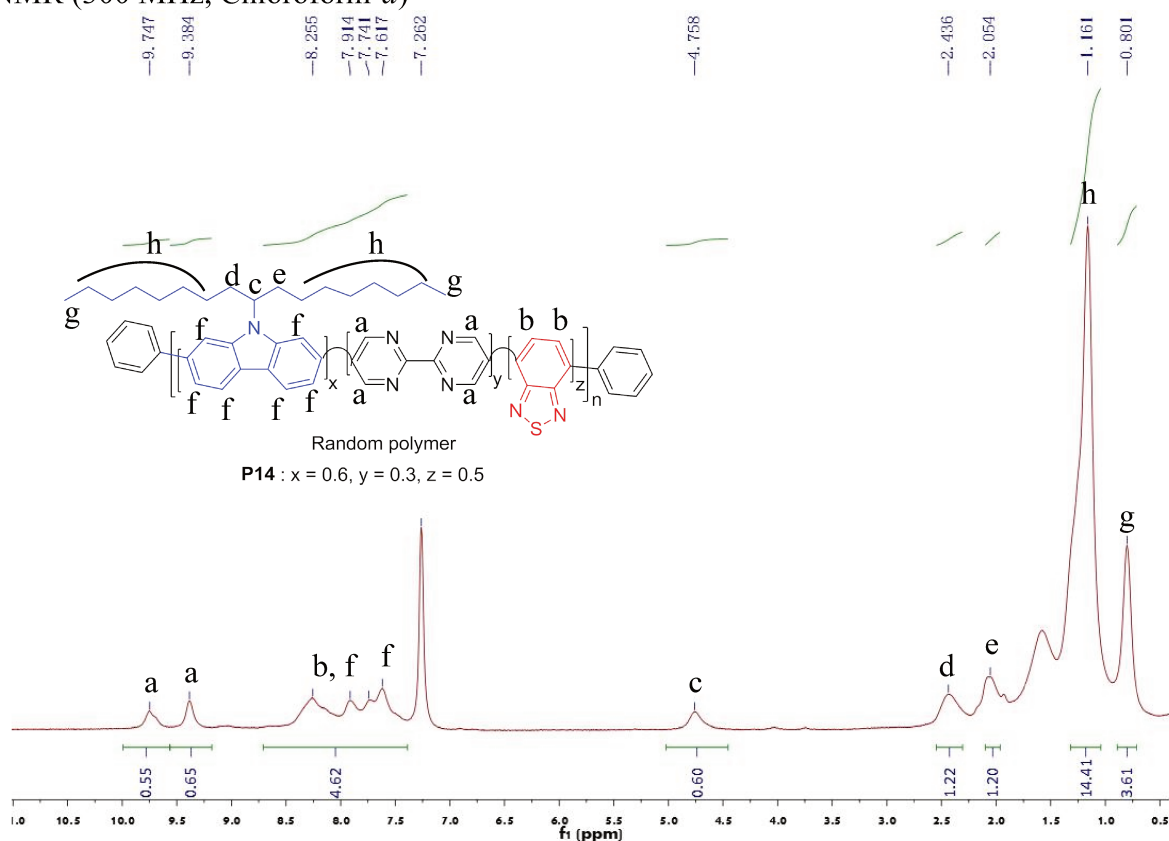
^1H NMR (300 MHz, Chloroform-*d*) ^{13}C NMR (75 MHz, Chloroform-*d*)

^1H NMR (300 MHz, Chloroform-*d*) ^{13}C NMR (75 MHz, Chloroform-*d*)

¹H NMR (300 MHz, Chloroform-*d*)

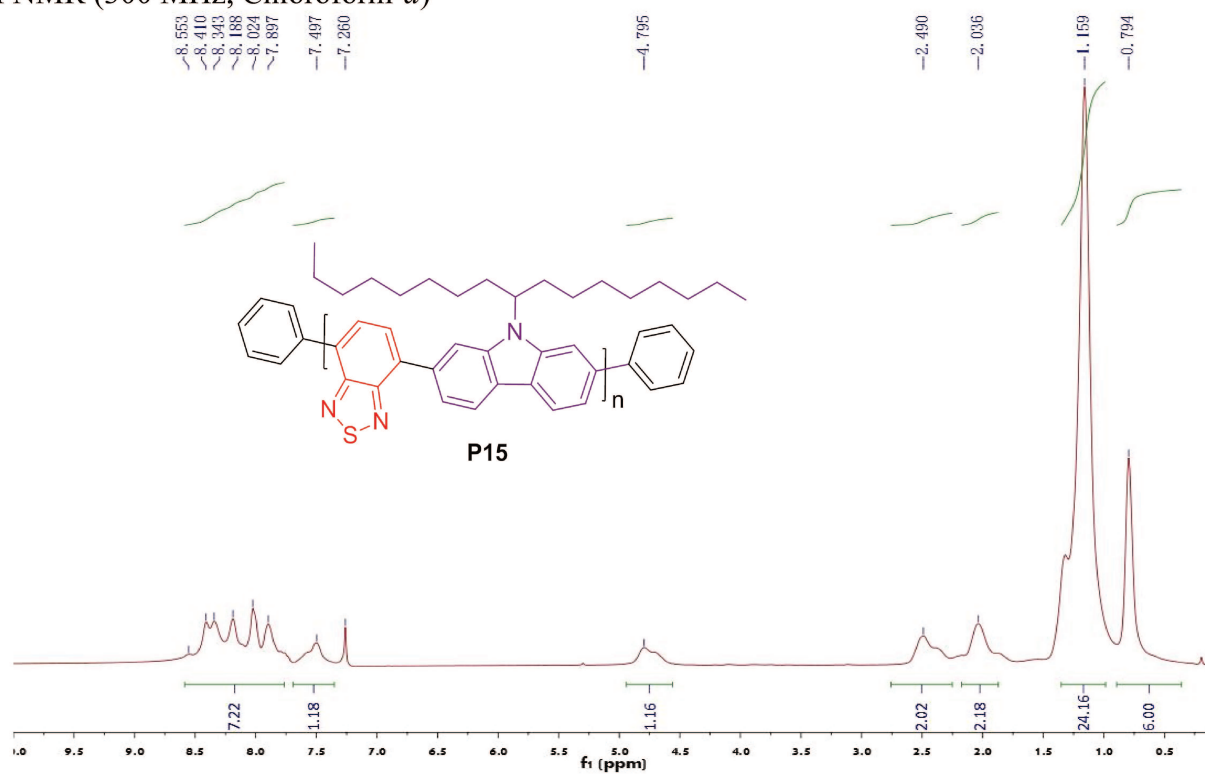
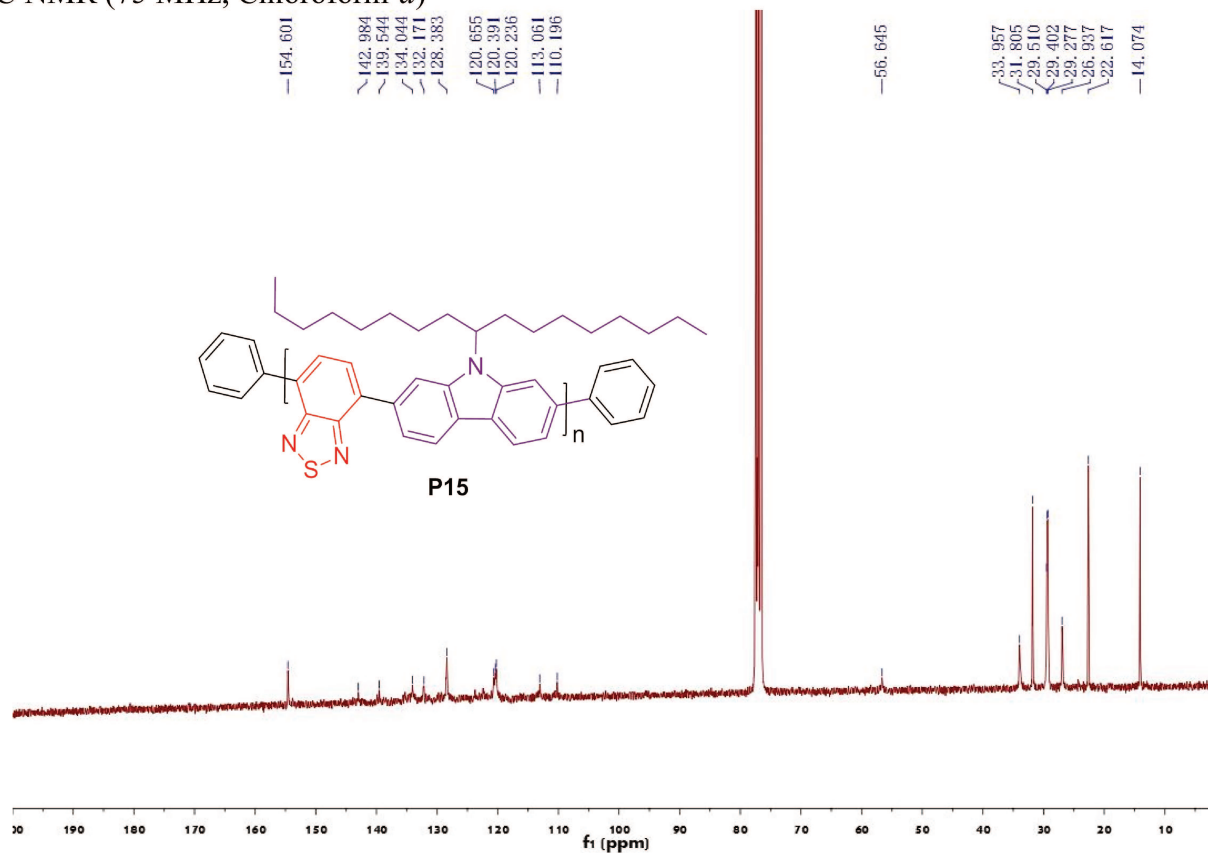
No.	Calculate from the structure	Show in the NMR spectrum
a	$4y = 4 * 0.4 = 1.6$	$0.7 + 0.9 = 1.6$
b[#]	$2z = 2 * 0.3 = 0.6$	Overlapped with "f", total = $1 + 1.7 = 2.7$
c	$1x = 1 * 0.3 = 0.3$	0.3
d	$2x = 2 * 0.3 = 0.6$	0.6
e	$2x = 2 * 0.3 = 0.6$	0.6
f[#]	$6x = 6 * 0.3 = 1.8$	Overlapped with "b", total = $1 + 1.7 = 2.7$
g	$6x = 6 * 0.3 = 1.8$	1.8
h	$24x = 24 * 0.3 = 7.2$	7.2

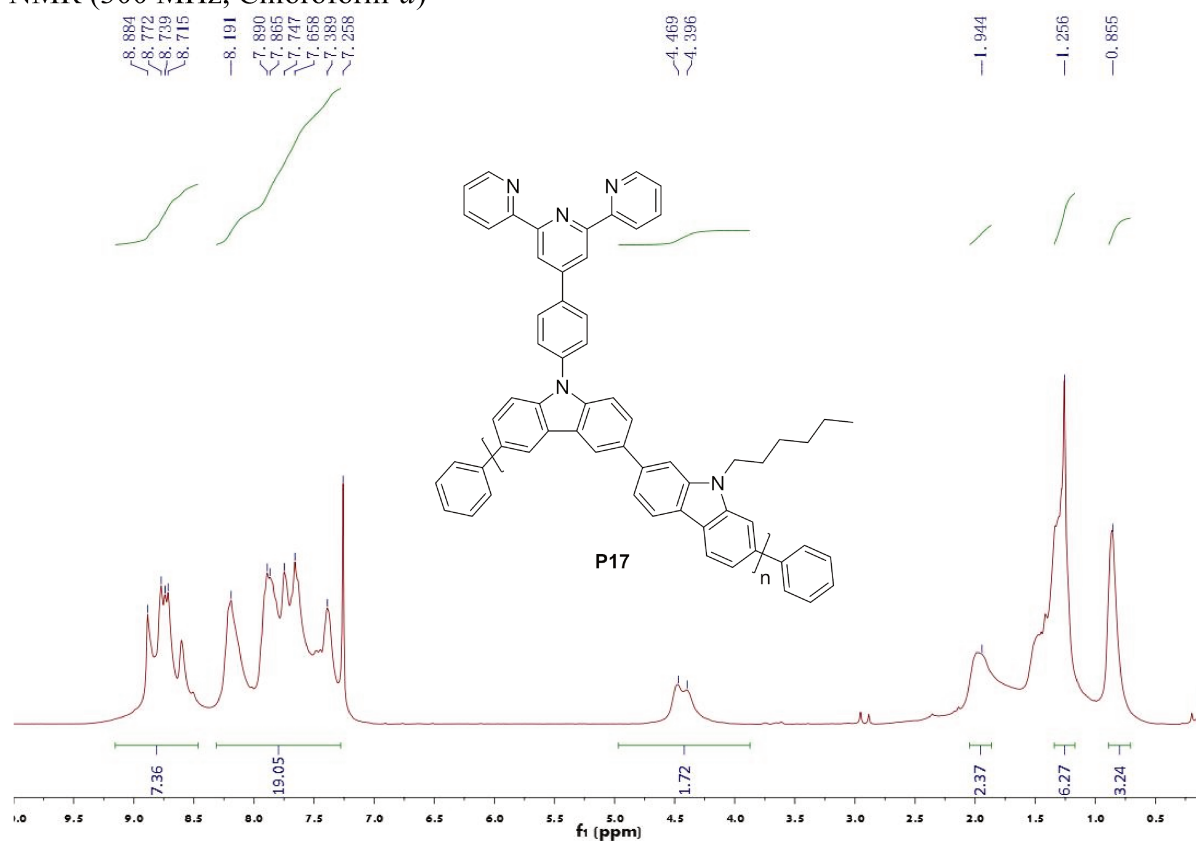
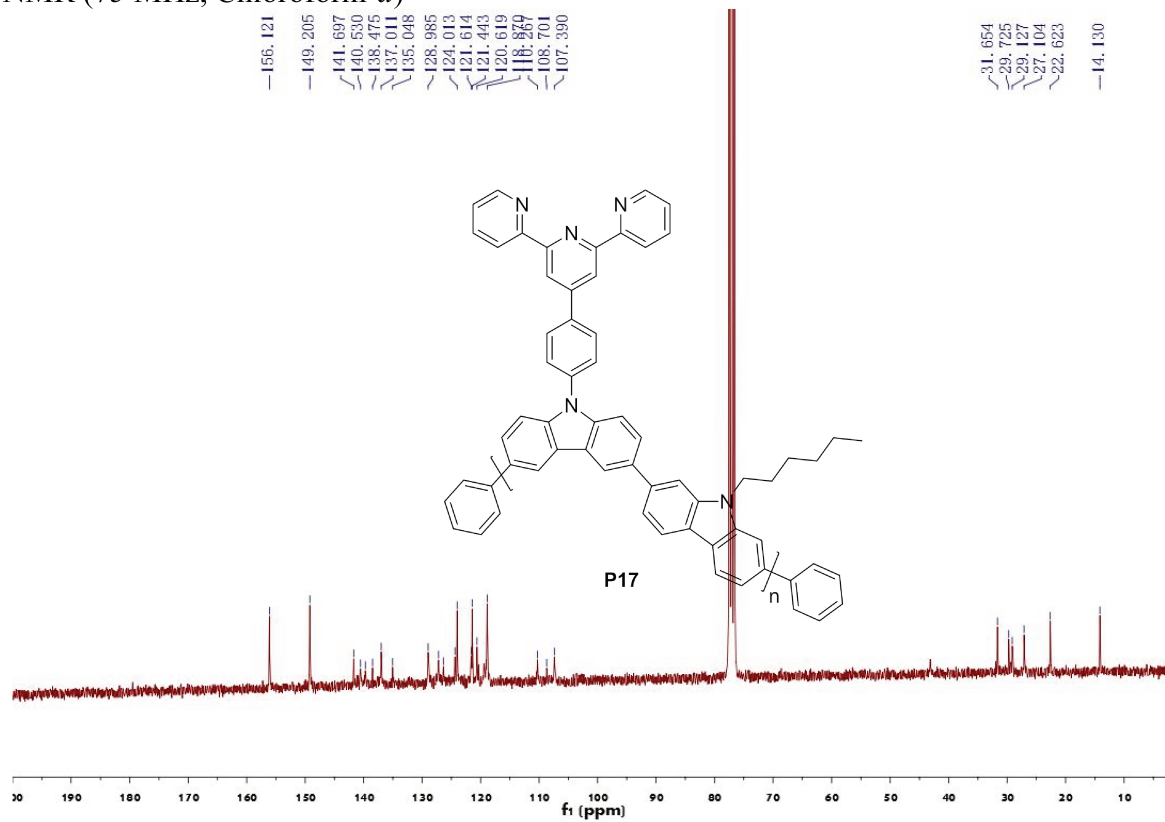
[#] 0.3 more from the NMR spectrum than "b + f" may comes from the end caping benzene unit.

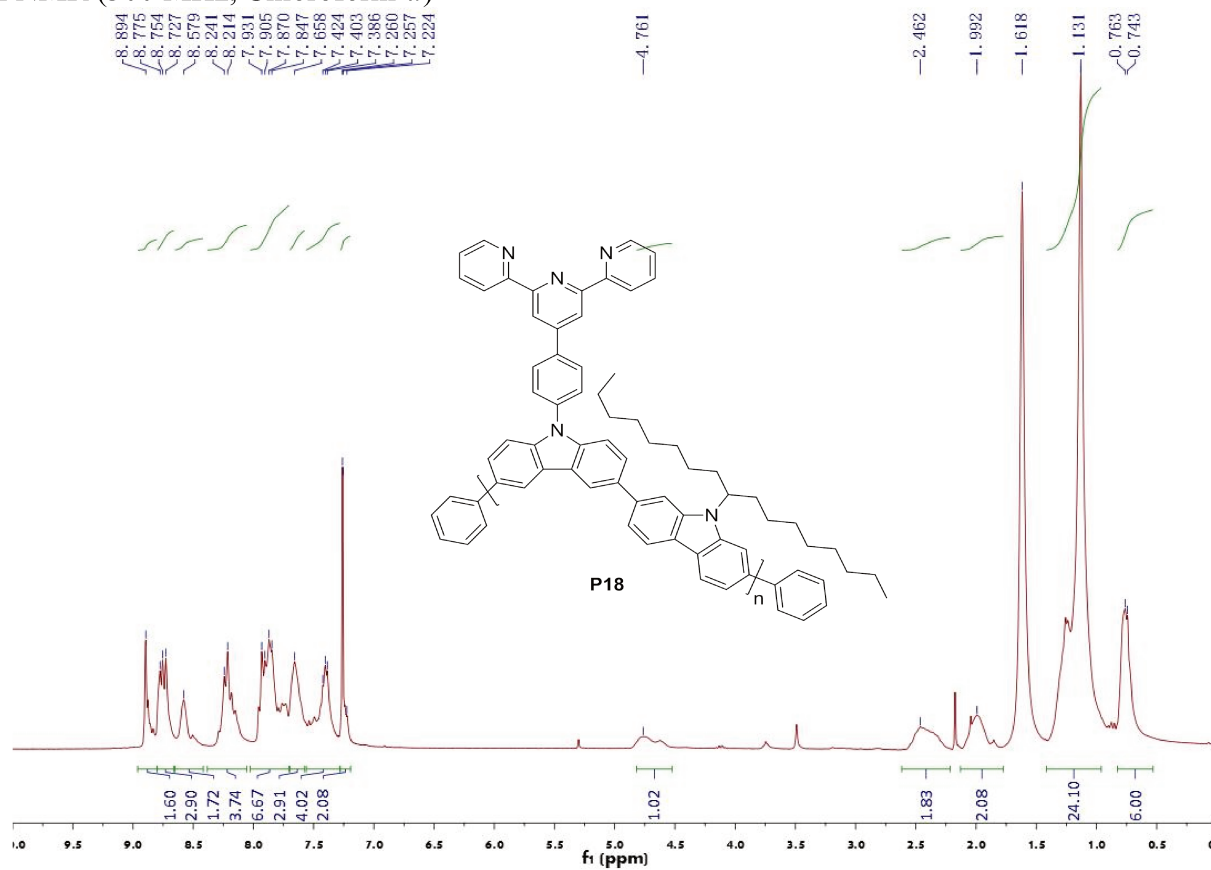
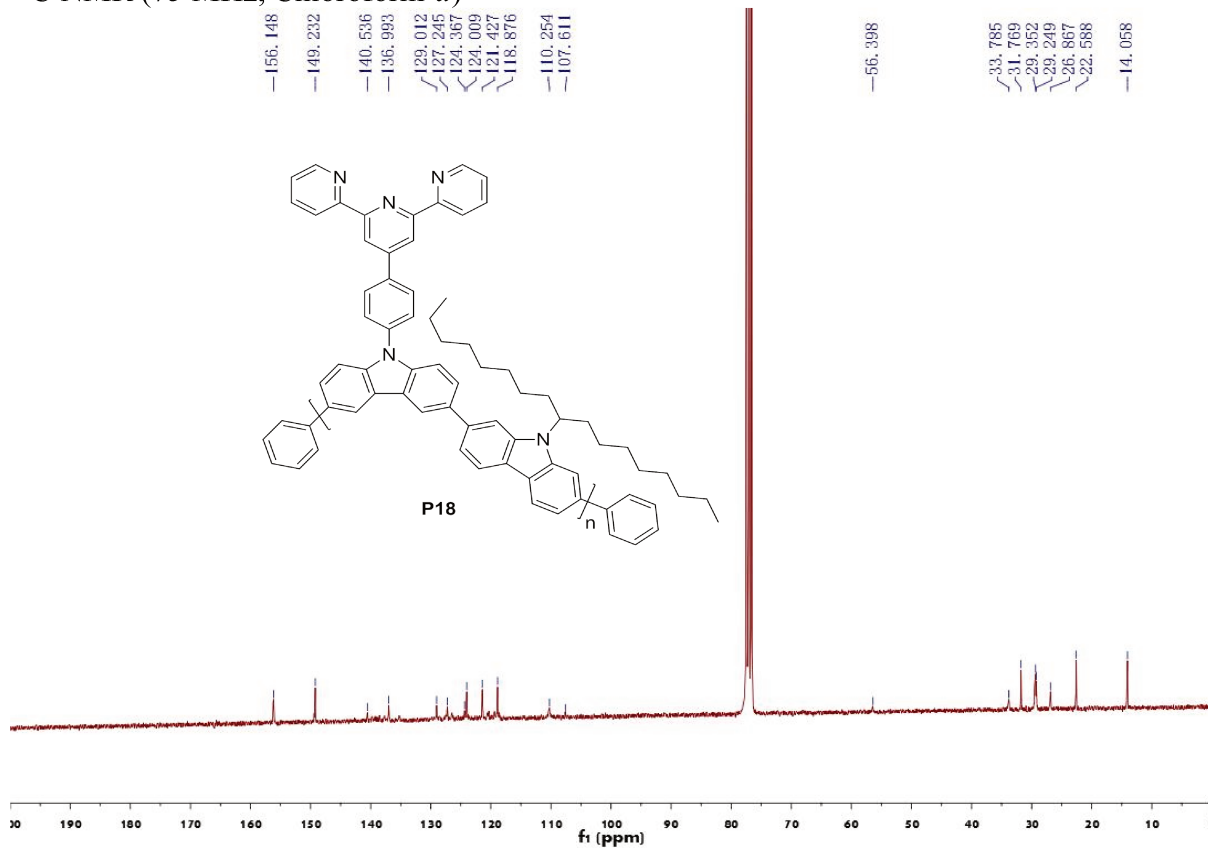
¹H NMR (300 MHz, Chloroform-*d*)

No.	Calculate from the structure	Show in the NMR spectrum
a	$4y = 4 * 0.3 = 1.2$	$0.55 + 0.65 = 1.2$
b	$2z = 2 * 0.5 = 1.0$	Overlapped with "f", total = 4.62
c	$1x = 1 * 0.6 = 0.6$	0.6
d[#]	$2x = 2 * 0.6 = 1.2$	1.22
e[#]	$2x = 2 * 0.6 = 1.2$	1.20
f	$6x = 6 * 0.6 = 3.6$	Overlapped with "b", total = 4.62
g[#]	$6x = 6 * 0.6 = 3.6$	3.61
h	$24x = 24 * 0.6 = 14.4$	14.41

[#] 0.2 more from the NMR spectrum than "b + f" may comes from the end capping benzene unit.

^1H NMR (300 MHz, Chloroform-*d*) ^{13}C NMR (75 MHz, Chloroform-*d*)

^1H NMR (300 MHz, Chloroform-*d*) ^{13}C NMR (75 MHz, Chloroform-*d*)

^1H NMR (300 MHz, Chloroform-*d*) ^{13}C NMR (75 MHz, Chloroform-*d*)

Appendix III List of publications and conferences

Peer reviewed publications

1. Xinyang Wang, **Qiqiao Lin**, Sasikumar Ramachandran, Gaëlle Pembouong, Robert B. Pansu, Bérengère Lebental, Gaël Zucchi*. Optical chemosensors for metal ions in aqueous medium with polyfluorene derivatives: sensitivity, selectivity and regeneration. **2018**. *Sensors & Actuators, B: Chemical*, **2019**, 286:521-532. DOI: [10.1016/j.snb.2019.01.013](https://doi.org/10.1016/j.snb.2019.01.013).
2. **Qiqiao Lin**, Gaël Zucchi* *et al.* Novel conjugated polymeric luminescent material with bipyrimidine as acceptor. **2019**, in preparation.
3. **Qiqiao Lin**, Gaël Zucchi* *et al.* Bipyrimidine-based luminescent conjugated polymers with improved photostability. **2019**, in preparation.
4. **Qiqiao Lin**, Gaël Zucchi* *et al.* Novel single conjugated polymer for white light emission. **2019**, in preparation.

Conference proceedings

Winners of Nobel Prize in chemistry in Académie des sciences, 7 March **2016**, at Institut de France.

2nd Journée de l'Ecole Doctorale 2MIB, held on 8 November **2016**, at CEA - INSTN, Paris.

7th Congrès LPICM, held on 2-4 Octobre, **2017**, at PIRIAC-SUR-MER, France. ([Poster](#))

LPICM_PhD day 2017, held on 23 January, **2017**, at Amphi Cauchy, l'X, Paris. ([Poster and oral presentation](#))

3rd Journée de l'Ecole Doctorale 2MIB, held on 17 Octobre **2017**, at ENS Paris-Saclay. ([Poster](#))

LPICM_PhD day 2018, held on 4 April, **2018**, at Amphi MONGE, l'X, Paris. ([Poster and oral presentation](#))

4th Journée de l'Ecole Doctorale 2MIB, held on 18 October **2018**, at IUT d'Orsay, Paris. ([Poster](#))

2nd International Workshop on Biophotonics and Optical Angular Momentum (BIOAM). Ecole polytechnique, Palaiseau, France. 25-26 October, **2018**.

LPICM_PhD day 2019, held on 15 April, **2019**, at Amphi Becquerel, l'X, Paris. ([Poster and oral presentation](#))

5th Journée de l'Ecole Doctorale 2MIB, held on 11 June **2019**, at l'Université d'EVRY, Paris. ([Oral presentation](#))

Journée du Groupe Français des Luminophores, held on 20 June **2019**, at Polygone scientifique, CNRS, Grenoble, France. ([Oral presentation](#))

Titre : Matériaux hybrides luminescents pour l'éclairage à LED

Mots clés : Polymères conjugués, 2,2'-bipyrimidine, Synthèse, Matériaux hybrides, Éclairage LED

Résumé : Cette thèse visait à concevoir et à synthétiser des matériaux hybrides organiques-inorganiques à luminescence contrôlée et à les étudier en tant que luminophores pour l'éclairage à LED. L'objectif final était d'obtenir une source de lumière blanche. En effet, les LED blanches commerciales sont constituées d'un dispositif émetteur bleu recouvert d'un luminophore jaune. La combinaison de ces deux couleurs produit une lumière blanche. Cependant, cette lumière n'est pas de bonne qualité car il lui manque une composante rouge. Cela entraîne un mauvais rendu des couleurs des objets éclairés par ces sources de lumière. Dans notre travail, des polymères conjugués de différentes couleurs d'émission ont été obtenus avec succès. En particulier, plusieurs émetteurs de blanc ont pu être isolés.

Dans cette thèse, non seulement les procédures de synthèse et les caractérisations chimiques sont présentées en détail, mais également les études des propriétés photophysiques des polymères, en solution et à l'état solide. Des études à l'état solide ont été effectuées sur les polymères et sur les polymères dispersés dans une matrice polymère. Ces études ont permis d'identifier les facteurs limitants quant aux utilisations pratiques de ces matériaux. Des solutions ont été proposées pour améliorer les performances d'émission et de stabilité des matériaux. De plus, ces travaux ont permis d'introduire la 2,2'-bipyrimidine comme nouvelle unité constitutrice pour le développement de polymères conjugués.

Title : Luminescent hybrid materials for LED lighting

Keywords : Conjugated polymers, 2,2'-bipyrimidine, Synthesis, Hybrid materials, LED lighting

Abstract : This thesis aimed at designing and synthesizing organic-inorganic hybrid materials with controlled luminescence and at investigating them as phosphors for LED lighting. The final goal was to obtain a white source of light. Indeed, commercial white LEDs are made up of a blue emitting device covered with a yellow phosphor. Combining these two colors yields white light. However, this light is not of good quality as it lacks some red component. This results in a bad rendering of the colors of objects illuminated by these sources of light. In our work, conjugated polymers with different emission colors have successfully been obtained. In particular, several single white emitters have been isolated.

In this PhD thesis, not only the synthetic procedures and chemical characterizations are presented in detail, but also the studies of the photophysical properties of the polymers, either in solution or in the solid state. Solid state studies were performed on the bulk polymers and on the polymers dispersed into a polymeric matrix. These studies have lead to identify the limiting factors that could hamper the use of the materials. Solutions have been proposed to improve the materials performance and stability. Furthermore, 2,2'-bipyrimidine has been introduced as a new synthon for designing and developing conjugated polymers.